Stony Brook University

Design, synthesis, and biological evaluation of novel taxoid-based drug conjugates and theranostic imaging agents towards tumor-targeted chemotherapy

A Dissertation Presented

by

Jacob G. Vineberg

to

The Graduate School

in Partial Fulfillment of the

Requirements

for the Degree of

Doctor of Philosophy

in

Chemistry

Stony Brook University

August 2014

Stony Brook University

The Graduate School

Jacob G. Vineberg

We, the dissertation committee for the above candidate for the

Doctor of Philosophy degree, hereby recommend

acceptance of this dissertation.

Iwao Ojima
Dissertation Advisor
Distinguished Professor, Department of Chemistry

Dale Drueckhammer
Chairperson of Defense
Professor, Department of Chemistry

Ming-Yu Ngai
Third Member of Dissertation Committee
Assistant Professor, Department of Chemistry

Susan B. Horwitz
Outside Committee Member
Distinguished Professor, Department of Molecular Pharmacology
Albert Einstein College of Medicine

This dissertation is accepted by the Graduate School

Charles Taber
Dean of the Graduate School

Abstract of the Dissertation

Design, synthesis, and biological evaluation of novel taxoid-based drug conjugates and theranostic imaging agents towards tumor-targeted chemotherapy

by

Jacob G. Vineberg

Doctor of Philosophy

in

Chemistry

Stony Brook University

2014

Cancer remains the second leading cause of death in the United States, accounting for nearly a quarter of all deaths, and is exceeded only by heart disease. Traditional chemotherapy uses highly potent cytotoxic agents to kill rapidly dividing cancer cells, relying on the premise that these fast-growing cancer cells are more likely to be killed by these drugs. Despite the profound impact of traditional chemotherapy, lack of tumor-specificity continues to be a serious issue for cancer treatment. Paclitaxel and docetaxel are among the most widely used chemotherapeutic agents, in particular against cancers such as ovarian, breast, lung, and Kaposi's sarcoma; however, despite their high antitumor activity as microtubule-stabilizing agents, these drugs cause undesirable side effects as well as encounter drug resistance. Over the past decade, significant advancement has been made on the development of next-generation taxoids that circumvent these mechanisms of drug resistance and tumor-targeted drug delivery systems (TTDDSs) to selectively deliver these agents to the tumor microenvironment.

Receptors for vitamins, such as those for biotin and folic acid, are overexpressed on the cell surfaces of cancer cells to maintain sufficient vitamin uptake in order to sustain their rapid cell growth and enhanced proliferation. And so, novel tumor-targeting small-molecule drug conjugates (SMDCs) using vitamins (biotin or folic acid) as tumor-targeting modules (TTMs) and next-generation taxoid SB-T-1214 as the cytotoxic agent connected through biocleavable linker systems have been designed, synthesized, and evaluated both *in vitro* and *in vivo*.

Internalization studies *in vitro* using flow cytometry, confocal fluorescence microscopy, and cell viability assays against vitamin-receptor positive and negative cell lines exhibited excellent target-specificity of the conjugates. Furthermore, a biotin conjugate of next-generation fluorotaxoid, SB-T-12822-5, on a self-immolative disulfide linker was designed, synthesized, and used in ^{19}F NMR studies to investigate the mechanism of linker cleavage and the factors that influence plasma stability and metabolic stability by real-time monitoring with ^{19}F NMR.

A series of biotin- and taxoid-based SMDCs was developed through a highly versatile TTDDS, consisting of 1,3,5-triazine as the key tripod splitter module, self-immolative disulfide linkers with polyethylene glycol oligomers to improve water solubility, and a propargylamino arm for the attachment of (a) camptothecin as a second cytotoxic agent (targeted combination chemotherapy), (b) folic acid as a second TTM (dual-targeting conjugate), or (c) an imaging agent (fluorescence or PET theranostics). These conjugates were evaluated against cancer cell lines known to overexpress the biotin receptor and demonstrated efficient internalization, target-specificity, and high potency.

Three PET tracers were developed as companion imaging agents for SB-T-1214 and the biotin-linker-taxoid series. Rapid methylation via Stille coupling of methyl iodide provided an efficient synthetic route for a [^{11}C]-labeled SB-T-1214. Two [^{18}F]-labeled biotin tracers, a small-molecule diagnostic tracer and a theranostic drug conjugate, were also developed for PET imaging.

Table of Contents

Chapter 1

Synthesis and Applications of Enantiomerically Pure β-Lactams

Chapter 2

Paclitaxel, Taxanes, and Next-Generation Taxoids

Chapter 3

Site-Specific Prodrug Activation and Self-Immolative Disulfide Linkers

Chapter 4

Biotin-Linker-Taxoid Tumor-targeting Drug Conjugates

Chapter 5

Double-Warhead Conjugates for Taxoid-Camptothecin Targeted Combination Chemotherapy

Chapter 6

Taxoid-based Tumor-targeting Theranostic Conjugates Bearing a Potential ^{18}F-PET Radiotracer

Chapter 7

Development of Novel ^{11}C- and ^{18}F-labeled Radiotracers for PET Imaging

Chapter 8

Folate-Linker-Taxoid Tumor-targeting Drug Conjugates

Appendices

List of Figures

Chapter 1

Chapter 2

Chapter 3

Chapter 4

Chapter 5

Chapter 6

Chapter 7

Chapter 8

List of Schemes

Chapter 1

Chapter 2

Chapter 3

Chapter 4

Chapter 5

Chapter 6

Chapter 7

Chapter 8

List of Tables

Chapter 2

Chapter 3

Chapter 4

Chapter 5

Chapter 6

Chapter 7

Chapter 8

List of Abbreviations

β-LSM	β-Lactam Synthon Method
δ	chemical shift
Δ	difference
λ	wavelength
3-FABS	three fluorines atoms for biochemical screening
4TI	murine mammary gland carcinoma cell line
A121	human ovarian carcinoma cell line
A2780	human ovarian cancer cell line
A549	human non-small cell lung cancer cell line
AA	arachidonic acid
ABC	ATP-binding cassette
ABL	Abelson murine leukemia viral oncogene
Ac	acetyl
AD	asymmetric dihydroxylation
ADC	antibody-drug conjugate
Am	amyl
ATCC	American Type Culture Collection
ATP	adenosine triphosphate
Bcl	B-cell lymphoma
BLT	biotin-linker-taxoid
BMS	Bristol-Myers Squibb
Bn	benzyl
Boc	butoxycarbonyl
BR	biotin receptor
Bu	butyl
C	centigrade; carbon
CAN	cerium(IV) ammonium nitrate
CD	cluster of differentiation
cDNA	complementary deoxyribonucleic acid
CFM	confocal fluorescence microscopy
CFPAC-1	human pancreatic carcinoma cell line
CML	chronic myelogenous leukemia
Colo-26	murine colon cancer cell line
CPT	camptothecin
CRADA	Cooperative Research and Development Agreement
CuAAC	copper(I)-catalyzed azide-alkyne cycloaddition
CX-1	human colon adenocarcinoma cell line
CYP	cytochrome p450
d	doublet
DAB	deacetylbaccatin
dd	doublet of doublets
DHA	docosahexaenoic acid
DHFR	dihydrofolate reductase
$(DHQD)_2PHAL$	hydroquinidine 1,4-phthalazinediyl diether

DIC	*N*,*N'*-diisopropylcarbodiimide
DIPEA	*N*,*N*-diisoproylethylamine
DLAR	Division of Laboratory Animal Resources at Stony Brook University
DLD-1	human colon carcinoma cell line
DMAP	4-(dimethylamino)pyridine
DMEM	Dulbecco's Modified Eagle medium
DMF	*N*,*N*-dimethylformamide
DMS	dimethyl sulfide
DMSO	dimethyl sulfoxide
DNA	deoxyribonucleic acid
ds	double-stranded
dt	doublet of triplets
DV	double-vitamin
DW	double-warhead
EC	Endocyte
EDC	1-ethyl-3-(3-dimethylaminopropyl)carbodiimide
ee	enantiomeric excess
EGFR	epidermal growth factor receptor
EM	electron microscopy
ESI	electrospray ionization
Et	ethyl
eV	electronvolt
FDA	U.S. Food and Drug Administration
FDG	2-[^{18}F]fluoro-2-deoxy-D-glucose
FITC	fluorescein isothiocyanate
FLT	3'-deoxy-3'-fluorothymidine
FR	folate-receptor
g	gram
GDP	gross domestic product
GE	gastroesophageal
gem	geminal
gp-60	glycoprotein 60
GSH	glutathione reduced form
GTP	guanoside-5'-triphosphate
h	hour
HeLa	human cervical cancer cell line (first derived from Henrietta Lacks)
HER2	human epidermal growth
HIF	hypoxia-inducible factor receptor 2
His	histidine
HMPT	hexamethylphosphorous triamide
HPLC	high-performance liquid chromatography
HRMS	high-resolution mass spectrometry
HSA	human serum albumin
HT-29	human colon cancer cell line
Hz	hertz
IC_{50}	half-maximum inhibitory concentration

ID8	murine ovarian cancer cell line
J	coupling constant
JC	murine mammary gland carcinoma cell line
k	kilo- (scale)
K_{222}	kryptofix-222
L	liter
L1210FR	murine leukemia cell line
L1210	murine leukemia cell line
LA	linoleic acid
LC	liquid chromatography
LDA	lithium diisopropylamide
LHMDS	lithium bis(trimethylsilyl)amide
LNA	α-linolenic acid
m	milli- (scale); multiplet (NMR)
M	mega- (scale); molar
μ	micro- (scale)
m/z	mass-to-charge ratio
mAb	monoclonal antibody
MAD	mitotic arrest deficient
MAP	microtubule-associated protein
MCF-7	human breast carcinoma cell line
MCF-7R	(see NCI/ADR-RES)
MDAH-B231	human breast carcinoma cell line
MDA-MB-435	human metastatic melanoma cell line
MDR	multidrug resistant
Me	methyl
min	minute
MMT060562	murine mammary gland carcinoma cell line
mol	mole
MRI	magnetic resonance imaging
Ms	mesyl (4-methanesulfonyl)
MS	mass spectrometry
MTT	3-(4,5-dimethylthiazol-2-yl)-2,5-diphenyltetrazolium bromide
MTX	mitoxantrone resistance gene
MX-1	human breast carcinoma cell line
n	nano- (scale)
NCI	National Cancer Institute
NCI/ADR-RES	platinum-resistant metastatic ovarian cancer cell line
NHS	*N*-hydroxysuccinimide
NMR	nuclear magnetic resonance
NSCLC	non-small cell lung cancer
p	*para*
P815	murine lymphoblast-like mastocytoma cell line
PANC-1	human pancreatic carcinoma cell line
PBS	phosphate buffered saline
PDGF-R	platelet-derived growth factor receptor

PEG	polyethylene glycol
PET	positron emission tomography
PFP	pentafluorophenyl
Pgp	P-glycoprotein
Ph	phenyl
PMP	*para*-methoxyphenyl
ppm	parts per million
PTX	paclitaxel (Taxol®)
PUFA	polyunsaturated fatty acid
py	pyridine
q	quartet
Raf	rapidly accelerated fibrosarcoma
RD995	murine spindle cell carcinoma
REDOR	rotational echo double resonance
R_f	retention factor
RME	receptor-mediated endocytosis
RNA	ribonucleic acid
RPMI	Roswell Park Memorial Institute medium
s	singlet
S	aqueous solubility promoted
SAR	structure-activity relationship
SB-T	Stony Brook taxoid
SCID	severe combined immunodeficient
SET	single-electron transfer
SIL	self-immolative linker
SMDC	small-molecule drug conjugate
SMVT	sodium-dependent multivitamin transporter
SpA	società per azioni
SPARC	secreted protein acidic and rich in cysteine
SPECT	single-photon emission computed tomography
SS	disulfide bond
Su	succinimide
SW	surrogate-warhead
t	time; triplet (NMR)
t	*tert*
TBAF	tetrabutylammonium fluoride
TBDMS	*tert*-butyldimethylsilyl
TES	triethylsilyl
TFA	trifluoroacetic acid
TFAA	trifluoroacetic anhydride
TIC	total ion current
TIPS	triisopropylsilyl
THF	tetrahydrofuran
TLC	thin-layer chromatography
TMS	trimethylsilyl
TOF	time-of-flight

Ts	tosyl (4-toluenesulfonyl)
TS	thymidylate synthase
TTDDS	tumor-targeted drug delivery system
TTM	tumor-targeting module
US	ultrasound
UV	ultraviolet
VEGF	vascular endothelial growth factor
VLB	vinblastine
WI38	normal human lung fibroblast

Acknowledgments

I would like to express my sincerest gratitude to my dissertation advisor, Distinguished Professor Iwao Ojima, for welcoming me into his research group and guiding me with unparalleled dedication, mentorship, and opportunities to grow as a scientist. I am quite fortunate to have received my training in a multidisciplinary laboratory, such as your own, and a first hand look at discovery chemistry and the many aspects of pharmaceutical sciences. You have provided me with the core skill sets of a synthetic organic and medicinal chemist that I intend on carrying with me in my future journeys. And of course, I would like to thank both you and Mrs. Yoko Ojima for your generous hospitality during the annual 4th of July BBQ and Thanksgiving Eve parties at your home.

I would also like to thank my dissertation committee members, Professor Frank W. Fowler, Professor Dale Drueckhammer, and Professor Ming-Yu Ngai, for their participation in constructive discussions, and sharing their experiences and a passion for chemistry with me throughout my graduate school career. I would also like to extend my utmost appreciation with tremendous respect to Distinguished Professor Susan B. Horwitz for her willingness to serve as an outside committee member on my dissertation committee. I am truly fortunate to have such an influential and groundbreaking scientist in Taxol chemotherapy review and discuss my work in taxoid-based targeted chemotherapy.

An unexpected and fortuitous venture into the world of radiochemistry could not have been made possible without those at the Department of Chemistry at Brookhaven National Laboratory. In particular, I would like to thank Professor Joanna S. Fowler for providing me with the opportunity to work with her research group and showing genuine and sincere interest in my research and career. I would also like to thank Dr. Sung Won Kim, Mr. David Alexoff, Dr. Michael Schueller, Hui Wang, Colleen Shea, and Youwen Xu for all of their training, support, and guidance. In addition, I would like to thank Dr. Jacob Hooker, Dr. Ramesh Neelamegan, and Dr. Osasere Evbuomwan of Harvard Medical School and Martinos Imaging Facility of Massachusetts General Hospital for inviting me to do some ^{18}F radiochemistry in Boston and showing me the wonders of PET imaging.

Graduate school and the doctoral experience relies on a continuous cycle of mentorship and passing knowledge from one generation of students to the next. Thus, I would like to thank former co-worker and Ojima group alumnus, Dr. Joshua D. Seitz, for taking me under his wing, showing me the ropes, and demonstrating not only in his words, but also without details, never details, what it takes to be a chemist, scientist, and professional in business and action. The training and guidance that I received was only surpassed by our friendship.

It has been a wonderful experience working with the many members of the Ojima research group: in particular, the cancer team members: Dr. Edison S. Zuniga, Dr. William Berger, Dr. Anushree Kamath, Tao Wang, Ying-Jen Chen, Longfei Wei, Xin Wang, and Brendan Lichtenthal. It was a great pleasure working with you all. In addition, the infectious disease, organometallics, and anti-inflammatory team members: Dr. Kunal Kumar, Dr. Gary Teng, Dr. Chi-Feng Lin, Dr. Chih-Wei Chien, Dr. Divya Awasthi, Dr. Alex A. Athan, Bora Park, Yang Zang, Simon Tong, Krupa Haranahalli, Edwin "Ricky" Lazo, Dr. Eduard Melief, Dr. Soumya Chowdhury, Dr. Tadashi Honda, Dr. Suqing Zheng, Dr. Motohiro Takahashi, Dr. Akiro Saito, and Dr. Wei Li. I wish you all the best of luck and success in your future endeavors. And of course, the undergraduate research assistants: Adele Whaley, Virghinya Patrecya, Evan "Balboa" Herlihy, Jonathan "Puerto Rico Bob" Khan, and Katherine Maffucci. Some of you

produced more β-lactam than others. Finally, Mrs. Patricia Marinaccio, from my first day until the last, you put the "family" in the Ojima group family with your perpetual thought, kindness, and resilience without interruption.

I would like to acknowledge and thank the many members of the Department of Chemistry and collaborators within the Stony Brook University community for their contributions to the completion of this dissertation. Dr. Béla Ruzsicska, for teaching me something about mass spectrometry and Habs ice hockey, I hope that Montréal brings home the Cup, though not at the Islanders' expense; Dr. Jim Marecek and Dr. Francis Picart, for their love and keen understanding of the intricacies of NMR spectrometry; Dr. Galina Botchkina, Ms. Rebecca Rowehl, and Dr. Anne Savitt, for their expertise in cell culture and cancer cell biology; Mrs. Roxanne Brockner, for allowing me use the air-conditioned conference room; Dr. Guo-Wei Tian, for training me in confocal fluorescence microscopy; Dr. Tom Zimmerman and Jean Rooney, for coordinating live-animal studies. In addition, I would like to thank my colleagues, both students and faculty, in the Department of Chemistry at Stony Brook University.

I would like to acknowledge the financial support from the National Cancer Institute (CA 103313 to I.O.) and State University of New York at Stony Brook.

Most importantly, I would like to thank my friends and family for all their continuous love and support not only during my four years at Stony Brook University, but throughout my entire life. My friends, some from my days in St. Louis and others from home, Dr. Dharmesh Tank, Mr. Ross Goldberg, Señor Ben Kellison, Sean Lee, Marc Dolgow, there was never a dull moment, indeed. To Susannah, my supporter, my best friend, and my love, you have given me something to look forward to each and every week of this journey, and you have stood by me every step of the way. To both of my parents, Allyn and Ariela, you have always invested your lives in me during high times and low and showed me that I can accomplish anything. I am who I am because of you both, and I cherish everything you have given me.

Vita

Education

State University of New York at Stony Brook, Stony Brook, NY
PhD, Organic Chemistry, 2014

Washington University in St. Louis, St. Louis, MO
B.A. Chemistry (*conc.* in biochemistry), 2010

Peer-reviewed Publications

Vineberg, J.G.[1]; Zuniga, E.S.; Kamath, A.; Chen, Y.-J.; Seitz, J.D.; Lichtenthal, B.; Ojima, I. Tumor-targeted drug delivery system for dual-warhead drug conjugates. *J. Med. Chem.*, **2014**, *57* (13), 5777-5791.

Seitz, J.D.[1]; **Vineberg, J.G.**[1]; Wei, L; Khan, J.F.; Lichtenthal, B.; Lin, C.-F.; Ojima, I. Design, Synthesis and Application of Fluorine-labeled Taxoids as ^{19}F NMR Probes for the Metabolic Stability Assessment of Tumor-targeted Drug Delivery Systems. *J. Fluor. Chem.*, Submitted.

Ojima, I.; Kumar, K.; Awasthi, D.; **Vineberg, J.G.** Drug discovery targeting cell division proteins, microtubules, and FtsZ. *Bioorg. Med. Chem.,* **2014**, DOI: 10.1016/j.bmc.2014.02.036

Seitz, J.D.; **Vineberg, J.G.**; Zuniga, E.S.; Ojima, I. Fluorine-containing taxoid anticancer agents and their tumor-targeted drug delivery. *J. Fluor. Chem.* **2013**, *152*, 157-165.

Selected Presentations

Vineberg, J.G.; Wang, T.; Seitz, J.D.; Fowler, J.S.; Ojima, I. Development of robust tumor-targeting drug delivery system (TDDSS) platform and its applications to novel taxane-based drug conjugates with biotin as the tumor-targeting module. *The 247th American Chemical Society National Meeting,* March 16-20, 2014, Dallas, TX. Abstract of Papers, MEDI-235 (Oral).

Vineberg, J.G.; Zuniga, E.S.; Fowler, J.S.; Ojima, I. Taxoid-based tumor-targeting chemotherapeutic agents bearing an imaging module. *The 245th American Chemical Society National Meeting*, April 7-11, 2013, New Orleans, LA. Abstract of Papers, MEDI-271 (Oral).

Vineberg, J.G.; Zuniga, E.S.; Ojima, I. Synthesis and biological evaluation of novel dual-warhead tumor-targeting drug conjugates bearing a taxoid and a camptothecin. *The 244th American Chemical Society National Meeting*, August 19-23, 2012, Philadelphia, PA. Abstract of Papers, MEDI-306.

Certification Programs

Chemical Biology Training Program, Department of Chemistry, Stony Brook University, 2012

Fundamentals of the Bioscience Industry Program, Center for Biotechnology, Stony Brook University, 2014

Honors and Awards

Chemistry Award for Excellence in Doctoral Research, Department of Chemistry, Stony Brook University, 2014

Memberships

New York Academy of Sciences, Dec 2013 – Present

American Chemical Society, Aug 2012 – Present

Tau Kappa Epsilon Fraternity – Xi Chapter, April 2008 – Present

Chapter 1

Synthesis and Applications of Enantiomerically Pure β-Lactams

Chapter Contents

§1.1 Introduction

§1.1.1 β-Lactam Synthon Method (β-LSM)

Over the past half-century, the β-lactam structure has attracted significant research interest in pharmaceutical development. First recognized for their uses as antimicrobial agents, β-lactam antibiotics, such as penicillins, cephalosporins, monobactams, and carbapenems, have become the primary treatment options for bacterial infections and remain one of the most significant advances in modern medicine (Figure 1.1).[1] More recently, β-lactams have emerged as versatile synthetic intermediates in the synthesis of unnatural amino acids, dipeptides, and β-amino acids.[2] The development of the "β-Lactam Synthon Method" in the late 1970s and early 1980s by Ojima and co-workers demonstrated that enantiopure β-lactams could serve as powerful tools in medicinal chemistry.[3]

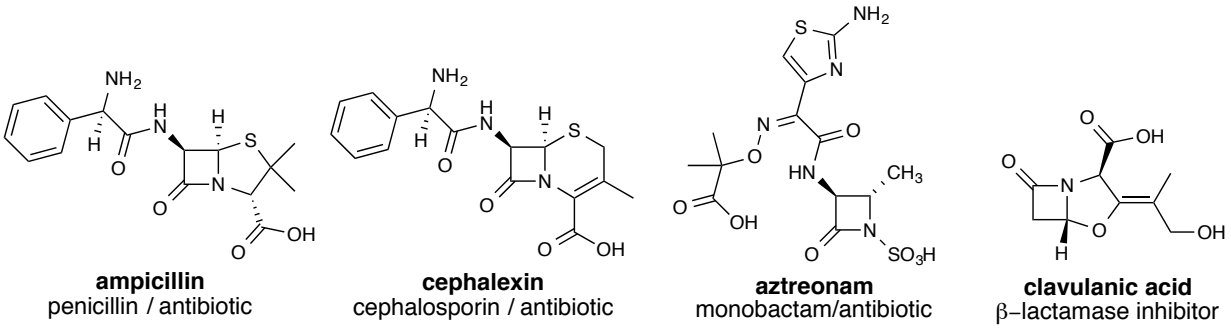

Figure 1.1. Chemical structures of some medicinally active β-lactams.

The β-LSM has since been employed in the synthesis of numerous medicinally active compounds, such as paclitaxel and next-generation taxoid anticancer agents, cryptophycins, and indolizidine alkaloids, which contain substituted isoserine β-amino acids.[3] These chiral isoserine moieties can be obtained from the ring-opening of enantiopure 3-hydroxy-β-lactams at the N–C(O) bond.[4] Cleavage of the β-lactam ring usually occurs through the N–C(O) bond by nucleophilic acyl substitution, however due to the highly strained conformation of the four-membered heterocycle, ring opening can occur at any of the four bonds.[2, 4-6]

Various synthetic methods towards the synthesis of enantiomerically pure β-lactams have been reported,[3] however the two most common approaches are the ketene-imine Staudinger [2+2] cycloaddition[7] followed by chemoenzymatic resolution (Section 1.2.1) and the lithium chiral ester enolate-imine cyclocondensation (Section 1.3.1).[8] The focus of these β-lactam syntheses was guided by the synthesis of highly potent taxoid-based anticancer agents.

§1.1.2 Semisynthesis of Taxane-based Anticancer Agents *via* the β-Lactam Synthon Method

Paclitaxel (Taxol®), docetaxel (Taxotere®), and cabazitaxel (Jevtana®) are three highly potent taxane anticancer agents, which contain phenylisoserine side chains that can be introduced semi-synthetically to a common tetracyclic baccatin core via the β-LSM (Figure 1.2).

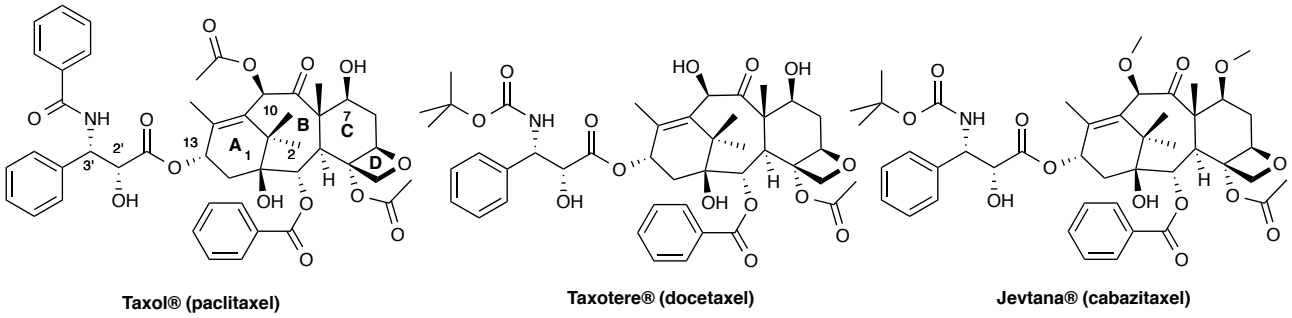

Figure 1.2. Chemical structures of taxane anticancer agents: paclitaxel, docetaxel, and cabazitaxel.

Highly efficient chiral ester enolate-imine cyclocondensation giving 3-hydroxy-4-aryl-β-lactams with excellent enantiomeric purity was successfully applied to the asymmetric synthesis of optically pure paclitaxel and docetaxel.[9] (3*S*,4*R*)-*N*-Acylated-3-(1-ethoxyethoxy)-4-phenyl-2-azetidinone, which was readily prepared from 3-hydroxy-4-phenyl-β-lactam, was coupled to various protected baccatin IIIs, followed by deprotection to give enantiomerically and diastereomerically pure paclitaxel and docetaxel in excellent yields.[9]

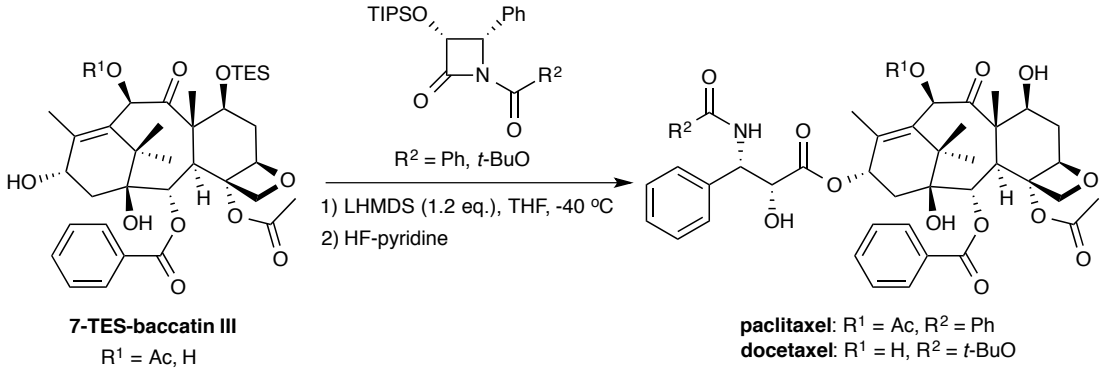

Scheme 1.1. The semisynthesis of paclitaxel and docetaxel by the Ojima-Holton coupling protocol.

The application of the β-LSM to the C13 side-chains of paclitaxel and docetaxel became known as the Ojima-Holton coupling protocol (Scheme 1.1).[10] The Ojima-Holton coupling reaction has allowed for a facile and efficient means for the semisynthesis of next-generation taxoids, some of which possess higher potency and better bioavailability than paclitaxel and docetaxel, and a much clearer understanding of the structure-activity relationship (SAR) for the taxane class.[10] Based on these SAR studies, β-lactams (+)**1-6** and (+)**1-20** with *N*-*t*-Boc and C4-isobutenyl or difluorovinyl moieties, respectively, were synthesized (Figure 1.3).

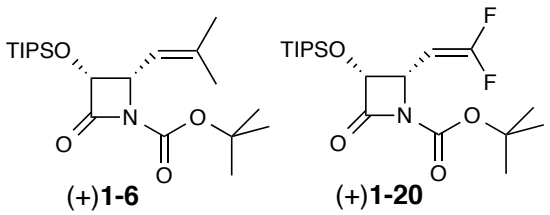

Figure 1.3. Chemical structures of β-lactams (+)**1-6** and (+)**1-20**.

§1.2 Synthesis of Enantiopure β-Lactams

§1.2.1 Staudinger [2+2] Ketene-Imine Cycloaddition Reaction followed by Kinetic Enzymatic Resolution

In 1907, Herman Staudinger developed the first synthetic route towards the synthesis of the β-lactam *via* a thermal [2+2] cycloaddition of the Schiff base (imine) derived from aniline and benzaldehyde with diphenylketene.[7] The most accepted mechanism takes place in a stepwise process, in which the imine nitrogen, as a nucleophile, attacks the ketene carbon to form a zwitterionic intermediate, which undergoes an electrocyclic conrotatory ring closure giving two new stereocenters at the C3 and C4 positions of the lactam.[11] Since the ketene is generated *in situ* in the Staudinger [2+2] reaction, various experimental factors such as temperature, solvent, base, and chloride anion can influence the stereochemical outcomes.[12] Molecular modeling (*ab initio*) at the RHF/6-31G* and MP2/6-31G*//6-31G* theory levels showed that electrocyclic conrotatory ring closure proceeds under stereoselective control as the rate-determining step, in which an *exo* attack from *E*-imines preferentially leads to the formation of *cis*-β-lactams, whereas *Z*-imines give *trans* isomers.[11, 13]

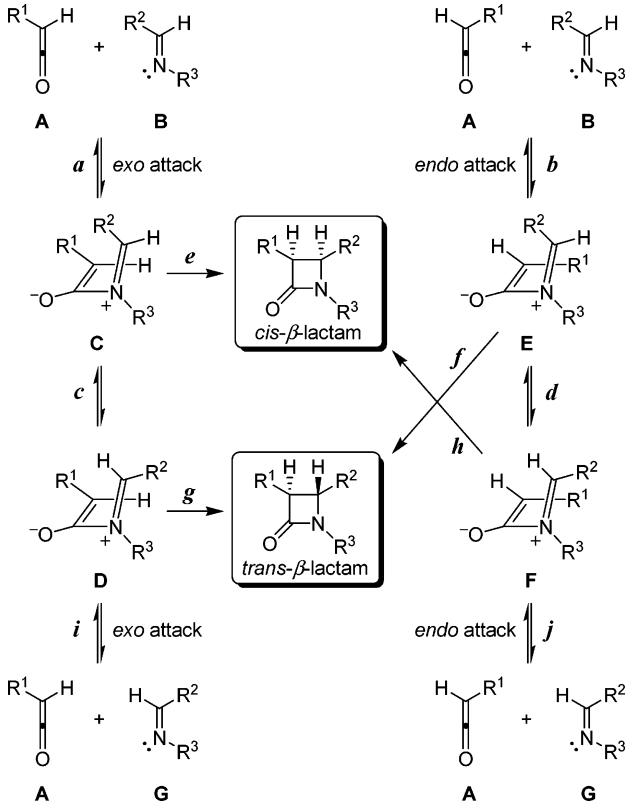

Figure 1.4. Pathways for formation of *cis*- and *trans*-β-lactams. Reprinted from reference [12].

However, since isomerization may occur at the zwitterionic intermediate, the relative rates between direct ring closure and isomerization determine the stereochemical outcome of the reaction (Figure 1.4).[12] Thus, both the torquoelectronic effect of ring closure and the electronic effects of the imine determine the stereochemical outcomes of the Staudinger [2+2] reaction (Figure 1.5).[11, 12]

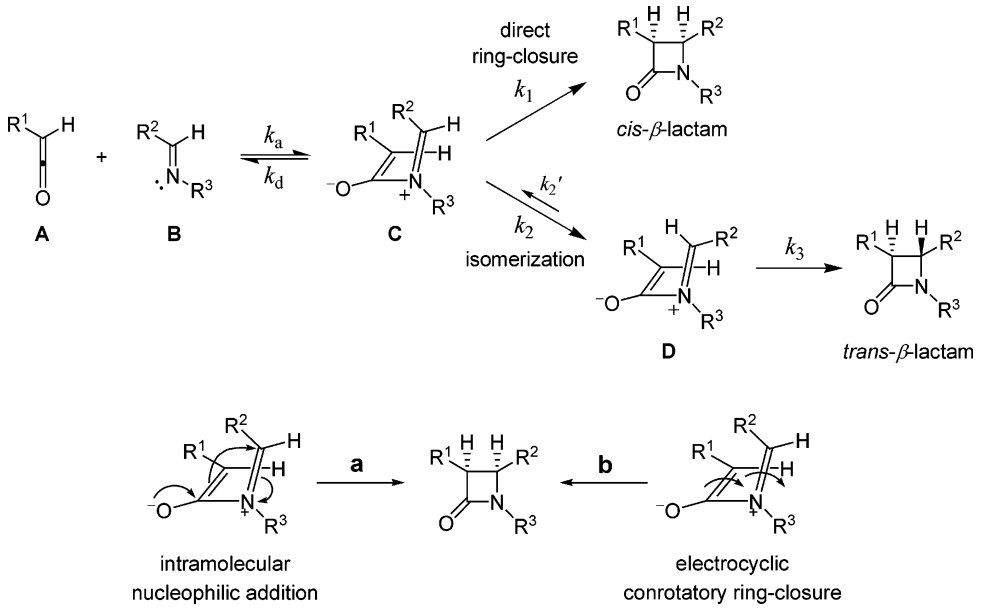

Figure 1.5. Suggested model for the relative stereoselectivity in the Staudinger reaction. Adapted from reference [12].

Although asymmetric Staudinger [2+2] reactions have recently been reported,[14] enantiopure β-lactams can be obtained from racemic mixtures by kinetic enzymatic resolution with various lipases.[15]

§1.2.2 Synthesis of Enantiomerically-Enriched β-Lactams *via* Staudinger Reaction Followed by Enzymatic Resolution

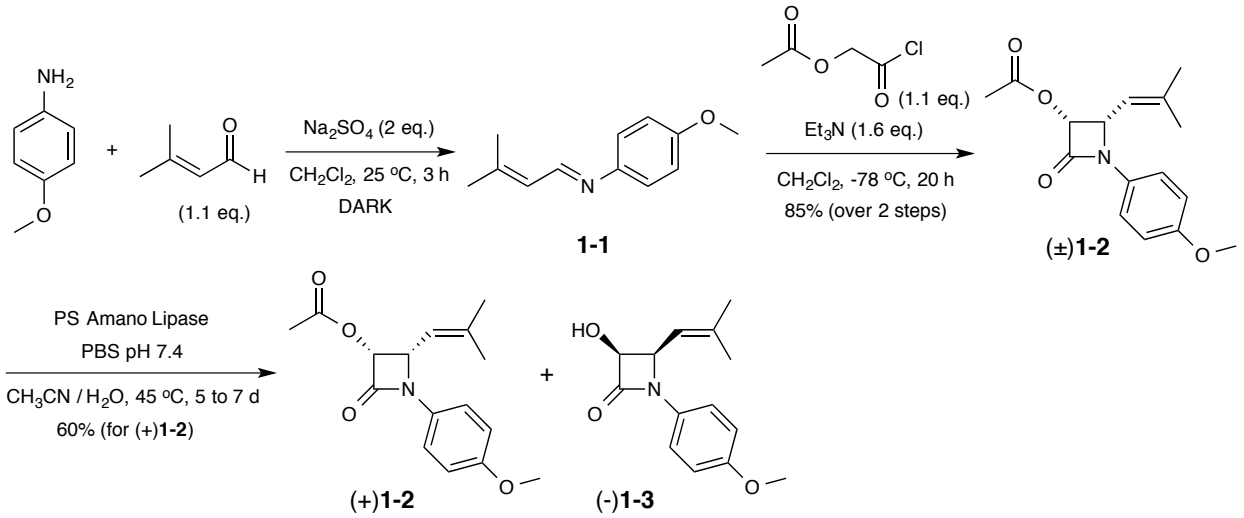

Scheme 1.2. Synthesis of enantiopure (+)**1-2** by Staudinger [2+2] cycloaddition followed by kinetic enzymatic resolution.

The synthesis of racemic *cis*-β-lactam (±)**1-2**, shown in Scheme 1.2, began with the formation of imine **1-1** from *p*-anisidine and 3-methyl-2-butenal in the presence of sodium sulfate in quantitative yield, the product of which was used immediately in the subsequent reaction without further purification. Imine **1-1** was added to the ketene generated *in situ* from acetoxyacetyl chloride and triethylamine at low temperature under anhydrous conditions to

generate racemic β-lactam (±)**1-2** in good yield (85% over 2 steps) in an exclusively *cis*-stereochemical outcome. The C3 acetate of the (-)-enantiomer was selectively hydrolyzed with PS Amano Lipase, derived from *Burkholderia cepacia*, allowing for selective preservation of (+)**1-2** in excellent enantiopurity (>99% ee). A co-solvent system of acetonitrile and phosphate buffered solution was used to accommodate the solubility of **1-2** as well as the physiological conditions required for optimal enzymatic function.

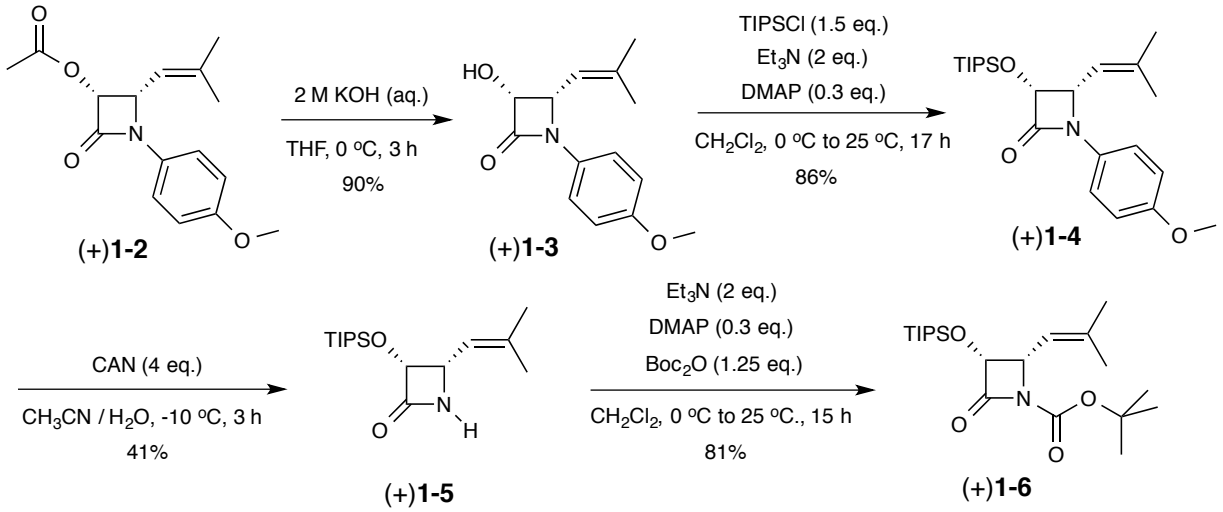

Scheme 1.3. Preparation of (+)**1-6** by removal of PMP group, followed by acylation with *t*-Boc.

Basic hydrolysis of the C3 acetate group of (+)**1-2** followed by subsequent TIPS protection afforded (+)**1-4** in excellent yield (77% over 2 steps). The C4 isobutenyl group of (+)**1-4** can be modified through various synthetic methods towards the development of novel β-lactams and isoserine taxoid side-chains (Section 1.4.1).

The *p*-methoxyphenyl (PMP) group was oxidatively cleaved by ceric ammonium nitrate (CAN) to give (+)**1-5** in modest yield. The CAN mechanism takes places through two oxidative single electron transfers (SET), the first of which generates a radical cation at the *para* position that is susceptible to nucleophilic attack by water and the loss of methanol; and the second of which leads to cleavage of the C–N bond to afford (+)**1-5** and loss of quinone. The resulting free amide was treated with di-*tert*-butyl dicarbonate and triethylamine to give (+)**1-6** in excellent yield (81%), shown in Scheme 1.3. Enantiopure β-lactam (+)**1-6** was used in the semisynthesis of next-generation taxoids SB-T-1214, SB-T-1216, SB-T-121602, SB-T-121405, and SB-T-121606 (Chapter 2).

§1.2.3 Lithium Chiral Ester Enolate-Imine Cyclocondensation

While the Staudinger [2+2] reaction provides an efficient synthetic path to *cis*- or *trans*-β-lactams, an inefficient and lengthy chemoenzymatic kinetic resolution is required to produce highly enantiopure β-lactams. The lithium chiral ester enolate-imine cyclocondensation provides a direct route towards highly enantioenriched β-lactams.[8] Treatment of a chiral ester with LDA generates a chiral enolate *in situ*, which can attack an imine to afford a lithiated β-amino chiral ester intermediate. This intermediate subsequently undergoes ring closure to regenerate the chiral auxiliary and give β-lactams in high enantiomeric purity (Scheme 1.4).

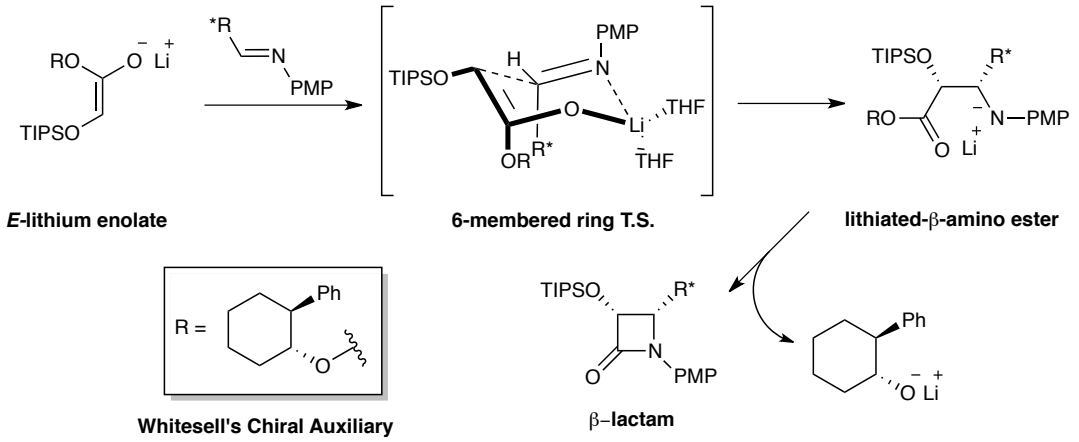

Scheme 1.4. Mechanism for lithium chiral ester enolate-imine cyclocondensation reaction. Adapted from reference [9].

A screening of various chiral auxiliaries and *O*-protecting groups that provide steric hinderance in the transition state showed that the combination of (-)-*trans*-2-phenylcyclohexyl and TIPS as substituents leads to the exclusive formation of *cis*-β-lactams in very high enantiopurity.[9]

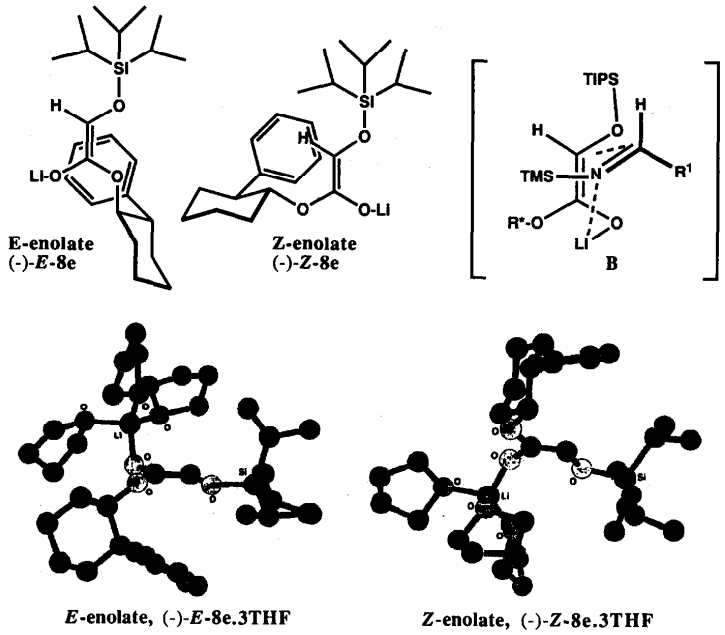

Figure 1.6. Formation of *E*- or *Z*-enolates using MACROMODEL molecular modeling. Reprinted from reference [9].

There are two proposed mechanistic pathways for the lithium chiral ester enolate-imine cyclocondensation: (1) *E*-enolate formation followed by a chair-like transition state; (2) and *Z*-enolate formation followed by a boat-like transition state. The chiral auxiliary positioned in the *endo* position of the chair-like transition state derived from the *E*-enolate leads to more favorable asymmetric induction than in the *exo* position of the boat-like transition state generated by the *Z*-enolate.[9] In addition, molecular mechanics calculations (MM2) for both *E*- and *Z*-enolates performed using MACROMODEL program indicated that the *E*-enolate was more thermodynamically favorable by 2.5 kcal/mol.[9] The bulky (-)-*trans*-2-phenyl-1-cyclohexyl chiral

auxiliary directs the approach of the *N*-(*p*-methoxyphenyl)-imine from the *si*-face of the *E* enolate to adopt the six-membered chair-like transition state, which is stabilized by coordination of the lithium counterion to both the enolate oxygen and the imine nitrogen. (Figure 1.6).[9]

§1.2.4 Synthesis of Whitesell' Chiral Auxiliary: *trans*-2-Phenylcyclohexanol

First used by Whitesell as a chiral auxiliary,[16] enantiomerically pure trans-2-phenylcyclohexanol has been used in numerous asymmetric transformations, such as asymmetric azo-ene reactions,[17] [4+2]-cycloaddition reactions,[18] ketene-olefin [2+2]-reactions,[19] enolate-imine cyclocondensations,[9] Pauson-Khand reactions,[20] palladium annulations,[21] and Reformatsky reactions.[22] Like (±)**1-2**, the enantiopure (-)**1-8** was first synthesized relying on an enzymatic resolution; however, chromatographic purification was required, making scale-up impractical.[23] A slight modification to the route first published by King and Sharpless[24] via the osmium-catalyzed asymmetric dihydroxylation (AD) reaction of 1-phenyl-1-cyclohexene provided a facile synthetic route towards (-)**1-8** in high enantiopurity (>99% ee) without the need for chromatography.

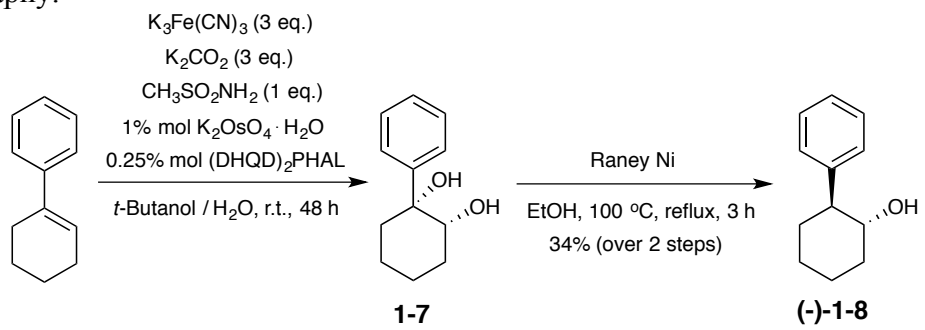

Scheme 1.5. Synthesis of Whitesell's chiral auxiliary.

The synthesis of (-)**1-8** began with the Sharpless asymmetric dihydroxylation (AD) of 1-phenyl-1-cyclohexene to give **1-7** in nearly quantitative yield. Reductive benzylic dehydroxylation of crude diol **1-7** gave the desired chiral auxiliary (-)**1-8** in modest yield (34% over 2 steps) in high optical purity (>99% ee), following recrystallization from pentane (Scheme 1.5).

§1.2.5 Chiral Ester Synthesis

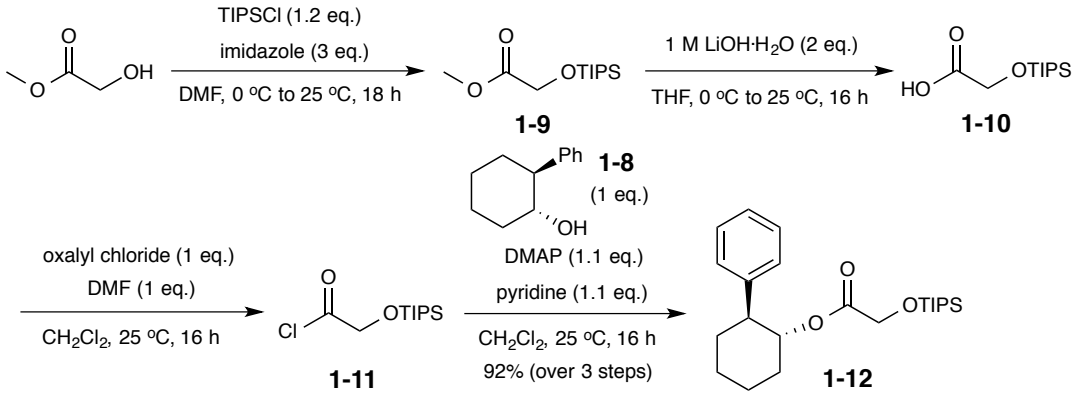

Scheme 1.6. First synthetic route towards chiral ester.

The synthesis of chiral ester **1-12** was performed *via* two synthetic routes. The first method, shown in Scheme 1.6, began with the TIPS protection of methyl glycolate, followed by basic hydrolysis of the methyl ester and treatment with oxalyl chloride and DMF to afford **1-11**. While the protection proceeded in excellent yield, the hydrolysis and subsequent acid-base work-up as well as acyl chloride formation resulted in some nontrivial deprotection of TIPS and generation of hexaisopropyldisilyloxane, which was found to interfere with the cyclocondensation reaction. Removal of the impurity by chromatographic purification was impractical since its R_f and that of chiral ester **1-12** were too close for efficient separation on a large scale.

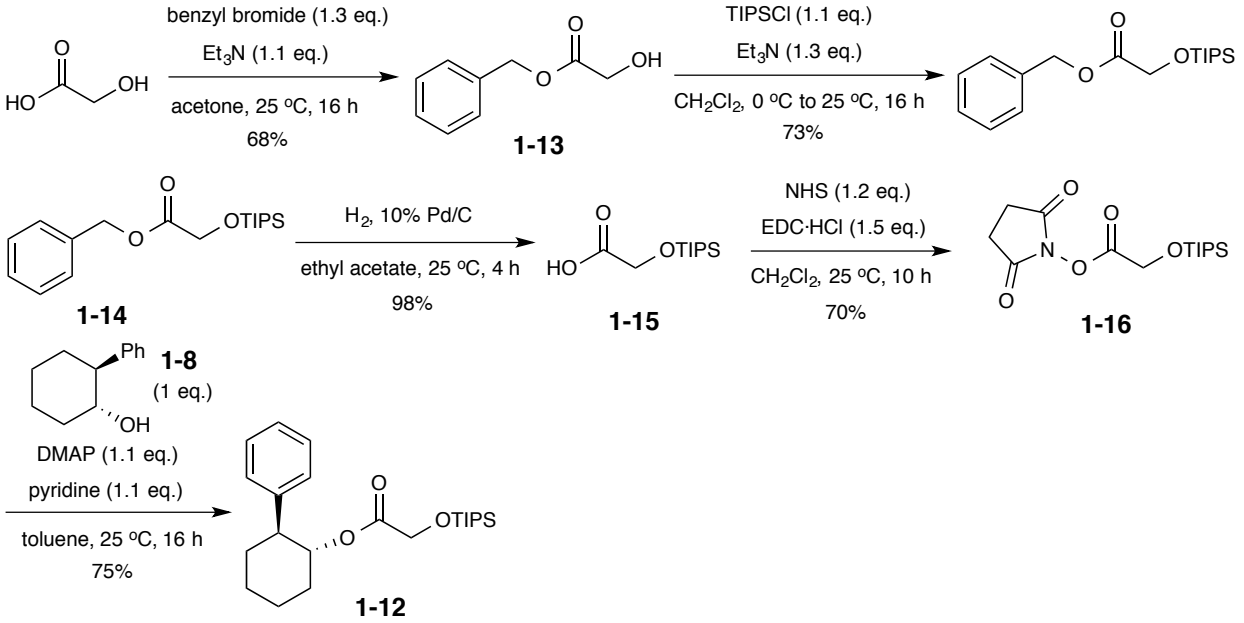

Scheme 1.7. Second synthetic route towards chiral ester.

The second synthetic route (Scheme 1.7) began with selective benzylation of the carboxylic acid of glycolic acid followed by TIPS protection of the alcohol to afford **1-14** in high yield following chromatographic purification (50% over 2 steps). Hydrogenolysis of the benzyl ester followed by formation of the activated succinimide ester gave **1-16** in excellent yield (98%), following recrystallization in hexanes. Coupling to (-)**1-8** under basic conditions gave chiral ester **1-12** in good yield (75%).

§1.2.6 Synthesis of (+)1-4 *via* Chiral Ester Enolate-Imine Cyclocondensation

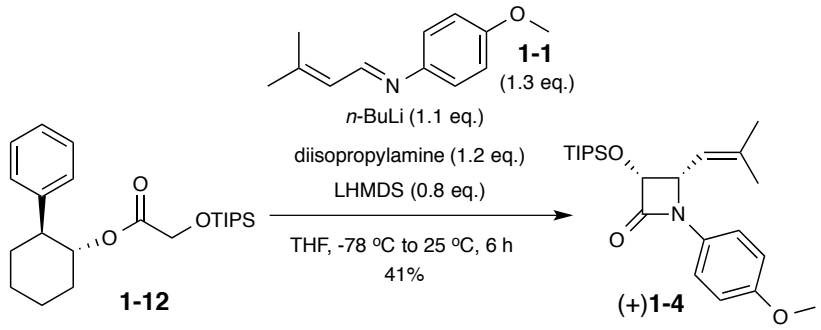

Scheme 1.8. Lithium chiral ester-enolate imine cyclocondensation.

The enantiopure β-lactam was synthesized from the cyclocondensation of the *E*-enolate generated *in situ* from chiral ester **1-12** and imine **1-1** in modest yield and high enantiopurity (>98% ee). The six-membered transition state indicates that the addition of the enolate to the imine proceeds through the less hindered *si*-face, leading to the stereoselective and enantiopure product *via* a lithiated-β-amino ester intermediate (Scheme 1.8). Cyclization of this intermediate and regeneration of the chiral auxiliary was facilitated by the addition of LHMDS at warmer temperatures.

§1.3 Difluorovinyl and Trifluoromethyl β-Lactams

§1.3.1 Synthesis of 4-Difluorovinyl β-Lactam

The synthesis of difluorovinyl β-lactam (+)**1-20** was carried out over four steps from versatile intermediate (+)**1-4.** Its applications in the semisynthesis of next-generation fluorotaxoids are discussed in Section 2.3.

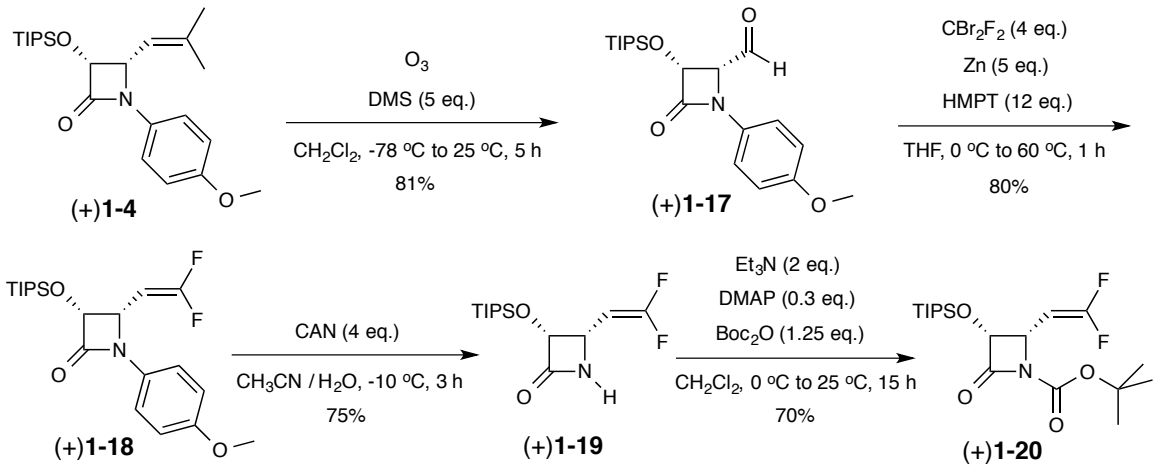

Scheme 1.9. Ozonolysis of isobutenyl group of (+)**1-4** followed by Wittig reaction to install difluorovinyl unit, subsequent PMP removal, and acylation with *t*-Boc.

Ozonolysis of (+)**1-4** resulted in alkene cleavage to give (+)**1-17** in high yield (81%). Chromatographic purification of (+)**1-17** was performed on alumina gel to avoid degredation of the C4 aldehyde. The difluorovinyl group was installed using a modified Wittig-type reaction with CBr_2F_2 and hexamethylphosphorous triamide (HMPT) in the presence of Zn to afford difluorovinyl β-lactam (+)**1-18** in good yield. Removal of the PMP group with CAN and subsequent protection of (+)**1-19** with *t*-Boc produced the desired difluorovinyl β-lactam (+)**1-20** in excellent yield (Scheme 1.9). Enantiopure β-lactam (+)**1-20** was used in the semisynthesis of next-generation fluorotaxoid SB-T-12854 (Section 2.3.3)

§1.3.2 Preparation of Trifluoromethyl-β-lactams

Enantiopure 1-acyl-3-hydroxy-4-CF_3-azetidin-2-ones were prepared according to literature method by Dr. Chi-Feng Lin.[25] The synthetic route towards CF_3-β-lactams is shown in Scheme 1.10.

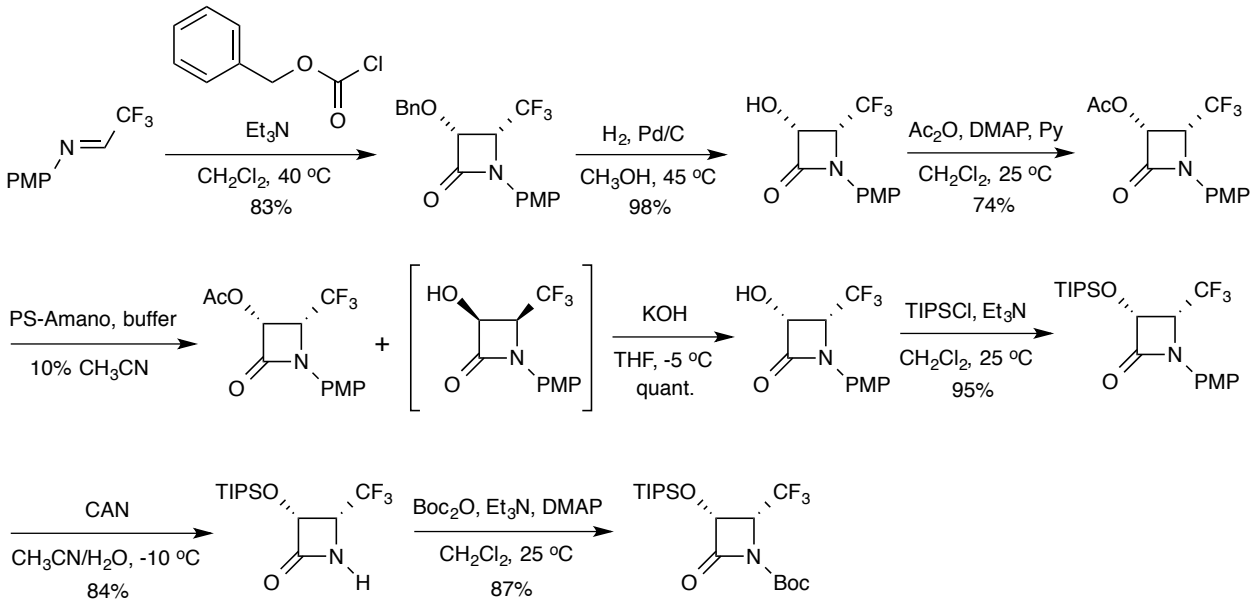

Scheme 1.10. Preparation of trifluoromethyl-β-lactam. Adapted from reference [25].

For the synthesis of 4-trifluoromethyl-β-lactams, the [2+2] ketene-imine cycloaddition of *N*-PMP-trifluoroacetaldimine and benzyloxyacetyl chloride at 40 °C gave racemic *cis*-3-benzyloxy-4-trifluoromethylazetidin-2-one. The β-lactam was converted to the corresponding 3-acetoxy-β-lactam through hydrogenolysis, followed by acetylation. Enzymatic optical resolution of the racemic mixture with "PS Amano" lipase gave kinetically resolved (+)-3-AcO-4-CF_3-β-lactam. The resulting acetate was hydrolyzed under basic conditions, and the C3 hydroxyl was protected with TIPS. Removal of the PMP group with CAN, followed by acylation with *t*-Boc gave the final trifluoromethyl-β-lactam. The applications of CF_3-β-lactams towards next-generation fluorotaxoids and linker stability studies will be discussed in Chapters 2 & 3.

§1.4. Summary

β-lactams have emerged as versatile synthetic intermediates in pharmaceutical development. The β-Lactam synthon method allows for efficient incorporation of β-lactams into medicinally active compounds, including the semisynthesis of taxane-based anticancer agents. Desired *N*-*t*-Boc and C4-isobutenyl β-lactam (+)**1-6** and C4-difluorovinyl β-lactam (+)**1-20** were synthesized *via* the Staudinger [2+2] reaction followed by kinetic enzymatic resolution and the lithium chiral ester enolate-imine cyclocondensation in high enantiomeric excess towards the semisynthesis of next-generation taxoids. The applications of these β-lactams towards the synthesis of next-generation taxoids will be discussed in Chapter 2.

§1.5 Experimental Section

§1.5.1 Caution

Some of the reagents have been designated as hazardous materials including, but not limited to, explosives, gases, flammable liquid and combustible liquid, flammable solid or dangerous when wet, oxidizer or organic peroxide, poison inhalation hazard, irritant or corrosive.

Osmium tetraoxide is extremely hazardous in case of ingestion and very hazardous in case of inhalation. All appropriate precautions, such as the use of gloves, goggles, labware, and fume hood, must be taken while handling these compounds at all times.

§1.5.2 General Information

^{1}H, ^{13}C, and ^{19}F NMR spectra were measured on a Varian 300, 400, 500, or 600 MHz NMR spectrometer or Bruker 300, 400, or 500 MHz NMR spectrometer. Hexafluorobenzene was used as an external standard for ^{19}F NMR analysis. Melting points were measured on a Thomas-Hoover capillary melting point apparatus and are uncorrected. TLC was performed on Sorbent Technologies aluminum-backed Silica G TLC plates (Sorbent Technologies, 200 μm, 20 x 20 cm), and column chromatography was carried out on silica gel 60 (Merck, 230-400 mesh ASTM). Purity and enantiomeric excess were determined with a Shimadzu L-2010A HPLC HT series HPLC assembly, using a Chiracel OD-H (4.6 mm x 250 mm) with hexanes-isopropanol gradient solvent system. Two analytical conditions were used and noted as part of the characterization data and purity, i.e., HPLC (1): flow rate 0.6 mL/min, isocratic 15% isopropanol for the 20 min period; HPLC (2): flow rate 0.4 mL/min, isocratic 2% isopropanol for the 25 min period.

§1.5.3 Materials

The chemicals were purchased from Sigma-Aldrich, Fisher Scientific, and VWR International, and used as received or purified before use by standard methods. Tetrahydrofuran was freshly distilled from sodium and benzophenone. Dichloromethane was also distilled immediately prior to use under nitrogen from calcium hydride.

§1.5.4 Experimental Procedure

4-Methoxy-*N*-(3-methyl-2-buten-1-ylidene)-benzenamine [1-1]:[26]
To a solution of *p*-anisidine (6.0 g, 0.0487 mol), recrystallized from EtOH, and anhydrous Na_2SO_4 (13.834 g, 0.0974 mol) in CH_2Cl_2 (100 mL) was added 3-methyl-2-butenal (5.1 mL, 0.0538 mol), and the mixture was allowed to react for 3 h at room temperature with stirring in the absence of light. The reaction mixture was filtered to remove the Na_2SO_4 and then concentrated *in vacuo* in the absence of heat to afford **1-1** as a dark red liquid, which was immediately used in the next step without further purification. ^{1}H NMR (300 MHz, $CDCl_3$) δ 1.96 (s, 3H), 2.01 (s, 3H), 3.81 (s, 3H), 6.20 (d, J = 9.3 Hz, 1H), 6.89 (d, J = 8.7 Hz, 2H), 7.12 (d, J = 9.0 Hz, 2H), 8.37 (d, J = 9.6 Hz, 1H). All data are in agreement with literature values.[26]

(±)-*cis*-1-(4-Methoxyphenyl)-3-acetoxy-4-(2-methylprop-1-enyl)azetidin-2-one [(±)1-2]:[27]
To a solution of **1-1** (crude) in CH_2Cl_2 (50 mL) at -78 °C was added Et_3N (10.8 mL, 0.0779 mmol), and the mixture was stirred for 15 min. Then, to the cooled solution was added acetoxyacetyl chloride (6.3 mL, 0.0585 mol) in CH_2Cl_2 (10 mL) by a jacketed addition funnel, cooled to -78 °C, and the mixture was allowed to react for 10 h at room temperature. The reaction was quenched with saturated NH_4Cl (10 mL), and the mixture was washed with brine (3 x 10 mL). The organic layer was dried over $MgSO_4$ and concentrated *in vacuo* to afford a dark orange oil. Purification of the crude product by column chromatography on silica gel with

hexanes/ethyl acetate (4:1) as eluent gave racemic β-lactam, (±)**1-2** (12.018 g, 85% over 2 steps) as a white solid; ^{1}H NMR (300 MHz, $CDCl_3$) δ 1.79 (s, 3H), 1.82 (s, 3H), 2.12 (s, 3H), 3.79 (s, 3H), 4.97 (dd, *J* = 4.8 Hz, 9.6 Hz, 1H), 5.14 (d, *J* = 9.6 Hz, 1H), 5.81 (d, *J* = 4.8 Hz, 1H), 6.86 (d, *J* = 9.3 Hz, 2H), 7.32 (d, *J* = 8.7 Hz, 2H). All data are in agreement with literature values.[27]

(3*S*,4*R*)-1-(4-Methoxyphenyl)-3-acetoxy-4-(2-methylprop-1-enyl)azetidin-2-one [(+)**1-2]:**[25]
To solution of (±)**1-2** (5.835 g, 0.0207 mmol) in 10% CH_3CN in phosphate buffered saline (pH 7.4) (800 mL) was added 20% wt PS Amano Lipase (1.167 g), and the mixture was allowed to react for 5 d at 45 °C with stirring by a mechanical stirrer. Reaction progress was monitored by TLC and ^{1}H NMR until 50% conversion was observed. The reaction was allowed to cool to room temperature, and the mixture was extracted with CH_2Cl_2 (3 x 100 mL). The combined organic layers were dried over $MgSO_4$ and concentrated *in vacuo* to give a yellow solid. Purification of the crude product by column chromatography on silica gel with hexanes/ethyl acetate (4:1) as eluent gave (+)**1-2** (1.685 g, 60%) as a white solid; ^{1}H NMR (300 MHz, $CDCl_3$) δ 1.79 (s, 3H), 1.82 (s, 3H), 2.12 (s, 3H), 3.79 (s, 3H), 4.97 (dd, *J* = 4.8 Hz, 9.6 Hz, 1H), 5.14 (d, *J* = 9.6 Hz, 1H), 5.81 (d, *J* = 4.8 Hz, 1H), 6.86 (d, *J* = 9.0 Hz, 2H), 7.32 (d, *J* = 8.0 Hz, 2H). HPLC (1): (+)**1-2**: t = 15.0, >98.4% ee; (-)**1-2**: t = 10.6 min, <1.6% ee. All data are in agreement with literature values.[25]

(3*R*,4*S*)-1-(4-Methoxyphenyl)-3-hydroxy-4-(2-methylprop-1-enyl)azetidin-2-one: [(+)**1-3]:**[27]
To a cooled solution of (+)**1-2** (1.582 g, 5.47 mmol) in THF (20 mL) was added an aqueous solution of 2 M KOH (20 mL), and the mixture was allowed to react at 0 °C for 4 h with stirring. The reaction was quenched with saturated NH_4Cl (20 mL), and the mixture was extracted with CH_2Cl_2 (3 x 50 mL). The combined organic layers were washed with brine (3 x 20 mL), dried over $MgSO_4$, and concentrated *in vacuo* to afford (+)**1-3** (1.217 g, 90%) as a white solid, which was immediately used in the next step without further purification. ^{1}H NMR (300 MHz, $CDCl_3$) δ 1.86 (s, 6H), 2.86 (bs, 1H), 3.78 (s, 3H), 4.89 (dd, *J* = 4.8, 9.3 Hz, 1H), 5.03 (d, *J* = 4.8 Hz, 1H), 5.27 (d, *J* = 9.3 Hz, 1H), 6.84 (d, *J* = 9.0 Hz, 2H), 7.31 (d, *J* = 9.0 Hz, 2H). All data are in agreement with literature values.[27]

(3*R*,4*S*)-1-(4-Methoxyphenyl)-3-triisopropylsilyloxy-4-(2-methylprop-1-enyl)azetidin-2-one [(+)**1-4]:**[27]
To a cooled solution of (+)**1-3** (1.120 g, 4.53 mmol) and DMAP (0.166 g, 1.36 mmol) in CH_2Cl_2 (45 mL) was added Et_3N (1.26 mL, 9.06 mmol) followed by TIPSCl (1.452 mL, 6.795 mmol), and the mixture was allowed to warm to room temperature and react for 17 h with stirring. The reaction was quenched with saturated NH_4Cl (10 mL), and the mixture was extracted with CH_2Cl_2 (3 x 20 mL). The combined organic layers were washed with brine (3 x 20 mL), dried over $MgSO_4$, and concentrated *in vacuo* to afford a yellow oil. Purification of the crude product by column chromatography on silica gel with hexanes/ethyl acetate (9:1) as eluent gave (+)**1-4** (1.565 g, 86%) as a white solid; ^{1}H NMR (600 MHz, $CDCl_3$) δ 1.09 (m, 21H), 1.79 (s, 3H), 1.85 (s, 3H), 3.77 (s, 3H), 4.81 (dd, *J* = 5.1 Hz, 9.9 Hz, 1H), 5.05 (d, *J* = 5.1 Hz, 1H), 5.33 (d, *J* = 9.9 Hz, 1H), 6.84 (d, *J* = 9.0 Hz, 2H), 7.32 (d, *J* = 9.0 Hz, 2H). All data are in agreement with literature values.[27]

(3*R*,4*S*)-3-Triisopropylsilyloxy-4-(2-methylprop-1-enyl)azetidin-2-one [(+)1-5]:[26]
To a cooled solution of (+)**1-4** (0.775 g, 1.99 mmol) in CH_3CN (32 mL) was added cerium ammonium nitrate (4.375 g, 7.98 mmol) in H_2O (30 mL) by slow addition, and the mixture was allowed to react for 3 h at -10 °C with stirring. The reaction mixture was extracted with ethyl acetate (3 x 20 mL) and washed with saturated $NaHSO_3$ (3 x 20 mL). The combined organic layers were washed with brine (3 x 30 mL), dried over $MgSO_4$, and concentrated *in vacuo* to afford a dark brown oil. Purification of the crude product by column chromatography on silica gel with hexanes/ethyl acetate (4:1) as eluent gave (+)**1-5** (0.233 g, 41%) as a white solid; ^{1}H NMR (300 MHz, $CDCl_3$) δ 1.05 (m, 21H), 1.69 (s, 3H), 1.76 (s, 3H), 4.45 (dd, *J* = 4.2, 9.6 Hz, 1H), 5.00 (m, 1H), 5.32 (d, *J* = 9.6 Hz, 1H), 5.78 (bs, 1H). All data are in agreement with literature values.[26]

(3*R*,4*S*)-1-(*tert*-Butoxycarbonyl)-3-triisopropylsilyloxy-4-(2-methylprop-1-enyl)azetidin-2-one [(+)1-6]:[26]
To a cooled solution of (+)**1-5** (0.219 g, 0.737 mmol) and DMAP (0.027 g, 0.221 mmol) in CH_2Cl_2 (4 mL) was added Et_3N (0.2 mL, 1.47 mmol) followed by Boc_2O (0.204 g, 0.922 mmoL) in CH_2Cl_2 (2 mL), and the mixture was allowed to react for 15 h at room temperature with stirring. The reaction was quenched with saturated NH_4Cl (10 mL), and the mixture was extracted with CH_2Cl_2 (3 x 20 mL). The combined organic layers were washed with brine (3 x 20 mL), dried over $MgSO_4$, and concentrated *in vacuo* to afford a yellow oil. Purification of the crude product by column chromatography on silica gel with hexanes/ethyl acetate (19:1) as eluent gave (+)**1-6** (0.239 g, 81%) as a colorless oil; ^{1}H NMR (500 MHz, $CDCl_3$) δ 1.07 (m, 21H), 1.51 (s, 9H), 1.79 (d, *J* = 1.3 Hz, 3H), 1.81 (d, *J* = 1.3 Hz, 3H), 4.78 (dd, *J* = 5.8 Hz, 9.9 Hz, 1H), 5.00 (d, *J* = 5.8 Hz, 1H), 5.31 (d, *J* = 9.9 Hz, 1H); ^{13}C NMR (400 MHz, $CDCl_3$) δ 12.0, 17.7, 18.4, 26.2, 28.2, 57.0, 82.7, 118.6, 139.7, 148.3, 166.5. All data are in agreement with literature values.[26]

(1*R*,2*R*)-*cis*-1-Phenyl-1,2-cyclohexanediol [1-7]:[28]
To a cooled solution of potassium ferricyanide (62.366 g, 0.189 mol), K_2CO_3 (26.226 g, 0.189 mol), and methanesulfonamide (6.024 g, 0.0633 mol) in *tert*-butanol–H_2O (2:3) (170 mL) was added potassium osmate (VI) dihydrate (60 mg, 0.163 mmol) and $(DHQD)_2PHAL$ (0.470 g, 0.603 mmol), and the mixture was allowed to react for 10 min at 0 °C with stirring. To the solution was added 1-phenyl-1-cyclohexene (10 mL, 0.0628 mmol), and the mixture was allowed to react for 48 °C at room temperature with stirring. The reaction mixture was extracted with ethyl acetate (3 x 150 mL) and subsequently filtered to remove solid impurities. The combined organic layers were washed with an aqueous solution of 2 M KOH (100 mL), dried over $MgSO_4$, and concentrated *in vacuo* to afford **1-7** (11.667 g, crude) as an off-white solid, which was used immediately in the next step without further purification. ^{1}H NMR (600 MHz, $CDCl_3$) δ 1.3-1.6 (m, 9H), 2.69 (bs, 1H), 3.95 (dt, *J* = 4.0, 11.0 Hz, 1H), 7.27 (t, *J* = 7.5 Hz, 1H), 7.35 (t, *J* = 7.8 Hz, 2H), 7.49 (d, *J* = 8.1 Hz, 2H). All data are in agreement with literature values.[28]

(-)-*trans*-2-Phenyl-cyclohexanol [1-8]:[28]
To a solution of **1-7** (crude) in EtOH (120 mL), equipped with a condenser and mechanical stirrer, was added W-2 Raney nickel (200 mL), and the mixture was allowed to react for 3 h at 100 °C with stirring. The reaction was allowed to cool to 40 °C, and the mixture was filtered

over celite and concentrated *in vacuo* to afford a white solid. The product was recrystallized from pentane to afford **1-8** (3.649 g, 34 % over two steps) as white needles; ^{1}H NMR (600 MHz, $CDCl_3$) δ 1.83 (m, 2H), 1.94 (m, 2H), 2.36 (m, 2H), 2.56 (m, 2H), 6.28 (m, 1H), 7.36 (t, *J* = 7.5 Hz, 1H), 7.45 (t, *J* = 7.5 Hz, 2H), 7.53 (d, *J* = 8.1 Hz, 2H); HPLC (2): t = 24.5 min, >99.4% ee. All data are in agreement with literature values. All data are in agreement with literature values.[28]

2-(Triisopropylsiloxy)acetic acid methyl ester [1-9]:[29]
To a cooled solution of methyl glycolate (4.8 mL, 0.0631 mmol) and imidazole (12.857 g, 0.1889 mol) in DMF (30 mL) was added TIPSCl (16.2 mL, 0.0757 mol), and the mixture was allowed to react for 18 h at room temperature with stirring. The reaction was quenched with saturated NH_4Cl (10 mL), and the mixture was extracted with ethyl acetate (3 x 30 mL). The combined organic layers were washed with brine (3 x 20 mL), dried over $MgSO_4$, and concentrated *in vacuo* to afford **1-9** (16.258, crude) as a yellow liquid, which was immediately used in the next step without further purification. ^{1}H NMR (300 MHz, $CDCl_3$) δ 1.00 (m, 21H), 3.66 (s, 3H), 4.25 (s, 2H). All data are in agreement with literature values.[29]

2-(Triisopropylsilyloxy)acetic acid [1-10]:[30]
To a cooled solution **1-9** (crude) in THF (120 mL) was added an aqueous solution of 1 M $LiOH{\cdot}H_2O$ (120 mL, 0.120 mol), and the mixture was allowed to react for 16 h at room temperature with stirring. The reaction mixture was extracted with CH_2Cl_2 (3 x 20 mL), and the pH of the aqueous phase was adjusted to 2 with 1 *N* HCl. The acidified aqueous layer was once again extracted with CH_2Cl_2 (3 x 20 mL). The combined organic layers were washed with brine (3 x 20 mL), dried over $MgSO_4$, and concentrated *in vacuo* to afford **1-10** (9.941 g, crude) as a yellow liquid, which was immediately used in the next step without further purification. ^{1}H NMR (300 MHz, $CDCl_3$) δ 1.06 (m, 21H), 4.30 (s, 2H). MS (ESI) *m/z* for $C_{11}H_{23}O_3Si^-$ calcd: 232.1. Found: 232.1. All data are in agreement with literature values.[30]

2-(Triisopropylsilyloxy)acetyl chloride [1-11]:[31]
To a solution of **1-10** (crude) in CH_2Cl_2 (125 mL) was added oxalyl chloride (4.8 mL, 55.60 mmol) followed by DMF (0.5 mL, 6.49 mmol), and the mixture was allowed to react for 16 h at room temperature with stirring. The reaction mixture was directly concentrated *in vacuo* to afford **1-11** (10.44 g, crude) as an orange liquid, which was immediately used in the next step without further purification. ^{13}C NMR (400 MHz, $CDCl_3$) δ 11.86, 17.65, 70.15, 172.63. All data are in agreement with literature values.[31]

2-(Triisopropylsilyloxy)acetic acid (1*R*,2*S*)-2-phenylcyclohexyl ester [1-12]:[9]
To a solution of **1-8** (3.63 g, 0.0206 mol) and DMAP (2.81 g, 0.0227 mol) in CH_2Cl_2 (50 mL) was added pyridine (2.5 mL, 0.0227 mmol) followed by **1-11** (7.802, 0.0309 mol) and the mixture was allowed to react for 16 h at room temperature. The reaction was quenched with saturated $NaHCO_3$ (20 mL), and the mixture was washed with saturated $CuSO_4$ (3 x 20 mL) and brine (3 x 20 mL). The organic layer was dried over $MgSO_4$ and concentrated *in vacuo* to afford a yellow liquid. Purification of the crude product by column chromatography on silica gel with hexanes/ethyl acetate (33:1) as eluent gave **1-12** (7.429 g, 92%) as a colorless oil; ^{1}H NMR (500 MHz, $CDCl_3$) δ 1.00 (m, 21H), 1.48 (m, 4H), 1.80 (m, 1H), 1.87 (m, 1H), 1.96 (m, 1H), 2.17 (m, 1H), 2.69 (dt, *J* = 9.0, 12.5 Hz, 1H), 3.94 (d, *J* = 16.5 Hz, 1H), 4.10 (d, *J* = 16.5 Hz, 1H), 5.10 (dt,

J = 4.0, 11.0 Hz, 1H), 7.19 (m, 3H), 7.26 (m, 2H). All data are in agreement with literature values.[9]

Benzyl glycolate [1-13]:[32]
To a solution of glycolic acid (2.5 g, 0.032 mol) in acetone (30 mL) was added Et_3N (5 mL, 0.036 mmol) followed by benzyl bromide (5.0 g, 0.042 mol), and the mixture was allowed to react for 16 h at room temperature with stirring. The reaction mixture was directly concentrated *in vacuo* to afford a yellow oil. The oil was dissolved in H_2O (20 mL) and extracted with ethyl acetate (3 x 20 mL). The combined organic layers were washed with brine (3 x 50 mL), dried over $MgSO_4$, and concentrated *in vacuo* to give **1-13** (3.298 g, 68%) as a colorless liquid; ^{1}H NMR (300 MHz, $CDCl_3$) 4.20 (s, 2H), 5.23 (s, 2H), 7.37 (m, 5H). All data are in agreement with literature values.[32]

2-(Triisopropylsiloxy)acetic acid benzyl ester [1-14]:[30]
To a solution of **1-13** (3.056 g, 18.41 mmol) and DMAP (0.250 g, 1.84 mmol) in CH_2Cl_2 (45 mL) was added Et_3N (3.3 mL, 23.93 mmol) followed by TIPSCl (5.0 mL, 20.25 mmol), and the mixture was allowed to react for 16 h at room temperature with stirring. The reaction was quenched with saturated NH_4Cl (10 mL) and diluted with H_2O (20 mL). The reaction mixture was extracted with CH_2Cl_2 (3 x 20 mL). The combined organic layers were washed with brine (3 x 20 mL), dried over $MgSO_4$, and concentrated *in vacuo* to give a yellow oil. Purification of the crude product by column chromatography on silica gel with hexanes/ethyl acetate (99:1) as eluent gave **1-14** (4.329 g, 73%) as a colorless oil; ^{1}H NMR (500 MHz, $CDCl_3$) 1.06 (d, *J* = 6.4 Hz, 18H), 1.12 (m, 3H), 4.36 (s, 2H), 5.19 (s, 2H), 7.34 (m, 5H). All data are in agreement with literature values.[30]

2-(Triisopropylsiloxy)acetic acid [1-15]:[30]
To a solution of **1-14** (3.196 g, 9.93 mmol) in ethyl acetate (130 mL) was added 20% w/w palladium on carbon (0.640 g), and the mixture was purged with N_2 and set under H_2 for 4 h at room temperature with stirring. The reaction mixture was filtered over celite and concentrated *in vacuo* to give **1-15** (2.257 g, 98%) as a colorless liquid; ^{1}H NMR (400 MHz, $CDCl_3$) 1.10 (m, 21H), 4.31 (s, 2H). All data are in agreement with literature values.[30]

2-Triisopropylsiloxy-acetic succinate ester [1-16]:
To a solution of **1-15** (1.670 g, 7.20 mmol) and HOSu (0.993 g, 8.64 mmol) in CH_2Cl_2 (35 mL) was added EDC·HCl (2.073 g, 10.797 mmol) in CH_2Cl_2 (10 mL), and the mixture was allowed to react for 12 h at room temperature with stirring. The reaction was quenched with saturated NH_4Cl (10 mL) and diluted with H_2O (3 x 10 mL). The reaction mixture was extracted with CH_2Cl_2 (3 x 20 mL). The combined organic layers were dried over $MgSO_4$ and concentrated *in vacuo* to afford a yellow oil. Recrystallization from hexanes gave **1-16** (1.653 g, 70%) as a white solid; ^{1}H NMR (300 MHz, $CDCl_3$) δ 1.08 (m, 21H), 2.84 (s, 4H), 4.67 (s, 2H). HRMS for $C_{15}H_{28}NO_5Si^+$ calcd: 330.1731. Found: 330.1738 (Δ = 2.1 ppm).

(3*R*,4*S*)-1-(4-Methoxyphenyl)-4-(2-methyl-1-propen-1-yl)-3-triisopropylsilyloxy-2-azetidinone [(+)1-4]:[9]
To a cooled solution of 2 M lithium diisopropylamide (2.5 mL, 5.0 mmol) in THF (10 mL) was added **1-12** (1.275 g, 3.26 mmol) by slow addition over 30 min. To the reaction vessel was added

neat **1-1** (0.803 g, 4.24 mmol) by slow addition over 1 h, and the mixture was allowed to react for 2 h at -78 °C with stirring. To the reaction mixture was added 1 M LHMDS (2.5 mL, 2.50 mmol), and the mixture was allowed to warm to -40 °C and react for 2 h with stirring. The reaction was quenched with saturated NH_4Cl (10 mL), diluted with H_2O (10 mL), and allowed to warm to 25 °C. The reaction mixture was extracted with ethyl acetate (3 x 30 mL). The combined organic layers were washed with brine (3 x 30 mL), dried over $MgSO_4$, and concentrated *in vacuo* to afford a brown oil. Purification of the crude product by column chromatography on silica gel with hexanes/ethyl acetate (3:1) as eluent gave (+)**1-4** (0.735 g, 41%) as a white solid; ^{1}H NMR (600 MHz, $CDCl_3$) δ 1.10 (m, 21H), 1.79 (s, 3H), 1.85 (s, 3H), 3.77 (s, 3H), 4.80 (dd, *J* = 4.8 Hz, 9.9 Hz, 1H), 5.05 (d, *J* = 4.8 Hz, 1H), 5.33 (d, *J* = 9.9 Hz, 1H), 6.83 (d, *J* = 9.0 Hz, 2H), 7.32 (d, *J* = 9.0 Hz, 2H). HPLC (1): (+)**1-4**: t = 14.5, >99.6% ee. All data are in agreement with literature values.[9]

(3*R*,4*S*)-1-(4-Methoxyphenyl)-4-oxo-3-(triisopropylsiloxy)azetidin-2-one [(+)**1-17]:**[25]
A solution of (+)**1-4** (1.426 g, 3.53 mmol) in CH_2Cl_2 (150 mL) was purged with O_2 and cooled to -78 °C. Ozone was bubbled into the solution at an oxygen flow rate of ¼ and an ozonolysis setting of 8, and the mixture was allowed to react for 5 h at -78 °C with stirring until the solution turned light blue. Ozone flow was stopped, and after 30 min dimethyl sulfide (3 mL, 17.6 mmol) was added, and the mixture was allowed to warm to room temperature. The reaction mixture was concentrated *in vacuo* to afford a yellow liquid. The liquid was dissolved in ethyl acetate (50 mL) and washed with H_2O (3 x 10 mL) and brine (3 x 10 mL). The organic layer was dried over $MgSO_4$ and concentrated *in vacuo* to afford a yellow liquid. Purification of the crude product by column chromatography on alumina gel with hexanes/ethyl acetate (3:1) as eluent gave (+)**1-17** (1.075 g, 81%) as a white solid; ^{1}H NMR (600 MHz, $CDCl_3$) 1.09 (m, 21 H), 3.79 (s, 3H), 4.46 (m, 1H), 5.31 (d, *J* = 4.8 Hz, 1H), 6.87 (d, *J* = 9.0 Hz, 2H), 7.27 (d, *J* = 9.0 Hz, 2H), 9.77 (d, *J* = 4.2 Hz, 1H). All data are in agreement with literature values.[25]

(3*R*,4*S*)-4-(2,2-Difluoroethenyl)-1-(4-methoxyphenyl)-3-(triisopropylsiloxy)azetidin-2-one [(+)**1-18]:**[33]
To a cooled solution of (+)**1-17** (0.800 g, 2.12 mmol) in THF (120 mL) was added Zn powder (0.700 g, 10.5 mmol); and in a second vessel, to a cooled solution of dibromodifluoromethane (0.8 mL, 8.75 mmol) in THF (60 mL) was added hexamethylphosphorous triamide (4.1 mL, 25.8 mmol) to form a white precipitate. The contents of the second vessel were immediately added to the suspension in the former flask, and the mixture was sealed and allowed to react for 40 min at 60 °C with stirring. The reaction mixture was filtered over celite and concentrated *in vacuo* to afford a red oil. The oil was dissolved in ethyl acetate (100 mL) and washed with H_2O (3 x 10 mL) and brine (3 x 10 mL). The organic layer was dried over $MgSO_4$ and concentrated *in vacuo* to afford an orange oil. Purification of the crude product by column chromatography on silica gel with hexanes/ethyl acetate (3:1) as eluent gave (+)**1-18** (0.700 g, 80%) as a white solid; ^{1}H NMR (600 MHz, $CDCl_3$) δ 1.10 (m, 21H), 3.79 (s, 3H), 4.53 (dd, *J* = 10, 24.9 Hz, 1H), 4.83 (m, 1H), 5.14 (d, *J* = 5.1 Hz, 1H), 6.86 (d, *J* = 9.0 Hz, 2H), 7.33 (d, *J* = 9.0 Hz, 2H). All data are in agreement with literature values.[33]

(3*R*,4*S*)-4-(2,2-Difluoroethenyl)-3-(triisopropylsiloxy)azetidin-2-one [(+)**1-19]:**[33]
To a cooled solution of (+)**1-18 (**0.668 g, 1.63 mmol) in CH_3CN (30 mL) was added ammonium cerium(IV) nitrate (3.63 g, 6.62 mmol) in H_2O (30 mL) by slow addition, and the mixture was

allowed to react for 3 h at -10 °C with stirring. The reaction mixture was extracted with ethyl acetate (3 x 30 mL). The combined organic layers were washed with $NaHSO_3$ (3 x 30 mL) and brine (3 x 30 mL), dried over $MgSO_4$, and concentrated *in vacuo* to afford a dark brown oil. Purification of the crude product by column chromatography on silica gel with hexanes/ethyl acetate (2:1) as eluent gave (+)**1-19** (0.370 g, 75%) as white needles; ^{1}H NMR (600 MHz, $CDCl_3$) δ 1.09 (m, 21H), 4.13 (m, 1H), 4.55 (m, 1H), 5.07 (m, 1H), 5.85 (bs, 1H). All data are in agreement with literature values.[33]

(3*R,4*S)-1-(*tert*-Butoxycarbonyl)-4-(2,2-difluoroethenyl)-3-(triisopropylsiloxy)azetidin-2-one [(+)1-20]:[33]

To a cooled solution of (+)**1-19** (0.370 g, 1.213 mmol) and DMAP (0.044 g, 0.364 mmol) in CH_2Cl_2 (7 mL) was added Et_3N (0.35 mL, 2.426 mmol) followed by Boc_2O (0.332 g, 1.52 mmol) in CH_2Cl_2 (1.5 mL), and the mixture was allowed to react for 14 h at room temperature with stirring. The reaction was quenched with saturated NH_4Cl (10 mL), and the mixture was extracted with CH_2Cl_2 (3 x 30 mL). The combined organic layers were washed with brine (3 x 30 mL), dried over $MgSO_4$, and concentrated *in vacuo* to afford a red liquid. Purification of the crude product by column chromatography on silica gel with hexanes/ethyl acetate (19:1) as eluent gave (+)**1-20** (0.341 g, 70%) as a colorless oil; ^{1}H NMR (600 MHz, $CDCl_3$) δ 1.14 (m, 21H), 1.51 (s, 9H), 4.51 (dd, J = 10.2, 24.0 Hz, 1H), 4.75 (m, 1H), 5.05 (d, J = 5.4 Hz, 1H). All data are in agreement with literature values.[33]

§1.6.0 References

1. Drawz, S. M.; Bonomo, R. A. Three decades of beta-lactamase inhibitors. *Clin. Microbiol. Rev.* **2010,** 23, 160-201.
2. Ojima, I. Recent advances in the β-Lactam Synthon Method. *Acc. Chem. Res.* **1995,** 28, 383-389.
3. Kamath, A.; Ojima, I. Advances in the chemistry of beta-lactam and its medicinal applications. *Tetrahedron* **2012,** 68, 10640-10664.
4. Palomo, C.; Aizpurua, J. M.; Ganboa, I.; Oiarbide, M. From beta-lactams to alpha- and beta-amino acid derived peptides. *Amino Acids* **1999,** 16, 321-343.
5. Del Buttero, P.; Molteni, G.; Roncoroni, M. Reductive ring opening of 2-azetidinones promoted by sodium borohydride. *Tetrahedron Lett.* **2006,** 47, 2209-2211.
6. Alcaide, B.; Martin-Cantalejo, Y.; Rodriguez-Lopez, J.; Sierra, M. New reactivity patterns of the beta-lactam ring: tandem C3-C4 bond breakage-rearrangement of 4-acyl- or 4-imino-3,3-dimethoxy-2-azetidinones promoted by stannous chloride (SnCl2-2H2O). *J. Org. Chem.* **1993,** 58, 4767-4770.
7. Staudinger, H. Justus Liebigs Ann. Chem. *Liebigs Ann. Chem.* **1907,** 356, 51.
8. Ojima, I.; Habus, I. Asymmetric synthesis of β-lactams by chiral ester enolate-imine condensation. *Tetrahedron Lett.* **1990,** 31, 4289-4292.
9. Ojima, I.; Habus, I.; Zhao, M.; Zucco, M.; Park, Y. H.; Sun, C. M.; Brigaud, T. New and efficient approaches to the semisynthesis of Taxol and its C-13 side chain analogs by means of β-lactam Synthon Method. *Tetrahedron* **1992,** 48, 6985-7012.
10. Ojima, I.; Slater, J. C.; Michaud, E.; Kuduk, S. D.; Bounaud, P. Y.; Vrignaud, P.; Bissery, M. C.; Veith, J. M.; Pera, P.; Bernacki, R. J. Syntheses and structure-activity relationships of the

second-generation antitumor taxoids: exceptional activity against drug-resistant cancer cells. *J. Med. Chem.* **1996,** 39, 3889-3896.
11. Lopez, R.; Sordo, T. L.; Sordo, J. A.; Gonzalez, J. Torquoelectronic effect in the control of stereoselectivity of ketene-imine cycloaddition reactions. *J. Org. Chem.* **1993,** 58, 7036-7037.
12. Jiao, L.; Liang, Y.; Xu, J. Origin of the relative stereoselectivity of the beta-lactam formation in the Staudinger reaction. *J. Am. Chem. Soc.* **2006,** 128, 6060-6069.
13. Palomo, C.; Aizpurua, J. M.; Ganboa, I.; Oiarbide, M. Asymmetric synthesis of β-Lactams by Staudinger Ketene-Imine Cycloaddition Reaction. *Eur. J. Org. Chem.* **1999,** 12, 3223-3235.
14. Lee, E. C.; Hodous, B. L.; Bergin, E.; Shih, C.; Fu, G. C. Catalytic asymmetric Staudinger reactions to form beta-lactams: an unanticipated dependence of diastereoselectivity on the choice of the nitrogen substituent. *J. Am. Chem. Soc.* **2005,** 127, 11586-11587.
15. Brieva, R.; Crich, J. Z.; Sih, C. Chemoenzymatic synthesis of the C-13 side chain of Taxol: Optically-active 3-hydroxy-4-phenyl β-lactam derivatives. *J. Org. Chem.* **1993,** 58, 1068-1075.
16. Whitesell, J. K.; Chen, H.-H.; Lawrence, R. M. trans-2-Phenylcyclohexanol: A powerful and readily available chiral auxiliary. *J. Org. Chem.* **1985,** 50, 4663.
17. Brimble, M. A.; Lee, C. K. Y. Asymmetric azo-ene reactions using the chiral azo-enophile di-(-)-(1R, 2S)-2-phenyl-1-cyclohexyl diazenedicarboxylate. *Tetrahedron: Asymmetry* **1998,** 9, 873-884.
18. Denmark, S. E.; Hurd, A. R.; Sacha, H. J. Tandem [4+2]/[3+2] cycloadditions of nitroalkenes. 13. The synthesis of (-)-detoxinine. *J. Org. Chem.* **1997,** 62, 1668-1674.
19. De Azevedo, M. B. M.; Murta, M. M.; Greene, A. E. Novel, enantioselective lactone construction. First synthesis of methylenolactocin, antitumor antibiotic from Penicillium sp. *J. Org. Chem.* **1992,** 57, 4567-4569.
20. Castro, J.; Moyano, A.; Pericas, M. A.; Riera, A.; Greene, A. E.; Alvarez-Larena, A.; Piniella, J. F. Asymmetric Approach to (+)-beta-Cuparenone by Intramolecular Pauson-Khand Reaction. *J. Org. Chem.* **1996,** 61, 9016-9020.
21. Chassaing, C.; Haudrechy, A.; Langois, Y. Asymmetric palladium annulation: formal synthesis of (+)-huperzine A. *Tetrahedron Lett.* **1999,** 40, 8805-8809.
22. Shankar, B. B.; Kirkup, M. P.; McCombie, S. W.; Clader, J. W.; Ganguly, A. K. Synthesis of an optically pure 3-unsubstituted β-lactam using an asymmetric Reformatsky reaction and its conversion to cholesterol absorption inhibitors. *Tetrahedron Lett.* **1996,** 37, 4095-4098.
23. Carpenter, B. E.; Hunt, I. R.; Keay, B. R. A short efficient preparation of (+) and (−)-trans-2-phenylcyclohexanol. *Tetrahedron: Asymmetry* **1996,** 7, 3107-3108.
24. King, S. B.; Sharpless, K. B. An efficient synthesis of enantiomerically pure trans-2-phenylcyclohexanol. *Tetrahedron Lett.* **1994,** 35, 5611-5612.
25. Kuznetsova, L. U., I.M.; Pepe, A.; Zanardi, I.; Wu, X.; Ojima, I. Trifluoromethyl- and difluoromethyl-β-lactams as useful building blocks for the synthesis of fluorinated amino acids, dipeptides, and fluoro-taxoids. *J. Fluor. Chem.* **2004,** 125, 487-500.
26. Ojima, I.; Fumero-Oderda, C. L.; Kuduk, S. D.; Ma, Z.; Kirikae, F.; Kirikae, T. Structure-activity relationship study of taxoids for their ability to activate murine macrophages as well as inhibit the growth of macrophage-like cells. *Bioorg. Med. Chem.* **2003,** 11, 2867-2888.

27. Kuznetsova, L. V.; Pepe, A.; Ungureanu, I. M.; Pera, P.; Bernacki, R. J.; Ojima, I. Syntheses and Structure-Activity Relationships of Novel 3'-Difluoromethyl and 3'-Trifluoromethyl-Taxoids. *J. Fluor. Chem.* **2008,** 129, 817-828.
28. Gonzalez, J. A., C.; Truesdale, L. Synthesis of (+)-(1S,2R)- and (-)-(1R,2S)-trans-2-phenylcyclohexanol via Sharpless Asymmetric Dihydroxylation (AD). *Org. Synth.* **2002,** 79, 93.
29. Brenner, S.; Goelet, P.; Millward, S. W.; Stackhouse, J. Drug conjugates and methods of designing the same. *US Patent No. WO2001013958 A2* **2000**.
30. Hongwu, Y.; Ballard, C. E.; Boyle, P. D.; Wang, B. An inexpensive carbohydrate derivative used as a chiral auxiliary in the synthesis of α-hydroxy carboxylic acids. *Tetrahedron* **2002,** 58, 7663-7679.
31. Batchelor, M. J.; Bebbington, D.; Bemis, G.; Fridman, W.; Gillespie, R. J.; Golec, J.; Gu, Y.; Lauffer, D. J.; Livingston, D.; Matharu, S. Inhibitors of interleukin-1β converting enzyme. *US Patent No. WO9722619 A2* **1997**.
32. Macrae, M. X.; Blake, S.; Mayer, M.; Yang, J. Nanoscale ionic diodes with tunable and switchable rectifying behavior. *J. Am. Chem. Soc.* **2010,** 132, 1766-1767.
33. Kuznetsova, L.; Sun, L.; Chen, J.; Zhao, X.; Seitz, J.; Das, M.; Li, Y.; Veith, J. M.; Pera, P.; Bernacki, R. J.; Xia, S.; Horwitz, S. B.; Ojima, I. Synthesis and Biological Evaluation of Novel 3'-Difluorovinyl Taxoids. *J. Fluor. Chem.* **2012,** 143, 177-188.

Chapter 2

Paclitaxel, Taxanes, and Next-Generation Taxoids

Chapter Contents

§2.1 Introduction

"Down to their innate molecular core, cancer cells are hyperactive, survival-endowed, scrappy, fecund, inventive copies of ourselves."

- Siddhartha Mukherjee, *The Emperor of All Maladies*

§2.1.1 Cancer

Cancer is a classification of diseases characterized by uncontrolled growth and spread of abnormal cells. Malignant cells can spread to nearby tissues by local invasion, circulation through the blood stream, intravasation through the walls of nearby lymph or blood vessels, or implant into distant tissues by a process called "metastasis." While all cancers involve the malfunction of the genes responsible for cell division and growth, approximately 5% are derived from inherited genetic traits. The remaining majority of cancer incidents result from damage done to genes over the course aging. External risk factors include, but are not limited to, smoking tobacco, sunlight exposure, ionizing radiation, certain chemical exposure, poor diet, lack of physical activity, and obesity.[1]

Cancer remains the second leading cause of death in the United states, accounting for nearly a quarter of all deaths, and is exceeded only by heart disease; about 1.6 million cases were expected to be diagnosed in 2013, and of these over 580,000 people were expected to die from the disease.[2, 3] The lifetime probability of developing cancer is approximately 1 in 2 for men and 1 in 3 for women (Figure 2.1), and the total economic loss impacted by cancer is estimated at $895 billion, or 1.5% of the global gross domestic product (GDP).[1]

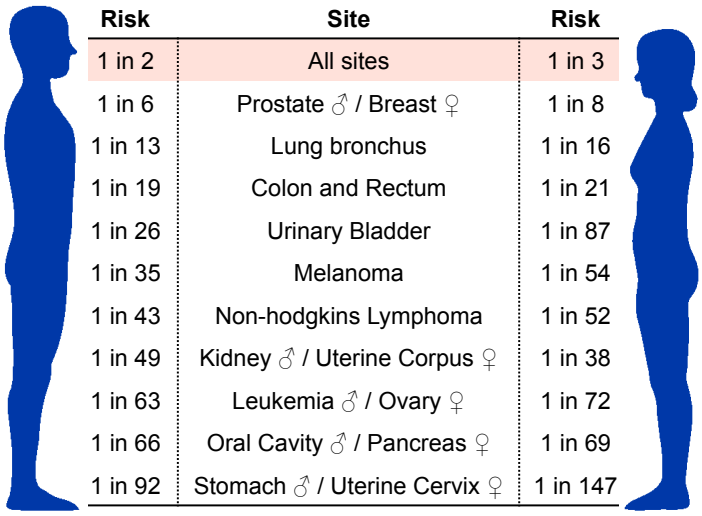

Risk	Site	Risk
1 in 2	All sites	1 in 3
1 in 6	Prostate ♂ / Breast ♀	1 in 8
1 in 13	Lung bronchus	1 in 16
1 in 19	Colon and Rectum	1 in 21
1 in 26	Urinary Bladder	1 in 87
1 in 35	Melanoma	1 in 54
1 in 43	Non-hodgkins Lymphoma	1 in 52
1 in 49	Kidney ♂ / Uterine Corpus ♀	1 in 38
1 in 63	Leukemia ♂ / Ovary ♀	1 in 72
1 in 66	Oral Cavity ♂ / Pancreas ♀	1 in 69
1 in 92	Stomach ♂ / Uterine Cervix ♀	1 in 147

Figure 2.1 Lifetime probability of developing cancer by gender, 2007-2009. Adapted from reference [1].

Significant advances in cancer treatment have been made over the past several decades. Awareness of the disease and external risk factors have contributed to a reduction in cancer incidence rates.[1] Over the past 40 years, a 50% reduction in per capita cigarette consumption has led to a 30% reduction in the male lung cancer death rate.[1] Furthermore, early detection diagnostic methods though practices such as annual mammograms and periodic colonoscopies

have contributed to the great improvements in five-year relative cancer survival rates for breast and colorectal cancers, at 90% and 65%, respectively.[1] However, despite these advances, the five-year survival rates for most cancers remain extremely low, like pancreatic cancer (6%), lung and bronchial cancer (17%), and ovarian cancer (43%).[1]

Primary cancer treatment options include surgery, chemotherapy, radiation, immunotherapy, hormonal suppression, gene therapy, and targeted therapy. Depending on the progression of the disease and tumor accessibility, either a single method or a series of the above listed treatment options can be employed to combat malignant tissue or to augment

§2.1.2 Chemotherapy

Traditional chemotherapy uses potent cytotoxic agents to target the molecular processes of cell division and exploit of the increased rate of cell division in cancer cells. There are many classes of chemotherapeutic agents, including microtubule stabilizing agents (i.e., paclitaxel), topoisomerase inhibitors (i.e., topotecan, irinotecan), thymidylate synthase inhibitors (5-fluorouracil), DNA alkylating agents (cisplatin), and protein kinase inhibitors (Gleevec®). Often, two or more drugs are used in combination (combination chemotherapy) to block different processes of cell division based on non-overlapping mechanisms of action. However, these highly potent drugs lack selectivity towards cancer cells that often leads to undesired side effects, such as vomiting, hair loss, a compromised immune system, bleeding, and fatigue.

Table 2.1. Top selling cancer drugs in the U.S. in 2013.[a]

Rank	Drug	Company	Indication	Class	Target
1	Rituxan (rituximab)	Biogen Idec, Genentech	non-Hodgkin lymphoma	monoclonal antibody	CD20
2	Avastin (bevacizumab)	Genentech	metastatic colorectal cancer	monoclonal antibody	VEGF-A
3	Herceptin (trastuzumab)	Genentech	breast cancer	monoclonal antibody	HER2/neu receptor
4	Gleevec (imatinib)	Novartis	leukemia	tyrosine-kinase inhibitor	ABL, CD117, PDGF-R
5	Alimta (pemetrexed)	Eli Lilly	pleural mesothelioma, NSCLC	antifolate	TS, DHFR
6	Xeloda (capecitabine)	Genentech	colorectal cancer	antimetabolite	TS inhibitor

[a]Source: Drugs.com U.S. Pharmaceutical Sales - 2013

A list of the top selling cancer drugs in 2013 is provided in Table 2.1. In addition to these highly successful chemotherapeutic agents, many more compounds that had been developed earlier are available off patent or as generics and, moving forward, numerous promising candidates are currently undergoing clinical evaluation. The area of research in this dissertation, however, was focused on microtubule stabilizing agents and, in particular, Taxol® (paclitaxel) and its relative taxanes.

§2.2 Paclitaxel (Taxol®) and the Taxane Class

§2.2.1 Discovery of Paclitaxel and its Mechanism of Action

Taxol (paclitaxel) was first isolated by Wall and Wani from the bark of *Taxus brevifolia* as a natural diterpenoid, and its structure was published in 1971 (Figure 2.2).[4] Despite its complex structure, low availability from natural source, and poor water solubility, subsequent development with NCI revealed excellent antitumor activity against human solid tumor xenografts, including CX-1 colon and MX-1 breast tumor xenografts, leading to preclinical formuation and eventual clinical development.[5]

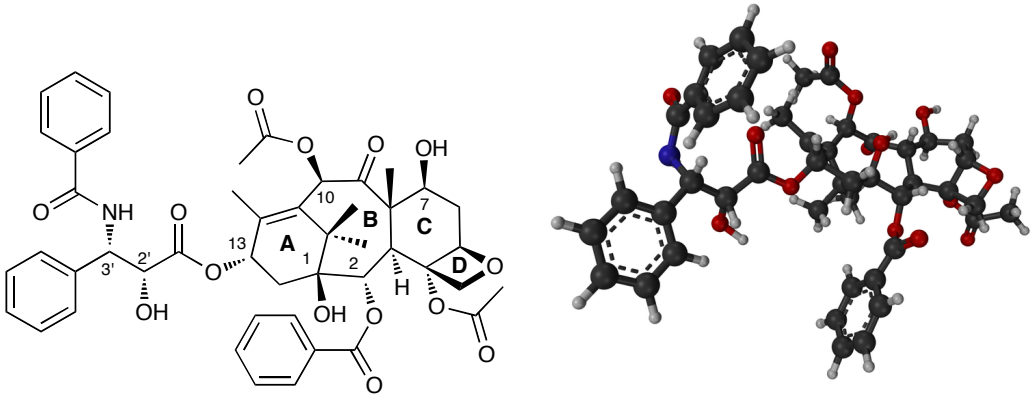

Figure 2.2 Chemical structure (*left*) and 3D depiction of paclitaxel (*right*).

Taxol entered Phase I clinical trials against advanced ovarian carcinoma and melanoma in 1984 and encountered some resistance due to its formulation as an emulsion with Cremophor EL®, resulting in allergic responses and at least one death in clinical trial patients.[6] Adjustments to the infusion period and premedication regimen overcame these problems, as the drug demonstrated increased cytotoxicity and *in vivo* activity on prolonged exposure.[5] Phase II clinical trials with the lengthened infusion period proved to be successful in 1985, and the first definitive results were reported in pivotal clinical trials against drug-refractory ovarian cancer in 1989,[7] and breast cancer in 1991.[8] In 1989, Bristol-Myers Squibb (BMS) was awarded a 7-year period of exclusivity by NCI under the Cooperative Research and Development Agreement (CRADA) in return for their investment in development, and the drug was marketed under the brand name Taxol®.[5] Taxol was approved by the U.S. Food and Drug Administration (FDA) for the treatment of refractory ovarian cancer in 1992, refractory or anthracycline-resistant breast cancer in 1994, Kaposi's sarcoma in 1997, and non-small cell lung cancer in 1998.[5] Taxol is currently being evaluated in Phase II and III clinical trials for additional indications as well as in combination with other drugs.

Taxol consists of a tetracyclic baccatin III skeleton – cyclohexene (A ring), cyclooctane (B ring), cyclohexane (C ring), and oxetane (D ring) – and an *N*-benzoylphenylisoserine side chain. With eleven chiral centers, fourteen oxygen atoms, and a single nitrogen atom, the chemical structure of taxol is given in Figure 2.2.

The mechanism of action of taxol as a promotor of tubulin polymerization was discovered by Dr. Susan Horwitz and co-workers in 1979.[9] Unlike vinblastine and vincristine, known inhibitors of tubulin polymerization, taxol was the first identified microtubule-stabilizing agent, a groundbreaking discovery that led to the development of other agents such as

epothilones and discodemolide that have a similar mechanism of action.[5] Microtubules consist of two polypeptide subunits, α- and β-tubulin, approximately 440 amino acids in length (ca. 50 kDa), that together form the tubulin heterodimer.[9] Tubulin heterodimers polymerize in the presence of guanoside-5'-triphosphate (GTP), magnesium ions (Mg^{2+}), and microtubule-associated proteins (MAPs) to form the microtubule, which consists of 13 protofilaments with an average diameter of 23 nm. However, upon interaction with taxol, the resulting microtubule contains 12 protofilaments and is stable under depolymerization conditions. The assembly and disassembly of microtubules are responsible for the formation of the mitotic spindle, a necessary process in cell division. Taxol promotes polymerization of tubulin heterodimers to microtubules, binding in an approximately equimolar ratio, stabilizes the formed microtubule, and inhibits the disassembly of the mitotic spindle (Figure 2.3).[9] This process arrests mitosis in the G_2/M phase, leading to nonsegregation of chromosomes during cell division and eventual apoptosis.[9]

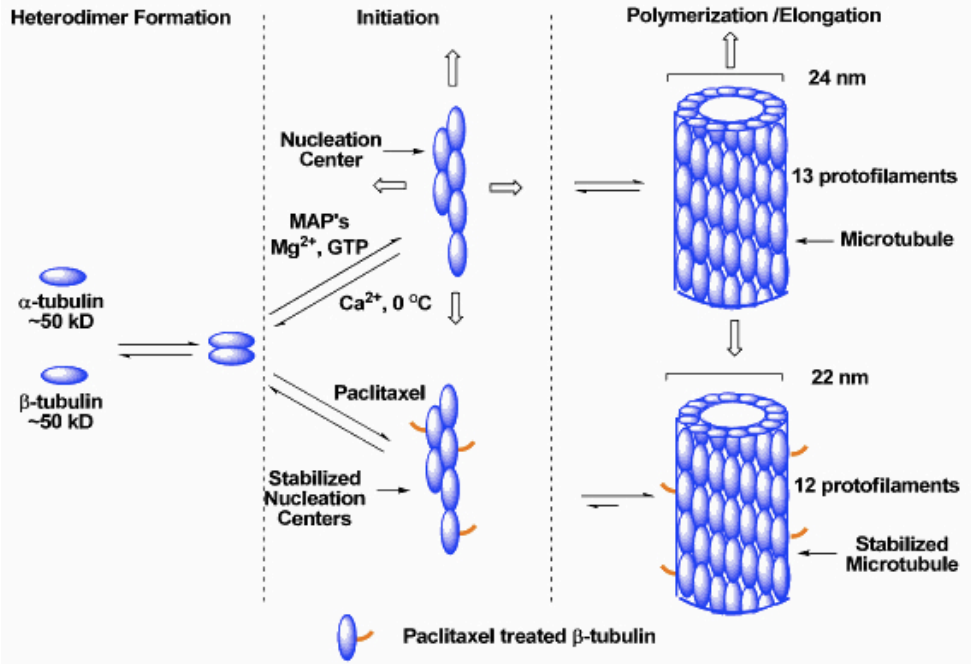

Figure 2.3. Microtubule formation in the presence of Taxol®. Adapted from reference [10].

In addition to its interaction with tubulin, taxol has demonstrated several minor biological effects, such as its ability to inactivate the anti-apoptotic protein Bcl-2.[5] Taxol both binds to and induces phosphorylation of Bcl-2, which was suggested to occur through activation of Raf-1 kinase following drug-induced disruptions of microtubules.[11-13] In spite of its effect on Bcl-2 and production of cytokines, it has been proposed that all significant effects of taxol are directly derived from its interaction with tubulin.[5]

§2.2.2 Docetaxel and Cabazitaxel

Docetaxel (Taxotere®), a semi-synthetic analogue of paclitaxel, was shown to have excellent activity, better than paclitaxel in some cases, and was developed in parallel to taxol. Docetaxel entered Phase I clinical trials in 1990, and was approved by the U.S. FDA for treatment of advanced breast cancer in 1996,[14] non small-cell lung cancer (NSCLC) in 1999,[15] and head and neck cancer in 2006.[16] Recently, cabazitaxel (Jevtana®), another semi-synthetic

taxane, received U.S. FDA approval for hormone-refractory metastatic prostate cancer in 2009,[17] and is in Phase III clinical trials for breast cancer.[18] The chemical structures of docetaxel and cabazitaxel are illustrated in Figure 2.4.

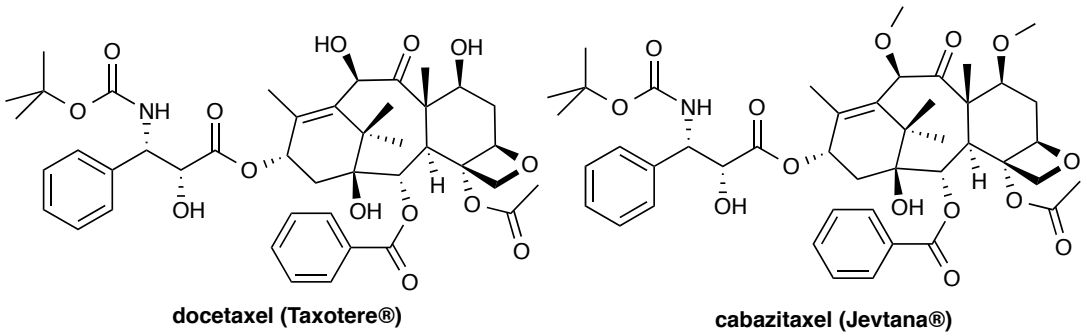

Figure 2.4. Chemical structures of docetaxel (*left*) and cabazitaxel (*right*).

§2.2.3 Production of Paclitaxel

The natural source of taxol is from the bark of *Taxus brevifolia*, the pacific yew tree. However, environmental concerns arose due to its non-renewable process for extraction and the location of the natural habitat of the endangered spotted owl within the yew forest, limiting taxol supply from this source.[5, 19] The first reported total syntheses of taxol were performed concurrently by Holton[20] and Nicolaou[21] in 1994, and since then by Danishefsky,[22] Wender,[23] Kuwajima,[24] Mukaiyama,[25] and Takahashi.[26] In spite of these impressive synthetic accomplishments, none of the above synthetic routes proved to be efficient or economical for large-scale production.

A semi-synthetic approach from 10-deacetylbaccatin III (10-DAB III), discovered by Potier and co-workers to be abundant and renewable in the needles of the European Yew, *Taxus baccata*, led to the commercial synthesis of taxol.[27] With the identical tetracyclic framework as taxol, modified 10-DAB III was coupled to an enantiomerically pure *N*-phenylisoserine side chain in 1988 by Potier and Green, however harsh conditions were required for 50% conversion and epimerization was observed at the C2' position.[27] Later, the installation of the taxol side chain to the baccatin core was concurrently accomplished by Holton[20] and Ojima[28] by the Ojima-Holton coupling protocol between a modified 10 DAB III and enantiopure β-lactam (Scheme 2.1).

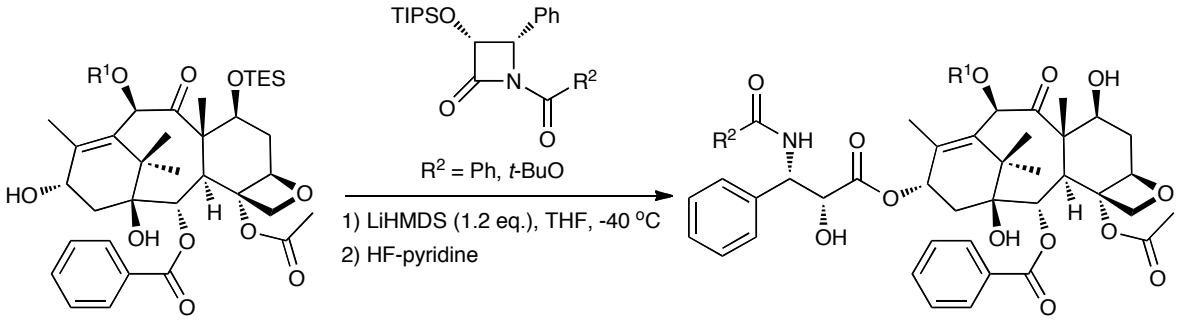

Scheme 2.1. Semi-synthesis of paclitaxel and docetaxel by the Ojima-Holton coupling protocol.

§2.2.4 Structure-Activity Relationship (SAR) Study of Taxanes

The discovery of 10-DAB III as a semi-synthetic precursor towards the semi-synthesis of taxol and next-generation taxoids led to the exploration of structure-activity relationship (SAR) studies within the taxane class. An overview of SAR studies on taxol is shown in Figure 2.5.

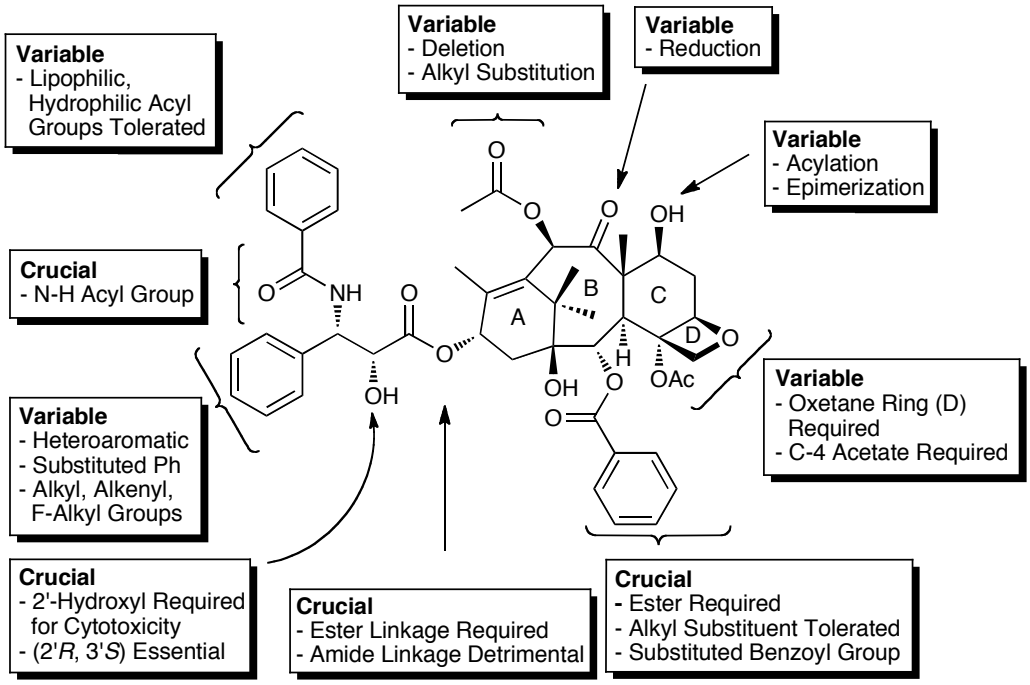

Figure 2.5. Overview of previously conducted SAR studies on paclitaxel (See Figure 2.2 for atom numbering)

While the substitution pattern of aromatic acylation at C2 is optimal for biological activity, modified benzoyl groups at C2 bearing *meta*-substituents can be tolerated and have even been shown to greatly increase the potency and binding affinity of the taxoid.[29]

The C4 acyl group is essential for activity; removal of the C4 acetate leads to loss of activity.[30] However, re-acylation of C4 with various acyl groups showed improved activity, such as the C4 carbonate as BMS-188797[31] and its *tert*-butoxy analog as BMS-275183,[32] in Phase I and Phase II clinical trials, respectively (Figure 2.6).

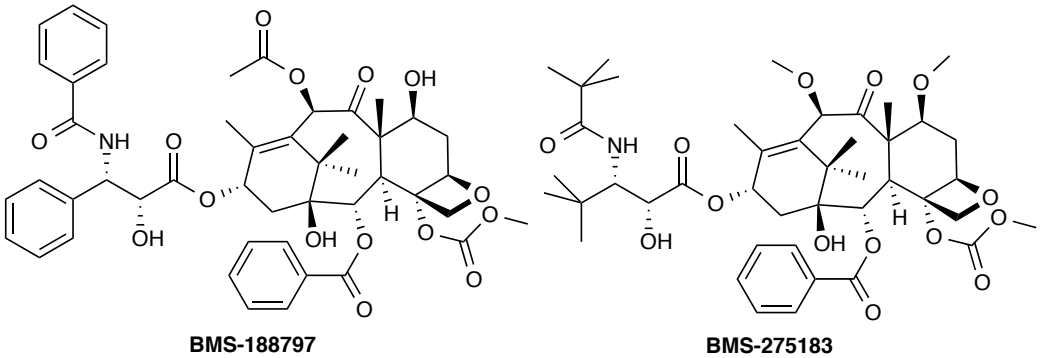

Figure 2.6. Chemical structures of BMS-188797 (left) and BMS-275183 (right).

The most readily modified functional group in the baccatin core is the C7 hydroxyl group.[5] If the C2' hydroxyl is suitably protected, the C7 hydroxy can be selectively derivatized with various acyl,[33] ether,[34] and thioether groups. Numerous C7 prodrugs of taxol have been reported as well, including water-soluble phosphate and polyethylene glycol (PEG) derivatives.[35]

While changes at the C10 position do not contribute significantly bioactivity, small acyl groups are optimal. However, alterations in this position can alter the efficacy of the compound against multidrug resistant (MDR) cell lines, as the C10 position is involved in recognition by the Pgp-efflux pump,[36] discussed in Section 2.2.4. Additionally, deacetylation at the C10 position can be found in the FDA approved docetaxel.[37] The C7,C10-dimethoxy analog of docetaxel, known as cabazitaxel, was prepared from 10-DAB III and demonstrated excellent activity in combination with prednisone against certain prostate and breast cancer.[5, 38]

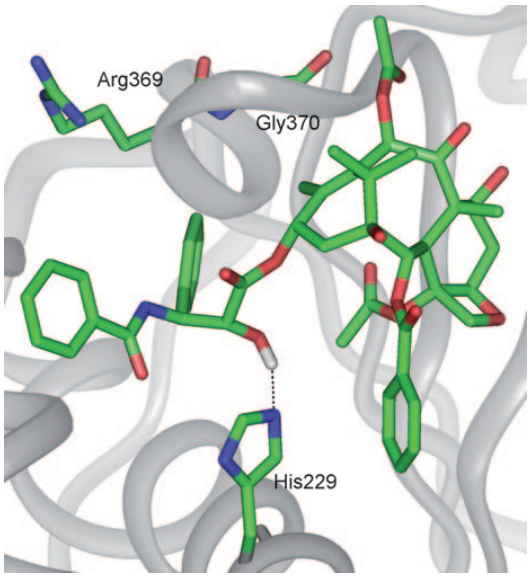

Figure 2.7. Proposed binding conformation of REDOR-taxol in 1JFF cryo-EM structure of Zn^{2+}-stabilized α,β-tubulin dimer with paclitaxel bound. Reprinted from reference [39].

Previous SAR studies have shown that modifications to the isoserine side chain can result in increased potency compared to taxol. Replacement of the C13 ester with an amide moiety results in complete loss of activity, whereas epimerization of the C2'-hydroxyl and C3'-amide moiety leads to compromised activity. The C2'-hydroxyl group participates as a hydrogen bonding donor with β-tubulin residue, His227, and as a hydrogen bond acceptor with Arg369 to promote microtubule binding (Figure 2.7).[40] The *N*-phenyl group can be substituted with lipophilic or hydrophilic acyl groups, such as *tert*-butyoxycarbonyl in docetaxel, to improve potency. Furthermore, through modifications to β-lactam precursors prior to Ojima-Holton coupling, it was observed that the C3' position is variable and non-essential for maintaining drug activity.

Certain modifications to the baccatin scaffold are not tolerated, such as disruption of the oxetane ring or removal of the C1 hydroxyl.[41] Also, the free C2' hydroxy is essential for bioactivity. The hydroxylated baccatin III derivative 14β-hydroxy-10-DAB III, isolated from *Taxus wallichiana* leaves, led to semi-synthetic taxane ortataxel, which is in Phase II clinical trials against taxane-resistant breast cancer.[42, 43]

§2.2.5 Multidrug Resistance (MDR)

Several transmembrane transporter proteins, termed ATP-binding cassette (ABC) transporters or efflux pumps, have been shown to be involved in tumor resistance to chemotherapeutic agents, utilizing adenosine triphosphate (ATP) hydrolysis to provide the energy for biological processes.[44] P-glycoprotein (Pgp), a broad spectrum multidrug efflux pump that has 12 transmembrane domains and two ATP-binding sites (Figure 2.8), is the primary ABC-transporter involved in export of neutral and cationic hydrophobic compounds (i.e. vinblastine, vincristine, doxorubicin, duanorubicin, etoposide, and paclitaxel) from the cell.[44] Tumor cells that develop resistance through a multidrug resistance (MDR) mechanism often develop cross-resistance to structurally unrelated natural products,[45] and thus resistance to chemotherapy remains an obstacle in cancer treatment. Malignant cells that display this MDR phenotype usually contain an amplified gene, *mdr1*, which encodes for P-glycoprotein.[45-47] While the primary binding target of taxol is tubulin and the microtubule spindle, the levels of various spindle assembly proteins, such as MAD2, BUBR1, Synuclein-gamma, and Aurora A play a role in chemoresistance to taxol.[5]

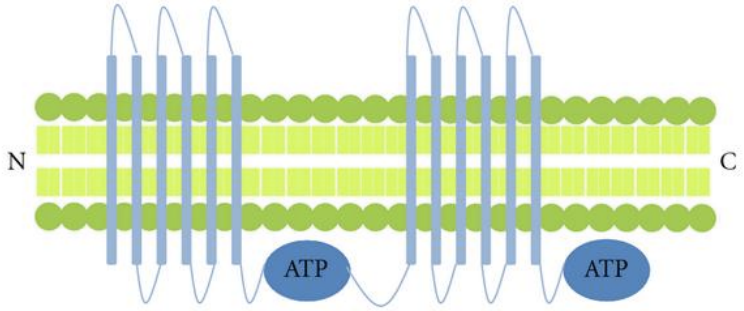

Figure 2.8. Structure of P-glycoprotein (Pgp) – this ABC transporter consists of 12 transmembrane domains and 2 ATP binding sites. Reprinted from reference [44].

While taxol and docetaxel have had a significant impact on chemotherapy and are very effective against solid tumors, such as breast, ovarian, and lung carcinomas, these agents have shown limited efficacy against colon, pancreatic, melanoma, and renal cancers, in which MDR is expressed.[48] Cabazitaxel, with C10 methoxy substitution, is a poor substrate for Pgp, and is much less subjected to drug resistance than taxol and docetaxel.[17]

§2.3.0 Next-Generation Taxoids

§2.3.1 Second-Generation Taxoids

Structure-activity relationship (SAR) studies on paclitaxel and docetaxel established that the C3'-phenyl group is a non-essential functionality for taxane antitumor activity.[49] In a SAR study in which a series of 3'-alkyl and 3'-alkenyl taxoids were assessed, the 10-acetyl (R = Ac) analogs demonstrated two to three times improved cytotoxicity than 10-unmodified (R = H) analogs against drug-sensitive and drug-resistant (MDR) cancer cell lines.[49] This new series of taxoids, bearing C3'- and C10 modifications, termed *second-generation taxoids*, were two orders of magnitude more potent than paclitaxel and docetaxel against drug-resistant human breast cancer cells MCF-7R.[49]

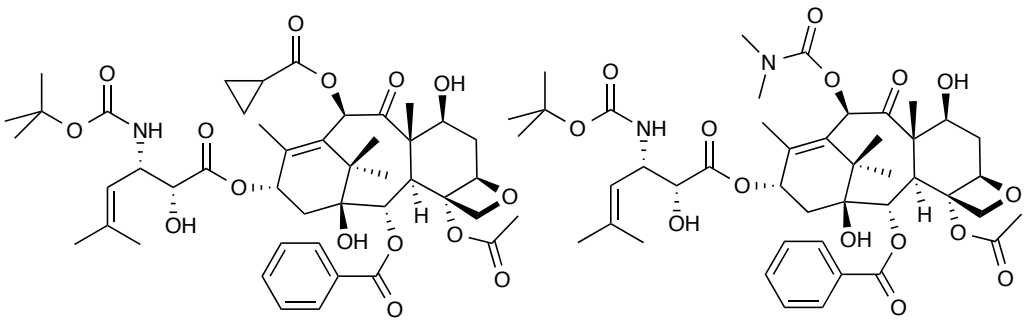

Figure 2.9. Chemical structures of second-generation taxoids SB-T-1214 (left) and SB-T-1216 (right).

A series of new 3'-(2-methyl-1-propenyl) taxoids with modifications at C10 demonstrated excellent activity against human cancer cell lines.[49] Among these taxoids, SB-T-1214 and SB-T-1216, illustrated in Figure 2.9, demonstrated exceptional potency, possessing two orders of magnitude better activity than paclitaxel and docetaxel.[49] The improved activity has been attributed to the C10 modifications with cyclopropanecarbonyl and *N,N*-dimethylcarbamoyl groups in comparison with the corresponding 10-acetyl taxoids, such as SB-T-1212 (Table 2.2).[49]

Table 2.2. Cytotoxicities (IC_{50}, nM) of second-generation taxoids against cancer cell lines. Adapted from reference [49].

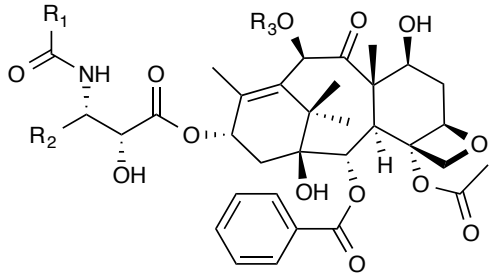

Taxoid	R_1	R_2	R_3	A121[a]	A549[b]	HT-29[c]	MCF-7[d]	NCI/ADR-RES[e]
paclitaxel	Ph	Ph	Ac	6.3	3.6	3.6	1.7	299
docetaxel	*N*-Boc	Ph	H	1.2	1.0	1.2	1.0	235
SB-T-1102	*N*-Boc	CH_2-$C(CH_3)_2$	Ac	3.8	0.98	3.2	4.0	36
SB-T-1212	*N*-Boc	$CH=C(CH_3)_2$	Ac	0.46	0.27	0.63	0.55	12
SB-T-1213	*N*-Boc	$CH=C(CH_3)_2$	EtCO	0.12	0.29	0.31	0.18	2.2
SB-T-1214	*N*-Boc	$CH=C(CH_3)_2$	*c*-PrCO	0.26	0.57	0.36	0.20	2.1
SB-T-1216	*N*-Boc	$CH=C(CH_3)_2$	$(CH_3)_2NCO$	0.30	0.60	0.5	0.13	4.9

[a]Human ovarian carcinoma cell line; [b]Human non-small cell lung cancer cell line; [c]Human colon cancer cell line; [d]Human breast cancer cell line; [e]Platinum-resistant metastatic ovarian cancer cell line; [f]Cells were incubated with a taxoid for 72 h at 37 °C with a 5% CO_2 atmosphere.

Three next-generation taxoids (SB-T-1214, SB-T-121303 and SB-T-110203) were assayed against two paclitaxel-resistant cell line subtypes (1A9PTX10 and 1A9PTX22) of human ovarian carcinoma cell line, 1A9, a parental clone of human ovarian cell line A2780.[29] These sublines bear point mutations in class I β-tubulin that confer resistance to paclitaxel binding.[50] All three taxoids exhibited high potency against these cell lines, demonstrating that these next-generation taxoids may in fact circumvent paclitaxel-drug resistance arising from point mutations in tubulin.[29]

A preliminary study on the *in vivo* antitumor activity of SB-T-1214 against pancreatic tumor xenograft CFPAC-1 revealed that following treatment with SB-T-1214 (20 mg/kg x 3 dose in Tween80/EtOH/PBS), no traces of cancer cells remained after 8 weeks and only inflammatory infiltrate and fibrotic tissue were present.[29] Against drug-resistant human colon tumor xenograft (Pgp+) DLD-1 in severe combined immunodeficient (SCID) mice, treatment with SB-T-1214 (20 mg/kg x 3 dose) resulted in complete tumor regression in 5 of 5 mice with limited observed systemic toxicity and weight loss, whereas paclitaxel not at all effective.[29]

Both SB-T-1216 and paclitaxel, at death-inducing concentrations, exerted a similar effect on the formation of interphase microtubule bundles in sensitive MDA-MB-435 and NCI/ADR-RES cells.[51] However, cell death induced in both cell lines resulted in different cell-cycle distribution between paclitaxel and SB-T-1216.[51] While treatment with paclitaxel led to the accumulation of cells in the G_2/M phase, the effect of SB-T-1216 was characterized by the accumulation of hypodiploid cells, not in the G_2/M phase.[51] This result suggests that second-generation taxoid, SB-T-1216, induces cell death via a pathway differing from M-phase block and can induce apoptosis independent of mitotic arrest.[51]

§2.3.2 C3'-Difluorovinyl Taxoids

The site specific incorporation of fluorine in next-generation taxoids was employed to investigate its effects on cytotoxicity and metabolic stability.[52] Fluorinated paclitaxel and docetaxel analogs have been synthesized to augment metabolic stability as well as to observe by ^{19}F NMR the solution phase and protein-bound conformations of Taxol.[53]

Studies on the metabolism of next-generation taxoids bearing a C3'-(2-methyl-1-propenyl) group have revealed that the allylic methyls can be hydroxylated by CYP3A4.[54] Metabolic analyses on paclitaxel and docetaxel *in vivo* showed that the C3'-phenyl and the C3'*N*-*t*-Boc groups are hydroxylated by CYP3A4, respectively, and that the C6 methylene is hydroxylated by CYP2C.[55, 56] Similarly, the C3'-(2-methyl-1-propenyl) group on SB-T-1214 can undergo a similar mechanism of hydroxylation by CYP3A4 (Figure 2.10).[54]

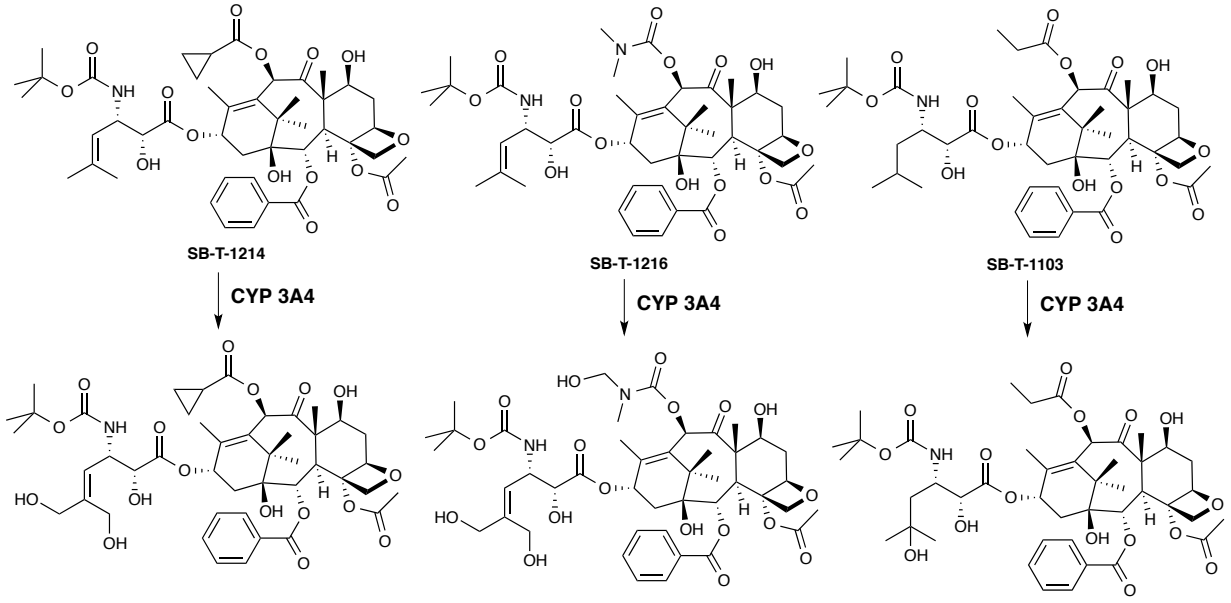

Figure 2.10. Metabolic hydroxylation of the second-generation taxoids by P450 enzymes. Adapted from reference [57].

To prevent the allylic hydroxylation of next-generation taxoids, a difluorovinyl group was introducted *in lieu* of the C3'-(2-methyl-1-propenyl) group.[57] The replacement of the carbon-hydrogen bond with the carbon-fluorine bond can effectively block metabolic pathways *via* hydroxylation of C-H bonds, specifically by the cytochrome P-450 family of enzymes. The H_3C–*F* bond is 5.0 kcal/mol stronger than the H_3C–*H* bond, providing increased stability. The strategic incorporation of fluorine into metabolic sites is referred to as the "block effect" and has been employed to improve the pharmacokinetics of drug candidates. Thus, C3'-difluorovinyl taxoids were prepared from β-lactam (+)**1-20**.

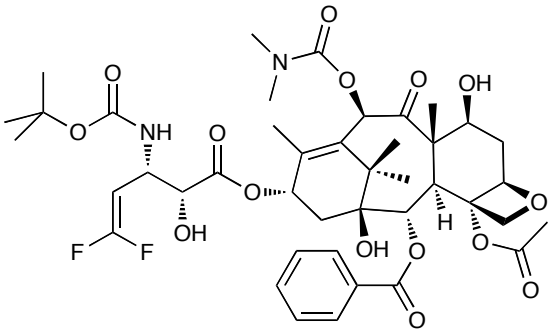

SB-T-12854

Figure 2.11. Chemical structure of second-generation fluorotaxoid, SB-T-12854.

Of the C3'-difluorovinyl second-generation taxoids, SB-T-12854 (Figure 2.11), a C3'-difluorovinyl analog of SB-T-1216, has demonstrated one to three orders of magnitude greater potency in comparison with paclitaxel in drug-sensitive and drug-resistant cancer cell lines (Table 2.3).[57] With resistance factors as low as 1.7, this class of taxoids appears unaffected by MDR.[57]

Table 2.3. Cytotoxicities (IC_{50}, nM) of second-generation fluorotaxoids against cancer cell lines. Adapted from reference [57].

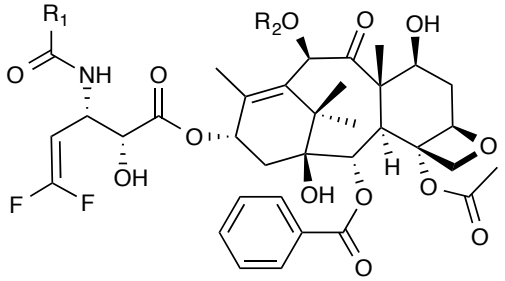

Taxoid	R_1	R_2	MCF-7[a]	NCI/ADR[b]	HT-29[c]	PANC-1[d]
paclitaxel	Ph	Ac	1.2	300	3.6	25.7
docetaxel	*N*-Boc	H	0.83	235	-	-
SB-T-12851	*N*-Boc	Ac	0.099	0.95	0.41	1.19
SB-T-12852	*N*-Boc	*c*-PrCO	0.12	6.03	0.85	5.85
SB-T-12853	*N*-Boc	EtCO	0.12	1.2	0.34	0.65
SB-T-12854	*N*-Boc	$(CH_3)_2NCO$	0.13	4.27	0.46	1.58

[a]Human breast carcinoma cell line; [b]Platinum-resistant metastatic human ovarian cancer cell line; [c]Human Caucasian colon adenocarcinoma cell line; [d]Human pancreatic carcinoma cell line; [e]Cells were incubated with a taxoid for 72 h at 37 °C with a 5% CO_2 atmosphere.

Additionally, metabolic studies revealed little to no observation of CYP3A4 hydroxylation at the C3' and C6 positions, indicating that the C3'-difluorovinyl taxoids are not susceptible to oxidative metabolism.[57] In addition to their metabolic stability, these fluorotaxoids have exhibited remarkable activity *in vitro*, inducing apoptosis by the activation of caspases 2, 8, and 9.[58]

§2.3.3 Semi-synthesis of Second-generation Taxoids: SB-T-1214, SB-T-1216, and SB-T-12854

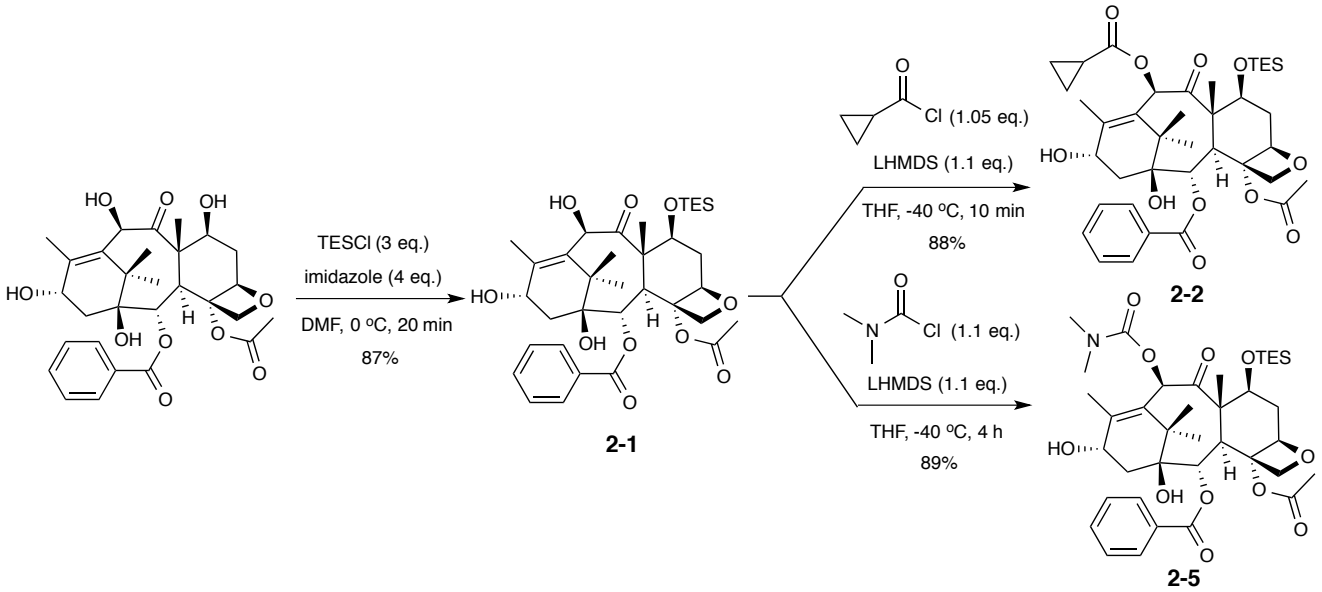

Scheme 2.2. Protection of C7 hydroxyl of 10-DAB III with TES and subsequent acylation reactions.

First, silyl protection of the C7 hydroxyl was achieved by treating 10-deacetylbaccatin III with chlorotriethylsilane (3 equiv.) in the presence of imidazole (4 equiv) to give **2-1** in high yield (87%). Minor di- and tri-TES protection was observed on TLC. Acylation of the C10 hydroxyl with cyclopropanecarbonyl chloride or *N*,*N*-dimethylcarbamoyl chloride in the presence of lithium bis(trimethylsilyl)amide (LHMDS) afforded modified baccatins **2-2** and **2-5**, respectively, in high yields (88-89%). Reaction progress was carefully monitored by TLC to limit di-substitution at the C13 hydroxyl group. The synthesis of modified baccatins **2-2** and **2-5** is illustrated in Scheme 2.2.

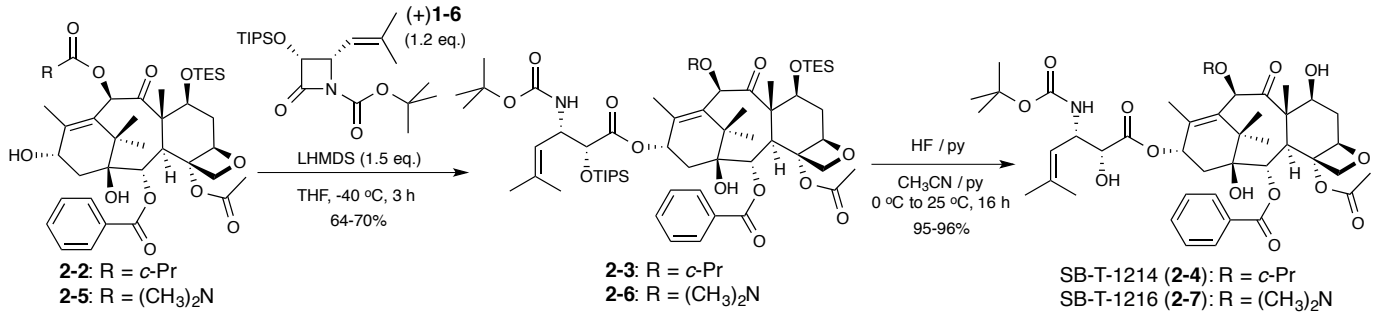

Scheme 2.3. Coupling of β-lactam (+)**1-6** to 7-TES-10-acyl-baccatins by Ojima-Holton protocol and deprotection of silyl groups to give SB-T-1214 (**2-4**) and SB-T-1216 (**2-7**).

The C13 isoserine side chain of the taxoid skeleton with C3'-(2-methyl-1-propenyl) and C3'*N*-*t*-Boc groups was introduced to by the Ojima-Holton coupling reaction. Coupling of β-lactam (+)**1-6** to 7-TES-10-acyl-baccatins **2-2** and **2-5** in the presence of LHMDS gave di-silyl protected taxoids **2-3** and **2-6** in good yields (64-70%). Deprotection of the silyl groups with HF-pyridine afforded SB-T-1214 (**2-4**) and SB-T-1216 (**2-7**) in excellent yields (95-96%), shown in Scheme 2.3. Recrystallization from hexanes and ethyl acetate afforded both taxoids in >98% purity by reverse-phase HPLC analysis.

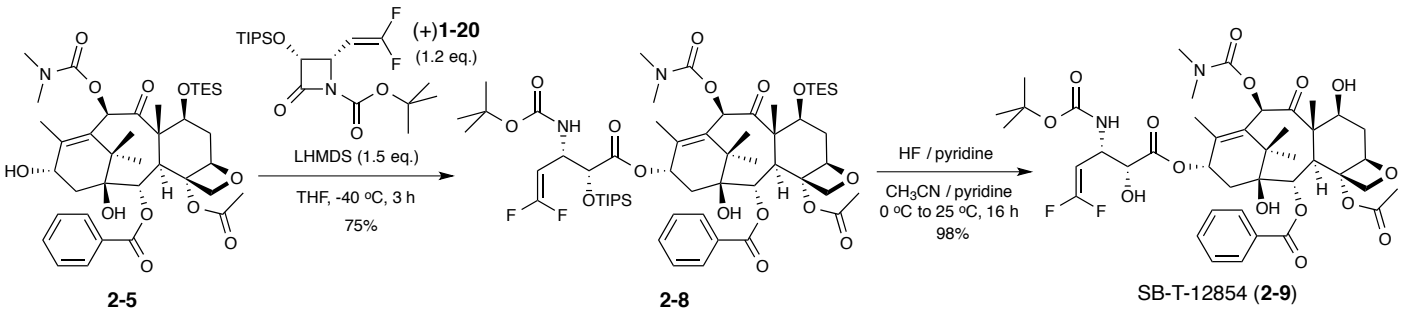

Scheme 2.4. Ojima-Holton coupling reaction followed by deprotection of silyl groups with HF-pyridine to give SB-T-12854 (**2-9**).

Difluorovinyl β-lactam (+)**1-20** was coupled to **2-5** under a similar protocol to afford **2-8** in good yield (75%), and deprotection of the silyl groups with HF-pyridine gave C3'-difluorovinyl taxoid SB-T-12854 (**2-9**) in nearly quantitative yield (98%), shown in Scheme 2.4. Chromatographic purification and recrystallization with hexanes and diethyl ether afforded SB-T-12854 in >98% purity by reverse-phase HPLC analysis.

§2.3.4 Third-Generation Taxoids

Additional SAR studies indicated that taxoids with *meta*-substituted C2-benzoate modifications demonstrated remarkable potency against drug-sensitive and drug-resistant (Pgp+) cancer cell lines, with a resistance-to-sensitivity (R/S) ratio below three in most cases and less than one in three cases.[59] Some of these C2-benzoate modified taxoids were found to have up to 3 orders of magnitude higher potency than paclitaxel and docetaxel against drug-resistant cell lines (Table 2.4).[59] These highly potent and efficacious taxanes can virtually circumvent the Pgp-mediated MDR and have been termed *third-generation taxoids*.[59] Of these third-generation taxoids, SB-T-121602, has demonstrated picomolar activity against human colon cancer cell line, HT-29, as well as excellent activity against breast and pancreatic cancer.[60]

Table 2.4. Cytotoxicities (IC_{50}, nM) of third-generation taxoids against cancer cell lines. Adapted from reference [48].

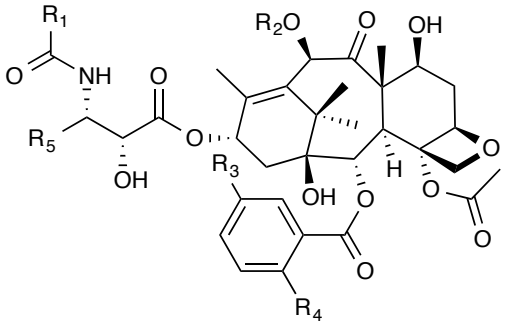

Taxoid	R_1	R_2	R_3	R_4	R_5	MCF-7[a]	LCC6-MDR[b]	HT-29[c]	CFPAC-1[d]
paclitaxel	Ph	Ac	H	H	Ph	1.7	346	12	68
docetaxel	*N*-Boc	H	H	H	Ph	1.0	120	-	-
SB-T-11033	*N*-Boc	EtCO	OCH_3	H	*i*-Bu	0.36	0.80	-	-
SB-T-121303	*N*-Boc	EtCO	OCH_3	H	$CH{=}C(CH_3)_2$	0.36	0.90	-	0.89
SB-T-121313	*N*-Boc	EtCO	OCH_3	OCH_3	$CH{=}C(CH_3)_2$	0.30	-	0.56	0.025
SB-T-121602	*N*-Boc	$(CH_3)_2NCO$	CH_3	H	$CH{=}C(CH_3)_2$	0.08	-	0.003	0.31

[a]Human breast carcinoma cell line; [b]Human ovarian cancer cell line; [c]Human Caucasian colon adenocarcinoma cell line; [d]Human pancreatic carcinoma cell line; [e]Cells were incubated with a taxoid for 72 h at 37 °C with a 5% CO_2 atmosphere.

To advance the current SAR understanding of *meta*-substituted C2-benzoates in third-generation taxoids, a series of third-generation taxoids with C2-*m*-CF_3-benzoate and C2-*m*-OCF_3-benzoate was synthesized. Novel third-generation fluorotaxoid, SB-T-12822-5 was designed as a chemical tool for ^{19}F NMR experiments involving linker conjugation at the C2'-hydroxyl (Chapter 3).

§2.3.5 Synthesis of Third-Generation Taxoids

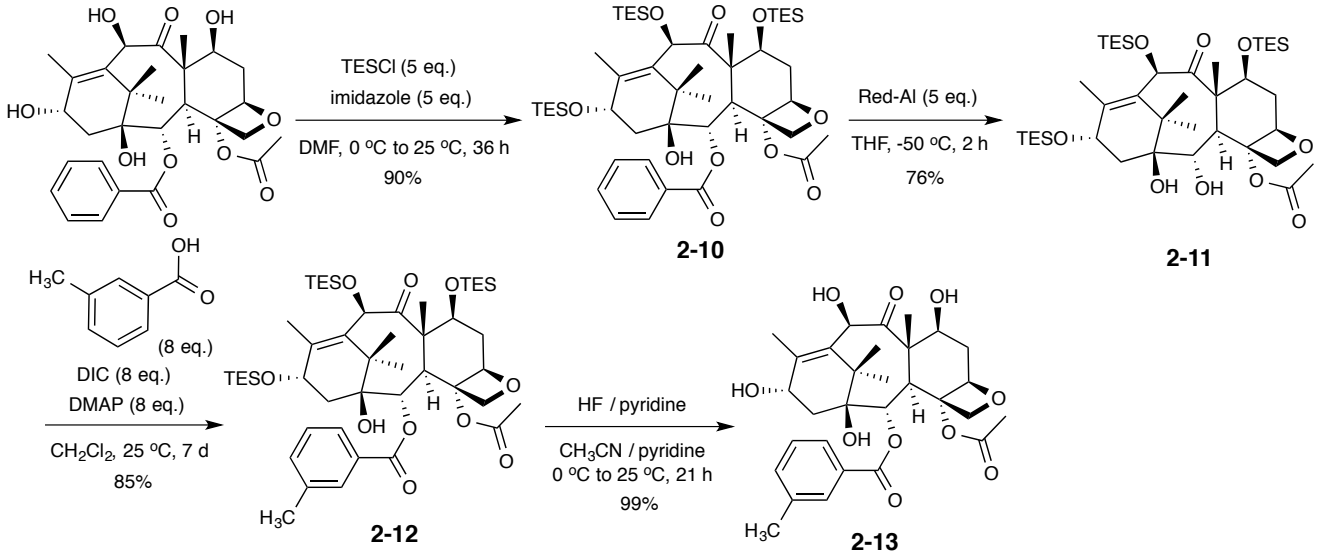

Scheme 2.5. Modifications to the C2 benzoate of 10-DAB III.

The synthesis of third-generation taxoid SB-T-121602 (**2-17**) was performed over eight steps from 10 DAB III. The C7, C10, and C13 hydroxyl groups of 10 DAB III were first protected with TES to afford **2-10** in excellent yield (90%); the C1 hydroxyl remains unreactive towards large silyl groups due its configuration in the 3D structure of baccatin (Figure 2.2) and appears to be unnecessary for the activity of paclitaxel.[41] Selective reductive cleavage of the C2-benzoate with Red-Al, which coordinates to the C1 hydroxyl and delivers the hydride to the C2-ester while preserving of the C4 acetate, gave **2-11** in good yield (76%). Coupling to the desired *m*-substituted benzoic acid to **2-11** in the presence of diisopropylcarbodiimide afforded **2-12** in high yield (85%). Reaction durations for coupling at the C2 position varies depending on the substituted benzoic acid, ranging from one to seven days. Deprotection of the silyl groups with HF-pyridine gave the C2-benzoate-*m*-CH_3 substituted 10-DAB III derivative **2-13** in quantitative yield.

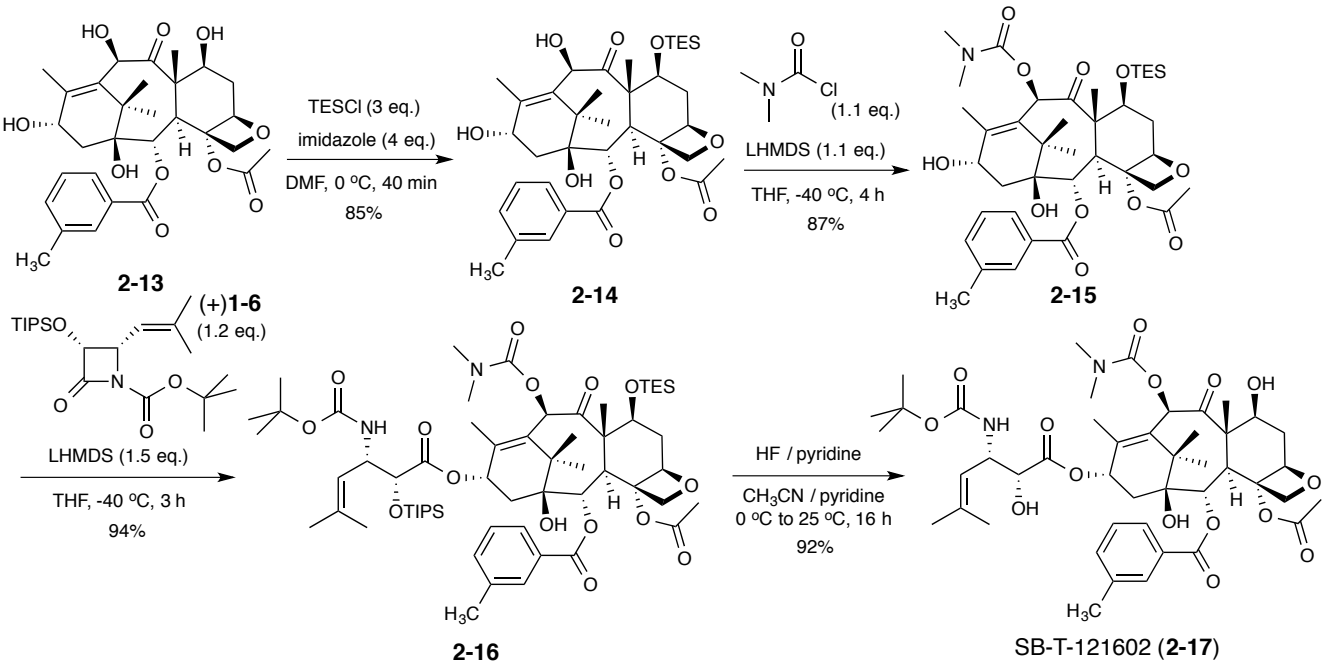

Scheme 2.6. Synthesis of C2-*m*-CH_3 third-generation taxoid: SB-T-121602 (**2-17**).

Protection of **2-13** with TES in the presence of imidazole gave **2-14** in high yield (85%), and acylation of the C10 hydroxyl with *N*,*N*-dimethylcarbamoyl chloride in the presence of LHMDS gave **2-15** in high yield (87%). The C13 isoserine side chain with C3'-isobutenyl and C3'*N*-*t*-Boc groups was introduced by Ojima-Holton coupling of β-lactam (+)**1-6** to 7-TES-10-acyl-10-DAB III (**2-15**) in the presence of LHMDS to afford **2-16** in excellent yield (94%). Deprotection of the silyl groups with HF-pyridine afforded SB-T-121602 (**2-17**) in excellent yields (92%). The synthesis of SB-T-121602 is illustrated in Scheme 2.6. Recrystallization from hexanes and ethyl acetate afforded SB-T-121602 in >98% purity by reverse-phase HPLC analysis.

§2.3.6 Synthesis of C2-*m*-CF_3 Third-generation Fluorotaxoids

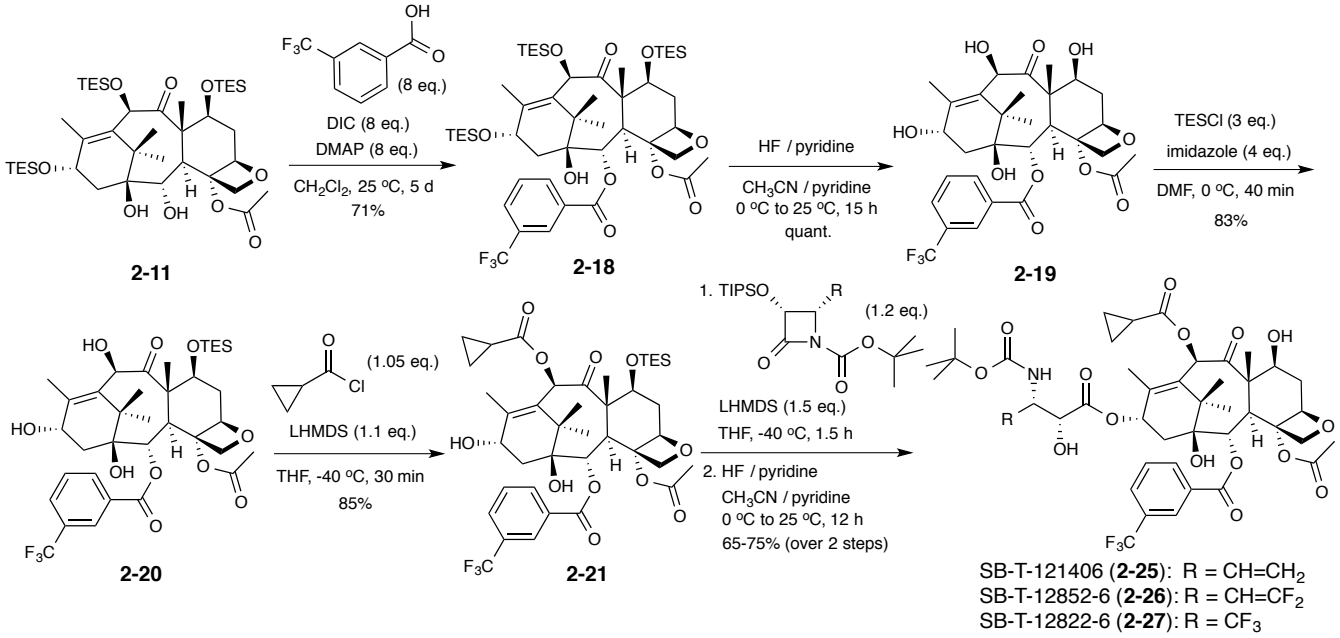

Scheme 2.7. Synthesis of C2-*m*-CF_3 taxoids: SB-T-121406 (**2-25**), SB-T-12852-6 (**2-26**), and SB-T-12822-6 (**2-27**)

Synthesis of third-generation fluorotaxoids with modified C2-*m*-(trifluoromethyl)-benzoates was performed by a similar synthetic route as that for SB-T-121602. Coupling of tri-TES protected baccatin III (**2-11**) with 3-(trifluoromethyl)benzoic acid in the presence of DIC and DMAP gave **2-18** in good yield (71%). Deprotection of the silyl groups with HF-pyridine gave baccatin **2-19** in quantitative yield, and protection of the C7 hydroxyl with TES in the presence of imidazole gave **2-20** in high yield (83%). Acylation of the C10 hydroxyl with cyclopropanecarbonyl chloride in the presence of LHMDS afforded **2-21** in high yield (85%). Coupling of β-lactams (+)**1-6**, (+)**1-20**, and CF_3-β-lactam to the C13 hydroxyl in the presence of LHMDS of **2-21** gave protected taxoids **2-22**, **2-23**, and **2-24** in high yields (81-87%). Deprotection of the silyl groups with HF-pyridine afforded SB-T-121406 (**2-25**), SB-T-12852-6 (**2-26**), and SB-T-12822-6 (**2-27**) in high yields (80-86%) shown in Scheme 2.7. Chromatographic purification and recrystallization with hexanes and ethyl acetate afforded the three fluorotaxoids in >98% purity by reverse-phase HPLC analysis.

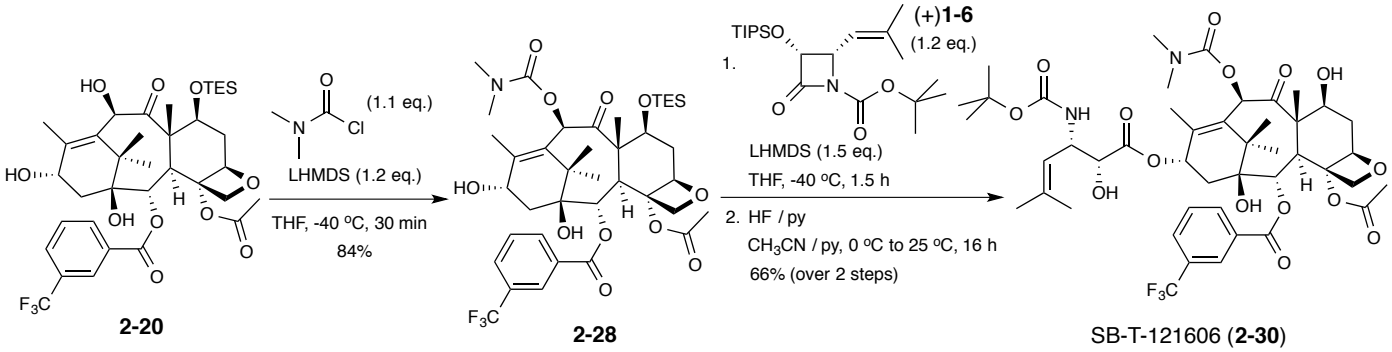

Scheme 2.8. Synthesis of C2-*m*-CF_3 third-generation fluorotaxoid: SB-T-121606 (**2-30**).

For the synthesis of SB-T-121606, acylation of the C10 hydroxyl of **2-20** with *N,N*-dimethylcarbamoyl chloride in the presence of LHMDS gave **2-28** in high yield (84%). Coupling of β-lactam (+)**1-6** to the C13 hydroxyl of **2-28** in the presence of LHMDS, followed by deprotection of the silyl groups with HF-pyridine gave SB-T-121606 (**2-30**) in good yield (66% over 2 steps), shown in Scheme 2.8. Chromatographic purification and recrystallization with hexanes and ethyl acetate afforded SB-T-121606 in >98% purity by reverse-phase HPLC analysis.

§2.3.7 Synthesis of C2-*m*-OCF_3 Third-generation Fluorotaxoid: SB-T-12822-5.

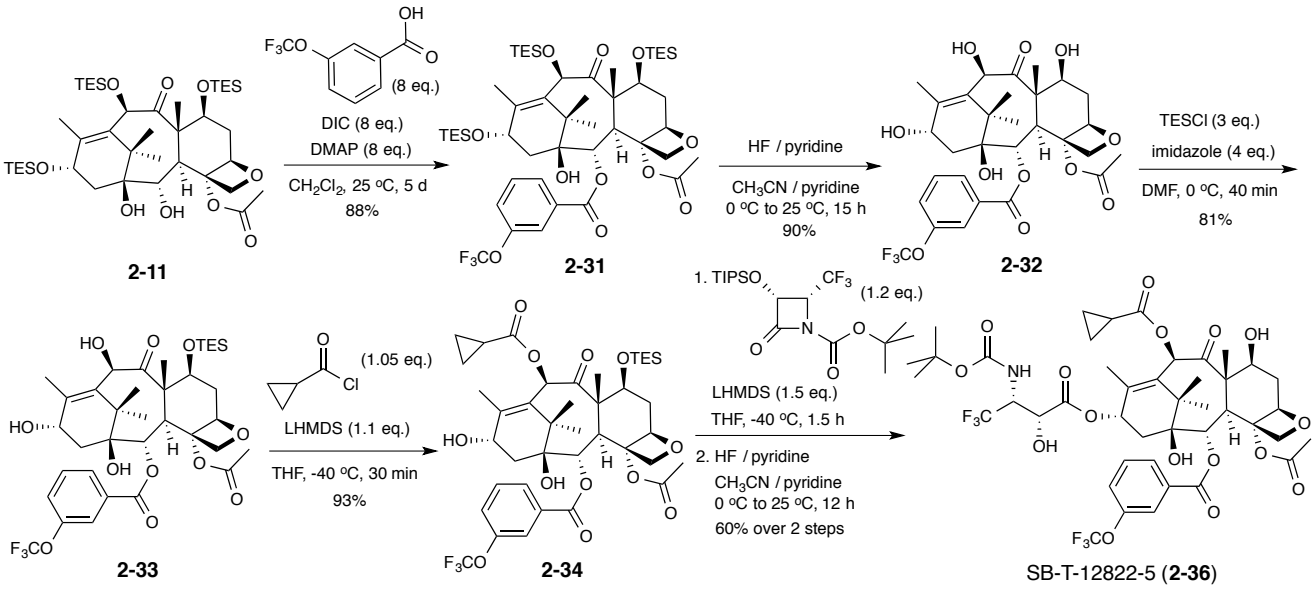

Scheme 2.9. Synthesis of C2-*m*-OCF_3 third-generation fluorotaxoid: SB-T-12822-5 (**2-36**). Adapted from reference [61].

Synthesis of third-generation fluorotaxoid, SB-T-12822-5, shown in Scheme 2.9, with modified C2-*m*-(trifluoromethoxy)-benzoates was performed by a similar synthetic route as that for SB-T-121602. Coupling of tri-TES protected baccatin (**2-11**) with 3-(trifluoromethyoxy)benzoic acid in the presence of DIC and DMAP gave **2-31** in high yield (88%). Deprotection of the silyl groups with HF-pyridine gave baccatin **2-32** in excellent yield (90%), and protection of the C7 hydroxyl with TES in the presence of imidazole gave **2-33** in high yield (81%). Acylation of the C10 hydroxyl with cyclopropanecarbonyl chloride in the presence of LHMDS afforded **2-34** in excellent (93%). Coupling of CF_3-β-lactam to the C13 hydroxyl of **2-34** gave protected taxoids **2-35** in modest yield (69%). Deprotection of the silyl groups with HF-pyridine afforded SB-T-12822-5 (**2-36**), in high yield (87%). Chromatographic purification and recrystallization with hexanes and ethyl acetate afforded SB-T-12822-5 in >98% purity by reverse-phase HPLC analysis.[61]

§2.3.8 Biological Evaluation of Third-generation Fluorotaxoids

The potencies of third-generation fluorotaxoids SB-T-121406, SB-T-121606, SB-T-12822-6, and SB-T-12852-6, were evaluated *in vitro* against human breast carcinoma cell line, MCF-7, and platinum-resistant metastatic ovarian cancer cell line, ID8. The cytotoxicity assays

were performed by MTT method.[62] As controls for comparison, paclitaxel and docetaxel were evaluated as well. The results for 72 h drug incubation are given in Table 2.5.

Table 2.5. Cytotoxicities (IC_{50}, nM) of third-generation fluorotaxoids against cancer cell lines.[c,d]

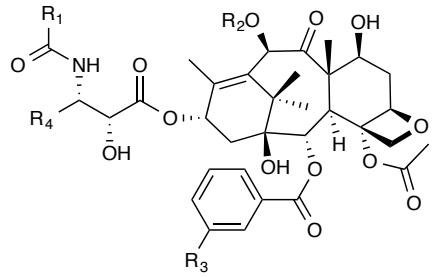

Compound	R_1	R_2	R_3	R_4	MCF-7[a]	NCI/ADR-RES[b]
paclitaxel	Ph	Ac	H	Ph	3.31 ± 1.09	271 ± 81
docetaxel	*N*-Boc	H	H	Ph	0.73 ± 0.01	519 ± 126
SB-T-121405[d]	*N*-Boc	*c*-PrCO	OCF_3	$CH{=}C(CH_3)_2$	0.19 ± 0.05	0.59 ± 0.11
SB-T-121406	*N*-Boc	*c*-PrCO	CF_3	$CH{=}C(CH_3)_2$	10.1 ± 4.9	59.9 ± 12.2
SB-T-12822-6	*N*-Boc	*c*-PrCO	CF_3	CF_3	3.79 ± 1.21	67.1 ± 19.6
SB-T-12852-6	*N*-Boc	*c*-PrCO	CF_3	$CH{=}C(CH_3)_2$	25.2 ± 15.3	61.4 ± 8.7

[a]Human breast carcinoma cell line; [b]Platinum-resistant metastatic ovarian cancer cell line; [c]Cells were incubated with a taxoid for 72 h at 37 °C in a 5% CO_2 atmosphere; [d]Synthesis of SB-T-121405 and cytotoxicity assay were performed by Xin Wang.

As anticipated, both paclitaxel and docetaxel were found to be highly potent against MCF-7 with IC_{50} values of 3.31 and 0.73 nM, respectively, and two to three orders of magnitude less potent against multidrug resistant cancer cell line NCI/ADR-RES with IC_{50} values of 271 and 519 nM, respectively. Third-generation fluorotaxoid with C2-*m*-OCF_3 (SB-T-121405) showed improved activity compared to paclitaxel and docetaxel against MCF-7 with a sub-nanomolar IC_{50} value of 0.19 nM and a marked improvement in activity against drug resistant cell line NCI/ADR-RES also with a submolar IC_{50} value of 0.59 nM. Third-generation fluorotaxoids with C2-*m*-CF_3 modifications (SB-T-121406, SB-T-121606, SB-T-12822-6, and SB-T-12852-6) showed high activity against MCF-7 with IC_{50} values ranging from 4-25 nM and reduced potency against NCI/ADR-RES with IC_{50} values ranging from 59-67 nM.

The results indicate through structure-activity relationship (SAR) studies a marked improvement in potency with the addition of *m*-OCF_3 on the C2-benzoate ring against MCF-7 breast cancer cell line. Furthermore, the incorporation of *m*-OCF_3 in SB-T-121405 appears to circumvent drug resistance shown by its sub-nanomolar activity against NCI/ADR-RES. While addition of a C2-*m*-CF_3 group to the taxoid skeleton increases the overall potency compared to paclitaxel and docetaxel, it appears that its incorporation contributes less to overall potency than the C2-*m*-OCF_3 substitution. This difference may be attributable to the more rigid nature of the trifluoromethyl group, whereas the trifluoromethoxy group is both more rotatable and perpendicular and may better accommodate tubulin-binding interactions.

§2.4. Fluorescence-labeled Taxoids

A series of fluorescently labeled taxoids was synthesized and employed to study the interaction of taxanes with the tubulin/microtubule system and visualize microtubule dynamics through fluorescence spectroscopy.[63, 64] Most taxane-based fluorescent probes have been prepared through the introduction of a fluorophore, such as fluorescein or rhodamine, at the C7 position, since the C7 and other "northern hemisphere" substituents have been shown not to interfere with taxane-tubulin interactions.[64]

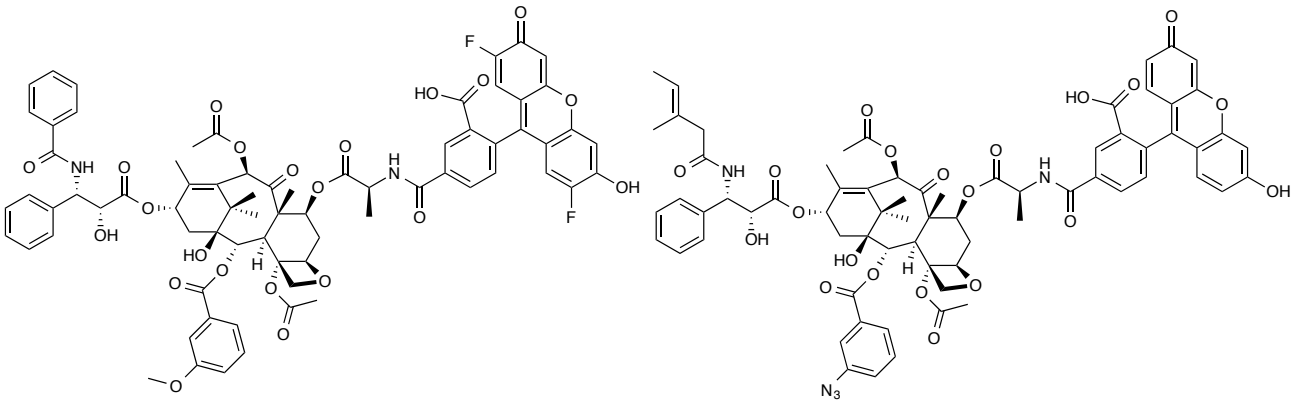

Figure 2.12. Chemical structures of two fluorescently labeled taxoids. Adapted from reference [64].

§2.4.1 Synthesis of Taxol-7-Fluorescein

The fluorescein moiety, 6-tethered fluorescein isobutyl ester, was obtained from Tao Wang. The synthesis was carried out in three steps from commercially available fluorescein. First, fluorescein was converted to the methyl ester, and Mitsunobu coupling with *tert*-butyl 4-hydroxybutanoate afforded a modified fluorescein diester. Selective deprotection with trifluoroacetic acid gave the 6-tethered fluorescein isobutyl ester, which used in the synthesis of 7-fluorescein-tethered paclitaxel.

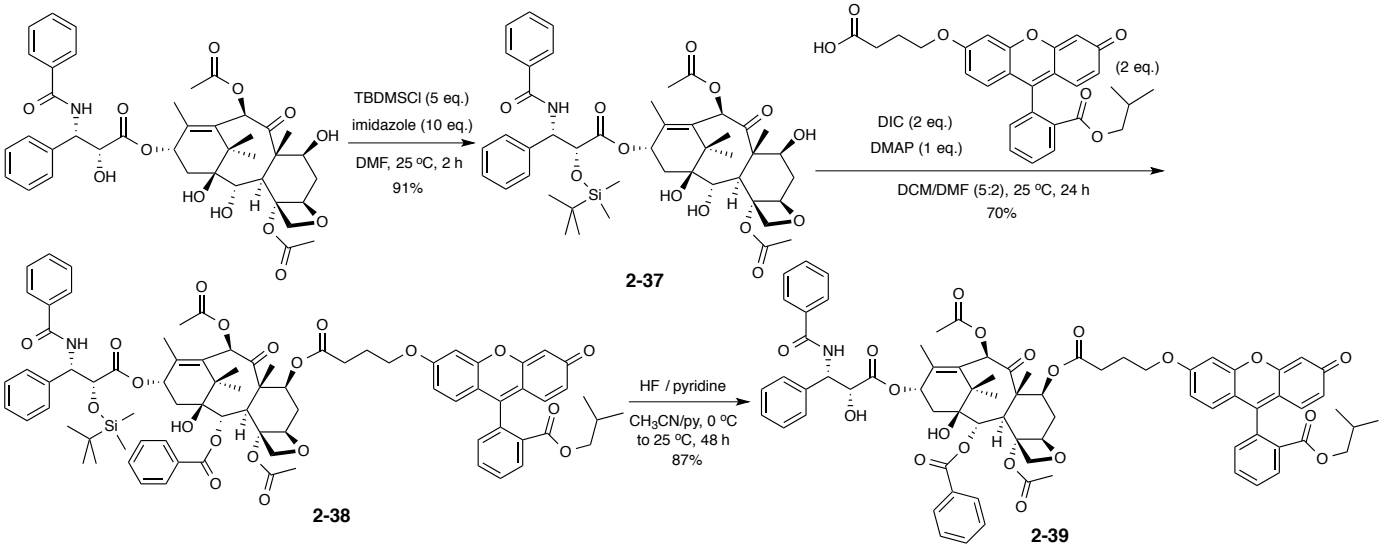

Scheme 2.10. Protection of C2' hydroxyl with TBDMS, coupling of 4-isobutanoyl-fluorescein to C7 hydroxyl, and subsequent deprotection with HF-pyridine to give Taxol-7-fluorescein (**2-39**).

The C2'-hydroxy group of paclitaxel was protected with TBDMS in the presence of imidazole to afford **2-37** in excellent yield (91%), which was coupled to 6-tethered fluorescein isobutyl ester in the presence of DIC and DMAP, followed by silyl deprotection with HF-pyridine to give **2-39** in good yield (61% over 2 steps), 7-fluorescein-tethered paclitaxel. The biological evaluation of Taxol-7-fluorescein (**2-39**) for non-specific internalization is discussed later in Chapter 4.

§2.5 Summary

Paclitaxel and docetaxel are among the most widely used chemotherapeutic agents, in particular against cancers such as ovarian, breast, lung, and Kaposi's sarcoma. Despite their high antitumor activity as microtubule-stabilizing agents, these drugs cause undesirable side effects as well as encounter drug resistance. New next-generation taxane anticancer agents that show several orders of magnitude greater potency than paclitaxel or docetaxel against MDR cancer cells (second-generation taxoids) or that can virtually circumvent the Pgp-mediated MDR (third-generation taxoids) were designed and synthesized. A series third-generation fluorotaxoids (SB-T-121406, SB-T-121606, SB-T-12822-6, and SB-T-12852-6) with modifications to the C2-benzoate with *m*-OCF_3 and *m*-CF_3 substituents was designed and synthesized by the Ojima-Holton coupling protocol from enantiomerically pure β-lactams towards advancement of structure-activity relationship (SAR) studies. The biological evaluation of these third-generation fluorotaxoids showed a marked improvement in potency with the addition of C2-*m*-OCF_3 to the taxoid skeleton, as well as greatly increased potency against MDR cancer cells compared to paclitaxel and docetaxel. While incorporation of the C2-*m*-CF_3 group increased the potency as well, the trifluoromethyl substituent contributed to an increase in potency less so than its trifluoromethoxy counterpart. Finally, a fluorescent probe of taxol, Taxol-7-fluroescein, was designed and synthesized, and later used in Chapter 4 to observe non-specific internalization of the taxoid by confocal fluorescence microscopy across cancer and normal cell types.

§2.6 Experimental

§2.6.1 Caution

Taxoids have been identified as potent cytotoxic agents. Thus, all drugs and structurally related compounds and derivatives must be considered mutagens and potential reproductive hazards for both males and females. All appropriate precautions, such as the use of gloves, goggles, labware, and fume hood, must be taken while handling the compounds at all times.

§2.6.2 General Information

^{1}H, ^{13}C, and ^{19}F NMR spectra were measured on a Varian 300, 400, 500, or 600 MHz NMR spectrometer or Bruker 300, 400, or 500, or 700 MHz NMR spectrometer. Hexafluorobenzene was used as an external standard for ^{19}F NMR analysis. Melting points were measured on a Thomas-Hoover capillary melting point apparatus and are uncorrected. TLC was performed on Sorbent Technologies aluminum-backed Silica G TLC plates (Sorbent Technologies, 200 μm, 20 x 20 cm), and column chromatography was carried out on silica gel 60 (Merck, 230-400 mesh ASTM). Purity was determined with a Shimadzu L-2010A HPLC HT

series HPLC assembly, using a Kinetex PFP column (4.6 mm x 100 mm, 2.6 μm) with acetonitrile-water gradient solvent system. One analytical condition was used and noted as part of the characterization and purity data, i.e., HPLC: flow rate 0.4 mL/min, 5% acetonitrile from 0→1 min, and a gradient of 5→95% acetonitrile for the 1-25 min period. High resolution mass spectrometry analysis was carried out on an Agilent LC-UV-TOF mass spectrometer at the Institute of Chemical Biology and Drug Discovery, Stony Brook, NY or at the Mass Spectrometry Laboratory, University of Illinois at Urbana-Champaign, Urbana, IL.

§2.6.3 Materials

The chemicals were purchased from Sigma-Aldrich, Fisher Scientific, and VWR International, and used as received or purified before use by standard methods. Tetrahydrofuran was freshly distilled from sodium and benzophenone. Dichloromethane was also distilled immediately prior to use under nitrogen from calcium hydride. 10-Deacetylbaccatin III and paclitaxel were obtained from Indena, SpA, Italy. (3*R*,4*R*)-1-(*tert*-Butoxycarbonyl)-3-triisopropylsiloxy-4-trifluoromethylazetidin-2-one was prepared according to literature methods.[65]

§2.6.4 Experimental Procedure

10-Deacetyl-7-triethylsilylbaccatin III [2-1]:[27, 66]
To a cooled solution of 10-deacetylbaccatin III (0.501 g, 0.919 mmol) and imidazole (0.256 g, 3.68 mmol) in DMF (9 mL) was added TESCl (0.46 mL, 2.76 mmoL), and the mixture was allowed to react at 0 °C for 20 min with stirring. The reaction was quenched with saturated NH_4Cl (10 mL) and diluted with H_2O (10 mL), and the reaction mixture was extracted with ethyl acetate (3 x 30 mL). The combined organic layers were washed with brine (3 x 20 mL), dried over $MgSO_4$, and concentrated *in vacuo* to afford a white solid. Purification of the crude product by column chromatography on silica gel with hexanes/ethyl acetate (3:1) as eluent gave **2-1** (0.529 g, 87%) as a white solid; ^{1}H NMR (300 MHz, $CDCl_3$) δ 0.55 (m, 6H), 0.93 (m, 9H), 1.06 (s, 6H), 1.63 (s, 1H), 1.69 (bs, 1H), 1.72 (s, 3H), 1.89 (m, 1H), 2.07 (s, 3H), 2.24 (m, 2H), 2.27 (s, 3H), 2.47 (m, 1H), 3.93 (d, *J* = 7.2 Hz, 1H), 4.15 (d, *J* = 8.4 Hz, 1H), 4.27 (s, 1H), 4.30 (d, *J* = 8.4 Hz, 1H), 4.40 (dd, *J* = 6.9, 10.9 Hz, 1H), 4.84 (m, 1H), 4.95 (d, *J* = 8.4 Hz, 1H), 5.16 (d, *J* = 2.1 Hz, 1H), 5.59 (d, *J* = 6.9 Hz, 1H), 7.49 (t, *J* = 7.8 Hz, 2H), 7.59 (d, *J* = 7.5 Hz, 1H), 8.09 (d, *J* = 7.5 Hz, 2H). All data are in agreement with literature values.[25]

10-Cyclopropanecarbonyl-10-deacetyl-7-triethylsilylbaccatin III [2-2]:[49]
To a cooled solution of **2-1** (0.525 g, 0.796 mmol) in THF (6 mL) was added 1 M LHMDS (0.9 mL, 0.876 mmoL) followed by cyclopropanecarbonyl chloride (77 μL, 0.836 mmol), and the mixture was allowed to react for 10 min at -50 °C with stirring. The reaction was allowed to warm to -40 °C and was quenched with saturated NH_4Cl (10 mL) and diluted with H_2O (10 mL). The reaction mixture was extracted with ethyl acetate (3 x 30 mL). The combined organic layers were washed with brine (3 x 30 mL), dried over $MgSO_4$, and concentrated *in vacuo* to afford a white solid. Purification of the crude product by column chromatography on silica gel with hexanes/ethyl acetate (3:1) as eluent gave **2-2** (0.508 g, 88%) as a white solid; ^{1}H NMR (300 MHz, $CDCl_3$) δ 0.55 (m, 6H), 0.91 (m, 9H), 0.99 (m, 4H), 1.04 (s, 3H), 1.20 (s, 3H), 1.64 (s, 3H), 1.86 (m, 1H), 2.14 (s, 3H), 2.19 (m, 1H), 2.23 (m, 2H), 2.24 (s, 3H), 2.51 (m, 1H), 3.88 (d, *J* =

6.9 Hz, 1H), 4.09 (d, *J* = 8.4 Hz, 1H), 4.29 (d, *J* = 8.4 Hz, 1H), 4.47 (dd, *J* = 6.9, 10.1 Hz, 1H), 4.82 (bt, 1H), 4.96 (d, *J* = 7.8 Hz, 1H), 5.63 (d, *J* = 6.9 Hz, 1H), 6.96 (s, 1H) 7.47 (t, *J* = 7.8 Hz, 2H), 7.60 (t, *J* = 7.5 Hz, 1H), 8.11 (d, *J* = 7.2 Hz, 2H). All data are in agreement with literature values.[49]

10-Cyclopropanecarbonyl-3'-dephenyl-3'-(2-methyl-2-propenyl)-7-triethylsilyl-2'-triisopropylsilyldocetaxel [2-3]:[49]

To a cooled solution of **2-2** (0.260 g, 0.361 mmol) and β-lactam (+)**1-6** (0.188 g, 0.469 mmol) in THF (9 mL) was added 1 M LHMDS (0.47 mL, 0.469 mmol), and the mixture was allowed to react for 3 h at -40 °C with stirring. The reaction was diluted with H_2O (10 mL), and the mixture was extracted with ethyl acetate (3 x 30 mL). The combined organic layers were washed with brine (3 x 30 mL), dried over $MgSO_4$, and concentrated *in vacuo* to afford a white solid. Purification of the crude product by column chromatography on silica gel with hexanes/ethyl acetate (9:1) as eluent gave **2-3** (0.277 g, 70%) as a white solid; ^{1}H NMR (300 MHz, $CDCl_3$) δ 0.55 (m, 6H), 0.85 (dd, *J* = 5.4, 6.6 Hz, 2H), 0.93 (m, 9H), 0.95 (m, 2H), 1.11 (m, 21H), 1.20 (s, 3H), 1.23 (s, 3H), 1.34 (s, 9H), 1.67 (s, 3H), 1.73 (m, 1H), 1.75 (s, 3H), 1.79 (d, *J* = 1.2 Hz, 3H), 1.89 (m, 1H), 2.01 (s, 3H), 2.36 (s, 3H), 2.37 (m, 2H), 2.50 (m, 1H), 3.82 (d, *J* = 6.9 Hz, 1H), 4.14 (d, *J* = 8.4 Hz, 1H), 4.30 (d, *J* = 8.4 Hz, 1H), 4.42 (d, *J* = 2.7 Hz, 1H), 4.44 (dd, *J* = 6.9, 10.1 Hz, 1H), 4.75 (m, 2H), 4.96 (d, *J* = 7.5 Hz, 1H), 5.34 (d, *J* = 8.9 Hz, 1H), 5.67 (d, *J* = 6.5 Hz, 1H), 6.18 (t, *J* = 8.0 Hz, 1H), 6.30 (s, 1H), 7.47 (t, *J* = 6.0 Hz, 2H), 7.58 (t, *J* = 8.0 Hz, 1H), 8.09 (d, *J* = 7.5 Hz, 2H). All data are in agreement with literature values.[49]

10-Cyclopropanecarbonyl-3'-dephenyl-3'-(2-methyl-2-propenyl)docetaxel (SB-T-1214) [2-4]:[49]

To a cooled solution of **2-3** (0.178 g, 0.158 mmol) in CH_3CN-pyridine (1:1) (11 mL) was added HF-pyridine (1.85 mL), and the reaction mixture was allowed to warm from 0 °C to room temperature and react for 22 h with stirring. The reaction was diluted with H_2O (20 mL), and the mixture was extracted with ethyl acetate (3 x 30 mL). The combined organic layers were washed with saturated $CuSO_4$ (3 x 30 mL) and brine (3 x 30 mL), dried over $MgSO_4$, and concentrated *in vacuo* to afford a white solid. Purification of the crude product by column chromatography on silica gel with hexanes/ethyl acetate (1:9) as eluent gave SB-T-1214 (**2-4**) (0.129 g, 96%) as a white solid; ^{1}H NMR (600 MHz, $CDCl_3$), δ 0.99 (m, 2H), 1.10 (m, 2H), 1.14 (s, 3 H), 1.25 (s, 3H), 1.34 (s, 9H), 1.67 (s, 3H), 1.71 (m, 1H), 1.75 (s, 6H), 1.84 (m, 1H), 1.89 (s, 3H,), 2.35 (s, 3H), 2.37 (bs, 1H), 2.53 (m, 1H), 2.61 (d, *J* = 3.6 Hz, 1H), 3.40 (d, *J* = 5.4 Hz, 1H), 3.80 (d, *J* = 6.9 Hz, 1H), 4.13 (d, *J* = 8.4 Hz, 1H), 4.15 (m, 1H), 4.30 (d, *J* = 8.4 Hz, 1H), 4.41 (m, 1H), 4.73 (d, *J* = 2.4 Hz, 1H), 4.79 (t, *J* = 8.4 Hz, 1H), 4.96 (d, *J* = 8.4 Hz, 1H), 5.31 (d, *J* = 8.1 Hz, 1H), 5.66 (d, *J* = 6.9 Hz, 1H), 6.16 (t, *J* = 8.8 Hz, 1H), 6.30 (s, 1H), 7.47 (t, *J* = 7.5 Hz, 2H), 7.61 (t, *J* = 7.8 Hz, 1H), 8.10 (d, *J* = 7.2 Hz, 2H); ^{13}C NMR (150 MHz, $CDCl_3$) δ 9.1, 9.4, 9.5, 13.0, 14.9, 18.5, 21.9, 22.4, 25.7, 26.7, 28.2, 35.5, 35.6, 43.2, 45.6, 51.6, 58.6, 72.2, 72.3, 73.7, 75.0, 75.4, 76.5, 77.0, 77.5, 79.2, 80.0, 81.1, 84.4, 120.7, 128.6, 129.2, 130.1, 133.0, 133.6, 137.9, 142.6, 155.4, 166.9, 170.1, 175.1, 203.9. HPLC: t = 20.7 min, purity >98%. All data are in agreement with literature values.[49]

10-Deacetyl-10-*N,N*-dimethylcarbamoyl-7-triethylsilylbaccatin III [2-5]:[49]

To a cooled solution of **2-1** (0.201 g, 0.305 mmol) in THF (6 mL) was added 1 M LHMDS (0.35 mL, 0.35 mmol) followed by *N,N*-dimethylcarbamoyl chloride (36 μL, 0.336 mmol), and the

mixture was allowed to react for 4 h at -40 °C with stirring. Reaction progress was monitored by TLC (CH_2Cl_2/CH_3OH = 19:1). The reaction was quenched with saturated NH_4Cl (10 mL) and diluted with H_2O (10 mL). The reaction mixture was extracted with ethyl acetate (3 x 30 mL). The combined organic layers were washed with brine (3 x 30 mL), dried over $MgSO_4$, and concentrated *in vacuo* to afford a colorless oil. Purification of the crude product by column chromatography on silica gel with hexanes/ethyl acetate (3:1) as eluent gave **2-5** (0.202, 89%) as a white solid; ^{1}H NMR (600 MHz, CDCl3) δ 0.59 (m, 6 H), 0.92 (t, *J* = 7.8 Hz, 9H), 1.06 (s, 3H), 1.20 (s, 3H), 1.69 (s, 3H), 1.89 (m, 1H), 2.25 (s, 3H), 2.27 (m, 2H), 2.29 (s, 3H), 2.53 (m, 1H), 2.94 (s, 3H), 3.08 (s, 3H), 3.91 (d, *J* = 7.2 Hz, 1H), 4.15 (d, *J* = 8.4 Hz, 1H), 4.30 (d, *J* = 8.4 Hz, 1H), 4.50 (dd, *J* = 6.6, 10.2 Hz, 1H), 4.84 (m, 1H), 4.97 (d, *J* = 9.0 Hz, 1H), 5.64 (d, *J* = 7.2 Hz, 1H), 6.39 (s, 1H), 7.48 (t, *J* = 7.2 Hz, 2H), 7.60 (t, *J* = 7.8 Hz, 1H,), 8.11 (d, *J* = 7.2 Hz, 2H). All data are in agreement with literature values.[49]

3'-Dephenyl-10-*N*,*N*-dimethylcarbamoyl-3'-(2-methyl-2-propenyl)-7-triethylsilyl-2'-triisopropylsilyldocetaxel [2-6]:[49]

To a cooled solution of **2-5** (0.200 g, 0.270 mmol) and β-lactam (+)**1-6** (0.200 g, 0.325 mmol) in THF (7 mL) was added 1 M LHMDS (0.35 mL, 0.350 mmol), and the mixture was allowed to react for 3 h at -40 °C with stirring. The reaction was diluted with H_2O (10 mL), and the mixture was extracted with ethyl acetate (3 x 30 mL). The combined organic layers were washed with brine (3 x 30 mL), dried over $MgSO_4$, and concentrated *in vacuo* to afford a yellow oil. Purification of the crude product by column chromatography on silica gel with hexanes/ethyl acetate (3:2) as eluent gave **2-6** (0.192 g, 64%) as a white foam; ^{1}H NMR (300 MHz, $CDCl_3$) δ 0.60 (m, 6H), 0.92 (t, *J* = 8.1 Hz, 9H), 1.10 (m, 21H), 1.19 (s, 3H), 1.22 (s, 3H), 1.34 (s, 9H), 1.69 (s, 3H), 1.75 (s, 3H), 1.79 (s, 3H), 1.88 (t, *J* = 13.2 Hz, 1H), 2.06 (s, 3H), 2.27 (m, 1H), 2.36 (s, 3H), 2.37 (m, 1H), 2.51 (m, 1H), 2.94 (s, 3H), 3.06 (s, 3H), 3.86 (d, *J* = 7.2 Hz, 1H), 4.20 (d, *J* = 8.4 Hz, 1H), 4.30 (d, *J* = 8.4 Hz, 1H), 4.43 (d, *J* = 2.7 Hz, 1H) 4.48 (dd, *J* = 6.6, 10.2 Hz, 1H), 4.78 (m, 2H), 4.94 (d, *J* = 8.1 Hz, 1H), 5.33 (d, *J* = 8.1 Hz, 1H), 6.10 (bt, 1H), 6.40 (s, 1H), 7.46 (t, *J* = 7.8 Hz, 2H), 7.60 (t, *J* = 7.5 Hz, 1H), 8.11 (d, *J* = 7.2 Hz, 2H). All data are in agreement with literature values.[49]

3'-Dephenyl-10-*N*,*N*-dimethylcarbamoyl)-3'-(2-methyl-2-propenyl)docetaxel (SB-T-1216) [2-7]:[49]

To a cooled solution of **2-6** (0.158 g, 0.140 mmol) in CH_3CN-pyridine (1:1) (30 mL) was added HF-pyridine (1.4 mL), and the reaction mixture was allowed to warm from 0 °C to room temperature and react for 24 h with stirring. The reaction was diluted with H_2O (20 mL), the reaction mixture was extracted with ethyl acetate (3 x 30 mL). The combined organic layers were washed with saturated $CuSO_4$ (3 x 30 mL) and brine (3 x 30 mL), dried over $MgSO_4$, and concentrated *in vacuo* to afford a yellow oil. Purification of the crude product by column chromatography on silica gel with hexanes/ethyl acetate (1:4) as eluent gave SB-T-1216 (**2-7**) (0.114 g, 95%) as a white solid; ^{1}H NMR (500 MHz, $CDCl_3$) δ 1.15 (s, 3H), 1.24 (s, 3H), 1.34 (s, 9H), 1.66 (s, 3H), 1.76 (s, 6H), 1.87 (t, *J* = 13.2 Hz, 1H), 1.91 (s, 3H), 2.27 (m, 1H), 2.35 (s, 3H), 2.37 (m, 1H), 2.53 (m, 1H), 2.95 (s, 3H), 3.04 (s, 3H), 3.22 (d, *J* = 3 Hz, 1H), 3.46 (bs, 1H), 3.81 (d, *J* = 7 Hz, 1H), 4.18 (d, *J* = 8.4 Hz, 1H), 4.20 (d, *J* = 2.4 Hz, 1H), 4.29 (d, *J* = 8.4 Hz, 1H), 4.45 (m, 1H), 4.74 (bt, *J* = 7.5 Hz, 1H), 4.82 (d, *J* = 8 Hz, 1H), 4.97 (d, *J* = 9.5 Hz, 1H), 5.31 (d, *J* = 8.5 Hz, 1H,), 5.65 (d, *J* = 6.6 Hz, 1H), 6.18 (t, *J* = 8.5 Hz, 1H), 6.25 (s, 1H), 7.50 (t, *J* = 7.8

Hz, 2H), 7.60 (t, *J* = 7.5 Hz, 1H), 8.09 (d, *J* = 7.2 Hz, 2H). HPLC: t = 20.5 min, purity >98%. All data are in agreement with literature values.[49]

3'-Dephenyl-3'-(2,2-difluoroethenyl)-10-*N,N*-dimethylcarbamoyl-7-triethylsilyl-2'-triisopropylsilyldocetaxel [2-8]:[57]

To a cooled solution of **2-5 (**0.530 g, 0.710 mmol) and β-lactam (+)**1-20** (0.341 g, 0.836 mmol) in THF (18 mL) was added 1 M LHMDS (0.9 mL, 0.900 mmol), and the mixture was allowed to react for 2 h at -40 °C with stirring. The reaction was diluted with H_2O (20 mL), and the mixture was extracted with ethyl acetate (3 x 30 mL). The combined organic layers were washed with brine (3 x 30 mL), dried over $MgSO_4$, and concentrated *in vacuo* to afford a colorless oil. Purification of the crude product by column chromatography on silica gel with hexanes/ethyl acetate (9:1) as eluent gave **2-8** (0.618 g, 75%) as a white solid; ^{1}H NMR (600 MHz, $CDCl_3$) δ 0.60 (m, 6H), 0.92 (t, *J* = 7.8 Hz, 9H), 1.12 (m, 21H), 1.20 (s, 3H), 1.23 (s, 3H), 1.31 (s, 9H), 1.69 (s, 3H), 1.88 (t, *J* = 13.2 Hz, 1H), 2.06 (s, 3H), 2.23 (m, 1H), 2.35 (s, 3H), 2.37 (m, 1H), 2.50 (m, 1H), 2.94 (s, 3H), 3.07 (s, 3H), 3.81 (d, *J* = 6.6 Hz, 1H), 4.19 (d, *J* = 8.4 Hz, 1H), 4.30 (d, *J* = 8.4 Hz, 1H), 4.47 (dd, *J* = 6.6, 10.2 Hz, 1H), 4.50 (m, 1H), 4.52 (d, *J* = 1.8 Hz, 1H), 4.86 (m, 1H), 4.94 (d, *J* = 8.4 Hz, 1H), 5.65 (d, *J* = 6.6 Hz, 1H), 6.18 (t, *J* = 8.5 Hz, 1H), 6.40 (s, 1H), 7.43 (t, *J* = 7.5 Hz, 2H), 7.60 (t, *J* = 7.2 Hz, 1H), 8.11 (d, *J* = 7.2 Hz, 2H). All data are in agreement with literature values.[57]

3'-Dephenyl-3'-(2,2-difluoroethenyl)-10-*N,N*-dimethylcarbamoyldocetaxel (SB-T-12854) [2-9]:[57]

To a cooled solution of **2-8** (0.570 g, 0.503 mmol) in CH_3CN-pyridine (1:1) (35 mL) was added HF-pyridine (5.7 mL), and the reaction was allowed to warm from 0 °C to room temperature and react for 17 h with stirring. The reaction was diluted with H_2O (30 mL), and the mixture was extracted with ethyl acetate (3 x 30 mL). The combined organic layers were washed with saturated $CuSO_4$ (3 x 30 mL) and brine (3 x 30 mL), dried over $MgSO_4$, and concentrated *in vacuo* to afford a crude, white solid. Purification of the crude product by column chromatography on silica gel with hexanes/ethyl acetate (1:9) as eluent gave SB-T-12854 (**2-9**) (0.426 g, 98%) as a white solid; ^{1}H NMR (600 MHz, $CDCl_3$) δ 1.16 (s, 3H), 1.26 (s, 3H), 1.31 (s, 9H), 1.68 (s, 3H), 1.89 (t, *J* = 13.2 Hz, 1H), 1.91 (s, 3H), 2.30 (m, 1H), 2.38 (m, 1H), 2.39 (s, 3H), 2.53 (m, 1H), 2.95 (s, 3H), 3.05 (s, 3H), 3.22 (d, *J* = 3 Hz, 1H), 3.42 (d, *J* = 4.8 Hz, 1H), 3.81 (d, *J* = 6.6 Hz, 1H), 4.18 (d, *J* = 8.4 Hz, 1H), 4.20 (d, *J* = 4.2 Hz, 1H), 4.30 (d, *J* = 8.4 Hz, 1H), 4.45 (m, 1H), 4.57 (m, 1H), 4.88 (bs, 1H), 4.98 (d, *J* = 8.4 Hz, 1H), 5.66 (d, *J* = 6.6 Hz, 1H), 6.26 (bs, 2H), 7.50 (t, *J* = 7.2 Hz, 2H), 7.61 (t, *J* = 7.2 Hz, 1H), 8.12 (d, *J* = 7.2 Hz, 2H). HPLC: t = 20.6 min, purity >97%. All data are in agreement with literature values.[57]

10-Deacetyl-7,10,13-tris(triethylsilyl)baccatin III [2-10]:[29]

To a cooled solution of 10-deacetylbaccatin III (0.499 g, 0.917 mmol) and imidazole (0.312 g, 4.59 mmol) in DMF (1.7 mL) was added TESCl (0.77 mL, 4.59 mmol), and the mixture was allowed to warm from 0 °C to room temperature and react for 72 h with stirring. The reaction was quenched with saturated NH_4Cl (10 mL) and diluted with H_2O (10 mL). The reaction mixture was extracted with ethyl acetate (3 x 30 mL). The combined organic layers were washed with brine (3 x 30 mL), dried over $MgSO_4$, and concentrated *in vacuo* to afford a white solid. Purification of the crude product by column chromatography on silica gel with hexanes/ethyl acetate (9:1) as eluent gave **2-10** (0.736 g, 90%) as a white solid; ^{1}H NMR (600 MHz) δ 0.57 (m,

18H), 0.93 (m, 27H), 1.04 (s, 3H), 1.13 (s, 3H), 1.20 (s, 3H), 1.67 (s, 3H), 1.88 (m, 1H), 2.00 (s, 3H), 2.10 (m, 1H), 2.19 (m, 1H), 2.28 (s, 3H), 2.54 (m, 1H), 3.86 (d, J = 6.8 Hz, 1H), 4.14 (d, J = 8.2 Hz, 1H), 4.29 (d, J = 8.0 Hz, 1H), 4.48 (dd, J = 6.8, 10.2 Hz, 1H), 4.95 (m, 2H), 5.20 (s, 1H), 5.62 (d, J = 7.2 Hz, 1H), 7.46 (t, J = 7.6 Hz, 2H), 7.58 (t, J = 7.2 Hz, 1H), 8.09 (d, J = 7.2 Hz, 1H). All data are in agreement with literature values.[29]

10-Deacetyl-2-debenzoyl-7,10,13-tris(triethylsilyl)baccatin III [2-11]:[29]
To a cooled solution of **2-10** (0.736, 0.831 mmol) in THF (16 mL) was added sodium bis(2-methoxyethoxy)aluminum hydride (0.78 mL, 4.15 mmol), and the mixture was allowed to react for 1½ h at -50 °C with stirring. The reaction was quenched with saturated NH_4Cl (10 mL) and diluted with H_2O (10 mL). The reaction mixture was extracted with ethyl acetate (3 x 30 mL). The combined organic layers were washed with brine (3 x 30 mL), dried over $MgSO_4$, and concentrated *in vacuo* to afford a colorless liquid. Purification of the crude product by column chromatography on silica gel with hexanes/ethyl acetate (3:1) as eluent gave **2-11** (0.492 g, 76%) as a white foam; ^{1}H NMR (600 MHz, $CDCl_3$) δ 0.57 (m, 18 H), 0.93 (m, 27H), 1.09 (s, 3H), 1.16 (s, 3H), 1.62 (s, 3H), 1.89 (m, 3H), 2.02 (s, 3H), 2.07 (m, 1H), 2.29 (s, 3H), 2.44 (d, J = 6.3 Hz, 1H), 2.52 (m, 1H), 3.40 (d, J = 7.2, 1H), 3.87 (t, J = 6.6 Hz, 1H), 4.35 (dd, J = 6.6, 10.2 Hz, 1H), 4.56 (d, J = 8.4 Hz, 1H), 4.63 (d, J = 8.4 Hz, 1H), 4.95 (m, 2H), 5.11 (s, 1H). All data are in agreement with literature values.[29]

10-Deacetyl-2-debenzoyl-2-(3-methylbenzoyl)-7,10,13-tris(triethylsilyl)baccatin III [2-12]:[29]
To a solution of **2-11** (0.425 g, 0.543 mmol), 3-methylbenzoic acid (0.591 g, 4.34 mmol), and DMAP (0.530 g, 4.34 mmol) in CH_2Cl_2 (5 mL) was added DIC (0.7 mL, 4.34 mmol), and the mixture was allowed to react for 7 d at room temperature with stirring. The reaction was quenched with saturated NH_4Cl (10 mL) and diluted with H_2O (10 mL). The reaction mixture was extracted with ethyl acetate (3 x 30 mL). The combined organic layers were washed with brine (3 x 30 mL), dried over $MgSO_4$, and concentrated *in vacuo* to afford a white solid. Purification of the crude product by column chromatography on silica gel with hexanes/ethyl acetate (4:1) as eluent gave **2-12** (0.417 g, 85%) as a white solid; ^{1}H NMR (600 MHz, $CDCl_3$) δ 0.63 (m, 18 H), 0.99 (m, 27 H), 1.04 (s, 3H), 1.13 (s, 3H), 1.19 (d, J = 2.4 Hz, 3H), 1.67 (s, 3H), 1.89 (t, J = 10.8 Hz, 1H), 1.98 (s, 3H), 2.10 (m, 1H), 2.24 (m, 1H), 2.27 (s, 3H), 2.41 (s, 3H), 2.52 (m, 1H), 3.86 (d, J = 7.2 Hz, 1H), 4.14 (d, J = 8.4 Hz, 1H), 4.28 (d, J = 8.4 Hz, 1H), 4.42 (dd, J = 6.6, 10.2 Hz, 1H), 4.92 (m, 2H), 5.20 (s, 1H), 5.61 (d, J = 7.2 Hz, 1H), 7.36 (t, J = 7.5 Hz, 1H), 7.41 (d, J = 7.2 Hz, 1H), 7.92 (d, J = 7.8 Hz, 1H), 7.93 (s, 1H). HRMS for $C_{48}H_{81}O_{10}Si_3^+$ calcd: 901.5132. Found: 901.5135 (Δ = 0.3 ppm). All data are in agreement with literature values.[29]

10-Deacetyl-2-debenzoyl-2-(3-methylbenzoyl)baccatin III [2-13]:[29]
To a cooled solution of **2-12** (0.345 g, 0.383 mmol) in CH_3CN-pyridine (1:1) (21 mL) was added HF-pyridine (3.45 mL), and the mixture was allowed to warm from 0 °C to room temperature and react for 21 h with stirring. The reaction was diluted with H_2O (20 mL), and the mixture was extracted with ethyl acetate (3 x 30 mL). The combined organic layers were washed with saturated $CuSO_4$ (3 x 30 mL) and brine (3 x 30 mL), dried over $MgSO_4$, and concentrated *in vacuo* to afford a white solid. Purification of the crude product by column chromatography on silica gel with hexanes/ethyl acetate (1:9) as eluent gave **2-13** (0.212 g, 99%) as a white solid; ^{1}H NMR (600 MHz, $CDCl_3$) δ 1.10 (s, 6H), 1.74 (s, 3H), 1.83 (t, J = 13.2 Hz, 1H), 2.02 (s, 3H),

2.28 (m, 2H), 2.29 (s, 3H), 2.42 (s, 3H), 2.61 (m, 1H), 4.01 (d, *J* = 7.2 Hz, 1H), 4.14 (d, *J* = 8.4 Hz, 1H), 4.27 (m, 1H), 4.32 (d, *J* = 8.4 Hz, 1H), 4.87 (bs, 1H), 4.98 (d, *J* = 9 Hz, 1H), 5.25 (s, 1H,) 5.62 (d, *J* = 7.2 Hz, 1H), 7.36 (t, *J* = 7.2 Hz, 1H), 7.41 (d, *J* = 7.2 Hz, 1H), 7.90 (d, *J* = 7.8 Hz, 1H), 7.93 (s, 1H). HRMS for $C_{30}H_{39}O_{10}^+$ calcd: 559.2538. Found: 559.2537 (Δ = -0.2 ppm). All data are in agreement with literature values.[29]

2-Debenzoyl-2-(3-methylbenzoyl)-7-triethylsilyl 10-deacetylbaccatin III [2-14]:
To a cooled solution of **2-13** (0.195 g, 0.370 mmol) and imidazole (0.100 g, 1.47 mmol) in DMF (4 mL) was added TESCl (0.19 mL, 1.11 mmol), and the mixture was allowed to react for 40 min at 0 °C with stirring. The reaction was quenched with saturated NH_4Cl (10 mL) and diluted with H_2O (10 mL). The reaction mixture was extracted with ethyl acetate (3 x 30 mL). The combined organic layers were washed with brine (3 x 30 mL), dried over $MgSO_4$, and concentrated *in vacuo* to afford a white solid. Purification of the crude product by column chromatography on silica gel with hexanes/ethyl acetate (3:1) as eluent gave **2-14** (0.198 g, 85%) as a white solid; ^{1}H NMR (600 MHz, $CDCl_3$) δ 0.56 (m, 6H), 0.93 (t, *J* = 8.4 Hz, 9H), 1.09 (s, 6H), 1.73 (s, 3H), 1.89 (m, 1H), 2.02 (s, 3H), 2.27 (m, 2H), 2.29 (s, 3H), 2.42 (s, 3H), 2.50 (m, 1H), 3.95 (d, *J* = 6.6 Hz, 1H), 4.14 (d, *J* = 8.4 Hz, 1H), 4.32 (d, *J* = 8.4 Hz, 1H), 4.41 (dd, *J* = 6.6, 10.2 Hz, 1H), 4.87 (bs, 1H), 4.96 (d, *J* = 9.6 Hz, 1H), 5.17 (s, 1H), 5.58 (d, *J* = 7.2 Hz, 1H), 7.35 (t, *J* = 7.2 Hz, 1H), 7.40 (d, *J* = 7.2 Hz, 1H), 7.89 (d, *J* = 7.8 Hz, 1H), 7.93 (s, 1H). HRMS for $C_{36}H_{53}O_{10}Si^+$ calcd: 673.3403. Found: 673.3407 (Δ = 0.6 ppm).

2-Debenzoyl-10-(*N,N*-dimethylcarbamoyl)-2-(3-methylbenzoyl)-7-*O*-(triethylsilyl)-10-deacetylbaccatin III [2-15]:
To a cooled solution of **2-14** (0.192 g, 0.285 mmol) in THF (5.7 mL) was added 1 M LHMDS (0.35 mL, 0.35 mmol) followed by *N,N*-dimethylcarbamoyl chloride (35 μL, 0.371 mmol), and the mixture was allowed to react for 2 h at -40 °C with stirring. Reaction progress was monitored via TLC (CH_2Cl_2/CH_3OH = 19:1). The reaction was quenched with saturated NH_4Cl (10 mL) and diluted with H_2O (10 mL). The reaction mixture was extracted with ethyl acetate (3 x 30 mL). The combined organic extracts were washed with brine (3 x 30 mL), dried over $MgSO_4$, and concentrated *in vacuo* to afford a white solid. Purification of the crude product by column chromatography on silica gel with hexanes/ethyl acetate (3:1) as eluent gave **2-15** (0.183 g, 87%) as a white solid; ^{1}H NMR (600 MHz, $CDCl_3$) δ 0.57 (m, 6H), 0.93 (m, 9H), 1.05 (s, 3H), 1.19 (s, 3H), 1.68 (s, 3H), 1.89 (t, *J* = 13.2 Hz, 1H), 2.02 (s, 3H), 2.26 (m, 2H), 2.29 (s, 3H), 2.42 (s, 3H), 2.50 (m, 1H), 2.93 (s, 3H), 3.06 (s, 3H), 3.90 (d, *J* = 6.6 Hz, 1H), 4.14 (d, *J* = 8.4 Hz, 1H), 4.30 (d, *J* = 8.4 Hz, 1H), 4.48 (dd, *J* = 6.6, 10.2 Hz, 1H), 4.83 (m, 1H), 4.96 (d, *J* = 9.6 Hz, 1H), 5.62 (d, *J* = 7.2 Hz, 1H), 6.38 (s, 1H), 7.35 (t, *J* = 7.2 Hz, 1H), 7.40 (d, *J* = 7.8 Hz, 1H), 7.90 (d, *J* = 7.8 Hz, 1H), 7.94 (s, 1H). HRMS for $C_{39}H_{58}NO_{11}Si^+$ calcd: 744.3774. Found: 744.3774 (Δ = 0 ppm).

2-Debenzoyl-3'-dephenyl-10-(*N,N*-dimethylcarbamoyl)-2-(3-methylbenzoyl)-3'-(2-methyl-2-propen-1-yl)-7-*O*-(triethylsilyl)-2'-*O*-(triisopropylsilyl)docetaxel [2-16]:
To a cooled solution of **2-15** (0.173 g, 0.233 mmol) and β-lactam (+)**1-6** (0.140 g, 0.350 mmol) in THF (6 mL) was added 1 M LHMDS (0.3 mL, 0.3 mmol), and the mixture was allowed to react for 2 h at -40 °C with stirring. The reaction was diluted with H_2O (10 mL), and the mixture was extracted with ethyl acetate (3 x 30 mL). The combined organic extracts were washed with brine (3 x 30 mL), dried over $MgSO_4$, and concentrated *in vacuo* to afford a pale yellow oil.

Purification of the crude product by column chromatography on silica gel with hexanes/ethyl acetate (6:1) as eluent gave **2-16** (0.250 g, 94%) as a white solid; ^{1}H NMR (600 MHz, $CDCl_3$) δ 0.57 (m, 6H), 0.93 (t, *J* = 7.8 Hz, 9H), 1.11 (m, 21H), 1.20 (s, 3H), 1.22 (s, 3H), 1.34 (s, 9H), 1.67 (s, 3H), 1.75 (s, 3H) 1.78 (s, 3H) 1.89 (t, *J* = 13.2 Hz, 1H), 2.02 (s, 3H), 2.26 (m, 2H), 2.29 (s, 3H), 2.42 (s, 3H), 2.51 (m, 1H), 2.94 (s, 3H), 3.06 (s, 3H), 3.87 (d, *J* = 6.6 Hz, 1H), 4.19 (d, *J* = 8.4 Hz, 1H), 4.30 (d, *J* = 8.4 Hz, 1H), 4.44 (d, *J* = 3 Hz, 1H), 4.49 (dd, *J* = 6.6, 10.2 Hz, 1H), 4.80 (m, 2H), 4.95 (d, *J* = 9.6 Hz, 1H), 5.34 (d, *J* = 8.4 Hz, 1H), 5.68 (d, *J*=7.2 Hz, 1H), 6.10 (t, *J* = 8.4 Hz, 1H), 6.40 (s, 1H), 7.34 (t, *J* = 7.2 Hz, 1H), 7.40 (d, *J* = 7.8 Hz, 1H), 7.90 (d, *J* = 7.8 Hz, 1H), 7.94 (s, 1H). HRMS for $C_{60}H_{97}N_2O_{15}Si_2^+$ calcd: 1141.6422. Found: 1141.6434 (Δ = 1.1 ppm).

2-Debenzoyl-3'-dephenyl-10-(*N,N*-dimethylcarbamoyl)-2-(3-methylbenzoyl)-3'-(2-methyl-2-propen-1-yl)docetaxel (SB-T-121602) [2-17]:

To a cooled solution of **2-16** (0.238 g, 0.208 mmol) in CH_3CN-pyridine (1:1) (15 mL) was added HF-pyridine (2.4 mL), and the mixture was allowed to warm from 0 °C to room temperature and react for 21 h with stirring. The reaction was diluted with H_2O (30 mL), and the mixture was extracted with ethyl acetate (3 x 30 mL). The combined organic layers were washed with saturated $CuSO_4$ (3 x 30 mL) and brine (3 x 30 mL), dried over $MgSO_4$, and concentrated *in vacuo* to afford a white solid. Purification of the crude product by column chromatography on silica gel with hexanes/ethyl acetate (1:9) as eluent gave SB-T-121602 (**2-17**) (0.166 g, 92%) as a white solid; ^{1}H NMR (300 MHz, $CDCl_3$), δ 1.15 (s, 3H), 1.24 (s, 3H), 1.34 (s, 9H), 1.66 (s, 3H), 1.75 (s, 3H), 1.76 (s, 3H), 1.87 (t, *J* = 12.5 Hz, 1H), 1.91 (s, 3H), 2.05 (m, 2H), 2.35 (s, 3H), 2.41 (s, 3H), 2.53 (m, 1H), 2.95 (s, 3H), 3.04 (s, 3H), 3.43 (bs, 1H), 3.81 (d, *J* = 6.5 Hz, 1H), 4.17 (d, *J* = 8.4 Hz, 1H), 4.20 (d, *J* = 3.0 Hz, 1H), 4.30 (d, *J* = 8.4 Hz, 1H), 4.44 (bs, 1H), 4.74 (bt, *J* = 8.0 Hz, 1H), 4.81 (d, *J* = 8.0 Hz, 1H), 4.97 (d, *J* = 9.0 Hz, 1H), 5.32 (d, *J* = 8.1 Hz, 1H), 5.63 (d, *J* = 7.2 Hz, 1H), 6.18 (bt, *J* = 8.0 Hz, 1H), 6.25 (s, 1H), 7.34 (t, *J* = 7.5 Hz, 1H), 7.40 (d, *J* = 7.8 Hz, 1H), 7.89 (d, J=7.5 Hz, 1H), 7.93 (s, 1H), ^{13}C NMR (100 MHz) δ 9.3, 15.0, 18.5, 21.3, 22.2, 22.3, 25.7, 26.8, 28.2, 35.4, 36.0, 36.6, 43.2, 45.6, 51.6, 58.5, 72.5, 73.8, 75.1, 76.2, 76.3, 76.5, 79.3, 79.9, 81.2, 84.2, 120.7, 127.3, 128.5, 129.2, 130.8, 133.2, 134.4, 137.8, 138.3, 142.9, 155.4, 156.1, 167.1, 169.9, 173.1, 205.7. HPLC: t = 21.2 min, purity >98%. HRMS for $C_{45}H_{63}N_2O_{15}^+$ calcd: 871.4223. Found: 871.4231 (Δ = 0.9 ppm).

10-Deacetyl-2-debenzoyl-2-[3-(trifluoromethyl)benzoyl]-7,10,13-tris(triethylsilyl)baccatin III [2-18]:

To a solution of **2-11** (0.809 g, 1.033 mmol), 3-(trifluoromethyl)benzoic acid (1.572 g, 8.268 mmol), and DMAP (0.991 g, 8.268 mmol) in CH_2Cl_2 (10 mL) was added DIC (1.3 mL, 8.393 mmol), and the mixture was allowed to react for 5 d at room temperature with stirring. The reaction was quenched with H_2O (10 mL), and the mixture was extracted with CH_2Cl_2 (3 x 30 mL). The combined organic layers were washed with brine (3 x 30 mL), dried over $MgSO_4$, and concentrated *in vacuo* to give a yellow solid. Purification of the crude product by column chromatography on silica gel with hexanes/ethyl acetate (9:1) as eluent gave **2-18** (0.570 g, 71%) as a white solid; R_f = 0.75 (hexanes/ethyl acetate = 3:1); mp 160-162 °C; ^{1}H NMR (700 MHz, $CDCl_3$) δ 0.65 (m, 18H), 1.02 (m, 27H), 1.15 (s, 3H), 1.22 (s, 3H), 1.51 (s, 1H), 1.68 (s, 3H), 1.91 (m, 1H), 2.01 (s, 3H), 2.12 (m, 1H), 2.25 (m, 1H), 2.30 (s, 3H), 2.55 (m, 1H), 3.91 (d, *J* = 7.7 Hz, 1H), 4.16 (d, *J* = 8.4 Hz, 1H), 4.24 (d, *J* = 8.4 Hz, 1H), 4.44 (dd, *J* = 6.3, 10.5 Hz, 1H), 4.93 (t, *J* = 8.4 Hz, 1H), 4.98 (d, *J* = 7.7 Hz, 1H), 5.22 (s, 1H), 5.61 (d, *J* = 7.7 Hz, 1H), 7.65 (t, *J*

= 7.7 Hz, 1H), 7.87 (d, *J* = 8.4 Hz, 2H), 8.29 (d, *J*=7.7 Hz, 1H), 8.46 (s, 1H); ^{13}C NMR (175 MHz, $CDCl_3$) δ 5.83, 5.25, 5.98, 6.86, 6.96, 10.42, 14.58, 20.59, 22.12, 26.29, 37.25, 39.80, 42.92, 46.96, 58.20, 68.23, 72.67, 75.76, 76.15, 76.46, 79.80, 80.74, 84.01, 122.88, 124.43, 126.85, 129.32, 129.91, 130.58, 130.90, 131.10, 131.28, 133.37, 135.60, 139.57, 165.54, 169.95, 205.80; ^{19}F NMR (376 MHz, $CDCl_3$) δ -62.97 (s, 3H). HRMS for $C_{48}H_{78}F_3O_{10}Si_3^+$ calcd: 955.4849. Found: 955.4851 (Δ = 0.2 ppm).

10-Deacetyl-2-debenzoyl-2-[3-(trifluoromethyl)benzoyl]baccatin III [2-19]:
To a cooled solution of **2-18** (0.570 g, 0.578 mmol) in CH_3CN-pyridine (1:1) (60 mL) was added HF-pyridine (5.7 mL), and the mixture was allowed to warm from 0 °C to room temperature and react for 10 h with stirring. The reaction was diluted with H_2O (30 mL), and the mixture was extracted with ethyl acetate (3 x 30 mL). The combined organic layers were washed with saturated $CuSO_4$ (3 x 30 mL) and brine (3 x 30 mL), dried over $MgSO_4$, and concentrated *in vacuo* to afford **2-19** (0.356 g, 99%) as a white solid; R_f = 0.1 (hexanes/ethyl acetate = 3:1); ^{1}H NMR (500 MHz, CD_3OD) δ 1.11 (s, 3H), 1.12 (s, 3H), 1.73 (s, 3H), 1.84 (m, 1H), 2.07 (d, *J* = 1.5 Hz, 3H), 2.25 (dd, *J* = 7.0, 8.5 Hz, 1H), 2.30 (s, 3H), 2.39 (dd, *J* = 7.0, 8.5 Hz, 1H), 2.49 (m, 1H), 4.03 (d, *J* = 7.0 Hz, 1H), 4.21 (dd, J_{AB} = 8.0, 12.0 Hz, 2H), 4.30 (dd, *J* = 6.5, 11.0 Hz, 1H), 4.83 (t, *J* = 7.5 Hz, 1H), 5.06 (d, *J* = 7.5 Hz, 1H), 5.35 (s, 1H), 5.64 (d, *J* = 7.0 Hz, 1H), 7.78 (t, *J* = 7.7 Hz, 1H), 7.98 (d, *J* = 7.0 Hz, 1H), 8.37 (d, *J* = 8.0 Hz, 1H), 8.48 (s, 1H); ^{13}C NMR (125 MHz, CD_3OD) δ 8.91, 13.07, 13.89, 19.40, 19.46, 21.16, 25.79, 36.14, 39.31, 42.53, 57.47, 60.14, 66.70, 71.40, 74.86, 75.73, 76.06, 78.02, 80.62, 84.52, 120.66, 122.82, 124.98, 126.29, 127.14, 129.48 130.26, 130.52, 130.78, 131.04, 131.31, 133.20, 134.28, 143.00, 164.65, 170.46, 171.58, 210.29; ^{19}F NMR (376 MHz, $CDCl_3$) δ -62.90 (s, 3H). HRMS for $C_{30}H_{36}F_3O_{10}^+$ calcd: 613.2255. Found: 613.2259 (Δ = 0.7 ppm).

10-Deacetyl-2-debenzoyl-2-[3-(trifluoromethyl)benzoyl]-7-triethylsilyl-baccatin III [2-20]:
To a cooled solution of **2-19** (0.200 g, 0.330 mmol) and imidazole (0.168 g, 1.2 mmol) in DMF (3.3 mL) was added TESCl (0.25 mL, 1.0 mmol), and the mixture was allowed to react for 40 min at 0 °C with stirring. The reaction was diluted with H_2O (30 mL) and extracted with ethyl acetate (3 x 30 mL). The combined organic layers were washed with brine (3 x 30 mL), dried over $MgSO_4$, and concentrated *in vacuo* to give a yellow oil. Purification of the crude product by column chromatography on silica gel with hexanes/ethyl acetate (4:1) as eluent gave **2-20** (0.196 g, 83%) as a white solid; R_f = 0.7 (hexanes/ethyl acetate = 1:1); ^{1}H NMR (500 MHz, $CDCl_3$) δ 0.71 (m, 6H), 1.04 (t, *J* = 8.0 Hz, 9H), 1.13 (s, 3H), 1.19 (s, 3H), 1.49 (d, *J* = 7.5 Hz, 1H), 1.54 (s, 1H), 1.78 (s, 3H), 1.86 (m, 1H), 2.06 (d, *J* = 1.0 Hz, 3H), 2.16 (m, 1H), 2.26 (m, 1H), 2.32 (s, 3H), 3.99 (d, *J* = 7.0 Hz, 1H), 4.19 (d, *J* = 8.5 Hz, 1H), 4.20 (d, *J* = 1.0 Hz, 1H), 4.28 (d, *J* = 8.5 Hz, 1H), 4.32 (m, 1H), 4.98 (t, *J* = 7.5 Hz, 1H), 5.02 (d, *J* = 7.5 Hz, 1H), 5.29 (d, *J* = 1.0 Hz, 1H), 5.64 (d, *J* = 7.0 Hz, 1H), 7.67 (t, *J* = 7.7 Hz, 1H), 7.90 (d, *J* = 8.0 Hz, 1H), 8.30 (d, *J* = 7.5 Hz, 1H), 8.46 (s, 1H); ^{13}C NMR (125 MHz, $CDCl_3$) δ 4.80, 6.90, 9.92, 15.03, 20.81, 22.01, 26.31, 36.89, 40.31, 42.73, 46.62, 57.53, 68.28, 71.97, 74.98, 75.88, 76.35, 79.81, 80.58, 84.09, 120.40, 122.54, 124.71, 126.80, 126.83, 129.45, 130.11, 130.14, 130.36, 130.90, 131.17, 131.43, 131.69, 133.38, 133.41, 144.30, 165.48, 170.06, 211.93; ^{19}F NMR (376 MHz, $CDCl_3$) δ -62.99 (s, 3F). HRMS for $C_{36}H_{50}F_3O_{10}Si^+$ calcd: 727.3120. Found: 727.3127 (Δ = 1.0 ppm).

10-Cyclopropanecarbonyl-10-deacetyl-2-debenzoyl-2-[3-(trifluoromethyl)benzoyl]-7-triethylsilyl-baccatin III [2-21]:
To a cooled solution of **2-20** (0.081 g, 0.111 mmol) in THF (3 mL) was added 1 M LHMDS (112 μL, 0.120 mmol) followed by cyclopropanecarbonyl chloride (10 μL, 0.117 mmol), and the mixture was allowed to react for 30 min at -40 °C with stirring. The reaction was quenched with H_2O (20 mL), and the mixture was extracted with ethyl acetate (3 x 30 mL). The combined organic layers were washed with brine (3 x 30 mL), dried over $MgSO_4$, and concentrated *in vacuo* to give a yellow oil. Purification of the crude product by column chromatography on silica gel with hexanes/ethyl acetate (4:1) as eluent gave **2-21** (0.075 g, 85%) as a white solid; R_f = 0.75 (hexanes/ethyl acetate = 1:1); ^{1}H NMR (500 MHz, $CDCl_3$) δ 0.57 (m, 6H), 0.89 (m, 2H), 0.92 (m, 9H), 1.02 (m, 1H), 1.05 (s, 3H), 1.18 (m, 1H), 1.20 (s, 3H), 1.25 (m, 3H), 1.56 (s, 3H), 1.76 (m, 1H), 1.87 (m, 1H), 2.05 (d, *J* = 5.0 Hz, 1H), 2.20 (m, 3H), 2.26 (s, 1H), 2.27 (m, 3H), 2.53 (m, 1H), 3.90 (d, *J* = 7.0 Hz, 1H), 4.12 (d, *J* = 8.4 Hz, 1H), 4.24 (d, *J* = 8.4 Hz, 1H), 4.48 (dd, *J* = 6.5 Hz, 10.5 Hz, 1H), 4.84 (m, 1H), 4.98 (d, *J* = 8.0 Hz, 1H), 5.61 (d, *J* = 7.0 Hz, 1H), 7.63 (t, *J* = 7.5 Hz, 1H), 7.86 (d, *J* = 8.0 Hz, 1H), 8.28 (d, *J* = 8.0 Hz, 1H), 8.45 (s, 1H); ^{13}C NMR (125 MHz, $CDCl_3$) δ 5.29, 6.80, 8.62, 8.75, 9.92, 13.03, 14.98, 20.13, 22.42, 26.85, 29.72, 37.21, 38.14, 42.72, 47.31, 58.58, 67.93, 72.39, 75.31, 75.51, 76.39, 78.98, 80.82, 84.24, 122.56, 124.72, 126.84, 126.87, 126.90, 126.93, 129.41, 130.11, 130.14, 130.33, 131.13, 131.39, 132.64, 133.43, 143.99, 165.57, 170.73, 173.18, 202.21; ^{19}F NMR (376 MHz, $CDCl_3$) δ -62.89 (s, 3F); HRMS for $C_{40}H_{54}F_3O_{11}Si^+$ calcd: 795.3382. Found: 795.3387 (Δ = 0.6 ppm).

2-Debenzoyl-3'-dephenyl-10-(cyclopropanecarbonyl)-2-[3-(trifluoromethyl)benzoyl]-7-triethylsilyl-2'-triisopropylsilyl-3'-(2-methyl-1-propenyl)docetaxel [2-22]:
To a cooled solution of **2-21** (0.023 g, 0.0289 mmol) and β-lactam (+)**1-6** (0.025 g, 0.0625 mmol) in THF (1.5 mL) was added 1 M LHMDS (50 μL, 0.050 mmol), and the mixture was allowed to react for 1½ h at -40 °C with stirring. The reaction was diluted with H_2O (10 mL), and the mixture was extracted with ethyl acetate (3 x 20 mL). The combined organic layers were washed with brine (3 x 10 mL), dried over $MgSO_4$, and concentrated *in vacuo* to give a colorless oil. Purification of the crude product by column chromatography on silica gel with hexanes/ethyl acetate (4:1) as eluent gave **2-22** (0.030 g, 87%) as a white solid; R_f = 0.7 (hexanes/ethyl acetate = 3:1); ^{1}H NMR (500 MHz, $CDCl_3$) δ 0.59 (m, 6H), 0.92 (m, 2H), 0.94 (m, 9H), 1.14 (m, 21H), 1.22 (s, 3H), 1.27 (s, 3H), 1.36 (s, 9H), 1.45 (m, 1H), 1.71 (s, 3H), 1.77 (s 6H), 1.91 (m, 1H), 2.05 (s, 3H), 2.38 (s, 3H), 2.39 (m, 1H), 2.55 (m, 1H), 3.89 (d, *J* = 6.5 Hz, 1H), 4.19 (d, *J* = 8.4 Hz, 1H), 4.29 (d, *J* = 4.8 Hz, 1H), 4.44 (d, *J* = 2 Hz, 1H), 4.48 (dd, *J* = 6.5, 10.5 Hz, 1H), 4.77 (m, 1H), 4.84 (m, 1H), 5.00 (d, *J* = 9.0 Hz, 1H), 5.35 (d, *J* = 8.5 Hz, 1H), 5.70 (d, *J* = 7.0 Hz, 1H), 6.06 (bt, 1H), 6.52 (s, 1H), 7.67 (t, *J* = 7.2 Hz, 1H), 7.89 (d, *J* = 7.5 Hz, 1H), 8.33 (d, *J* = 8.0 Hz, 1H), 8.48 (s, 1H); ^{13}C NMR (125 MHz, $CDCl_3$) δ 5.32, 6.78, 8.70, 8.81, 10.00, 12.57, 12.96, 14.38, 17.91, 18.05, 18.42, 21.28, 22.28, 25.66, 26.23, 28.26, 29.72, 35.31, 37.14, 43.24, 46.74, 52.04, 58.31, 72.00, 72.27, 74.79, 75.30, 75.52, 76.39, 78.91, 79.40, 81.05, 84.30, 121.92, 122.58, 124.75, 126.74, 129.46, 130.10, 130.12, 130.34, 131.01, 131.28, 131.13, 133.63, 136.34, 141.19, 155.21, 165.34, 169.70, 172.02, 173.08, 202.04.

2-Debenzoyl-3'-dephenyl-10-(cyclopropanecarbonyl)-2-[3-(trifluoromethyl)benzoyl]-7-triethylsilyl-2'-triisopropylsilyl-3'-(difluorovinyl)docetaxel [2-23]:
To a solution of **2-21** (0.023 g, 0.0289 mmol) and β-lactam (+)**1-20** (0.025 g, 0.0625 mmol) in THF at -40 °C was added 1 M LHMDS (50 μL, 0.050 mmol), and the mixture was allowed to

react for 1½ at -40 °C with stirring. The reaction was diluted with H_2O (10 mL), and the mixture was extracted with ethyl acetate (3 x 20 mL). The combined organic layers were washed with brine (3 x 10 mL), dried over $MgSO_4$, and concentrated *in vacuo* to give a colorless oil. Purification of the crude product by column chromatography on silica gel with hexanes/ethyl acetate (4:1) as eluent gave **2-23** (0.028 g, 81%), as a white solid; R_f = 0.7 (3:1 hexanes/ethyl acetate); ^{1}H NMR (400 MHz, $CDCl_3$) δ 0.58 (m, 6H), 0.92 (m, 9H), 0.93 (m, 2H), 1.13 (m, 21H), 1.21 (s, 3H), 1.25 (s, 3H), 1.31 (s, 9H), 1.70 (s, 3H), 1.77 (m, 1H), 1.90 (m, 1H), 2.03 (s, 3H), 2.33 (m, 2H), 2.37 (s, 3H), 2.54 (m, 1H), 3.87 (d, *J* = 7.2 Hz, 1H), 4.17 (d, *J* = 8.4 Hz, 1H), 4.27 (d, *J* = 8.4 Hz, 1H), 4.46 (m, 1H), 4.51 (d, *J* = 2 Hz, 2H), 4.87 (m, 1H), 4.98 (m, 2H), 5.68 (d, *J* = 7.2 Hz, 1H), 6.12 (bt, 1H), 6.50 (s, 1H), 7.67 (t, *J* = 8 Hz, 1H), 7.88 (d, *J* = 8 Hz, 1H), 8.32 (d, *J* = 8 Hz, 1H), 8.47 (s, 1H); ^{13}C NMR (100 MHz, $CDCl_3$) δ 5.30, 6.75, 8.70, 8.81, 9.98, 12.56, 12.95, 14.32, 17.95, 18.04, 21.29, 21.12, 26.31, 28.11, 35.21, 37.13, 43.25, 46.75, 58.33, 71.92, 72.26, 74.73, 75.53, 76.38, 78.96, 81.06, 84.26, 126.95, 129.48, 130.20, 133.48, 140.60, 154.95, 165.55, 169.69, 171.14, 173.12, 201.88; ^{19}F NMR (376 MHz, $CDCl_3$) δ -62.95 (s, 3F), -84.58 (m, 1F), -86.25 (d, *J* = 40.4 Hz, 1F).

2-Debenzoyl-3'-dephenyl-10-(cyclopropanecarbonyl)-2-[3-(trifluoromethyl)benzoyl]-7-triethylsilyl-2'-triisopropylsilyl-3'-(trifluoromethyl)docetaxel [2-24]:
To a cooled solution of **2-21** (0.023 g, 0.0289 mmol) and (3*R*,4*R*)-1-(*tert*-butoxycarbonyl)-3-triisopropylsiloxy-4-trifluoromethylazetidin-2-one (0.025 g, 0.0625 mmol) in THF (1.5 mL) was added 1 M LHMDS (50 μL, 0.050 mmol), and the mixture was allowed to react for 1½ h at -40 °C with stirring. The reaction was diluted with H_2O (10 mL), and the mixture was extracted with ethyl acetate (3 x 30 mL). The combined organic extracts were washed with brine (3 x 30 mL), dried over $MgSO_4$, and concentrated *in vacuo* to give a yellow oil. Purification of the crude product by column chromatography on silica gel with hexanes/ethyl acetate (4:1) as eluent gave **2-24** (0.029 g, 83%) as a white solid; R_f = 0.7 (hexanes/ethyl acetate = 3:1); ^{1}H NMR (700 MHz, $CDCl_3$) δ 0.58 (m, 6H), 0.93 (m, 9H), 0.97 (m, 2H), 1.14 (m, 21H), 1.20 (s, 3H), 1.26 (s, 3H), 1.28 (s, 1H), 1.32 (s, 9H), 1.63 (s, 2H), 1.71 (s, 3H), 1.78 (m, 1H), 1.91 (m, 1H), 2.05 (s, 3H), 2.33 (m, 2H), 2.36 (s, 3H), 2.54 (m, 1H), 3.87 (d, *J* = 7.0 Hz, 1H), 4.18 (d, *J* = 8.4 Hz, 1H), 4.28 (d, *J* = 8.4 Hz, 1H), 4.48 (dd, *J* = 6.5, 10.5 Hz, 1H), 4.67 (m, 1H), 4.94 (s, 1H), 4.96 (d, *J* = 9.8 Hz, 1H), 5.18 (d, *J* = 10.5 Hz, 1H), 5.68 (d, *J* = 7.0 Hz, 1H), 6.10 (t, *J* = 9.1 Hz, 1H), 6.50 (s, 1H), 7.67 (t, *J* = 7.7 Hz, 1H), 7.89 (d, *J* = 7.7 Hz, 1H), 8.33 (d, *J* = 7.7 Hz, 1H), 8.48 (s, 1H); ^{13}C NMR (175 MHz, $CDCl_3$) δ 5.30, 6.74, 8.68, 8.81, 10.03, 12.73, 12.95, 14.26, 17.81, 17.93, 21.32, 22.17, 26.23, 27.94, 35.24, 37.12, 43.26, 46.79, 58.33, 70.04, 72.23, 72.40, 74.67, 75.55, 76.36, 79.02, 81.10, 81.15, 84.27, 121.26, 122.81, 123.16, 124.35, 124.76, 125.90, 127.06, 127.09, 127.11, 129.46, 130.10, 130.17, 131.04, 131.23, 131.42, 131.61, 133.43, 133.56, 140.26, 155.11, 165.53, 169.81, 170.58, 173.10, 201.74; ^{19}F NMR (376 MHz, $CDCl_3$) δ -62.98 (s, 3F), -72.51 (d, *J* = 8.4 Hz, 3F).

2-Debenzoyl-3'-dephenyl-10-(cyclopropanecarbonyl)-2-[3-(trifluoromethyl)benzoyl]-3'-(2-methyl-1-propenyl)docetaxel (SB-T-121406) [2-25]:
To a cooled solution of **2-22** (0.027 g, 0.023 mmol) in CH_3CN-pyridine (1:1) (2.3 mL) was added HF-pyridine (0.3 mL), and the reaction was allowed to warm from 0 °C to room temperature and react for 15 h with stirring. The reaction was diluted with H_2O (10 mL), and the mixture was extracted with ethyl acetate (3 x 10 mL). The combined organic layers were washed with saturated $CuSO_4$ (3 x 10 mL) and brine (3 x 10 mL), dried over $MgSO_4$, and concentrated *in*

vacuo to give a colorless oil. Purification of the crude product by column chromatography on silica gel with hexanes/ethyl acetate (1:4) as eluent gave SB-T-121406 (**2-25**) (0.018 g, 86%) as a white solid; R_f = 0.2 (hexanes/ethyl acetate = 3:1); ^{1}H NMR (500 MHz, $CDCl_3$) δ 1.00 (m, 2H), 1.13 (m, 2H), 1.16 (s, 3H), 1.24 (m, 1H), 1.26 (s, 3H), 1.33 (s, 9H), 1.67 (s, 3H), 1.70 (s, 1H), 1.72 (s, 3H), 1.76 (s, 3H), 1.77 (m, 1H), 1.86 (m, 1H), 1.90 (s, 3H), 2.33 (s, 3H), 2.41 (m, 1H), 2.55 (m, 1H), 2.60 (d, *J* = 3.9 Hz, 1H), 3.32 (m, 1H), 3.83 (d, *J* = 7.1 Hz, 1H), 4.15 (d, *J* = 8.2 Hz, 1H), 4.18 (d, *J* = 7.0 Hz, 1H), 4.25 (d, *J* = 8.2 Hz, 1H), 4.41 (m, 1H), 4.71 (m, 1H), 4.73 (s, 1H), 4.98 (d, *J* = 7.8 Hz, 1H), 5.32 (d, *J* = 5.9 Hz, 1H), 5.64 (d, *J* = 7.2 Hz, 1H), 6.13 (t, *J* = 8.5 Hz, 1H), 6.31 (s, 1H), 7.64 (t, *J* = 7.8 Hz, 1H), 7.87 (d, *J* = 7.8 Hz, 1H), 8.29 (d, *J* = 7.8 Hz, 1H), 8.43 (s, 1H); ^{13}C NMR (125 MHz, $CDCl_3$) δ 9.23, 9.46, 13.04, 15.03, 18.42, 21.91, 22.11, 25.67, 26.62, 28.21, 29.72, 35.41, 35.50, 43.17, 45.68, 51.63, 58.53, 72.29, 72.48, 73.64, 75.42, 75.64, 76.30, 79.30, 79.92, 81.04, 84.47, 120.46, 122.55, 124.72, 126.81, 129.51, 130.20, 131.12, 131.39, 132.68, 133.57, 138.13, 142.97, 155.41, 165.40, 169.96, 175.17, 203.85; ^{19}F NMR (376 MHz, $CDCl_3$) δ -62.84 (s, 3F); HRMS for $C_{46}H_{59}F_3NO_{15}^+$ calcd: 922.3831. Found: 922.3845 (Δ = 1.5 ppm); HPLC: t = 22.6 min, purity >98%.

2-Debenzoyl-3'-dephenyl-10-(cyclopropanecarbonyl)-2-[3-(trifluoromethyl)benzoyl]-3'-(difluorovinyl)docetaxel (SB-T-12852-6) [2-26]:

To a cooled solution of **2-23** (0.026 g, 0.022 mmol) in CH_3CN-pyridine (1:1) (2.2 mL) was added HF-pyridine (0.3 mL), and the mixture was allowed to warm from 0 °C to room temperature and react for 15 h with stirring. The reaction was diluted with H_2O (10 mL), and the mixture was extracted with ethyl acetate (3 x 10 mL). The combined organic layers were washed with saturated $CuSO_4$ (3 x 10 mL) and brine (3 x 10 mL), dried over $MgSO_4$, and concentrated *in vacuo* to give a colorless oil. Purification of the crude product by column chromatography on silica gel with hexanes/ethyl acetate (1:4) as eluent gave SB-T-12852-6 (**2-26**) (0.016 g, 80%) as a white solid; R_f = 0.2 (hexanes/ethyl acetate = 3:1); ^{1}H NMR (500 MHz, $CDCl_3$) δ 0.91 (m, 1H), 1.03 (m, 2H), 1.16 (m, 2H), 1.19 (s, 3H), 1.29 (s, 3H), 1.32 (s, 9H), 1.71 (s, 3H), 1.72 (s, 1H), 1.81 (m, 1H), 1.90 (m, 1H), 1.92 (s, 3H), 2.28 (m, 2H), 2.40 (s, 3H), 2.58 (m, 1H), 2.63 (m, 1H), 3.49 (d, *J* = 5.3 Hz, 1H), 3.86 (d, *J* = 7.1 Hz, 1H), 4.18 (d, *J* = 8.2 Hz, 4.28 (s, 1H), 4.29 (d, *J* = 8.2 Hz, 1H), 4.44 (m, 1H), 4.60 (dd, *J* = 8.6, 24.6 Hz, 1H), 4.87-4.93 (m, 2H), 5.01 (d, *J* = 8.2 Hz, 1H), 5.67 (d, *J* = 7.2 Hz, 1H), 6.23 (t, *J* = 8.1 Hz, 1H), 6.33 (s, 1H), 7.69 (t, *J* = 7.8 Hz, 1H), 7.90 (d, *J* = 8.0 Hz, 1H), 8.33 (d, *J* = 7.7 Hz, 1H), 8.47 (s, 1H); ^{13}C NMR (125 MHz, $CDCl_3$) δ 9.26, 9.48, 13.03, 14.98, 22.07, 26.71, 28.09, 29.71, 35.34, 35.50, 43.18, 45.67, 58.54, 72.26, 72.71, 73.12, 75.33, 75.63, 76.29, 79.29, 80.42, 81.04, 84.45, 120.32, 122.49, 124.66, 126.82, 127.00, 129.54, 130.06, 130.23, 130.98, 131.25, 131.51, 131.77, 132.99, 133.46, 142.40, 154.24, 154.83, 156.56, 158.87, 165.57, 170.18, 172.50, 175.13, 203.71; ^{19}F NMR (376 MHz, $CDCl_3$) δ -85.72 (d, *J* = 35.6 Hz, 1F), -83.78 (dd, *J* = 25.5, 35.6 Hz, 1F), -62.94 (s, 3F); HRMS for $C_{44}H_{53}F_6NO_{15}^+$ calcd: 930.3330. Found: 930.3330 (Δ = 0 ppm); HPLC: t = 22.5 min, purity >97%.

2-Debenzoyl-3'-dephenyl-10-(cyclopropanecarbonyl)-2-[3-(trifluoromethyl)benzoyl]-3'-(trifluoromethyl)docetaxel (SB-T-12822-6) [2-27]:

To a cooled solution of **2-24** (0.028 g, 0.024 mmol) in CH_3CN-pyridine (1:1) (2.4 mL) was added HF-pyridine (0.3 mL), and the mixture was allowed to warm from 0 °C to room temperature and react for 15 h with stirring. The reaction was diluted with H_2O (10 mL), and the mixture was extracted with ethyl acetate (3 x 10 mL). The combined organic layers were washed with saturated $CuSO_4$ (3 x 10 mL) and brine (3 x 10 mL), dried over $MgSO_4$, and concentrated *in*

vacuo to give a colorless oil. Purification of the crude product by column chromatography on silica gel with hexanes/ethyl acetate (1:4) as eluent gave SB-T-12822-6 (**2-27**) (0.017 g, 81%) as a white solid; R_f = 0.2 (hexanes/ethyl acetate = 3:1); ^{1}H NMR (700 MHz, $CDCl_3$) δ 0.90 (m, 2H), 1.03 (m, 2H), 1.19 (s, 6H), 1.27 (s, 6H), 1.31 (s, 9H), 1.68 (bs, 1H), 1.70 (s, 3H), 1.81 (m, 1H), 1.90 (bt, 1H), 1.92 (s, 3H), 2.33 (m, 2H), 2.39 (s, 3H), 2.60 (m, 2H), 3.39 (bs, 1H), 3.86 (d, *J* = 7.7 Hz, 1H), 4.18 (d, *J* = 8.4 Hz, 1H), 4.29 (d, *J* = 8.4 Hz, 1H), 4.43 (bs, 1H), 4.72 (s, 1H), 4.77 (m, 1H), 4.99 (d, *J* = 9.1 Hz, 1H), 5.21 (d, *J* = 10.5 Hz, 1H), 5.66 (d, *J* = 7 Hz, 1H), 6.25 (bt, *J* = 8.8, 1H), 6.32 (s, 1H), 7.69 (t, *J* = 7.7 Hz, 1H), 7.90 (d, *J* = 7.7 Hz, 1H), 8.33 (d, *J* = 7.7 Hz, 1H), 8.47 (s, 1H); ^{13}C NMR (175 MHz, $CDCl_3$) δ 9.25, 9.43, 9.50, 13.00, 14.11, 14.87, 15.26, 21.97, 22.08, 22.69, 26.70, 27.91, 29.36, 29.66, 29.70, 31.59, 31.93, 35.35, 35.46, 43.18, 45.68, 58.54, 65.86, 68.08, 72.22, 73.38, 75.22, 75.65, 76.28, 79.30, 81.16, 81.29, 84.47, 121.23, 122.77, 123.13, 124.32, 124.73, 125.87, 127.06, 129.53, 130.00, 130.22, 130.24, 131.12, 131.31, 131.50, 131.69, 133.30, 133.40, 141.79, 154.57, 165.61, 170.14, 171.79, 175.10, 203.54; HRMS for $C_{43}H_{52}F_6NO_{15}^+$ calcd: 936.3236. Found: 936.3227 (Δ = -1.0 ppm); HPLC: t = 19.6 min, purity >97%.

10-Deacetyl-2-debenzoyl-10-(*N,N*-dimethylcarbamoyl)-2-[3-(trifluoromethyl)benzoyl]-7-(triethylsilyl)baccatin III [2-28]:

To a solution of **2-20** (0.040 g, 0.0551 mmol) in THF (1.2 mL) was added 1 M LHMDS (66 μL, 0.0660 mmol), followed by *N,N*-dimethylcarbamoyl chloride (7 μL, 0.0680 mmol), and the mixture was allowed to react for 4 h at -40 °C with stirring. Reaction progress was monitored by TLC (CH_2Cl_2/CH_3OH = 19:1). The reaction was quenched with saturated NH_4Cl (5 mL), and the mixture was diluted with H_2O (5 mL) and extracted with ethyl acetate (3 x 15 mL). The combined organic layers were washed with brine (3 x 30 mL), dried over $MgSO_4$, and concentrated *in vacuo* to afford a colorless oil. Purification of the crude product by column chromatography on silica gel with hexanes/ethyl acetate (3:1) as eluent gave **2-28** (0.037 g, 84%) as a white solid; ^{1}H NMR (400 MHz, $CDCl_3$) δ 0.63 (m, 6H), 0.94 (t, *J* = 8.0 Hz, 9H), 1.07 (s, 3H), 1.21 (s, 3H), 1.24 (m, 1H), 1.70 (s, 3H), 1.89 (m, 1H), 2.20 (m, 2H), 2.27 (s, 3H), 2.29 (s, 3H), 2.56 (m, 1H), 2.96 (s, 3H), 3.10 (s, 1H), 3.93 (d, *J* = 6.9 Hz, 1H), 4.16 (d, *J* = 8.4 Hz, 1H), 4.26 (d, *J* = 8.4 Hz, 1H), 4.51 (dd, *J* = 6.9, 10.6 Hz, 1H), 4.85 (m, 1H), 4.99 (d, *J* = 8.8 Hz, 1H), 5.64 (d, *J* = 7.1 Hz, 1H), 6.41 (s, 1H), 7.65 (t, *J* = 7.8 Hz, 1H), 7.87 (d, *J* = 7.7 Hz, 1H), 8.29 (m, 1H), 8.47 (s, 1H); ^{19}F NMR (376 MHz, $CDCl_3$) δ -62.89 (s, 3F).

2-Debenzoyl-3'-dephenyl-10-(*N,N*-dimethylcarbamoyl)-3'-(2-methyl-2-propenyl)-2-[3-(trifluoromethyl)benzoyl]- docetaxel (SB-T-121606) [2-30]:

To a solution of **2-28** (0.037 g, 0.0462 mmol) and β-lactam (+)**1-6** (0.022 g, 0.0554 mmol) in THF (1.5 mL) was added 1 M LHMDS (69 μL, 0.0690 mmol), and the mixture was allowed to react for 1½ h at -40 °C with stirring. The reaction was diluted with H_2O (10 mL), and the mixture was extracted with ethyl acetate (3 x 20 mL). The combined organic layers were washed with brine (3 x 10 mL), dried over $MgSO_4$, and concentrated *in vacuo* to give a colorless oil. Purification of the crude product by column chromatography on silica gel with hexanes/ethyl acetate (4:1) as eluent gave **2-29** (0.043 g, 78%) as a white solid; R_f = 0.7 (hexanes/ethyl acetate = 3:1). To a cooled solution of **2-29** (0.043 g, 0.0360 mmol) in CH_3CN-pyridine (1:1) (3.6 mL) was added HF-pyridine (0.45 mL), and the mixture was allowed to warm from 0 °C to room temperature and react for 16 h with stirring. The reaction mixture was diluted with H_2O (10 mL), and the mixture was extracted with ethyl acetate (3 x 10 mL). The combined organic layers were

washed with saturated $CuSO_4$ (3 x 10 mL) and brine (3 x 10 mL), dried over $MgSO_4$, and concentrated *in vacuo* to give a colorless oil. Purification of the crude product by column chromatography on silica gel with hexanes/ethyl acetate (1:4) as eluent gave SB-T-121606 (**2-30**) (0.028 g, 85%) as a white solid; R_f = 0.2 (hexanes/ethyl acetate = 3:1); ^{1}H NMR (700 MHz, $CDCl_3$) δ 1.16 (s, 3H), 1.25 (m, 5H), 1.33 (s, 9H), 1.67 (s, 3H), 1.73 (s, 3H), 1.76 (s, 3H), 1.87 (m, 2H), 1.92 (s, 3H), 2.34 (s, 3H), 2.41 (m, 1H), 2.54 (m, 1H), 2.96 (s, 3H), 3.04 (s, 3H), 3.83 (d, *J* = 7.1 Hz, 1H), 4.15 (d, *J* = 8.4 Hz, 1H), 4.18 (s, 1H), 4.25 (d, *J* = 8.4 Hz, 1H), 4.44 (dd, *J* = 6.9, 10.8 Hz, 1H), 4.72 (t, *J* = 7.8 Hz, 1H), 4.76 (m, 1H), 4.99 (d, *J* = 9.4 Hz, 1H), 5.32 (d, *J* = 7.6 Hz, 1H), 5.64 (d, *J* = 7.1 Hz, 1H), 6.14 (t, *J* = 9.0 Hz, 1H), 6.27 (s, 1H), 7.63 (t, *J* = 7.8 Hz, 1H), 7.86 (d, *J* = 7.7 Hz, 1H), 8.28 (d, *J* = 7.7 Hz, 1H), 8.44 (s, 1H); ^{13}C NMR (175 MHz, $CDCl_3$) δ 9.30, 15.05, 18.41, 20.10, 22.18, 25.66, 26.74, 28.20, 28.23, 29.70, 35.37, 35.45, 36.03, 36.65, 43.16, 45.64, 51.60, 58.45, 72.49, 73.64, 75.75, 76.20, 76.28, 79.34, 79.87, 81.09, 84.64, 120.47, 121.30, 122.85, 124.40, 125.95, 126.80, 126.83, 129.48, 130.16, 130.18, 130.22, 130.94, 131.13, 131.31, 131.50, 132.97, 133.55, 138.09, 143.18, 155.40, 156.13, 165.39, 169.91, 173.34, 205.61; HRMS for $C_{45}H_{60}F_3N_2O_{15}^+$ calcd: 925.3940. Found: 925.3945 (Δ = 0.5 ppm).

10-Deacetyl-2-debenzoyl-2-[3-(trifluoromethoxy)benzoyl]-7,10,13-tris(triethylsilyl)baccatin III [2-31]:[61]

To a solution **2-11** (0.398 g, 0.508 mmol), 3-(trifluoromethoxy)benzoic acid (0.838 g, 4.07 mmol), and DMAP (0.497 g, 4.07 mmol) in CH_2Cl_2 (10 mL) was added DIC (0.63 mL, 4.07 mmol), and the mixture was allowed to react for 10 h at room temperature with stirring. The reaction was quenched with saturated NH_4Cl (10 mL) and diluted with H_2O (10 mL), and the mixture was extracted with ethyl acetate (3 x 30 mL). The combined organic layers were washed with brine (3 x 30 mL), dried over $MgSO_4$, and concentrated *in vacuo* to give a yellow solid. Purification of the crude product by column chromatography on silica gel with hexanes/ethyl acetate (6:1) as eluent gave **2-31** (0.435 g, 88%) as a white solid; R_f = 0.9 (hexanes/ethyl acetate = 3:1); ^{1}H NMR (500 MHz, $CDCl_3$) δ 0.64 (m, 18H), 0.99 (m, 27H), 1.12 (s, 3H), 1.19 (s, 3H), 1.50 (s, 1H), 1.65 (s, 3H), 1.88 (t, *J* = 10.6 Hz, 1H), 1.98 (s, 3H), 2.10 (m, 1H), 2.19 (m, 1H), 2.27 (s, 3H), 2.53 (m, 1H), 3.86 (d, *J* = 7.0 Hz, 1H), 4.13 (d, *J* = 8.2 Hz, 1H), 4.25 (d, *J* = 8.2 Hz, 1H), 4.40 (dd, *J* = 6.6, 10.3 Hz, 1H), 4.94 (m, 2H), 5.19 (s, 1H), 5.59 (d, *J* = 7.2 Hz, 1H), 7.43 (d, *J* = 9.0 Hz, 1H), 7.52 (t, *J* = 8.0 Hz, 1H), 7.98 (s, 1H), 8.02 (d, *J* = 7.8 Hz, 1H); ^{13}C NMR (125 MHz, $CDCl_3$) δ 4.80, 5.21, 5.94, 6.85, 6.95, 10.40, 14.59, 20.55, 22.17, 26.29, 37.23, 39.71, 42.93, 46.88, 58.19, 68.22, 72.61, 75.74, 76.09, 76.46, 79.63, 80.72, 84.01, 122.03, 126.03, 128.53, 130.17, 131.62, 135.61, 139.55, 149.21, 165.64, 169.99, 205.64; ^{19}F NMR (282 MHz, $CDCl_3$) δ -58.48 (s, 3F); HRMS for $C_{48}H_{78}F_3O_{11}Si_3^+$ calcd: 971.4799. Found: 971.4806 (Δ = 0.7 ppm).

10-Deacetyl-2-debenzoyl-2-[3-(trifluoromethoxy)benzoyl]baccatin III [2-32]:[61]

To a cooled solution of **2-31** (0.573 g, 0.590 mmol) in CH_3CN-pyridine (1:1) (40 mL) was added HF-pyridine (5.7 mL), and the mixture was allowed to warm from 0 °C to room temperature and react for 13 h with stirring. The reaction was quenched with 10% citric acid (15 mL) and diluted with H_2O (10 mL), and the mixture was extracted with ethyl acetate (3 x 30 mL). The combined organic layers were washed with saturated $CuSO_4$ (3 x 30 mL) and brine (3 x 30 mL), dried over $MgSO_4$, and concentrated *in vacuo* to give **2-32** (0.333 g, 90%) as a white solid; R_f = 0.1 (hexanes/ethyl acetate = 3:1); ^{1}H NMR (500 MHz, DMSO-d_6) δ 0.97 (s, 3H), 0.98 (s, 3H), 1.57 (s, 3H), 1.69 (m, 1H), 1.94 (s, 3H), 2.18 (d, *J* = 8.3 Hz, 1H), 2.21 (s, 3H), 2.32 (m, 1H), 3.86 (d,

J = 7.1 Hz, 1H), 4.06 (s, 2H), 4.13 (m, 1H), 4.52 (s, 1H), 4.66 (m, 1H), 4.97 (d, *J* = 8.3 Hz, 1H), 5.05 (d, *J* = 7.1 Hz, 1H), 5.17 (d, *J* = 2.6 Hz, 1H), 5.28 (d, *J* = 4.6 Hz, 1H), 5.43 (d, *J* = 7.1 Hz, 1H), 7.76 (s, 1H), 7.77 (t, *J* = 8.1 Hz, 1H), 7.96 (s, 1H), 8.06 (dt, *J* = 1.7, 7.0 Hz, 1H); ^{13}C NMR (125 MHz, DMSO-d_6) δ 10.16, 15.34, 20.58, 22.53, 27.22, 37.04, 42.88, 46.96, 57.49, 66.47, 71.41, 74.87, 75.88, 76.06, 77.40, 80.56, 84.18, 121.91, 126.52, 129.06, 131.62, 132.86, 134.89, 142.07, 148.79, 164.27, 169.89, 210.70; ^{19}F NMR (376 MHz, DMSO-d_6) δ -56.92 (s, 3F); HRMS for $C_{30}H_{36}F_3O_{11}^+$ calcd: 629.2204. Found: 629.2207 (Δ = 0.5 ppm).

10-Deacetyl-2-debenzoyl-2-[3-(trifluoromethoxy)benzoyl]-7-triethylsilyl-baccatin III [2-33]:[61]

To a cooled solution of **2-32** (0.333 g, 0.530 mmol) and imidazole (0.144 g, 2.12 mmol) in DMF (5.3 mL) was added TESCl (0.3 mL, 1.59 mmol), and the mixture was allowed to react for 30 min at 0 °C with stirring. The reaction was quenched with saturated NH_4Cl (10 mL) and diluted with H_2O (10 mL), and the mixture was extracted with ethyl acetate (3 x 30 mL). The combined organic layers were washed with brine (3 x 30 mL), dried over $MgSO_4$, and concentrated *in vacuo* to give a colorless oil. Purification of the crude product by column chromatography on silica gel with hexanes/ethyl acetate (3:2) as eluent gave **2-33** (0.320 g, 81%) as a white solid; R_f = 0.75 (hexanes/ethyl acetate = 1:1); ^{1}H NMR (500 MHz, $CDCl_3$) δ 0.54 (m, 6H), 0.93 (t, *J* = 8.0 Hz, 9H), 1.07 (s, 6H), 1.72 (s, 3H), 1.89 (dt, *J* = 2.1, 12.6 Hz, 1H), 2.07 (s, 3H), 2.08 (t, *J* = 5.3 Hz, 1H), 2.25 (t, *J* = 8.1 Hz, 2H), 2.26 (s, 3H), 2.47 (m, 1H), 3.95 (d, *J* = 6.9 Hz, 1H), 4.14 (d, *J* = 8.2 Hz, 1H), 4.24 (d, *J* = 2.1 Hz, 1H), 4.28 (d, *J* = 8.2 Hz, 1H), 4.41 (dd, *J* = 7.0, 10.6 Hz, 1H), 4.86 (m, 1H), 4.96 (d, *J* = 7.9 Hz, 1H), 5.16 (d, *J* = 2.1 Hz, 1H), 5.57 (d, *J* = 7.0 Hz, 1H), 7.45 (d, *J* = 8.1 Hz, 1H), 7.52 (t, *J* = 7.9 Hz, 1H), 7.98 (s, 1H), 8.03 (dt, *J* = 1.1, 7.7 Hz, 1H); ^{13}C NMR (125 MHz, $CDCl_3$) δ 5.13, 6.72, 9.86, 15.19, 19.43, 22.39, 26.83, 37.17, 38.44, 42.61, 46.96, 57.89, 67.85, 72.91, 74.64, 75.34, 78.85, 80.63, 84.23, 122.12, 126.10, 128.50, 130.21, 131.41, 134.98, 141.89, 149.22, 149.24, 165.54, 170.77, 210.24; ^{19}F NMR (376 MHz, $CDCl_3$) δ -57.86 (s, 3F); HRMS for $C_{36}H_{50}F_3O_{11}Si^+$ calcd: 743.3069. Found: 743.3072 (Δ = 0.4 ppm).

10-(Cyclopropanecarbamoyl)-10-deacetyl-2-debenzoyl-2-[3-(trifluoromethoxy)benzoyl]-7-triethylsilyl-baccatin III [2-34]:[61]

To a cooled solution of **2-33** (0.240 g, 0.323 mmol) in THF (3.2 mL) was added 1 M LHMDS in THF (0.35 mL, 0.350 mmol) followed by cyclopropanecarbonyl chloride (31 μL, 0.340 mmol), and the mixture was allowed to react for 10 min at -40 °C with stirring. The reaction was quenched with saturated NH_4Cl (10 mL) and diluted with H_2O (10 mL), and the mixture was extracted with ethyl acetate (3 x 30 mL). The combined organic layers were washed with brine (3 x 30 mL), dried over $MgSO_4$, and concentrated *in vacuo* to give a crude yellow oil. Purification of the crude product by column chromatography on silica gel with hexanes/ethyl acetate (3:2) as eluent gave **2-34** (0.245 g, 93%) as a white solid; R_f = 0.8 (hexanes/ethyl acetate = 1:1); ^{1}H NMR (500 MHz, $CDCl_3$) δ 0.57 (m, 6H), 0.90 (m, 2H), 0.91 (t, *J* = 8.0 Hz, 9H), 1.05 (s, 3H), 1.19 (s, 3H), 1.67 (s, 3H), 1.75 (m, 1H), 1.87 (dt, *J* = 2.0, 12.3 Hz, 1H), 2.08 (m, 1H), 2.19 (s, 3H), 2.24 (m, 2H), 2.26 (s, 3H), 2.53 (m, 1H), 3.89 (d, *J* = 7.0 Hz, 1H), 4.12 (d, *J* = 8.0 Hz, 1H), 4.27 (d, *J* = 8.0 Hz, 1H), 4.47 (dd, *J* = 6.7, 10.3 Hz, 1H), 4.84 (m, 1H), 4.96 (d, *J* = 8.2 Hz, 1H), 5.61 (d, *J* = 7.1 Hz, 1H), 6.46 (s, 1H), 7.45 (d, *J* = 8.1 Hz, 1H), 7.53 (t, *J* = 8.0 Hz, 1H), 8.00 (s, 1H), 8.05 (dt, *J* = 1.2, 7.8 Hz, 1H); ^{13}C NMR (125 MHz, $CDCl_3$) δ 5.23, 6.74, 8.57, 8.71, 9.87, 12.98, 14.17, 14.93, 20.07, 21.04, 22.44, 26.80, 37.15, 38.07, 42.68, 47.23, 53.40, 58.55, 60.39, 67.88, 72.31, 75.27, 75.47, 76.35, 78.84, 80.76, 84.21, 122.15, 126.12, 128.52, 130.21,

131.40, 132.60, 143.99, 149.22, 165.60, 170.72, 173.17, 202.24; ^{19}F NMR (376 MHz, $CDCl_3$) δ -57.86 (s, 3F); HRMS for $C_{40}H_{54}F_3O_{12}Si^+$ calcd: 811.3331. Found: 811.3336 (Δ = 0.6 ppm).

2-Debenzoyl-3'-dephenyl-10-(cyclopropanecarbamoyl)-2-[3-(trifluoromethoxy)benzoyl]-7-triethylsilyl-2'-triisopropylsilyl-3'-(trifluoromethyl)docetaxel [2-35]:[61]
To a cooled solution of **2-34** (0.245 g, 0.302 mmol) and (3*R*,4*R*)-1-(*tert*-butoxycarbonyl)-3-triisopropylsiloxy-4-trifluoromethylazetidin-2-one (0.155 g, 0.369 mmol) in THF (5 mL) was added 1 M LHMDS in THF (0.4 mL, 0.4 mmol), and the mixture was allowed to react for 3 h at -40 °C with stirring. The reaction was quenched with NH_4Cl (10 mL) and diluted with H_2O (10 mL), and the mixture was extracted with ethyl acetate (3 x 30 mL). The combined organic layers were washed with brine (3 x 30 mL), dried over $MgSO_4$, and concentrated *in vacuo* to give a yellow oil. Purification of the crude product by column chromatography on silica gel with hexanes/ethyl acetate (4:1) as eluent gave **2-35** (0.254 g, 69%) as a white solid; R_f = 0.5 (hexanes/ethyl acetate = 5:1); ^{1}H NMR (500 MHz, $CDCl_3$) δ 0.55 (m, 6H), 0.90 (t, *J* = 8.0 Hz, 9H), 0.92 (m, 2H), 1.11 (m, 21H), 1.17 (s, 3H), 1.22 (s, 3H), 1.31 (s, 9H), 1.58 (m, 3H), 1.68 (s, 3H), 1.75 (m, 1H), 1.88 (m, 1H), 2.01 (s, 3H), 2.30 (m, 1H), 2.32 (s, 3H), 2.50 (m, 1H), 3.84 (d, *J* = 7.1 Hz, 1H), 4.17 (d, *J* = 8.7 Hz, 1H), 4.29 (d, *J* = 8.4 Hz, 1H), 4.45 (dd, *J* = 6.7, 10.5 Hz, 1H), 4.65 (m, 1H), 4.91 (s, 1H), 4.93 (t, *J* = 16.6 Hz, 1H), 5.17 (d, *J* = 10.6 Hz, 1H), 5.65 (d, *J* = 7.6 Hz, 1H), 6.07 (t, *J* = 8.5 Hz, 1H), 6.47 (s, 1H), 7.45 (d, *J* = 7.5 Hz, 1H), 7.55 (t, *J* = 8.0 Hz, 1H), 8.01 (s, 1H), 8.06 (d, *J* = 7.8 Hz, 1H); ^{13}C NMR (125 MHz, $CDCl_3$) δ 5.27, 6.73, 8.70, 8.83, 10.02, 12.70, 12.93, 14.18, 14.25, 17.79, 17.92, 21.29, 22.22, 26.50, 27.92, 35.19, 37.09, 43.23, 46.71, 58.33, 70.01, 72.18, 72.44, 72.66, 75.48, 76.36, 78.84, 81.12, 84.26, 122.20, 126.11, 128.57, 130.32, 131.26, 133.59, 140.25, 149.26, 155.12, 165.54, 169.87, 170.61, 173.14, 201.81; ^{19}F NMR (376 MHz, $CDCl_3$) δ -57.98 (s, 3F), -72.55 (s, 3F); HRMS for $C_{58}H_{86}F_6NO_{16}Si_2^+$ calcd: 1222.5384. Found: 1222.5383 (Δ = 0.1 ppm).

2-Debenzoyl-3'-dephenyl-10-(cyclopropanecarbamoyl)-2-[3-(trifluoromethoxy)benzoyl]-3'-(trifluoromethyl)docetaxel (SB-T-12822-5) [2-36]:[61]
To a cooled solution of **2-35** (0.190 g, 0.155 mmol) in CH_3CN-pyridine (1:1) (10 mL) was added HF-pyridine (1.9 mL), and the mixture was allowed to warm from 0 °C to room temperature and react for 12 h with stirring. The reaction was quenched with 10% citric acid (10 mL) and diluted with H_2O (10 mL), and the mixture was extracted with ethyl acetate (3 x 30 mL). The combined organic layers were washed with saturated $CuSO_4$ (3 x 30 mL) and brine (3 x 30 mL), dried over $MgSO_4$, and concentrated *in vacuo* to give a colorless oil. Purification of the crude product by column chromatography on silica gel with hexanes/ethyl acetate (3:7) as eluent gave SB-T-12822-5 (**2-36**) (0.128 g, 87%) as a white solid; R_f = 0.45 (hexanes/ethyl acetate = 1:1); ^{1}H NMR (500 MHz, $CDCl_3$) δ 1.00 (m, 2H), 1.14 (m, 2H), 1.15 (s, 3H), 1.24 (s, 3H), 1.31 (s, 9H), 1.67 (s, 3H), 1.78 (m, 1H), 1.85 (m, 1H), 1.88 (s, 3H), 2.32 (t, *J* = 12.7 Hz, 2H), 2.35 (s, 3H), 2.54 (m, 1H), 2.60 (d, *J* = 4.1 Hz, 1H), 3.43 (d, *J* = 4.6 Hz, 1H), 3.81 (d, *J* = 7.0 Hz, 1H), 4.16 (d, *J* = 8.4 Hz, 1H), 4.28 (d, *J* = 8.4 Hz, 1H), 4.40 (m, 1H), 4.69 (d, *J* = 4.0 Hz, 1H), 4.74 (m, 1H), 4.95 (d, *J* = 7.9 Hz, 1H), 5.22 (d, *J* = 7.9 Hz, 1H), 5.22 (d, *J* = 10.8 Hz, 1H), 5.63 (d, *J* = 7.1 Hz, 1H), 6.21 (t, *J* = 8.0 Hz, 1H), 6.29 (s, 1H), 7.46 (d, *J* = 7.4 Hz, 1H), 7.56 (t, *J* = 8.0 Hz, 1H), 8.00 (s, 1H), 8.06 (d, *J* = 7.8 Hz, 1H); ^{13}C NMR (125 MHz, $CDCl_3$) δ 9.30, 9.54, 13.03, 13.73, 14.22, 14.89, 19.14, 21.05, 21.09, 22.00, 22.14, 26.70, 27.93, 30.65, 35.34, 35.48, 43.20, 45.66, 53.46, 58.55, 60.45, 64.42, 68.06, 72.19, 73.46, 75.25, 75.63, 76.32, 79.17, 81.15, 81.34, 84.50, 122.34, 126.28, 128.60, 130.43, 131.15, 133.34, 141.82, 149.33, 154.65, 165.65, 170.22, 171.88, 175.16, 203.65;

^{19}F NMR (470 MHz, $CDCl_3$) δ -57.96 (s, 3F), -73.39 (d, *J* = 8.0 Hz, 3F); HRMS for $C_{43}H_{52}F_6NO_{16}^+$ calcd: 952.3185. Found: 952.3199 (Δ =1.5 ppm); HPLC: t = 23.0 min, purity >98%.

2'-(*tert*-Butyldimethylsilyl)-Taxol [2-37]:[63]

To a solution of paclitaxel (0.306 g, 0.36 mmol) and imidazole (0.243 g, 3.58 mmol) in DMF (1 mL) was added TBDMSCl (0.270 g, 1.79 mmol), and the mixture was allowed to react for 2 h at room temperature with stirring. The reaction mixture was diluted with ethyl acetate (30 mL). The organic layer was washed with H_2O (3 x 30 mL) and brine (3 x 30 mL), dried over $MgSO_4$, and concentrated *in vacuo* to afford a colorless oil. Purification of the crude product by column chromatography on silica gel with hexanes/ethyl acetate (1:1) as eluent gave **2-37** (0.315 g, 91%) as a white solid; ^1H NMR (300 MHz, $CDCl_3$) δ -0.29 (s, 3H), -0.05 (s, 3H), 0.80 (s, 9H), 1.14 (s, 3H), 1.24 (s, 3H), 1.25 (m, 1H), 1.69 (s, 3H), 1.88 (m, 1H), 1.90 (s, 3H), 2.04 (bs, 1H), 2.14 (dd, *J* = 8.1, 15.3 Hz, 1H), 2.25 (s, 3H, 10-OAc), 2.40 (dd, *J* = 9.6, 15.3 Hz, 1H), 2.49 (m, 1H), 2.57 (m, 1H), 2.58 (s, 3H), 3.83 (d, *J* = 6.9 Hz, 1H), 4.22 (d, *J* = 8.1 Hz, 1H), 4.33 (d, *J* = 8.7 Hz, 1H), 4.44 (m, 1H), 4.66 (d, *J* = 2.1 Hz, 1H), 4.99 (d, *J* = 8.1 Hz, 1H), 5.69 (d, *J* = 7.2 Hz, 1H), 5.72 (d, *J* = 7.5 Hz, 1H), 6.27 (m, 1H), 6.29 (s, 1H), 7.09 (d, *J* = 9.0 Hz, 1H), 7.34 (m, 3H), 7.41 (m, 4H), 7.52 (m, 3H), 7.61 (t, *J* = 7.2 Hz, 1H), 7.73 (d, *J* = 7.5 Hz, 2H), 8.14 (d, *J* = 7.2 Hz, 2H). All data are in agreement with literature values.[63]

2'-TBDMS-7-[4-[9-(2-isobutoxycarbonylphenyl)-3-oxo-3H-xanthen-6-yloxy]butanoyl]-paclitaxel [2-38]:

To a solution of **2-37** (0.038 g, 0.039 mmol), 4-(butanoyl)fluorescein isobutyl ester (0.037 g, 0.078 mmol), and DMAP (0.005 g, 0.039 mmol) in CH_2Cl_2-DMF (2:1) (2 mL) was added DIC (12 μL, 0.078 mmol), and the mixture was allowed to react for 24 h at room temperature with stirring. The reaction mixture was directly concentrated *in vacuo* to afford an orange oil. Purification of the crude product by column chromatography on silica gel with 2% CH_3OH in CH_2Cl_2 as eluent gave **2-38** (0.039 g, 70%) as a yellow solid; ^1H NMR (500 MHz, $CDCl_3$) δ -0.30 (s, 3H), -0.03 (s, 3H), 0.70 (m, 6H), 0.80 (s, 9H), 1.16 (s, 3H), 1.22 (s, 3H), 1.61 (m, 4H), 1.79 (s, 1H), 1.82 (s, 3H), 1.87 (m, 1H), 1.98 (s, 3H). 2.13 (m, 5H), 2.49 (m, 2H), 2.54 (t, *J* = 7.1 Hz, 1H), 2.58 (s, 3H), 2.61 (m, 1H), 3.73 (m, 1H), 3.79 (d, *J* = 6.9 Hz, 1H), 3.99 (m, *J* = 7.0 Hz, 1H), 4.12 (m, 2H), 4.21 (d, *J* = 8.5 Hz, 1H), 4.35 (d, *J* = 8.5 Hz, 1H), 4.67 (s, 1H), 4.97 (d, *J* = 9.2 Hz, 1H), 5.64 (dd, *J* = 7.2, 10.6 Hz, 1H), 5.74 (dd, *J* = 7.0, 18.9 Hz, 1H), 6.26 (t, *J* = 9.6 Hz, 1H), 6.27 (s, 1H), 6.47 (bs, 1H), 6.56 (d, *J*=9.1 Hz, 1H), 6.74 (d, *J* = 8.9 Hz, 1H), 6.89 (t, *J* = 8.7 Hz, 2H), 6.96 (s, 1H), 7.09 (d, *J* = 9.0 Hz, 1H), 7.32 (m, 4H), 7.40 (m, 4H), 7.52 (m, 3H), 7.61 (t, *J* = 7.5 Hz, 1H), 7.67 (t, *J* = 7.9 Hz, 1H), 7.72 (t, *J* = 7.4 Hz, 1H), 7.75 (d, *J* = 7.1 Hz, 2H), 8.13 (d, *J* = 7.1 Hz, 2H), 8.26 (d, *J* = 7.8 Hz, 1H). ^{13}C NMR (125 MHz, $CDCl_3$) δ -5.79, -5.14, 10.93, 14.66, 18.14, 18.88, 20.75, 21.43, 23.03, 23.52, 23.77, 25.55, 26.38, 27.53, 30.36, 33.46, 35.62, 42.23, 43.38, 46.86, 55.07, 55.70, 67.92, 71.33, 71.80, 71.89, 74.49, 75.10, 75.24, 76.50, 78.66, 80.96, 83.95, 101.83, 105.74, 115.23, 117.92, 126.41, 127.03, 128.01, 128.80, 128.94, 129.07, 129.66, 130.24, 130.54, 130.85, 131.31, 131.85, 132.54, 132.65, 133.79, 134.12, 134.23, 138.28, 140.97, 156.85, 159.01, 167.00, 169.06, 169.98, 171.48, 172.06, 202.09. HRMS for $C_{81}H_{90}NO_{20}Si^+$ calcd: 1424.5820. Found: 1424.5829 (Δ = 0.6 ppm).

7-[4-[9-(2-isobutoxycarbonylphenyl)-3-oxo-3H-xanthen-6-yloxy]butanoyl]-paclitaxel [2-39]: To a cooled solution of **2-38** (0.025 g, 0.017 mmol) in CH_3CN-pyridine (1:1) (1.1 mL) was added HF-pyridine (0.3 mL), and the mixture was allowed to warm from 0 °C to room temperature and react for 48 h with stirring. The reaction was quenched with H_2O (10 mL), and the mixture was extracted with ethyl acetate (3 x 30 mL). The combined organic layers were washed with saturated $CuSO_4$ (3 x 20 mL) and brine (3 x 20 mL), dried over $MgSO_4$, and concentrated *in vacuo* to afford an orange oil. Purification of the crude product by column chromatography on silica gel with 2% CH_3OH in CH_3OH as eluent gave **2-39** (0.020 g, 87%) as an orange solid; ^{1}H NMR (500 MHz, $CDCl_3$) δ 0.68 (m, 6H), 0.88 (m, 2H), 1.14 (s, 3H), 1.25 (s, 3H), 1.62 (m, 1H), 1.82 (s, 3H), 1.88 (m, 2H), 2.04 (s, 3H), 2.11 (d, *J* = 3.0 Hz, 3H), 2.33 (m, 2H), 2.35 (m, 2H), 2.41 (s, 3H), 2.57 (m, 2H), 3.78 (m, 2H), 4.20 (d, *J* = 8.5 Hz, 1H), 4.26 (m, 2H), 4.35 (d, *J* = 8.5 Hz, 1H), 4.87 (d, *J* = 2.1 Hz, 1H), 4.97 (d, *J* = 9.3 Hz, 1H), 5.69 (d, *J* = 6.9 Hz, 1H), 5.80 (m, 2H), 6.18 (t, *J* = 8.9 Hz, 1H), 6.27 (s, 1H), 6.67 (d, *J* = 9.4 Hz, 2H), 6.79 (d, *J* = 9.0 Hz, 1H), 6.96 (m, 2H), 7.31 (m, 2H), 7.40 7.63 (t, *J* = 7.4 Hz, 1H), 7.46 (m, 2H), 7.53 (m, 3H), 7.69 (t, *J* = 7.8 Hz, 1H), 7.74 (t, *J* = 7.5 Hz, 1H), 7.84 (d, *J* = 7.2 Hz, 2H), 8.12 (d, *J* = 7.3 Hz, 2H), 8.28 (d, *J* = 7.6 Hz, 1H). ^{13}C NMR (125 MHz, $CDCl_3$) δ 10.87, 14.73, 18.85, 20.76, 20.91, 22.52, 22.97, 23.47, 26.39, 27.50, 29.31, 29.69, 30.92, 33.47, 35.60, 43.24, 47.19, 55.27, 56.10, 67.94, 71.57, 71.87, 73.34, 74.31, 75.46, 76.40, 78.52, 80.89, 83.93, 100.84, 105.31, 114.84, 115.65, 117.20, 127.26, 127.98, 128.52, 128.73, 128.79, 129.08, 129.84, 130.16, 130.39, 130.58, 130.75, 131.32, 132.56, 133.78, 133.96, 135.06, 137.82, 138.69, 138.74, 140.91, 148.00, 155.31, 159.38, 164.53, 166.84, 167.16, 169.01, 170.36, 172.60, 202.14. HRMS for $C_{75}H_{76}NO_{20}^+$ calcd: 1310.4955. Found: 1310.4961 (Δ = 0.5 ppm).

Cell Culture.

All cell lines were obtained from ATCC unless otherwise noted. Cells were cultured in RPMI-1640 cell culture medium (Gibco), supplemented with 10% (v/v) heat-inactivated fetal bovine serum (FBS) and 1% (v/v) penicillin and streptomycin (PenStrep) at 37 °C in a humidified atmosphere with 5% CO_2. Human breast carcinoma cell line, MCF-7, and metastatic ovarian MDR cancer cell line, NCI/ADR-RES, were cultured as monolayers on 100 mm tissue culture dishes in supplemented RPMI-1640 cell culture medium. Cells were harvested, collected by centrifugation at 850 rpm for 5 min, and resuspended in fresh culture medium. Cell cultures were routinely divided by treatment with trypsin (TrypLE, Gibco) as needed every 2-4 days and collected by centrifugation at 850 rpm for 5 min. The cells were resuspended in fresh cell culture medium, containing varying cell densities for subsequent biological experiments and analysis.

In Vitro Cytotoxicity Assays.

The cytotoxicities (IC_{50}, nM) of paclitaxel, SB-T-1214, and next-generation taxoids were evaluated against various cancer cell lines by means of the standard quantitative colorimetric MTT assay.[62] The inhibitory activity of each compound is represented by the IC_{50} value, which is defined as the concentration required for inhibiting 50% of the cell growth. Cells were harvested, collected, and resuspended in 100 μL cell culture medium (RPMI-1640) at a concentrations ranging from 0.5-1.5 x 10^4 cells per well in a 96-well plate.

For the MTT assay of paclitaxel, SB-T-1214, or a next-generation taxoid, cells were resuspended in 200 μL medium with 8,000 to 10,000 cells per well of a 96-well plate and incubated at 37 °C for 24 h before drug treatment. In DMSO stock solutions, each drug or conjugate was diluted to a series of concentrations in cell culture medium to prepare test

solutions. After removing the old medium, these test solutions were added to the wells in the 96-well plate to give the final concentrations ranging from 0.5 to 5,000 nM (100 μL), and the cells were subsequently cultured at 37 °C for 48 of 72 h.

After removing the test medium, fresh solution of MTT in PBS (40 μL of 0.5 mg MTT/mL) was added to the wells, and the cells were incubated at 37 °C for 3 h. The MTT solution was then removed, and the resulting insoluble violet formazan crystals were dissolved in 0.1 N HCl in isopropanol with 10% Triton X-100 (40 μL) to give a violet solution. The spectrophotometric absorbance measurement of each well in the 96-well plate was run at 570 nm using a Labsystems Multiskan Ascent microplate reader. The IC_{50} values and their standard errors were calculated from the viability-concentration curve using Four Parameter Logistic Model of *Sigmaplot*. The concentration of DMSO per well was ≤1% in all cases. Each experiment was run in triplicate.

§2.7 References

1. Cancer Statistics 2013: A Presentation from the American Cancer Society, ©2013. American Cancer Society, Inc.
2. *American Cancer Society. Cancer Facts & Figures 2013*; Atlanta: American Cancer Society, 2013.
3. Heron, M. Deaths: leading causes for 2009. *Natl. Vital Stat. Rep.* **2012,** 61, 1-95.
4. Wani, M. C.; Taylor, H. L.; Wall, M. E.; Coggon, P.; McPhail, A. T. Plant antitumor agents. VI. The isolation and structure of taxol, a novel antileukemic and antitumor agent from Taxus brevifolia. *J. Am. Chem. Soc.* **1971,** 93, 2325-2327.
5. Cragg, G. M.; Kingston, D. G. I.; Newman, D. J. *Anticancer agents from natural products*. CRC Press: 2011.
6. Weiss, R. B.; Donehower, R. C.; Wiernik, P. H.; Ohnuma, T.; Gralla, R. J.; Trump, D. L.; Baker, J. R., Jr.; Van Echo, D. A.; Von Hoff, D. D.; Leyland-Jones, B. Hypersensitivity reactions from taxol. *J. Clin. Oncol.* **1990,** 8, 1263-1268.
7. McGuire, W. P.; Rowinsky, E. K.; Rosenshein, N. B.; Grumbine, F. C.; Ettinger, D. S.; Armstrong, D. K.; Donehower, R. C. Taxol: a unique antineoplastic agent with significant activity in advanced ovarian epithelial neoplasms. *Ann. Intern. Med.* **1989,** 111, 273-279.
8. Holmes, F. A.; Walters, R. S.; Theriault, R. L.; Forman, A. D.; Newton, L. K.; Raber, M. N.; Buzdar, A. U.; Frye, D. K.; Hortobagyi, G. N. Phase II trial of taxol, an active drug in the treatment of metastatic breast cancer. *J. Natl. Cancer Inst.* **1991,** 83, 1797-1805.
9. Schiff, P. B.; Fant, J.; Horwitz, S. B. Promotion of microtubule assembly in vitro by taxol. *Nature* **1979,** 277, 665-667.
10. Zhao, X. Design, synthesis and biological evaluation of novel taxane-based anticancer agents and their applications to tumor-targeting drug delivery systems (Doctoral Dissertation). State University of New York at Stony Brook, 2009.
11. Haldar, S.; Chintapalli, J.; Croce, C. M. Taxol induces bcl-2 phosphorylation and death of prostate cancer cells. *Cancer Res.* **1996,** 56, 1253-1255.
12. Blagosklonny, M. V.; Giannakakou, P.; el-Deiry, W. S.; Kingston, D. G.; Higgs, P. I.; Neckers, L.; Fojo, T. Raf-1/bcl-2 phosphorylation: a step from microtubule damage to cell death. *Cancer Res.* **1997,** 57, 130-135.

13. Rodi, D. J.; Janes, R. W.; Sanganee, H. J.; Holton, R. A.; Wallace, B. A.; Makowski, L. Screening of a library of phage-displayed peptides identifies human bcl-2 as a taxol-binding protein. *J. Mol. Biol.* **1999,** 285, 197-203.
14. Bissery, M. C.; Nohynek, G.; Sanderink, G. J.; Lavelle, F. Docetaxel (Taxotere): a review of preclinical and clinical experience. Part I: Preclinical experience. *Anti-cancer Drugs* **1995,** 6, 339-355.
15. Gueritte, F. General and recent aspects of the chemistry and structure-activity relationships of taxoids. *Curr. Pharm. Des.* **2001,** 7, 1229-1249.
16. FDA; (2014). FDA approves new treatment for advanced head and neck cancer [Press Release]. Retrieved from http://www.fda.gov/NewsEvents/Newsroom/PressAnnouncements/2006/ucm108771.htm.
17. Galsky, M. D.; Dritselis, A.; Kirkpatrick, P.; Oh, W. K. Cabazitaxel. *Nat. Rev. Drug Discov.* **2010,** 9, 677-678.
18. Pivot, X.; Koralewski, P.; Hidalgo, J. L.; Chan, A.; Goncalves, A.; Schwartsmann, G.; Assadourian, S.; Lotz, J. P. A multicenter phase II study of XRP6258 administered as a 1-h i.v. infusion every 3 weeks in taxane-resistant metastatic breast cancer patients. *Ann. Oncol.* **2008,** 19, 1547-1552.
19. Chase, M. Cancer drug may save many human lives - at a cost of rare trees. *Wall Street J.* 1991, p A8.
20. Holton, R. A.; Somoza, C.; Kim, B. K.; Liang, F.; Biediger, R. J.; Boatman, P. D.; Shindo, M.; Smith, C. C.; Kim, S. First total synthesis of taxol: 1. Functionalization of the B-ring. *J. Am. Chem. Soc.* **1994,** 116, 1597-1598.
21. Nicolaou, K. C.; Yang, Z.; Liu, J. J.; Ueno, H.; Nantermet, P. G.; Guy, R. K.; Claiborne, C. F.; Renaud, J.; Couladouros, E. A.; Paulvannan, K.; et al. Total synthesis of taxol. *Nature* **1994,** 367, 630-634.
22. Danishefsky, S.; Masters, J.; Young, W.; Link, J.; Snyder, L.; Magee, T.; Jung, D.; Isaacs, R.; Bornmann, W.; Alaimo, C.; Coburn, C.; Grandi, M. Total synthesis of Baccatin III and Taxol. *J. Am. Chem. Soc.* **1996,** 118, 2843-2859.
23. Wender, P. A.; Badham, N.; Conway, S.; Floreancig, P.; Glass, T.; Granicher, C.; Houze, J. B.; Janichen, J.; Lee, D.; Marquess, D.; McGrane, P. L.; Meng, W.; Muccairo, T. P.; Muhlebach, M.; Natchus, M. G.; Paulsen, H.; Rawlins, D. B.; Satkofsky, J.; Shuker, A. J.; Sutton, J. C.; Taylor, R. E.; Tomooka, K. The Pinene Path to Taxanes. 5. Stereocontrolled synthesis of a versatile taxane precursor. *J. Am. Chem. Soc.* **1997,** 119, 2755-2756.
24. Morihira, K.; Hara, R.; Kawahara, S.; Nishimori, T.; Kashima, H.; Nakamura, N.; Kusama, H.; Kuwajima, I. Enantioselective total synthesis of taxol. *J. Am. Chem. Soc.* **1998,** 120, 12980-12981.
25. Mukaiyama, T.; Shiina, I.; Iwadare, H.; Saitoh, M.; Nishimura, T.; Ohkawa, N.; Sakoh, H.; Nishimura, K.; Tani, Y.; Hsagawa, M.; Yamada, K.; Saitoh, K. Asymmetric total synthesis of taxol. *Chem. Eur. J.* **1999,** 5, 121-161.
26. Doi, T.; Fuse, S.; Miyamoto, S.; Nakai, K.; Sasuga, D.; Takahashi, T. A formal total synthesis of taxol aided by an automated synthesizer. *Chem. Asian J.* **2006,** 1, 370-383.
27. Denis, J.; Greene, A. A highly efficient, practical approach to natural Taxol. *J. Am. Chem. Soc.* **1988,** 110, 5917-5919.
28. Ojima, I.; Habus, I.; Zhao, M.; Zucco, M.; Park, Y. H.; Sun, C. M.; Brigaud, T. New and efficient approaches to the semisynthesis of Taxol and its C-13 side chain analogs by means of β-lactam Synthon Method. *Tetrahedron* **1992,** 48, 6985-7012.

29. Ojima, I.; Chen, J.; Sun, L.; Borella, C. P.; Wang, T.; Miller, M. L.; Lin, S.; Geng, X.; Kuznetsova, L.; Qu, C.; Gallager, D.; Zhao, X.; Zanardi, I.; Xia, S.; Horwitz, S. B.; Mallen-St Clair, J.; Guerriero, J. L.; Bar-Sagi, D.; Veith, J. M.; Pera, P.; Bernacki, R. J. Design, synthesis, and biological evaluation of new-generation taxoids. *J. Med. Chem.* **2008,** 51, 3203-3221.
30. Neidigh, K. A.; Gharpure, M. M.; Rimoldi, J. M.; Kingston, D. G. I.; Jiang, Y. Q.; Hamel, E. Synthesis and biological evaluation of 4-deacetylpaclitaxel. *Tetrahedron Lett.* **1994,** 35, 6839-6842.
31. du Bois, A.; Jung, B.; Loehr, A.; Schaller-Kranz, T.; Cohen, M.; Frickhofen, N. A phase I and pharmacokinetic study of novel taxane BMS-188797 and cisplatin in patients with advanced solid tumors. *Br. J. Cancer* **2006,** 94, 79-84.
32. Bröeker, L. E.; de Vos, F. Y. F. L.; van Groeningen, C. J.; Kuenen, B. C.; Gall, H. E.; Woo, M. H.; Voi, M.; Gietema, J. A.; de Vries, E. G. E.; Gianccone, G. Phase I trial with BMS-275183, a novel oral taxane with promising antitumor activity. *Clin. Cancer Res.* **2006,** 12, 1760-1767.
33. Doggrell, S. A. Clinical trials in restenosis with 7-hexanoyltaxol and paclitaxel-eluting stents. *Expert Rev. Cardiovasc. Ther.* **2004,** 2, 745-752.
34. Altstadt, T. J.; Fairchild, C. R.; Golik, J.; Johnston, K. A.; Kadow, J. F.; Lee, F. Y.; Long, B. H.; Rose, W. C.; Vyas, D. M.; Wong, H.; Wu, M. J.; Wittman, M. D. Synthesis and antitumor activity of novel C-7 paclitaxel ethers: discovery of BMS-184476. *J. Med. Chem.* **2001,** 44, 4577-4583.
35. Ryu, B. Y.; Sohn, J. S.; Hess, M.; Choi, S. K.; Choi, J. K.; Jo, B. W. Synthesis and anti-cancer efficacy of rapid hydrolysed water-soluble paclitaxel pro-drugs. *J. Biomater. Sci. Polym. Ed.* **2008,** 19, 311-324.
36. Chen, S.-H.; Fairchild, C.; Mamber, S. W.; Farina, V. Taxol structure-activity relationships: Synthesis and biological evaluation of 10-deoxytaxol. *J. Org. Chem.* **1993,** 58, 2927-2928.
37. Lyseng-Williamson, K. A.; Fenton, C. Docetaxel. *Drugs* **2005,** 65, 2513-2531.
38. Attard, G.; Greystoke, A.; Kaye, S.; De Bono, J. Update on tubulin-binding agents. *Pathol. Biol. (Paris)* **2006,** 54, 72-84.
39. Ojima, I. Use of fluorine in the medicinal chemistry and chemical biology of bioactive compounds--a case study on fluorinated taxane anticancer agents. *ChemBioChem* **2004,** 5, 628-635.
40. Ojima, I.; Kumar, K.; Awasthi, D.; Vineberg, J. G. Drug discovery targeting cell division proteins, microtubules and FtsZ. *Bioorg. Med. Chem.* **2014,** 2014.02.036 [Epub ahead of print] (March 5, 2014).
41. Kingston, D. G.; Chordia, M. D.; Jagtap, P. G.; Liang, J.; Shen, Y. C.; Long, B. H.; Fairchild, C. R.; Johnston, K. A. Synthesis and Biological Evaluation of 1-Deoxypaclitaxel Analogues. *J. Org. Chem.* **1999,** 64, 1814-1822.
42. Geney, R.; Chen, J.; Ojima, I. Recent advances in the new generation taxane anticancer agents. *Med. Chem.* **2005,** 1, 125-139.
43. Beer, M.; Lenaz, L.; Amadori, D. Phase II study of ortataxel in taxane-resistant breast cancer. *J. Clin. Oncol.* **2008,** 26, 1066.
44. Wind, N. S.; Holen, I. Multidrug resistance in breast cancer: from in vitro models to clinical studies. *Int. J. Breast Cancer* **2011,** 2011, 1-12.
45. Goldstein, L. J. MDR1 gene expression in solid tumours. *Eur. J. Cancer* **1996,** 32A, 1039-1050.

46. Mechetner, E.; Kyshtoobayeva, A.; Zonis, S.; Kim, H.; Stroup, R.; Garcia, R.; Parker, R. J.; Fruehauf, J. P. Levels of multidrug resistance (MDR1) P-glycoprotein expression by human breast cancer correlate with in vitro resistance to taxol and doxorubicin. *Clin. Cancer Res.* **1998,** 4, 389-398.
47. Riordan, J. R.; Deuchars, K.; Kartner, N.; Alon, N.; Trent, J.; Ling, V. Amplification of P-glycoprotein genes in multidrug-resistant mammalian cell lines. *Nature* **1985,** 316, 817-819.
48. Ojima, I.; Zuniga, E. S.; Berger, W. T.; Seitz, J. D. Tumor-targeting drug delivery of new-generation taxoids. *Future Med. Chem.* **2012,** 4, 33-50.
49. Ojima, I.; Slater, J. C.; Michaud, E.; Kuduk, S. D.; Bounaud, P. Y.; Vrignaud, P.; Bissery, M. C.; Veith, J. M.; Pera, P.; Bernacki, R. J. Syntheses and structure-activity relationships of the second-generation antitumor taxoids: exceptional activity against drug-resistant cancer cells. *J. Med. Chem.* **1996,** 39, 3889-3896.
50. Giannakakou, P.; Sackett, D. L.; Kang, Y.-K.; Zhan, Z.; Buters, J. T. M.; Fojo, T.; Poruchynsky, M. S. Paclitaxel-resistant human ovarian cancer cells have mutant β-tubulins that exhibit impaired paclitaxel-driven polymerization. *J. Biol. Chem.* **1997,** 272, 17118-17125.
51. Kovar, J.; Ehrlichova, M.; Smejkalova, B.; Zanardi, I.; Ojima, I.; Gut, I. Comparison of cell death-inducing effect of novel taxane SB-T-1216 and paclitaxel in breast cancer cells. *Anticancer Res.* **2009,** 29, 2951-2960.
52. Ojima, I.; Inoue, T.; Chakravarty, S. Enantiopure fluorine-containing taxoids: potent anticancer agents and versatile probes for biomedical problems. *J. Fluor. Chem.* **1999,** 97, 3-10.
53. Sun, L.; Simmerling, C.; Ojima, I. Recent advances in the study of the bioactive conformation of taxol. *ChemMedChem* **2009,** 4, 719-731.
54. Gut, I.; Ojima, I.; Vaclavikova, R.; Simek, P.; Horsky, S.; Linhart, I.; Soucek, P.; Kondrova, E.; Kuznetsova, L. V.; Chen, J. Metabolism of new-generation taxanes in human, pig, minipig and rat liver microsomes. *Xenobiotica* **2006,** 36, 772-792.
55. Marre, F.; Sanderink, G. J.; de Sousa, G.; Gaillard, C.; Martinet, M.; Rahmani, R. Hepatic biotransformation of docetaxel (Taxotere) in vitro: involvement of the CYP3A subfamily in humans. *Cancer Res.* **1996,** 56, 1296-1302.
56. Monsarrat, B.; Mariel, E.; Cros, S.; Gares, M.; Guenard, D.; Gueritte-Voegelein, F.; Wright, M. Taxol metabolism. Isolation and identification of three major metabolites of taxol in rat bile. *Drug Metab. Dispos.* **1990,** 18, 895-901.
57. Kuznetsova, L.; Sun, L.; Chen, J.; Zhao, X.; Seitz, J.; Das, M.; Li, Y.; Veith, J. M.; Pera, P.; Bernacki, R. J.; Xia, S.; Horwitz, S. B.; Ojima, I. Synthesis and Biological Evaluation of Novel 3'-Difluorovinyl Taxoids. *J. Fluor. Chem.* **2012,** 143, 177-188.
58. Voborilova, J.; Nemcoa-Furstova, V.; Neubauerova, J.; Ojima, I.; Zanardi, I.; Gut, I.; Kovar, J. Cell death induced by novel fluorinated taxanes in drug-sensitive and drug-resistant cancer cells. *Invest. New Drugs* **2011,** 29, 411-423.
59. Ojima, I.; Das, M. Recent advances in the chemistry and biology of new generation taxoids. *J. Nat. Prod.* **2009,** 72, 554-565.
60. Ojima, I. Tumor-targeting drug delivery of chemotherapeutic agents. *Pure Appl. Chem.* **2011,** 83, 1685-1698.
61. Seitz, J. D.; Vineberg, J. G.; Wei, L.; Khan, J. F.; Lichtenthal, B.; Feng, C.-F.; Ojima, I. Design, synthesis, and application of fluorine-labeled taxoids as 19F NMR probes for the metabolic stability assessment of tumor-targeted drug delivery systems. *J. Fluor. Chem.* **2014**, Submitted.

62. Mosmann, T. Rapid colorimetric assay for cellular growth and survival: application to proliferation and cytotoxicity assays. *J. Immunol. Methods* **1983,** 65, 55-63.
63. Chen, S.; Zhao, X.; Chen, J.; Kuznetsova, L.; Wong, S. S.; Ojima, I. Mechanism-based tumor-targeting drug delivery system. Validation of efficient vitamin receptor-mediated endocytosis and drug release. *Bioconjug. Chem.* **2010,** 21, 979-987.
64. Li, X.; Barasoain, I.; Matesnz, R.; Diaz, J. F.; Fang, W.-S. Synthesis and biological activities of high affinity taxane-based fluorescent probes. *Bioorg. Med. Chem. Lett.* **2009,** 19, 751-754.
65. Kuznetsova, L. U., I.M.; Pepe, A.; Zanardi, I.; Wu, X.; Ojima, I. Trifluoromethyl- and difluoromethyl-β-lactams as useful building blocks for the synthesis of fluorinated amino acids, dipeptides, and fluoro-taxoids. *J. Fluor. Chem.* **2004,** 125, 487-500.
66. Mangatal, L.; Adeline, M.; Guenard, D.; Gueritte-Voegelein, F.; Potier, P. Application of the vicinal oxyamination reaction with asymmetric induction to the hemisynthesis of Taxol and analogues. *Tetrahedron* **1989,** 45, 4177-4190.

Chapter 3

Site-Specific Prodrug Activation and Self-Immolative Disulfide Linkers

Chapter Contents

§3.1 Introduction

§3.1.1 Targeted Chemotherapy

Traditional chemotherapy uses highly potent cytotoxic agents to kill rapidly dividing cancer cells, relying on the premise these fast-growing cancer cells are more likely to be killed by the drug. However, these traditional chemotherapeutic agents lack cell specificity and kill indiscriminately, affecting normal cells that divide rapidly, such as those in hair follicles, gastrointestinal tract, and bone marrow, leading to undesired and severe side effects (Figure 3.1).[1]

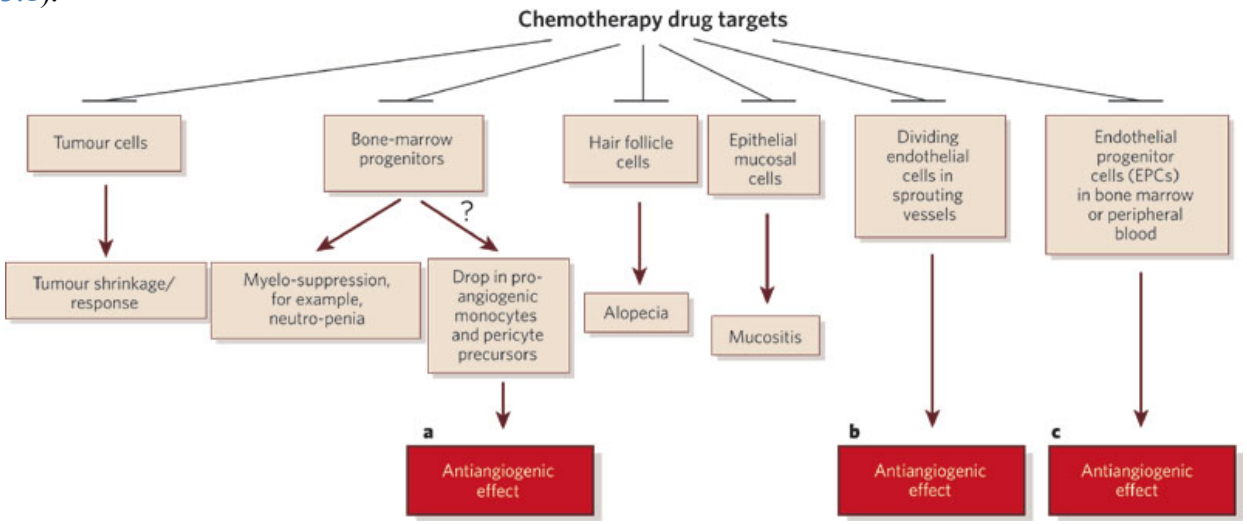

Figure 3.1. Non-specific targeting and severe side effects of traditional chemotherapy. Reprinted from reference [1].

There are two main approaches in targeted chemotherapy: (1) the development of molecularly targeted drugs, specific to abnormal proteins, signaling pathways or other biomarkers that are fundamental to the cancer itself; and (2) the attachment of tumor-targeting modules (TTMs) to highly potent cytotoxic agents. Two recent examples of "molecularly targeted molecules" include: Herceptin® (trastuzumab), a monoclonal antibody that interferes with human epidermal growth factor receptor 2 (HER2), which is amplified/overexpressed in several human cancers, received U.S. FDA approval for treatment of node-positive, HER2-overexpressing breast cancer in 2006 and HER2-overexpressing metastatic gastric or gastroesophageal (GE) junction adenocarcinoma in 2010;[2] Gleevec® (imatinib mesylate), a *BCR-ABL* tyrosine-kinase inhibitor, most notably received U.S. FDA approval for treatment of chronic myelogenous leukemia (CML) in 2001, illustrated in Figure 3.2.[3]

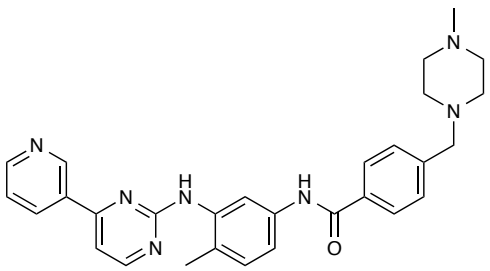

Gleevec® (imatinib)

Figure 3.2. Chemical structure of Gleevec®.

In the latter approach, a tumor-targeting drug delivery system consists of a tumor recognition moiety and cytotoxic agent connected directly or through a suitable linker system to form a drug conjugate.[4] The drug conjugate should be stable during blood circulation and systemically nontoxic; however, upon internalization into the tumor, the active agent should be released within the tumor microenvironment.[4]

§3.2 PUFA-targeted Taxol Prodrugs

§3.2.1 Polyunsaturated Fatty Acids

Lipids, such as fats, oils, and waxes, are categorized into several subgroups including fatty acids, phospholipids, eicosanoids, glycolipids, triacylglycerols, and sterols.[5] While primarily recognized for their role in energy storage, lipids also contribute to structural and signaling roles in cell biology and biochemistry.[5] Polyunsaturated fatty acids (PUFAs), found in deep-water fish (*n*-3 PUFAs) and vegetable oils (*n*-6 PUFAs), are composed of hydrocarbon chains of variable length, with more than one double bond, a methyl group at one end of the chain, and a carboxyl group at the other.[5] PUFAs are utilized in cellular signaling pathways, lipid peroxidation and oxidative stress, fatty acid metabolism, epigenetic regulation, and energy storage.[6-8] Furthermore, PUFA uptake is substantially elevated in malignant tissues.[9] Numerous PUFA-targeted prodrugs, such as DHA-paclitaxel (Taxoprexin®), have been developed by conjugation of PUFAs to cytotoxic agents as an effective method for targeted drug delivery.[9]

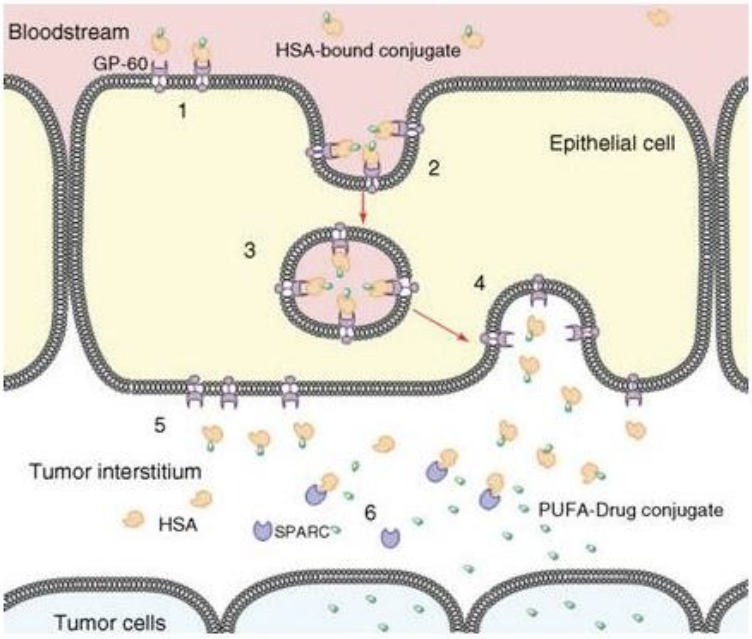

Figure 3.3. Internalization of a PUFA-targeted prodrug by gp60-mediated transcytosis. Reprinted from reference [9].

PUFA-targeted prodrug delivery proceeds through glycoprotein 60 (gp-60) mediated transcytosis (Figure 3.3).[9] The fatty acid component of a PUFA drug conjugate readily binds to human serum albumin (HSA) to form a HSA–drug conjugate complex, which enhances tumor-specific accumulation of the drug, solubilizes the hydrophobic drug conjugate, and lowers the

rate of clearance.[9] Once in the bloodstream, the HSA-complex binds to gp-60 on the tumor epithelial cell surface, upon which ligand binding initiates transcytosis. Vesicles containing protein–drug conjugate complex are transported across the cell, and fusion across the interstitial cell wall occurs; at which point, the HSA–drug conjugate complex is released into the tumor interstitium.[9] Binding of "secreted protein acidic and rich in cysteine" (SPARC) to HSA causes release of the PUFA-targeted prodrug, which permeates into tumor cells.[9]

Once internalized into the tumor interstitium, certain PUFAs and their metabolites affect cellular signaling pathways; for example, cellular growth of MCF-7 breast cancer is inhibited by treatment with omega-3 fatty acids (*n*-3), but not omega-6 fatty acids (*n*-6).[9, 10] Populations that consume significant amounts of *n*-3 PUFAs, such as DHA and LNA, have a lower rate of cancer incidence than populations that have diets rich in *n*-6 PUFAs, like LA and AA.[5, 9] Thus, PUFA-targeted prodrug conjugates may lead not only to accumulation of the cytotoxic agent in the tumor microenvironment, but also synergism between the PUFA-targeting component and the drug.[9]

§3.2.2 DHA-paclitaxel

Doxosahexaenoic acid (DHA) is an omega-3, C22 natural fatty acid with six *cis* double bonds.[11] A constituent of membranes and a precursor for metabolic and biochemical pathways, DHA is found in human milk and is classified as a nutritional additive by the U.S. FDA.[11] Based on its safety profile, DHA contributes little if any additional toxicity to drug conjugates.

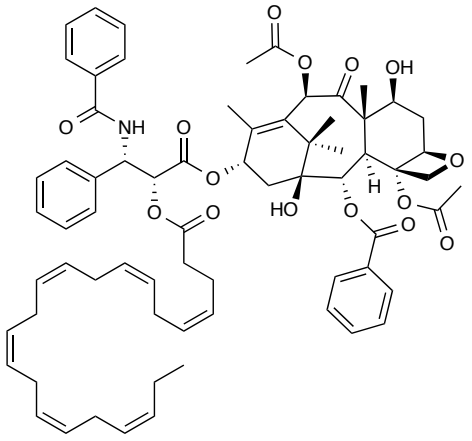

Taxoprexin® (DHA-paclitaxel)

Figure 3.4. Chemical structure of DHA-paclitaxel.

DHA-paclitaxel (Figure 3.4) was synthesized from paclitaxel and DHA in a single step which covalently links DHA to paclitaxel at the C2' hydroxyl position.[11] As shown in previous SAR studies (Section 2.2.4), acylation of the C2' hydroxyl significantly diminishes the *in vitro* bioactivity of paclitaxel and masks its cytotoxicity as a prodrug until the C2'-ester is metabolized.[12] Despite the hydrophobic nature of DHA, the fatty acid conjugate was more soluble than paclitaxel in 10% Cremophor EL/10% ethanol/80% saline.[11] Preclinical studies of DHA-paclitaxel in immune-deficient nude mice demonstrated increased activity relative to paclitaxel and the potential for a superior therapeutic ratio.[13] Phase I clinical studies demonstrated a well defined and manageable side-effect profile at the recommended Phase II dose of 1100 mg/m^2, with a small volume of distribution, long terminal half-life, and slow

system clearance.[13] In Phase II trial, 36 patients with metastatic melanoma were treated, 4 patients had a partial response, and 13 had stabilization of the disease.[13, 14] DHA-paclitaxel entered Phase III clinical trials as Taxoprexin® in 2010 for the treatment of metastatic malignant melanoma.[13]

§3.2.3 PUFA-targeted Next-generation Taxoid Prodrugs

One of the drawbacks of paclitaxel is its lack of efficacy against drug-resistant tumors such as colon, pancreatic, melanoma, and renal cancers, in which MDR is expressed.[15] While DHA-paclitaxel has not demonstrated substrate specificity to Pgp, upon release, paclitaxel will be recognized by the efflux pump and removed from the cell.[15] In contrast, next-generation taxoids have exhibited 2-3 orders of magnitude higher potency than paclitaxel against cancer cells expressing MDR.[15]

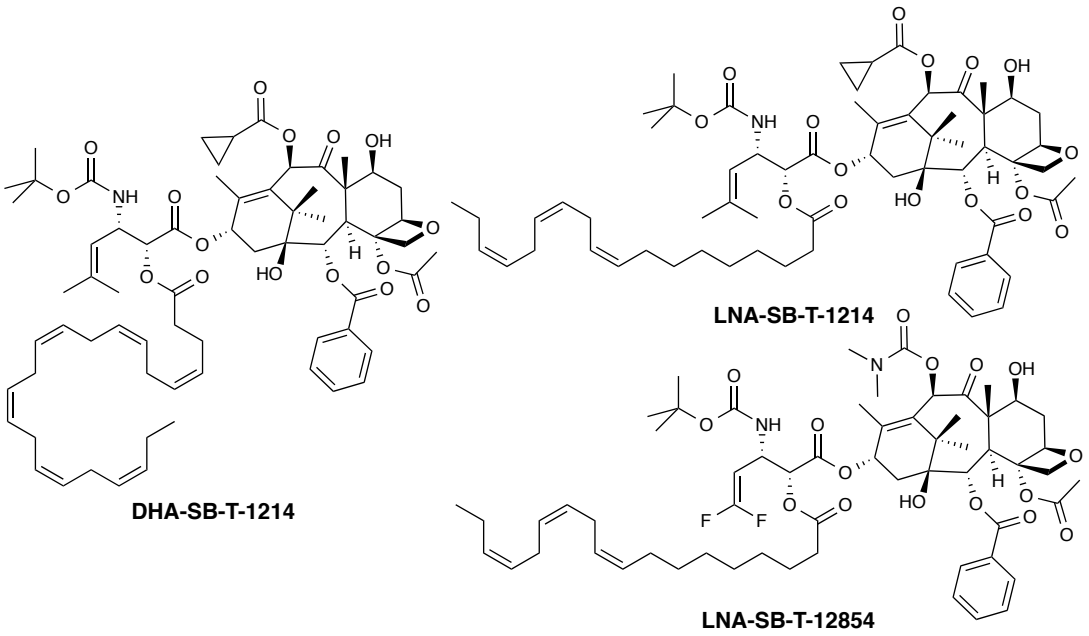

Figure 3.5. Chemical strucutres of DHA-SB-T-1214, LNA-SB-T-1214, LNA-SB-T-12854.

PUFA-targeted taxoid conjugates of docosahexaenoic acid (DHA), linolenic acid (LNA), and linoleic acid (LA) were synthesized and their efficacy assessed in preclinical *in vivo* studies against drug-sensitive human ovarian tumor xenograft (Pgp-) A121 and drug-resistant human colon xenograft (Pgp+) DLD-1.[15] Of these next-generation fatty acid conjugates, DHA–SB-T-1214 achieved complete tumor regression of DLD-1 in five of five mice at 80 mg/kg dose administered on days 5, 8, and 11 (total dose 240 mg/kg; tumor growth delay > 187 days), whereas paclitaxel and DHA–paclitaxel were ineffective against the drug-resistant tumor xenograft (Figure 3.6).[15]

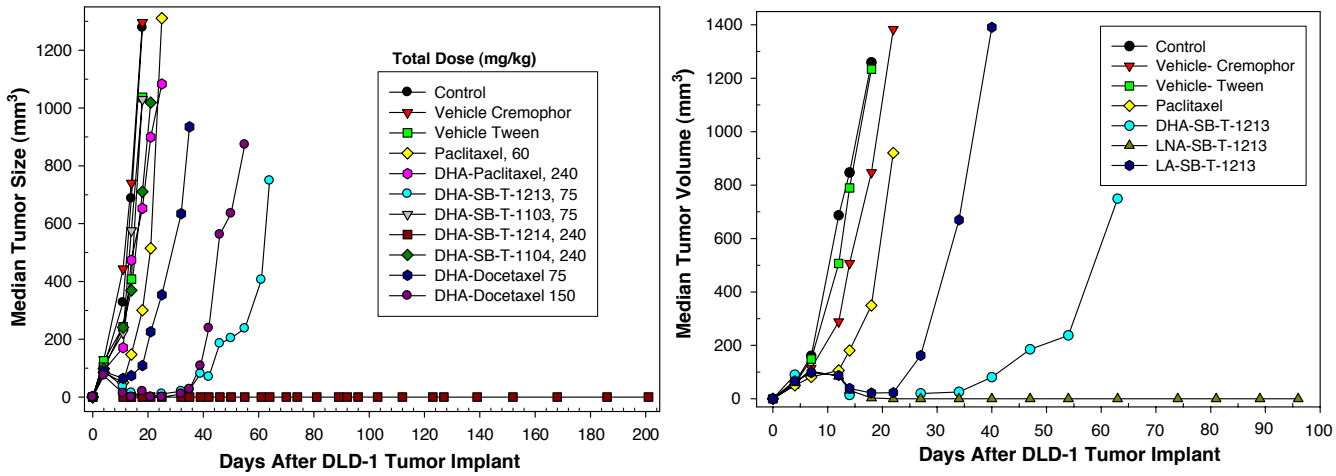

Figure 3.6. Effect of DHA-taxoid conjugates (left) and antitumor effect of PUFA-taxoid conjugates delivered intravenous to SCID mice bearing a Pgp+ human colon tumor xenograft (Pgp+) DLD-1 (right). Adapted from reference [15].

Conjugates of SB-T-1213 with DHA, LNA, and LA were assessed for efficacy against DLD-1 colon tumor xenograft (Figure 3.6).[15] DHA-SB-T-1213 delayed tumor growth for more than 186 days and caused complete tumor regression in all surviving mice (four of five) at 30 mg/kg x 3; LNA-SB-T-1213 delayed tumor growth for more than 109 days and exhibited complete regression in two of five mice; and LA-SB-T-1213 did not demonstrate meaningful efficacy.[15] This study revealed the marked difference between *n*-3 PUFAs (DHA, LNA) and *n*-6 PUFA (LA).[15]

§3.2.4 Synthesis of LNA-targeted Taxoid Prodrugs

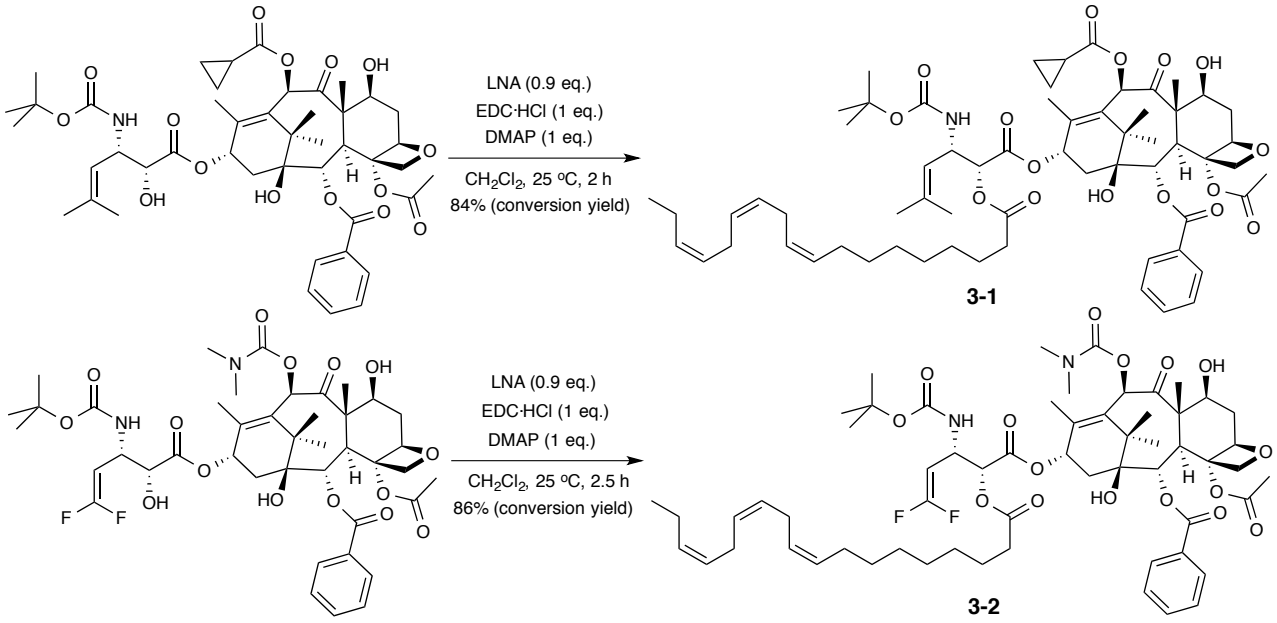

Scheme 3.1. Synthesis of LNA–SB-T-1214 (**3-1**) and LNA–SB-T-12854 (**3-2**).

The syntheses of linolenic (LNA)-targeted taxoid prodrugs of SB-T-1214 and SB-T-12854 were performed *via* coupling of the C2' hydroxyl of the taxoid to the free carboxyl group of the PUFA in the presence of EDC·HCl and DMAP (Scheme 3.1). Conjugates **3-1** (LNA–SB-T-1214) and **3-2** (LNA–SB-T-12854) were obtained in modest yields (47-52%) with high conversion yields (84-86%), and the PUFA-drug conjugates were stored under inert conditions at -20 °C to prevent allylic oxidation.

§3.2.5 Preclinical *In Vivo* Evaluation of LNA-targeted Taxoid Prodrugs

LNA-SB-T-1214 (**3-1**) and LNA-SB-T-12854 (**3-2**) were evaluated *in vivo* in SCID mice bearing MX-1 human breast carcinoma tumor xenografts. The PUFA-taxoid conjugates were formulated with ethanol:Solutol® HS 15 (1:1) in stock solutions at concentrations of 50 mg/mL and diluted with saline to 200 µL total volume. These animal studies were conducted by Jean Rooney and Dr. Thomas Zimmerman at the Division of Laboratory Animal Resources (DLAR) at Stony Brook University and coordinated by Dr. Joshua D. Seitz.

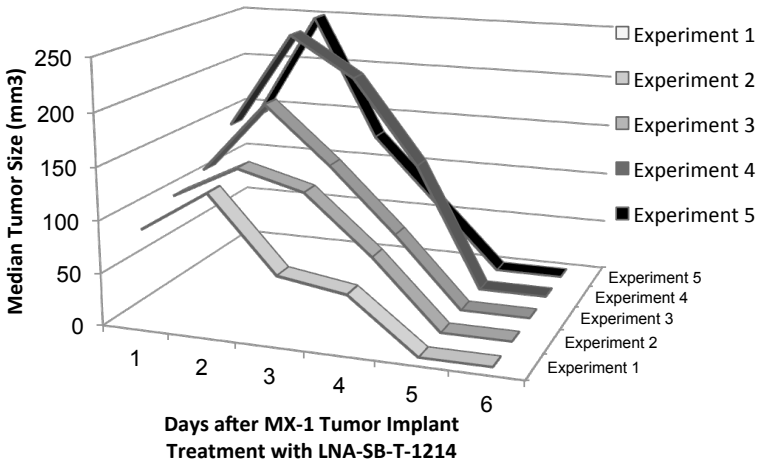

Figure 3.7. Effect of LNA-SB-T-1214 on human breast carcinoma xenograft MX-1. Adapted from reference [16].

LNA-SB-T-1214 (**3-1**) was highly effective against MX-1 tumor xenografts and induced complete tumor regressions in five of five mice, shown in Figure 3.7. In one particular mouse (Experiment 5), treatment with LNA-SB-T-1214 was able to eradicate a tumor that had grown to approximately 250 mm^3 prior to conjugate administration. Paclitaxel was also evaluated as a control, and, though significantly reducing tumor growth, it also demonstrated extremely high toxicity against all mice.

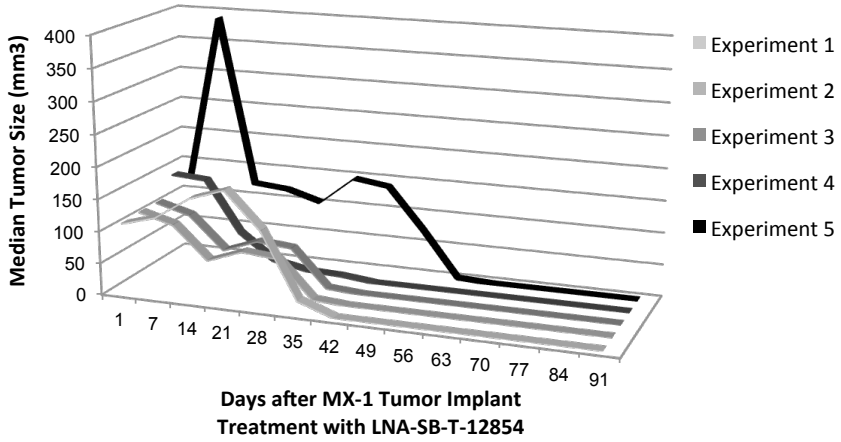

Figure 3.8. Effect of LNA-SB-T-12854 on human breast carcinoma xenograft MX-1. Adapted from reference [16].

LNA-SB-T-12854 (**3-2**) was also evaluated in SCID mice bearing MX-1 tumor xenografts and found to be highly effective, inducing complete tumor regressions in five of five mice (Figure 3.8). The PUFA-fluorotaxoid conjugate was tested against a control, ethanol:Solutol® HS 15 (1:1) vehicle, and SB-T-1214. These animal studies were conducted by Jean Rooney and Dr. Thomas Zimmerman at the Division of Laboratory Animal Resources (DLAR) at Stony Brook University and coordinated by Dr. Joshua D. Seitz.

For mice treated with LNA-SB-T-12854, complete tumor regression was observed in five of five mice, including tumors that had grown to be over 400 mm^3 in median diameter, with survival up to 90 days. Though, despite tumor remission, toxicity was observed for treatment with LNA-SB-T-12854 as all five mice encountered significant weight loss. This increased toxicity may be attributed to the unique pharmacokinetic and metabolic profile of C3'-difluorovinyl taxoids.

§3.3 Mechanism-based Self-immolative Disulfide Linkers

§3.3.1 Linker Systems in Targeted Chemotherapy

Tumor-targeted drug delivery and site-specific prodrug activation have emerged as primary strategies in targeted chemotherapy. Numerous TTMs have been identified and used in drug conjugates to directly transport the cytotoxic agent to cancer cells with target-specificity and high efficiency. While the drug is covalently connected to a TTM–linker system, its activity and toxicity is masked by site-specific prodrug deactivation. Once internalized inside the tumor microenvironment, a chemical change occurs resulting in cleavage of the linker and release of the active agent.[17] At least one chemical bond must be broken during prodrug activation. This linker bond should be stable in the bloodstream and healthy tissue in order to avert premature linker cleavage.[17] Furthermore, at the tumor site, a rapid and irreversible cleavage of the linker-bond must take place, releasing the drug efficiently in its active form.[17]

Direct linkages may be too labile and prone to hydrolysis, in the case of ester bonds, or too stable, such as amides or ethers.[17] More complex linker structures employ crosslinkers or spacers to act as a bridge gap between drugs and tumor-targeting modules, which may or may not bear orthogonal functional groups. Without the introduction of a specific cleavage point, these crosslinkers display the same disadvantages as their basic counterparts. Thus, an additional structural unit, termed a trigger, allows for tumor-specific cleavable moieties to be introduced

into drug conjugates. Various triggers have been characterized and employed, including proteolytically cleavable peptides, disulfides for reductive cleavage, or acid-sensitive hydrazone groups.[17]

§3.3.2 Self-Immolative Disulfide Linkers

The tumor microenvironment is characterized by unique biochemical and pathophysiological properties: upregulation of certain proteases, such as cathepsins or MMPs, acidic pH in tumor tissue and in endosomes and lysosomes, and a higher intracellular concentration of reducing agents such as glutathione and thioredoxin.[17] These cancer-specific properties can be exploited as "triggers" by incorporation of a chemical bond labile only in the presence of these unique environments.[17]

Self-immolative linkers (SILs) function as both a spacer between the drug and tumor-targeting module and a point of cleavage for prodrug release. Three criteria exist for the classification of SILs: (1) drug-linker bond must remain stable under most physiological conditions; (2) the trigger-linker bond must remain stable, except under conditions unique to the tumor microenvironment where drug release is intended to take place; 3) following breakage of the trigger-linker bond, a chemical process leads to rapid and irreversible cleavage of the drug-linker bond.[17] Cyclization strategies for cleavage often rely on the formation of five- and six-membered lactones, lactams, ureas, or carbamates, energetically favorable processes.[4]

Disulfide bonds have attracted much attention as crosslinkers due to their stability normal physiological conditions and strong reducing environment within the tumor microenvironment. Glutathione, an intracellular reducing agent, was found at a concentration 1,000 times greater in tumors than in blood plasma.[4, 18] This gradient provides a natural trigger for disulfide linker cleavage in disulfide-linker containing drug-conjugates.

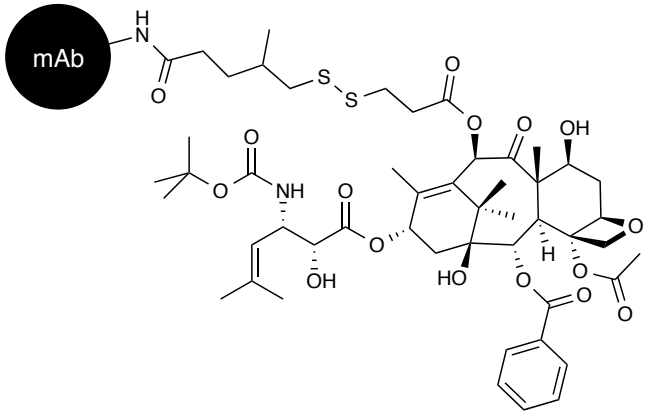

Figure 3.9. Chemical structure of mAb-12136.

First-generation self-immolative disulfide linkers, based on an alkyl disulfide moiety, were employed in monoclonal antibody–drug conjugates, in which a self-immolative disulfide linker was connected to a second-generation taxoid with modified sulfhydrylalkanoyl group at the C10 hydroxyl and murine monoclonal antibody (mAb) directed against human epidermal growth factor hormone (EGFR).[19] This mAb–SB-T-12136 immunoconjugate (Figure 3.9) showed remarkable antitumor activity against human squamous cancer xenografts in SCID

mice.[20] However, in this first-generation design, the original taxoid molecule was not released because of the compromised modification at the C10 position.[4]

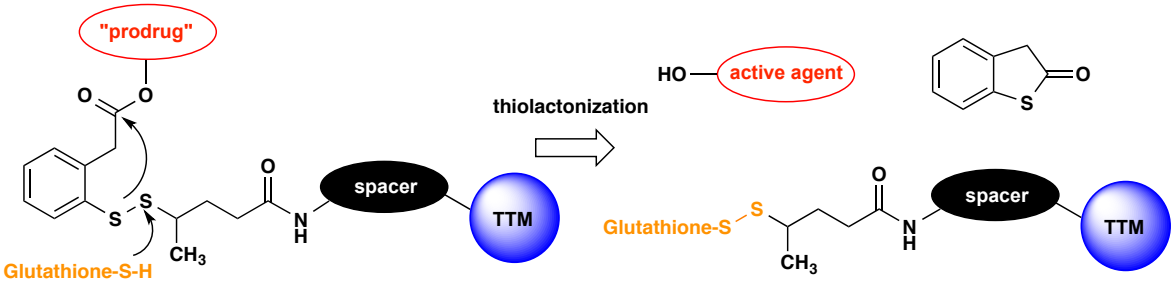

Figure 3.10. Glutathione-triggered thiolactonization of second-generation self-immolative disulfide linkers. Adapted from reference [4].

Second-generation mechanism-based disulfide linkers, which can be connected to various cytotoxic agents as well as targeting moieities, allow for facile and efficient release of the active agent in its desired form. Similarly, these bifunctional linkers are designed to remain stable during circulation but readily cleave inside the tumor microenvironment.[4] The linker disulfide bond is readily cleaved by endogenous thiols such as thioredoxin or glutathione (GSH), the concentration of which ranges from 1-2 μM in circulating human blood plasma but 2-8 mM in tumor tissues,[18, 21] allowing for facile and efficient drug release inside tumor cells. The strategic design of placing a phenyl group proximal to the disulfide bond leads to a cascade process in which the nucleophilic attack of these thiols on the disulfide moiety results in the process of thiolactonization and drug release. In this second-generation linker design, methyl and dimethyl substituents were included proximal to the disulfide bond to lengthen its circulation half-life.

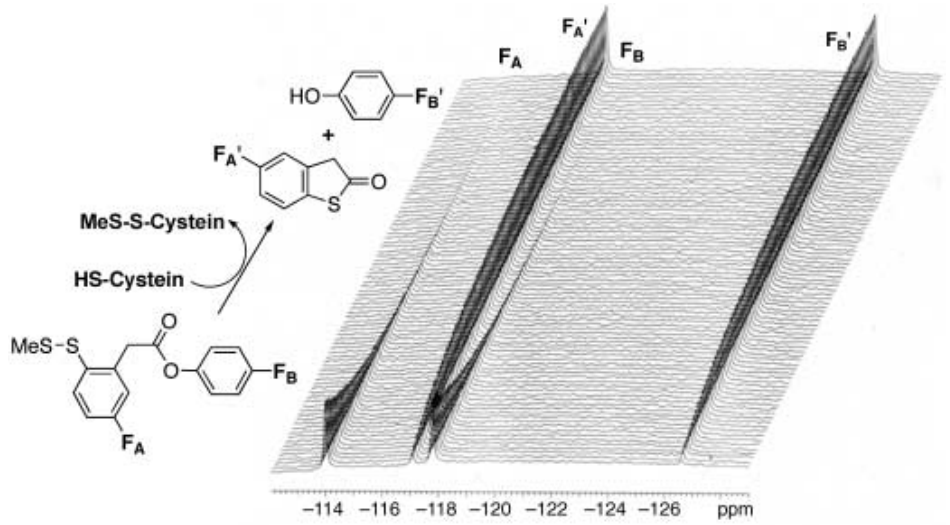

Figure 3.11. A model system for the mechanism-based drug release using cysteine as the trigger for thiolactonization. Reprinted from reference [22].

A model system to validate the glutathione-triggered disulfide cleavage was developed using ^{19}F NMR.[22] The absence of fluorine-19 in biorelevant molecules and media allows for direct observation and monitoring of fluorinated compounds. Strategic incorporation of fluorine at the *para*-position on the disulfide linker directs disulfide cleavage by an endogenous thiol,

such as cysteine, to generate the thiophenolate intermediate prior to thiolactonization.[22] This process of thiolactonization was validated by time-resolved ^{19}F NMR in a model system in which two distinct fluorine signals were monitored for changes in chemical shifts (Figure 3.11).

§3.3.3 Synthesis of 4C-chain Methyl-Branched Disulfide Linker

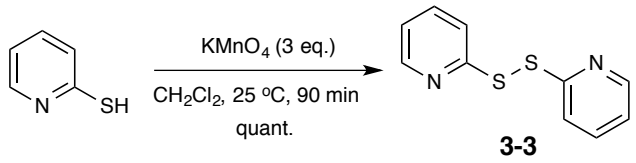

Scheme 3.2. Oxidation of pyridine-2-thol with potassium permanganate.

Synthesis of the 4-carbon chain methyl-branched disulfide linker (Me-SS-Linker) began with the preparation of two thiol-disulfide exchange intermediates: (1) first, with pyridinyldisulfanylpyridine, (2) then followed by sulfhydrylphenyl acetic acid. Oxidation of pyridine-2-thiol with potassium permanganate gave **3-3**, the first exchange intermediate, in quantitative yield (Scheme 3.2).

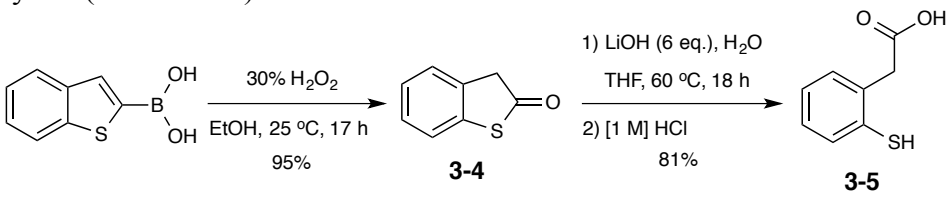

Scheme 3.3. Synthesis of 2-sulfhydrylphenyl acetic acid (**3-5**).

Oxidation of 2-benzothienylboronic acid with hydrogen peroxide gave the corresponding thiolactone **3-4** in excellent yield (95%), which was hydrolyzed under basic conditions, followed by an acid-base workup to afford **3-5** in good yield (81%), shown in Scheme 3.3. Sulfhydrylphenyl acetic acid must be stored under inert conditions at or below -20 °C to avoid degradation.

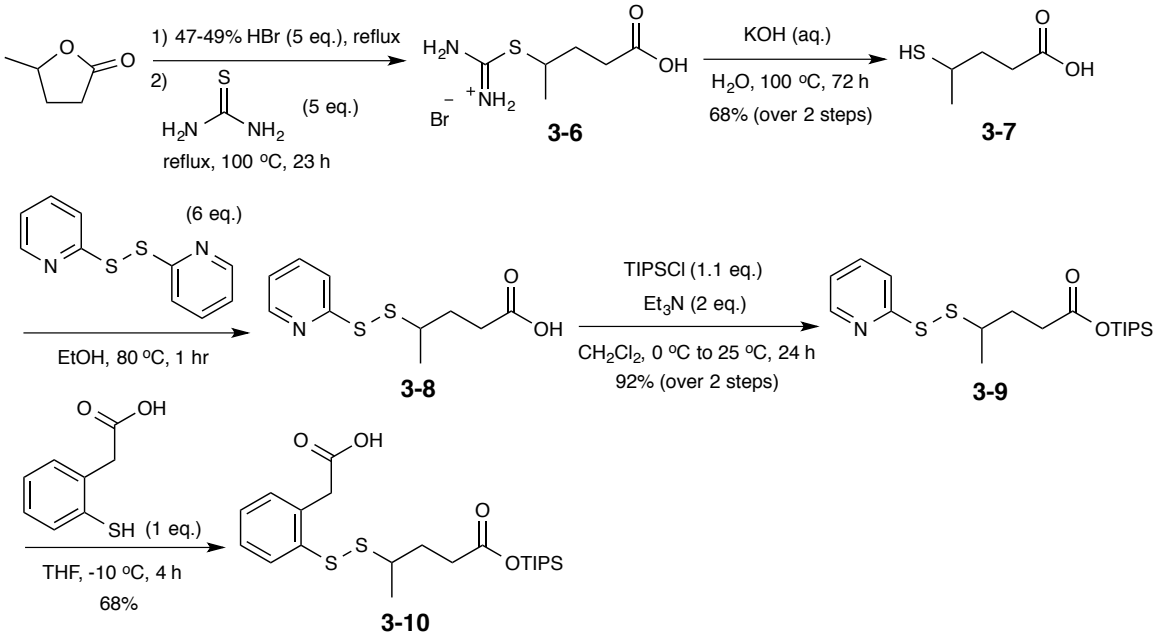

Scheme 3.4. Synthesis of methyl-branched disulfide linker (Me-SS-Linker) (**3-10**).

Synthesis of methyl-branched 4C-chain linker **3-10** was carried out in five steps (Scheme 3.4). Nucleophilic acid-catalyzed ring opening substitution of γ-valerolactone with thiourea gave salt **3-6**, which underwent basic hydrolysis to give **3-7** in modest yield (68% over 2 steps). The free thiol of **3-7** was subjected to disulfide exchange with excess **3-3** to afford **3-8**, which was protected with TIPS to give **3-9** in excellent yield (92% over 2 steps). Remaining **3-3** was removed by trituration with hexanes prior to chromatography. The second thiol-disulfide exchange between **3-5** and **3-9** gave metastable linker **3-10** in good yield (68%). Temperature must be kept at -10 °C lest the intrinsic acidity of the carboxylic acid deprotect the TIPS group. Linker **3-10** must be stored under inert conditions at or below -20 °C and should be used promptly to avoid decomposition.

§3.3.4 Synthesis SB-T-1214–(Me-SS-Linker)-Construct

The free acid of the four-carbon chain methyl-branched disulfide linker **3-10** was coupled to the C2' hydroxyl group of SB-T-1214 in the presence of EDC·HCl and DMAP to give **3-11** in good yield (77%), shown in Scheme 3.5. Reaction progress was closely monitored by TLC to minimize di-substitution at the C7 hydroxyl group. When DIC was used as the coupling reagent, the diisoproylurea byproduct was removed by filtration with diethyl ether. Alternatively, EDC·HCl may be used as the coupling reagent, though the rate of reaction is slower.

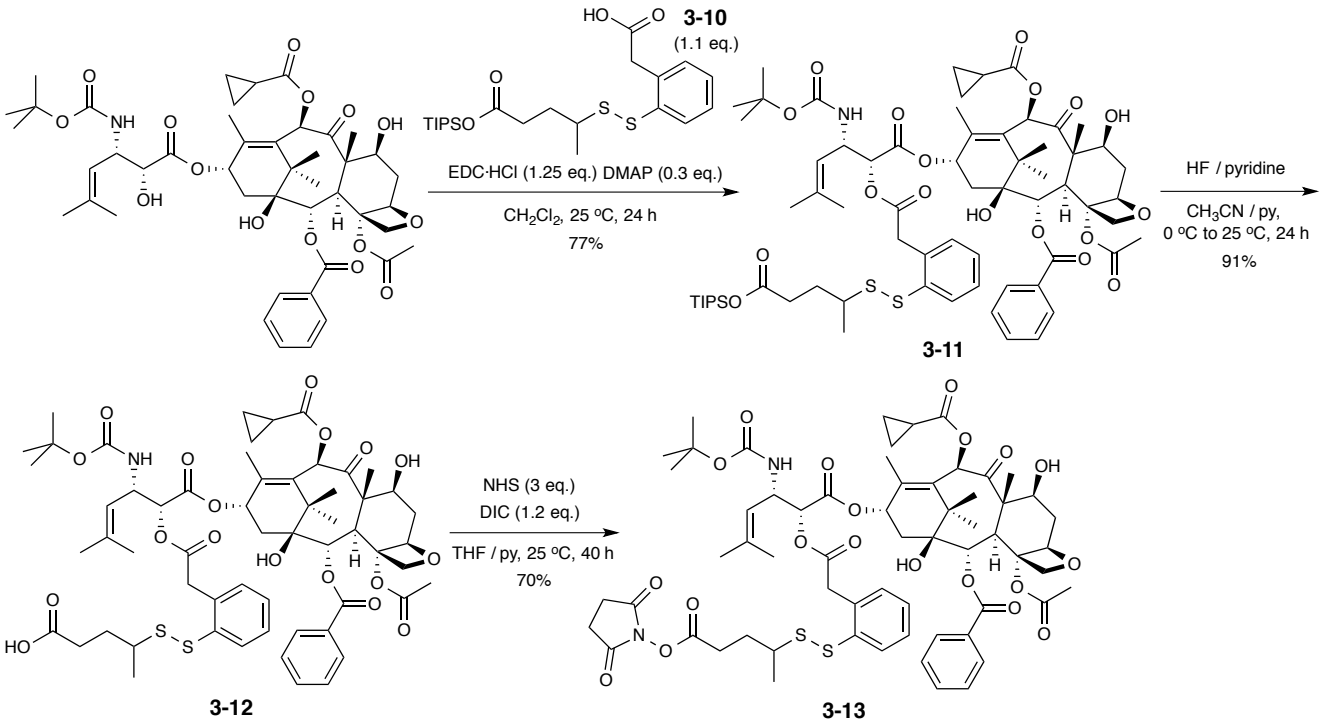

Scheme 3.5. Synthesis of SB-T-1214-(Me-SS-Linker)-OSu (**3-13**).

Deprotection of the silyl group of **3-11** in the presence of HF-pyridine gave **3-12** in excellent yield (91%), and the free carboxylic acid of **3-12** was activated with *N*-hydroxysuccinimide in the presence of DIC to afford **3-13** in good yield (70%). Purification by

column chromatography gave the activated drug–linker in sufficient purity for subsequent reactions.

§3.3.5 Synthesis of 4C-chain *gem*-Dimethyl-branched Disulfide Linker

Preparation of the four-carbon chain *gem*-dimethyl-branched disulfide linker **3-20** follows a similar synthetic path as that of the methyl-branched linker: (1) synthesis of the parent propanic acid chain, followed by two subsequent thiol-disulfide exchanges.

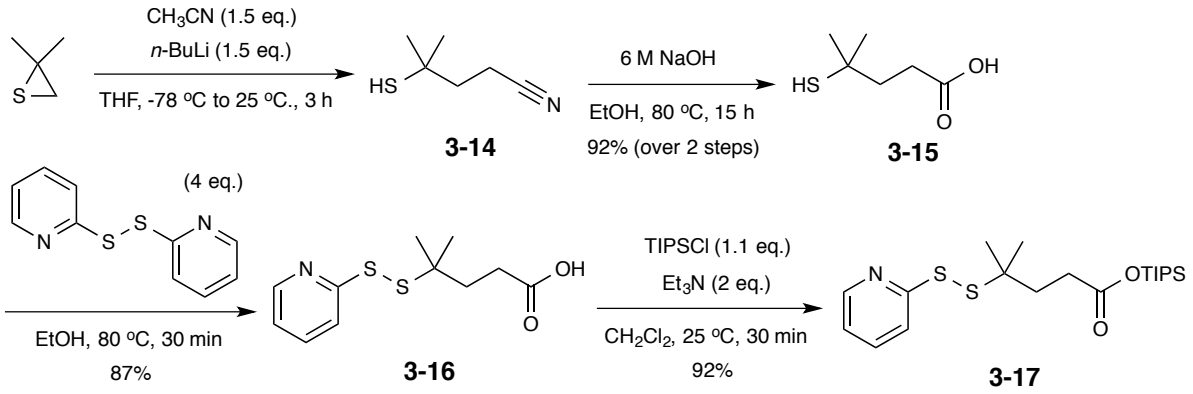

Scheme 3.6. Synthesis of Me_2-SS-Linker intermediate **3-17**.

Stoichiometric acetonitrile was converted *in situ* to the lithiated acetonitrile salt in the presence of *n*-BuLi at -78 °C; lithiated acetonitrile nucleophilically opens three-membered heterocycle isobutylene sulfide to give crude **3-14**, which was isolated through acid-base workup. Nitrile **3-14** was hydrolyzed under basic conditions to give the corresponding carboxylic acid **3-15** in excellent yield (92% over 2 steps), and the corresponding thiol **3-15** was subjected to a thiol-disulfide exchange with excess **3-3** to give **3-16** in high yield (87%). Protection of the carboxylic acid of **3-16** with TIPS gave **3-17** in excellent yield (92%), shown in Scheme 3.6.

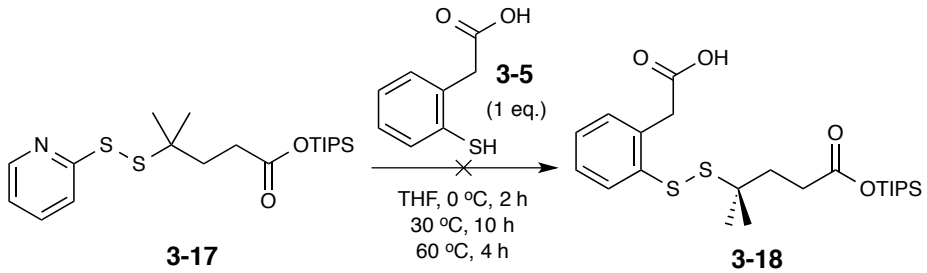

Scheme 3.7. First attempt at synthesis of *gem*-dimethyl-branched disulfide linker (**3-18**).

However, the subsequent thiol-disulfide exchange with **3-5** did not proceed at 0 or 30 °C (Scheme 3.7), according to TLC and mass spectrometry. At 60 °C, the reaction appeared to proceed, though while mass spectrometry indicated a single mass, ^{1}H NMR revealed that two compounds were present. This may be attributed to a transfer of the TIPS group to the free acid or the presence of rotamers. Thus, an alternative synthetic route was explored.

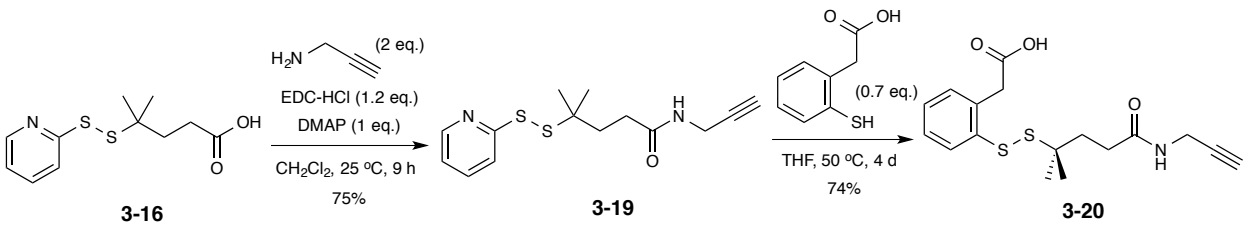

Scheme 3.8. Second attempt at synthesis of *gem*-dimethyl-branched disulfide linker (**3-20**).

The second attempt involved direct coupling of propargylamine with the free carboxylic acid of **3-16** in the presence of EDC·HCl and DMAP to give **3-19** in good yield (75%). The functionalized amide serves as an orthogonal protecting group; though, unlike TIPS, the amide remains stable during the second disulfide exchange in the presence of heat. The subsequent thiol-disulfide exchange between **3-5** and **3-19** gave **3-20** in good yield (74%), however reaction progress was slow over four days at 50 °C. Reaction optimization is currently in progress, however this synthetic route appears to be a viable alternative for preparation of *gem*-dimethyl-branched disulfide linker. The synthesis of **3-20** is illustrated in Scheme 3.8.

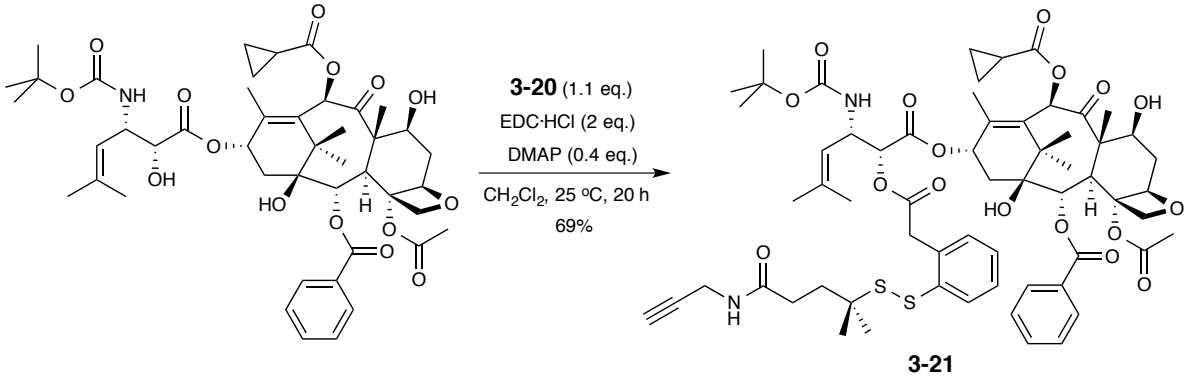

Scheme 3.9. Synthesis of SB-T-1214–(Me_2-SS-Linker)-Alkyne (**3-21**).

The free acid of the four-carbon chain *gem*-dimethyl-branched disulfide linker **3-20** was coupled to the C2' hydroxyl group of SB-T-1214 in the presence of EDC·HCl and DMAP to give **3-21** in good yield (69%), shown in Scheme 3.9.

§3.4 Drug Release and Linker Studies

§3.4.1. Rational Design: ^{19}F NMR Probe

Fluorine-19 nuclear magnetic resonance (NMR) spectroscopy allows for direct observation of fluorinated compounds and their metabolites in biological systems without background signal from the tissue or medium due to the absence of fluorine in living systems.[23] Furthermore, fluorine-19 has a natural abundance of 100% and has a sensitivity to NMR detection that is 83% that of the sensitivity of ^{1}H, allowing for a strong NMR signal with negligible background noise.[24] Recently, the "three fluorine atoms for biochemical screening" (3-FABS) technique has emerged as a useful biochemical tool with heightened sensitivity by labeling a substrate with a CF_3 moiety and using ^{19}F NMR spectroscopy for subsequent analysis of biochemical or enzymatic processes.[25-28]

Previously, our laboratory designed BLT-F_2, shown in Figure 3.12, as a ^{19}F NMR probe for the metabolic stability assessment of tumor-targeted drug delivery systems. BLT-F_2 consists of biotin as the tumor-targeting moiety, next-generation fluorotaxoid SB-T-12145 with site specific incorporation of fluorine at the *meta* position of the C2 benzoate moiety, and a self-immolative disulfide linker.[28] Another fluorine was introduced to the 4-position of the linker ring, i.e. *para* to the disulfide moiety. Time-resolved ^{19}F NMR analysis of BLT-F_2 revealed a stepwise mechanism for release of the fluorotaxoid, generating the anticipated thiolate intermediate (**3-A**) as a detectable and transient species, as well as indicated a profound effect of the fluorine *para* to the disulfide group on the rate of linker cleavage and thiolactonization (Figure 3.12). Additionally, the use of excipient (Solutol HS 15) in formulation of BLT-F_2 was shown to drastically slow down the rate of linker cleavage. The synthesis and corresponding ^{19}F NMR experiments using BLT-F_2 were performed by co-worker Dr. Joshua D. Seitz.

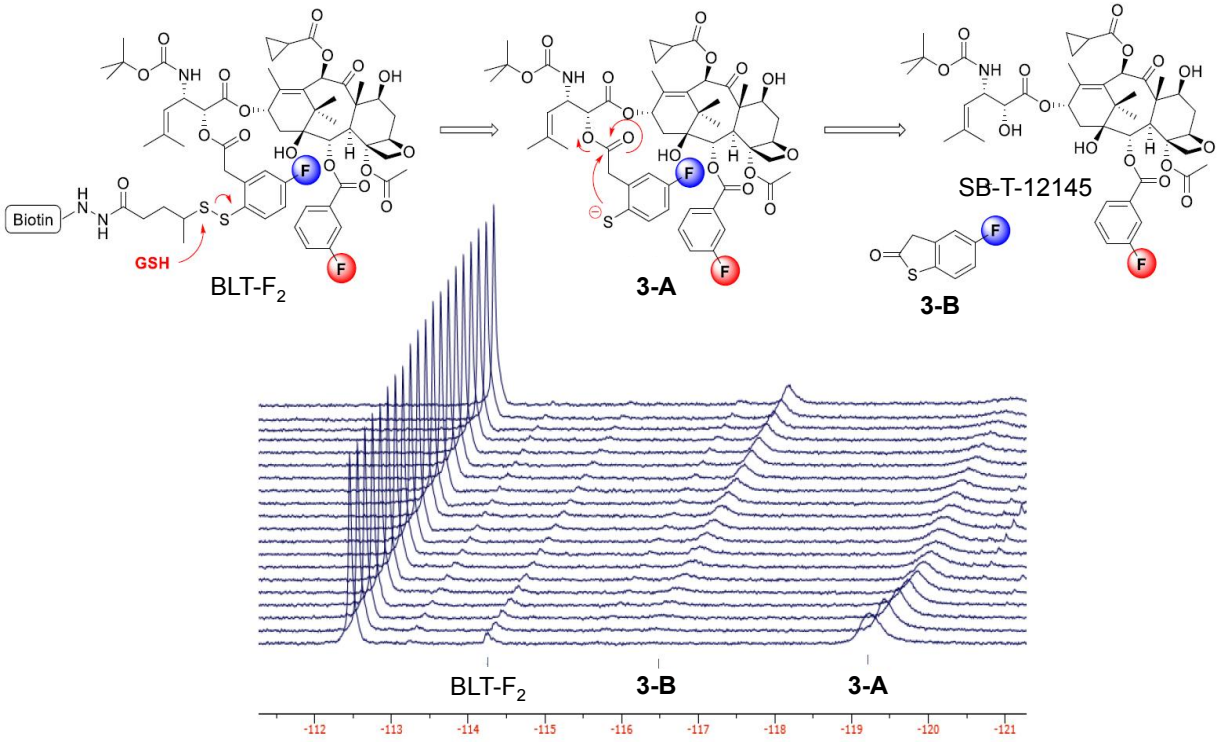

Figure 3.12. Time-resolved ^{19}F NMR spectra for the disulfide linker cleavage and thiolactonization process of BLT-F_2 (2.5 mM) in 30% DMSO in D_2O beginning at 1 h after the addition of 6 equivalents of GSH at 25 °C with 15 min intervals (128 scans/spectrum) (Performed by Dr. Joshua Seitz). Reprinted from reference [28].

However, attempts to use BLT-F_2 in cell culture medium or blood plasma were hampered by its poor solubility in aqueous media and low signal intensity of the probe. Thus, BLT-S-F_6 (**3-24**) was designed as a more sensitive ^{19}F NMR probe using 3-FABS with higher solubility using polyethylene glycol oligomers in aqueous media than BLT-F_2.

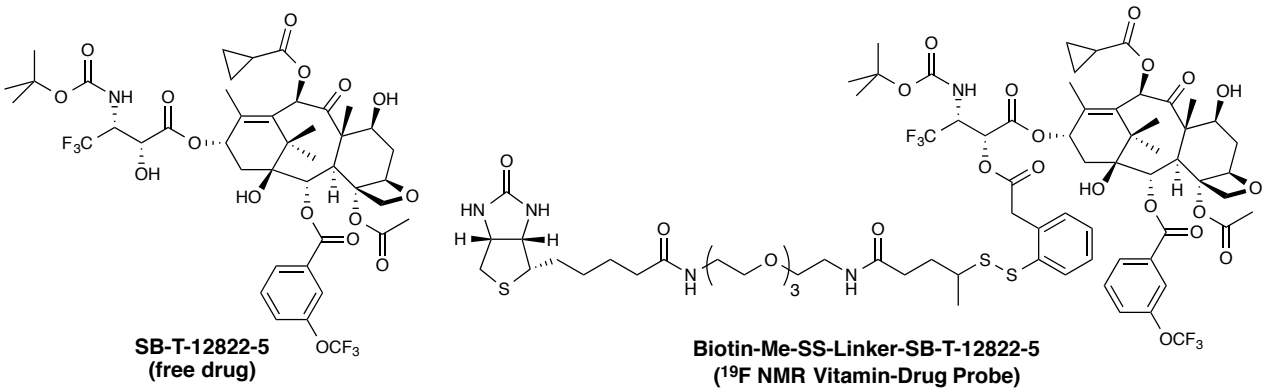

Figure 3.13. Third-generation fluorotaxoid SB-T-12822-5 (**2-36**) (left) and BLT-S-F_6 (**3-23**) (right), as chemical probe for ^{19}F NMR. Adapted from reference [28].

Upon conjugation to a vitamin-linker system at the C2' hydroxyl (Figure 3.13), the C3'-trifluoromethyl moiety undergoes a chemical shift of approximately 0.3 ppm in $CDCl_3$, from -73.40 ppm (free drug) to -73.11 ppm (prodrug), shown in Figure 3.14. The C2-*m*-OCF_3 substituent was included as an internal reference for ^{19}F NMR study. Trifluoromethyl groups, using 3-FABS, rather than single-fluorine substituents, allow for the use of lower concentrations by providing an enhanced signal and peak sensitivity.

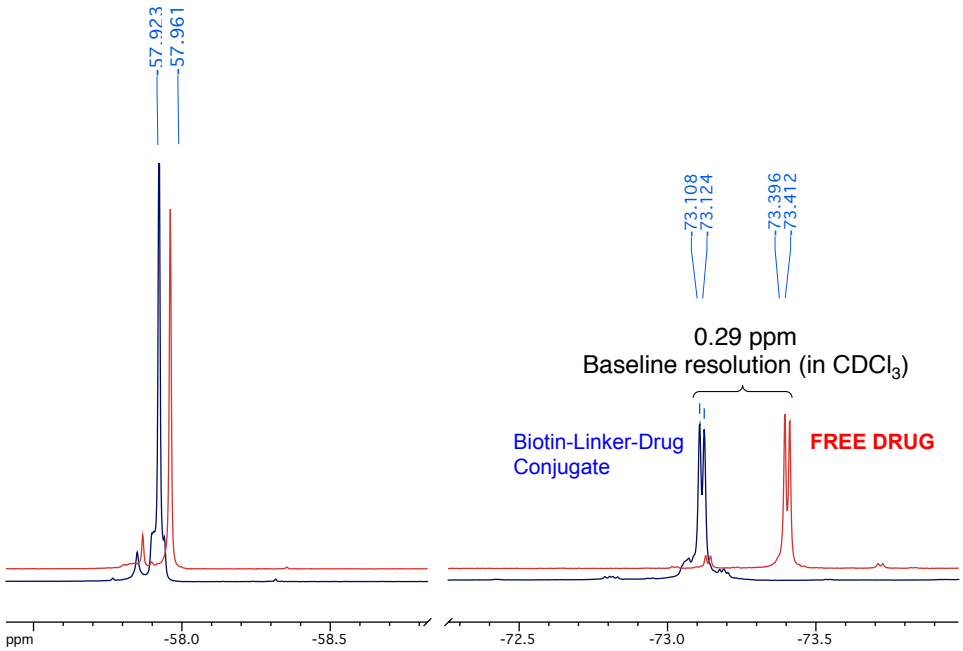

Figure 3.14. ^{19}F NMR Spectrum of SB-T-12822-5 (**2-36**) and BLT-S-F_6 (**3-23**), showing a 0.29 ppm chemical shift upon conjugation to C2' in $CDCl_3$. Reprinted from reference [28].

§3.4.2 Synthesis of ^{19}F NMR Probe: BLT-S-F$_6$

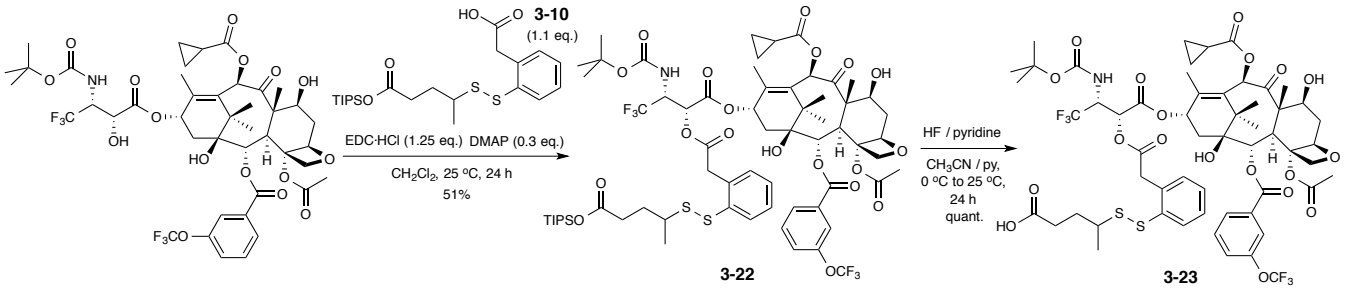

Scheme 3.10. Synthesis of SB-T-12822-5–(Me-SS-Linker)-COOH (**3-22**).

Similar to the synthesis of **3-12,** the free acid of linker **3-10** was coupled to the C2' hydroxyl of SB-T-12822-5 in the presence of EDC·HCl and DMAP to give **3-22** in modest yield (51%), and the TIPS group was efficiently removed with HF-pyridine to afford **3-23** in quantitative yield, shown in Scheme 3.10. Interestingly, both ^{1}H and ^{19}F NMR spectra for **3-23** indicated the presence of conformational isomers, indicated by two sets of analogous peaks at certain positions, such as C10, C3'-CF_3, and C2-*m*-OCF_3. This duplicate set was observed for the free acid **3-12** as well, but not in the subsequent steps of amidation or esterification.

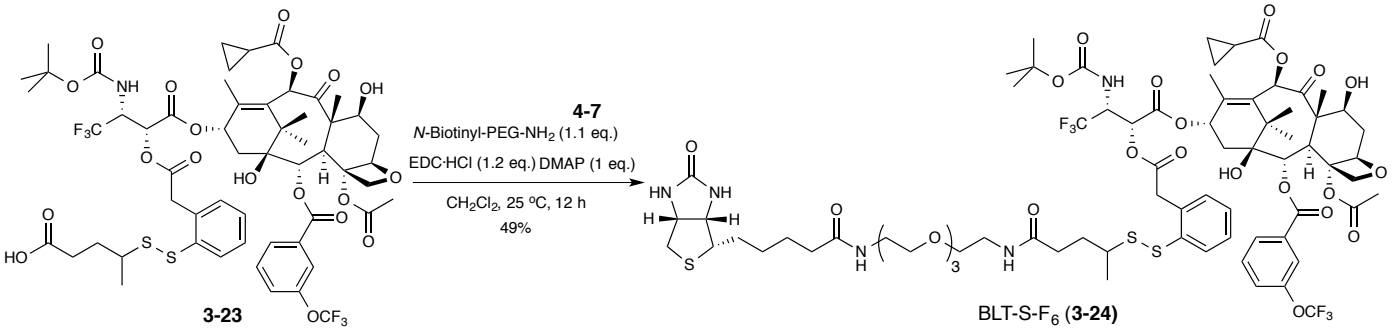

Scheme 3.11. Synthesis of Biotin-(Me-SS-Linker)-SB-T-12822-5 (BLT-S-F_6) (**3-24**).

The free terminal acid of prodrug **3-22** was coupled to *N*-biotinyl-PEG-NH_2 (**4-7**) in the presence of EDC·HCl and DMAP to afford **3-24** in modest yield (49%), shown in Scheme 3.11 Discussions on the use of vitamins, such as biotin, as a tumor-targeting module in targeted chemotherapy, as well as the synthesis of **4-7** are included in Chapter 4.

§3.4.3 Effects of Solvent Systems and Drug Formulations on the ^{19}F NMR Chemical Shifts of the Fluorine Signals at the 3'-Position of BLT-S-F$_6$ (3-24) and SB-T-12822-5 (2-36).

The C3'-CF_3 and C2-*m*-OCF_3 groups of BLT-S-F_6 (**3-24**) and released taxoid SB-T-12822-5 (**2-36**) were used as quantitative reporter signals for ^{19}F NMR to determine the effects of solvent systems and drug formulations on their chemical shifts. The changes in ^{19}F NMR chemical shifts were measured on a 400 MHz NMR spectrometer in various solvent and formulation systems.

Table 3.1. ^{19}F NMR chemical shifts (ppm) of BLT-S-F$_6$ (3-24) in various formulations. Adapted from reference [28].

Entry	Formulation	Ratio	*m*-OCF_3 **2-36**	*m*-OCF_3 **3-24**	|Δ *m*-OCF_3|	CF_3 **2-36**	CF_3 **3-24**	|Δ CF_3|
1	$CDCl_3$	100	-57.961	-57.923	0.038	-73.404	-73.116	0.288
2	blood plasma:D_2O: EtOH:polysorbate 80	84:10:4:2	-58.074	-58.074	0	-72.838	-72.048	0.210
3	RPMI-1640:D_2O: EtOH:polysorbate 80	84:10:4:2	-57.906	-57.906	0	-72.705	-72.911	0.206
4	D_2O:EtOH:polysorbate 80	94:4:2	-57.888	-57.888	0	-72.702	-72.889	0.187
5	saline:EtOH:D_2O	50:40:10	-58.419	-58.436	0.017	-73.342	-73.412	0.070
6	PBS:EtOH:D_2O	50:40:10	-58.413	-58.431	0.018	-73.339	-73.404	0.065
7	DMSO:D_2O	70:30	-56.459	-56.431	0.028	-71.115	-71.068	0.047
8	D_2O:EtOH	60:40	-58.417	-58.436	0.019	-73.361	-73.407	0.046
9	D_2O:solutol HS15:EtOH	84:8:8	-58.047	-58.047	0	-72.910	-72.910	0

Samples of BLT-S-F$_6$ (**3-24**) and fluorotaxoid SB-T-12822-5 (**2-36**) were prepared in various biologically relevant aqueous media with or without excipient, and the ^{19}F NMR chemical shifts were recorded. The results are provided in Table 3.1. The largest difference in chemical shifts of the C3'-CF_3 signals of BLT-S-F$_6$ (**3-24**) and free taxoid SB-T-12822-5 (**2-36**) was observed when 2% polysorbate 80 (Tween® 80) was used as a surfactant in formulation (Entries 2–4), with as large as 0.21 ppm difference with baseline resolution in blood plasma solution (Entry 2). However, in contrast, no appreciable change was Solutol HS 15 was used as an excipient (Entry 9). These results showed that different excipients in formulation affect the microenvironment of BLT-S-F$_6$.

In the absence of excipient, the ^{19}F NMR chemical shift differences between the C3'-CF_3 groups of BLT-S-F$_6$ (**3-24**) and free taxoid SB-T-12822-5 (**2-36**) in solutions of either saline or PBS in ethanol and D_2O were 0.065–0.070 ppm (Entries 5 and 6) and in aqueous DMSO or ethanol solutions were 0.046–0.047 (Entries 7 and 8). For the C2-*m*-OCF_3 signals, no chemical shift was observed in the presence of excipient, either polysorbate 80 or Solutol HS 15; though, in the absence of excipient, small changes were detected ranging from 0.02–0.04 ppm.

§3.4.4 Assessment of Stability and Reactivity of BLT-S-F$_6$ in Blood Plasma by ^{19}F NMR

The stability and reactivity of BLT-S-F$_6$ (**3-24**) in 86% human blood plasma, 10% D_2O, 2% ethanol, and 2% polysorbate 80 at 37 °C was evaluated by ^{19}F NMR using the C3'-CF_3 signals of BLT-S-F$_6$ (**3-24**) and released SB-T-12822-5 (**2-36**) as reporter signals. In these conditions, BLT-S-F$_6$ (**3-24**) remained quite stable with less than 10% release of the fluorotaxoid via disulfide linker cleavage and thiolactonization for 48 h at 37 °C, shown in Figure 3.15. This result implies that the theoretical half-life of BLT-S-F$_6$ and other similar TTDDSs containing this methyl-branched self-immolative disulfide linker under these conditions would be on the order of weeks in human blood plasma.

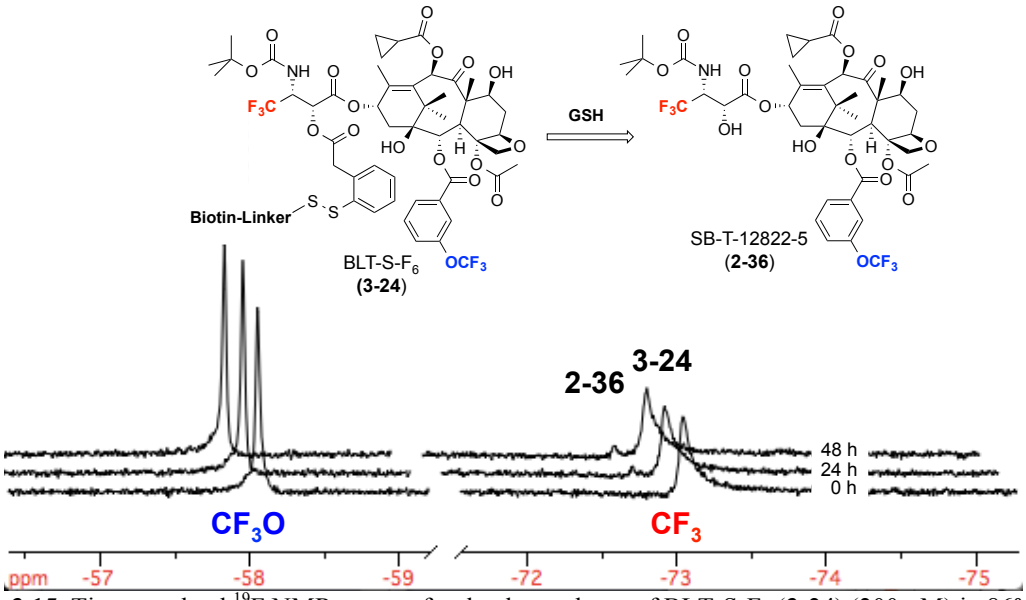

Figure 3.15. Time-resolved ^{19}F NMR spectra for the drug release of BLT-S-F_6 (**3-24**) (200 μM) in 86% blood plasma, 10% D_2O, 2% ethanol, and 2% polysorbate 80 at 37 °C without supplemental GSH at 0, 24, and 48 h (2048 scans/spectrum). The signals of 2-*m*-OCF_3 (*left*) and 3'-CF_3 (*right*) for BLT-S-F_6 (**3-24**) and free taxoid SB-T-12822-5 (**2-36**) are shown, which indicates minimal drug release after 48 h. Reprinted from reference [28].

As a control study, 100 equivalents of supplemental GSH (20 mM) were added to BLT-S-F_6 in the same formulation (86% blood plasma, 10% D_2O, 2% ethanol, 2% polysorbate 80), and the reaction of disulfide cleavage was monitored by ^{19}F NMR with one-hour intervals. Greater than 98% of the C3'-CF_3 signal for BLT-S-F_6 (**3-24**) disappeared and the corresponding signal for the released taxoid appeared within 10 hours at 37 °C, shown in Figure 3.16. As anticipated, there was no observable change in chemical shift in the C2-*m*-OCF_3 signal.

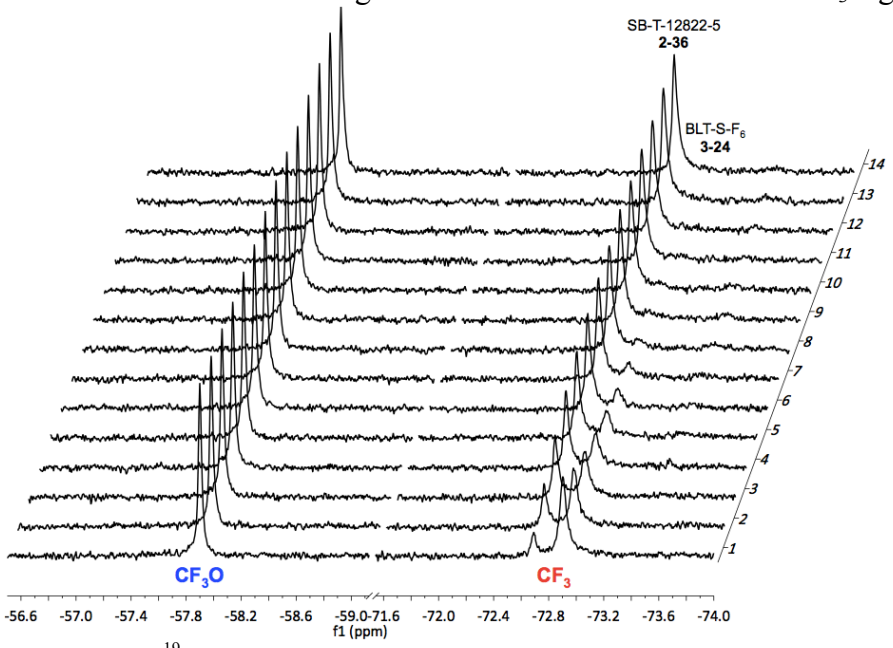

Figure 3.16. Time-resolved ^{19}F NMR spectra for the drug release of BLT-S-F_6 (**3-24**) (200 μM) in 86% blood plasma, 10% D_2O, 2% ethanol, and 2% polysorbate 80 at 30 min after the addition of 100 equivalents of GSH at 37 °C with 1 h intervals (1024 scans/spectrum) for 13 h. The signals of 2-*m*-OCF_3 (*left*) and 3'-CF_3 (*right*) are shown, which indicate complete drug release after 13.5 h. Reprinted from reference [28].

The normalized changes in integration of the C3'-CF_3 peaks of BLT-S-F_6 (**3-24**) with 100 equivalents of GSH in 86% blood plasma, 10% D_2O, 2% ethanol, 2% polysorbate 80 and released SB-T-12822-5 (**2-36**) were plotted against time and shown in Figure 3.17. The normalized integration values and raw experimental data are provided in Table 3.2. The half-life of BLT-S-F_6 (**3-24**) in these conditions was calculated to be approximately 3 h. Since the intracellular level of glutathione is typically 2-10 mM,[18, 29] these conditions allow for estimation of the half-life of this self-immolative disulfide linker in the cytosolic compartments following internalization by RME.

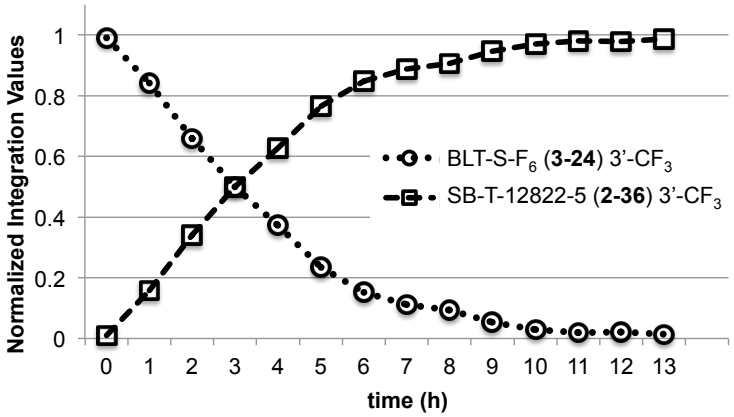

Figure 3.17. Normalized changes in integration of 3'-CF_3 peaks of BLT-S-F_6 (**3-24**) with 100 equivalents of GSH in 86% blood plasma, 10% D_2O, 2% ethanol, 2% polysorbate 80 and released taxoid SB-T-12822-5 (**2-36**). Reprinted from reference [28].

Table 3.2.[a] Experimental data and normalized values for Figure 3.17. Adapted from reference [28].

time (h)	Normalized Integration for BLT-S-F_6 (**3-24**)	Normalized Integration for SB-T-12822-5 (**2-36**)
0	1	0
1	0.841018667 (0.6803)	0.158981333 (0.1286)
2	0.658950264 (0.5750)	0.341049736 (0.2976)
3	0.500068503 (0.3650)	0.499931497 (0.3649)
4	0.37350062 (0.2709)	0.62649938 (0.4544)
5	0.23476298 (0.1976)	0.76523702 (0.6441)
6	0.152388797 (0.1295)	0.847611203 (0.7203)
7	0.110911486 (0.0926)	0.889088514 (0.7423)
8	0.094353851 (0.1001)	0.905646149 (0.9608)
9	0.054218871 (0.0489)	0.945781129 (0.8530)
10	0.028866218 (0.0249)	0.971133782 (0.8377)
11	0.019893467 (0.0183)	0.980106533 (0.9016)
12	0.020392911 (0.0191)	0.979607089 (0.9175)
13	0.014137708 (0.0131)	0.985862292 (0.9135)

[a]Time-resolved ^{19}F NMR integration values for 3'-CF_3 of BLT-S-F_6 (**3-24**) and released SB-T-12822-5 (**2-36**) beginning with a 200 μM solution of BLT-S-F_6 with supplemental glutathione (100 equiv.) at 37 °C starting at t = 0 (control, without GSH) to 13 h in blood plasma-D_2O-ethanol-polysorbate 80 (86:10:2:2) with spectra every 1 h (1024 scans/spectrum).

Linker cleavage of BLT-S-F_6 (**3-24**) and drug release of SB-T-12822-5 with 100 equivalents of GSH in 96% D_2O, 2% ethanol, and 2% polysorbate 80 at 37 °C was significantly slower than that under the same conditions in blood plasma – only 50% drug release was observed at approximately 4 days by ^{19}F NMR analysis (Figure 3.18). Similar to the results observed for BLT-F_2 in the presence of Solutol HS 15, once again the presence of excipient slows the rate of disulfide cleavage in aqueous D_2O formulations. However, blood plasma contains many proteins that are absent in the D_2O formulations and likely interact with the excipient, leading to dissociation of the excipient from the SMDC and rendering the disulfide bond more available for thiol-disulfide exchange with supplemental GSH.

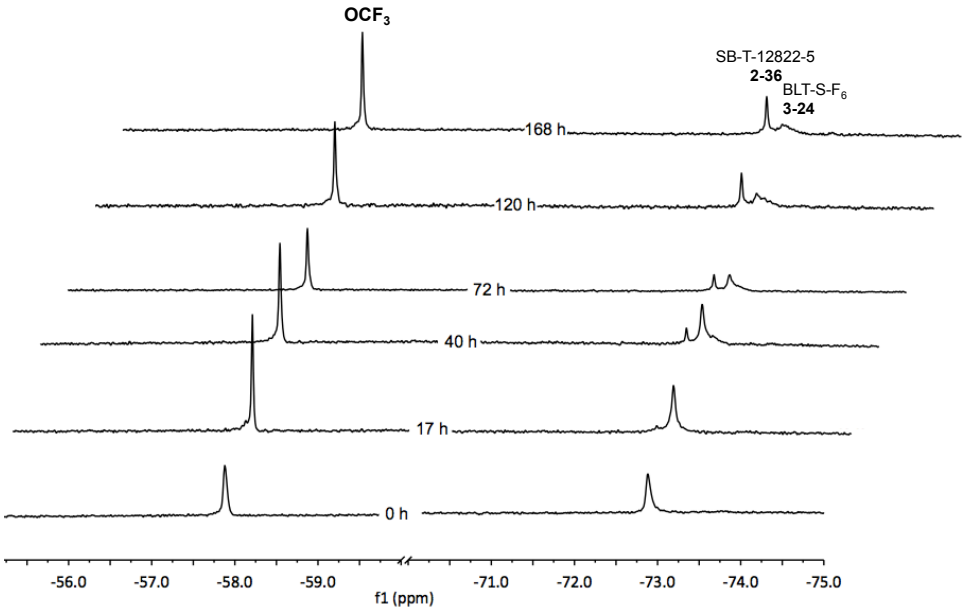

Figure 3.18. ^{19}F NMR spectra (>512 of scans) showing chemical shifts of a 200 μM solution of BLT-S-F_6 (**3-24**) and released SB-T-12822-5 (**2-36**) with 100 equivalents of GSH in D_2O-ethanol-polysorbate 80 (96:2:2) at 0, 17, 40, 72, 120, and 168 h, indicating a $t_{1/2}$ of approximately 4 d. Reprinted from reference [28].

Formulation and time-resolved ^{19}F NMR experiments on BLT-S-F_6 (**2-36**) were performed primarily by co-worker Longfei Wei, with assistance from co-worker Brendan Lichtenthal. Undergraduate research assistant Jonathan F. Khan assisted in the scale-up synthesis of SB-T-12822-5.

§3.5.0 Summary

Tumor-targeted drug delivery uses potent chemotherapeutic drugs connected to tumor-targeting modules via biocleavable linker systems to selectively target cancer cells while avoiding normal healthy tissue. These biocleavable linker systems rely on tumor-specific triggers to activate prodrug release in the tumor microenvironment. Mechanism-based self-immolative disulfide linkers have been developed for site-specific prodrug activation triggered by higher concentrations of endogenous thiols in cancer cells. These linkers have been coupled to the C2' hydroxyl of next-generation taxoids in an efficient and scalable synthetic route. Both methyl- and dimethyl-disulfide linkers have been designed and synthesized to introduce steric hinderance

proximal to the disulfide to prolong the half-life of the linker. From these taxoid-based prodrugs, numerous tumor-targeting drug conjugates have been constructed, discussed in later chapters.

Previously, our laboratory designed and synthesized BLT-F_2, a tumor-targeted drug delivery conjugate containing biotin as the tumor-targeting moiety, next-generation fluorotaxoid SB-T-12145 with site specific incorporation of fluorine at the *meta* position of the C2-benzoate moiety, and a self-immolative disulfide linker. Another fluorine was introduced to the 4-position of the linker ring, i.e. *para* to the disulfide moiety. Time-resolved ^{19}F NMR analysis of BLT-F_2 revealed a stepwise mechanism for release of the fluorotaxoid, generating the anticipated thiolate intermediate (**3-A**) as a detectable and transient species, as well as indicated a profound effect of the fluorine *para* to the disulfide group on the rate of linker cleavage and thiolactonization.

BLT-S-F_6 was designed with heightened sensitivity using 3-FABS and polyethylene glycol oligomers to enhance aqueous solubility. The stability of the disulfide linker of BLT-S-F_6 in blood plasma was assessed using ^{19}F NMR, and the linker system was shown to be quite stable in blood plasma with less than 10% cleavage and drug release after two days – the half-life of BLT-S-F_6 in blood plasma was estimated to be on the order of weeks with supplemental glutathione, whereas SB-T-12822-5 was released much faster ($t_{1/2}$ = 3 h) in the presence of excess supplemental glutathione (20 mM). This concentration of GSH is indicative of the level in tumors and may provide a fair representation of drug release in cancer cells.

§3.6.0 Experimental

§3.6.1 Caution

Taxoids have been identified as potent cytotoxic agents. Thus, all drugs and structurally related compounds and derivatives must be considered mutagens and potential reproductive hazards for both males and females. All appropriate precautions, such as the use of gloves, goggles, labware, and fume hood, must be taken while handling the compounds at all times.

§3.6.2 General Information

^{1}H, ^{13}C, and ^{19}F NMR spectra were measured on a Varian 300, 400, 500, or 600 MHz NMR spectrometer or Bruker 300, 400, or 500 MHz NMR spectrometer. Hexafluorobenzene was used as an external standard for ^{19}F NMR analysis. Melting points were measured on a Thomas-Hoover capillary melting point apparatus and are uncorrected. TLC was performed on Sorbent Technologies aluminum-backed Silica G TLC plates (Sorbent Technologies, 200 μm, 20 x 20 cm), and column chromatography was carried out on silica gel 60 (Merck, 230-400 mesh ASTM). Purity was determined with a Shimadzu L-2010A HPLC HT series HPLC assembly, using a Kinetex PFP column (4.6 mm x 100 mm, 2.6 μm) with acetonitrile-water gradient solvent system. One analytical condition was used and noted as part of the characterization and purity data, i.e., HPLC: flow rate 0.5 mL/min, a gradient of 5→95% acetonitrile for the 0-12 min period and 95% acetonitrile for the 11-15 min period. Low resolution mass spectrometry was performed on an Agilent LC-MSD mass spectrometer at the Institute of Chemical Biology and Drug Discovery, Stony Brook, NY. High resolution mass spectrometry analysis was carried out on an Agilent LC-UV-TOF mass spectrometer at the Institute of Chemical Biology and Drug Discovery, Stony Brook, NY or at the Mass Spectrometry Laboratory, University of Illinois at Urbana-Champaign, Urbana, IL.

§3.6.3 Materials

The chemicals were purchased from Sigma-Aldrich, Fisher Scientific, and VWR International, and used as received or purified before use by standard methods. Tetrahydrofuran was freshly distilled from sodium and benzophenone. Dichloromethane was also distilled immediately prior to use under nitrogen from calcium hydride.

§3.6.4 Experimental Procedure

LNA–SB-T-1214 [3-1]:
To a solution of SB-T-1214 (0.133 g, 0.156 mmol), α-linolenic acid (42 μL, 0.140 mmol), and DMAP (0.019 g, 0.156 mmol) in CH_2Cl_2 (2 mL) was added EDC·HCl (0.030 g, 0.156 mmol) in CH_2Cl_2 (1 mL), and the mixture was allowed to react for 2 h at room temperature with stirring. The reaction was diluted with CH_2Cl_2 (20 mL), and the mixture was washed with saturated NH_4Cl (3 x 20 mL) and brine (3 x 20 mL). The organic layer was dried over $MgSO_4$ and concentrated *in vacuo* to afford a clear oil. Purification of the crude product by column chromatography on silica gel with hexanes/ethyl acetate (3:2) as eluent gave **3-1** (0.073 g, 47%) as a waxy white solid. SB-T-1214 (0.065 g) was recovered from the reaction, resulting in a 84% conversion yield. ^{1}H NMR (300 MHz, $CDCl_3$) δ 0.99 (m, 5H), 1.16 (s, 6H), 1.26 (s, 6H), 1.36 (s, 17H), 1.68 (s, 6H), 1.77 (s, 7H), 1.88 (m, 1H), 1.94 (s, 3H), 2.09 (m, 1H), 2.35 (m, 2H), 2.39 (s, 3H), 2.46 (m, 2H), 2.55 (m, 2H), 2.82 (m, 1H), 3.82 (d, *J* = 6.6 Hz, 1H), 4.19 (d, *J* = 8.4 Hz, 1H), 4.32 (d, *J* = 8.4 Hz, 1H), 4.46 (m, 1H), 4.84 (m, 1H), 4.98 (m, 3H), 5.19 (m, 1H), 5.37 (m, 1H), 5.68 (d, *J* = 7.2 Hz, 1H), 6.20 (bt, 1H), 6.31 (s, 1H), 7.50 (t, *J* = 7.5 Hz, 2H), 7.63 (t, *J* = 7.2 Hz, 1H), 8.12 (d, *J* = 7.2 Hz, 2H). HRMS (TOF) for $C_{63}H_{88}NO_{16}^+$ calcd: 1114.6098. Found: 1114.6084 (Δ = -1.3 ppm).

LNA–SB-T-12854 [3-2]:
To a solution of SB-T-12854 (0.171 g, 0.203 mmol), α-linolenic acid (61 μL, 0.203 mmol), DMAP (0.025 g, 0.203 mmol) in CH_2Cl_2 (2.5 mL) was added EDC·HCl (0.039 g, 0.203 mmol) in CH_2Cl_2 (1 mL), and the mixture was allowed to react for 2½ h at room temperature with stirring. The reaction was diluted with CH_2Cl_2 (20 mL), and the mixture was washed with saturated NH_4Cl (3 x 20 mL) and brine (3 x 20 mL). The organic layer was dried over $MgSO_4$ and concentrated *in vacuo* to afford a clear oil. Purification of the crude product by column chromatography on silica gel with hexanes/ethyl acetate (1:1) as eluent gave **3-2** (0.125 g, 56%) as a white solid; mp 84-86 °C; SB-T-12854 (0.059 g) was recovered from the reaction, resulting in a 86% conversion yield. ^{1}H NMR (600 MHz, $CDCl_3$) 0.98 (t, *J* = 7.2 Hz, 3H), 1.15 (s, 3H), 1.25 (s, 3H), 1.31 (s, 9H), 1.32 (m, 8H), 1.67 (s, 3H), 1.68 (m, 2H), 1.88 (t, *J* = 13.2 Hz, 1H), 1.96 (s, 3H), 2.07 (m, 4H), 2.22 (m, 1H), 2.36 (m, 1H), 2.39 (s, 3H), 2.47 (m, 2H), 2.54 (m, 1H), 2.81 (t, *J* = 6.0 Hz, 4H), 2.96 (s, 3H), 3.03 (s, 3H), 3.21 (d, *J* = 3.6 Hz, 1H), 3.82 (d, *J* = 7.8 Hz, 1H), 4.18 (d, *J* = 8.4 Hz, 1H), 4.31 (d, *J* = 8.4 Hz, 1H), 4.41 (dd, *J* = 9.0 Hz, 25.5 Hz, 1H), 4.49 (m, 1H), 4.93 (m, 1H), 4.99 (d, *J* = 7.8 Hz, 1H), 5.06 (m, 2H), 5.36 (m, 6H), 5.67 (d, *J* = 6.6 Hz, 1H), 6.25 (s, 1H), 6.28 (t, *J* = 8.4 Hz, 1H), 7.50 (t, *J* = 7.2 Hz, 2H), 7.61 (t, *J* = 7.2 Hz, 1H), 8.13 (d, *J* = 7.2 Hz, 2H); ^{13}C NMR (125 MHz, $CDCl_3$) δ 9.4, 14.1, 14.3, 14.8, 20.5, 22.2, 22.5, 22.5, 24.7, 25.5, 25.6, 26.9, 27.2, 28.1, 29.0, 29.1, 29.14, 29.6, 31.6, 33.6, 35.3, 35.4, 36.0, 36.6, 43.2, 45.5, 58.4, 71.8, 72.5, 75.3, 76.1, 79.4, 81.0, 84.7, 127.1, 127.8, 128.2, 128.3, 128.7, 129.2, 130.2, 132.0, 133.6, 156.1, 167.2, 172.5, 205.8; ^{19}F NMR (282 MHz, $CDCl_3$) δ -83.58 (dd, *J* =

23.8 Hz, 34.8 Hz, 1F), -85.36 (d, J = 34.8 Hz, 1F); HRMS (TOF) for $C_{60}H_{83}F_2N_2NaO_{16}^+$ [M+ Na^+] calcd: 1147.5525. Found: 1147.5519 (Δ = -0.5 ppm).

2,2'-dithiobis-pyridine [3-3]:[30]
To a solution of pyridine-2(1*H*)-thione (2.921 g, 0.025 mol) in CH_2Cl_2 (250 mL) was added $KMnO_4$ (13.14 g, 0.083 mol), and the mixture was allowed to react for 1½ h at room temperature with vigorous stirring. The reaction mixture was filtered over celite and concentrated *in vacuo* to afford a yellow oil. Purification of the crude product by column chromatography on silica gel with hexanes/ethyl acetate (9:1) as eluent gave **3-3** (2.772 g, 96%) as a white needles; ^{1}H NMR (500 MHz, $CDCl_3$) δ 7.13 (m, 2H), 7.64 (m, 4H), 8.48 (d, J = 4.8 Hz, 2H). All data are in agreement with literature values.[30]

(3*H*)-Benzo[b]thiophen-2-one [3-4]:[31]
To a solution of 2-benzothienylboronic acid (2.004 g, 11.23 mmol) in EtOH (55 mL) was added H_2O_2 (16 mL), and the mixture was allowed to react for 16 h at room temperature with stirring. The reaction mixture was extracted with CH_2Cl_2 (3 x 50 mL). The combined organic layers were dried over $MgSO_4$ and concentrated *in vacuo* to afford a dark red oil. Purification of the crude product by column chromatography on silica gel with hexanes/ethyl acetate (9:1) as eluent gave **3-4** (1.808 g, 95%) as a brown solid; ^{1}H NMR (600 MHz, $CDCl_3$) δ 3.97 (s, 2H), 7.21 (dd, J = 7.2 Hz, 1H), 7.30 (dd, J = 8.4 Hz, 2H), 7.34 (d, J = 7.8 Hz, 1H). All data are in agreement with literature values.[31]

(2-Mercaptophenyl)acetic acid [3-5]:[32]
To a solution of **3-4** (1.800 g, 12.05 mmol) in THF (25 mL) heated to 60 °C under reflux was added an aqueous solution of 3 M LiOH (25.0 mL, 75.0 mmol), and the mixture was allowed to react for 18 h at 60 °C with stirring. The reaction was allowed to cool to room temperature and diluted with H_2O (25 mL). The pH of the aqueous phase was adjusted to 2 with 1 *N* HCl. The organic layer was separated, and the aqueous layer was extracted with CH_2Cl_2 (3 x 30 mL). The combined organic layers were washed with brine (3 x 50 mL), dried over $MgSO_4$, and concentrated *in vacuo* to afford a yellow oil. Purification of the crude product by column chromatography on silica gel with hexanes/ethyl acetate (2:1) as eluent gave **3-5** (1.643 g, 81%) as a white solid; ^{1}H NMR (600 MHz, $CDCl_3$) δ 3.49 (s, 1H), 3.82 (s, 2H), 7.16-7.20 (m, 2H), 7.24 (m, 1H), 7.40 (m, 1H). All data are in agreement with literature values.[32]

4-Mercaptopentanoic acid [3-7]:[33]
A solution of γ-valerolactone (4 mL, 0.042 mmol) and thiourea (15.9 g, 0.210 mol) in 48% HBr in H_2O (23 mL) was allowed to react for 24 h at 100 °C under reflux conditions with stirring. The reaction was allowed to cool to room temperature and diluted with H_2O (20 mL). The aqueous layer was washed with CH_2Cl_2 (3 x 30 mL) and diethyl ether (3 x 30 mL) to give thiourea salt **3-6** in the aqueous layer. The pH of the aqueous phase was adjusted to 13 with KOH (s), and the basic solution was allowed to react for 24 h at 100 °C under reflux conditions with stirring. The reaction was allowed to cool to room temperature and diluted with H_2O (20 mL). The pH was adjusted to 2 with 1 *N* HCl, and the acidified solution was extracted with CH_2Cl_2 (3 x 50 mL). The combined organic layers were dried over $MgSO_4$ and concentrated *in vacuo* to afford **3-7** (3.822 g, 68% over two steps) as a pungent yellow oil; ^{1}H NMR (500 MHz,

$CDCl_3$) δ 1.38 (d, *J* = 7.0 Hz, 3H), 1.45 (d, *J* = 7.0 Hz, 1H), 1.78 (m, 1H), 1.99 (m, 1H), 2.54 (m, 2H), 2.96 (m, 1H); All data are in agreement with literature values.[33]

Triisopropylsilyl-4-(pyridin-2-yldisulfanyl)pentanoate [3-9]:[34]
To a solution of **3-7** (0.709 g, 5.29 mmol) in EtOH (25 mL) was added **3-3** (7 g, 31.7 mmol) in EtOH (100 mL), and the mixture was allowed to react for 2 h at 80 °C under reflux with stirring. The reaction was allowed to cool to room temperature, and the mixture was concentrated *in vacuo* to afford a yellow precipitate. Excess **3-3** was removed by trituration with hexanes. Purification of the crude product by column chromatography on silica gel with hexanes/ethyl acetate (9:1) as eluent gave mixture of **3-8** along with pyridine-2-thiol. The product was taken directly to the subsequent TIPS-protection. To a cooled solution of the **3-8** in CH_2Cl_2 (50 mL) was added Et_3N (2.1 mL, 15.1 mmol) and TIPSCl (1.93 mL, 9.04 mmol), and the mixture was allowed to warm from 0 °C to room temperature and react for 24 h with stirring. The reaction mixture was concentrated *in vacuo* to afford a yellow oil. Purification of the crude product by column chromatography on silica gel with hexanes/ethyl acetate (2:1) as eluent gave **3-9** (2.706, 92% over 2 steps) as a colorless oil; ^{1}H NMR (600 MHz, $CDCl_3$) δ 1.06 (m, 21 H), 1.34 (d, *J* = 7.2 Hz, 3H), 1.89 (m, 1H), 2.00 (m, 1H), 2.51 (m, 2H), 3.03 (m, 1H), 7.06 (t, *J* = 7.8 Hz, 1H), 7.62 (t, *J* = 7.8 Hz, 1H), 7.72 (d, *J* = 7.8 Hz, 1H), 8.44 (d, *J* = 3.0 Hz, 1H); HRMS for $C_{19}H_{34}NO_2S_2Si^+$ calcd: 400.1795. Found: 400.1788 (Δ = -1.8 ppm). All data are in agreement with literature values.[34]

2-(2-5-Oxo-triisopropylsilyloxypentan-2-yl)disulfanylphenylacetic acid [3-10]:[34]
To a cooled solution of **3-9** (0.300 g, 0.752 mmol) in THF (1.5 mL) was added **3-5** (0.130 g, 0.752 mmol) in THF (1.5 mL), and the mixture was allowed to react for 2 h at -10 °C with stirring. The reaction mixture was concentrated *in vacuo* to afford a yellow oil. Purification of the crude product by column chromatography on silica gel with hexanes/ethyl acetate (3:1) as eluent gave **3-10** (0.166 g, 68%) as a pale yellow oil; ^{1}H NMR (500 MHz, $CDCl_3$) δ 1.05 (d, *J* = 7.5 Hz, 18H), 1.25 (d, *J* = 6.5 Hz, 3H), 1.26 (m, 3H), 1.81 (m, 1H), 1.96 (m, 1H), 2.41 (m, 2H), 2.90 (m, 1H), 3.90 (s, 2H), 7.21 (m, 2H), 7.29 (m, 1H), 7.79 (d, *J* = 7.5 Hz, 1H); ^{13}C NMR (125 MHz, $CDCl_3$) δ 11.88, 17.79, 20.26, 31.04, 33.14, 38.92, 45.18, 127.53, 128.34, 130.15, 130.84, 133.17, 133.20, 137.77, 173.56, 175.70; HRMS for $C_{22}H_{37}O_4S_2Si^+$ calcd: 457.1897. Found: 457.1892 (Δ = -1.1 ppm). All data are in agreement with literature values.[34]

SB-T-1214-(Me-SS-Linker)-OTIPS [3-11]:[35]
To a solution of SB-T-1214 (**2-4**) (0.600 g, 0.703 mmol), **3-10** (0.350 g (0.768 mmol), and DMAP (0.038 g, 0.308 mmol) in CH_2Cl_2 (15 mL) was added DIC (135 µL, 0.877 mmol), and the mixture was allowed to react for 24 h at room temperature with stirring. The reaction was quenched with saturated NH_4Cl (15 mL) and diluted with H_2O (10 mL), and the mixture was washed with brine (3 x 20 mL). The organic layer was dried over $MgSO_4$ and concentrated *in vacuo* to afford a yellow oil. The diisopropylurea byproduct was removed by filtration with diethyl ether. Purification of the crude product by column chromatography on silica gel with hexanes/ethyl acetate (2:1) as eluent gave **3-11** (0.697, 77%) as a white solid; ^{1}H NMR (400 MHz, $CDCl_3$) δ 0.97 (m, 2H), 1.06 (d, *J* = 7.2 Hz, 18H), 1.14 (m, 5H), 1.25 (s, 6H), 1.30 (d, *J* = 6.8 Hz, 3H), 1.33 (s, 9H), 1.66 (s, 3H), 1.69 (s, 3H), 1.72 (s, 3H), 1.76 (m, 2H), 1.85 (m, 1H), 1.90 (s, 3H), 1.93 (m, 2H), 2.30 (m, 2H), 2.35 (s, 3H), 2.42 (m, 2H), 2.53 (m, 2H), 2.59 (m, 1H), 2.94 (m, 1H), 3.81 (d, *J* = 7.2 Hz, 1H), 3.94 (dd, *J* = 1.7, 16.8 Hz, 1H), 4.10 (dd, *J* = 1.7, 16.8

Hz, 1H), 4.18 (d, *J* = 8.4 Hz, 1H), 4.30 (d, *J* = 8.4 Hz, 1H), 4.42 (m, 1H), 4.79 (d, *J* = 8.4 Hz, 1H), 4.92 (s, 1H), 4.96 (d, *J* = 7.2 Hz, 1H), 5.07 (d, *J* = 8.4 Hz, 1H), 5.67 (d, *J* = 7.2 Hz, 1H), 6.19 (t, *J* = 8.7 Hz, 1H), 6.28 (s, 1H), 7.26 (m, 3H), 7.47 (t, *J* = 7.9 Hz, 2H), 7.60 (t, *J* = 7.4 Hz, 1H), 7.80 (d, *J* = 7.4 Hz, 1H), 8.11 (d, *J* = 7.1 Hz, 2H); HRMS for $C_{67}H_{94}NO_{18}S_2Si^+$ calcd: 1292.5676. Found: 1292.5676 (Δ = 0 ppm).

SB-T-1214-(Me-SS-Linker)-COOH [3-12]:[35]
To a cooled solution of **3-11** (0.649 g, 0.502 mmol) in CH_3CN-pyridine (1:1) (50 mL) was added HF-pyridine (6.5 mL), and the mixture was allowed to warm from 0 °C to room temperature and react for 24 h at room temperature with stirring. The reaction was quenched with 10% citric acid (10 mL), and the mixture was extracted with ethyl acetate (3 x 30 mL). The combined organic layers were washed with saturated $CuSO_4$ (3 x 20 mL) and brine (3 x 20 mL), dried over $MgSO_4$, and concentrated *in vacuo* to afford a colorless oil. Purification of the crude product by column chromatography on silica gel with hexanes/ethyl acetate (1:4) as eluent gave **3-12** (0.516 g, 91%) as a white solid. Yields ranged from 83%-91%. ^{1}H NMR (500 MHz, $CDCl_3$) δ 1.02 (m, 2H), 1.16 (m, 2H), 1.18 (m, 3H), 1.29 (s, 6H), 1.39 (s, 9H), 1.70 (s, 3H), 1.75 (s, 3H), 1.76 (s, 3H), 1.80 (m, 2H), 1.89 (bt, 1H), 1.93 (s, 3H) 1.94 (m, 2H), 2.39 (m, 2H), 2.42 (s, 3H), 2.56 (m, 1H), 3.03 (m, 1H), 3.83 (m, 1H), 3.96 (dd, *J* = 1.7, 16.8 Hz, 1H), 4.15 (dd, *J* = 1.7, 16.8 Hz, 1H), 4.20 (d, *J* = 8.4 Hz, 1H), 4.34 (d, *J* = 8.5 Hz, 1H), 4.45 (m, 1H), 5.00 (m, 3H), 5.18 (d, *J* = 7.1 Hz, 1H), 5.70 (d, *J* = 7.2 Hz, 1H), 6.25 (m, 1H), 6.32 (m, 1H), 7.33 (m, 3H), 7.51 (t, J = 7.8 Hz, 2H), 7.63 (t, J = 7.5 Hz, 1H), 7.84 (d, *J* = 7.8 Hz, 1H), 8.14 (d, *J* = 7.1 Hz, 2H), 8.66 (bs, 1H); HRMS for $C_{58}H_{74}NO_{18}S_2^+$ calcd: 1136.4342. Found: 1136.4365 (Δ = 2.0 ppm).

SB-T-1214-(Me-SS-Linker)-OSu [3-13]:[35]
To a solution of **3-12** (0.500 g, 0.441 mmol) and *N*-hydroxysuccinimide (0.160 g, 1.32 mmol) in THF-pyridine (1:1) (8 mL) was added EDC·HCl (0.100 g, 0.485 mmol), and the mixture was allowed to react for 36 h at room temperature with stirring. The reaction was quenched with saturated NH_4Cl (15 mL), and the mixture was extracted with CH_2Cl_2 (3 x 30 mL). The combined organic layers were washed with brine (3 x 30 mL), dried over $MgSO_4$, and concentrated *in vacuo* to afford a yellow oil. Purification of the crude product by column chromatography on silica gel with hexanes/ethyl acetate (1:1) as eluent gave **3-13** (0.376 g, 70%) as a white solid; ^{1}H NMR (500 MHz, $CDCl_3$) δ 0.98 (m, 2H), 1.12 (m, 2H), 1.14 (s, 3H), 1.25 (m, 3H), 1.31 (dd, *J* = 4.8, 6.8 Hz, 3H), 1.33 (s, 2H), 1.34 (s, 9H), 1.66 (s, 3H), 1.71 (s, 3H), 1.73 (s, 3H), 1.86 (t, *J* = 13.8 Hz, 1H), 1.90 (s, 3H), 1.97 (m, 2H), 2.32 (m, 2H), 2.35 (s, 3H), 2.53 (m, 1H), 2.64 (t, *J* = 7.0 Hz, 2H), 2.83 (s, 4H), 2.99 (m, 1H), 3.80 (d, *J* = 7.2 Hz, 1H), 3.97 (dd, *J* = 1.7, 16.8 Hz, 1H), 4.08 (dd, *J* = 1.7, 16.8 Hz, 1H), 4.13 (m, 1H), 4.18 (d, *J* = 8.4 Hz, 1H), 4.30 (d, *J* = 8.4 Hz, 1H), 4.42 (m, 1H), 4.81 (m, 1H), 4.92 (s, 1H), 4.96 (d, *J* = 8.5 Hz, 1H), 5.09 (d, *J* = 8.5 Hz, 1H), 5.67 (d, *J* = 7.2 Hz, 1H), 6.18 (t, *J* = 8.5 Hz, 1H), 6.28 (s, 1H), 7.30 (m, 3H), 7.47 (t, *J* = 7.8 Hz, 2H), 7.60 (t, *J* = 7.4 Hz, 1H), 7.79 (d, *J* = 8.2 Hz, 1H), 8.11 (d, *J* = 7.5 Hz, 2H). ^{13}C NMR (125 MHz, $CDCl_3$) δ 9.19, 9.39, 9.58, 13.04, 13.75, 14.23, 14.87, 18.54, 19.15, 20.40, 22.25, 22.45, 23.51, 25.61, 25.75, 26.70, 28.24, 30.26, 30.66, 35.45, 35.51, 38.80, 42.29, 43.20, 45.60, 58.48, 64.40, 71.83, 72.16, 75.01, 75.22, 75.49, 76.42, 79.31, 80.97, 84.52, 119.98, 128.03, 128.48, 128.66, 129.29, 130.21, 130.64, 130.69, 131.00, 132.40, 133.45, 133.63, 154.94, 156.89, 167.01, 168.16, 169.10, 169.64, 170.19, 170.21, 175.12, 204.18; HRMS for $C_{62}H_{77}N_2O_{20}S_2^+$ calcd: 1233.4506. Found: 1233.4496 (Δ = -0.8 ppm). HPLC: t = 14.1 min, purity > 98%.[35]

4-Mercapto-4-methylpentanenitrile [3-14]:[33]
To a cooled solution of *n*-BuLi (11 mL, 17.6 mmol) in THF (22 mL) at -78 °C was added CH_3CN (0.91 mL, 17.6 mmol), slowly and dropwise over 5 min, to pre-form the lithiated acetonitrile salt as a white precipitate. To the cooled suspension was added isobutylene sulfide (1.15 mL, 11.7 mmol) over 15 min by dropwise addition, and the mixture was allowed to react for 1 h at -78 °C with stirring. The reaction was allowed to warm to room temperature as a yellow oil formed at the bottom of the reaction flask. Reaction progress was monitored by mass spectrometry. The reaction mixture was cooled to 0 °C and acidified slowly with 0.5 *N* HCl (5 mL). The organic layer was separated, and the acidic aqueous layer was extracted with ethyl acetate (3 x 30 mL). The combined organic layers were dried over $MgSO_4$ and concentrated *in vacuo* to afford **3-14** (1.616 g, crude) as an amber oil; ^{1}H NMR (300 MHz, $CDCl_3$) δ 1.52 (s, 6H), 2.04 (t, *J* = 7.2 Hz, 2H), 2.85 (t, *J* = 7.2 Hz, 2H); MS (ESI) for $C_6H_{12}NS^+$ calc'd: 130.1. Found: 130.1. All data are in agreement with literature reported values.[33]

4-Mercapto-4-methylpropanoic acid [3-15]:[33]
To a solution of **3-14** (1.616 g, crude) in EtOH (7 mL) was added an aqueous solution of 6 M NaOH (2 mL), and the mixture was allowed to react for 15 h at 80 °C under reflux conditions with stirring. The reaction was diluted with H_2O (20 mL), and the mixture was extracted with hexanes/ethyl acetate (1:2) (3 x 30 mL). The aqueous layer was acidified to pH 2 with HCl (conc.) and extracted with ethyl acetate (3 x 30 mL). The combined organic layers were dried over $MgSO_4$ and concentrated *in vacuo* to give **3-15** (1.595 g, 92%) as an amber oil; ^{1}H NMR (300 MHz, $CDCl_3$) δ 1.41 (s, 6H), 1.94 (t, *J* = 7.8 Hz, 2H), 2.58 (t, *J* = 7.8 Hz, 2H); MS FIA$^-$ for $C_6H_{11}O_2S^-$ calc'd: 147.1. Found: 147.1. All data are in agreement with literature reported values.[33]

4-Methyl-4-(pyridinyl-2-disulfanyl)pentanoic acid [3-16]:
To a solution of **3-15** (0.890 g, 6.061 mmol) in EtOH (60 mL) was added **3-3** (4.0 g, 18.18 mmol), and the mixture was allowed to react for 2 h at 80 °C under reflux conditions with stirring. The reaction was allowed to cool to room temperature, and the mixture was concentrated *in vacuo* to give an orange oil. Purification of the crude product by column chromatography on silica gel with hexanes/ethyl acetate (3:1) as eluent gave **3-16** (1.344 g, 87%) as a yellow solid; R_f = 0.5 (hexanes/ethyl acetate = 1:1); ^{1}H NMR (300 MHz, $CDCl_3$) δ 1.31 (s, 6H), 1.96 (t, *J* = 7.8 Hz, 2H), 2.51 (t, *J* = 7.8 Hz, 2H), 7.09 (dd, *J* = 6.3 Hz, 1H), 7.64 (dd, *J* = 7.5 Hz, 1H), 7.75 (d, *J* = 8.1 Hz, 1H), 8.46 (d, *J* = 4.5 Hz, 1H); ^{13}C NMR (75 MHz, $CDCl_3$) δ 27.38, 29.86, 35.52, 51.73, 120.40, 120.78, 137.04, 149.21, 160.78, 178.46; HRMS for $C_{11}H_{17}NO_2S_2^+$ calcd: 258.0622. Found: 258.0619 (Δ = -1.2 ppm).

Triisopropylsiloxy-4-methyl-4-(pyridinyl-2-disulfanyl)pentanoate [3-17]:
To a cooled solution of **3-16** (0.295 g, 1.148 mmol) in CH_2Cl_2 (11 mL) was added Et_3N (0.32 mL, 2.296 mmol) followed by TIPSCl (0.27 mL, 1.263 mmol), and the mixture was allowed to warm from 0 °C to room temperature and react for 30 min with stirring. The reaction was diluted with H_2O (10 mL), and the mixture was extracted with CH_2Cl_2 (3 x 20 mL). The combined organic layers were dried over $MgSO_4$ and concentrated *in vacuo* to give a yellow oil. Purification of the crude product by column chromatography on silica gel with hexanes/ethyl acetate (24:1) as eluent gave **3-17** (0.475 g, 94%) as a colorless oil; R_f = 0.85 (hexanes/ethyl

acetate = 3:1); ^{1}H NMR (300 MHz, $CDCl_3$) δ 1.08 (m, 21H), 1.32 (s, 6H), 1.96 (t, *J* = 7.8 Hz, 2H), 2.48 (t, *J* = 7.8 Hz, 2H), 7.07 (m, 1H), 7.62 (t, *J* = 7.8 Hz, 1H), 7.75 (d, *J* = 8.1 Hz, 1H), 8.44 (d, *J* = 4.5 Hz, 1H); ^{13}C NMR (125 MHz, $CDCl_3$) δ 11.90, 17.81, 27.43, 31.63, 36.21, 51.77, 119.96, 120.58, 136.83, 149.33, 161.02, 173.32; HRMS for $C_{20}H_{36}NO_2S_2Si^+$ calcd: 414.1957. Found: 414.1954 (Δ = -0.7 ppm).

2-(2-[2-Methyl-5-oxo-triisopropylsilyloxy]pentan-2-yl)disulfanyl-3-phenylacetic acid [3-18]:
To a solution of **3-17** (0.456 g, 1.034 mmol) in THF (10 mL) was added **3-5** (0.173 g, 1.034 mmol), and the mixture was allowed to react for 3 h at 60 °C. Reaction progress was monitored by TLC and MS ([M–H$^+$] *m/z* 469). The reaction mixture was concentrated *in vacuo* to give a yellow oil. Purification of the crude product by column chromatography on silica gel with hexanes/ethyl acetate (13:1) as eluent gave **3-18** (0.110 g) as a colorless oil. ^{1}H and ^{13}C NMR indicated that two products were present, either due to TIPS transfer between acids or by the presence of rotamers; ^{1}H NMR (400 MHz, $CDCl_3$) δ 1.19 (m, 18H), 1.24 (s, 3H), 1.30 (m, 3H), 1.36 (s, 3H), 1.89 (t, *J* = 7.8 Hz, 1H), 2.02 (t, *J* = 7.8 Hz, 1H), 2.36 (t, *J* = 7.8 Hz, 1H), 2.50 (t, *J* = 7.8 Hz, 1H), 3.93 (s, 1H), 3.96 (s, 1H), 7.21 (s, 1H), 7.33 (m, 2H), 7.82 (m, 1H); ^{13}C NMR (100 MHz, $CDCl_3$) δ 11.89, 11.91, 27.55, 27.67, 31.45, 31.65, 36.02, 36.14, 38.88, 39.33, 51.85, 127.22, 128.15, 128.49, 129.26, 129.62, 130.75, 130.98, 132.59, 133.63, 135.39, 137.16, 138.01, 173.55, 173.58, 176.03, 176.14; HRMS for $C_{23}H_{39}O_4S_2Si^+$ calcd: 471.2029. Found: 471.2029 (Δ = 0 ppm).

N-Propargylamino-4-methyl-4-(pyridinyl-2-disulfanyl)pentanoate [3-19]:
To a solution of **3-16** (0.257 g, 1.0 mmol) in CH_2Cl_2 (10 mL) was added EDC·HCl (0.230 g, 1.2 mmol) and DMAP (0.122 g, 1.0 mmol) followed by propargylamine (128 μL, 2.0 mmol), and the mixture was allowed to react for 9 h at room temperature with stirring. The reaction was diluted with H_2O (20 mL) and CH_2Cl_2 (20 mL), and the mixture was washed with brine (3 x 10 mL). The organic layer was dried over $MgSO_4$ and concentrated *in vacuo* to give an orange oil. Purification of the crude product by column chromatography on silica gel with hexanes/ethyl acetate (3:2) as eluent gave **3-19** (0.216 g, 75%) as a yellow oil; R_f = 0.5 (hexanes/ethyl acetate = 1:1); ^{1}H NMR (500 MHz, $CDCl_3$) δ 1.33 (s, 6H), 1.99 (dt, *J* = 6.0, 8.5 Hz, 2H), 2.27 (t, *J* = 2.5 Hz, 1H), 2.36 (dt, *J* = 6.0, 8.5 Hz, 2H), 4.04 (dd, *J* = 2.5 Hz, 1H), 5.66 (bs, 1H), 7.12 (m, 1H), 7.65 (dt, *J* = 1.5, 7.5 Hz, 1H), 7.75 (d, *J* = 8.0 Hz, 1H), 8.48 (d, *J* = 4.0 Hz, 1H); ^{13}C NMR (125 MHz, $CDCl_3$) δ 27.58, 29.26, 32.08, 36.42, 52.00, 71.73, 79.48, 120.53, 120.86, 136.92, 149.44, 160.79, 172.01; HRMS for $C_{14}H_{19}N_2OS_2^+$ calcd: 295.0933. Found: 295.0943 (Δ = 3.4 ppm).

N-Propargylamino-4-methyl-3-(2-disulfanyl-1-phenylacetate)pentanoate [3-20]:
To a heated solution of **3-19** (0.177 g, 0.495 mmol) in THF (5 mL) at 55 °C was added **3-5** (0.058 g, 0.347 mmol) in THF (1 mL), and the mixture was allowed to react for 4 d at 55 °C with stirring. Reaction progress was monitored by mass spectrometry. The reaction mixture was concentrated *in vacuo* to give a yellow oil. Purification of the crude product by column chromatography on silica gel with hexanes/ethyl acetate (1:1) as eluent gave **3-20** (0.110 g, 74%) as a yellow oil; R_f = 0.3 (hexanes/ethyl acetate = 2:3); contains **3-19**; ^{1}H NMR (500 MHz, $CDCl_3$) δ 1.27 (s, 6H), 1.81 (m, 2H), 2.09 (m, 2H), 2.24 (t, *J* = 2.5 Hz, 1H), 3.87 (dd, *J* = 2.5 Hz, 2H), 3.98 (s, 2H), 7.33 (m, 3H), 7.85 (d, *J* = 7.5 Hz, 1H); ^{13}C NMR (125 MHz, $CDCl_3$) 27.53, 29.21, 32.14, 36.32, 52.84, 71.55, 79.50, 113.80, 120.63, 127.71, 128.14, 131.41, 133.99, 137.79, 172.68; HRMS for $C_{17}H_{20}NO_3S_2^-$ calcd: 350.0890. Found: 350.0900 (Δ = 2.9 ppm).

SB-T-1214-(Me_2-SS-Linker)-Alkyne [3-21]:
To a solution of SB-T-1214 (**2-4**) (0.076 g, 0.089 mmol), **3-20** (0.035 g, 0.099 mmol), and DMAP (0.006 g, 0.027 mmol) in CH_2Cl_2 (1 mL) was added EDC·HCl (0.030 g, 0.190 mmol), and the mixture was allowed to react for 20 h at room temperature with stirring. The reaction mixture was concentrated *in vacuo* to give a yellow oil. Purification of the crude product by column chromatography on silica gel with hexanes/ethyl acetate/acetic acid (53:46:1) as eluent gave **3-21** (0.073 g, 69%) as a white solid; R_f = 0.4 (hexanes/ethyl acetate/acetic acid = 59:40:1); ^{1}H NMR (500 MHz, $CDCl_3$) δ 0.92 (m, 2H), 1.02 (m, 2H), 1.18 (s, 3H), 1.27 (s, 3H), 1.28 (s, 6H), 1.33 (s, 3H), 1.38 (s, 9H), 1.69 (s, 3H), 1.76 (s, 3H), 1.77 (s, 3H), 1.80 (m, 2H), 1.89 (bt, 1H), 1.94 (s, 3H), 2.05 (m, 1H), 2.08 (s, 3H), 2.27 (t, *J* = 2.5 Hz, 1H), 2.37 (m, 1H), 2.38 (s, 3H), 2.56 (m, 2H), 3.82 (d, *J* = 7.0 Hz, 1H), 3.84 (ddd, *J* = 2.5, 2.5, 17.5 Hz, 1H), 3.93 (ddd, *J* = 2.5, 2.5, 17.5 Hz), 4.06 (d, *J* = 16.5 Hz, 1H), 4.18 (d, *J* = 16.5 Hz, 1H), 4.21 (d, *J* = 8.4 Hz, 1H), 4.33 (d, *J* = 8.4 Hz, 1H), 4.45 (dd, *J* = 6.5, 11.0 Hz, 1H), 4.97 (d, *J* = 11.0 Hz, 1H), 5.00 (m, 2H), 5.21 (bs, 1H), 5.43 (bs, 1H), 5.70 (d, *J* = 7.0 Hz, 1H), 6.22 (t, *J* = 8.7 Hz, 1H), 6.32 (s, 1H), 7.31 (m, 3H), 7.51 (t, *J* = 7.5 Hz, 2H), 7.63 (t, *J* = 7.5 Hz, 1H), 7.84 (d, *J* = 7.0 Hz, 1H), 8.14 (d, *J* = 7.0 Hz, 2H); ^{13}C NMR (125 MHz, $CDCl_3$) δ 9.19, 9.41, 9.56, 13.02, 14.89, 18.55, 22.20, 22.49, 22.78, 26.70, 27.23, 28.04, 28.25, 29.11, 29.72, 31.87, 35.46, 36.23, 38.82, 43.20, 45.65, 52.42, 58.48, 71.52, 71.83, 72.14, 75.19, 75.46, 76.41, 79.28, 79.64, 81.01, 84.49, 119.93, 128.09, 128.27, 128.66, 129.25, 130.19, 131.31, 131.42, 132.52, 133.66, 137.65, 137.92, 143.39, 155.00, 167.02, 168.18, 169.63, 170.83, 172.09, 175.13, 204.09; HRMS for $C_{62}H_{79}N_2O_{17}S_2^+$ calcd: 1187.4815. Found: 1187.4826 (Δ = 0.9 ppm).

SB-T-12822-5-(Me-SS-Linker)-OTIPS [3-22]:[28]
To a solution of SB-T-12822-5 (**2-36**) (0.100 g, 0.105 mmol), **3-10** (0.058 g, 0.115 mmol), and DMAP (0.006 g, 0.031 mmol) in CH_2Cl_2 (10 mL) was added DIC (18 μL, 0.115 mmol), and the mixture was allowed to react for 12 h at room temperature with stirring. The reaction was quenched with saturated NH_4Cl (10 mL) and diluted with H_2O (10 mL), and the mixture was extracted with CH_2Cl_2 (3 x 30 mL). The combined organic layers were washed with brine (3 x 30 mL), dried over $MgSO_4$, and concentrated *in vacuo* to afford a yellow oil. The diisopropylurea byproduct was removed by filtration with Et_2O. Purification of the crude product by column chromatography on silica gel with hexanes/ethyl acetate (2:1) as eluent gave **3-22** (0.075, 51%) as a white solid; R_f = 0.4 (hexanes/ethyl acetate = 2:1); ^{1}H NMR (500 MHz, $CDCl_3$) δ 0.97 (m, 2H), 1.08 (d, *J* = 7.5 Hz, 18H), 1.25 (m, 3H), 1.26 (s, 3H), 1.31 (d, *J* = 7.5 Hz, 3H), 1.36 (s, 9H), 1.69 (s, 3H), 1.80 (m, 1H), 1.92 (s, 3H), 2.30 (m, 1H), 2.35 (s, 3H), 2.46 (m, 2H), 2.57 (m, 1H), 2.65 (d, *J* = 3.5 Hz, 1H), 2.97 (m, 1H), 3.87 (m, 4H), 4.01 (bs, 2H), 4.09 (m, 1H), 4.18 (d, *J* = 8.0 Hz, 1H), 4.31 (d, *J* = 8.0 Hz, 1H), 4.45 (m, 1H), 4.92 (m, 1H), 4.99 (d, *J* = 9.0 Hz, 1H), 5.22 (d, *J* = 10.0 Hz, 1H), 5.37 (s, 1H), 5.66 (d, *J* = 7.0 Hz, 1H), 6.22 (t, *J* = 9.5 Hz, 1H), 6.30 (s, 1H), 7.21 (m, 3H), 7.48 (d, *J* = 8.0 Hz, 1H), 7.59 (t, *J* = 8.0 Hz, 1H), 7.84 (d, *J* = 7.5 Hz, 1H), 8.04 (s, 1H), 8.09 (d, *J* = 7.5 Hz, 1H); ^{13}C NMR (125 MHz, $CDCl_3$) δ 9.23, 9.47, 9.55, 11.88, 12.99, 14.79, 15.30, 17.79, 19.14, 20.52, 21.99, 22.21, 23.36, 24.70, 26.64, 27.92, 30.95, 33.00, 35.26, 35.38, 36.64, 38.48, 43.15, 45.61, 46.03, 58.47, 64.40, 65.89, 69.30, 72.15, 72.37, 75.30, 75.76, 76.24, 79.36, 81.00, 81.58, 84.54, 122.31, 126.21, 127.71, 128.49, 128.55, 130.19, 130.89, 130.72, 131.21, 132.38, 132.76, 137.51, 142.77, 149.31, 154.67, 156.83, 165.65, 166.21, 169.39, 169.67, 173.00, 175.11, 203.85; ^{19}F NMR (470 MHz, $CDCl_3$) δ -57.95 (s, 3F), -73.31 (d, *J* = 8.0 Hz, 3F); HRMS for $C_{65}H_{86}F_6NO_{19}S_2Si^+$ calcd: 1390.4903. Found: 1390.4882 (Δ= -1.5 ppm).

SB-T-12822-5-(Me-SS-Linker)-COOH [3-23]:[28]
To a cooled solution of **3-22** (0.035 g, 0.025 mmol) in CH_3CN-pyridine (1:1) (8 mL) was added HF-pyridine (0.4 mL), and the mixture was allowed to warm from 0 °C to room temperature and react for 10 h with stirring. The reaction was quenched with 10% citric acid (10 mL) and diluted with H_2O (10 mL), and the mixture was extracted with ethyl acetate (3 x 20 mL). The combined organic layers were washed with saturated $CuSO_4$ (3 x 20 mL) and brine (3 x 20 mL), dried over $MgSO_4$, and concentrated *in vacuo* to afford **3-22** (0.031, quant.) as a white solid; conformational isomers present; R_f = 0.2 (hexanes/ethyl acetate); ^{1}H NMR (500 MHz, $CDCl_3$) δ 0.91 (m, 2H), 1.11 (m, 3H), 1.26 (s, 3H), 1.28 (m, 3H), 1.35 (s, 4.5H), 1.36 (s, 4.5H), 1.79 (m, 4H), 1.90 (s, 1.5H), 1.91 (s, 1.5H), 2.30 (m, 3H), 2.42 (s, 1.5H), 2.39 (s, 1.5H), 2.65 (m, 2H), 2.94 (m, 0.5 H), 3.02 (m, 0.5 H), 4.00 (dd, *J* = 9.0, 17.0 Hz, 1H), 4.08 (d, *J* = 7.0 Hz, 1H), 4.15 (d, *J* = 7.0 Hz, 1H), 4.31 (d, *J* = 8.0 Hz, 2H), 4.43 (m, 1H), 4.93 (m, 1H), 5.00 (d, *J* = 9.0 Hz, 1H), 5.35 (dd, *J* = 10.5, 16.0 Hz, 1H), 5.48 (s, 0.5 H), 5.52 (s, 0.5 H), 5.66 (d, *J* = 7.0 Hz, 1H), 6.24 (m, 1H), 6.29 (s, 0.5H), 6.30 (s, 0.5H), 7.26 (m, 3H), 7.35 (m, 1H), 7.48 (d, *J* = 8.0 Hz, 1H), 7.59 (t, *J* = 8.0 Hz, 1H), 7.84 (d, *J* = 7.5 Hz, 1H), 8.03 (s, 1H), 8.08 (d, *J* = 8.0 Hz, 1H); ^{13}C NMR (125 MHz, $CDCl_3$) δ 9.25, 9.47, 9.56, 11.75, 11.86, 13.01, 13.73, 14.15, 14.22, 14.73, 14.74, 17.22, 19.14, 20.11, 20.21, 21.09, 21.91, 22.12, 22.16, 22.68, 22.72, 26.61, 26.65, 27.92, 29.39, 29.72, 30.65, 31.61, 31.95, 35.26, 35.42, 38.45, 43.13, 45.38, 45.75, 45.87, 52.36, 52.61, 53.22, 55.95, 58.45, 60.44, 64.40, 69.41, 69.48, 72.14, 79.29, 81.21, 81.28, 81.57, 81.61, 84.42, 122.32, 126.22, 127.57, 127.63, 127.92, 128.53, 128.80, 129.75, 130.04, 130.40, 130.89, 131.22, 132.32, 132.76, 137.20, 137.59, 142.73, 149.32, 154.70, 154.78, 157.21, 165.63, 166.45, 169.55, 170.73, 175.14, 175.18, 195.28, 203.75; ^{19}F (470 MHz, $CDCl_3$) δ -57.95 (s, 3F), -73.09 (d, *J* = 8 Hz, 1.5H), -73.15 (d, *J* = 1.5H); HRMS for $C_{56}H_{69}F_6N_2O_{19}S_2^+$ [M+NH_4^+] calcd: 1251.3835. Found: 1251.3820 (Δ= -1.2 ppm).

Biotin-PEG-(SS-Linker)-SB-T-12822-5 (BLT-S-F_6) [3-24]:[28]
To a solution of **3-23** (0.035 g, 0.0251 mmol), *N*-biotinyl-PEG-NH_2 (**4-7**) (0.015 g, 0.036 mmol), and DMAP (0.004 g, 0.033 mmol) in $CHCl_3$ (3.3 mL) was added EDC·HCl (0.009 g, 0.049 mmol), and the mixture was allowed to react for 12 h at room temperature with stirring. The reaction mixture was concentrated *in vacuo* to give a yellow oil. Purification of the crude produt by column chromatography on silica gel with 8% CH_3OH in CH_2Cl_2 as eluent gave **3-23** (0.023 g, 49%) as a white solid; R_f = 0.38 (CH_2Cl_2/CH_3OH = 9:1); ^{1}H NMR (500 MHz, $CDCl_3$) δ 1.02 (t, *J* = 8.0 Hz, 2H), 1.18 (s, 3H), 1.28 (s, 3H), 1.30 (d, *J* = 6.8 Hz, 3H), 1.37 (s, 9H), 1.48 (m, 4H), 1.73 (m, 9H), 1.91 (m, 4H), 1.92 (s, 3H), 2.34 (m, 4H), 2.35 (s, 3H), 2.36 (m, 1H), 2.48 (t, *J* = 7.5 Hz, 2H), 2.55 (m, 1H), 2.75 (d, *J* = 12.5 Hz, 1H), 2.92 (m, 1H), 2.93 (dd, *J* = 4.5, 12.5 Hz, 1H), 3.20 (m, 2H), 3.46 (m, 4H), 3.59 (t, *J* = 5.0 Hz, 2H), 3.66 (m, 10H), 3.83 (d, *J* = 7.0 Hz, 1H), 4.01 (m, 2H), 4.09 (dd, *J* = 3.5, 6.5 Hz, 1H), 4.19 (d, *J* = 8.5 Hz, 1H), 4.35 (m, 5H), 4.54 (m, 1H), 4.94 (m, 1H), 4.99 (d, *J* = 9.0 Hz, 1H), 5.20 (s, 2H), 5.39 (s, 1H), 5.57 (t, *J* = 11.0 Hz, 1H), 5.66 (d, *J* = 7.0 Hz, 1H), 5.78 (s, 1H), 6.17 (s, 1H), 6.20 (t, *J* = 8.0 Hz, 1H), 6.33 (s, 1H), 6.51 (m, 1H), 6.75 (bt, 1H), 7.28 (m, 2H), 7.35 (m, 1H), 7.48 (d, *J* = 8.0 Hz, 1H), 7.59 (t, *J* = 7.5 Hz, 1H), 7.83 (d, *J* = 7.5 Hz, 1H), 8.03 (s, 1H), 8.08 (d, *J* = 8.0 Hz, 1H); ^{13}C NMR (125 MHz, $CDCl_3$) δ 9.21, 9.39, 9.62, 13.04, 14.74, 20.62, 20.97, 22.03, 22.52, 25.14, 22.52, 25.14, 25.54, 26.59, 27.96, 28.05, 28.12, 28.27, 28.31, 29.73, 31.31, 33.42, 33.50, 35.32, 35.64, 35.84, 38.44, 39.10, 30.15, 40.52, 42.86, 43.18, 45.85, 46.33, 47.85, 53.46, 55.32, 55.32, 55.50, 58.38, 60.19, 61.78, 69.41, 69.94, 70.00, 70.08, 70.36, 71.92, 72.47, 75.30, 75.71, 76.25, 79.20, 81.08, 81.52,

84.53, 122.29, 126.18. 127.79, 128.54, 130.40, 130.50, 130.55, 130.86, 131.26, 132.64, 132.92, 137.59, 142.29, 149.30, 153.96, 154.82, 163.42, 163.64, 165.59, 166.44, 170.00, 172.43, 173.33, 173.33, 174.04, 174.85, 203.75; ^{19}F NMR (470 MHz, $CDCl_3$) δ -57.92 (s, 3F), -73.11 (d, J = 7.5 Hz, 3F); HRMS for $C_{74}H_{98}F_6N_5O_{23}S_3^+$ calcd: 1634.5713. Found: 1634.5698 (Δ= -0.9 ppm).

^{19}F NMR Experiments

^{19}F NMR experiments were performed on a Brüker Nanobay 400 MHz NMR spectrometer operating at a ^{19}F Larmor frequency of 376 MHz with $BBFO_{PLUS}$ 5 mm probe (^{1}H–^{19}F) at 25 °C or 37 °C. ^{19}F NMR spectra were recorded using a pulse sequence of proton decoupling with a spectral width of 15,040 Hz (40 ppm), an acquisition time of 0.8 s, and a relaxation delay of 1.0 s. The obtained spectra were analyzed with TOPSPIN 3.0 (Brüker).

Formulation Experiments on BLT-S-F_6

Stock solutions of SB-T-12822-5 (**2-36**) and BLT-S-F_6 (**3-34**) were prepared by dissolving each compound in ethanol to the final concentration of 10 mM. In each experiment, an aliquot of the prepared stock solution (10 μM) was diluted with various volumes of aqueous media (PBS, saline, cell culture medium or blood plasma), 0-8% ethanol and/or excipient (solutol HS 15 or polysorbate 80), and 10% D_2O (50 μL) to the final volume of 500 μL. Formulations with excipients were performed with a 500 μL sample volume in an NMR tube with D_2O as the NMR reference solvent. Chemical shift differences were determined by comparison of the recorded chemical shifts of the 2-*m*-OCF_3 and 3'-CF_3 groups for mixtures of SB-T-12822-5 and BLT-S-F_6 in each formulation.

Time-resolved ^{19}F NMR Analysis of BLT-S-F_6

For linker stability and reactivity studies in human blood plasma, supplemental glutathione (100 equivalents) was dissolved in 200 μM solutions of BLT-S-F_6 with 86% blood plasma, 10% D_2O, 2% ethanol, 2% polysorbate (500 μL). Time-resolved ^{19}F NMR spectra, representing disulfide bond cleavage and drug release, were recorded in real-time at 37 °C beginning at 30 min after the GSH addition by measuring one spectrum every 1 h (1024 scans/spectrum) over a 13 h period (total of 13 spectra). The rate of drug release was monitored by measuring the integration ratio of the C3'-CF_3 peaks of BLT-S-F_6 (**3-24**) and SB-T-12822 (**2-36**). The normalized integration ratios indicating drug release were plotted as a function of time.

§3.7.0 References

1. Ferrara, N.; Kerbel, R. S. Angiogenesis as a therapeutic target. *Nature* **2005,** 438, 967-974.
2. Le, X. F.; Pruefer, F.; Bast, R. C., Jr. HER2-targeting antibodies modulate the cyclin-dependent kinase inhibitor p27Kip1 via multiple signaling pathways. *Cell Cycle* **2005,** 4, 87-95.
3. Goldman, J. M.; Melo, J. V. Chronic myeloid leukemia--advances in biology and new approaches to treatment. *N. Engl. J. Med.* **2003,** 349, 1451-1464.
4. Ojima, I. Guided molecular missiles for tumor-targeting chemotherapy--case studies using the second-generation taxoids as warheads. *Acc. Chem. Res.* **2008,** 41, 108-119.
5. Colquhoun, A.; Miyake, J. A.; Benadiba, M. Fatty acids, eicosanoids, and cancer. *Nutr. Thera. Metabol.* **2009,** 27, 105-112.

6. Schonberg, S. A.; Lundemo, A. G.; Fladvad, T.; Holmgren, K.; Bremseth, H.; Nilsen, A.; Gederaas, O.; Tvedt, K. E.; Egeberg, K. W.; Krokan, H. E. Closely related colon cancer cell lines display different sensitivity to polyunsaturated fatty acids, accumulate different lipid classes and downregulate sterol regulatory element-binding protein 1. *FEBS J.* **2006,** 273, 2749-2765.
7. Lauritzen, L.; Hansen, H. S.; Jorgensen, M. H.; Michaelsen, K. F. The essentiality of long chain n-3 fatty acids in relation to development and function of the brain and retina. *Prog. Lipid Res.* **2001,** 40, 1-94.
8. Schonberg, S. A.; Rudra, P. K.; Noding, R.; Skorpen, F.; Bjerve, K. S.; Krokan, H. E. Evidence that changes in Se-glutathione peroxidase levels affect the sensitivity of human tumour cell lines to n-3 fatty acids. *Carcinogenesis* **1997,** 18, 1897-904.
9. Seitz, J. D. Drug Conjugates with Polyunsaturated Fatty Acids. In *Drug Deliver in Oncology: From Basic Research to Cancer Therapy*, First ed.; Kratz, F., Ed. Wiley-VCH Verlag GmbH & Co. KGaA: Germany, 2012; Vol. 3, pp 1323-1357.
10. Grammatikos, S.; Subbaiah, P.; Victor, T.; Miller, W. n-3 and n-6 fatty acid processing and growth effects in neoplastic and non-cancerous human mammary epithelial cell lines. *Brit. J. Cancer* **1994,** 70, 219-227.
11. Bradley, M. O.; Swindell, C. S.; Anthony, F. H.; Witman, P. A.; Devanesan, P.; Webb, N. L.; Baker, S. D.; Wolff, A. C.; Donehower, R. C. Tumor targeting by conjugation of DHA to paclitaxel. *J. Control. Release* **2001,** 74, 233-236.
12. Mellado, W.; Magri, N. F.; Kingston, D. G.; Garcia-Arenas, R.; Orr, G. A.; Horwitz, S. B. Preparation and biological activity of taxol acetates. *Biochem. Biophys. Res. Commun.* **1984,** 124, 329-336.
13. Bedikian, A. Y.; DeConti, R. C.; Conry, R.; Agarwala, S.; Papadopoulos, N.; Kim, K. B.; Ernstoff, M. Phase 3 study of docosahexaenoic acid-paclitaxel versus dacarbazine in patients with metastatic malignant melanoma. *Ann. Oncol.* **2010,** 22, 787-793.
14. Bradley, M. O.; Webb, N. L.; Anthony, F. H.; Devanesan, P.; Witman, P. A.; Hemamalini, S.; Chander, M. C.; Baker, S. D.; He, L.; Horwitz, S. B.; Swindell, C. S. Tumor targeting by covalent conjugation of a natural fatty acid to paclitaxel. *Clin. Cancer Res.* **2001,** 7, 3229-3238.
15. Kuznetsova, L.; Chen, J.; Sun, L.; Wu, X.; Pepe, A.; Veith, J. M.; Pera, P.; Bernacki, R. J.; Ojima, I. Syntheses and evaluation of novel fatty acid-second-generation taxoid conjugates as promising anticancer agents. *Bioorg. Med. Chem. Lett.* **2006,** 16, 974-977.
16. Seitz, J. D.; Vineberg, J. G.; Ojima, I. Synthesis of a next-generation taxoid by rapid methylation amenable for [11C]-labeling. *J. Org. Chem.*, To be submitted shortly.
17. Warnecke, A. Site-Specific Prodrug Activation and the Concept of Self-Immolation. In *Drug Delivery in Oncology: From Basic Research to Cancer Therapy*, 1 ed.; Kratz, F., Ed. Wiley-VCH Verlag GmbH & Co. KGaA: Germany, 2012; Vol. 2, pp 553-589.
18. Zheng, Z. B.; Zhu, G.; Tak, H.; Joseph, E.; Eiseman, J. L.; Creighton, D. J. N-(2-hydroxypropyl)methacrylamide copolymers of a glutathione (GSH)-activated glyoxalase i inhibitor and DNA alkylating agent: synthesis, reaction kinetics with GSH, and in vitro antitumor activities. *Bioconjug. Chem.* **2005,** 16, 598-607.
19. Ojima, I.; Geng, X.; Wu, X.; Qu, C.; Borella, C. P.; Xie, H.; Wilhelm, S. D.; Leece, B. A.; Bartle, L. M.; Goldmacher, V. S.; Chari, R. V. Tumor-specific novel taxoid-monoclonal antibody conjugates. *J. Med. Chem.* **2002,** 45, 5620-5623.
20. Jaracz, S.; Chen, J.; Kuznetsova, L. V.; Ojima, I. Recent advances in tumor-targeting anticancer drug conjugates. *Bioorg. Med. Chem.* **2005,** 13, 5043-5054.

21. Chen, J.; Chen, S.; Zhao, X.; Kuznetsova, L. V.; Wong, S. S.; Ojima, I. Functionalized single-walled carbon nanotubes as rationally designed vehicles for tumor-targeted drug delivery. *J. Am. Chem. Soc.* **2008,** 130, 16778-16785.
22. Ojima, I. Use of fluorine in the medicinal chemistry and chemical biology of bioactive compounds--a case study on fluorinated taxane anticancer agents. *ChemBioChem* **2004,** 5, 628-635.
23. Wolf, W.; Albright, M. J.; Silver, M. S.; Weber, H.; Reichardt, U.; Sauer, R. Fluorine-19 NMR spectroscopic studies of the metabolism of 5-fluorouracil in the liver of patients undergoing chemotherapy. *Magn. Reson. Imaging* **1987,** 5, 165-169.
24. Gerig, J. T. Fluorine nuclear magnetic resonance of fluorinated ligands. *Methods Enzymol.* **1989,** 177, 3-23.
25. Dalvit, C.; Ardini, E.; Flocco, M.; Fogliatto, G. P.; Mongelli, N.; Veronesi, M. A general NMR method for rapid, efficient, and reliable biochemical screening. *J. Am. Chem. Soc.* **2003,** 125, 14620-14625.
26. Marek, P.; Yirmiya, R.; Liebeskind, J. C. Genetic influences on brain stimulation-produced analgesia in mice: II. Correlation with brain opiate receptor concentration. *Brain Res* **1990,** 507, 155-7.
27. Liebeskind, L. S.; Fengl, R. W. 3-Stannylcyclobutenediones as nucleophilic cyclobutenedione equivalents. Synthesis of substituted cyclobutenediones and cyclobutenedione monoacetals and the beneficial effect of catalytic copper iodide on the Stille reactio. *J. Org. Chem.* **1990,** 55, 5359-5364.
28. Seitz, J. D.; Vineberg, J. G.; Wei, L.; Khan, J. F.; Lichtenthal, B.; Feng, C.-F.; Ojima, I. Design, synthesis, and application of fluorine-labeled taxoids as 19F NMR probes for the metabolic stability assessment of tumor-targeted drug delivery systems. *J. Fluor. Chem.* **2014**, Submitted.
29. Appenzeller-Herzog, C. Glutathione- and non-glutathione-based oxidant control in the endoplasmic reticulum. *J. Cell. Sci.* **2011,** 124, 847-855.
30. Shaabani, A. Potassium Permanganate Oxidation of Organic Compounds. *Synth. Commun.* **2005,** 35, 571-580.
31. Bordwell, F. G. Heterocyclic Aromatic Anions with 4n+2 pi Electrons. *J. Org. Chem.* **1991,** 56, 4218-4223.
32. Chen, S.; Zhao, X.; Chen, J.; Kuznetsova, L.; Wong, S. S.; Ojima, I. Mechanism-based tumor-targeting drug delivery system. Validation of efficient vitamin receptor-mediated endocytosis and drug release. *Bioconjug. Chem.* **2010,** 21, 979-987.
33. Widdison, W. C.; Wilhelm, S. D.; Cavanagh, E. E.; Whiteman, K. R.; Leece, B. A.; Kovtun, Y.; Goldmacher, V. S.; Xie, H.; Steeves, R. M.; Lutz, R. J.; Zhao, R.; Wang, L.; Blattler, W. A.; Chari, R. V. Semisynthetic maytansine analogues for the targeted treatment of cancer. *J. Med. Chem.* **2006,** 49, 4392-4408.
34. Banerjee, P. S.; Zuniga, E. S.; Ojima, I.; Carrico, I. S. Targeted and armed oncolytic adenovirus via chemoselective modification. *Bioorg. Med. Chem. Lett.* **2011,** 21, 4985-4988.
35. Vineberg, J. G.; Zuniga, E. S.; Kamath, A.; Chen, Y. J.; Seitz, J. D.; Ojima, I. Design, Synthesis and Biological Evaluations of Tumor-Targeting Dual-Warhead Conjugates for a Taxoid-Camptothecin Combination Chemotherapy. *J. Med. Chem.* **2014,** 57, 5777-5791.

Chapter 4

Biotin-Linker-Taxoid Tumor-targeting Drug Conjugates

Chapter Contents

§4.1 Introduction

§4.1.1 Vitamins in Targeted Drug Delivery

Vitamins are essential nutrients that are not produced in sufficient quantities in living systems and are obtained externally through the diet.[1] Classified by their biological or chemical activity, rather than by structure, vitamins consist of numerous classes, including the B vitamins.[1] B vitamins (i.e. biotin, folic acid, niacin, etc.) are a group of water-soluble vitamins that serve as cofactors for numerous processes involved in cell metabolism.[2] All living cells depend on vitamins for survival, but cancer cells require certain vitamins substantially more than most normal cells do in order to sustain their rapid cell growth and enhanced proliferation.[3-5] Thus, receptors for these vitamins are overexpressed on the cell surfaces of cancer cells to maintain sufficient vitamin uptake.[3-5] The increased expression level of these cell surface receptors has emerged as a tumor-specific biomarker for tumor-targeted drug delivery, as well as the identification and imaging of tumor cells.[6-12]

§4.1.2 Biotin as a Tumor-targeting Module

Of these B-class vitamins, D-(+)-biotin (vitamin B_7, vitamin H, coenzyme R) acts as a coenzyme for five-biotin-dependent carboxylases in the single-carbon transfer of bicarbonate to organic acids in mediating the covalent binding of bicarbonate to organic acids.[2] Biotin also plays a role in epigenetic regulation via cellular signaling, fats and amino acids metabolism, fatty acid synthesis, and energy production.[2, 13] Synthesized by microorganisms and plants, and present at low concentrations relative to most vitamins in the food supply, like all vitamins, biotin is obtained by mammals through the diet.[14] Biotin is internalized by carrier-mediated uptake *via* the sodium-dependent multivitamin transporter (SMVT), which was confirmed by the cloned expression of a murine cDNA coding for SMVT in human-derived HeLa cells.[13, 15] This uptake elucidates the heightened efficacy of biotin in mammals.[13, 15, 16]

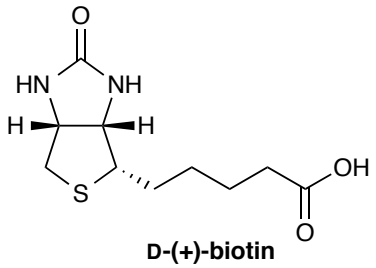

Figure 4.1. The chemical structure of D-(+)-biotin.

Russell-Jones et al. examined the effect of vitamin-targeting on the accumulation of rhodamine-labeled polymers in various tumors and reported that those cancer cells that over-expressed receptors for folic acid and vitamin B_{12} also demonstrated over-expression for biotin receptors (Table 4.1).[4] Furthermore, this study indicated that the receptors for biotin were even more overexpressed than those for folic acid and vitamin B_{12} on the surface of some cancer cells, such as L1210FR, Colo-26, P815, RD995, 4TI, JC, and MMT060562.[4] The relative uptake of vitamin-targeted rhodamine-labeled polymers in various tumor cell lines is given in Table 4.1.

Table 4.1. Relative uptake of folate-, cobalamin-, and biotin-targeted rhodamine-labeled polymers in various tumor cell lines Adapted from reference [4].

Tumor	Mouse	Type	Folate	Cbl	Biotin
HCT-116	Balb/C-Nu	Colon	–	–	–
L1210	DBA/2	Leukemia	+/–	+/–	–
L1210FR	DBA/2	Leukemia	++	+	+++
Ov2008	Balb/C-Nu	Ovarian	+++	–	++
ID8	C57/BI	Ovarian	+++	–	++
Ovcar-3		Ovarian	+++	–	++
Colo-26	Balb/C	Colon	+/–	++	+++
P815	DBA/2	Mastocytoma	+/–	++	+++
M109	Balb/C	Lung	+	+++	+++
RENCA	Balb/C	Renal cell	+	+++	+++
RD995	C3H/HeJ	Renal cell	+	++	+++
4TI	Balb/C	Breast	+	++	+++
JC	Balb/C	Breast	+	++	+++
MMT060562	Balb/C	Breast	+	++	+++

The relative uptake of the vitamin-targeted rhodamine-labeled polymers can be categorized into three, distinct classifications: (1) 0157, BW5147, B16, LL-2, and HCT-116 demonstrated no heightened efficacy; (2) L1210, Ov2008, ID8, and Ovcar exhibited enhanced efficacy of both folate and biotin receptors; and (3) Colo-26, P815, M109, RENCA, RD995, 4T1, JC, and MMT060562 displayed enhanced efficacy of both vitamin B_{12} and biotin.[4] Thus, the biotin receptor has become a new target for tumor-targeted drug delivery.

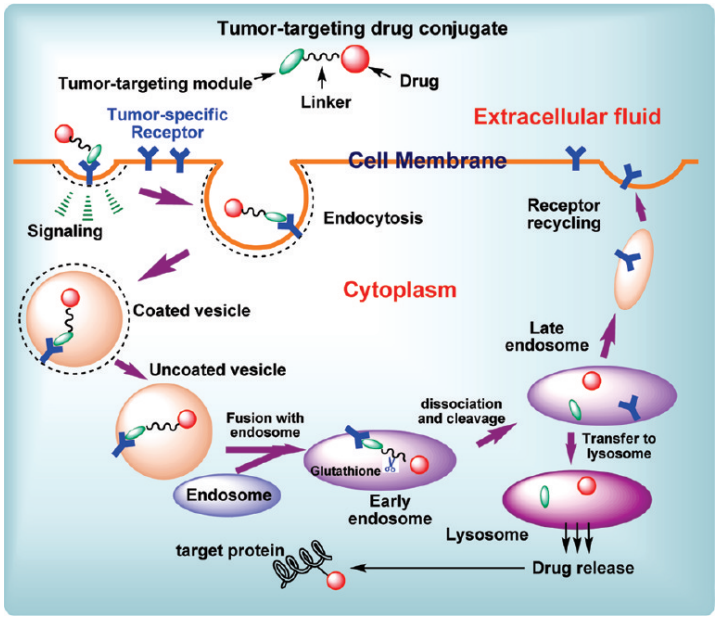

Figure 4.2. Receptor-mediated endocytosis and intracellular drug release. Reprinted from reference [6].

Biotin uptake has been shown to be Na^+, pH, and temperature dependent, but energy independent, through the biotin receptor by receptor-mediated endocytosis (RME), illustrated in Figure 4.2.[16] After a biotin conjugate binds to the cell surface receptor, a signaling cascade is

initiated, and an invagination of the plasma membrane leads to the formation and internalization of a coated vesicle containing the conjugate. This internalized vesicle fuses with the endosome, as the conjugate is transferred from the early endosome to the lysosome, which is acidic in pH and contains elevated concentrations of endogenous thiols, such as glutathione (GSH) and thioredoxin. Previously, biotin RME was validated using CFM and quantified using flow cytometry, as demonstrated with biotin-NHNH-FITC.[6]

§4.2 Biotin-Linker-Taxoid SMDCs

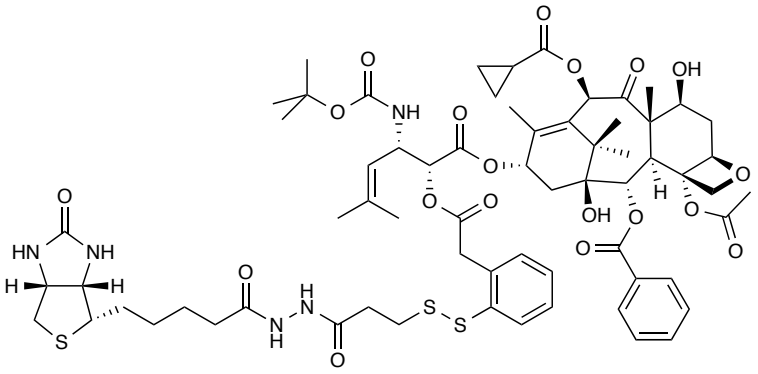

Figure 4.3. The chemical structure of the original biotin-linker-taxoid conjugate. Adapted from reference [6].

The structure of the original biotin-linker-taxoid (BLT) conjugate, an efficient mechanism-based tumor-targeting drug delivery system, based on tumor-specific biotin receptor-mediated endocytosis, is shown in Figure 4.3. This BLT design consists of biotin as the tumor-targeting module connected to a next-generation taxoid (SB-T-1214) through a self-immolative disulfide linker and a hydrazide spacer.[6] The conjugate demonstrated high potency (IC_{50} 8.8 nM) and target-specificity towards biotin receptor overexpressing (BR+) cancer cell line L1210FR (murine leukemia), while those against L1210 (murine leukemia) and WI38 (normal lung fibroblast), cell lines that do not overexpress the biotin receptor (BR-), were 59–65 times less potent.[6] SB-T-1214 was tested against the same three cell lines, and did not differentiate between BR+ and BR-, highlighting both the non-specific activity of the taxoid and the high target-specificity of the biotin conjugate.[6]

The original BLT design contained a 3-carbon disulfide linker, which was found to lack sufficient stability in aqueous media and decompose due to a retro-Michael reaction, forming an α,β-unsaturated ketone and the free disulfide. In a second-generation self-immolative disulfide linker design, a 4-disulfanylpentanoic acid moiety was incorporated to prevent this decomposition pathway. In this study, linkers bearing a 4-disulfanylpentanoic acid moieties are more stable than disulfanylpropanoic acid moieties and exhibit about one order of magnitude longer half-life than the latter design.[17] Thus, these longer disulfide linkers were synthesized and incorporated into next-generation BLT tumor-targeting drug conjugates.

§4.2.1 Synthesis of Biotin-(SS-Linker)-Taxoid: Methyl-branched Disulfide Linker

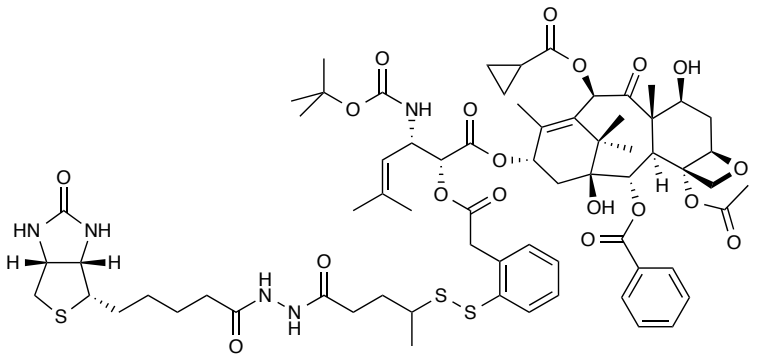

BLT (**4-3**)

Figure 4.4. The chemical structure of biotin-(SS-linker)-taxoid: methyl-branched disulfide linker (**4-3**).

Next-generation biotin-(SS-Linker)-taxoid **4-3** consists of biotin as the tumor-targeting module connected to SB-T-1214 through a methyl-branched 5-carbon self-immolative disulfide linker and a hydrazine spacer. The structure is shown in Figure 4.4.

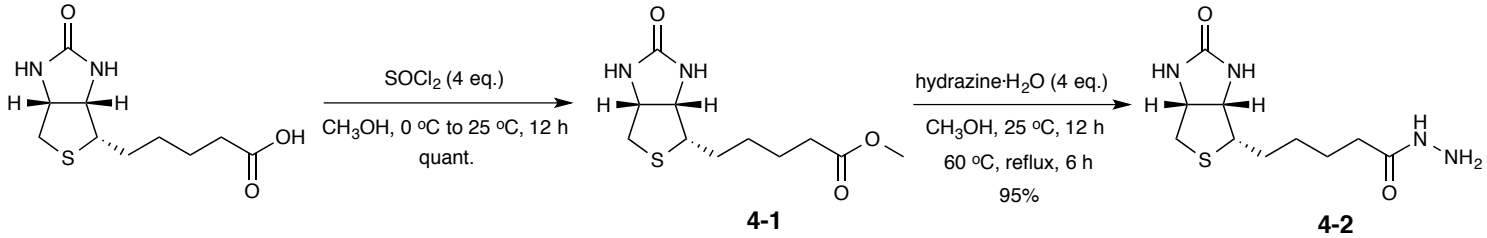

Scheme 4.1. Synthesis of biotinylhydrazine (**4-2**).

Biotin was first converted to its methyl ester **4-1** through its acyl chloride in the presence of thionyl chloride and methanol in quantitative yield (Scheme 4.1). The methyl ester was refluxed with excess hydrazine in methanol to afford biotinylhydrazine (**4-2**) in excellent yield (95%).

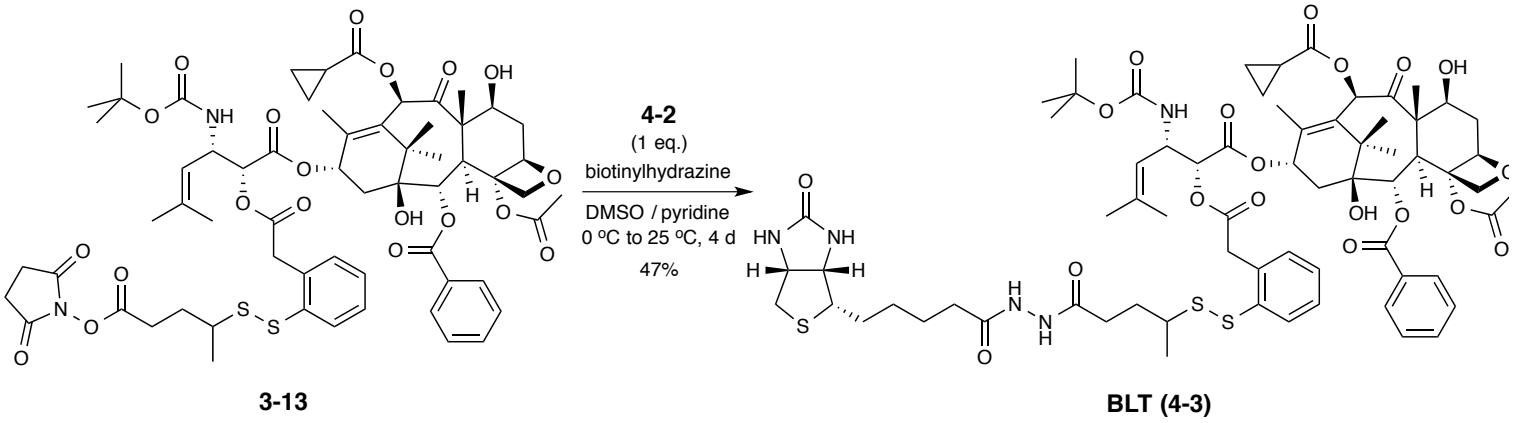

Scheme 4.2. Synthesis of biotin-(SS-Linker)-taxoid (**4-3**).

SB-T-1214-(SS-linker) activated ester construct **3-13** was coupled to **4-2** in the presence of pyridine. The reaction proceeded slowly at room temperature, but afforded **4-3** in moderate yield in >98% HPLC purity. This material was used for *in vitro* biological evaluation against BR+ cancer cell lines (Section 4.4) and *in vivo* testing in a SCID mice bearing MX-1 tumor xenograft (Section 4.5).

§4.2.2 Polyethylene Glycol Spacers

Polyethylene glycol (PEG) is a water soluble, nontoxic, non-immunogenic, and biocompatible polymer that has been approved by the U.S. Food and Drug Administration for human intravenous, oral, and dermal applications, and is employed in drug conjugates to enhance bioavailability, stability, safety, and efficacy of the cytotoxic agents.[18, 19] Many chemical functional groups can be modified with PEG, including, but not limited to amines, thiols, hydroxyls, and amides via acylation, alkylation or various other chemical and enzymatic methods.[20] However, there are three primary limitations in the use of PEG chains: (1) the synthetic polymer, polyethylene glycol, is polydisperse and contains a varying number of monomer units, in turn resulting in drug conjugates with varying molecular weights and differing biological properties, in body-residence times and immunogenicity; (2) while PEG is typically excreted by the renal pathway, higher molecular weight PEGs tend to accumulate in the liver and result in macromolecule-induced nephritic syndrome;[20] and (3) increasing the size of PEG spacers can significantly reduce tumor penetration, leading to reductions in conjugate accumulation in the tumor.[21] Thus, in order to maximize the advantage of PEG while circumventing these limitations, small-chain PEG derivatives of tetraethylene glycol were incorporated into our drug conjugates. And due to the poor solubility of taxoid-based drug conjugates, PEG conjugation was selected as a method to improve pharmacokinetic profile by reducing the rate clearance and improving overall conjugate solubility.

§4.2.3 Synthesis of Biotin-(SS-Linker)-PEG-Taxoid: BLT-S

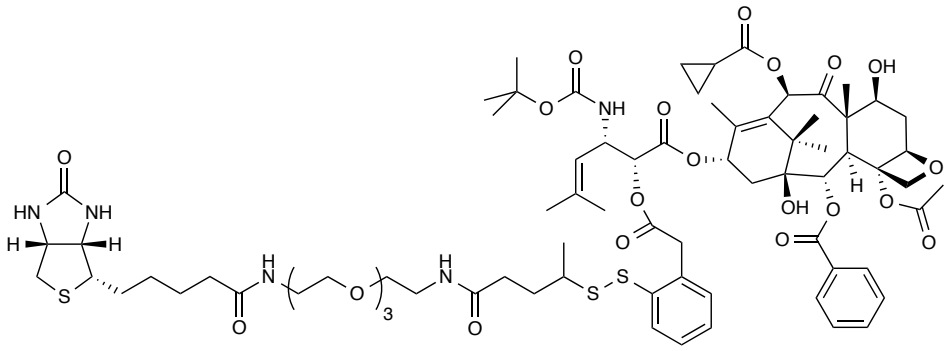

BLT-S (**4-8**)

Figure 4.5. The chemical structure of biotin-PEG-(SS-linker)-taxoid (**4-8**) with methyl-branched disulfide linker.

PEGylated biotin-PEG-(SS-Linker)-taxoid (**4-8**) consists of biotin as the tumor-targeting module connected to SB-T-1214 through a methyl-branched 5-carbon self-immolative disulfide linker and a polyethylene glycol intramolecular spacer. The structure is shown in Figure 4.5.

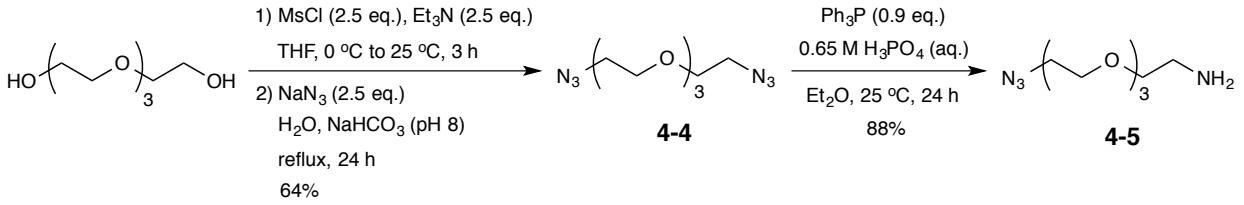

Scheme 4.3. Synthesis of 11-azido-3,6,9-trioxaundecan-1-amine (**4-5**).

Tetraethylene glycol was reacted with methanesulfonyl chloride in the presence of triethylamine to give dimesylate intermediate, which was adjusted to pH 8 and treated with sodium azide under reflux conditions to give **4-4** in good yield.[22] A selective two-phase mono-Staudinger reduction of diazide **4-4** in the presence of triphenylphosphine gave **4-5** in very good yield (88%).[22]

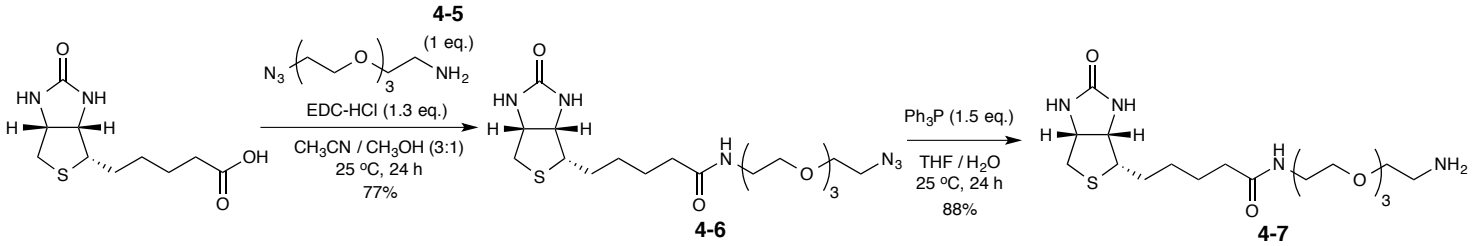

Scheme 4.4. Synthesis of *N*-biotinyl-PEG-NH_2 (**4-7**).

Coupling of biotin and **4-5** in the presence of EDC·HCl gave azide **4-6** in good yield (77%). The azide of **4-6** was reduced under Staudinger conditions in the presence of triphenylphosphine to give **4-7** in excellent yield (88%). Sufficient washing of the aqueous layer with toluene, followed by lyophilization of the aqueous layer gave **4-7** as a white solid. Unlike biotinylhydrazine, which lacked solubility in many organic solvents, *N*-biotinyl-PEG-amine is soluble in most organic solvents, including $CHCl_3$, and aqueous media.

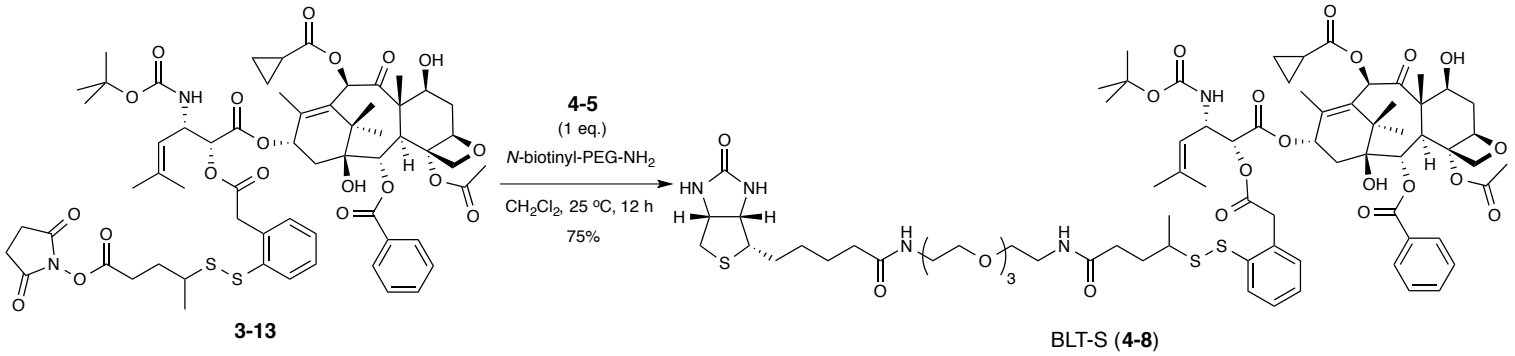

Scheme 4.5. Synthesis of biotin-PEG-(SS-Linker)-taxoid (**4-8**).

SB-T-1214-(SS-linker) activated ester construct **3-13** was coupled to **4-7** in chloroform to give **4-8** in good yield (72%). This reaction proceeded notably faster than the reaction with biotinylhydrazine at room temperature, affording **4-8** in in >98% HPLC purity. This material was used for *in vitro* biological evaluation against BR+ cancer cell lines (Section 4.4) and *in vivo* testing in a SCID mice bearing MX-1 tumor xenograft (Section 4.5) as well.

§4.2.4 Synthesis of Biotin-(SS-Linker)-Taxoid: *gem*-Dimethyl-branched Disulfide Linker

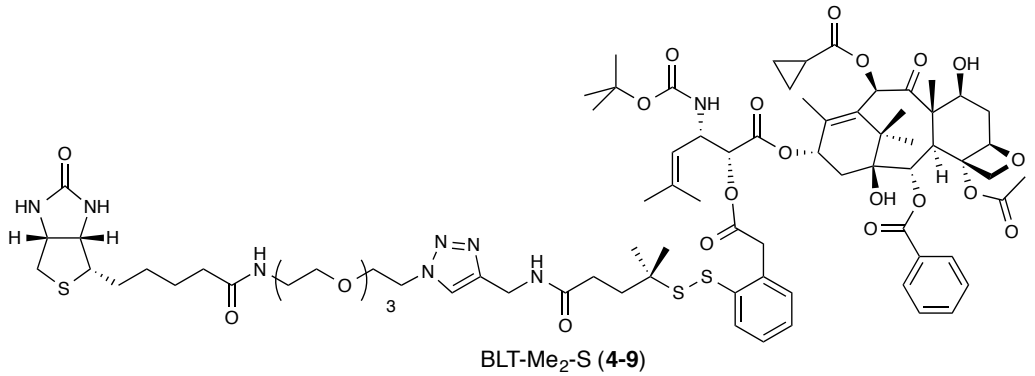

BLT-Me_2-S (**4-9**)

Figure 4.6. The chemical structure of biotin-PEG-(*gem*-Me_2-SS-linker)-taxoid: *gem*-dimethyl-branched disulfide linker (**4-9**).

Biotin-PEG-(*gem*-Me_2-SS-Linker)-taxoid (**4-9**) consists of biotin as the tumor-targeting module connected to SB-T-1214 through a germinal dimethyl-branched 5-carbon self-immolative disulfide linker and a polyethylene glycol intramolecular spacer. The structure is shown in Figure 4.6.

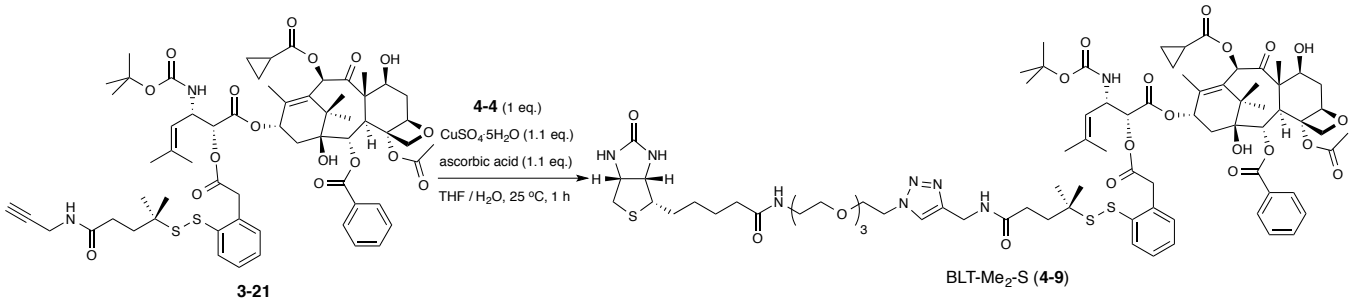

Scheme 4.6. Synthesis of biotin-PEG-(*gem*-Me_2-SS-Linker)-taxoid (**4-9**).

SB-T-1214-(*gem*-Me_2-SS-linker)-alkyne **3-21** was reacted with azide **4-6** in the presence of cupric sulfate and ascorbic acid under "click" chemistry conditions to give **4-9**. Reaction progress was monitored by TLC and mass spectrometry. The copper(I) catalyst for the 1,3-dipolar cycloaddition of the azide and terminal acetylene is generated *in situ* from copper(II) sulfate using ascorbic acid as the reducing agent. However, the product was lost during workup and subsequent column chromatography, likely due to the high polarity of the compound on silica gel column. Optimization of reaction conditions and purification methods are currently on-going in our laboratory.

§4.3 Overexpression of BR in Cancer Cells

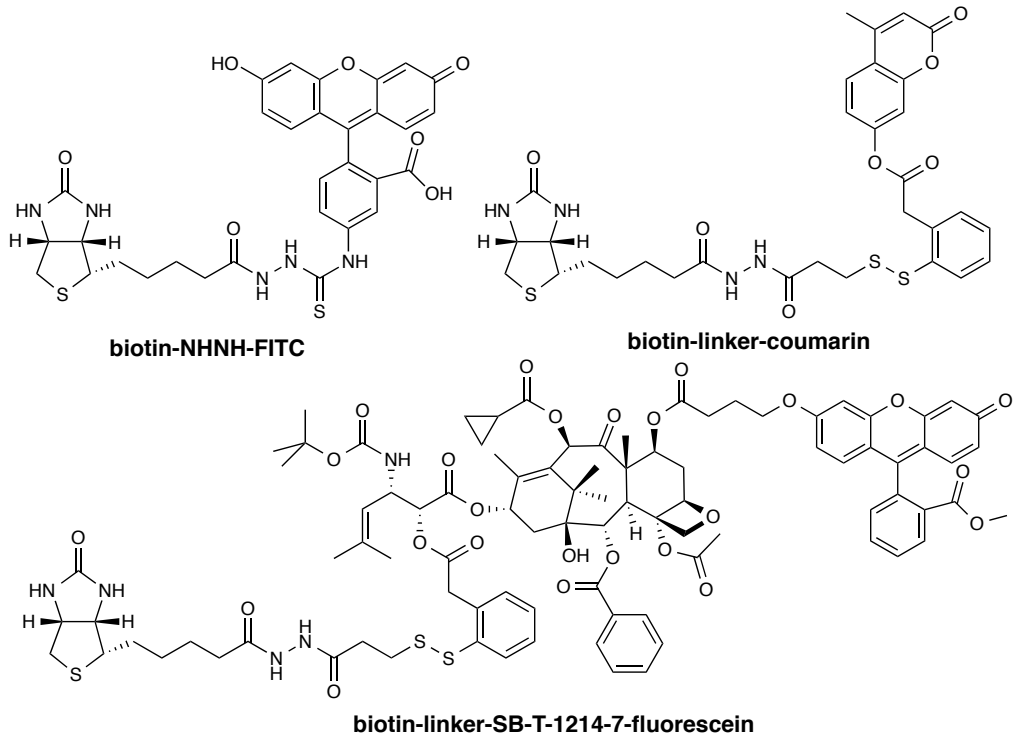

Figure 4.7. Chemical structures of fluorescent and fluorogenic probes to monitor and validate biotin RME.

Following the identification of the biotin receptor as a tumor-specific biomarker, three fluorescent and fluorogenic probes were designed and synthesized in order to monitor and validate receptor-mediated endocytosis of the biotin conjugate, drug release, and drug-binding to the target protein (Figure 4.7).[6] The first probe, biotin-NHNH-FITC, demonstrated the RME of biotin conjugates through competition, inhibition, and temperature-dependence studies, shown below in Figure 4.8.[6]

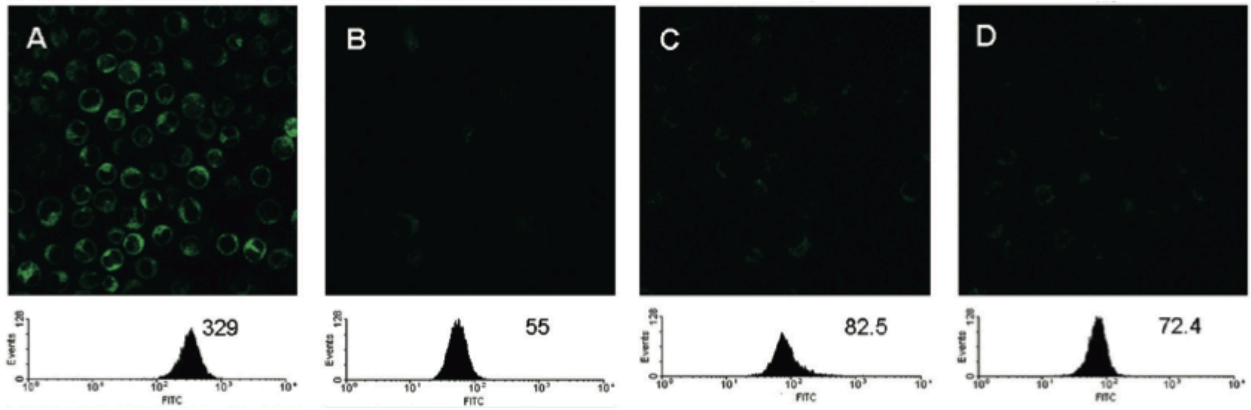

Figure 4.8. CFM and flow cytometry analysis of L1210FR cells after treatment with 100 nM biotin-NHNH-FITC for 3 h under different conditions: (A) 37 °C; (B) 4 °C; (C) 0.05% NaN_3, 37 °C; (D) pretreated with 2 mM biotin, 37 °C. The geometric mean of the fluorescence intensity in cells following treatment is given with the flow cytometry histogram. Reprinted from reference [6].

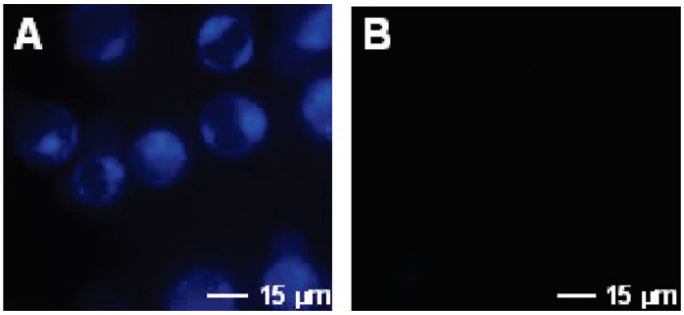

Figure 4.9. CFM images of L1210FR cells after treatment with biotin-linker-coumarin showing: (A) epifluorescence, following addition of GSH-OEt. Reprinted from reference [6].

The second probe, biotin-linker-coumarin, was designed to observe linker cleavage upon release of fluorogenic coumarin, shown in Figure 4.9.[6] The third probe, biotin-linker-SB-T-1214-fluorescein, was used to examine the cell specificity in BR+ (L1210FR) and BR- (L1210 and WI38) cell lines.[6] These probes demonstrated the target-specificity of drug conjugates to the biotin receptor as well as the mechanism-based intracellular drug release.[6]

§4.3.1 Synthesis of Biotin-PEG-FITC

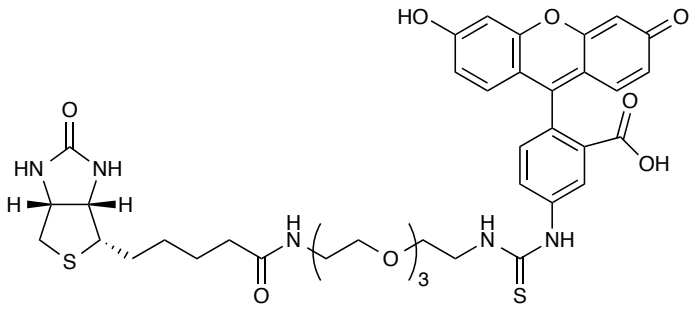

Figure 4.10. Chemical structure of biotin-PEG-FITC.

Similar to the PEGylation of biotin-PEG-(SS-linker)-taxoid, a more water-soluble fluorescent probe, biotin-PEG-FITC (**4-10**), was designed and synthesized. The structure is shown in Figure 4.10.

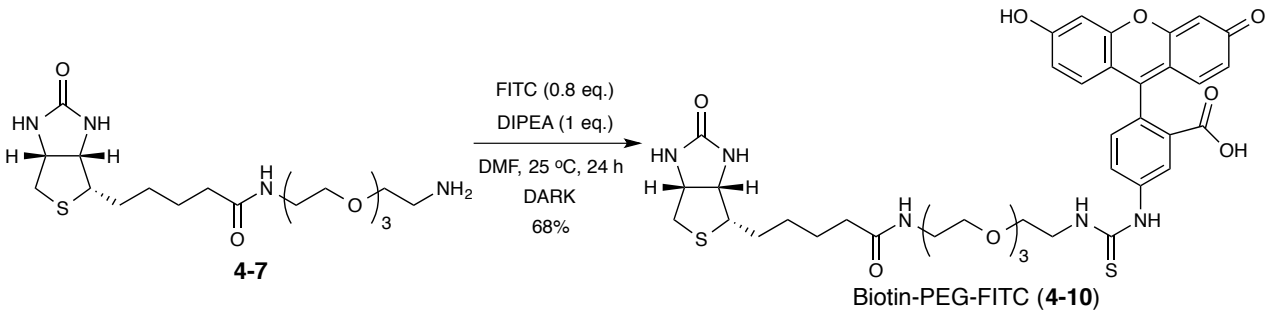

Scheme 4.7. Synthesis of biotin-PEG-FITC.

Coupling of fluorescein isothiocyanate (FITC) to **4-7** in the presence of DIPEA gave fluorescent probe **4-10** in good yield (68%), shown in Scheme 4.7. The reaction was run in the dark in the absence of heat due to the light-sensitive nature of fluorescein and its derivatives. Compound **4-10** should be stored at -20 °C or below to avoid fluorescence quenching.

§4.3.2 Flow cytometry and CFM analysis of Biotin-PEG-FITC

Fluorescent biotin-PEG-FITC probe **4-10** was used to assess the BR expression levels in several human cancer cell lines by means of flow cytometry and confocal fluorescence microscopy (CFM). As illustrated in Figure 4.11, internalization of **4-10** into MX-1 and MCF-7 (human breast carcinoma), ID8 (murine ovarian carcinoma), L1210FR and L1210 (murine leukemia cell lines), and WI38 (normal lung fibroblast) was monitored at 0, 1, and 3 h periods.

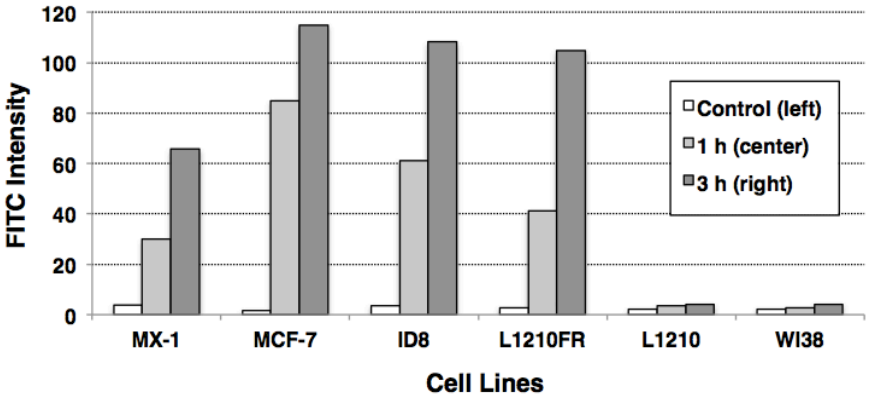

Figure 4.11. Internalization of biotin-PEG-FITC (**4-10**) into various cell lines at 0, 1, and 3 h at 37 °C. Fluorescence intensity is a geometric mean of values obtained from a flow cytometry histogram for each cell line. Reprinted from reference [23].

Previously, ID8 and L1210FR were identified as BR+ cell lines, and L1210 and WI-38 were found to be BR- cell lines.[6] However, in this study, MX-1 (BR^{++}) and MCF-7 (BR^{+++}) were newly identified as cell lines that overexpress the biotin receptor. As anticipated, the BR expression level is negligible in known BR- cell line, L1210, and normal human lung fibroblast, WI38. The flow cytometry histograms as well as the corresponding CFM images of biotin-PEG-FITC are shown in Figure 4.12 as examples.

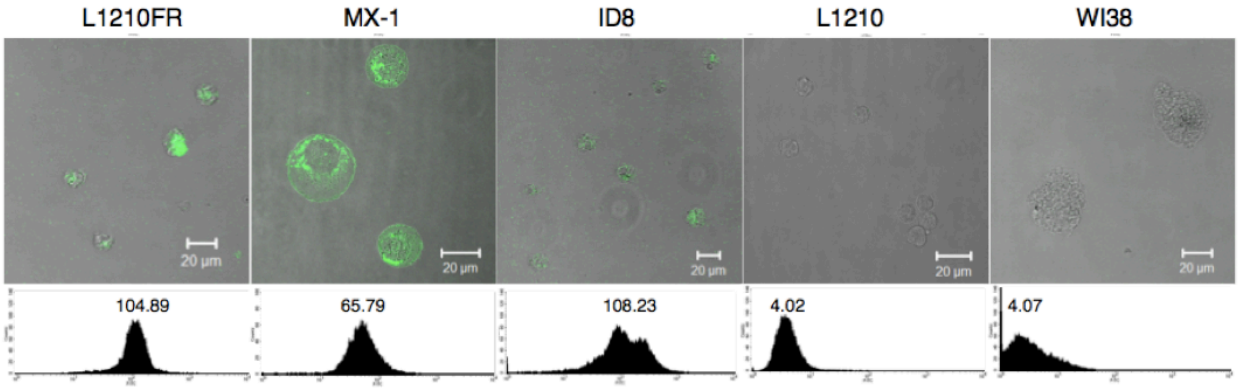

Figure 4.12. Internalization of 5 µM **4-10** for 3 h at 37 °C based on flow cytometry and CFM analysis in various cancer and normal cell lines from *left* to *right*: L1210FR (BR^{+++}), MX-1 (BR^{++}), ID8 (BR^{+++}), L1210 (BR-), WI38 (BR-).

To validate the non-specific internalization of the taxane class towards normal and cancer cell lines, paclitaxel-7-fluorescein (**2-39**) was designed and synthesized. Figure 4.13 shows the non-specific internalization of the taxoid by passive diffusion across various BR+ and BR- cell lines.

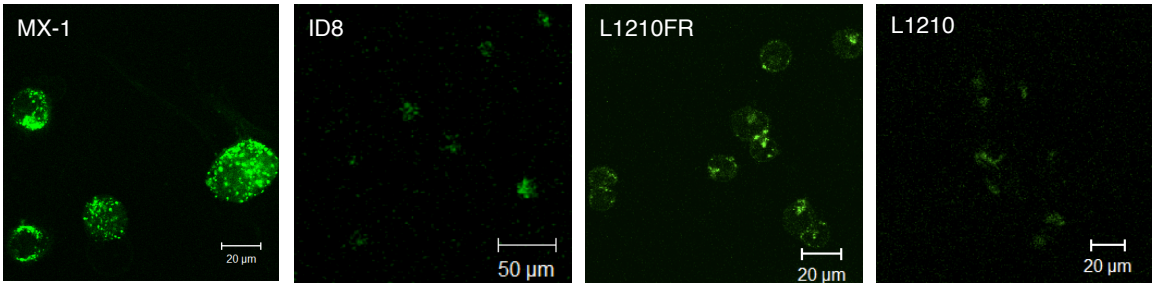

Figure 4.13. Nonspecific internalization of 5 µM paclitaxel-7-fluorescein (**2-39**) against various cell lines for 3 h at 37 °C with 5% CO_2 atmosphere.

§4.4 Biological Evaluation of Biotin-Linker-Taxoid In Vitro

The potency and efficacy of biotin-linker-taxoid conjugate **4-3** were evaluated *in vitro* against various BR+ and BR- cell lines. The cytotoxicity assays of BLT (**4-3**) against MX-1, ID8, and L1210FR (BR+ cell lines) and L1210 and WI38 (BR- cell lines) were performed by MTT method.[24] As controls, paclitaxel and parent taxoid SB-T-1214 were assayed as well. The results for 48 h drug incubation with no supplemental GSH-OEt are given in Table 4.2.

Table 4.2. Cytotoxicities (IC_{50}, nM) of paclitaxel, SB-T-1214, and BLT (4-3) against BR+ and BR- cell lines at 37 °C for 48 h.

Compound	MX-1[a]	ID8[b]	L1210FR[c]	L1210[d]	WI38[e]
paclitaxel[f]	7.23	14.36	38.7	77.1	61.4
SB-T-1214[f]	4.13	0.17	4.18	7.05	5.23
BLT (**4-3**)[f]	15.4	4.32	13.4	481	670

[a]Human breast carcinoma cell line (BR+); [b]Murine ovarian carcinoma cell line (BR+); [c]Murine lymphocytic leukemia cell line (BR+); [d]Murine lymphocytic leukemia cell line (BR-); [e]Human lung fibroblast cell line (BR-); [f]Cells were incubated with a drug or conjugate at 37 °C for 48 h.

As anticipated, the two taxoids were non-specific across all five cell lines, with SB-T-1214 possessing one to two orders of magnitude greater potency than paclitaxel, giving IC_{50} values ranging from 0.17–7 nM and 7–77.1 nM, respectively. Furthermore, BLT (**4-3**) demonstrated excellent target specificity against BR+ cell lines with IC_{50} values in a range of 4–15 nM, possessing one to two orders of magnitude greater potency than those against L1210 and WI38. However, in the absence of supplemented GSH-OEt, the potency of **4-3** remained slightly below that of its parent taxoid by ½ to 1½ orders of magnitude.

To evaluate the complete potency of BLT conjugate **4-3**, two experiments were designed to introduce supplemental GSH-OEt. In the first experiment (Table 4.3, Exp 2), glutathione ethyl ester (GSH-OEt) was added to the re-suspended cancer cells after the cells had been incubated with **4-3** for 24 h, followed by washing of the drug media with phosphate-buffered saline (PBS) and additional incubation for 48 h in fresh cell culture media; it should be noted that the re-suspended cancer cells only included BLT internalized in the first 24 h period. Under these

conditions, BLT demonstrated an approximate two-fold increase in potency compared to its 48 h incubation without supplemental GSH-OEt in BR+, whereas only a negligible increase in potency in WI38 (BR-) was observed. The results are given in Table 4.3, Exp. 2.

Table 4.3. Cytotoxicities (IC_{50}, nM) of paclitaxel, SB-T-1214, and BLT (4-3) in the presence of GSH-OEt after internalization.

Compound	MX-1[a]			L1210FR[c]			WI38[e]		
	Exp 1[b]	Exp 2[d]	Exp 3[f]	Exp 1[b]	Exp 2[d]	Exp 3[f]	Exp 1[b]	Exp 2[d]	Exp 3[f]
paclitaxel	4.07 ± 0.80			35.6 ± 8.2			131 ± 19		
SB-T-1214	2.66 ± 0.16			2.32 ± 1.41			4.89 ± 2.24		
BLT (**4-3**)	4.66 ± 0.87	3.85 ± 0.14	2.40 ± 0.18	12.3 ± 2.8	5.15 ± 2.85	2.92 ± 2.34	645 ± 97	590 ± 164	11.0 ± 3.1

[a,c,e]See captions for cell lines in Table 4.2; [b]Cells were incubated with a drug or conjugate at 37 °C in a 5% CO_2 atmosphere for 72 h; [d]Cells were initially incubated with **4-3** at 37 °C in a 5% CO_2 atmosphere for 24 h, followed by washing of the drug media with PBS, then addition of GSH-OEt (6 equiv. to conjugate) for drug release and additional incubation for 48 h; [f]Cells were initially incubated with **4-3** 37 °C in a 5% CO_2 atmosphere for 24 h, followed by addition of GSH-OEt (6 equiv. to conjugate) for drug release and additional incubation for 48 h. Total drug or conjugate incubation was 72 h for all experiments.

In the next experiment (Table 4.3, Exp 3), glutathione ethyl ester (GSH-OEt) was added to the re-suspended cancer cells after the cells had been incubated with **4-3** for 24 h, and the cells were incubated for additional for 48 h; it should be noted that the re-suspended cancer cells only included BLT internalized in the first 24 h period plus the additional released taxoid in the latter 48 h period. Under these conditions, BLT demonstrated an additional increase in potency compared to the results from "Exp 2" and its 48 h incubation without supplemental GSH-OEt in BR+, whereas there was a negligible increase in potency in WI38 (BR-). These results, given in Table 4.3, Exp. 3, indicate that after 24 h some BLT remains outside the cell. IC_{50} values for **4-3** under "Exp 3" conditions reached as low as 2.4 nM.

§4.5 Biotin-Linker-Taxoid In Vivo Studies

The biological activity of BLT was evaluated *in vivo* by treating severe combined immunodeficient (SCID) female Swiss Webster athymic nude mice bearing established, human MX-1 tumor xenografts intravenously with BLT and SB-T-1214 as comparison. Dosage for BLT was administered to three mice at 20 mg/kg per week x 4, and to two mice at 40 mg/kg per week x 2; SB-T-1214 was administered to five mice at 20 mg/kg per week x 3, followed by 40 mg/kg x 4 (Figure 4.14). It should be noted that the total dose administered to all five mice remained constant at 80 mg/kg for BLT; whereas the dose regimen for SB-T-1214 was escalated from 20 mg/kg to 40 mg/kg over time.

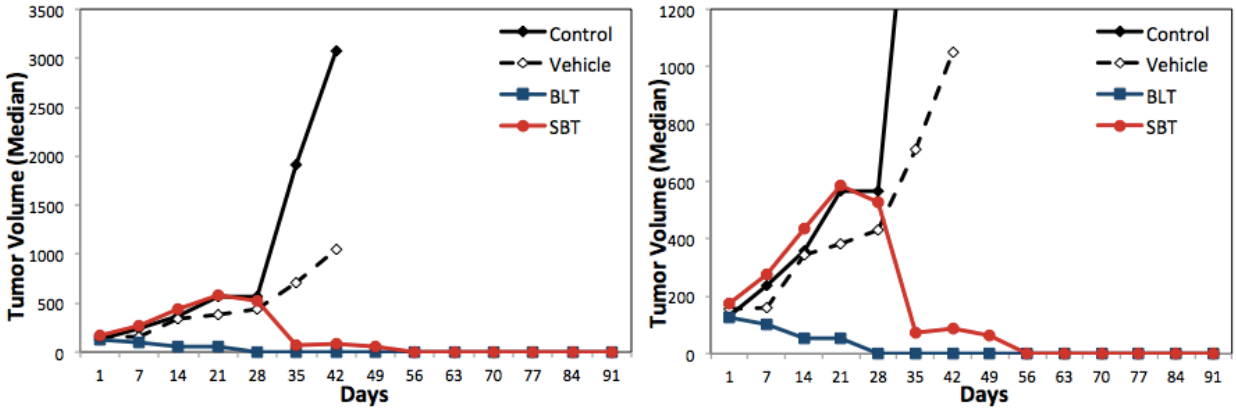

Figure 4.14. Average tumor volumes for 5 surviving SCID female Swiss Webster athymic nude mice bearing MX-1 tumor xenograft with the following dose regimen – SB-T-1214: 20 mg/kg, q7d x 3 + 40 mg/kg x 4; BLT: (a) 20 mg/kg, q7d x 4 (3 studies), (b) 40 mg/kg, q7d x 2 (2 studies). Right image is enlarged scale of left image. Adapted from reference [25].

BLT demonstrated potent antitumor activity, and all mice receiving treatment with the biotin conjugate achieved complete tumor regression after Day-28, whereas complete tumor regression was achieved in three of five mice treated with SB-T-1214. Furthermore, excluding two mice that experienced erratic tumor growth as a result of direct injection of MX-1 cells in the xenograft protocol, the mice treated with SB-T-1214 experienced only moderate weight loss during or following therapy, demonstrating a significant reduction in toxicity to normal cells. For treatment with BLT, one mouse experienced some statistically relevant weight loss. These results underline the *in vivo* application of biotin-mediated tumor-targeting. Future studies involving optimized formulation and dosing regimens and next-generation BLT conjugates are currently underway. These animal studies were conducted by Jean Rooney and Dr. Thomas Zimmerman at the Division of Laboratory Animal Resources (DLAR) at Stony Brook University and coordinated by Dr. Joshua D. Seitz.

§4.6 Design of a [^{18}F]Biotin-PEG$_3$-F for PET Imaging

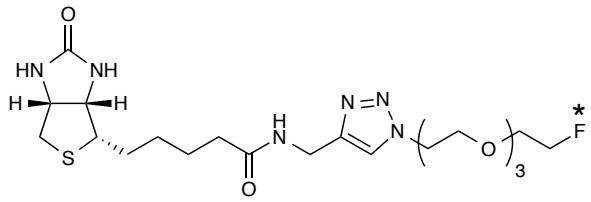

[^{18}F]biotin-PEG-F **(4-20)**

Figure 4.15. Chemical structure of [^{18}F]biotin-PEG-F.

To evaluate the biodistribution of biotin and its derivatives *in vivo*, we developed a fluorine-18 labeled derivative of biotin, [^{18}F]biotin-PEG$_3$-F, for imaging by positron emission tomography (PET). During this development, the chemical synthesis and radiosynthesis of the compound was reported in the literature by Claesener and co-workers.[26] The chemical structure of [^{18}F]biotin-PEG$_3$-F (**4-20**) is shown in Figure 4.15.

§4.6.1 Cold Synthesis of Fluorine-labeled Biotin Derivatives

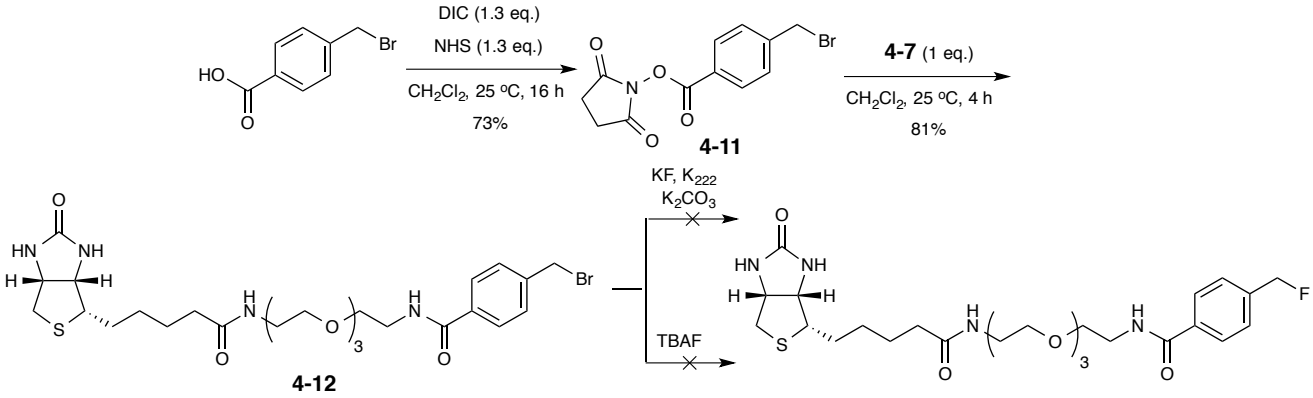

Scheme 4.8. Synthesis of biotin-PEG$_3$-Bn-Br (**4-12**) and unsuccessful subsequent fluorination.

The first design towards a fluorine-labeled biotin PET tracer began with a benzyl bromide tether. First, activation of α-bromo-*p*-toluic acid with NHS in the presence of DIC gave **4-11** in good yield (73%). Coupling of **4-11** to biotin-PEG$_3$-NH$_2$ (**4-7**) gave biotin-PEG$_3$-Bn-Br **4-12** in good yield (81%). However, fluorination of the benzyl bromide in the presence of either (1) KF, Kryptofix 222, and K_2CO_3 or (2) TBAF did not afford the desired product. Thus, an alternate design was explored.

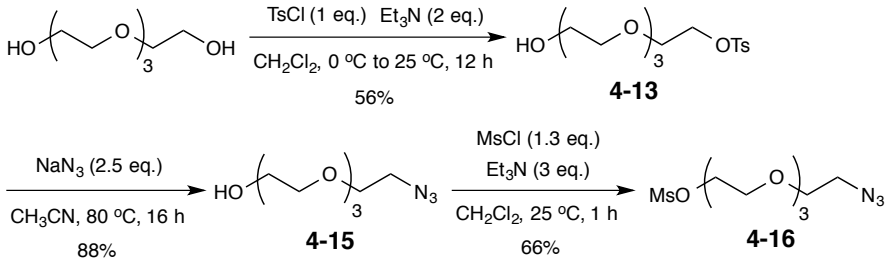

Scheme 4.9. Synthesis of 11-azido-3,6,9-trioxaundecanyl-1-methylsulfonate (**4-16**)

In the second design (Figure 4.15), biotin derivative **4-20** consists of a fluorine-labeled polyethylene glycol oligomer connected by amide linkage to the carboxyl terminus of biotin. First, tetraethylene glycol was treated with one equivalent of toluenesulfonyl chloride in the presence of triethylamine to give **4-13** in modest yield (56%), as well as the di-tosylated product **4-14** in 20% yield. Nucleophilic substitution of the mono-tosylate of **4-13** with sodium azide gave **4-15** in excellent yield (88%), followed by conversion of **4-15** to the corresponding mesylate **4-16**, shown in Scheme 4.9.

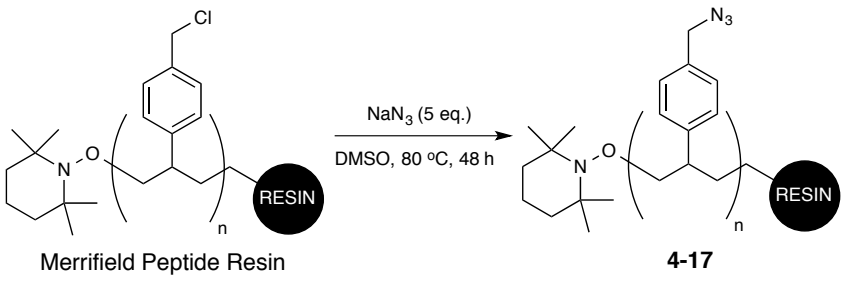

Scheme 4.10. Synthesis of Alkyne Scavenger Resin (**4-17**).

For additional ease in purification of "click" chemistry reactions, an alkyne scavenger was prepared by treatment of Merrifield Peptide Resin, swollen in DMSO, with sodium azide to give **4-17**, shown in Scheme 4.10. Infrared spectroscopy (IR) showed the signature carbon-azide stretch at 2050 cm^{-1}.

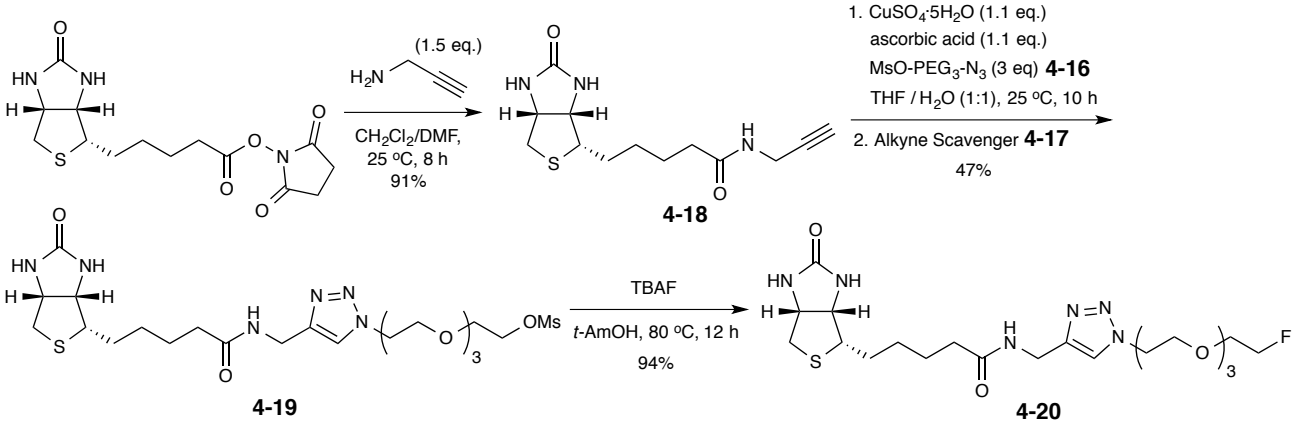

Scheme 4.11. Synthesis of biotin-PEG-F (**4-20**) as a potential PET radiotracer.

Coupling of propargylamine to biotin succinimide ester gave **4-18** in excellent yield (91%). Then, biotin derivative **4-18** was subjected to a "click" reaction with **4-16** in the presence of cupric sulfate and ascorbic acid to give the corresponding biotin-PEG_3-OMs (**4-19)** in modest yield (47%). The alkyne scavenger **4-17** was added to the reaction to quench any unreacted starting material and facilitate purification. Finally, **4-19** was treated with tetrabutylammonium fluoride in *tert*-amyl alcohol to give biotin-PEG-F (**4-20**) in excellent yield (94%), shown in Scheme 4.11. The radiosynthesis, analytical HPLC, and semi-preparative HPLC purification of **[^{18}F]4-20** will be discussed later in Chapter 7.

§4.7 Summary

Cell surface biotin receptors are overexpressed in certain cancers to maintain sufficient vitamin uptake and, thus, these receptors may serve as useful biomarkers for tumor-targeted drug delivery. A biotin fluorescence probe, biotin-NHNH-FITC, was developed to elucidate the target-specificity and internalization of biotin conjugates via the biotin receptor by receptor-mediated endocytosis. A novel biotin-fluorescence probe, biotin-PEG-FITC, was designed and synthesized to identify additional cancer cell lines that overexpress the biotin receptor. Human breast carcinoma cell lines, MX-1 and MCF-7, demonstrated efficient uptake of the probe based on flow cytometry histograms and confocal fluorescence microscopy imaging, and both have been newly identified as BR^+ cancer cell lines.

Previously, a biotin-linker-taxoid (BLT) small-molecule drug conjugate, which consists of next-generation taxoid SB-T-1214 as the cytotoxic agent, a self-immolative disulfide linker for target specific drug release, and biotin as the tumor-targeting module, was developed. This biotin-based small-molecule drug conjugate (SMDC) demonstrated excellent target specificity and high potency against BR+ tumor types both *in vitro* and *in vivo*. A next-generation biotin receptor-targeted and taxoid-based drug conjugate, BLT-S, which included a methyl-branched disulfide linker and polyethylene glycol oligomers, was designed and synthesized with the intent

of increasing its pharmacokinetic profile by lengthening its half-life during circulation and improving its aqueous solubility. In addition, a conjugate with dimethyl-branched self-immolative disulfide linker (BL_2T-S) was designed and synthesized as well for even more prolonged half-life during circulation, however reaction optimization and purification methods are currently under development.

A fluorine-18 labeled derivative of biotin, [^{18}F]biotin-PEG-F, was developed to evaluate the biodistribution of biotin and its derivatives *in vivo* by positron emission tomography. The radiosynthesis and purification of [^{18}F]biotin-PEG-F will be discussed later in Chapter 7.

§4.8 Experimental

§4.8.1 Caution

Taxoids have been identified as potent cytotoxic agents. Thus, these drugs and all structurally related compounds and derivatives must be considered mutagens and potential reproductive hazards. Appropriate precautions, such as the use of gloves, goggles, labware, and fume hood, must be taken while handling these compounds at all times.

§4.8.2 General Methods

^{1}H and ^{13}C NMR spectra were measured on a Varian 300, 400, or 500 MHz spectrometer or a Bruker 400 or 500 MHz NMR spectrometer. Melting points were measured on a Thomas-Hoover capillary melting point apparatus and are uncorrected. TLC was performed on Sorbent Technologies aluminum-backed Silica G TLC plates (Sorbent Technologies, 200 μm, 20 x 20 cm), and column chromatography was carried out on silica gel 60 (Merck, 230-400 mesh ASTM). High resolution mass spectrometry analysis was carried out on an Agilent LC-UV-TOF mass spectrometer at the Institute of Chemical Biology and Drug Discovery, Stony Brook, NY or at the Mass Spectrometry Laboratory, University of Illinois at Urbana-Champaign, Urbana, IL.

§4.8.3 Materials

The chemicals were purchased from Sigma-Aldrich, Fisher Scientific, and VWR International, and used as received or purified before use by standard methods. Tetrahydrofuran was freshly distilled from sodium and benzophenone. Dichloromethane was also distilled immediately prior to use under nitrogen from calcium hydride. 4-*N,N*-dimethylaminocinnamaldehyde solution was used as a TLC stain for biotin derivatives, and H_2SO_4 (conc.) in ethanol was used for taxoid derivatives. *N*-succinimido-biotin was prepared according to literature method.[27]

§4.8.4 Experimental procedure

Biotin methyl ester [4-1]:[28]
To a cooled solution of D-(+)-biotin (0.325 g, 1.33 mmol) in CH_3OH (10 mL) was added thionyl chloride (0.4 mL, 5.32 mmol), and the mixture was allowed to warm from 0 °C to room temperature and react for 12 h with stirring. The solution immediately turned colorless and transparent. The reaction mixture was concentrated *in vacuo* to afford **4-1** (0.344 g, quant.) as a

white-solid. The product was taken directly to the subsequent step without further purification. ^{1}H NMR (300 MHz, $CDCl_3$) δ 1.47 (m, 2H), 1.67 (m, 4H), 2.53 (t, *J* = 7.2 Hz), 2.87 (d, *J* = 12.8 Hz, 1H), 2.94 (dd, *J* = 5.0 Hz, 12.8 Hz, 1H), 3.21 (t, *J* = 5.0 Hz, 1H), 3.68 (s, 3H), 4.44 (dd, *J* = 4.4, 8.0 Hz, 1H), 4.65 (dd, *J* = 4.4, 8.0 Hz). All data are in agreement with literature values.[28]

Biotinylhydrazine [4-2]:[28]
To a solution of **4-1** (0.342 g, 1.32 mmol) in CH_3OH (7 mL) was added hydrazine monohydrate (0.25 mL, 5.32 mmol), and the mixture was allowed to react for 12 h at room temperature with stirring, and then at 60 °C for 5 h under reflux. The precipitate was collected by filtration, and the collected solution was concentrated *in vacuo* and combined with the collected precipitate to afford **4-2** (0.344 g, 95%) as a white solid. The product was taken directly to the subsequent step without further purification. ^{1}H NMR (300 MHz, D_2O) δ 1.26 (m, 2H), 1.36-1.60 (m, 4H), 2.25 (t, *J* = 7.5 Hz, 2H), 2.62 (d, *J* = 12.8 Hz, 1H), 2.84 (dd, *J* = 5.0, 12.8 Hz, 1H), 3.18 (m, 1H), 4.27 (dd, *J* = 4.4, 8.0 Hz, 1H), 4.45 (dd, *J* = 4.4, 8.0 Hz, 1H); ^{13}C NMR (125 MHz, DMSO-d_6) δ 25.74, 28.49, 28.70, 33.56, 39.90, 55.89, 59.67, 61.51, 163.21, 173.81. All data are in agreement with literature values.[28]

Biotin-(Me-SS-Linker)-SB-T-1214 (BLT) [4-3]:
To a cooled solution of **3-13** (0.069 g, 0.269 mmol) in DMSO-pyridine (3:1) (3 mL) was added **4-2** (0.336 g, 0.269 mmol), and the mixture was allowed to warm from 0 °C to room temperature and react for 4 d with stirring. Purification of the reaction mixture by column chromatography on silica gel with 7% CH_3OH in CH_2Cl_2 as eluent gave **4-3** (0.175 g, 47%) as a white solid; ^{1}H NMR (400 MHz, CD_3OD) δ 1.02 (m, 2H), 1.10 (m, 2H), 1.20 (s, 6H), 1.30 (d, J = 6.8 Hz, 3H), 1.44 (s, 9H), 1.49 (m, 2H), 1.63 (m, 4H), 1.68 (s, 3H), 1.76 (s, 3H), 1.78 (s, 3H), 1.81 (m, 3H), 1.94 (s, 3H), 1.99 (m, 2H), 2.28 (t, *J* = 7.6 Hz, 2H), 2.35 (m, 2H), 2.41 (s, 3H), 2.48 (m, 2H), 2.71 (d, *J* = 12.7 Hz, 1H), 2.93 (dd, *J* = 5.0, 12.7 Hz, 1H), 2.98 (m, 1H), 3.22 (m, 1H), 3.87 (d, *J* = 7.2 Hz, 1H), 4.03 (d, *J* = 2.4, 16.7, 1H), 4.13 (d, *J* = 1.8, 16.7 Hz, 1H), 4.20 (d, J = 8.4 Hz, 1H), 4.24 (d, *J* = 8.4 Hz, 1H), 4.32 (m, 2H), 4.50 (dd, *J* = 4.4, 8.0 Hz, 1H), 4.59 (s, 2H), 4.94 (d, *J* = 2.4 Hz, 2H), 5.03 (d, *J* = 7.6 Hz, 1H), 5.28 (bs, 1H), 5.69 (d, *J* = 7.2 Hz, 1H), 6.16 (bt, *J* = 9.0 Hz, 1H), 6.48 (s, 1H), 7.33 (m, 3H), 7.53 (t, *J* = 8.0 Hz, 2 Hz), 7.66 (t, *J* = 7.4 Hz, 1H), 7.83 (d, *J* = 7.8 Hz, 1H), 8.15 (d, *J* = 7.2 Hz, 2H); ^{13}C NMR (125 MHz, CD_3OD) δ 7.81, 7.84, 9.06, 12.41, 13.64, 17.27, 19.46, 19.57, 20.99, 21.89, 24.73, 24.98, 25.59, 27.41, 27.96, 28.14, 30.61, 30.90, 32.98, 35.35, 36.14, 38.13, 39.03, 39.67, 43.20, 45.78, 45.90, 46.68, 49.32, 55.54, 57.88, 60.25, 61.85, 70.92, 71.58, 74.92, 75.18, 75.34, 76.06, 77.70, 79.11, 80.93, 84.49, 119.83, 127.51, 128.06, 128.30, 129.75, 130.01, 130.09, 130.12, 131.01, 133.19, 133.37, 133.53, 137.28, 137.40, 137.54, 141.24, 156.09, 164.75, 166.20, 168.91, 170.08, 170.10, 170.89, 172.67, 173.47, 173.72, 203.76; HRMS (TOF) for $C_{68}H_{90}N_5O_{19}S_3^+$ calcd: 1376.5387. Found: 1376.5397 (Δ = 0.7 ppm).

1,11-Diazido-3,6,9-trioxaundecane [4-4]:[22]
(JGV-01-137)
To a cooled solution of tetraethylene glycol (8.9 mL, 51.5 mmol) and methanesulfonyl chloride (9.9 mL, 128.7 mmol) in THF (40 mL) was added Et_3N (17 mL, 128.7 mmol), and the mixture was allowed to warm from 0 °C to room temperature and react for 3 h with stirring. The reaction was diluted with H_2O (20 mL) to dissolve the formed precipitate, and the pH of the reaction mixture was adjusted to 8 by addition of $NaHCO_3$(s) followed by NaN_3 (8.4 g, 128.7 mmol). The reaction mixture was concentrated *in vacuo*, and the remaining aqueous solution was heated for

24 h at 100 °C under reflux with stirring. The reaction mixture was extracted with Et_2O (5 x 100 mL). The combined organic layers were washed with brine (3 x 20 mL), dried over $MgSO_4$, and concentrated *in vacuo* to give **4-4** (8.051 g, 64%) as a light yellow liquid; ^{1}H NMR (600 MHz, $CDCl_3$) δ 3.39 (t, *J* = 4.8 Hz, 4 H), 3.68 (m, 12H). All data are in agreement with literature values.[22]

11-Azido-3,6,9-trioxaundecan-1-amine [4-5]:[22]
To a solution of **4-4** (8.051 g, 0.033 mol) in 0.65 M H_3PO_4 (80 mL) was added Ph_3P (7.78 g, 0.030 mol) in Et_2O (60 mL), and the mixture was allowed to react for 24 h at room temperature with stirring. The aqueous layer was separated and washed with Et_2O (3 x 100 mL). To the aqueous layer was added KOH (6 g), and the basic solution was cooled at 4 °C for 16 h, forming triphenylphosphine (TPPO) as a white precipitate. TPPO was removed by gravity filtration, and the product was extracted from the aqueous layer with CH_2Cl_2 (10 x 50 mL). The combined organic layers were concentrated *in vacuo* to give **4-5** (6.602 g, 88%) as a yellow liquid; ^{1}H NMR (600 MHz, $CDCl_3$) δ 1.67 (bs, 2H), 2.87 (t, *J* = 5.4 Hz), 3.40 (t, *J* = 4.8 Hz, 2H), 3.52 (t, *J* = 5.1 Hz, 2H, PEG), 3.68 (m, 10H, PEG). All data are in agreement with literature values.[22]

Biotin-PEG$_3$-azide [4-6]:[29]
To a solution of D-(+)-biotin (1.200 g, 7.023 mmol) and **4-5** (1.531 g, 7.023 mmol) in DMF (70 mL) was added EDC·HCl (0.900 g, 9.130 mmol), and the mixture was allowed to react for 24 h at room temperature with stirring. The reaction mixture was concentrated *in vacuo* to afford a yellow oil. Purification of the crude product by column chromatography on silica gel with 8% CH_3OH in CH_2Cl_2 as eluent gave **4-6** (1.688 g, 77%) as a white solid; ^{1}H NMR (500 MHz, $CDCl_3$) δ 1.44 (m, 2H), 1.68 (m, 2H), 1.76 (m, 2H), 2.23 (t, *J* = 7.5, 2H), 2.74 (d, *J* = 12.5 Hz, 1H), 2.91 (dd, *J* = 5.0, 12.5 Hz, 1H), 3.14 (m, 1H), 3.40 (t, *J* = 5.0 Hz, 2H), 3.43 (m, 2H), 3.56 (t, *J* = 5.0 Hz, 2H), 3.62-3.68 (m, 10H), 4.32 (dd, *J* = 4.8, 8.1 Hz, 1H), 4.50 (dd, *J* = 4.8, 8.1 Hz, 1H), 5.39 (s, 1H), 6.37 (s, 1H), 6.71 (m, 1H). All data are in agreement with literature values.[29]

Biotin-PEG$_3$-amine [4-7]:[30]
To a solution of **4-6** (0.899 g, 2.025 mmol) and Ph_3P (0.797 g, 3.037 mmol) in THF (20 mL) was added H_2O (0.7 mL), and the mixture was allowed to react for 16 h at room temperature with stirring. The reaction mixture was concentrated *in vacuo*, diluted with H_2O (10 mL), and washed with toluene (5 x 30 mL). The aqueous layer was concentrated *in vacuo* by azeotropic distillation with THF to afford **4-8** (0.741 g, 88%) as a white solid; ^{1}H NMR (300 MHz, D_2O). δ 1.27 (m, 2H), 1.48 (m, 4H), 2.12 (t, *J* = 7.2 Hz, 2H), 2.62 (d, *J* = 12.9 Hz, 1H), 2.83 (dd, *J* = 5.1, 12.9 Hz, 1H), 2.80 (m, 2H), 3.18 (m, 1H), 3.23 (t, *J* = 5.1 Hz, 2H), 3.41-3.55 (m, 12H), 4.27 (dd, *J* = 4.8, 8.1 Hz, 1H), 4.45 (dd, *J* = 4.8, 8.1 Hz, 1H). All data are in agreement with literature values.[30]

Biotin-PEG$_3$-Me-SS-Linker-SB-T-1214 (BLT-S) [4-8]:
To a solution of **3-13** (36 mg, 0.0289 mmol) in CH_2Cl_2 (1 mL) was added **4-7** (12 mg, 0.0289 mmol) in CH_2Cl_2 (1 mL), and the mixture was allowed to react for 6 h at room temperature with stirring. The reaction mixture was concentrated *in vacuo* to give an off-white solid. Purification of the crude product by column chromatography with 10% CH_3OH in CH_2Cl_2 as eluent gave **4-8** (32 mg, 72%) as a white solid; ^{1}H NMR (500 MHz, CD_3OD) δ 0.93 (m, 1H), 1.03, (m, 2H), 1.06 (m, 1H), 1.11 (m, 1H), 1.21 (s, 6H), 1.31 (d, *J* = 6.8 Hz, 3H), 1.45 (s, 9H), 1.68 (s, 3H), 1.69 (m, 4H), 1.78 (s, 3H), 1.80 (s, 3H), 1.95 (s, 3H), 2.23 (t, *J* = 7.4 Hz, 2H), 2.30 (m, 2H), 2.41 (s, 3H),

2.49 (m, 2H), 2.72 (d, *J* = 12.8 Hz, 1H), 2.91 (m, 1H), 2.94 (dd, *J* = 5.0, 12.8 Hz, 1H), 3.21 (m, 1H), 3.38 (m, 2H), 3.56 (m, 4H), 3.67 (m, 8H), 3.88 (d, *J* = 7.1 Hz, 1H), 4.05 (dd, *J* = 2.8, 16.7 Hz, 1H), 4.14 (d, *J* = 16.7 Hz, 1H), 4.23 (m, 2H), 4.32 (dd, *J* = 4.4, 8.0 Hz, 1H), 4.35 (m, 1H), 4.50 (m, 1H), 4.95 (s, 2H), 5.04 (d, *J* = 9.2 Hz, 1H), 5.31 (bs, 1H), 5.70 (d, *J* = 7.2 Hz, 1H), 6.71 (m, 1H), 6.49 (s, 1H), 6.92 (d, *J* = 7.8 Hz, 1H), 7.32 (m, 1H), 7.35 (m, 2H), 7.54 (t, *J* = 7.7 Hz, 2H), 7.67 (t, *J* = 7.4 Hz, 1H), 7.84 (m, 1H), 8.16 (d, *J* = 7.6 Hz, 2H); ^{13}C NMR (125 MHz, CD_3OD) δ 7.75, 7.78, 9.02, 12.38, 13.64, 17.25, 19.50, 19.54, 20.97, 21.86, 24.70, 25.46, 25.58, 27.39, 28.11, 28.39, 31.33, 31.36, 32.79, 32.91, 35.36, 36.14, 38.11, 38.96, 39.67, 43.20, 45.88, 45.97, 46.67, 55.61, 57.88, 60.22, 61.92, 69.15, 69.22 69.84, 70.21, 70.92, 71.54, 74.92, 75.19, 75.31, 76.05, 77.69, 79.07, 80.93, 84.48, 119.88, 127.60, 128.02, 128.78, 129.75, 130.03, 130.12, 130.16, 131.09, 131.14, 156.10, 164.69, 166.19, 168.88, 170.02, 173.65, 173.75, 174.69, 203.75. HRMS for $C_{76}H_{106}N_5O_{22}S_3^+$ calcd: 1536.6486. Found: 1536.6427 (Δ = -3.8 ppm)

Biotin-PEG$_3$-*gem*-dimethyl-SS-Linker-SB-T-1214 [4-9]:
To a solution of **3-21** (24 mg, 0.0202 mmol), **4-6** (9 mg, 0.222 mmol), and ascorbic acid (4.4 mg, 0.222 mmol) in THF (0.8 mL) was added $CuSO_4{\cdot}H_2O$ (5 mg, 0.222 mmol) in H_2O (0.2 mL), and the mixture was allowed to stir for 48 h at room temperature with stirring. The reaction was diluted with H_2O (10 mL) and extracted with CH_2Cl_2 (3 x 20 mL). The combined organic layers were concentrated *in vacuo* to give an off-white solid. Purification of the crude product did not lead to the desired product. HRMS for $C_{80}H_{111}N_8O_{22}S_3^+$ calcd: 1631.6970. Found: 1631.6987 (Δ = 1.0 ppm). Reaction optimization and purification method develop is currently under development.

Biotin-PEG$_3$-FITC [4-10]:
To a solution of fluorescein isothiocyanate (FITC) (20 mg, 0.0502 mmol) and **4-7** (30 mg, 0.0717 mmol) in DMF (0.6 mL) was added DIPEA (14 μL, 0.0502 mmol), and the mixture was allowed to react for 48 h at room temperature in the dark with stirring. The reaction mixture was directly loaded onto a silica gel column. Purification of the reaction mixture by column chromatography on silica gel with 15% CH_3OH in CH_2Cl_2 as eluent gave **4-10** (27 mg, 68% yield) as an orange solid; mp 191-192 °C; ^{1}H NMR (500 MHz, CD_3OD) δ 1.40 (m, 2H), 1.62 (m, 2H), 1.69 (m, 2H), 2.19 (t, *J* = 7.4 Hz, 2H), 2.67 (d, *J* = 12.7 Hz, 1H), 2.88 (dd, *J* = 5.0, 12.7 Hz, 1H), 3.15 (m, 1H), 3.32 (m, 2H), 3.51 (t, *J* = 5.2 Hz, 2H), 3.59 (m, 2H), 3.63 (m, 2H), 3.68 (s, 4H), 3.71 (t, *J* = 5.2 Hz, 2H), 3.82 (bs, 2H), 4.26 (dd, *J* = 4.5, 7.9 Hz, 1H), 4.45 (dd, *J* = 4.5, 7.9 Hz, 1H), 6.55 (dd, *J* = 2.4, 8.8 Hz, 2H), 6.67 (d, *J* = 2.4 Hz, 2H), 6.69 (d, *J* = 8.8 Hz, 2H), 7.16 (d, *J* = 8.3 Hz, 1H), 7.77 (d, *J* = 7.8 Hz, 1H), 7.95 (bs, 1H), 8.15 (d, J = 1.7 Hz, 1H); ^{13}C NMR (125 MHz, CD_3OD) 7.21, 12.43, 15.43, 21.71, 24.82, 27.47, 27.73, 30.77, 34.74, 38.32, 39.05, 43.49, 45.89, 54.97, 59.61, 61.35, 68.58, 69.24, 69.32, 69.56, 69.61, 101.54, 109.74, 112.02, 123.99, 128.46, 140.43, 152.40, 164.11, 169.25, 174.15, 180.88; HRMS (TOF) for $C_{39}H_{46}N_5O_{16}S_2^+$ calcd: 808.2681. Found: 808.2691 (Δ = 1.2 ppm).

4-(Bromomethyl)-*N*-benzoate succinimide ester [4-11]:[31]
To a solution of α-bromo-*p*-toluic acid (1.500 g, 6.98 mmol) and HOSu (0.980 g, 8.37 mmol) in CH_2Cl_2 (50 mL) was added DIC (1.3 mL, 8.37 mmol), and the mixture was allowed to react for 16 h at room temperature with stirring. The reaction mixture was concentrated *in vacuo* to afford a white solid. Purification of the crude product by column chromatography on silica gel with hexanes/ethyl acetate (2:3) as eluent gave **4-11** as a white solid. The solid was recrystallized

from ethyl acetate and hexanes to afford **4-11** (1.589 g, 73%) as a white crystalline solid; ^{1}H NMR (300 MHz, DMSO-d_6) δ 2.94 (s, 4H), 4.86 (s, 2H), 7.76 (d, J = 8.2 Hz, 2H), 8.13 (d, J = 8.2 Hz, 2H). HRMS (TOF) for $C_{12}H_{11}NO_4Br^+$ calcd: 311.9871. Found: 311.9874 (Δ = 1.0 ppm).

Biotin-PEG$_3$-Bn-Br [4-12]:
To a solution of **4-7** (50 mg, 0.120 mmol) in CH_2Cl_2 (1 mL) was added **4-11** (37 mg, 0.120 mmol) in CH_2Cl_2 (1 mL), and the mixture was allowed to react for 4 h at room temperature with stirring. The reaction mixture was concentrated in vacuo to afford an off-white solid. Purification of the crude product by column chromatography on silica gel with 10% CH_3OH in CH_2Cl_2 as eluent gave **4-12** (59 mg, 81%) as a white solid; ^{1}H NMR (500 MHz, CD_3OD) δ 1.45 (t, J = 7.8 Hz, 2H), 1.65 (m, 2H), 1.75 (m, 2H), 2.23 (t, J = 7.2 Hz, 2H), 2.72 (d, J = 12.8 Hz, 1H), 2.93 (dd, J = 5.0, 12.8 Hz, 1H), 3.21 (m, 1H), 3.53 (t, J = 5.4 Hz, 2H), 3.61 (m, 4H), 3.69 (m, 10H), 4.31 (dd, J = 4.4, 8.0 Hz, 1H), 4.50 (dd, J = 4.4, 8.0 Hz, 1H), 4.63 (s, 2H), 7.54 (d, J = 8.3 Hz, 2H), 7.83 (d, J = 8.3 Hz, 2H); ^{13}C NMR (125 MHz, CD_3OD) δ 25.41, 28.09, 28.33, 31.50, 35.34, 38.94, 39.58, 39.62, 55.56, 60.26, 61.99, 69.13, 69.18, 69.82, 69.92, 70.19, 127.11, 127.33, 127.37, 128.38, 128.88, 129.32, 134.10, 141.93, 164.67, 168.29, 172.45, 174.69. HRMS for $C_{26}H_{40}BrN_4O_6S^+$ calcd: 615.1849. Found: 615.1846. (Δ = -0.5 ppm).

11-(*p*-Toluenesulfonyl)-3,6,9-trioxaundecan-1-ol [4-13]:[32]
To a cooled solution of tetraethylene glycol (7.0 g, 0.036 mol) in CH_2Cl_2 (35 mL) was added a solution of *p*-toluenesulfonyl chloride (6.87 g, 0.036 mol) and Et_3N (5.0 mL, 0.036 mol) in CH_2Cl_2 (35 mL), and the mixture was allowed to warm from 0 °C to room temperature and react for 16 h with stirring. The reaction was diluted with H_2O (30 mL), and the mixture was extracted with CH_2Cl_2 (3 x 20 mL). The combined organic layers were dried over $MgSO_4$ and concentrated *in vacuo* to afford a yellow oil. Purification of the crude product by column chromatography on silica gel with hexanes/ethyl acetate (1:1) as eluent gave **4-13** (7.002 g, 56%) as a colorless oil; ^{1}H NMR (300 MHz, $CDCl_3$) δ 2.43 (s, 3H), 3.58 (m, 14H), 4.15 (m, 2H), 7.33 (d, J = 8.2 Hz, 2H), 7.78 (d, J = 8.2 Hz, 2H). Also obtained by column purification was the di-tosylated product, **4-14** (3.593 g, 20%) as a yellow oil; ^{1}H NMR (300 MHz, $CDCl_3$) δ 2.44 (s, 6H), 3.57 (m, 8H), 3.68 (t, J = 4.8 Hz, 4H), 4.15 (m, 4H), 7.33 (d, J = 7.8 Hz, 4H), 7.78 (d, J = 8.1 Hz, 4H). All data are in agreement with literature values.[32]

11-Azido-3,6,9-trioxaundecan-1-ol [4-15]:[32]
A solution of **4-13** (2.377 g, 6.82 mmol) and NaN_3 (0.520 g, 7.85 mmol) in CH_3CN (50 mL) was heated for 16 h at 80 °C under reflux with stirring. The reaction was diluted with H_2O (10 mL), and the mixture was extracted with ethyl acetate (5 x 10 mL). The combined organic layers were dried over $MgSO_4$ and concentrated *in vacuo* to afford **4-15** (1.310 g, 88%) as a colorless oil; ^{1}H NMR (500 MHz, $CDCl_3$) δ 3.39 (t, J = 5.1 Hz, 2H), 3.60 (t, J = 5.1 Hz, 2H), 3.66 (m, 10 H), 3.71 (m, 2H). All data are in agreement with literature values.[32]

11-Azido-3,6,9-trioxaundecanyl-1-methylsulfonate [4-16]:[32]
To a cooled solution of **4-15** (1.237 g, 5.64 mmol) in CH_2Cl_2 (30 mL) at 0 °C was added Et_3N (2.4 mL, 16.93 mmol) and methanesulfonyl chloride (0.6 mL, 7.34 mmol), and the mixture was allowed to react for 1 h at 0 °C with stirring. The reaction was diluted with H_2O (15 mL), and the mixture was extracted with CH_2Cl_2 (3 x 30 mL). The combined organic layers were dried over $MgSO_4$ and concentrated *in vacuo* to afford an orange oil. Purification of the crude product by

column chromatography on silica gel with hexanes/ethyl acetate (2:3) as eluent gave **4-16** (1.103 g, 66%) as a colorless oil; ^{1}H NMR (300 MHz, $CDCl_3$) δ 3.07 (s, 3H), 3.38 (t, *J* = 5.1 Hz, 2H), 3.66 (m, 10H), 3.76 (m, 2H), 4.37 (m, 2H). All data are in agreement with literature values.[32]

Alkyne-Scavenger Resin [4-17]:[33]
A suspension of Merrifield Peptide Resin (1.0 g, 2.5-4 mmol/g) and NaN_3 (1.3 g, 12.5-20 mmol) in DMSO (10 mL) was heated at 80 °C for 3 d with stirring. The resin beads were filtered and washed with CH_2Cl_2 (6 x 30 mL), CH_3OH (6 x 30 mL), and Et_2O (6 x 30 mL). The beads were dried under vacuum for 24 h. FTIR (cm^{-1}) 2050 (sharp, C-azide).

N-Biotinylpropargylamine [4-18]:[34]
To a solution of *N*-succinimido-D-(+)-biotin (0.445 g, 1.305 mmol) in CH_2Cl_2-DMF (1:1) (13 mL) was added propargylamine (124 μL, 1.970 mmol), and the mixture was allowed to react for 8 h at room temperature. The reaction mixture was concentrated *in vacuo* to give a yellow oil. Purification of the crude product by column chromatography on silica gel with 10% CH_3OH in CH_2Cl_2 as eluent gave **4-18** (0.332 g, 91%) as a white solid; ^{1}H NMR (500 MHz, CD_3OD) δ 1.44 (m, 2H), 1.66 (m, 4H), 2.21 (t, *J* = 7.5 Hz, 2H), 2.36 (t, *J* = 7.5 Hz, 1H), 2.49 (t, *J* = 7.4 Hz, 1H), 2.57 (t, *J* = 2.5 Hz, 1H), 2.69 (d, *J* = 12.8 Hz, 1H), 2.92 (dd, J=5.0, 12.8 Hz, 1H), 3.20 (m, 1H), 3.93 (d, *J* = 2.5 Hz, 2H), 4.30 (dd, *J* = 4.4, 8.0 Hz, 1H), 4.84 (dd, *J* = 4.4, 8.0 Hz, 1H), 4.60 (s, 1H); ^{13}C NMR (125 MHz, CD_3OD), δ 25.31, 27.98, 28.06, 28.33, 35.10, 39.66, 55.58, 60.24, 61.97, 70.71, 79.29, 164.76, 174.27. All data are in agreement with literature values.[34]

Biotin-Triazole-PEG$_3$-Mesylate [4-19]:[26]
To a solution of **4-18** (0.060 g, 0.212 mmol), **4-16** (0.126 g, 0.423 mmol), and ascorbic acid (0.040 g, 0.233 mmol) in THF (0.8 mL) was added a solution of $CuSO_4 \cdot 5H_2O$ (0.057 g, 0.223 mmol) in H_2O (0.8 mL), and the mixture was allowed to react for 16 h at room temperature with stirring. Alkyne scavenger **4-17** was added to remove any unreacted **4-18**, and the mixture was stirred for 3 h. The reaction was diluted with H_2O (3 mL), and the mixture was extracted with CH_2Cl_2 (3 x 10 mL). The combined organic layers were dried over $MgSO_4$ and concentrated *in vacuo* to afford a yellow oil. Purification of the crude product by column chromatography on silica gel with 12% CH_3OH in CH_2Cl_2 as eluent gave **4-19** (0.058 g, 47%) as a yellow solid; ^{1}H NMR (500 MHz, CD_3OD) δ 1.43 (m, 2H), 1.64 (m, 4H), 2.23 (t, *J* = 7.2 Hz, 2H), 2.79 (d, J = 12.7 Hz, 1H), 2.92 (dd, *J* = 5.0, 12.7 Hz, 1H), 3.08 (s, 3H), 3.19 (m, 1H), 3.59 (m, 8H), 3.74 (m, 2H), 3.87 (t, *J* = 5.1 Hz, 2H), 4.29 (dd, J = 4.4, 8.0 Hz, 1H), 4.35 (m, 2H), 4.42 (s, 2H), 4.48 (d, *J* = 4.4, 8.0 Hz, 1H), 4.55 (t, *J* = 5.1 Hz, 2H), 7.90 (s, 1H); ^{13}C NMR (125 MHz, CD_3OD) δ 25.33, 28.05, 28.33, 34.20, 35.19, 36.08, 39.66, 50.05, 53.43, 60.23, 61.93, 68.71, 69.00. 69.62, 70.08, 70.10, 70.12, 70.19, 123.65, 144.70, 164.72, 174.52. HRMS (TOF) for $C_{22}H_{39}N_6O_8S_2^+$ calcd: 579.2265. Found: 579.2273 (Δ = 1.4 ppm). All data are in agreement with literature values.[26]

Biotin-PEG$_3$-F [4-20]:[26]
To a solution of **4-19** (3.2 mg, 8.65 μmol) in *tert*-AmOH-DMSO (3:2) (200 μL) was added 1 M TBAF in THF (30 μL), and the mixture was heated for 6 h at 80 °C under reflux with stirring. Reaction progress was monitored by mass spectrometry. Purification of the reaction mixture by column chromatography on silica gel with 15% CH_3OH in CH_2Cl_2 as eluent gave **4-20** (2.6 mg, 94%), as a waxy solid; ^{1}H NMR (500 MHz, CD_3OD) δ 1.34 (m, 2H), 1.62 (m, 2H), 1.77 (m, 2H), 2.27 (t, *J* = 7.5 Hz, 2H), 2.73 (d, *J* = 12.6 Hz, 1H), 2.95 (dd, *J* = 5.0, 12.6 Hz, 1H), 3.23 (m, 1H),

3.64 (m, 5H), 3.66 (m, 2H), 3.70 (m, 1H), 3.77 (m, 1H), 3.90 (t, J = 5.1 Hz, 2H), 4.32 (dd, J = 4.4, 8.0 Hz, 1H), 4.46 (s, 2H), 4.50 (m, 1H), 4.52 (dd, J = 4.4, 8.0 Hz, 1H), 4.58 (t, J = 5.1 Hz, 2H), 7.93 (s, 1H); ^{13}C NMR (125 MHz, CD_3OD) δ 16.85, 25.33, 28.05, 28.33, 34.18, 35.17, 38.06, 39.64, 50.03, 53.41, 55.58, 60.22, 61.92, 68.99, 70.04, 70.09, 70.12, 70.15, 70.25, 70.27, 82.06, 83.39, 123.65, 144.66, 164.70, 174.49. All data are in agreement with literature values.[26]

Cell Culture

All cell lines were obtained from ATCC unless otherwise noted. Cells were cultured in RPMI-1640 cell culture medium (Gibco) or DMEM culture medium (Gibco), both supplemented with 5% (v/v) heat-inactivated fetal bovine serum (FBS), 5% (v/v) NuSerum, and 1% (v/v) penicillin and streptomycin (PenStrep) at 37 °C in a humidified atmosphere with 5% CO_2. Murine leukemia cell lines L1210 and L1210FR (a gift from Dr. Gregory Russell-Jones, Access Pharmaceuticals Pty Ltd., Australia) were grown as a suspension in supplemented RPMI-1640. Human breast carcinoma, MX-1 and MCF-7, and murine ovarian carcinoma, ID8, cell lines were cultured as monolayers on 100 mm tissue culture dishes in a supplemented RPMI-1640 cell culture medium, and normal human lung fibroblast cell line WI-38 (ATCC) as a monolayer in a supplemented DMEM cell culture medium. Cells were harvested, collected by centrifugation at 850 rpm for 5 min, and resuspended in fresh culture medium. Cell cultures were routinely divided by treatment with trypsin (TrypLE, Gibco) as needed every 2-4 days and collected by centrifugation at 850 rpm for 5 min, and resuspended in fresh cell culture medium, containing varying cell densities for subsequent biological experiments and analysis.

Incubation of Cells with Biotin-PEG$_3$-FITC (4-10) and Taxol-7-Fluorescein (2-36).

Cell suspensions (3 mL) of MX-1, ID8, and WI38 at 5 x 10^5 cells/mL were added to each individual well of 6-well plates, and the plates were subsequently incubated overnight in the appropriate cell culture media. The cell culture media was replaced with 5 μM solutions of fluorescent probes **4-10** or **2-36** in cell culture media (3 mL). Then, the cells were incubated with probes **4-10** or **2-36** for 1 or 3 h at 37 °C. In the case of leukemia cell lines (L1210, L1210FR), probes **4-10** or **2-36** (1 mM) in DMSO (15 μM) were injected directly into fresh cell suspensions to give a final concentration of 5 μM, and cells were incubated for similar time intervals. Following incubation, the cells were removed by treatment with trypsin as needed, washed twice with phosphate buffered solution (PBS), collected by centrifugation, and resuspended in PBS (150 μL) for subsequent confocal fluorescence microscopy imaging or flow cytometry analysis.

Confocal Fluorescence Microscopy (CFM) Imaging of the Treated Cells

Cells treated as described above were resuspended in 150 μL of PBS after each experiment, and dropped onto an uncoated microslide with coverslip (MatTek Corp). CFM experiments were performed using a Zeiss LSM 510 META NLO two-photon laser scanning confocal microscope system, operating at a 488 nm excitation wavelength and at 527 ± 23 nm detecting emission wavelength using a 505-550 nm bandpass filter. Images were captured using a C-Apochromat 63x/1.2 water (corr.) objective. Acquired data were analyzed using LSM 510 Meta software.

Flow Cytometry Fluorescent Measurements of the Cells

Flow cytometry analysis of the cells treated with probes **4-10** or **2-36** was performed with a flow cytometer, FACSCalibur, operating at a 488 nm excitation wavelength and detecting 530 nm emission wavelengths with a 30 nm bandpass filter (515-545 nm range). Cells treated as described above were resuspended in 0.5 mL of PBS. Approximately 10,000 cells were counted for each experiment using *CellQuest 3.3* software (Becton Dickinson), and the distribution of FITC fluorescence was analyzed using *WinMDI 2.8* freeware (Joseph Trotter, Scripps Research Institute).

In Vitro Cytotoxicity Assays.

The cytotoxicities (IC_{50}, nM) of paclitaxel, SB-T-1214, and **4-3** were evaluated against various cancer cell lines by means of the standard quantitative colorimetric MTT assay.[24] The inhibitory activity of each compound is represented by the IC_{50} value, which is defined as the concentration required for inhibiting 50% of the cell growth. Cells were harvested, collected, and resuspended in 100 μL cell culture medium (RPMI-1640 or DMEM) at a concentrations ranging from 0.5-1.5 x 10^4 cells per well in a 96-well plate. For adhesive cell types, cells were allowed to descend to the bottom of the wells overnight, and appropriate fresh medium was added to each well upon removal of the old medium.

For the MTT assay of paclitaxel, SB-T-1214, and **4-3**, cells were resuspended in 200 μL medium with 8,000 to 10,000 cells per well of a 96-well plate and incubated at 37 °C for 24 h before drug treatment. In DMSO stock solutions, each drug or conjugate was diluted to a series of concentrations in cell culture medium to prepare test solutions. After removing the old medium, these test solutions were added to the wells in the 96-well plate to give the final concentrations ranging from 0.5 to 5,000 nM (100 μL), and the cells were subsequently cultured at 37 °C for 72 h. For the leukemia cell lines, cells were harvested, collected, and resuspended in the test solutions ranging from 0.5 to 5,000 nM (100 μL) at 0.5 to 0.8 x 10^4 cells per well in a 96-well plate and subsequently incubated at 37 °C for 72 h.

In a second series of experiments, cells were incubated with **4-3** at 37 °C for 24 h and the drug medium was removed. Then, treated cells were washed with PBS, and GSH-OEt (6 equivalents) in cell culture medium (200 μL) was added to the wells. These cells were incubated at 37 °C for an additional 48 h; i.e., the total incubation time was 72 h.

In a third series of experiments, cells were incubated with **4-3** at 37 °C for 24 h, and GSH-OEt (6 equivalents) in cell culture medium (100 μL) was directly added to the wells. These cells were incubated at 37 °C for an additional 48 h; i.e. the total incubation time was also 72 h.

For all experiments, after removing the test medium, fresh solution of MTT in PBS (40 μL of 0.5 mg MTT/mL) was added to the wells, and the cells were incubated at 37 °C for 3 h. The MTT solution was then removed, and the resulting insoluble violet formazan crystals were dissolved in 0.1 N HCl in isopropanol with 10% Triton X-100 (40 μL) to give a violet solution. The spectrophotometric absorbance measurement of each well in the 96-well plate was run at 570 nm using a Labsystems Multiskan Ascent microplate reader. The IC_{50} values and their standard errors were calculated from the viability-concentration curve using Four Parameter Logistic Model of *Sigmaplot*. The concentration of DMSO per well was ≤1% in all cases. Each experiment was run in triplicate.

§4.9.0 References

1. Sauberlich, H. E. Bioavailability of vitamins. *Prog. Food Nutr. Sci.* **1985,** 9, 1-33.
2. Zempleni, J.; Wijeratne, S. S.; Hassan, Y. I. Biotin. *Biofactors* **2009,** 35, 36-46.
3. Leamon, C. P. Folate-targeted drug strategies for the treatment of cancer. *Curr. Opin. Invest. Drugs* **2008,** 9, 1277-1286.
4. Russell-Jones, G.; McTavish, K.; McEwan, J.; Rice, J.; Nowotnik, D. Vitamin-mediated targeting as a potential mechanism to increase drug uptake by tumours. *J. Inorg. Biochem.* **2004,** 98, 1625-1633.
5. Lu, Y.; Low, P. S. Folate-mediated delivery of macromolecular anticancer therapeutic agents. *Adv. Drug Deliv. Rev.* **2002,** 54, 675-693.
6. Chen, S.; Zhao, X.; Chen, J.; Kuznetsova, L.; Wong, S. S.; Ojima, I. Mechanism-based tumor-targeting drug delivery system. Validation of efficient vitamin receptor-mediated endocytosis and drug release. *Bioconjug. Chem.* **2010,** 21, 979-987.
7. Chen, J.; Chen, S.; Zhao, X.; Kuznetsova, L. V.; Wong, S. S.; Ojima, I. Functionalized single-walled carbon nanotubes as rationally designed vehicles for tumor-targeted drug delivery. *J. Am. Chem. Soc.* **2008,** 130, 16778-16785.
8. Ojima, I. Guided molecular missiles for tumor-targeting chemotherapy--case studies using the second-generation taxoids as warheads. *Acc. Chem. Res.* **2008,** 41, 108-119.
9. Ojima, I.; Zuniga, E. S.; Berger, W. T.; Seitz, J. D. Tumor-targeting drug delivery of new-generation taxoids. *Future Med. Chem.* **2012,** 4, 33-50.
10. Leamon, C. P.; Reddy, J. A.; Klein, P. J.; Vlahov, I. R.; Dorton, R.; Bloomfield, A.; Nelson, M.; Westrick, E.; Parker, N.; Bruna, K.; Vetzel, M.; Gehrke, M.; Nicoson, J. S.; Messmann, R. A.; LoRusso, P. M.; Sausville, E. A. Reducing undesirable hepatic clearance of a tumor-targeted vinca alkaloid via novel saccharopeptidic modifications. *J. Pharmacol. Exp. Ther.* **2011,** 336, 336-343.
11. Vlahov, I. R.; Santhapuram, H. K.; Wang, Y.; Kleindl, P. J.; You, F.; Howard, S. J.; Westrick, E.; Reddy, J. A.; Leamon, C. P. An assembly concept for the consecutive introduction of unsymmetrical disulfide bonds: synthesis of a releasable multidrug conjugate of folic acid. *J. Org. Chem.* **2007,** 72, 5968-5972.
12. Fischer, C. R.; Muller, C.; Reber, J.; Muller, A.; Kramer, S. D.; Ametamey, S. M.; Schibli, R. [18F]fluoro-deoxy-glucose folate: a novel PET radiotracer with improved in vivo properties for folate receptor targeting. *Bioconjug. Chem.* **2012,** 23, 805-813.
13. Zempleni, J. Uptake, localization, and noncarboxylase roles of biotin. *Annu. Rev. Nutr.* **2005,** 25, 175-196.
14. McMahon, R. J. Biotin in metabolism and molecular biology. *Annu. Rev. Nutr.* **2002,** 22, 221-239.
15. Prasad, P. D.; Wang, H.; Kekuda, R.; Fujita, T.; Fei, Y. J.; Devoe, L. D.; Leibach, F. H.; Ganapathy, V. Cloning and functional expression of a cDNA encoding a mammalian sodium-dependent vitamin transporter mediating the uptake of pantothenate, biotin, and lipoate. *J. Biol. Chem.* **1998,** 273, 7501-7506.
16. Luo, S.; Kansara, V. S.; Zhu, X.; Mandava, N. K.; Pal, D.; Mitra, A. K. Functional characterization of sodium-dependent multivitamin transporter in MDCK-MDR1 cells and its utilization as a target for drug delivery. *Mol. Pharmacol.* **2006,** 3, 329-339.
17. Widdison, W. C.; Wilhelm, S. D.; Cavanagh, E. E.; Whiteman, K. R.; Leece, B. A.; Kovtun, Y.; Goldmacher, V. S.; Xie, H.; Steeves, R. M.; Lutz, R. J.; Zhao, R.; Wang, L.; Blattler,

W. A.; Chari, R. V. Semisynthetic maytansine analogues for the targeted treatment of cancer. *J. Med. Chem.* **2006,** 49, 4392-4408.
18. Harris, J. M.; Chess, R. B. Effect of pegylation on pharmaceuticals. *Nat. Rev. Drug Discov.* **2003,** 2, 214-221.
19. Cheng, T. L.; Chuang, K. H.; Chen, B. M.; Roffler, S. R. Analytical Measurement of PEGylated Molecules. *Bioconjug. Chem.* **2012,** 23, 881-889.
20. Veronese, F. M.; Pasut, G. PEGylation, successful approach to drug delivery. *Drug Discov. Today* **2005,** 10, 1451-1458.
21. Vlashi, E.; Kelderhouse, L. E.; Sturgis, J. E.; Low, P. S. Effect of folate-targeted nanoparticle size on their rates of penetration into solid tumors. *ACS Nano* **2013,** 7, 8573-8582.
22. Schwabacher, A. W.; Lane, J. W.; Schiesher, M. W.; Leigh, K. M.; Johnson, C. W. Desymmetrization reactions: Efficient preparation of unsymmetrically substituted linker molecules. *J. Org. Chem.* **1998,** 63, 1727-1729.
23. Vineberg, J. G.; Zuniga, E. S.; Kamath, A.; Chen, Y. J.; Seitz, J. D.; Ojima, I. Design, Synthesis and Biological Evaluations of Tumor-Targeting Dual-Warhead Conjugates for a Taxoid-Camptothecin Combination Chemotherapy. *J. Med. Chem.* **2014,** 57, 5777-5791.
24. Mosmann, T. Rapid colorimetric assay for cellular growth and survival: application to proliferation and cytotoxicity assays. *J. Immunol. Methods* **1983,** 65, 55-63.
25. Seitz, J. D.; Vineberg, J. G.; Ojima, I. Synthesis of a next-generation taxoid by rapid methylation amenable for [11C]-labeling. *J. Org. Chem.*, To be submitted shortly.
26. Claesener, M.; Breyholz, H. J.; Hermann, S.; Faust, A.; Wagner, S.; Schober, O.; Schafers, M.; Kopka, K. Efficient synthesis of a fluorine-18 labeled biotin derivative. *Nucl. Med. Biol.* **2012,** 39, 1189-1194.
27. Zhang, D.; Macinkovic, I.; Devarie-Baez, N. O.; Pan, J.; Park, C. M.; Carroll, K. S.; Filipovic, M. R.; Xian, M. Detection of protein S-sulfhydration by a tag-switch technique. *Angew. Chem. Int. Ed.* **2014,** 53, 575-581.
28. Wilchek, M.; Bayer, E. A. Biotin-containing reagents. *Methods Enzymol.* **1990,** 184, 123-138.
29. Fusz, S.; Srivatsan, S. G.; Ackermann, D.; Famulok, M. Photocleavable initiator nucleotide substrates for an aldolase ribozyme. *J. Org. Chem.* **2008,** 73, 5069-5077.
30. Borcard, F.; Godinat, A.; Staedler, D.; Blanco, H. C.; Dumont, A. L.; Chapuis-Bernasconi, C.; Scaletta, C.; Applegate, L. A.; Juillerat, F. K.; Gonzenbach, U. T.; Gerber-Lemaire, S.; Juillerat-Jeanneret, L. Covalent cell surface functionalization of human fetal osteoblasts for tissue engineering. *Bioconjug. Chem.* **2011,** 22, 1422-1432.
31. Li, J. L.; Wang, Y. X.; Tian, H. B.; Zhou, W.; Zhang, X. L.; Lin, Y. W.; Yin, D. Z. An improved radiochemical synthesis of N-succinimidyl 4-F-18-(fluoromethyl)benzoate and the labeling of IgG. *J. Radioanal. Nucl. Chem.* **2002,** 254, 415-419.
32. Luo, Z.; Ding, X.; Hu, Y.; Wu, S.; Xiang, Y.; Zeng, Y.; Zhang, B.; Yan, H.; Zhang, H.; Zhu, L.; Liu, J.; Li, J.; Cai, K.; Zhao, Y. Engineering a hollow nanocontainer platform with multifunctional molecular machines for tumor-targeted therapy in vitro and in vivo. *ACS Nano* **2013,** 7, 10271-10284.
33. Sachin, K.; Jadhav, V. H.; Kim, E. M.; Kim, H. L.; Lee, S. B.; Jeong, H. J.; Lim, S. T.; Sohn, M. H.; Kim, D. W. F-18 labeling protocol of peptides based on chemically orthogonal strain-promoted cycloaddition under physiologically friendly reaction conditions. *Bioconjug. Chem.* **2012,** 23, 1680-1686.

34. Rong, L.; Liu, L. H.; Chen, S.; Cheng, H.; Chen, C. S.; Li, Z. Y.; Qin, S. Y.; Zhang, X. Z. A coumarin derivative as a fluorogenic glycoproteomic probe for biological imaging. *Chem. Commun.* **2014,** 50, 667-669.

Chapter 5

Double-Warhead Conjugates for Taxoid-Camptothecin Targeted Combination Chemotherapy

Chapter Contents

§5.1.0 Introduction

§5.1.1 Combination Chemotherapy

Over the past several decades, combination chemotherapy has emerged as a primary treatment option for many types of cancers, some of which had previously been considered incurable (i.e. acute lymphocytic leukemia, Hodgkin's lymphoma).[1, 2] Combination chemotherapy involves the sequential delivery of two or more cytotoxic agents based on non-overlapping toxicities and mechanisms of action to augment therapeutic efficacy.[3, 4] Compared to the use of a single cytotoxic drug, the use of two or more properly selected agents in combination can lead to a decrease in systemic toxicity, as each drug can be administered at lower than typical doses, and an increase in efficacy due to synergistic or cooperative effects of the drugs on tumor eradication.[5] Furthermore, a sequential treatment with chemotherapeutic agents bearing different mechanisms of action has been shown to circumvent drug resistance and lead to synergistic enhancement of efficacy.[3, 6, 7]

§5.1.2 Camptothecins

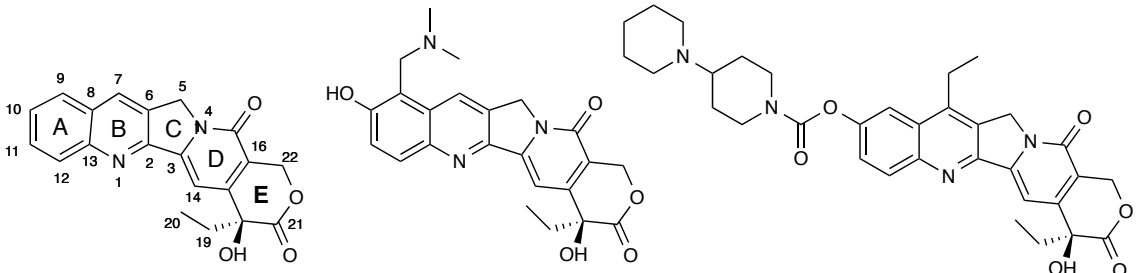

Figure 5.1. Chemical structures of camptothecin (CPT), topotecan, and irinotecan (CPT-11).

Camptothecin (CPT) and its derivatives are classified as topoisomerase I (topo I) inhibitors, which prevent the cleavage and reannealing of single-strand DNA (ssDNA) during replication and transcription.[8] These inhibitors increase the number of intracellular covalent topo I–DNA complexes, which interact with replication forks to induce irreversible double-strand DNA (dsDNA) cleavage.[9, 10] The dsDNA lesions are the target of camptothecin-induced cell death, resulting in inhibition of RNA transcription and apoptotic cell death.[9, 11] Among these agents are two water-soluble derivatives – topotecan and irinotecan, which received FDA approval as anticancer agents for the treatment of lung, colon, and ovarian cancers (Figure 5.1).[12]

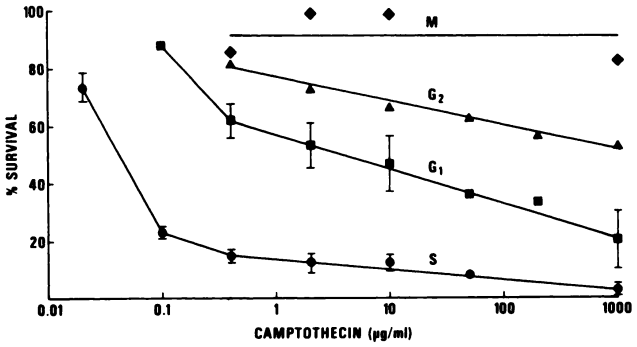

Figure 5.2. Camptothecin dose-survival curves of M, G1, S, and G2 cell phases. Reprinted from reference [13].

The mechanism of action by camptothecin is highly cell-cycle dependent, rendering cells in S phase 100- to 1000-times more sensitive then cells in the remaining phases of the cell cycle (Figure 5.2).[8, 13, 14] Pretreatment *in vitro* with taxanes and other microtubule stabilizing agents can increase the potency of topoisomerase I inhibitors by increasing topoisomerase I levels and the fraction of cells in the S phase, the target phase of the cell cycle by such inhibitors.[6]

Several camptothecin derivatives, such as camptothecin-20-ester(*S*), topotecan, and 9-glycineamido-20(*S*)-camptothecin hydrochloride, have been identified as small molecule inhibitors of hypoxia-inducible factor 1 (HIF-1) transcriptional activation pathway.[15] Comprised of HIF-1α and HIF-1β subunits,[16] HIF-1 is a transcriptional factor that regulates gene expression of proteins during hypoxic, or oxygen-deprived, conditions.[15, 17] These genes encode for proteins involved in angiogenesis, such as vascular endothelial growth factor (VEGF) and inducible nitric oxide synthase, as well as in anaerobic metabolism (glycolytic enzymes), and erythropoietin production.[15, 17] Overexpression of HIF-1α protein is associated with increased vascularity and tumor progression, and has been demonstrated in many human cancers.[16] For example, MX-1 (human breast cancer) cell line has demonstrated upregulated VEGF gene expression mediated by HIF-1 under hypoxic conditions both *in vitro* and *in vivo*.[18]

§5.1.3 Taxoid-Camptothecin Synergy

Combined regimens of a camptothecin and a taxoid have afforded conflicting results in previous preclinical evaluations.[8] While several studies demonstrated antagonistic effects, [9, 19] most others observed synergistic or additive effects.[20-23] Pre-exposure to paclitaxel or docetaxel against MCF-7 or MDAH-B231 human breast carcinoma cell lines resulted in a 10-fold reduction in the IC_{50} values of topotecan and 9-aminocamptothecin.[20] Furthermore, a two-fold up-regulation of topoisomerase I RNA was observed 24 hours following taxane exposure.[20] Reverse or simultaneous exposure to taxanes and camptothecins did not afford synergistic results, merely additive, indicating that the sequence of treatment may be essential.[6, 20]

As a class, camptothecins have encountered intrinsic drug resistance in certain colon cancer cell lines, as well as resistance that may be acquired in breast cancer cells.[24] Several mechanisms of camptothecin-related drug resistance have been described.[11, 24-26] Mutations or reduced expression that alter topoisomerase I levels can lead to a reduction in both the interactions and formation of the cleavable CPT-topoisomerase I complex.[11, 24] Overexpression of the Pgp efflux pump showed slight resistance to topotecan, however resistance towards camptothecin was not observed.[25] An additional ATP-binding cassette (ABC) half-transporter, encoded by the mitoxantrone resistance (MTX) gene, has been linked to camptothecin drug resistance.[24] It should be noted that drug resistance conferred by MXR does not include resistance to taxanes.[24]

§5.2 SB-T-1214 and Camptothecin

For the selection of two drugs for *in vitro* biological evaluations in combination and to investigate their synergistic or additive effects, selection was focused on a microtubule-stabilizing agent (taxanes) and a topoisomerase I inhibitor (camptothecins) due to their different and well-defined molecular targets, previously elucidated cell-cycle dependence, and extensive preclinical and clinical drug development. Next-generation taxoid, SB-T-1214, was selected as the microtubule-stabilizing agent, as it exhibits two to three orders of magnitude greater potency than paclitaxel and docetaxel against multidrug resistant and paclitaxel-resistant cancer cell lines and tumors.[27-30] Camptothecin was chosen as the topoisomerase I inhibitor due to its single reactive site – a tertiary hydroxyl – which, upon thiolactonization of a disulfide linker, is generated in an unmodified form. Thus, SB-T-1214 and camptothecin were subsequently evaluated as combination agents for *in vitro* cytotoxicity studies in BR+ cancer cell lines.

§5.2.1 Effect of Equimolar Combinations of SB-T-1214 and CPT on Cytotoxicity

The effect of equimolar combinations of SB-T-1214 and camptothecin on cytotoxicity was investigated using three different timings for drug administration: (a) simultaneous exposure (Entry 3), (2) first, SB-T-1214 for 24 h, followed by camptothecin (Entry 4), and (c) first, camptothecin for 24 h, followed by SB-T-1214 (Entry 5).[31] Single-drug administrations (Entries 1 and 2) and combinations were evaluated against human breast carcinoma (MX-1 and MCF-7), murine ovarian (ID8), and murine leukemia (L1210FR) cancer cell lines. The results are summarized in Table 5.1.

Table 5.1. Cytotoxicities (IC_{50}, nM) of SB-T-1214, CPT, and Their Equimolar Combinations against Cancer Cell Lines Overexpressing Biotin Receptor (BR+). Adapted from reference [31].

Entry	Conjugate	Time	MX-1[a]	MCF-7[b]	ID8[c]	L1210FR[d]
1[e]	SB-T-1214	72 h	2.01 ± 0.52	0.44 ± 0.18	1.11 ± 0.26	2.14 ± 1.30
2[e]	CPT	72 h	1,700 ± 200	65.1 ± 12.3	474 ± 101	510 ± 139
3[f]	SB-T-1214:CPT (1:1)	72 h	1.88 ± 0.14	0.40 ± 0.09	1.02 ± 0.17	4.14 ± 0.46
4[g]	SB-T-1214 then CPT	24 h 48 h	1.98 ± 0.29	0.33 ± 0.10	0.96 ± 0.14	3.51 ± 0.27
5[h]	CPT then SB-T-1214	24 h 48 h	>5,000	79.2 ± 12.4	110 ± 12	949 ± 116

[a]Human breast carcinoma cell line (BR+); [b]Human breast carcinoma cell line (BR+); [c]Murine ovarian carcinoma cell line (BR+); [d]Murine lymphocytic leukemia cell line (BR+); [e]Cells were incubated with a drug for 72 h at 37 °C; [f]Cells were incubated with an equimolar mixture of two drugs for 72 h at 37 °C; [g]Cells were incubated with SB-T-1214 at a given concentration for 24 h at 37 °C. Then, an equimolar amount of CPT was added and the cells were incubated for an additional 48 h at 37 °C; [h]Cells were incubated with CPT at a given concentration for 24 h at 37 °C. Then, an equimolar amount of SB-T-1214 was added and the cells were incubated for an additional 48 h at 37 °C.

For the single administration of each drug, the cytotoxicity of SB-T-1214 was 148–846 times more potent than that of camptothecin against all four evaluated cancer cell lines (Entries 1 and 2) in a 72 h drug incubation period. The order of exposure to these two drugs, i.e. (a) simultaneous delivery, (b) first, SB-T-1214 for 24 h followed by camptothecin, and (c) first, camptothecin for 24 h followed by SB-T-1214, exhibited a marked difference in potency. When the cells were exposed to camptothecin for 24 h, followed by equimolar concentrations of SB-T-1214 (Entry 5), significant increases in the IC_{50} values were observed compared to those values for

simultaneous exposure (Entry 3), and the values were even higher than those for camptothecin alone, except for that against ID8 cell line (Entry 2). These results clearly suggest that the two drugs act antagonistically in this case and that camptothecin appears to block the action of SB-T-1214, likely ascribed to cell cycle control, e.g. synchronization, by camptothecin, which leads to detrimental effects on the mechanism of action of the taxoid.[32] However, when the cells were exposed to an equimolar mixture of the two drugs (Entry 3) or to SB-T-1214 first for 24 h, followed by camptothecin (Entry 4), the IC_{50} values remained nearly the same as those for the single-drug administration of SB-T-1214 (Entry 1). These results indicate that in these two cases (Entries 3 and 4), SB-T-1214 and camptothecin act cooperatively, and SB-T-1214 may augment the effects of camptothecin.[31]

§5.3 Tumor-targeted Combination Chemotherapy

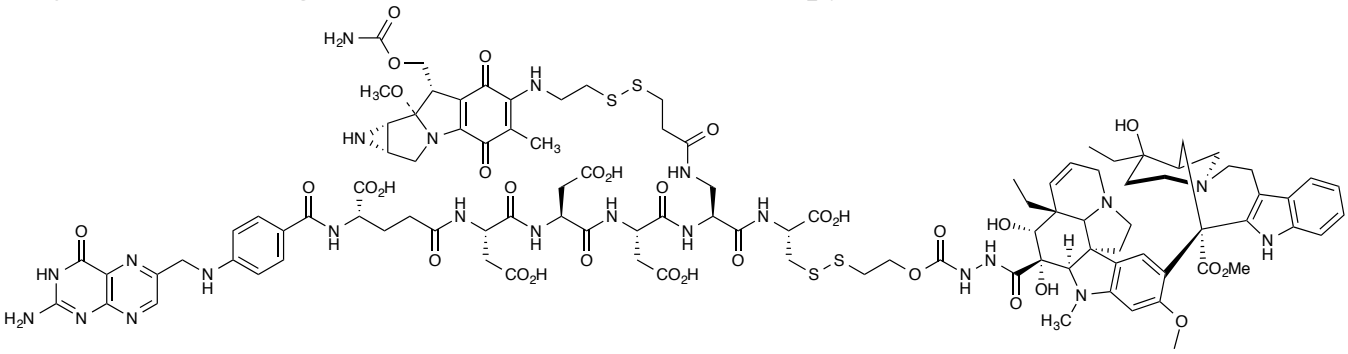

Figure 5.3. Chemical structure of EC0225, folate-based conjugate of dAc-VLB-mH and mitomycin C. Adapted from reference [33].

Traditional combination chemotherapy suffers from the same drawbacks of single-agent chemotherapy – lack of tumor specificity continues to be a serious problem for cancer treatment; thus, there is an urgent need for targeted combination chemotherapy. The first drug conjugate possessing two different biologically active agents, EC0225, was developed by Endocyte and reported in 2007, shown in Figure 5.3.[33] EC0225 bears both highly potent antimitotic agent desacetylvinblastine monohydrazide and chemically sensitive alkylating agent mitomycin C attached to a folate-polypeptide spacer unit via two disulfide-based linker systems.[33] EC0225 is in Phase I clinical trials for the treatment of hormone refractory or metastatic solid tumors.

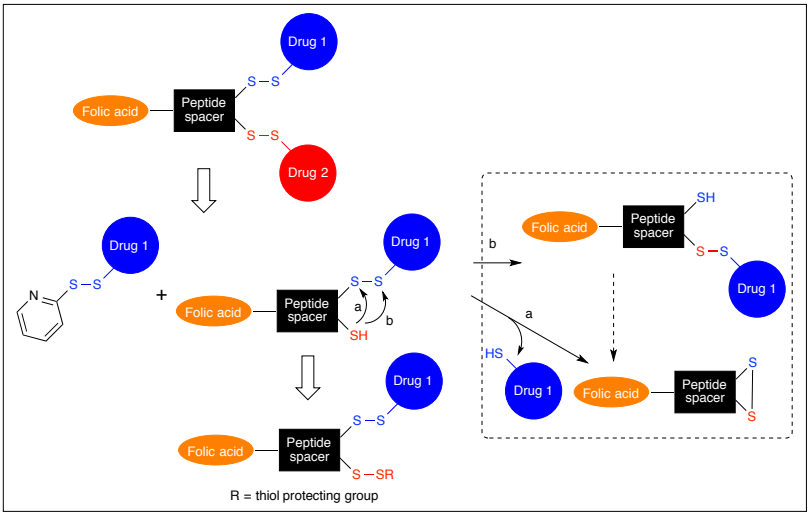

Figure 5.4. Major byproduct formation resulting from the addition of a second thiol-bearing drug to a FA-based drug delivery scaffold. Adapted from reference [33].

However, there are several notable limitations and areas for improvement in this double-warhead design. First, the disulfide release systems require modification to desacetylvinblastine with a hydrazide functionality, in turn reducing and limiting the potency of the drug conjugate. Second, installation of each cytotoxic agent proceeds *via* thiol-disulfide exchange and leads to undesired major side-product formation and poor yields, as illustrated in Figure 5.4. Finally, incorporation of additional water-solubilizing spacers, such as polyethylene glycol oligomers, may enhance the overall aqueous solubility of the drug conjugate.

§5.3.1 Design of Double-Warhead Biotin Conjugates for Combination Chemotherapy

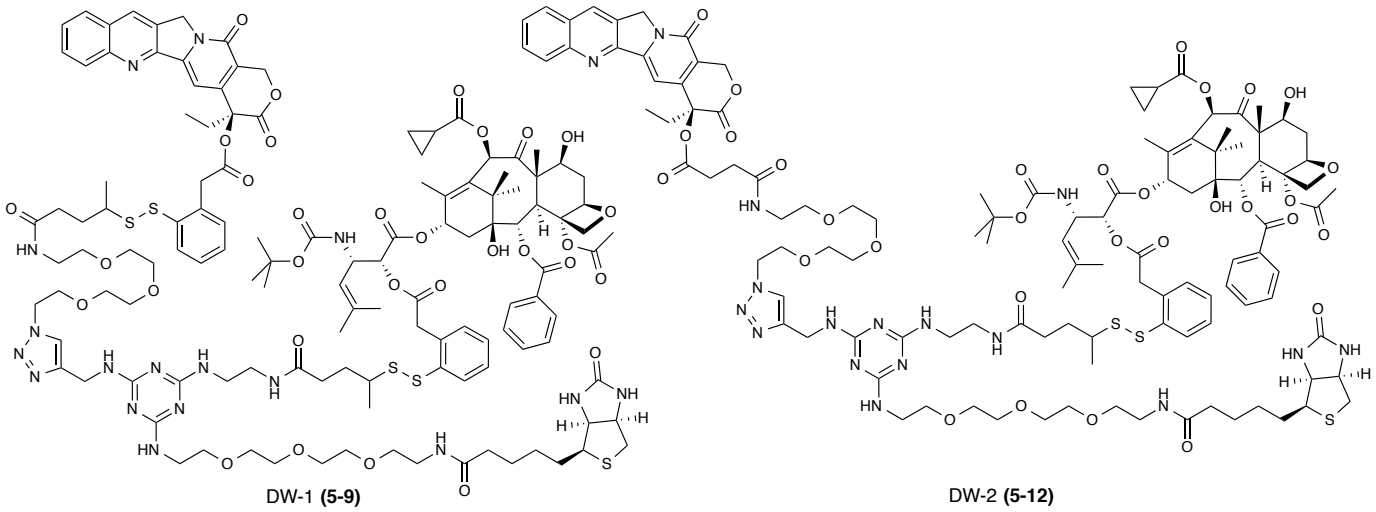

Figure 5.5. Chemical structures of double-warhead biotin conjugate of SB-T-1214 and camptothecin DW-1 (**5-9**) and DW-2 (**5-12**).

Double-warhead biotin conjugate of SB-T-1214 and camptothecin DW-1 (**5-9**) was designed through a versatile tumor-targeted drug delivery platform, consisting of 1,3,5-triazine as the tripod splitter module, self-immolative disulfide linkers with polyethylene glycol spacers to improve aqueous solubility, and a propargylamino arm for attachment of a second drug through orthogonal "click" chemistry. Another double-warhead conjugate DW-2 (**5-12**) bearing camptothecin with simple ester linkage was also designed to secure stepwise release. The chemical structures of DW-1 (**5-9**) and DW-2 (**5-12**) are illustrated in Figure 5.5.

§5.3.2 Synthesis of Double-Warhead Biotin Conjugates of Camptothecin and SB-T-1214

Synthesis of double-warhead conjugate DW-1 (**5-9**) was performed with the preparation of two components: (a) camptothecin-(SS-linker)-PEG-N_3 (**5-3**), (b) tumor-targeted drug delivery platform bearing biotin as the TTM and SB-T-1214 as the cytotoxic agent via 1,3,5-triazine splitter.

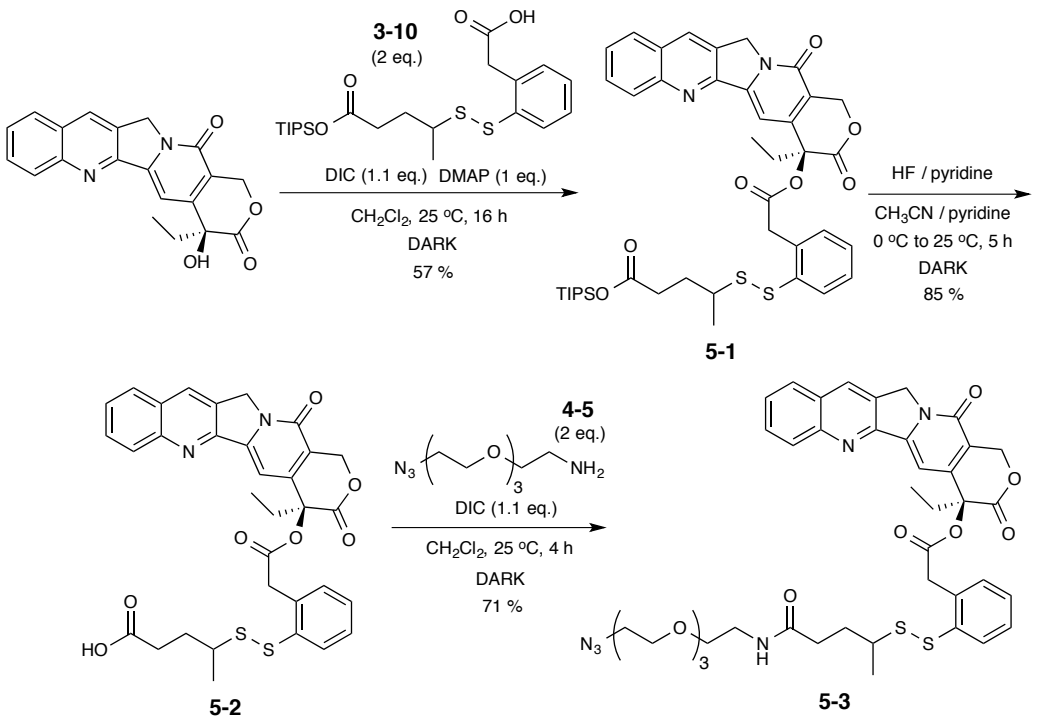

Scheme 5.1. Synthesis of camptothecin-(SS-linker)-PEG-N_3 (**5-3**).

The synthesis of camptothecin-(SS-linker)-PEG-N_3 is illustrated in Scheme 5.1. Coupling of camptothecin to disulfide linker **3-10** in the presence of DIC and DMAP in the dark gave the 20*S*-ester **5-1** in moderate yield (57%). The reaction was monitored by mass spectrometry, and excess **3-10** was used to push the reaction to completion. Also, dilute solvent conditions were used to accommodate the poor solubility of camptothecin hydrochloride in dichloromethane. Deprotection of the TIPS group with HF-pyridine afforded **5-2** in excellent yield (85%), and the corresponding acid was coupled to **4-5** in the presence of DIC to afford camptothecin-(SS-linker)-PEG-N_3 (**5-3**) in good yield (71%).

The tumor-targeted drug delivery platform bearing biotin as the TTM and SB-T-1214 as the cytotoxic agent via 1,3,5-triazine splitter was prepared from: (a) an ethylenediamine alkyl spacer, (b) *N*-biotinyl-PEG-NH_2 (**4-7**), (c) a modified 1,3,5-triazine core, and (d) SB-T-1214-(SS-linker)-OSu (**3-13**).

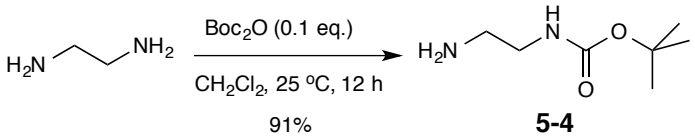

Scheme 5.2. Synthesis of *N*-Boc-ethylenediamine (**5-4**).

First, alkyl spacer *N*-Boc-ethylenediamine (**5-4**) was prepared by Boc protection, as illustrated in Scheme 5.2. Ethylenediamine was treated with di-*tert*-butyl dicarbonate as the limiting reagent to afford *N*-Boc-ethylenediamine (**5-4**) in excellent yield (91%).

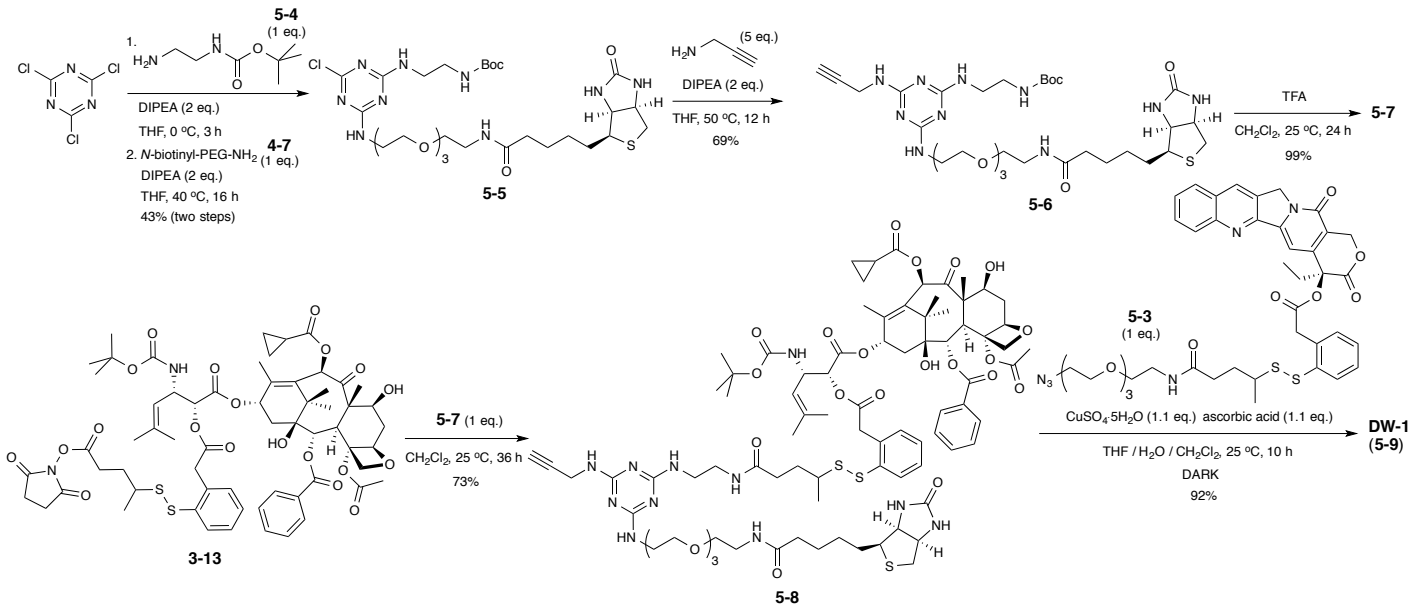

Scheme 5.3. Synthesis of double-warhead conjugate DW-1 (**5-9**).

Preparation of double-warhead conjugate DW-1 (**5-9**) is illustrated Scheme 5.3. First, cyanuric chloride was reacted with one equivalent of **5-4** in the presence of DIPEA at 0 °C, followed by the subsequent substitution reaction with one equivalent of **4-7** in the presence of DIPEA at 40 °C to afford **5-5** in moderate yield over two steps. Addition of propargylamine to **5-5** in the presence of DIPEA at 50 °C afforded fully functionalized triazine **5-6** in good yield (69%). Reaction progress was monitored by mass spectrometry, and additional equivalents of propargylamine were added as necessary. Deprotection of **5-6** with TFA gave **5-7** in quantitative yield, and the corresponding amine was coupled with SB-T-1214-(SS-linker)-OSu (**3-13**) in the presence of pyridine to give **5-8** in good yield (73%). Then, biotin-taxoid precursor **5-8** was subjected to a "click" reaction with camptothecin-(SS-linker)-PEG-N_3 (**5-3**) in the presence of copper(II) sulfate and ascorbic acid at 25 °C in the dark to give double-warhead conjugate DW-1 (**5-9**) in excellent yield (92%).

§5.3.3 Synthesis of Slow-release SB-T-1214–CPT Biotin Conjugates

In contrast to DW-1 (**5-9**), a second double-warhead conjugate, DW-2 (**5-12**), was designed for staggered drug release, with SB-T-1214 being released prior to camptothecin. Rather than connecting both drugs to identical self-immolative disulfide linkers, a more stable ester linkage was introduced to delay the release of camptothecin in the conjugate. The structure of DW-2 (**5-12**) is shown in Figure 5.5.

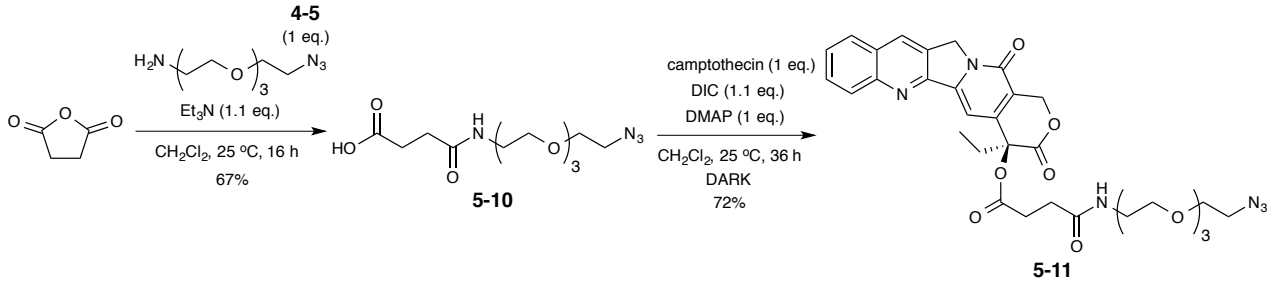

Scheme 5.4. Synthesis of CPT-PEG-N_3 (**5-11**).

The synthesis of slow-release camptothecin ester linker **5-11** is illustrated in Scheme 5.4. First, succinic anhydride was treated with **4-5** in the presence of triethylamine to give **5-10** in good yield (67%), and the corresponding spacer was coupled to camptothecin in the presence of DIC and DMAP in the dark to afford **5-11** in good yield (72%).

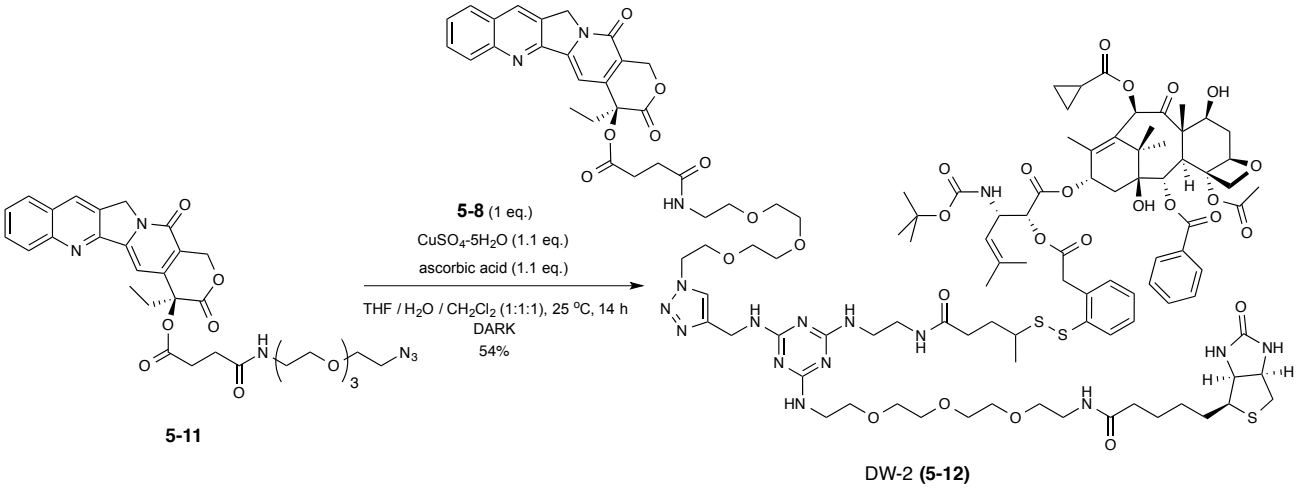

Scheme 5.5. Synthesis of double-warhead conjugate DW-2 (**5-12**).

Then, biotin-taxoid precursor **5-8** was subjected to a similar "click" reaction with azide **5-11** in the presence of copper(II) sulfate and ascorbic acid in the dark to give double-warhead conjugate DW-2 (**5-12**) in modest yield (54%), shown in Scheme 5.5.

§5.3.4 Synthesis of Surrogate-Warhead Biotin Conjugates

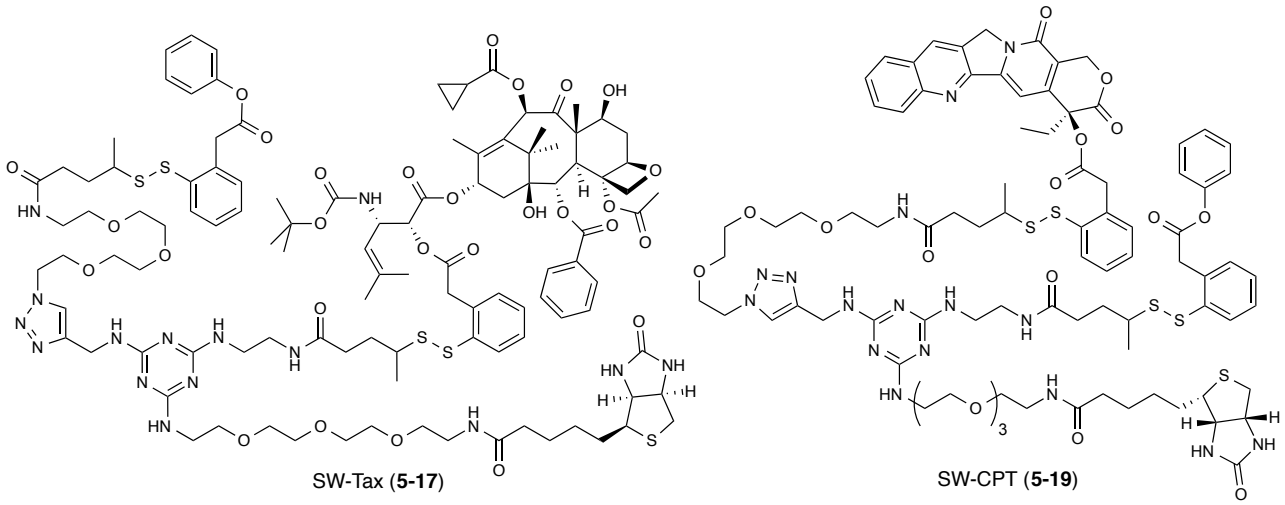

Figure 5.6. Chemical structures of single-warhead surrogate conjugates SW-Tax (**5-17**) and SW-CPT (**5-19**)

In addition to two double-warhead conjugates, two more drug conjugates were designed using the same platform, wherein one of the warheads was replaced with phenol as a surrogate: SW-Tax (**5-17**), a conjugate with SB-T-1214 and phenol; and SW-CPT (**5-19**), a conjugate with CPT and phenol. The chemical structures of the single-warhead surrogate conjugates are shown in Figure 5.6.

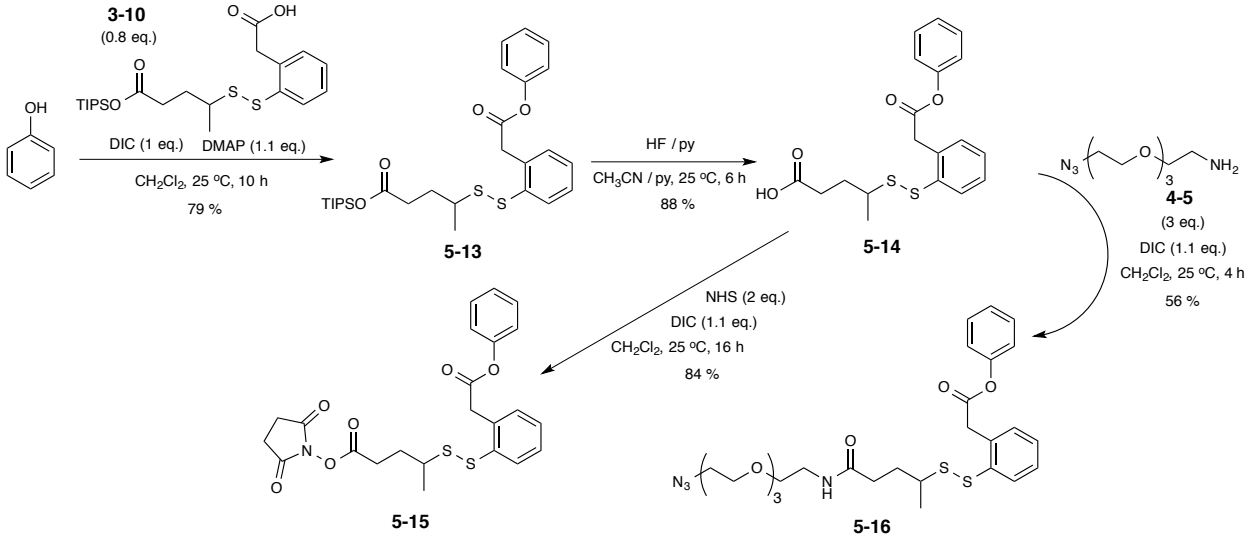

Scheme 5.6. Synthesis of phenol-(SS-linker)-OSu (**5-15**) and phenol-(SS-linker)-PEG-N_3 (**5-16**).

The phenol-(SS-linker)-PEG-N_3 component (**5-16**) was prepared in a similar synthetic route as **5-3**, shown in Scheme 5.6. First, coupling of phenol to disulfide linker **3-10** in the presence of DIC and DMAP gave **5-13** in good yield (79%). Deprotection of the TIPS group with HF-pyridine gave **5-14** in excellent yield (88%). From **5-14**, the free carboxylic acid was either activated with HOSu in the presence of DIC to give phenol-(SS-linker)-OSu (**5-15**) in good yield (84%) or coupled directly to **4-5** in the presence of DIC to afford **5-16** in modest yield (56%).

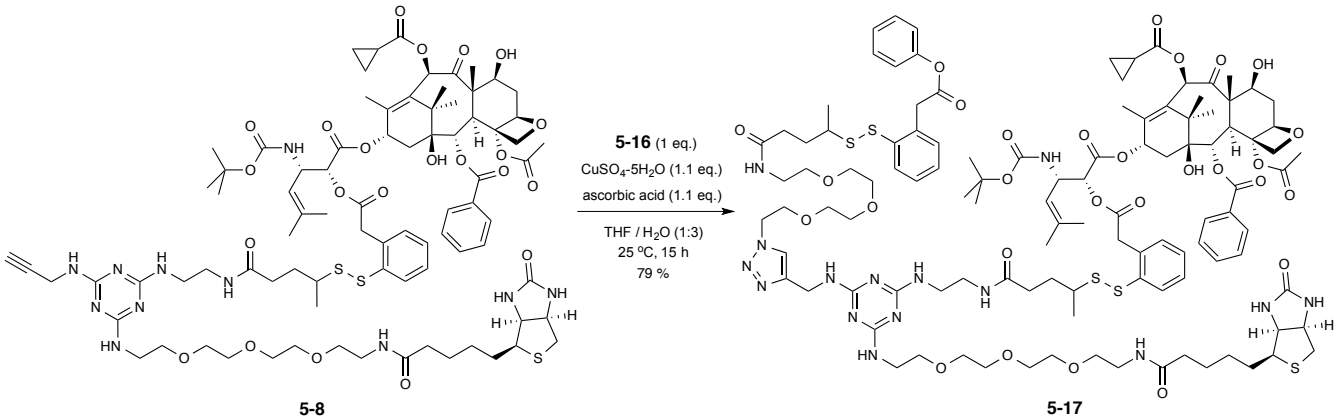

Scheme 5.7. Synthesis of single-warhead surrogate conjugate SW-Tax (**5-17**).

Next, biotin-taxoid precursor **5-8** was subjected to a "click" reaction with azide **5-16** in the presence of copper(II) sulfate and ascorbic acid to give single-warhead surrogate conjugate SW-Tax (**5-17**) in good yield (79%). The synthesis is shown in Scheme 5.7.

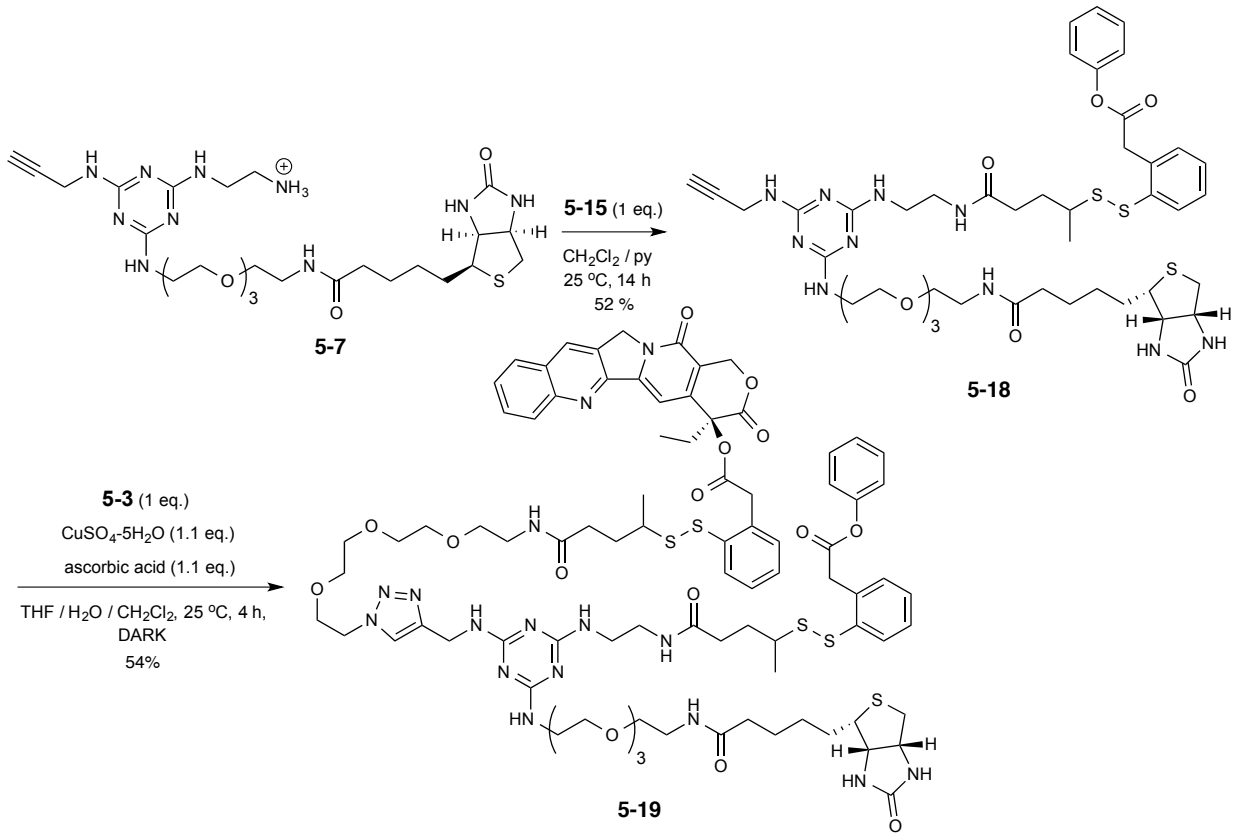

Scheme 5.8. Single-warhead surrogate conjugate SW-CPT (**5-19**).

For the preparation of SW-CPT (**5-19**), coupling of functionalized triazine **5-7** to phenol-(SS-linker)-OSu (**5-15**) in the presence of pyridine gave **5-18** in modest yield (52%), and **5-18** was subjected to a "click" reaction with azide **5-3** in the presence of copper(II) sulfate and ascorbic acid to afford SW-CPT (**5-19**) in modest yield (54%), shown in Scheme 5.8. Poor solubility of the

phenol derivatives may be responsible for the low yields in the above sequence, and additional optimization is currently ongoing.

§5.4 Biological Evaluation of DW Conjugates

The potency and efficacy of double-warhead conjugates DW-1 (**5-9**) and DW-2 (**5-12**), as well as surrogate-warhead conjugates SW-Tax (**5-17**) and SW-CPT (**5-19**), were evaluated by cytotoxicity assays against BR-positive cancer cell lines and BR-negative cell lines by MTT protocol.[34] The extent of drug release was also investigated using supplemental glutathione ethyl ester as a trigger for drug release following internalization of the conjugate. Internalization of DW-1 (**5-9**) was further investigated using confocal fluorescence microscopy.

§5.4.1 Internalization of DW-1 by CFM

Camptothecin possesses a unique intrinsic fluorescence emission derived from its substituted quinolone nucleus.[35] With an excitation wavelength (λ) of 360 nm, camptothecin produces an emission wavelength that can be detected at 440 nm (Figure 5.8). Upon conjugation to a linker or spacer at the C20 hydroxyl, the fluorescence properties of camptothecin remain unaltered.

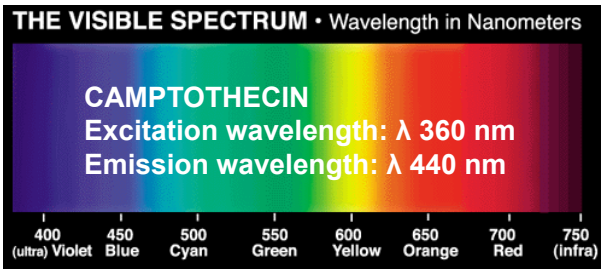

Figure 5.7. Fluorescence excitation and emission wavelengths of camptothecin.

The receptor-mediated internalization of double-warhead conjugate DW-1 (**5-9**) was examined by taking advantage of the intrinsic fluorescence of camptothecin, using confocal fluorescence microscopy (CFM). Murine ovarian (ID8) and human breast carcinoma (MCF-7) cancer cell lines were incubated with 10 μM DW-1 (**5-9**) at 37 °C for 10 h. After thorough washing of the drug media, the cells were analyzed by CFM. As shown in Figure 5.8, the intense signature blue fluorescence of camptothecin was observed in both cancer cell lines, confirming the efficient internalization of DW-1 (**5-9**).

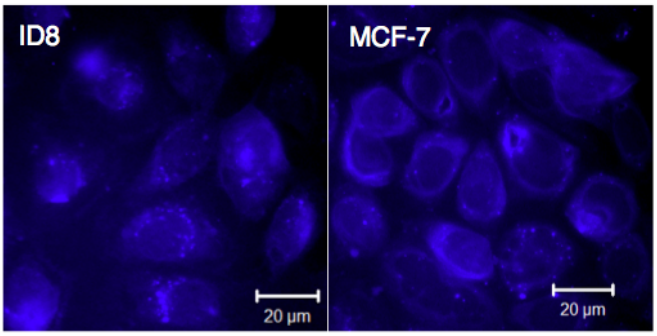

Figure 5.8. Confocal fluorescence microscopy images showing internalization of conjugate DW-1 (**5-9**) in ID8 (left) and MCF-7 (right) after incubation at 37 °C for 10 h. Reprinted from reference [31].

§5.4.2 Biological Evaluation of DW Conjugates for Cytotoxicity

The cytotoxicities of double-warhead conjugates DW-1 (**5-9**) and DW-2 (**5-12**), as well as their single-warhead surrogates SW-Tax (**5-17**) and SW-CPT (**5-19**) were evaluated in two experiments against four BR+ cancer cell lines – human breast carcinoma (MX-1 and MCF-7), murine ovarian (ID8), and murine leukemia (L1210FR) cell lines – as well as normal human lung fibroblast (WI38) cell line, using the standard MTT assay. The results are shown in Tables 5.2 and 5.3. Each free drug, SB-T-1214 and camptothecin, was also examined for comparison (Table 2, Entries 1 and 2, respectively).

Table 5.2. Cytotoxicities (IC_{50}, nM) of DW and SW conjugates against BR+ and BR- Cell Lines. Adapted from reference [31].

Entry	Conjugate	MX-1[a]	MCF-7[b]	ID8[c]	L1210FR[d]	WI38[e]
1[f]	SB-T-1214	2.01 ± 0.52	0.44 ± 0.18	1.11 ± 0.26	2.14 ± 1.30	5.89 ± 2.38
2[f]	CPT	1,700 ± 200	65.1 ± 12.3	474 ± 101	510 ± 139	786 ± 309
3[f]	DW-1 (**5-9**)	51.7 ± 5.1	19.0 ± 3.4	23.4 ± 4.7	39.1 ± 9.1	742 ± 166
4[f]	DW-2 (**5-12**)	65.1 ± 9.7	21.2 ± 2.9	25.6 ± 3.9	42.5 ± 8.9	868 ± 264
5[f]	SW-Tax (**5-17**)	66.9 ± 4.4	23.1 ± 1.8	26.7 ± 4.2	50.9 ± 15.9	941 ± 298
6[f]	SW-CPT (**5-19**)	>5,000	1,255 ± 172	>5000	319 ± 139	1,438 ± 364

[a-d]See captions for cell lines in Table 5.1. [e]Human lung fibroblast cell line (BR-); [f]Cells were incubated with a drug of conjugate at 37 °C for 72 h.

In the first experiment (Table 5.2), MX-1 (BR^{++}), MCF-7 (BR^{+++}), ID8 (BR^{+++}), and L1210FR (BR^{+++}) cancer cell lines were incubated with DW-1 (**5-9**), DW-2 (**5-12**), SW-Tax (**5-17**), and SW-CPT (**5-19**) for 72 h, and the cytotoxicity was determined by the corresponding IC_{50} values. The cytotoxicities of double-warhead conjugates DW-1 (**5-9**) and DW-2 (**5-12**) based on their IC_{50} values were determined to be in a range of 19–65 nM (Entries 3 and 4) against BR+ cancer cell lines, whereas that against normal cell lines WI38 (BR-) was found to be markedly lowered in a range of 742–868 nM. These results indicate that the conjugates demonstrated high-selectivity towards internalization into BR+ cancer cell lines by RME and that the drug was partially released inside cancer cells. Similarly, single-warhead surrogate SW-Tax (**5-17**) showed potency comparable to that of DW-2 (**5-12**), whereas SW-CPT (**5-19**) did not exhibit appreciable

cytotoxicity against MX-1 and ID8 or only exhibited weak potency against MCF-7 and WI38, with L1210FR as an exception (Entry 6).

For the conjugates bearing SB-T-1214 – that is, DW-1 (**5-9**), DW-2 (**5-12**), and SW-Tax (**5-17**) – the level of cytotoxicity was reduced compared to that of the free parent taxoid. Having already confirmed that these four cancer cell lines overexpress the biotin receptor and having demonstrated marked selectivity for BR+ cancer cell lines compared to normal WI38 (BR-) cell line, it is likely that the level of endogenous intracellular thiols is not sufficient to release the drugs by disulfide linker cleavage under *in vitro* conditions.

In the second experiment, glutathione ethyl ester (GSH-OEt) (6 mole equivalents to each conjugate) was added to the re-suspended cancer cells after the cells had been incubated with a conjugate for 24 h, followed by thorough washing with phosphate-buffered saline (PBS), and an additional 48 h incubation (Table 5.3). The re-suspended cancer cells only included conjugate internalized in the first 24 h period.

Table 5.3. Cytotoxicities (IC_{50}, nM) of DW-1 (5-9), DW-2 (5-12), SW-Tax (5-17), and SW-CPT (5-19) in the Presence of GSH-OEt Following Internalization. Adapted from reference [31].

Entry	Conjugate	MX-1[a]	MCF-7[b]	ID8[c]	L1210FR[d]	WI38[e]
1[f]	DW-1 (**5-9**)	9.80 ± 1.4	3.22 ± 0.84	5.66 ± 0.95	7.40 ± 3.48	705 ± 114
2[f]	DW-2 (**5-12**)	20.8 ± 2.2	9.39 ± 1.27	10.3 ± 1.7	13.7 ± 1.5	782 ± 132
3[f]	SW-Tax (**5-17**)	23.6 ± 4.6	9.87 ± 2.00	15.6 ± 3.0	14.4 ± 4.2	850 ± 100
4[f]	SW-CPT (**5-19**)	>5,000	538 ± 105	>2,390	177 ± 33	1,229 ± 219

*Cells were initially incubated with conjugates for 24 h, followed by washing of the drug media with PBS, then addition of GSH-OEt (6 equiv. to a conjugate) for drug release and additional incubation at 37 °C for 48 h.
[a-e]See captions for cell lines in Tables 5.1 and 5.2.

This protocol, shown in Table 5.3, including washing of the cells and addition of GSH-OEt did not lead to an increase in cytotoxicity for the conjugates in WI38 normal fibroblast cells, based on the comparison with the corresponding results in Table 5.2. Conjugate DW-1 (**5-9**) demonstrated IC_{50} values of 3.2–9.8 nM against four BR+ cell lines, whereas that against WI38 as 742 nM (Entry 1), a nearly two orders of magnitude difference between cancer and normal cells that can be attributed to the highly efficient biotin receptor-targeting by the conjugate. Furthermore, there was a moderate difference in potency between DW-1 (**5-9**) and DW-2 (**5-12**) (Entries 1 and 2), which can be attributed to full release of both SB-T-1214 and CPT in the first conjugate by disulfide linker cleavage versus incomplete release of CPT in the latter conjugate due to a more stable tertiary ester linkage between the linker and drug. Since single-warhead surrogate SW-Tax (**5-17**), bearing SB-T-1214 and phenol, exhibited a slightly weaker but comparable potency to that of DW-2 (**5-12**), it is likely that some camptothecin was released by hydrolysis of the tertiary ester linkage under these experimental conditions.

§5.5.0 Summary

Combination chemotherapy has emerged as a primary treatment option for many types of cancers, some of which had previously been considered incurable. Compared to the use of a single cytotoxic agent, the use of two or more properly selected drugs in combination can lead to a decrease in systemic toxicity and an increase in efficacy due to synergistic or cooperative effects of the drugs on tumor eradication. Sequential treatment with chemotherapeutic agents bearing

different mechanisms of action has been shown to circumvent drug resistance and lead to synergistic enhancement of efficacy. SB-T-1214 (next-generation taxoid) and camptothecin (topoisomerase I inhibitor) were evaluated in combination in against various BR-positive cancer cell lines, and the results indicate that the two agents act at least cooperatively in combination.

However, traditional combination chemotherapy suffers from the same drawbacks of single-agent chemotherapy – lack of tumor specificity. Thus, novel double-warhead drug conjugates of SB-T-1214 and camptothecin with biotin as the tumor-targeting module were designed and synthesized. Internalization by RME was confirmed by confocal fluorescence microscopy by exploiting the intrinsic fluorescence properties of camptothecin. The double-warhead conjugates, as well as surrogate-warhead conjugates with phenol as a substitute warhead, were evaluated *in vitro* against cancer cell lines that overexpress the biotin receptor, and the DW-conjugates demonstrated excellent target-specificity for the biotin receptor and high potency whereas they were nearly two orders of magnitude lower in potency against BR-negative normal cells. Addition of supplemental glutathione ethyl ester following conjugate incubation increased conjugate potency in BR+ cell lines whereas toxicity in normal cells remained unchanged, suggesting that normal *in vitro* physiological conditions do not completely reduce the disulfide linker, i.e. incomplete thiolactionization. The biological evaluation *in vitro* of DW-1 demonstrated positive results for its potential as a therapeutic candidate for BR-positive cancer cell lines, and preclinical studies in BR+ tumor-bearing mice will be carried out in due course.

§5.6 Experimental

§5.6.1 Caution

Taxoids and camptothecins have been identified as potent cytotoxic agents. Thus, all drugs and structurally related compounds and derivatives must be considered mutagens and potential reproductive hazards for both males and females. All appropriate precautions, such as the use of gloves, goggles, labware, and fume hood, must be taken while handling the compounds at all times.

§5.6.2 General Information

^{1}H and ^{13}C NMR spectra were measured on a Varian 300 MHz NMR spectrometer or Bruker 300, 400, or 500 MHz NMR spectrometer. Melting points were measured on a Thomas-Hoover capillary melting point apparatus and are uncorrected. TLC was performed on Sorbent Technologies aluminum-backed Silica G TLC plates (Sorbent Technologies, 200 μm, 20 x 20 cm), and column chromatography was carried out on silica gel 60 (Merck, 230-400 mesh ASTM). Purity was determined with a Shimadzu L-2010A HPLC HT series HPLC assembly, using a Kinetex PFP column (4.6 mm x 100 mm, 2.6 μm) with acetonitrile-water gradient solvent system. Two analytical conditions were used and noted as part of the characterization data and purity for literature unknown compounds, i.e., HPLC (1): flow rate 0.4 mL/min, a gradient of 15→95% acetonitrile for the 0-12 min period; HPLC (2): flow rate 0.5 mL/min, a gradient of 5→95% acetonitrile for the 0-12 min period and 95% acetonitrile for the 11-15 min period. High resolution mass spectrometry analysis was carried out on an Agilent LC-UV-TOF mass spectrometer at the Institute of Chemical Biology and Drug Discovery, Stony Brook, NY or at the Mass Spectrometry Laboratory, University of Illinois at Urbana-Champaign, Urbana, IL.

§5.6.3 Materials

The chemicals were purchased from Sigma-Aldrich, Fisher Scientific, and VWR International, and used as received or purified before use by standard methods. Tetrahydrofuran was freshly distilled from sodium and benzophenone. Dichloromethane was also distilled immediately prior to use under nitrogen from calcium hydride. 3-(4,5-Dimethylthiazol-2-yl)-2,5-diphenyltetrazolium bromide (MTT) was obtained from Sigma Chemical Co. Biological materials including RPMI-1640 and DMEM cell culture media, fetal bovine serum, NuSerum, PenStrep, and TrypLE were obtained from Gibco and VWR International, and used as received for cell-based assays.

§5.6.4 Experimental Procedure

CPT-Me-SS-Linker-OTIPS [5-1]:
To a solution of camptothecin (0.158 g, 0.431 mmol), **3-10** (0.489 g, 1.072 mmol), and DMAP (0.053 g, 0.431 mmol) in CH_2Cl_2 (20 mL) was added DIC (73 μL, 0.474 mmol), and the mixture was allowed to react at room temperature with stirring. The reaction mixture was cooled to 0 °C, and the urea by-product was removed via filtration. The filtrate was concentrated *in vacuo* to give a green solid. Purification of the crude product by column chromatography on silica gel with 1.5% CH_3OH in CH_2Cl_2 as eluent gave **5-1** (0.192 g, 57%) as an off-white solid; R_f = 0.75 (CH_2Cl_2/CH_3OH: 9/1); ^{1}H NMR (500 MHz, $CDCl_3$) δ 0.98 (t, *J* = 7.5 Hz, 3H), 1.05 (m, 21H), 1.45 (d, *J* = 6.8 Hz, 2H), 1.85 (m, 1H), 2.18 (m, 1H), 2.33 (m, 2H), 2.87 (m, 1H), 4.00 (dd, *J* = 4.5, 16.5 Hz, 1H), 4.02 (d, *J* = 22.0 Hz, 1H), 4.17 (dd, *J* = 9.2, 16.5 Hz, 1H), 5.21 (m, 2H), 5.38 (d, *J* = 17.2 Hz, 1H), 5.64 (d, *J* = 17.2 Hz, 1H), 7.21 (d, *J* = 2.5 Hz, 1H), 7.26 (m, 4H), 7.66 (t, *J* = 7.5 Hz, 1H), 7.85 (t, *J* = 8.0 Hz, 1H), 7.92 (d, *J* = 8.0 Hz, 1H), 8.27 (d, *J* = 8.5 Hz, 1H), 8.35 (s, 1H); ^{13}C NMR (125 MHz, $CDCl_3$) δ 7.60, 11.85, 17.78, 20.39, 20.98, 22.55, 23.53, 30.94, 31.78, 32.96, 38.59, 45.82, 49.92, 53.51, 67.13, 96.26, 120.18, 127.62, 127.67, 127.77, 127.92, 128.05, 128.13, 128.23, 128.27, 128.42, 129.69, 129.72, 129.94, 130.04, 130.40, 130.54, 130.59, 130.86, 130.89, 131.06, 132.56, 132.63, 134.65, 137.09, 137.44, 145.60, 146.20, 148.83, 152.30, 153.82, 157.27, 167.33, 169.91, 172.91; HRMS for $C_{42}H_{51}N_2O_7S_2Si^+$ calcd: 787.2901. Found: 787.2897 (Δ = -0.5 ppm).

CPT-Me-SS-Linker-OH [5-2]:
To a cooled solution of **5-1** (0.192 g, 0.244 mmol) in CH_3CN-pyridine (1:1) (30 mL) was added 70% HF-pyridine (3 mL) dropwise, and the mixture was allowed to warm from 0 °C to room temperature and react for 5 h with stirring. The reaction was quenched with 10% citric acid (10 mL) and diluted with H_2O (10 mL), and the mixture was extracted with CH_2Cl_2 (3 x 20 mL). The combined organic layers were washed with saturated $CuSO_4$ (60 mL), H_2O (60 mL), and brine (60 mL), dried over $MgSO_4$, and concentrated *in vacuo* to give a green solid. Purification of the crude product by column chromatography on silica gel with 1% CH_3OH in CH_2Cl_2 as eluent gave **5-2** (0.131 g, 85%) as a white solid; R_f = 0.1 (CH_2Cl_2/CH_3OH: 9/1); ^{1}H NMR (500 MHz, DMSO-d_6) δ 0.91 (t, *J* = 7.5 Hz, 3H), 1.05 (dd, *J* = 6.8, 8.4 Hz, 3 H), 1.53 (m, 1H), 1.70 (m, 1H), 2.18 (m, 4H), 2.88 (m, 1H), 4.05 (d, *J* = 16.5 Hz, 1H), 4.20 (dd, *J* = 4.0, 16.5 Hz, 1H), 5.30 (m, 2H), 5.46 (d, *J* = 17.2 Hz, 1H), 5.50 (d, *J* = 17.2 Hz, 1H), 7.10 (s, 1H), 7.27 (t, *J* = 7.5 Hz, 1H), 7.35 (m, 2H), 7.74 (m, 2H), 7.91 (t, *J* = 7.3 Hz, 1H), 8.15 (d, *J* = 8.0 Hz, 1H), 8.23 (d, *J* = 8.0 Hz, 1H), 8.70 (s, 1H), 12.10 (s, 1H); ^{13}C NMR (125 MHz, DMSO-d_6) δ 8.00, 20.13, 20.24, 30.69, 30.79, 30.86, 31.29,

31.35, 38.57, 45.75, 45.83, 50.70, 55.40, 66.78, 76.61, 95.61, 119.37, 127.95, 127.97, 128.17, 128.46, 128.89, 129.00, 129.57, 129.78, 129.86, 130.16, 130.84, 131.70, 131.96, 133.11, 133.16, 137.59, 137.63, 145.48, 146.41, 148.43, 152.71, 156.98, 167.51, 169.84, 174.22; HRMS for $C_{33}H_{31}N_2O_7S_2^+$ calcd: 631.1567. Found: 631.1561 (Δ = -0.9 ppm).

CPT-Me-SS-Linker-PEG$_3$-N$_3$ [5-3]:
To a solution of **5-2** (0.110 g, 0.175 mmol) and **4-5** (0.076 g, 0.349 mmol) in CH_2Cl_2 (60 mL) was added DIC (35 μL, 0.229 mmol), and the mixture was allowed to react for 4 h at room temperature with stirring. Purification of the reaction mixture by column chromatography on silica gel with 2% CH_3OH in CH_2Cl_2 as eluent gave **5-3** (0.103 g, 71%) as a pale-white solid; R_f = 0.85 (CH_2Cl_2/CH_3OH: 9/1); ^{1}H NMR (500 MHz, $CDCl_3$) δ 1.00 (m, 3H), 1.18 (d, *J* = 6.5 Hz, 3H), 1.74 (m, 4H), 2.04 (m, 1H), 2.21 (m, 1H), 2.33 (m, 1H), 2.82 (m, 1H), 3.34 (m, 1H), 3.40 (m, 2H), 3.49 (m, 2H), 3.61 (m, 2H), 3.69 (m, 10H), 4.04 (d, *J* = 16.5 Hz, 1H), 4.22 (dd, *J* = 4.0, 16.5 Hz, 1H), 5.31 (s, 2H), 5.42 (d, *J* = 17.3 Hz, 1H), 5.66 (dd, *J* = 1.4, 17.3 Hz, 1H), 5.98 (m, 1H), 7.25 (m, 5H), 7.72 (m, 2H), 7.89 (t, *J* = 7.4 Hz, 1H), 7.98 (d, *J* = 8.1 Hz, 1H), 8.30 (m, 1H), 8.42 (s, 1H); ^{13}C NMR (125 MHz, $CDCl_3$) δ 7.57, 14.20, 20.60, 20.73, 21.05, 23.50, 31.21, 31.42, 31.82, 33.50, 38.56, 39.10, 42.15, 46.36, 49.95, 50.67, 53.44, 60.39, 67.15, 69.74, 70.03, 70.23, 70.56, 70.61, 70.69, 96.30, 120.20, 120.29, 127.89, 128.01, 128.17, 128.19, 128.24, 128.46, 129.71, 130.62, 130.69, 131.12, 131.15, 131.21, 133.07, 137.55, 145.59, 146.22, 148.86, 152.32, 157.29, 167.32, 170.20, 171.14, 172.05, 172.12; HRMS for $C_{41}H_{47}N_6O_9S_2^+$ calcd: 831.2840. Found: 831.2838 (Δ = -0.2 ppm). HPLC (2): t = 12.4 min, purity > 95%.

***N*-(*tert*-Butoxycarbonyl)ethylenediamine [5-4]:**[36]
To a solution of ethylenediamine (13.8 mL, 0.206 mol) in CH_2Cl_2 (1000 mL) was added di-*tert*-butyl dicarbonate (4.49 g, 0.0206 mol) in CH_2Cl_2 (500 mL) dropwise over 30 min, and the mixture was allowed to react for 15 h at room temperature with stirring. The reaction mixture was concentrated in vacuo, redissolved in H_2O (50 mL), and extracted with CH_2Cl_2 (3 x 50 mL). The combined organic layers were dried over $MgSO_4$ and concentrated *in vacuo* to give **5-4** (3.007 g, 91%) as a colorless oil; ^{1}H NMR (300 MHz, $CDCl_3$) δ 1.60 (m, 9H), 2.64 (m, 4H). All data are in agreement with literature values.[36]

2-Chloro-4-(11-biotinylamino-3,6,9-trioxaundecyl)amino-6-(2-*N*-Boc-aminoethyl)amino-1,3,5-triazine [5-5]:
To a cooled solution of cyanuric chloride (0.414 g, 2.282 mmol) in THF (120 mL) at 0 °C was added a solution of **5-4** (0.366 g, 2.282 mmol) and DIPEA (0.6 mL, 3.432 mmol) in THF (2 mL), and the mixture was allowed to warm from 0 °C to room temperature and react for 3 h with stirring. Then, a solution of **4-7** (0.954 g, 2.282 mmol) and DIPEA (0.6 mL, 3.423 mmol) in THF (80 mL) was added to the reaction mixture and heated for 16 h at 67 °C under reflux. The reaction mixture was concentrated *in vacuo* to afford a red oil. Purification of the crude product by column chromatography on silica gel with 7% CH_3OH in CH_2Cl_2 as eluent gave **5-5** (0.645 g, 42%) as a white solid; mp 63-65 °C; ^{1}H NMR (300 MHz, CD_3OD) δ 1.34 (dt, *J* = 6.6, 12.6 Hz, 2H), 1.41 (s, 9H), 1.61 (m, 4H), 2.21 (t, *J* = 7.2 Hz, 2H), 2.69 (d, *J* = 12.6 Hz, 1H), 2.91 (dd, *J* = 5.0, 12.6 Hz, 1H), 3.20 (m, 3H), 3.37 (m, 4H), 3.54 (m, 4H), 3.63 (m, 10H), 4.29 (dd, *J* = 4.4, 8.0 Hz, 1H), 4.48 (dd, *J* = 4.4, 8.0 Hz, 1H); ^{13}C NMR (100 MHz, CD_3OD) δ 25.5, 27.4, 28.1, 28.4, 35.4, 39.0, 39.7, 40.2, 40.3, 40.6, 53.4, 54.2, 55.6, 60.2, 62.0, 69.2, 69.8, 70.19, 70.21, 78.7, 157.2, 164.7, 165.8,

168.1, 168.8, 174.7; HRMS (TOF) calcd for $C_{28}H_{49}ClN_9O_7S^+$: 690.3159. Found: 690.3157 (Δ = -0.3 ppm). HPLC (2): t = 10.0 min, purity >98%.

4-(11-Biotinylamino-3,6,9-trioxaundecyl)amino-6-(2-*N*-Boc-aminoethyl)amino-2-propargylamino-1,3,5-triazine [5-6]:
To a solution of **5-5** (0.794 g, 1.151 mmol) and DIPEA (0.4 mL, 2.302 mmol) in THF (12 mL) was added propargylamine (362 μL, 6.600 mmol), and the mixture was allowed to react for 12 h at 50 °C with stirring. Reaction progress was monitored by MS (ESI), and additional propargylamine was added as needed. The reaction mixture was cooled to 25 °C and concentrated *in vacuo* to afford an orange oil. Purification of the crude product by column chromatography on silica gel with 7% CH_3OH in CH_2Cl_2 as eluent gave **5-6** (0.560 g, 69%) as a light yellow solid; mp 66-68 °C; ^{1}H NMR (300 MHz, CD_3OD): δ 1.41 (m, 2H), 1.42 (s, 9H), 1.63 (m, 4H), 2.20 (t, *J* = 7.5 Hz, 2H), 2.52 (t, *J* = 2.4 Hz, 1H), 2.69 (d, *J* = 12.6 Hz, 1H), 2.91 (dd, *J* = 5.0, 12.6 Hz, 1H), 3.19 (m, 3H), 3.36 (t, *J* = 5.4 Hz, 4H), 3.54 (t, *J* = 5.4 Hz, 4H), 3.64 (m, 10H), 4.10 (bs, 2H), 4.27 (dd, *J* = 4.4, 8.0 Hz, 1H), 4.47 (dd, *J* = 4.4, 8.0 Hz, 1H); ^{13}C NMR (125 MHz, CD_3OD) δ 27.01, 28.94, 29.64, 29.93, 30.94, 36.89, 40.55, 41.21, 41.50, 41.56, 57.16, 61.77, 63.52, 70.74, 71.19, 71.40, 71.44, 71.73, 71.76, 158.76, 166.27, 176.30; HRMS (TOF) calcd for $C_{31}H_{53}N_{10}O_7S^+$: 709.3814. Found: 709.3814 (Δ = 0 ppm). HPLC (2): t = 10.0 min, purity >98%.

6-(2-Aminoethyl)amino-4-(11-biotinylamino-3,6,9-trioxaundecyl)amino-2-propargylamino-1,3,5-triazine TFA salt [5-7]:
To a solution of **5-6** (0.400 g, 0.564 mmol) in CH_2Cl_2 (6 mL) was added TFA (0.5 mL, 6.57 mmol), and the mixture was allowed to react for 48 h at room temperature with stirring. The reaction mixture was concentrated *in vacuo* to afford a yellow oil, which was triturated with Et_2O (20 mL) as the crude product (TFA salt) crashed out. The resulting solid was washed with Et_2O (4 x 20 mL) to afford **5-7** (0.408 g, quant.) as a white solid; ^{1}H NMR (400 MHz, CD_3OD) δ 1.42 (m, 2H), 1.63 (m, 4H), 2.20 (t, *J* = 7.2 Hz, 2H), 2.54 (m, 1H), 2.69 (d, *J* = 12.6 Hz, 1H), 2.92 (dd, *J* = 5.1, 12.6 Hz, 1H), 3.36 (t, *J* = 5.4 Hz, 4H), 3.54 (t, *J* = 5.4 Hz, 4H), 3.64 (m, 10H), 4.10 (bs, 2H), 4.30 (dd, *J* = 4.4, 8.0 Hz, 1H), 4.49 (dd, *J* = 4.4, 8.0 Hz, 1H), 4.68 (bs, 2H); ^{13}C NMR (100 MHz, CD_3OD) 25.46, 28.09, 28.34, 29.38, 35.33, 38.26, 38.94, 39.64, 39.95, 55.60, 60.25, 61.99, 69.17, 69.80, 69.95, 70.16, 112.74, 115.24, 118.15, 121.62, 161.58, 161.93, 164.68, 174.81. HRMS (TOF) calcd for $C_{26}H_{45}N_{10}O_5S^+$: 609.3290. Found: 609.3292 (Δ = 0.3 ppm).

4-(11-Biotinylamino-3,6,9-trioxaundecyl)amino-2-propargylamino-6-[2-(SB-T-1214-SS-linker)amidoethyl]amino-1,3,5-triazine [5-8]:
A solution of **3-13** (0.704 g, 0.564 mmol) and **5-7** (0.408 g, 0.564 mmol) in CH_2Cl_2-pyridine (4:1) (10 mL) was allowed to react for 36 h at room temperature with stirring. The reaction was quenched with saturated NH_4Cl (10 mL), and the reaction mixture was extracted with CH_2Cl_2 (3 x 20 mL). The combined organic layers were washed with brine (3 x 5 mL), dried over $MgSO_4$, and concentrated *in vacuo* to afford a yellow oil. Purification of the crude product by column chromatography on silica gel with 8% CH_3OH in CH_2Cl_2 as eluent gave **5-8** (0.806 g, 83%) as a white solid; mp 164-166 °C; ^{1}H NMR (500 MHz, CD_3OD) δ 0.86 (m, 2H), 0.98 (m, 2H), 1.17 (s, 6H), 1.26 (d, *J* = 6.8 Hz, 3H), 1.41 (s, 9H), 1.43 (m, 2H), 1.63 (m, 4H), 1.65 (s, 3H), 1.70 (m, 1H), 1.73 (s, 3H), 1.76 (s, 3H), 1.79 (m, 1H), 1.87 (m, 1H), 1.91 (s, 3H), 2.20 (t, *J* = 7.5 Hz, 2H), 2.25 (m, 4H), 2.38 (s, 3H), 2.45 (m, 2H), 2.65 (bs, 1H), 2.69 (d, *J* = 12.8 Hz, 1H), 2.86 (m, 1H), 2.90 (dd, *J* = 5.0, 12.8 Hz, 1H), 3.18 (m, 1H), 3.34 (m, 2H), 3.35 (t, *J* = 5.4 Hz, 2H), 3.52 (t, *J* = 5.4 Hz,

2H), 3.54 (m, 2H), 3.63 (m, 12H), 3.84 (d, *J* = 7.2 Hz, 1H), 4.02 (dd, *J* = 1.5, 16.7 Hz, 1H), 4.10 (d, *J* = 16.7 Hz, 1H), 4.17 (m, 2H), 4.20 (d, *J* = 8.4 Hz, 2H), 4.28 (dd, J = 4.4, 8.0 Hz, 1H), 4.30 (dd, *J* = 6.5, 10.6 Hz, 1H), 4.47 (dd, *J* = 4.4, 8.0 Hz, 1H), 4.8-4.9 (m, 3H), 4.99 (d, *J* = 8.9 Hz, 1H), 5.26 (bs, 1H), 5.67 (d, *J* = 7.2 Hz, 1H), 6.13 (bt, *J* = 8.5 Hz, 1H), 6.45 (s, 1H), 7.26 (m, 1H), 7.32 (m, 2H), 7.50 (t, *J* = 7.9 Hz, 2H), 7.63 (t, *J* = 7.5 Hz, 1H), 7.78 (m, 1H), 8.12 (d, *J* = 7.5 Hz, 2H); ^{13}C NMR (125 MHz, CD_3OD) δ 5.17, 5.21, 6.42, 7.76, 9.80, 10.42, 11.08, 14.64, 16.99, 17.03, 18.36, 19.26, 19.70, 22.09, 22.20, 22.87, 22.98, 24.79, 25.51, 25.76, 28.62, 28.75, 30.31, 30.39, 31.67, 31.78, 32.76, 33.52, 35.48, 36.36, 37.08, 40.60, 43.35, 44.07, 46.71, 53.00, 55.32, 57.65, 59.38, 66.59, 67.25, 67.32, 67.57, 68.39, 68.98, 72.32, 72.57, 72.72, 73.46, 75.09, 76.50, 78.35, 81.85, 117.21, 124.96, 125.41, 125.68, 127.15, 127.42, 128.50, 130.57, 130.85, 131.02, 134.71, 138.61, 153.50, 162.08, 163.61, 166.30, 167.46, 171.12, 172.18, 201.18. HRMS (TOF) for $C_{84}H_{116}N_{11}O_{22}S_3^+$ calcd: 1726.7453. Found: 1726.7432 (Δ = -1.2 ppm). HPLC (1): t = 12.0 min, purity > 98%.

Double-warhead Conjugate DW-1 [5-9]:
To a solution of **5-8** (40 mg, 0.0232 mmol) and ascorbic acid (4 mg, 0.0255 mmol) in THF (1 mL) was added **5-3** (0.019 g, 0.0232 mmol) in CH_2Cl_2 (1 mL) first, followed by an aqueous solution of $CuSO_4{\cdot}5H_2O$ (6.4 mg, 0.0244 mmol) (1 mL), and the mixture was allowed to react for 14 h at room temperature with stirring. The reaction was diluted with H_2O (5 mL), and the mixture was extracted with CH_2Cl_2 (3 x 10 mL). The combined organic layers were dried over $MgSO_4$ and concentrated *in vacuo* to give DW-1 (**5-9**) (54 mg, 92%) as an off-white solid; mp 138-139 °C; ^{1}H NMR (500 MHz, CD_3OD) δ 0.92 (m, 5H), 1.03 (m, 9H), 1.20 (s, 6H), 1.31 (m, 6H), 1.43 (s, 9H), 1.63 (m, 6H), 1.67 (s, 3H), 1.76 (s, 3H), 1.79 (s, 3H), 1.94 (s, 3H), 2.08 (t, *J* = 7.5 Hz, 1H), 2.24 (m, 8H), 2.40 (s, 3H), 2.47 (m, 1H), 2.71 (t, *J* = 12.8 Hz, 2H), 2.78 (m, 1H), 2.86 (m, 1H), 2.91 (dd, *J* = 5.5, 12.8 Hz, 1H), 3.19 (m, 1H), 3.26 (m, 1H), 3.37 (m, 2H), 3.45 (m, 2H), 3.63 (m, 24H), 3.81 (m, 6H), 4.08 (m, 2H), 4.10 (d, *J* = 16.7 Hz, 1H), 4.23 (m, 3H), 4.31 (m, 3H), 4.52 (m, 2H), 4.66 (m, 2H), 5.00 (t, *J* = 9.0 Hz, 2H), 5.32 (s, 2H), 5.35 (s, 1H), 5.60 (d, *J* = 16.7 Hz, 1H), 5.70 (m, 1H), 6.15 (bt, *J* = 8.5 Hz, 1H), 6.47 (s, 1H), 7.30 (m, 6H), 7.41 (d, *J* = 8.2 Hz, 1H), 7.53 (m, 2H), 7.65 (m, 2H), 7.74 (m, 3H), 7.92 (t, *J* = 8.0 Hz, 1H), 7.94 (bs, 1H), 8.08 (d, *J* = 8.0 Hz, 1H), 8.14 (d, *J* = 7.5 Hz, 2H), 8.27 (d, *J* = 8.5 Hz, 1H), 8.61 (s, 1H); ^{13}C NMR (125 MHz, DMSO-d_6) δ 7.99, 8.77, 8.85, 10.24, 13.16, 14.22, 14.25, 18.35, 20.08, 20.16, 20.47, 20.54, 20.74, 21.90, 23.00, 25.74, 25.96, 26.80, 28.51, 30.69, 30.89, 31.54, 31.64, 32.84, 34.87, 35.56, 38.51, 38.88, 41.14, 45.86, 46.69, 49.74, 50.72, 55.90, 57.96, 59.66, 61.50, 66.78, 69.52, 69.61, 69.98, 70.00, 70.07, 70.14, 70.19, 76.60, 77.21, 78.60, 80.00, 84.06, 95.59, 97.62, 119.37, 120.70, 125.38, 127.85, 128.17, 128.46, 128.87, 129.00, 130.17, 130.38, 130.83, 131.65, 131.96, 132.01, 133.03, 133.81, 133.89, 136.45, 137.33, 137.59, 137.63, 139.66, 139.97, 145.45, 145.49, 148.43, 151.93, 152.71, 155.39, 156.98, 157.24, 163.17, 165.59, 167.51, 169.27, 169.85, 170.07, 170.63, 171.73, 172.60, 178.58, 203.01; HRMS for $C_{125}H_{162}N_{17}O_{31}S_5^+$ calcd: 2557.0221; found: 2557.0207. (Δ = -0.5 ppm). HPLC (1): t = 11.3 min, purity >97%.

5-Aza-16-azido-8,11,14-trioxa-4-oxo-hexadecanoic acid [5-10]:
To a solution of succinic anhydride (0.183 g, 1.834 mmol) and **4-5** (0.400 g, 1.834 mmol) in CH_2Cl_2 (3 mL) was added Et_3N (25 μL, 0.1834 mmol), and the mixture was allowed to react for 16 h at room temperature with stirring. The reaction mixture was concentrated *in vacuo* to afford a yellow oil. Purification of the crude product by column chromatography on silica gel with 2% CH_3OH in CH_2Cl_2 as eluent gave **5-10** (0.389 g, 67%) as a colorless liquid; ^{1}H NMR (500 MHz,

$CDCl_3$) δ 2.54 (m, 2H), 2.67 (m, 2H), 3.40 (m, 2H), 3.45 (m, 2H), 3.55 (t, *J* = 5.0 Hz, 2H), 3.63 (m, 2H), 3.68 (m, 8H), 6.75 (bs, 1H); ^{13}C NMR (125 MHz, $CDCl_3$) δ 30.35, 30.99, 39.51, 50.68, 69.63, 69.93, 70.14, 70.44, 70.57, 70.65, 172.71, 175.29; HRMS for $C_{12}H_{23}N_4O_6^+$ calcd: 319.1612; found: 319.1622 (Δ = 3.2 ppm).

20-(5-Aza-16-azido-8,11,14-trioxa-4-oxo-hexadecanoic)camptothecin [5-11]:
To a solution of camptothecin (40 mg, 0.115 mmol), **5-10** (157 mg, 0.354 mmol), and DMAP (105 mg, 0.115 mmol) in CH_2Cl_2 (5 mL) was added DIC (30 μL, 0.127 mmol), and the mixture was allowed to react for 36 h at room temperature with stirring. The reaction mixture was cooled to 0 °C, and the precipitated urea by-product was removed by filtration. The filtrate was concentrated *in vacuo* to afford a yellow oil. Purification of the crude product by column chromatography on silica gel with 3% CH_3OH in CH_2Cl_2 as eluent gave **5-11** (53 mg, 72%) as an off-white solid; R_f = 0.55 (CH_2Cl_2/CH_3OH: 9/1); mp 100-101 °C; ^{1}H NMR (500 MHz, $CDCl_3$) δ 0.99 (t, *J* = 7.5 Hz, 3H), 2.20 (m, 1H), 2.51 (m, 2H), 2.88 (m, 2H), 3.36-3.45 (m, 6H), 3.55 (m, 2H), 3.60 (m, 2H), 3.63 (m, 6H), 5.28 (m, 2H), 5.38 (d, *J* = 17.1 Hz, 1H), 5.68 (d, *J* = 17.1 Hz, 1H), 6.31 (bs, 1H), 7.30 (s, 1H), 7.66 (t, *J* = 7.6 Hz, 1H), 7.84 (t, *J* = 7.8 Hz, 1H), 7.93 (d, *J* = 7.8 Hz, 1H), 8.25 (d, *J* = 8.6 Hz, 1H), 8.39 (s, 1H); ^{13}C NMR (125 MHz, $CDCl_3$) δ 7.58, 29.40, 30.67, 37.70, 39.31, 49.90, 50.63, 66.99, 69.67, 69.97, 70.16, 70.49, 70.54, 70.62, 76.12, 96.39, 119.90, 128.00, 128.13, 128.42, 129.66, 130.64, 131.11, 146.08, 146.19, 148.82, 152.34, 157.37, 176.54, 170.78, 171.93; HRMS for $C_{32}H_{37}N_6O_9^+$ calcd: 649.2617. Found: 649.2622 (Δ = 0.8 ppm). HPLC (2): t = 10.8 min, purity >98%.

Double-warhead Conjugate DW-2 [5-12]:
To a solution of **5-8** (12 mg, 6.95 μmol), **5-11** (5 mg, 6.95 μmol), and ascorbic acid (1.4 mg, 7.70 μmol) in THF (0.5 mL) was added an aqueous solution of $CuSO_4{\cdot}5H_2O$ (2 mg, 7.70 mmol) (0.1 mL), and the mixture was allowed to react for 10 h at room temperature with stirring. The reaction was diluted with H_2O (5 mL), and the mixture was extracted with CH_2Cl_2 (3 x 5 mL). The combined organic layers were concentrated in vacuo to afford a milky white solid. Purification of the crude product by column chromatography on silica gel with 10% CH_3OH in CH_2Cl_2 as eluent gave DW-2 (**5-12**) (12 mg, 54%) as a off-white solid; mp 143-145 °C; ^{1}H NMR (500 MHz, CD_3OD) δ 0.89 (m, 2H), 0.98 (m, 3H), 1.01 (t, *J* = 7.5 Hz, 3H), 1.07 (m, 2H), 1.15 (s, 3H), 1.16 (s, 3H), 1.25 (m, 6H), 1.40 (m, 2H), 1.40 (s, 9H), 1.60 (m, 4H), 1.64 (s, 3H), 1.73 (s, 3H), 1.74 (m, 3H), 1.75 (s, 3H), 1.86 (m, 2H), 1.90 (m, 3H), 2.01 (m, 1H), 2.20 (m, 7H), 2.38 (s, 3H), 2.42 (m), 2.53 (m), 2.68 (d, *J* = 12.8 Hz, 1H), 2.88 (m, 3H), 3.15 (m, 1H), 3.17 (bs, 2H), 3.34 (m, 2H), 3.39 (bt, *J* = 5.4 Hz, 2H), 3.43 (m, 4H), 3.52 (m, 6H), 3.62 (m, 10H), 3.73 (m, 2H, PEG), 3.80 (m, 1H), 3.83 (t, *J* = 7.3 Hz), 4.02 (d, *J* = 16.7 Hz, 1H), 4.06 (m, 1H), 4.20 (m, 3H), 4.28 (m, 2H), 4.38 (m, 1H), 4.48 (m, 3H), 4.91 (bs, 2H), 4.98 (t, *J* = 9.0 Hz, 1H), 5.26 (m, 1H), 5.31 (m, 2H), 5.45 (d, *J* = 16.7 Hz, 1H), 5.58 (d, *J* = 16.7 Hz, 1H), 5.66 (t, *J* = 6.7 Hz, 1H), 6.12 (bt, 1H), 6.43 (s, 1H), 6.45 (bs, 1H), 7.22 (m, 1H), 7.30 (m, 2H), 7.40 (s, 1H), 7.50 (t, *J* = 8.2 Hz, 2H), 7.63 (t, *J* = 7.4 Hz, 1H), 7.72 (m, 2H), 7.79 (m, 1H), 7.86 (t, *J* = 7.4 Hz, 1H), 7.93 (bs, 1H), 8.06 (d, *J* = 8.0 Hz, 1H), 8.11 (d, *J* = 7.8 Hz, 2H), 8.18 (d, *J* = 8.0 Hz, 1H), 8.61 (bs, 1H); ^{13}C NMR (125 MHz, CD_3OD) δ 6.70, 7.77, 7.82, 9.02, 12.41, 17.25, 19.61, 20.95, 21.88, 24.70, 25.09, 25.48, 25.58, 27.39, 28.09, 28.33, 28.33, 28.76, 30.75, 31.22, 35.34, 36.12, 38.04, 38.94, 43.20, 46.67, 50.26, 57.94, 60.24, 61.97, 66.32, 67.46, 69.03, 69.17, 69.84, 69.92, 69.95, 70.03, 70.20, 71.03, 73.25, 73.41, 74.90, 75.30, 75.59, 76.06, 76.41, 77.68, 78.07, 79.10, 80.95, 84.41, 87.85, 88.10, 96.77, 119.15, 119.81, 127.87, 128.00, 128.28, 128.41, 128.60, 129.74, 130.01, 130.62, 133.16, 137.31, 146.26, 146.96, 148.27,

157.59, 166.18, 167.97, 168.90, 170.05, 170.13, 170.92, 171.06, 172.63, 173.67, 173.72, 203.80; HRMS (TOF) calcd for $C_{116}H_{152}N_{17}O_{31}S_3^+$ calcd: 2374.9997. Found: 2374.9980 (Δ = -0.7 ppm). HPLC (1): t = 10.5 min, purity > 96%.

Phenol-(SS-Linker)-OTIPS [5-13]:
To a solution of phenol (135 mg, 1.434 mmol), **3-10** (545 mg, 1.195 mmol) and DMAP (14 mg, 0.119 mmol), in CH_2Cl_2 (15 mL) was added DIC (210 μL, 1.314 mmol), and the mixture was allowed to react for 10 h at room temperature with stirring. The reaction was quenched with saturated NH_4Cl (10 mL) and diluted with H_2O (5 mL), and the reaction mixture was extracted with CH_2Cl_2 (3 x 20 mL). The combined organic layers were dried over $MgSO_4$ and concentrated *in vacuo* to afford a yellow oil. Purification of the crude product by column chromatography on silica gel with hexanes/ethyl acetate (33:1) as eluent gave **5-13** (505 mg, 79%) as a colorless oil; R_f = 0.85 (hexanes/ethyl acetate: 3/1); ^{1}H NMR (400 MHz, $CDCl_3$) δ 1.06 (m, 21H), 1.30 (d, *J* = 6.8 Hz, 3H), 1.85 (m, 1H), 1.93 (m, 1H), 2.42 (m, 2H), 2.96 (m, 1H), 4.11 (s, 2H), 7.10 (d, *J* = 7.4 Hz, 2H), 7.21 (t, *J* = 7.4 Hz, 1H), 7.26 (t, *J* = 7.3 Hz, 1H), 7.31 (t, *J* = 7.3 Hz, 2H), 7.36 (t, *J* = 7.4 Hz, 2H), 7.82 (d, *J* = 7.9, 1H); ^{13}C NMR (100 MHz, $CDCl_3$) 11.89, 17.79, 20.57, 30.99, 33.03, 39.41, 46.11, 121.48, 125.84, 127.65, 128.27, 129.36, 130.23, 130.83, 133.38, 137.67, 150.79, 169.40, 173.01; HRMS (TOF) for $C_{28}H_{41}O_4S_2Si^+$ calcd: 533.2210. Found: 533.2222 (Δ = 2.3 ppm).

Phenol-(SS-Linker)-OH [5-14]
To a cooled solution of **5-13** (0.505 g, 0.947 mmol) in CH_3CN-pyridine (1:1) (80 mL) was added 70% HF/pyridine (5 mL), and the mixture was allowed to react for 6 h at room temperature with stirring. The reaction was quenched with 10% citric acid (20 mL), and the mixture was extracted with ethyl acetate (3 x 50 mL). The combined organic layers were washed with saturated $CuSO_4$ (3 x 50 mL) and brine (3 x 50 mL), dried over $MgSO_4$, and concentrated *in vacuo* to afford a pale-yellow oil. Purification of the crude product by column chromatography on silica gel with hexanes/ethyl acetate (1:1) as eluent gave **5-14** (0.314 g, 88%) as a colorless oil; R_f = 0.3 (hexanes/ethyl acetate: 1/1); ^{1}H NMR (500 MHz, $CDCl_3$) δ 1.29 (d, *J* = 6.8 Hz, 3H), 1.86 (m, 1H), 1.95 (m, 1H), 2.42 (m, 2H), 2.94 (m, 2H), 4.12 (s, 2H), 7.11 (d, *J* = 7.5 Hz, 2H), 7.21 (t, *J* = 7.5 Hz, 1H), 7.26 (m, 1H), 7.31 (t, *J* = 7.5 Hz, 2H), 7.35 (t, *J* = 7.5 Hz, 2H), 7.81 (d, *J* = 7.5 Hz, 1H); ^{13}C NMR (100 MHz, $CDCl_3$) δ 20.48, 30.35, 31.03, 39.42, 45.90, 121.47, 125.88, 127.80, 128.31, 129.39, 130.45, 130.94, 133.53, 137.51, 150.77, 169.50, 178.29; HRMS (TOF) for $C_{19}H_{21}O_4S_2^+$ calcd: 377.0876. Found: 377.0888 (Δ = 3.2 ppm).

Phenol-(SS-Linker)-OSu [5-15]:
To a solution of **5-14** (0.154 g, 0.410 mmol) and HOSu (0.141 g, 1.23 mmol) CH_2Cl_2 (1.6 mL) was added EDC·HCl (0.094 g, 0.493 mmol) in CH_2Cl_2 (1 mL), and the mixture was allowed to react for 16 h at room temperature with stirring. The reaction was quenched with saturated NH_4Cl (10 mL) and diluted with H_2O (10 mL), and the mixture was extracted with CH_2Cl_2 (3 x 20 mL). The combined organic layers were washed with brine (3 x 20 mL), dried over $MgSO_4$ and concentrated *in vacuo* to afford a yellow oil. Purification by of the crude product by column chromatography on silica gel with hexanes/ethyl acetate (1:1) as eluent gave **5-15** (0.162 g, 84%) as a colorless oil; R_f = 0.28 (hexanes/ethyl acetate: 1/1); ^{1}H NMR (500 MHz, $CDCl_3$) δ 1.30 (d, *J* = 6.8 Hz, 3H), 1.98 (m, 1H), 2.06 (m, 1H), 2.66 (t, *J* = 7.8 Hz, 2H), 2.82 (bs, 4H), 3.00 (m, 1H), 4.13 (s, 2H), 7.10 (d, *J* = 7.5 Hz, 2H), 7.21 (m, 1H), 7.26 (m, 1H), 7.34 (m, 4H), 7.82 (d, *J* = 7.5 Hz, 1H); ^{13}C NMR (125 MHz, $CDCl_3$) δ 20.41, 25.60, 28.31, 30.28, 39.44, 45.60, 121.50, 125.88, 127.92, 128.42, 129.41,

130.56, 130.94, 133.57, 137.43, 150.76, 168.16, 169.01, 169.46; HRMS (TOF) for $C_{23}H_{24}NO_6S_2^+$ calcd: 474.1040. Found: 474.1044 (Δ = 0.8 ppm).

Phenol-(SS-Linker)-PEG$_3$-N$_3$ [5-16]:
To a solution of **5-15** (0.149 g, 0.396 mmol) and **4-5** (0.259 g, 1.189 mmol) in CH_2Cl_2 (1 mL) was added DIC (67 μL, 0.436 mmol), and the mixture was allowed to react for 10 h at room temperature with stirring. The reaction mixture was concentrated *in vacuo* to give a yellow oil. Purification of the crude product by column chromatography on silica gel with 1.5% CH_3OH in CH_2Cl_2 as eluent gave **5-16** (0.127 g, 56%) as a colorless oil; R_f = 0.7 (CH_2Cl_2/CH_3OH: 9/1); ^{1}H NMR (500 MHz, $CDCl_3$) δ 1.34 (d, *J* = 6.8 Hz, 3H), 1.95 (m, 2H), 2.17 (t, *J* = 7.6 Hz, 1H), 2.57 (m, 1H), 2.94 (m, 1H), 3.40 (m, 2H), 3.49 (t, *J* = 5.3 Hz, 2H), 3.75 (m, 12H), 4.17 (s, 2H), 6.02 (bs, 1H), 7.14 (m, 2H), 7.25 (t, *J* = 7.5 Hz, 1H), 7.35 (m, 3H), 7.40 (t, *J* = 7.5 Hz, 2H), 7.82 (d, *J* = 7.5 Hz, 1H); ^{13}C NMR (125 MHz, $CDCl_3$) δ 20.88, 23.53, 31.31, 33.55, 39.44, 46.48, 50.69, 61.79, 69.78, 70.07, 70.24, 70.59, 70.64, 70.73, 72.50, 121.51, 125.94, 127.97, 128.24, 129.43, 130.87, 131.21, 133.86, 137.62, 150.76, 169.81, 172.17; HRMS (TOF) for $C_{27}H_{37}N_4O_6S_2^+$ calcd: 577.2149. Found: 577.2154 (Δ = 0.9 ppm).

Double-warhead conjugate with a taxoid and surrogate warhead, SW-Tax [5-17]:
To a solution of **5-8** (20 mg, 11.6 μmol), **5-16** (6.7 mg, 11.6 μmol), and ascorbic acid (2 mg, 12.7 μmol) in THF (1 mL) was added $CuSO_4{\cdot}5H_2O$ (3.2 mg, 12.7 μmol) in H_2O (0.25 mL), and the mixture was allowed to react for 15 h and room temperature with stirring. Purification of the lyophilized reaction mixture by column chromatography on silica gel with 10% CH_3OH in CH_2Cl_2 as eluent gave SW-Tax (**5-17**) (0.021 g, 79%) as a colorless solid; R_f = 0.3 (CH_2Cl_2/CH_3OH: 9/1); mp 125-127 °C; ^{1}H NMR (500 MHz, $CDCl_3$) δ 0.90 (m, 3H), 1.02 (bt, *J* = 8.0 Hz, 2H), 1.18 (s, 3H), 1.27 (s, 3H), 1.33 (d, *J* = 6.8 Hz, 6H), 1.29 (m, 2H), 1.37 (s, 9H), 1.43 (m, 2H), 1.49 (m, 2H), 1.66 (m, 4H), 1.69 (s, 3H), 1.75 (s, 3H), 1.78 (m, 2H), 1.93 (s, 3H), 2.17 (t, *J* = 7.4 Hz, 2H), 2.29 (m, 1H), 2.39 (s, 3H), 2.54 (m, 2H), 2.73 (d, *J* = 12.6 Hz, 1H), 2.90 (m, 2H), 2.92 (dd, J=5.0, 12.6 Hz, 1H), 3.15 (m, 1H), 3.41 (t, *J* = 5.0 Hz, 2H), 3.44 (t, *J* = 5.4 Hz, 2H), 3.49 (t, *J* = 5.4 Hz, 2H), 3.69 (m, 28H), 3.77 (t, *J* = 5.0 Hz, 1H), 3.83 (m, 1H), 4.17 (s, 2H), 4.20 (d, *J* = 8.4 Hz, 1H), 4.21 (m, 2H), 4.31 (d, *J* = 8.4 Hz, 1H), 4.33 (m, 1H), 4.42 (m, 1H), 4.51 (m, 1H), 5.00 (m, 2H), 5.16 (bs, 1H), 5.70 (d, *J* = 7.2 Hz, 1H), 6.06 (s, 1H), 6.20 (bt, 1H), 6.34 (s, 1H), 7.14 (d, *J* = 7.4 Hz, 1H), 7.23 (t, *J* = 7.4 Hz, 1H), 7.34 (m, 4H), 7.40 (t, *J* = 8.0 Hz, 2H), 7.50 (t, *J* = 7.8 Hz, 2H), 7.63 (t, *J* = 7.4 Hz, 1H), 7.81 (bs, 1H), 7.83 (d, *J* = 7.7 Hz, 1H), 8.13 (d, *J* = 7.7 Hz, 2H); ^{13}C NMR (125 MHz, $CDCl_3$) δ 9.17, 9.33, 9.63, 13.06, 14.81, 17.50, 18.53, 20.01, 20.43, 20.87, 22.07, 22.48, 23.51, 25.76, 26.61, 27.90, 28.26, 31.30, 33.54, 35.48, 39.12, 43.21, 45.88, 46.47, 50.68, 53.51, 55.49, 58.41, 60.24, 61.75, 69.67, 69.78, 70.05, 70.15, 70.22, 70.26, 70.32, 70.41, 70.58, 70.63, 70.67, 70.69, 70.71, 71.99, 72.49, 75.11, 75.47, 76.40, 78.90, 79.15, 79.83, 81.00, 84.48, 115.39, 117.71, 120.04, 121.50, 125.93, 127.95, 128.23, 128.37, 128.66, 128.84, 128.28, 129.60, 130.17, 130.85, 130.94, 131.20, 133.67, 133.85, 137.64, 150.75, 155.07, 162.94, 163.23, 166.97, 168.37, 169.80, 172.19, 173.39, 174.95, 204.09; HRMS for $C_{111}H_{152}N_{15}O_{28}S_5^+$ calcd: 2303.9529. Found: 2303.9480 (Δ = -2.1 ppm). HPLC (1): t = 11.0 min, purity >98%.

4-(11-Biotinylamino-3,6,9-trioxaundecyl)amino-6-[2-(camptothecin-SS-Linker)-amidoethyl]amino-2-propargylamino-1,3,5-triazine [5-18]:
To a solution of **5-7** (19 mg, 26.2 μmol) and **5-15** (12 mg, 26.2 μmol) in CH_2Cl_2 (1 mL) was added pyridine (1 mL), and the mixture was allowed to react for 10 h at room temperature with stirring.

The reaction mixture was concentrated *in vacuo* to give a yellow oil. Purification of the crude product by column chromatography on silica gel with 4% CH_3OH in CH_2Cl_2 as eluent gave **5-18** (13 mg, 52%) as a colorless oil; R_f = 0.4 (CH_2Cl_2/CH_3OH: 9/1); ^{1}H NMR (500 MHz, $CDCl_3$) δ 1.29 (d, *J* = 6.8 Hz, 3H), 1.43 (t, *J* = 7.7 Hz, 2H), 1.66 (m, 4H), 1.84 (m, 1H), 1.92 (m, 1H), 2.22 (m, 2H), 2.56 (bs, 1H), 2.72 (d, *J* = 12.8 Hz, 1H), 2.90 (m, 2H), 2.92 (dd, *J* = 5.0, 12.8 Hz, 1H), 3.19 (m, 1H), 3.38 (t, *J* = 5.4 Hz, 2H), 3.44 (bs, 2H), 3.56 (t, *J* = 5.4 Hz, 2H), 3.66 (m, 14H), 4.15 (bs, 2H), 4.20 (s, 2H), 4.30 (dd, *J* = 4.4, 8.0 Hz, 1H), 4.49 (dd, *J* = 4.4, 8.0 Hz, 1H), 7.14 (d, *J* = 7.8 Hz, 2H), 7.25-7.45 (m, 6H), 7.83 (d, *J* = 7.8 Hz, 1H), 8.55 (bs, 1H); ^{13}C NMR (125 MHz, $CDCl_3$) δ 19.57, 25.47, 28.09, 28.39, 31.27, 32.97, 35.35, 38.74, 39.00, 39.68, 46.00, 55.62, 60.22, 61.97, 69.18, 69.55, 69.84, 69.89, 70.18, 70.21, 120.99, 125.64, 127.67, 128.05, 128.27, 129.95, 130.34, 130.75, 131.21, 131.60, 134.01, 137.38, 148.66, 150.95, 164.73, 170.23, 174.75. HRMS for $C_{45}H_{63}N_{10}O_8S_3^+$ calcd: 967.3987. Found: 967.3991 (Δ = 0.4 ppm).

Double-warhead conjugate with camptothecin and a surrogate warhead, SW-CPT [5-19]:
To a solution of **5-18** (13 mg, 13.5 μmol), **5-11** (11 mg, 13.5 μmol), and ascorbic acid (2.6 mg, 14.9 μmol) in THF (1 mL) was added $CuSO_4{\cdot}5H_2O$ (3.7 mg, 14.9 μmol) in CH_3OH-H_2O (1:1) (1 mL), and the mixture was stirred for 4 h at room temperature with stirring. The reaction mixture was concentrated *in vacuo* and extracted with CH_2Cl_2 (3 x 10 mL). The combined organic layers were dried over $MgSO_4$ and concentrated *in vacuo* to give a yellow solid. Purification of the crude product by column chromatography on silica gel with 8% CH_3OH in CH_2Cl_2 as eluent gave SW-CPT (**5-19**) (13 mg, 54%) as a white solid; R_f = 0.38 (CH_2Cl_2/CH_3OH: 9/1); mp 127-128 °C; ^{1}H NMR (500 MHz, DMSO-d_6) δ 0.90 (t, *J* = 7.5 Hz, 3H), 1.03 (m, 2H), 1.20 (d, *J* = 6.8 Hz, 3H), 1.24 (s, 2H), 1.30 (m, 2H), 1.49 (m, 4H), 1.59 (m, 1.59), 1.71 (m, 2H), 1.84 (m, 1H), 2.07 (m, 4H), 2.17 (m, 4H), 2.57 (d, *J* = 12.8 Hz, 1H), 2.81 (m, 2H), 2.95 (m, 1H), 3.10 (m, 1H), 3.14 (m, 3H), 3.15 (m, 4H), 3.25 (m, 2H), 3.39 (t, *J* = 5.4 Hz, 4H), 3.43-3.49 (m, 20H), 3.77 (t, *J* = 5.0 Hz, 2H), 4.06 (t, 2H), 4.13 (m, 1H), 4.17 (m, 2H), 4.30 (m, 1H), 4.46 (m, 4H), 5.31 (m, 2H), 5.45 (d, *J* = 17.0 Hz, 1H), 5.50 (d, *J* = 17.0 Hz, 1H), 6.37 (s, 1H), 6.43 (s, 1H), 7.09 (s, 1H), 7.12 (d, *J* = 7.6 Hz, 2H), 7.24-7.44 (m, 9H), 7.73 (m, 3H), 7.88 (m, 4H), 8.14 (d, *J* = 8.1 Hz, 1H), 8.23 (d, *J* = 8.5 Hz, 1H), 8.69 (s, 1H); ^{13}C NMR (125 MHz, DMSO-d_6) δ 7.99, 20.06, 20.14, 20.51, 25.70, 28.51, 28.67, 30.69, 31.59, 32.83, 33.02, 35.56, 36.06, 45.85, 45.92, 46.18, 49.07, 49.66, 50.72, 55.41, 55.90, 59.65, 61.49, 66.78, 69.26, 69.52, 69.63, 69.99, 70.07, 70.14, 70.18, 70.22, 95.62, 119.36, 122.06, 126.41, 127.85, 128.04, 128.18, 128.46, 128.87, 129.00, 129.60, 129.73, 130.06, 130.17, 130.84, 131.66, 131.90, 131.96, 133.03, 133.83, 137.40, 137.63, 145.50, 146.42, 148.44, 150.91, 152.71, 156.99, 163.17, 166.15, 166.21, 167.53, 169.85, 171.74, 171.89, 172.58, 173.27; HRMS (TOF) for $C_{86}H_{109}N_{16}O_{17}S_5^+$ calcd: 1797.6755. Found: 1797.6705 (Δ = -2.8 ppm). HPLC (1): t = 8.6 min, purity >97%.

Cell Culture

All cell lines were obtained from ATCC unless otherwise noted. Cells were cultured in RPMI-1640 cell culture medium (Gibco) or DMEM culture medium (Gibco), both supplemented with 5% (v/v) heat-inactivated fetal bovine serum (FBS), 5% (v/v) NuSerum, and 1% (v/v) penicillin and streptomycin (PenStrep) at 37 °C in a humidified atmosphere with 5% CO_2. L1210 and L1210FR (a gift from Dr. Gregory Russell-Jones, Access Pharmaceuticals Pty Ltd., Australia) cells were grown as a suspension in supplemented RPMI-1640. LCC6-MDR, LCC6-WT, MX-1, MCF-7, and ID8 were cultured as monolayers on 100 mm tissue culture dishes in a supplemented RPMI-1640 cell culture medium, and WI-38 as a monolayer in a supplemented DMEM cell culture

medium. Cells were harvested, collected by centrifugation at 850 rpm for 5 min, and resuspended in fresh culture medium. Cell cultures were routinely divided by treatment with trypsin (TrypLE, Gibco) as needed every 2-4 days and collected by centrifugation at 850 rpm for 5 min, and resuspended in fresh cell culture medium, containing varying cell densities for subsequent biological experiments and analysis.

Confocal Fluorescence Microscopy Imaging of the Cells with DW-1 (5-9)

Cells treated as described above were re-suspended in 150 μL of PBS after each experiment, and dropped onto an uncoated microslide with coverslip (MatTek Corp.). Confocal fluorescence microscopy (CFM) experiments were performed using a Zeiss LSM 510 META NLO two-photon laser scanning confocal microscopy system, operating at a 488 nm excitation wavelength and at 527 ± 23 nm detecting emission wavelength using a 505-550 nm bandpass filter. Images were captured using a C-Apochromat 63x/1.2 water (corr.) objective. Images for DW-1 (**5-9**) were obtained using the camera mode with a filter set of 350 ± 25 nm excitation wavelength and 420 nm long pass emission wavelength. Acquired data were analyzed using LSM 510 Meta software.

***In Vitro* Cytotoxicity Assays**

The cytotoxicities (IC_{50}, nM) of SB-T-1214 and camptothecin were evaluated for single-agent administrations as well as for time-dependent administrations of equimolar combinations against various cancer cell lines by means of the standard quantitative colorimetric MTT assay.[34] The inhibitory activity of each compound is represented by the IC_{50} value, which is defined as the concentration required for inhibiting 50% of the cell growth. Cells were harvested, collected, and resuspended in 100 μL cell culture medium (RPMI-1640) at a concentrations ranging from 0.5-1.5 x 10^4 cells per well in a 96-well plate. For adhesive cell types, cells were allowed to descend to the bottom of the wells overnight, and appropriate fresh medium was added to each well upon removal of the old medium.

For the MTT assay of the time-dependent administrations of equimolar amounts of SB-T-1214 and camptothecin in a sequential manner, cells were re-suspended in 200 μL medium with 8,000 to 10,000 cells per well of a 96-well plate and incubated at 37 °C for 24 h before drug treatment. Two sets of serial dilutions of equimolar taxoid and camptothecin in sterile DMSO were added using the cell culture medium. The residual medium in each well were aspirated and the different drug solutions were added to each well of every column of the 96-well plate. After the addition of the first drug solution, the cells were incubated at 37 °C for 24 h. Then, the second drug solution was added, followed by incubation for additional 48 h at 37 °C.

For the MTT assay of paclitaxel, SB-T-1214, DW-1 (**5-9**), DW-2 (**5-12**), SW-Tax (**5-17**), and SW-CPT (**5-19**), cells were resuspended in 200 μL medium with 8,000 to 10,000 cells per well of a 96-well plate and incubated at 37 °C for 24 h before drug treatment. In DMSO stock solutions, each drug or conjugate was diluted to a series of concentrations in cell culture medium to prepare test solutions. After removing the old medium, these test solutions were added to the wells in the 96-well plate to give the final concentrations ranging from 0.5 to 5,000 nM (100 μL), and the cells were subsequently cultured at 37 °C for 48 of 72 h. For the leukemia cell lines, cells were harvested, collected, and resuspended in the test solutions ranging from 0.5 to 5,000 nM (100 μL) at 0.5 to 0.8 x 10^4 cells per well in a 96-well plate and subsequently incubated at 37 °C for 48 or 72 h.

The cytotoxicities (IC_{50}, nM) for conjugates DW-1 (**5-9**), DW-2 (**5-12**), SW-Tax (**5-17**), and SW-CPT (**5-19**) were evaluated in a similar manner. In DMSO stock solutions, each conjugate

was diluted to a series of concentrations in cell culture medium to prepare test solutions. After removing the old medium, these test solutions were added to the wells in the 96-well plate to give the final concentrations ranging from 0.5 to 5,000 nM (100 μL), and the cells were subsequently cultured at 37 °C for 72 h. For the leukemia cell lines, cells were harvested, collected, and re-suspended in the test solutions ranging from 0.5 to 5,000 nM (100 μL) at 0.5 to 0.8 x 10^4 cells per well in a 96-well plate and subsequently incubated at 37 °C for 72 h.

In another series of experiments, cells were incubated with a conjugate at 37 °C for 24 h and the drug medium was removed. Then, treated cells were washed with PBS, and GSH-OEt (6 equiv. to a conjugate) in cell culture medium (200 μL) was added to the wells. These cells were incubated at 37 °C for an additional 48 h, i.e., the total incubation time was 72 h.

For all experiments, after removing the test medium, fresh solution of MTT in PBS (40 μL of 0.5 mg MTT/mL) was added to the wells, and the cells were incubated at 37 °C for 3 h. The MTT solution was then removed, and the resulting insoluble violet formazan crystals were dissolved in 0.1 *N* HCl in isopropanol with 10% Triton X-100 (40 μL) to give a violet solution. The spectrophotometric absorbance measurement of each well in the 96-well plate was run at 570 nm using a Labsystems Multiskan Ascent microplate reader. The IC_{50} values and their standard errors were calculated from the viability-concentration curve using Four Parameter Logistic Model of *Sigmaplot*. The concentration of DMSO per well was ≤1% in all cases. Each experiment was run in triplicate.

§5.7 References

1. Lay, H. N.; Ekert, H.; Colebatch, J. H. Combination chemotherapy for children with acute lymphocytic leukemia who fail to respond to standard remission-induction therapy. *Cancer* **1975,** 36, 1220-1222.
2. Devita, V. T., Jr.; Serpick, A. A.; Carbone, P. P. Combination chemotherapy in the treatment of advanced Hodgkin's disease. *Ann. Intern. Med.* **1970,** 73, 881-895.
3. Rocha Lima, C.; Catapano, C. V.; Pacheco, D.; Sherman, C.; Oakhill, G.; Chaudhry, M.; Freeman, K. D.; Green, M. R. A phase I study of sequential administration of escalating doses of intravenous paclitaxel, oral topotecan, and fixed-dose oral etoposide in patients with solid tumors. *Cancer* **2004,** 100, 2671-2679.
4. Jensen, P. B.; Holm, B.; Sorensen, M.; Christensen, I. J.; Sehested, M. In vitro cross-resistance and collateral sensitivity in seven resistant small-cell lung cancer cell lines: preclinical identification of suitable drug partners to taxotere, taxol, topotecan and gemcitabin. *Br. J. Cancer* **1997,** 75, 869-877.
5. Zimmermann, G. R.; Lehar, J.; Keith, C. T. Multi-target therapeutics: when the whole is greater than the sum of the parts. *Drug. Discov. Today* **2007,** 12, 34-42.
6. Bahadori, H. R.; Green, M. R.; Catapano, C. V. Synergistic interaction between topotecan and microtubule-interfering agents. *Cancer Chemother. Pharmacol.* **2001,** 48, 188-196.
7. Whitacre, C. M.; Zborowska, E.; Gordon, N. H.; Mackay, W.; Berger, N. A. Topotecan increases topoisomerase IIalpha levels and sensitivity to treatment with etoposide in schedule-dependent process. *Cancer Res.* **1997,** 57, 1425-1428.
8. Murren, J. R.; Peccerillo, K.; DiStasio, S. A.; Li, X.; Leffert, J. J.; Pizzorno, G.; Burtness, B. A.; McKeon, A.; Cheng, Y. Dose escalation and pharmacokinetic study of irinotecan in combination with paclitaxel in patients with advanced cancer. *Cancer Chemother. Pharmacol.* **2000,** 46, 43-50.

9. Kaufmann, S. H.; Peereboom, D.; Buckwalter, C. A.; Svingen, P. A.; Grochow, L. B.; Donehower, R. C.; Rowinsky, E. K. Cytotoxic effects of topotecan combined with various anticancer agents in human cancer cell lines. *J. Natl. Cancer Inst.* **1996,** 88, 734-741.
10. Hsiang, Y. H.; Lihou, M. G.; Liu, L. F. Arrest of replication forks by drug-stabilized topoisomerase I-DNA cleavable complexes as a mechanism of cell killing by camptothecin. *Cancer Res.* **1989,** 49, 5077-5082.
11. Slichenmyer, W. J.; Rowinsky, E. K.; Donehower, R. C.; Kaufmann, S. H. The current status of camptothecin analogues as antitumor agents. *J. Natl. Cancer Inst.* **1993,** 85, 271-291.
12. Rothenberg, M. L. Topoisomerase I inhibitors: review and update. *Ann. Oncol.* **1997,** 8, 837-855.
13. Li, L. H.; Fraser, T. J.; Olin, E. J.; Bhuyan, B. K. Action of camptothecin on mammalian cells in culture. *Cancer Res.* **1972,** 32, 2643-2650.
14. Horwitz, S. B.; Horwitz, M. S. Effects of camptothecin on the breakage and repair of DNA during the cell cycle. *Cancer Res.* **1973,** 33, 2834-2836.
15. Rapisarda, A.; Uranchimeg, B.; Scudiero, D. A.; Selby, M.; Sausville, E. A.; Shoemaker, R. H.; Melillo, G. Identification of small molecule inhibitors of hypoxia-inducible factor 1 transcriptional activation pathway. *Cancer Res.* **2002,** 62, 4316-4324.
16. Rapisarda, A.; Uranchimeg, B.; Sordet, O.; Pommier, Y.; Shoemaker, R. H.; Melillo, G. Topoisomerase I-mediated inhibition of hypoxia-inducible factor 1: mechanism and therapeutic implications. *Cancer Res.* **2004,** 64, 1475-1482.
17. Robati, M.; Holtz, D.; Dunton, C. J. A review of topotecan in combination chemotherapy for advanced cervical cancer. *Ther. Clin. Risk Manag.* **2008,** 4, 213-218.
18. Marxsen, J. H.; Schmitt, O.; Metzen, E.; Jelkmann, W.; Hellwig-Burgel, T. Vascular endothelial growth factor gene expression in the human breast cancer cell line MX-1 is controlled by O2 availability in vitro and in vivo. *Ann. Anat.* **2001,** 183, 243-249.
19. Debernardis, D.; Cimoli, G.; Parodi, S.; Russo, P. Interactions between taxol and camptothecin. *Anticancer Drugs* **1996,** 7, 531-4.
20. Madden, T.; Newman, R. A.; Antoun, G.; Johansen, M. J.; Ali-Osman, F. Low-level taxane exposure increases the activity of topoisomerase I targeted agents. *Proc. Am. Assoc. Cancer Res.* **1998,** 39, 527.
21. Bissery, M. C.; Vrignaud, P.; Lavelle, F. In vivo evaluation of the docetaxel-irinotecan combination. *Proc. Am. Assoc. Cancer Res.* **1996,** 37, 378.
22. Chou, T. C.; Motzer, R. J.; Tong, Y.; Bosl, G. J. Computerized quantitation of synergism and antagonism of taxol, topotecan, and cisplatin against human teratocarcinoma cell growth: a rational approach to clinical protocol design. *J. Natl. Cancer Inst.* **1994,** 86, 1517-1524.
23. Pei, X. H.; Nakanishi, Y.; Takayama, K.; Bai, F.; Kawasaki, M.; Tsuruta, N.; Mizuno, K.; Hara, N. Effect of CPT-11 in combination with other anticancer agents in lung cancer cells. *Anticancer Drugs* **1997,** 8, 231-237.
24. Brangi, M.; Litman, T.; Ciotti, M.; Nishiyama, K.; Kohlhagen, G.; Takimoto, C.; Robey, R.; Pommier, Y.; Fojo, T.; Bates, S. E. Camptothecin resistance: role of the ATP-binding cassette (ABC), mitoxantrone-resistance half-transporter (MXR), and potential for glucuronidation in MXR-expressing cells. *Cancer Res.* **1999,** 59, 5938-5946.
25. Hoki, Y.; Fujimori, A.; Pommier, Y. Differential cytotoxicity of clinically important camptothecin derivatives in P-glycoprotein-overexpressing cell lines. *Cancer Chemother. Pharmacol.* **1997,** 40, 433-438.

26. Takahashi, T.; Fujiwara, Y.; Yamakido, M.; Katoh, O.; Watanabe, H.; Mackenzie, P. I. The role of glucuronidation in 7-ethyl-10-hydroxycamptothecin resistance in vitro. *Cancer Sci.* **1997,** 88, 1211-1217.
27. Ojima, I.; Slater, J. C.; Michaud, E.; Kuduk, S. D.; Bounaud, P. Y.; Vrignaud, P.; Bissery, M. C.; Veith, J. M.; Pera, P.; Bernacki, R. J. Syntheses and structure-activity relationships of the second-generation antitumor taxoids: exceptional activity against drug-resistant cancer cells. *J. Med. Chem.* **1996,** 39, 3889-3896.
28. Ojima, I.; Slater, J. C.; Kuduk, S. D.; Takeuchi, C. S.; Gimi, R. H.; Sun, C. M.; Park, Y. H.; Pera, P.; Veith, J. M.; Bernacki, R. J. Syntheses and structure-activity relationships of taxoids derived from 14 beta-hydroxy-10-deacetylbaccatin III. *J. Med. Chem.* **1997,** 40, 267-278.
29. Ojima, I.; Wang, T.; Miller, M. L.; Lin, S.; Borella, C.; Geng, X.; Pera, P.; Bernacki, R. J. Syntheses and structure-activity relationships of new second-generation taxoids. *Bioorg. Med. Chem. Lett.* **1999,** 9, 3423-3428.
30. Ojima, I.; Das, M. Recent advances in the chemistry and biology of new generation taxoids. *J. Nat. Prod.* **2009,** 72, 554-565.
31. Vineberg, J. G.; Zuniga, E. S.; Kamath, A.; Chen, Y. J.; Seitz, J. D.; Ojima, I. Design, Synthesis and Biological Evaluations of Tumor-Targeting Dual-Warhead Conjugates for a Taxoid-Camptothecin Combination Chemotherapy. *J. Med. Chem.* **2014,** 57, 5777-5791.
32. Pouillart, P.; Weiner, R.; Schwarzenberg, L.; Misset, J. L.; Oldham, R.; Amiel, J. L.; Mathe, G. Combination chemotherapy based on a model of cell recruitment by partial synchronization. *Med. Pediatr. Oncol.* **1975,** 1, 123-134.
33. Vlahov, I. R.; Santhapuram, H. K.; Wang, Y.; Kleindl, P. J.; You, F.; Howard, S. J.; Westrick, E.; Reddy, J. A.; Leamon, C. P. An assembly concept for the consecutive introduction of unsymmetrical disulfide bonds: synthesis of a releasable multidrug conjugate of folic acid. *J. Org. Chem.* **2007,** 72, 5968-5972.
34. Mosmann, T. Rapid colorimetric assay for cellular growth and survival: application to proliferation and cytotoxicity assays. *J. Immunol. Methods* **1983,** 65, 55-63.
35. Burke, T. G.; Mishra, A. K.; Wani, M. C.; Wall, M. E. Lipid bilayer partitioning and stability of camptothecin drugs. *Biochemistry* **1993,** 32, 5352-5364.
36. Mistry, S. N.; Baker, J. G.; Fischer, P. M.; Hill, S. J.; Gardiner, S. M.; Kellam, B. Synthesis and in vitro and in vivo characterization of highly beta1-selective beta-adrenoceptor partial agonists. *J. Med. Chem.* **2013,** 56, 3852-3865.

Chapter 6

Taxoid-based Tumor-targeting Theranostic Conjugates Bearing a Potential ^{18}F-PET Radiotracer

Chapter Contents

§6.1.0 Introduction

§6.1.1 Theranostics in Pharmaceutical Development

Over the past decade, significant advancement has been made in targeted chemotherapy with the development of tumor-targeted drug delivery systems (TTDDS), especially for monoclonal antibody-drug conjugates (ADCs),[1-6] and small-molecule drug conjugates (SMDCs)[6-13] that recognize tumor-specific biomarkers. One promising approach lies in the development of tumor-targeted drug delivery systems (TTDDS) in which tumor-recognition moieties and cytotoxic agents are conjugated through cleavable linker systems. While the drug is connected to a linker system as a drug conjugate, the linker must be designed to remain stable during circulation in blood, but readily cleavable within the tumor microenvironment.[6] With continuous development of novel TTDDSs, it is essential to design corresponding imaging modalities as "theranostic" tools – combining therapeutics and diagnostics – to detail the biochemical and physiological processes in living systems with enhanced sensitivity, spatial resolution, and tissue specificity.[14, 15]

Theranostic imaging delivers therapeutic drugs and diagnostic imaging agents simultaneously within the same dose and single-administration.[15] Prior to treatment with a chemotherapeutic agent, theranostic applications allow for a clearer understanding of the cellular phenotype(s) and heterogeneity of the tumor.[15-18] The use of theranostic agents enables scientists and clinicians to image and monitor the diseased tissue, delivery kinetics, and drug efficacy with improved tuning of the therapy and dose, overcoming the undesirable differences in biodistribution and selectivity that currently exist between individual imaging and cytotoxic agents.[15]

§6.1.2 Fluorine-18 for PET

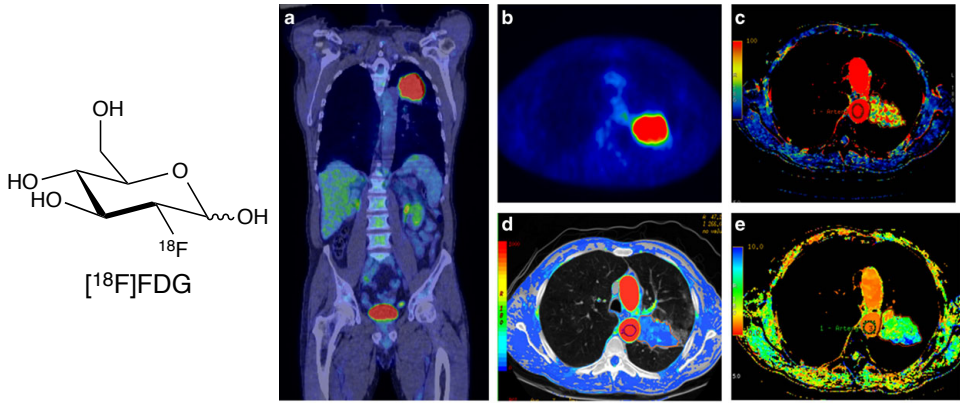

Figure 6.1. Chemical structure of [^{18}F]FDG (*left*) and (a) coronal fusion PET/CT image and (b) the axial PET image, (c) high ^{18}FDG uptake, and functional perfusion maps of (d) blood volume (BV) and (e) blood flow (BF) (*right*). Adapted from reference [19].

Positron emission tomography (PET) provides quantitative, real-time imaging of radiotracers in living systems and allows for *in vivo* biodistribution studies for a given radiotracer. Of these positron-emitting radioisotopes, fluorine-18 ($t_{1/2}$=110 min) is the most commonly used PET tracer in radiodiagnostics due to its prolonged half-life, which allows for multistep synthesis, and its short positron linear range in tissue (2.3 mm), which provides the

highest resolution of PET images of all the available positron emitters.[14] The development and use of 2-[^{18}F]fluoro-2-deoxy-D-glucose ([^{18}F]FDG) marked the beginning of target-specific imaging and diagnostic techniques with fluorine-18.[20] As an example, a PET image of a 68-year old male patient with a squamous cell carcinoma in the upper lobe of the left lung, treated with [^{18}F]FDG,[19] is shown in Figure 6.1. Recently, "click" chemistry by copper(I)-catalyzed azide-alkyne [3+2] cycloaddition (CuAAC) has been introduced as an orthogonal and efficient means for introduction of F-18 to biomolecules and radiopharmaceuticals.[21] However, there have been few reports of [^{18}F]-labeled biotin derivatives or TTDDSs in PET imaging for biodistribution studies in vivo.[22, 23] And so, we have selected the BR as the tumor-specific biomarker for these tumor-targeting theranostic drug conjugates.

§6.2 Biotin-based Theranostic Conjugates for Tumor Imaging

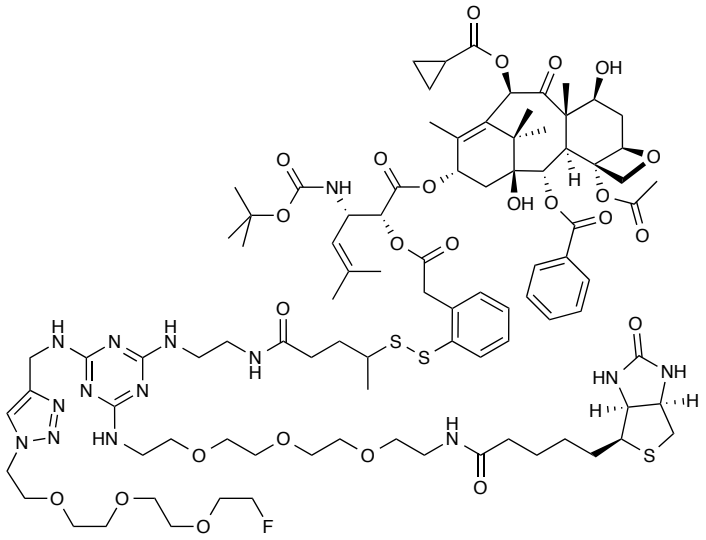

BLT-F **(6-4)**

Figure 6.2. Chemical structure for biotin-based tumor-targeting theranostic conjugate of SB-T-1214, BLT-F (**6-4**).

Novel tumor-targeting theranostic conjugate, BLT-F (**6-4**), which consists of next-generation taxoid (SB-T-1214) as the cytotoxic agent, a mechanism-based self-immolative disulfide linker, biotin as the TTM, polyethylene glycol oligomers to enhance aqueous solubility, 1,3,5-triazine as a splitter module, and a fluorine prosthetic as a potential ^{18}F-PET radiotracer, was designed and synthesized as a companion imaging agent for the biotin-linker-taxoid series. BLT-F (**6-4**) was synthesized from highly versatile biotin-based intermediate **5-8** and external fluorine prosthetic, F-PEG-N_3 (**6-3**) by rapid and efficient copper-catalyzed "click" chemistry. The chemical structure for BLT-F (**6-4**) is illustrated in Figure 6.2.

However, prior to the successful synthesis of BLT-F (**6-4**), the first attempt towards a fluorine-labeled theranostic conjugate involved a benzyl bromide moiety as a site for fluorination.

§6.2.1 First Attempt at Installation of an Imaging Modality

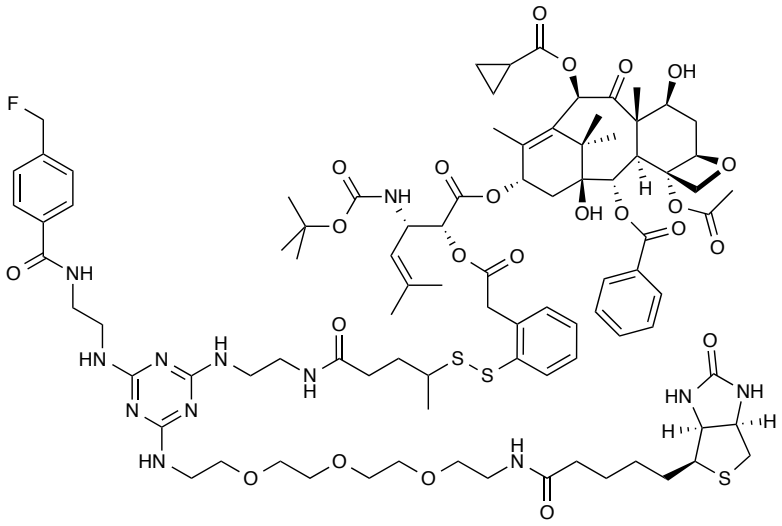

Figure 6.3. Proposed chemical structure for taxoid-based theranostic conjugate bearing a benzyl fluoride.

The original design to introduce a fluorine tether required the preparation of two components: (a) a modified triazine scaffold to accommodate a taxoid (SB-T-1214) and a tumor-targeting module (biotin) (**5-8**), introduced in Chapter 5, and (b) a benzyl bromide moiety as an imaging tether. The chemical structure is shown in Figure 6.3.

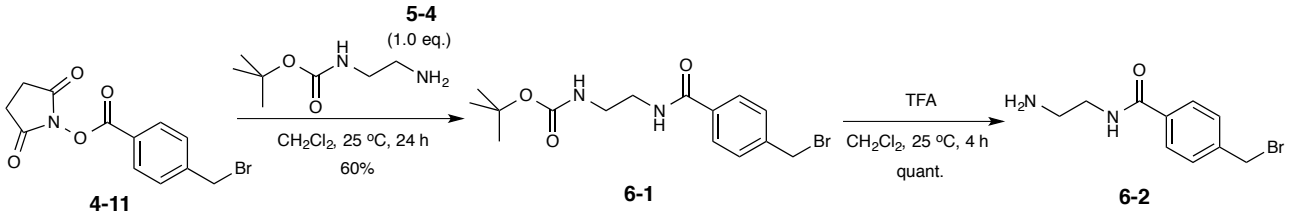

Scheme 6.1. Synthesis of *N*-[4-(bromomethyl)benzoyl]ethylenediamine (**6-2**).

Coupling of 4-(bromomethyl)-*N*-benzoate succinimide ester (**4-11**) with *N*-Boc-ethylenediamine (**5-4**) afforded **6-1** in moderate yield (60%). Removal of the Boc group with TFA gave *N*-[4-(bromomethyl)benzoyl]ethylenediamine **(6-2)** in quantitative yield. The synthesis of **6-2** is illustrated in Scheme 6.1.

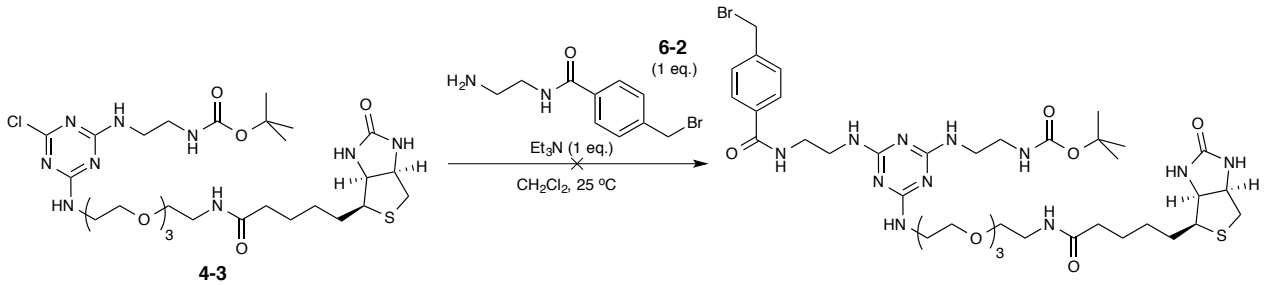

Scheme 6.2. Unsuccessful substitution of benzyl bromide **6-2** to di-substituted triazine intermediate **5-5**.

However, the substitution reaction of di-substituted triazine **5-5** with **6-2** was unsuccessful and afforded an undesired product (Scheme 6.2). Substitution of the triethylamine base at the benzyl position resulted in dehalogenation and generation of an undesired side-product, which was observed by mass spectrometry. The chemical structure of the proposed side-product is shown in Figure 6.5.

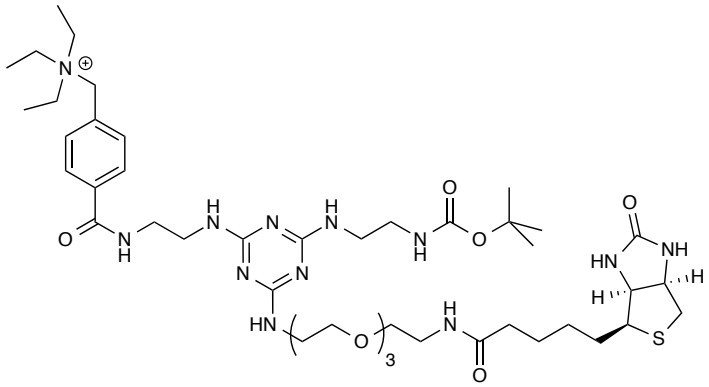

Figure 6.4. Chemical structure of side-product.

Thus, the benzyl bromide moiety did not possess sufficient stability for the subsequent reactions due to its lack of stability under basic conditions. The single-step fluorination approach was abandoned for a two-step synthetic strategy involving fluorination of an external prosthetic, followed by installation of the fluorinated-prosthetic.

§6.2.2 Cold Synthesis of Fluorine-labeled Theranostic Conjugate

The second design towards a fluorine-labeled theranostic conjugate, BLT-F (**6-4**), involved a two-step approach: first, fluorination of a prosthetic tether, followed by installation of the prosthetic to the conjugate via orthogonal "click" chemistry. For the fluorinated prosthetic, a polyethylene glycol oligomer bearing an azido group was selected to enhance the aqueous solubility of the conjugate. The chemical structure of BLT-F (**6-4**) is shown in Figure 6.2.

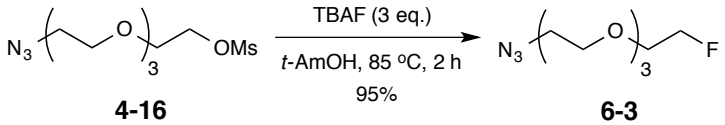

Scheme 6.3. Synthesis of 1-azido-2-[2-[2-[2-fluoroethoxy]ethoxy]ethoxy]ethane (**6-3**).

PEG derivative **4-16** was reacted with tetrabutylammonium fluoride in *tert*-amyl alcohol to give fluorinated prosthetic **6-3** in excellent yield (95%), shown in Scheme 6.3. While protic solvents are often not preferred for halide displacement reactions because of their partial positive charge and hydrogen-bonding capabilities, the use of *tert*-amyl alcohol as a reaction medium for nucleophilic fluorination has resulted in dramatic increases in rate and yield of reaction as well as decrease in side-product formation.[24] Complete conversion of the starting material was observed in under two hours by mass spectrometry. These rapid "cold" fluorination conditions seemed amenable to "hot" fluorination conditions and provided a benchmark for subsequent optimization with fluorine-18.

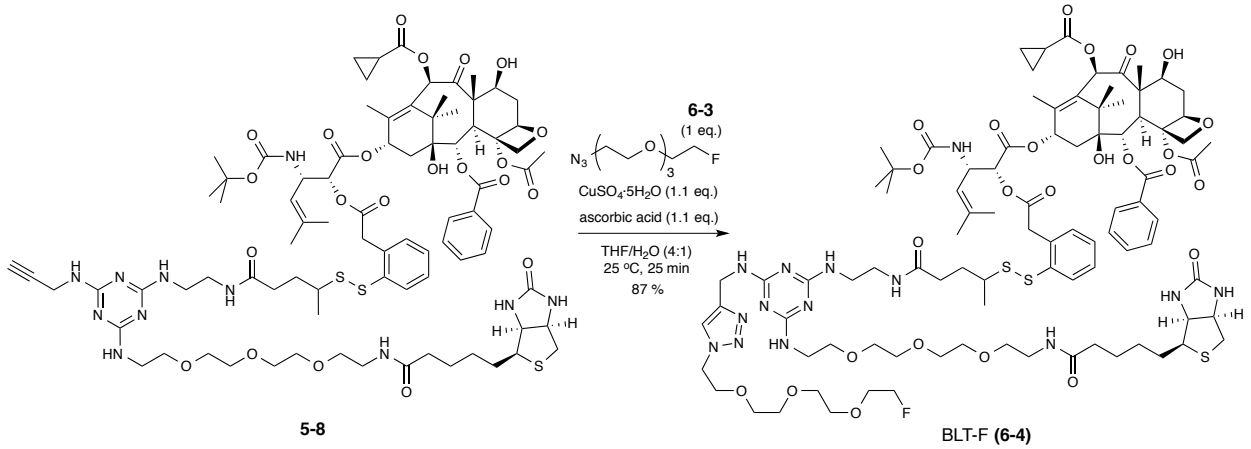

Scheme 6.4. Synthesis of BLT-F (**6-4**) by copper(I)-catalyzed "click" chemistry.

Next, highly versatile biotin-based drug delivery scaffold, **5-8**, consisting of SB-T-1214 connected to a self-immolative disulfide linker, 1,3,5-triazine as a tripod splitter module, biotin as a TTM, and a propargylamino arm, was subjected to a "click" reaction with fluorinated azide **6-3** in the presence of copper(II) sulfate and ascorbic acid to give theranostic conjugate BLT-F (**6-4**) in excellent yield (87%), shown in Scheme 6.4. Reaction progress was monitored by mass spectrometry, and complete conversion was observed in fewer than 25 minutes, shown in Figure 6.5. At 3 min, both starting material precursor **5-8** and BLT-F (**6-4**) can be observed in a 700-1000 *m/z* range, indicated by the presence of doubly charged species for each ($M+2H^+$), *m/z* 864.5 and 974.5, respectively. However, after 25 min, the peak at 864.5 disappeared, suggesting consumption of precursor **5-8**.

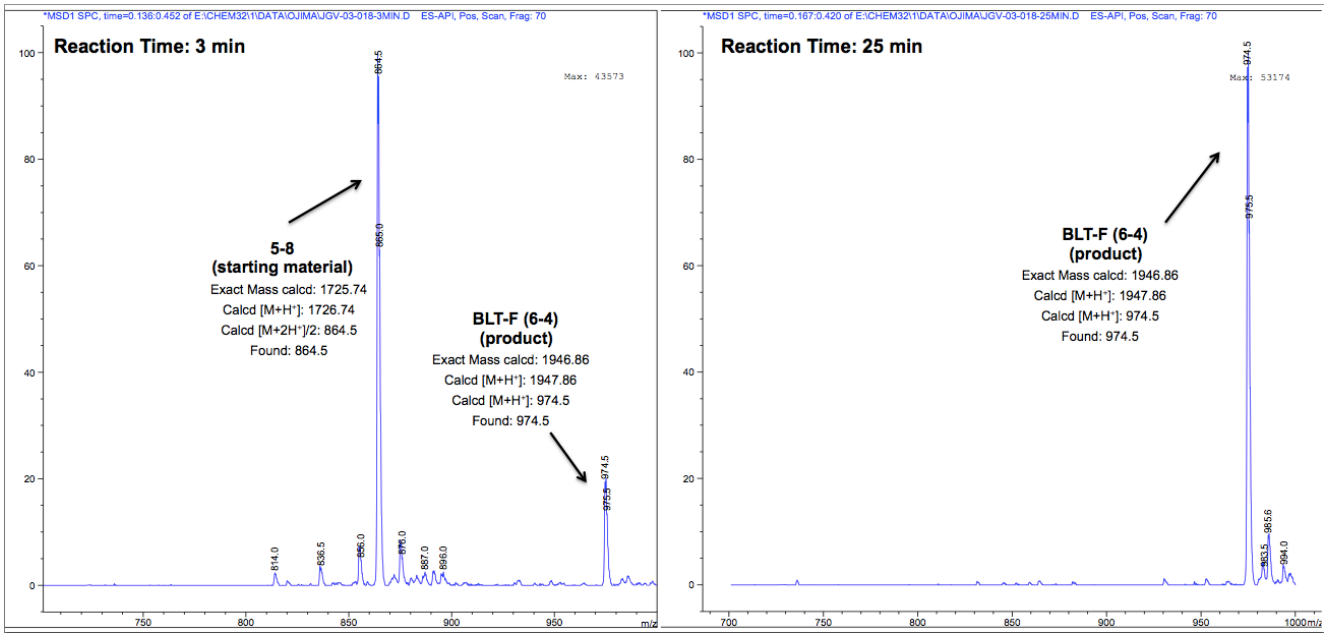

Figure 6.5. Mass spectrometry analysis of rapid "click" reaction to give BLT-F (**6-4**) in under 25 min.

Due to the solubility of ascorbic acid, and the Cu(I) and Cu(II) salts in aqueous media, BLT-F (**6-4**) was isolated by organic extraction and concentration *in vacuo*, followed by trituration with hexanes and ethyl acetate to give a BLT-F (**6-4**), as a white solid in >97% chemical purity by reverse-phase HPLC (Figure 6.6). Both regioisomers of the 1,3-dipolar cycloaddition were treated as a single compound.

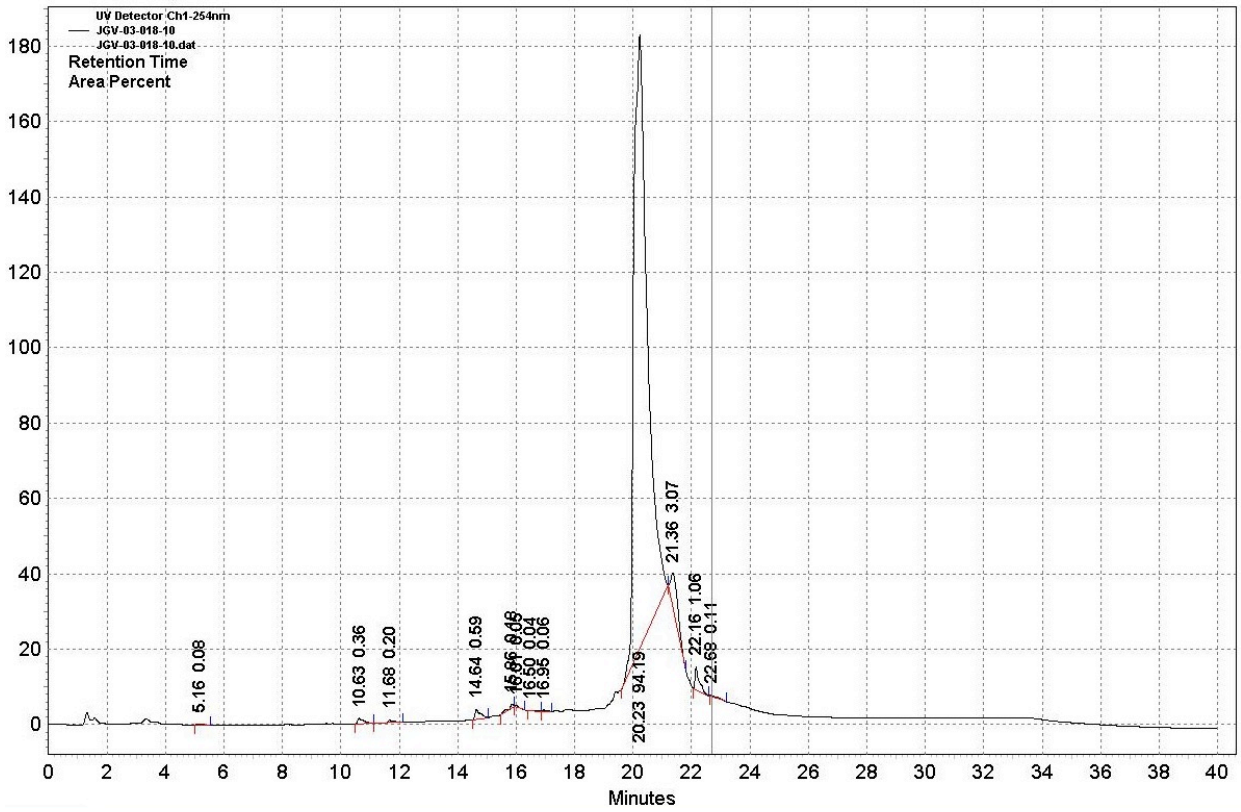

Figure 6.6. Reverse-phase HPLC chromatogram of BLT-F (**6-4**) indicating >97% chemical purity**.**

The optimization of "hot" fluorination conditions and analytical and semi-preparative HPLC method development towards the radiosynthesis of **[^{18}F]6-4** is discussed later in Chapter 7.

§6.2.3 Design of a Tumor-targeted Chemotherapeutic Agent for Fluorescence Imaging

Previously, our laboratory designed, synthesized, and used several fluorescent and fluorogenic probes for the BR by employing fluorescein isothiocyanate (FITC), fluorescein, and coumarin (Figure 4.7).[9] Among these probes, biotin-NHNH-FITC unambiguously verified the efficient process of receptor-mediated endocytosis (RME) by targeting the biotin receptor. Later, a more water-soluble derivative, biotin-PEG-FITC (**4-10**) was designed and synthesized, and numerous human breast cancer cell lines were found to overexpress the biotin receptor as well (Figure 4.11).

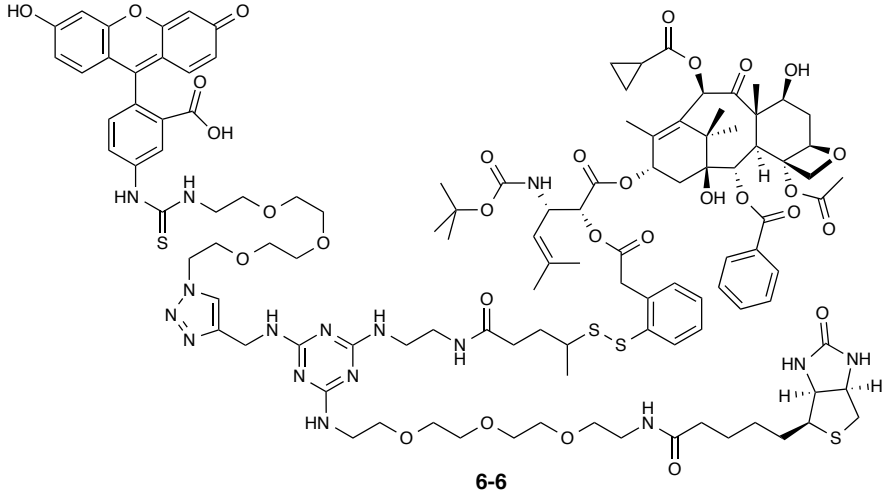

6-6

Figure 6.7. Chemical structure of FITC-labeled biotin conjugate (**6-6**) designed for fluorescence imaging.

Fluorescence-labeled conjugate **6-6** was designed and synthesized from the same TTDDS as double-warhead conjugates DW-1 (**5-9**) and DW-2 (**5-12**), as well as fluorine-labeled theranostic conjugate BLT-F (**6-4**), to validate efficient internalization by RME of this larger molecular weight drug delivery scaffold via the biotin receptor. The chemical structure of biotin-triazine-FITC-(SS-linker)-taxoid (**6-6**) is illustrated in Figure 6.7.

§6.2.4 Synthesis of Fluorescently Labeled Tumor-targeted Drug Delivery Platform

In a similar synthetic route as the fluorine-labeled biotin conjugate **6-4**, FITC-labeled biotin conjugate **6-6** was prepared from FITC-PEG-N_3 (**6-5**) and the biotin-based drug delivery scaffold (**5-8**) by "click" chemistry.

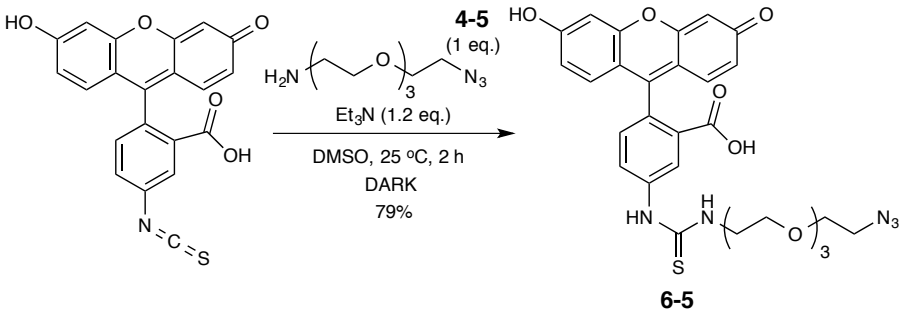

6-5

Scheme 6.5. Synthesis of FITC-PEG-N_3 (**6-5**).

Coupling of fluorescein isothiocyanate to **4-5** in the presence of triethylamine in the dark gave **6-5** in good yield (79%), shown in Scheme 6.5. The product was immediately purified by column chromatography on silica gel and stored under N_2 at -20 °C in the dark.

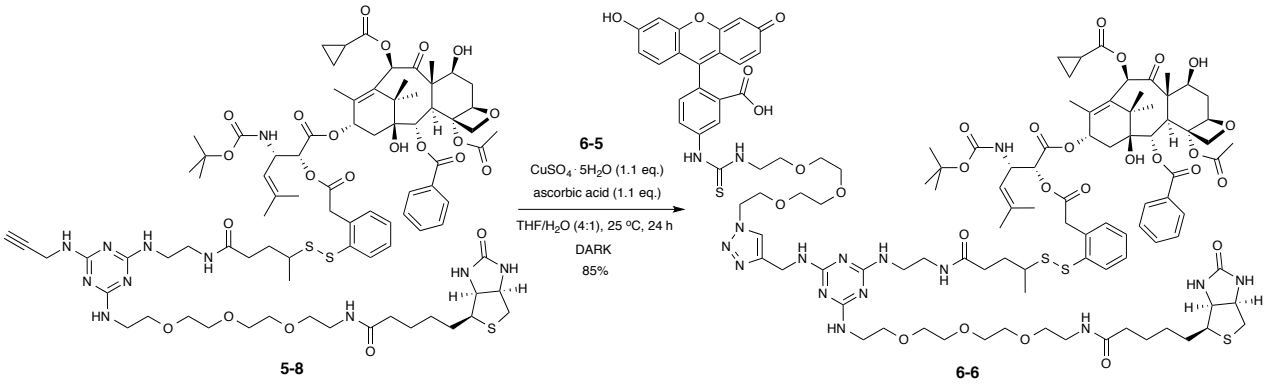

Scheme 6.6. Synthesis of FITC-labeled tumor-targeting theranostic conjugate (**6-6**).

Biotin-based drug delivery scaffold bearing a propargylamino arm, **5-8**, was subjected to a "click" reaction with fluorescence-labeled-PEG-azide, **6-5**, in the presence of copper(II) sulfate and ascorbic acid to give fluorescence-labeled biotin conjugate **6-6** in excellent yield (87%), shown in Scheme 6.6. Reaction progress was monitored by mass spectrometry, and both regioisomers were treated as a single compound. Probe **6-6** was stored under N_2 at -20 °C in the dark.

§6.3 Biological Evaluation of Biotin-based Theranostic Conjugates

Biological evaluation of fluorine-labeled theranostic conjugate **6-4** and fluorescence-labeled biotin conjugate **6-6** was performed by flow cytometry, confocal microscopy, and cytotoxicity assays by MTT protocol. The small-molecule biotin-PEG-FITC probe, **4-10**, was used as a reference for comparison with FITC-labeled biotin conjugate **6-6** to evaluate the size-effect of this TTDDS on internalization by RME via the biotin receptor. The potency and efficacy of theranostic conjugate, BLT-F (**6-4**), was evaluated alongside biotin-(Me-SS-linker)-taxoid **4-3** in a series of cell viability assays.

§6.3.1 Internalization of Theranostic Conjugates by Flow Cytometry and CFM

Fluorescent probe **6-6**, alongside biotin-PEG-FITC (**4-10**) as a small-molecule biotin probe, was administered to L1210FR (BR^{+++}), ID8 (BR^{+++}), MX-1 (BR^{++}), and at 5 μM concentration for 3 h at 37 °C. Internalization by receptor-mediated endocytosis (RME) was visualized by confocal fluorescence microscopy (CFM), and the fluorescence intensity was quantified using flow cytometry. Both **6-6** and **4-10** were efficiently internalized by RME as there was little appreciable difference between internalization of **4-10** and **6-6**, indicating that the larger size of **6-6** is not a limiting factor in RME via the biotin receptor. Probes **6-6** and **4-10** were also administered to L1210 and WI38 (BR^- cell lines), and as anticipated there was no fluorescence intensity observed from either probe following 3 h incubation. However, paclitaxel-7-fluorescein (**2-39**) demonstrated non-specific internalization across all five cell lines (Section 4.3.2). Thus, target-specific and efficient internalization of **6-6** by RME was validated. The confocal fluorescence microscopy images and flow cytometry histograms are shown in Figure 6.8.

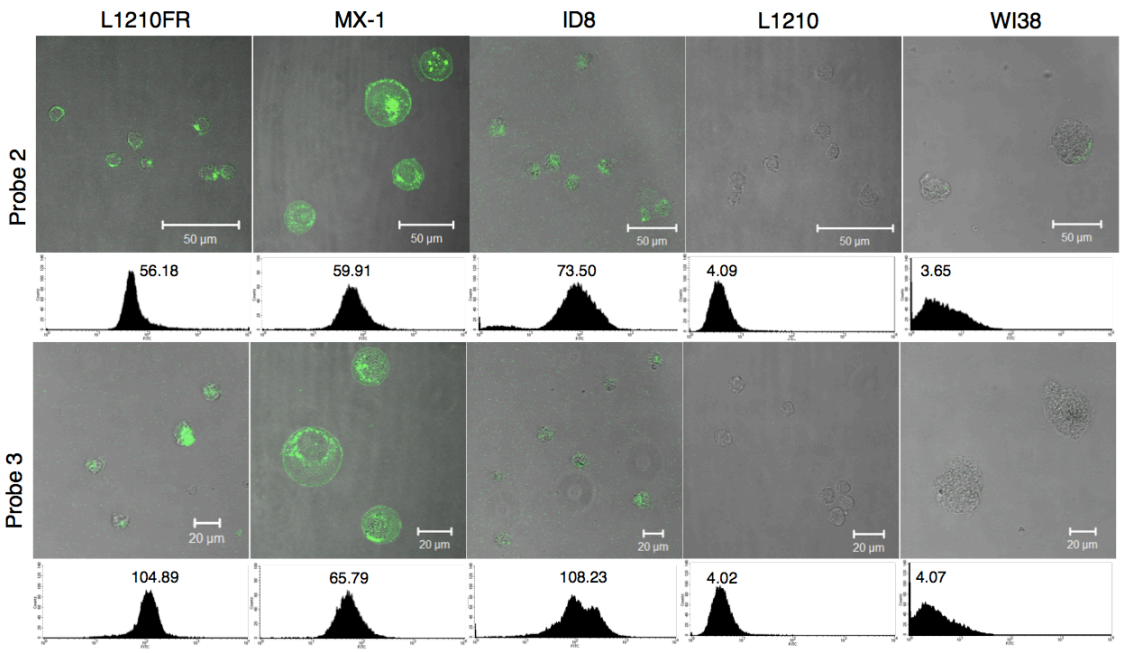

Figure 6.8. CFM images and flow cytometry histograms of 5 μM FITC-labeled TTDDS (**6-6**) (*top row*) and 5 μM biotin-PEG-FITC (**4-10**) (*bottom row*) in L1210FR (BR^{+++}), MX-1 (BR^{++}), ID8 (BR^{+++}), L1210 (BR–), and WI38 (BR–) cell lines at 37 °C for 3 h.

§6.3.2 Time-dependent Internalization Study in L1210FR and MX-1

The time-dependent internalization of fluorescent probe **6-6** in L1210FR and MX-1 was assessed at various time intervals ranging from 15 min to 24 h. Following incubation, the cells were washed thoroughly with phosphate-buffered saline (PBS) to remove the fluorescent media, and cleaved from the cell culture plate with trypsin. The cells were centrifuged twice and washed twice each time with PBS. Then, the cells were subjected to flow cytometry analysis. The results are illustrated in Figure 6.9.

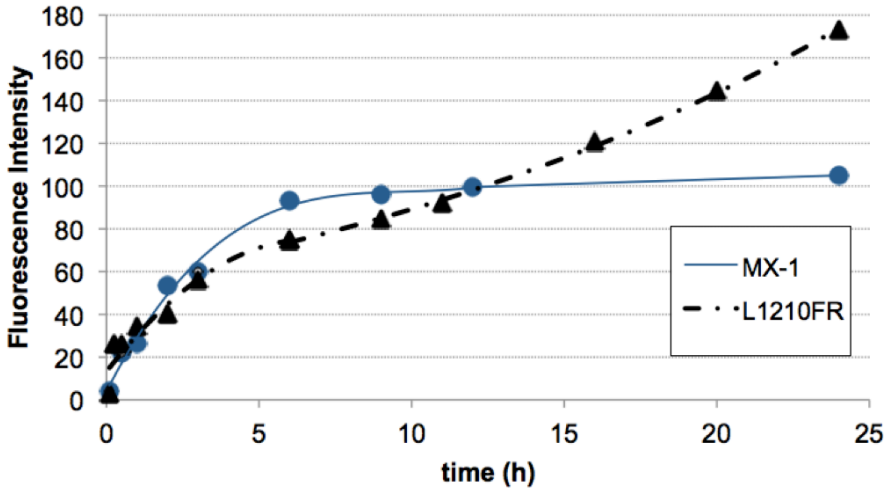

Figure 6.9. Time-dependent internalization of 5 μM **6-6** in L1210FR (BR^{+++}) and MX-1 (BR^{++}) at 37 °C based on flow cytometry histograms.

In both cell lines, the conjugate showed rapid cellular uptake by RME during the first 3 hours of incubation, which was quantified by the significant increase in fluorescence intensity based on flow cytometry histograms. Then, following this initial uptake, the rate of internalization slowed down likely due to saturation of cell-surface biotin receptors with conjugate **6-6** and internalized conjugate-receptor complexes. However, over time, the increase in fluorescence in L1210FR became significantly higher than that of MX-1, which can be attributed to a difference in the recycling rates of cell-surface vitamin receptors.[25]

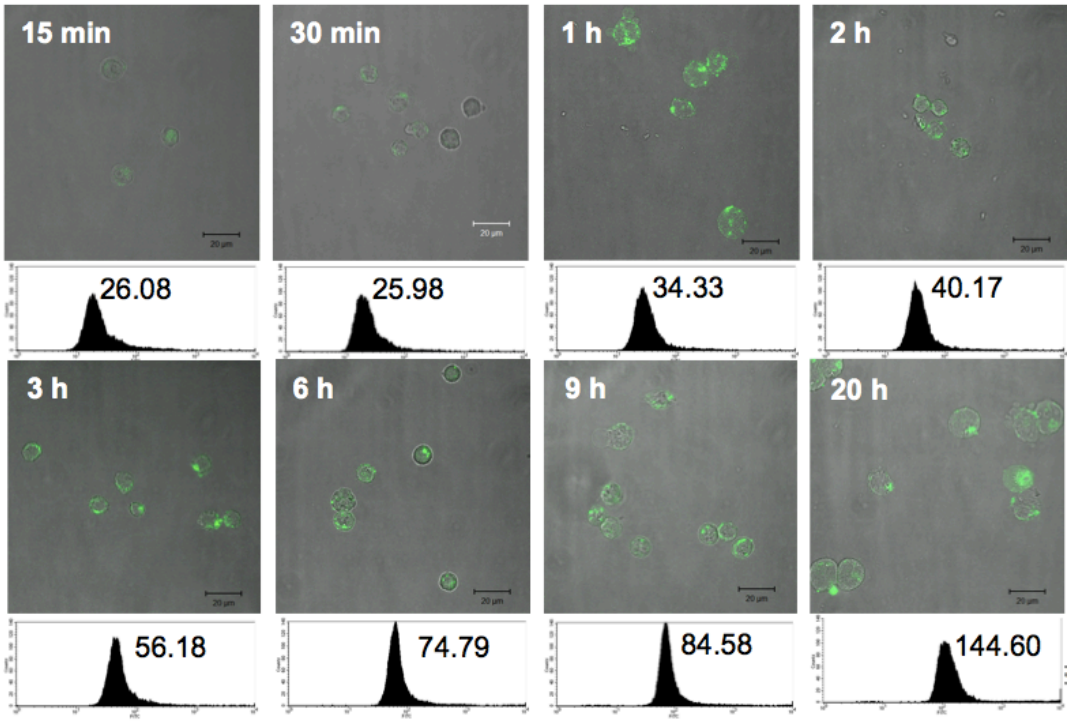

Figure 6.10. CFM images and flow cytometry histograms for time-dependent internalization of 5 μM **6-6** by RME in L1210FR (BR^{+++}) cell line at 37 °C for various time intervals.

The confocal fluorescence microscopy images and flow cytometry histograms for incubation of **6-6** in L1210FR and MX-1 are shown below in Figure 6.10 and Figure 6.11, respectively.

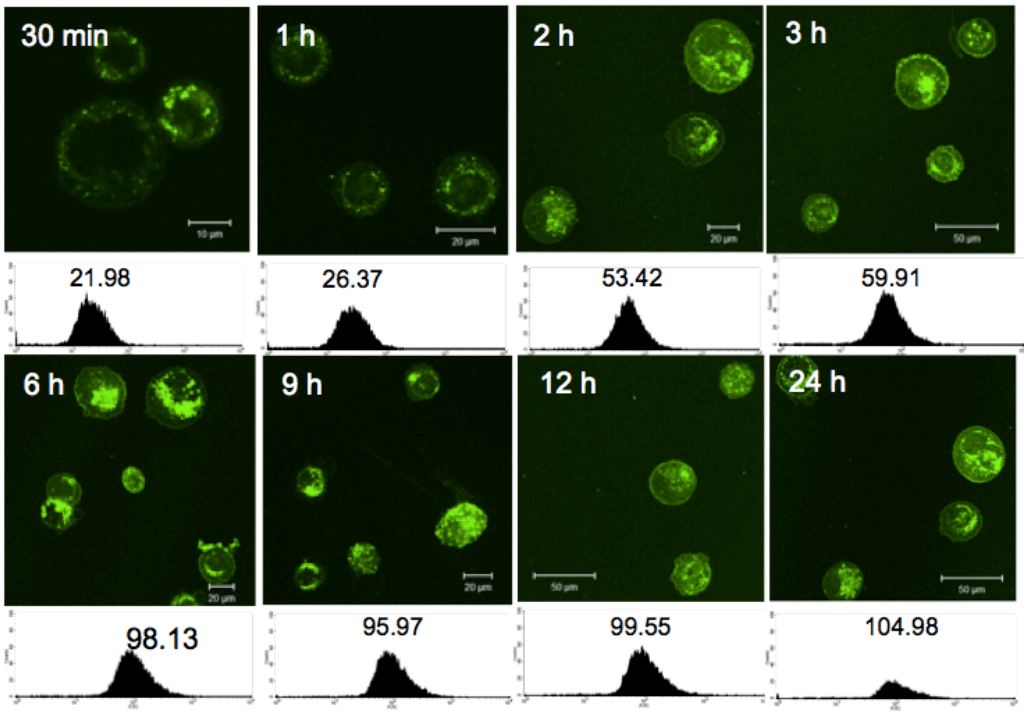

Figure 6.11. CFM images and flow cytometry histograms for time-dependent internalization of 5 μM **6-6** by RME in MX-1 (BR^{++}) cell line at 37 °C for various time intervals.

§6.3.3 Biological Evaluation of Theranostic Conjugates for Cytotoxicity

Cytotoxicities of theranostic conjugate BLT-F (**6-4**) and biotin-(SS-linker)-taxoid (**4-3**) were evaluated in three experiments against three BR+ cancer cell lines, L1210FR, MX-1, and ID8, and two BR- cell lines, L1210 and WI38, using the standard MTT assay. Results are summarized in Table 6.1 and Table 6.2. Paclitaxel and SB-T-1214 were also examined for comparison.

In the first experiment, L1210FR, MX-1, and ID8 (BR+) cancer cell lines were incubated with BLT-F (**6-4**) and BLT (**4-3**) for 48 h, and the corresponding IC_{50} values were determined. As Table 6.1 shows, the cytotoxicity of BLT-F (**6-4**) based on its IC_{50} values was determined to be in a range of 6–21 nM (Entry 3), while that against normal cell line WI38 (IC_{50} 709 nM) was two orders of magnitude weaker in potency. The results indicate that BLT-F (**6-4**) was selectively internalized into BR+ cancer cells via RME with partial release of the taxoid within the cancer cells. Biotin-linker-taxoid (**4-3**) showed similar results as that of BLT-F (**6-4**), in a range of 4–15 nM (Entry 4) with several orders of magnitude greater potency against BR+ cell lines than BR- cell lines. As expected, both SB-T-1214 and the parent taxoid showed non-specific activity against BR+ and BR- cell lines in the range of 0.1–7.0 nM, and 7–77 nM, respectively.

Table 6.1. Cytotoxicities (IC_{50}, nM) of paclitaxel, SB-T-1214, BLT-F (6-4), and BLT (4-3) Against BR+ and BR– Cell Lines at 37 °C for 48 h.

Entry	Compound	MX-1[a]	ID8[b]	L1210FR[c]	L1210[d]	WI38[e]
1[f]	paclitaxel	7.23 ± 0.68	14.36 ± 1.81	38.7 ± 17.7	77.1 ± 12.8	61.4 ± 12.7
2[f]	SB-T-1214	4.13 ± 2.59	0.17 ± 0.14	4.18 ± 1.8	7.05 ± 1.38	5.23 ± 0.27
3[f]	BLT-F (**6-4**)	21.2 ± 4.6	6.62 ± 0.86	14.7 ± 4.0	593 ± 123	709 ± 55
4[f]	BLT (**4-3**)	15.4 ± 4.2	4.32 ± 1.58	13.4 ± 6.8	481 ± 34	670 ± 89

[a]Human breast carcinoma cell line (BR+); [b]Murine ovarian carcinoma cell line (BR+); [c]Murine lymphocytic leukemia cell line (BR+); [d]Murine lymphocytic leukemia cell line (BR-); [e]Human lung fibroblast cell line (BR-);[f]Cells were incubated with a drug or conjugate at 37 °C for 48 h.

Table 6.2. Cytotoxicities (IC_{50}, nM) of paclitaxel, SB-T-1214, BLT-F (6-4), and BLT (4-3) with Supplemental GSH-OEt (6 equiv. to conjugate) After Internalization.

Entry	Compound	MX-1[a]			L1210FR[c]			WI38[e]		
		Exp 1[b]	Exp 2[d]	Exp 3[f]	Exp 1[b]	Exp 2[d]	Exp 3[f]	Exp 1[b]	Exp 2[d]	Exp 3[f]
1	paclitaxel	4.07 ± 0.80			35.6 ± 8.2			131 ± 19		
2	SB-T-1214	2.66 ± 0.16			2.32 ± 1.41			4.89 ± 2.24		
3	BLT-F (**6-4**)	6.27 ± 2.06	4.79 ± 0.12	2.56 ± 0.15	10.2 ± 3.0	6.60 ± 3.96	2.79 ± 1.43	682 ± 110	615 ± 97	12.9 ± 4.3
4	BLT (**4-3**)	4.66 ± 0.87	3.85 ± 0.14	2.40 ± 0.18	12.3 ± 2.8	5.15 ± 2.85	2.92 ± 2.34	645 ± 97	590 ± 164	11.0 ± 3.1

[a,c,e]See captions for cell lines in Table 6.1; [b]Cells were incubated with a drug or conjugate at 37 °C in a 5% CO_2 atmosphere for 72 h; [d]Cells were initially incubated with **6-4** or **4-3** at 37 °C in a 5% CO_2 atmosphere for 24 h, followed by washing of the drug media with PBS, then addition of GSH-OEt (6 equiv. to conjugate) for drug release and additional incubation for 48 h;[f]Cells were initially incubated with **6-6** of **4-3** at 37 °C in a 5% CO_2 atmosphere for 24 h, followed by addition of GSH-OEt (6 equiv. to conjugate) for drug release and additional incubation for 48 h. Total drug or conjugate incubation was 72 h for all experiments.

In the second experiment, glutathione ethyl ester (GSH-OEt; 6 mole equivalents to conjugate) was added to the resuspended cancer cells after the cells were incubated with BLT-F (**6-4**) or BLT (**4-3**) for 24 h, followed by thorough washing and removal of the old medium with PBS and an additional incubation period of 48 h, i.e., 72 h total incubation (Table 6.2). It should be noted that in this experiment the resuspended cancer cells only included conjugate internalized in the first 24 h period. As indicated in Table 6.2, washing of the cells and addition of GSH-OEt did not make any appreciable difference in the cytotoxicity of these conjugates against WI38 normal fibroblast cells, based on the comparison of the results in Table 2 with the 72 h incubation without the addition of GSH-OEt. BLT-F (**6-4**) demonstrated IC_{50} values of 6.6–11.6 nM in BR+ cell lines, L1210FR and MX-1, but 615 nM against WI38. Thus, this marked difference in cytotoxicity between cancer cells and normal cells in the presence of GSH is unambiguously attributed to the highly efficient target-specificity of conjugate **6-4** to BR+ cancer cell lines. Similar to the first experiment, conjugate BLT (**4-3**) showed comparable cytotoxicity results as that of BLT-F (**6-4**).

In the third experiment, glutathione ethyl ester was added directly to the cancer cells following 24 h incubation with BLT-F (**6-4**) or BLT (**4-3**), and incubated for a subsequent 48 h period, i.e., 72 h total incubation (Table 6.2). It should be noted that in this experiment the resuspended cancer cells included conjugate internalized in the first 24 h period as well as drug released outside the cell in the latter 48 h period. As indicated in Table 6.2, direct addition of GSH-OEt demonstrated an additional two-fold increase in potency for BLT-F (**6-4**) against BR+ cancer cell lines compared with the results from the second experiment, and a very significant increase in potency against normal cell line WI38 (IC_{50} 12.9 nM). This result indicates that not all of the conjugate was internalized by RME, and upon addition of GSH-OEt, the released taxoid underwent non-specific internalization into all cell lines. Again, biotin-linker-taxoid (**4-3**) showed analogous results.

§6.4.0 Summary

Two novel tumor-targeting theranostic conjugates, which consist of second-generation taxoid (SB-T-1214), self-immolative disulfide linkers for drug release, biotin as the TTM, 1,3,5-triazine scaffold as the splitter module, and either a fluorine-labeled prosthetic as a potential PET radiotracer (BLT-F, **6-4**) or a fluorescence tether for in vitro internalization studies (**6-6**), were designed and synthesized. “Cold material” BLT-F (**6-4**) was prepared in two steps from highly versatile tumor-targeting drug delivery scaffold bearing a terminal acetylene for orthogonal “click” chemistry. First, fluorination of a polyethylene glycol oligomer bearing a mesylate leaving group with tetrabutylammonium fluoride gave fluorine-labeled prosthetic for “click.” Then, the prosthetic was installed to the highly versatile intermediate by copper(I)-catalyzed azide-alkyne cycloaddition in under 25 min, a rapid and efficient synthesis, with complete conversion according to mass spectrometry.

The potency of BLT-F (**6-6**) was evaluated against MX-1, ID8, L1210FR (BR+: biotin receptor overexpressed) and L1210 and WI38 (BR-: normal) cell lines in the absence and presence of glutathione (GSH), an endogenous thiol that triggers intracellular drug release inside tumor cells. With supplemental GSH, BLT-F (**6-4**) exhibited IC_{50} values of 6.6–11.6 nM against all BR+ cancer cell lines, and 615 nM against WI38, a two-orders of magnitude higher selectivity to cancer cells. Internalization of **6-6** by receptor-mediated endocytosis (RME) via the biotin receptor was confirmed in L1210FR, MX-1 and ID8 by means of confocal fluorescence

microscopy (CFM) and flow cytometry analyses. For comparison, small-molecule biotin probe, biotin-PEG-FITC (**4-10**), was evaluated as well, and no appreciable difference in fluorescence intensity between **6-6** and **4-10** was observed, indicating that the larger size of **6-6** is not a major factor in its internalization. Also, time-dependent internalization studies on **6-6** in L1210FR and MX-1 demonstrated, first, rapid cellular uptake by RME, followed by receptor saturation, and then a gradual increase in conjugate internalization as receptors began to recycle. Thus, with target-specificity and high potency, BLT-F (**6-4**) may serve as a companion imaging agent as a theranostic conjugate for ^{18}F-PET imaging. The radiosynthesis of [^{18}F]BLT-F is discussed in Chapter 7.

§6.5.0 Experimental

§6.5.1 Caution

Taxoids have been identified as potent cytotoxic agents. Thus, these drugs and all structurally related compounds and derivatives must be considered mutagens and potential reproductive hazards. Appropriate precautions, such as the use of gloves, goggles, labware, and fume hood, must be taken while handling these compounds at all times.

§6.5.2 General Information

^{1}H, ^{13}C and ^{19}F NMR spectra were measured on a Varian 300 or 500 MHz spectrometer or a Bruker 500 MHz NMR spectrometer. Hexafluorobenzene was used as an external reference for ^{19}F NMR analysis. Melting points were measured on a Thomas- Hoover capillary melting point apparatus and are uncorrected. TLC was performed on Sorbent Technologies aluminum-backed Silica G TLC plates (Sorbent Technologies, 200 μm, 20 x 20 cm), and column chromatography was carried out on silica gel 60 (Merck, 230-400 mesh ASTM). Purity was determined with a Shimadzu L-2010A HPLC HT series HPLC assembly, using a Kinetex PFP column (4.6 mm x 100 mm, 2.6 μm) with acetonitrile-water or methanol-water solvent systems. One analytical condition was used and noted as a part of the characterization data for literature unknown compounds, i.e., HPLC (1): flow rate 0.6 mL/min, 30% methanol (isocratic). High-resolution mass spectrometry analysis was carried out on an Agilent LC-UV-TOF mass spectrometer at the Institute of Chemical Biology and Drug Discovery, Stony Brook, NY or at the Mass Spectrometry Laboratory, University of Illinois at Urbana-Champaign, Urbana, IL.

§6.5.3 Materials

The chemicals were purchased from Sigma-Aldrich, Fisher Scientific, and VWR International, and used as received or purified before use by standard methods. Tetrahydrofuran was freshly distilled from sodium and benzophenone. Dichloromethane was also distilled immediately prior to use under nitrogen from calcium hydride. 4-*N,N*-dimethylaminocinnamaldehyde solution was used as a TLC stain for biotin derivatives, and H_2SO_4 (conc.) in ethanol was used for taxoid derivatives.

§6.5.4 Experimental Procedure

***N*-[4-(Bromomethyl)benzoyl]-*N'*-(*tert*-butoxycarbonyl)-ethylenediamine [6-1]:**[26]
To a solution of **4-11** (0.450 g, 1.44 mmol) in CH_2Cl_2 (10 mL) was added **5-4** (0.230 g, 1.44 mmol) in CH_2Cl_2 (5 mL), and the mixture was allowed to react for 24 h at room temperature with stirring. The reaction mixture was concentrated *in vacuo* to afford an off-white solid. Purification of the crude product by column chromatography on silica gel with hexanes/ethyl acetate (1:1) as eluent gave **6-1** (0.307 g, 60%) as a white solid; ^{1}H NMR (300 MHz, DMSO) δ 1.41 (s, 9H), 3.13 (m, 2H), 3.31 (m, 2H), 4.78 (s, 2H), 6.96 (m, 1H), 7.56 (d, *J* = 8.2 Hz, 2H), 7.85 (d, *J* = 8.2 Hz, 2H), 8.52 (m, 1H). All data are in agreement with literature values.[26]

***N*-[4-(Bromomethyl)benzoyl]ethylenediamine [6-2]:**
To a solution of **6-1** (0.200 g, 0.586 mmol) in CH_2Cl_2 (5.6 mL) was added TFA (0.6 mL, 7.89 mmol), and the mixture was allowed to react for 4 h at room temperature with stirring. The reaction was quenched with $NaHCO_3$ (s), and the suspension was filtered to remove the solid. The filtrate was washed with CH_2Cl_2 (3 x 10 mL), and the combined organic layers were concentrated *in vacuo* to afford **6-2** (0.150 g, quant.), as a yellow oil. ^{1}H NMR (300 MHz, DMSO) δ 3.03 (m, 2H), 3.55 (m, 2H), 4.79 (s, 2H), 7.58 (d, *J* = 8.3 Hz, 2H), 7.89 (d, *J* = 8.3 Hz, 2H).

1-Azido-2-[2-[2-[2-fluoroethoxy]ethoxy]ethoxy]ethane [6-3]:[27]
To a solution of **4-16** (0.170 g, 0.572 mmol) in *tert*-amyl alcohol (6 mL) was added 1 M TBAF in THF (1.7 mL, 1.72 mmol), and the mixture was allowed to react for 2 h at 85 °C. The reaction was cooled to 25 °C and diluted with H_2O (10 mL), and the mixture was extracted with ethyl acetate (3 x 20 mL). The combined organic layers were washed with brine (3 x 10 mL), dried over $MgSO_4$, and concentrated *in vacuo* to afford a yellow liquid. Purification of the crude product by column chromatography on silica gel with 2% CH_3OH in CH_2Cl_2 as eluent gave **6-3** (0.120 g, 95%) as a colorless liquid; ^{1}H NMR (300 MHz, $CDCl_3$) δ 3.39 (t, *J* = 5.1 Hz, 2H), 3.67 (m, 10H), 3.75 (m, 2H), 4.57 (m, 2H); ^{13}C NMR (125 MHz, $CDCl_3$) δ 50.67, 70.01, 70.30, 70.45, 70.67, 70.79, 82.46, 83.81; ^{19}F NMR (282 MHz, $CDCl_3$) δ -45.56. All data are in agreement with literature values.[27]

Fluorine-labeled biotin conjugate designed for [^{18}F]-PET imaging (Cold Synthesis) [6-4]:
To a solution of **5-8** (27.8 mg, 17.4 mmol), **6-3** (4.2 mg, 19.1 μmol), and ascorbic acid (3.4 mg, 19.1 μmol) in THF (0.5 mL) was added $CuSO_4 \cdot 5H_2O$ (5 mg, 19.1 μmol) in H_2O (0.12 mL), and the mixture was allowed to react for 25 min at room temperature with stirring. Reaction progress was monitored by mass spectrometry. The reaction was diluted with H_2O (10 mL), and the mixture was extracted with CH_2Cl_2 (3 x 10 mL). The combined organic layers were dried over $MgSO_4$ and concentrated *in vacuo* to afford a milky white solid, which was triturated with hexanes (20 mL x 4) and ethyl acetate (20 mL x 4) to afford **6-4** (27 mg, 87%) as a white solid; regioisomers were treated as a single compound; mp 100-101 °C; ^{1}H NMR (500 MHz, CD_3OD) δ 0.90-1.02 (m, 7H), 1.08 (m, 1H), 1.16 (s, 3H), 1.17 (s, 3H), 1.24 (d, *J* = 6.8 Hz, 3H), 1.28 (m, 5H), 1.39 (m, 1H), 1.40 (s, 9H), 1.61 (m, 4H), 1.64 (s, 3H), 1.73 (s, 3H), 1.75 (s, 3H), 1.78 (m, 2H), 1.86 (m, 1H), 1.91 (s, 3H), 2.18 (t, *J* = 7.5 Hz, 2H), 2.22 (m, 3H), 2.38 (s, 3H), 2.54 (m, 2H), 2.68 (d, *J* = 12.8 Hz, 1H), 2.84 (m, 1H), 2.90 (dd, *J* = 5.0, 12.8 Hz, 1H), 3.16 (m, 1H), 3.34 (m, 3H), 3.41 (bs, 2H), 3.48 (m, 2H), 3.52 (t, *J* = 5.4 Hz, 2H), 3.61 (m, 4H), 3.65 (m, 20H), 3.71

(m, 2H), 3.85 (m, 3H), 4.00 (d, J = 16.8 Hz, 1H), 4.09 (d, J = 16.8 Hz, 1H), 4.20 (d, J = 8.4 Hz, 1H), 4.24 (d, J = 8.4 Hz, 1H), 4.27 (dd, J = 4.4 Hz, 8.0 Hz, 1H), 4.31 (m, 1H), 4.46 (m, 1H), 4.49 (m, 2H), 4.52 (m, 2H), 4.92 (bs, 2H), 5.00 (d, J = 8.4 Hz, 1H), 5.27 (bs, 1H), 5.67 (d, J = 7.2 Hz, 1H), 6.31 (bt, J = 8.5 Hz, 1H), 6.45 (s, 1H), 7.24 (m, 1H), 7.30 (m, 2H), 7.50 (t, J = 7.7 Hz, 2H), 7.63 (t, J = 7.5 Hz, 1H), 7.77 (m, 1H), 7.91 (bs, 1H), 8.12 (d, J = 7.5 Hz, 2H); ^{13}C NMR (125 MHz, CD_3OD) δ 7.79, 7.83, 9.05, 12.41, 13.04, 13.68, 14.04, 17.27, 19.59, 19.65, 20.97, 21.89, 22.30, 24.71, 25.47, 25.60, 27.41, 28.09, 28.37, 31.29, 31.35, 32.99, 33.08, 33.35, 36.15, 38.10, 38.99, 39.48, 39.77, 40.02, 43.21, 45.96, 46.06, 46.68, 50.09, 50.38, 55.69, 57.90, 60.20, 61.96, 65.52, 68.99, 69.19, 69.65, 69.74, 69.84, 69.90, 70.05, 70.13, 70.20, 70.23, 70.27, 70.93, 71.64, 74.94, 75.18, 75.33, 76.07, 79.31, 80.95, 82.10, 83.43, 84, 49, 119.83, 123.74, 127.58, 128.06, 128.30, 129.76, 130.02, 131.07, 132.79, 133.19, 133.45, 137.32, 141.18, 156.11, 164.68, 166.24, 168.94, 170.08, 170.97, 173.71, 174.01, 174.74, 203.78; ^{19}F NMR (282 MHz, CD_3OD) δ -46.92 (m, 1F); HRMS (TOF) for $C_{92}H_{132}N_{14}O_{25}FS_3^+$ calcd: 1947.8629. Found: 1947.8647 (Δ = 0.9 ppm). HPLC (1): t = 20.2 min, purity > 98%.

FITC-PEG-N_3 [6-5]:
To a solution of fluorescein isothiocyanate (0.200 g, 0.514 mmol) and **4-5** (0.131 g, 0.616 mmol) in DMSO (1 mL) was added Et_3N (75 μL, 0.514 mmol), and the mixture was allowed to react for 2 h at room temperature in the dark with stirring. The reaction mixture was directly concentrated *in vacuo* to afford a red oil. Purification of the crude product by column chromatography on silica gel with 7% CH_3OH in CH_2Cl_2 as eluent gave **6-5** (0.241 g, 79%) as an orange solid; ^{1}H NMR (500 MHz, DMSO-d_6) δ 3.42 (t, J = 5.0 Hz, 2H), 3.62 (m, 14H), 3.73 (bs, 2H), 6.57 (d, J = 2.3, 8.7 Hz, 2H), 6.62 (d, J = 8.7 Hz, 2H), 6.71 (d, J = 2.3 Hz, 2H), 7.22 (d, J = 8.3 Hz, 1H), 7.78 (d, J = 7.8 Hz, 1H), 8.13 (bs, 1H), 8.31 (s, 1H); ^{13}C NMR (125 MHz, DMSO-d_6) δ 44.19, 50.46, 68.90, 69.72, 70.15, 70.28, 79.65, 102.70, 110.18, 113.04, 116.79, 124.54, 127.30, 129.50, 129.86, 141.79, 147.61, 151.34, 159.94, 168.98, 180.99; HRMS (TOF) for $C_{29}H_{30}N_5O_8S^+$ calcd: 608.1810. Found: 608.1822 (Δ = 2.0 ppm).

FITC-labeled biotin conjugate for fluorescence imaging [6-6]:
To a solution of **5-8** (29.0 mg, 0.0167 mmol), **6-5** (10.2 mg, 0.0167 mmol), and ascorbic acid (3.3 mg, 0.0185 mmol) in THF (0.5 mL) was added $CuSO_4{\cdot}5H_2O$ (4.6 mg, 0.0185 mmol) in H_2O (0.1 mL), and the mixture was allowed to react for 24 h at room temperature in the dark with stirring. The reaction was diluted with H_2O (10 mL), and the mixture was extracted with CH_2Cl_2 (3 x 10 mL). The combined organic layers were dried over $MgSO_4$ and concentrated *in vacuo* to afford a yellow solid, which was re-dissolved in CH_2Cl_2 and CH_3OH (9:1) and lyophilized afford **6-6** (0.0331 g, 85%) as a yellow solid; ^{1}H NMR (500 MHz, DMSO-d_6) δ 0.92 (m, 2H), 1.00 (m, 2H), 1.10 (s, 3H), 1.22 (d, J = 6.8 Hz, 3H), 1.27 (s, 3H), 1.32 (m, 2H), 1.42 (s, 9H), 1.52 (m, 4H), 1.55 (s, 3H), 1.63 (s, 3H), 1.69 (m, 2H), 1.74 (s, 3H), 1.84 (s, 3H), 1.86 (m, 1H), 2.09 (t, J = 7.5 Hz, 2H), 2.20 (t, J = 7.0 Hz, 1H), 2.25 (m, 1H), 2.36 (s, 3H), 2.60 (d, J = 12.5, 1H), 2.86 (dd, J = 5.0, 12.5, 1H), 2.95 (m, 1H), 3.12 (m, 1H), 3.22 (m, 4H), 3.29 (m, 2H), 3.41 (t, J = 5.5 Hz, 4H), 3.53 (m, 18H), 3.62 (m, 2H), 3.71 (d, J = 7.2 Hz, 2H), 3.81 (m, 2H), 4.00 (s, 2H), 4.09 (m, 2H), 4.15 (m, 2H), 4.33 (m, 1H), 4.50 (m, 2H), 4.75 (m, 1H), 4.85 (d, J = 7.9 Hz, 1H), 4.96 (m, 3H), 5.20 (m, 1H), 5.52 (d, J = 7.2 Hz, 1H), 6.03 (m, 1H), 6.35 (s, 1H), 6.39 (s, 1H), 6.45 (s, 1H), 6.60 (dd, J = 2.3, 8.7 Hz, 2H), 6.64 (d, J = 8.7 Hz, 2H), 6.71 (d, J = 2.3 Hz, 2H), 7.25 (m, 2H) 7.30 (t, J = 7.7 Hz, 1H), 7.34 (m, 1H), 7.40 (t, J = 7.7 Hz, 1H), 7.57 (t, J = 7.7 Hz, 2H), 7.71 (t, J = 7.4 Hz, 1H), 7.76 (bs, 1H), 7.78 (d, J = 8.0 Hz, 1H), 7.85 (m, 1H), 7.90 (bs, 1H), 8.04 (d, J

= 7.6 Hz, 2H), 8.22 (bs, 1H); ^{13}C NMR (125 MHz, DMSO-d_6) δ 8.75, 8.83, 10.24, 13.15, 14.20, 14.23, 18.36, 19.64, 20.45, 20.52, 21.90, 22.99, 25.74, 25.95, 26.81, 28.50, 28.65, 31.57, 32.42, 32.98, 33.07, 35.56, 37.03, 38.31, 38.91, 40.91, 43.49, 46.04, 46.15, 46.69, 49.75, 55.39, 55.91, 57.96, 59.66, 61.50, 69.63, 70.02, 70.11, 70.19, 70.22, 70.89, 73.74, 75.00, 75.03, 75.06, 75.10, 75.12, 75.15, 75.27, 75.78, 77.22, 78.61, 80.88, 83.48, 84.07, 88.37, 102.71, 110.13, 110.45, 113.04, 120.71, 127.89, 128.83, 129.11, 129.50, 129.99, 130.40, 131.63, 133.32, 133.81, 133.87, 133.88, 136.45, 137.33, 137.35, 139.99, 152.37, 155.41, 159.94, 163.18, 165.50, 169.25, 170.07, 170.65, 171.92, 172.60, 172.64, 203.02; HRMS (TOF) calcd for $C_{113}H_{145}N_{16}O_{30}S_4^+$ calcd: 2333.9190. Found: 2333.9130 (Δ = -2.6 ppm).

Cell Culture.

All cell lines were obtained from ATCC unless otherwise noted. Cells were cultured in RPMI-1640 cell culture medium (Gibco) or DMEM culture medium (Gibco), both supplemented with 5% (v/v) heat-inactivated fetal bovine serum (FBS), 5% (v/v) NuSerum, and 1% (v/v) penicillin and streptomycin (PenStrep) at 37 °C in a humidified atmosphere with 5% CO_2. Murine leukemia cell lines L1210 and L1210FR (a gift from Dr. Gregory Russell-Jones, Access Pharmaceuticals Pty Ltd., Australia) were grown as a suspension in supplemented RPMI-1640. Human breast carcinoma, MX-1, and murine ovarian carcinoma, ID8 (obtained from Dr. Katherine Roby, University of Kansas Medical Center), cell lines were cultured as monolayers on 100 mm tissue culture dishes in a supplemented RPMI-1640 cell culture medium, and normal human lung fibroblast cell line WI-38 as a monolayer in a supplemented DMEM cell culture medium. Cells were harvested, collected by centrifugation at 850 rpm for 5 min, and resuspended in fresh culture medium. Cell cultures were routinely divided by treatment with trypsin (TrypLE, Gibco) as needed every 2-4 days and collected by centrifugation at 850 rpm for 5 min, and resuspended in fresh cell culture medium, containing varying cell densities for subsequent biological experiments and analysis.

Incubation of Cells with FITC-labeled biotin conjugate (6-6).

Cell suspensions (3 mL) of MX-1, ID8, and WI38 at 5 x 10^5 cells/mL were added to each individual well of 6-well plates, and subsequently incubated overnight in the appropriate cell culture media. The cell culture media was replaced with 5 μM solutions of **6-6** in cell culture media (3 mL). Then, the cells were incubated with each probe for various time intervals ranging from 30 min to 24 h at 37 °C. In the case of leukemia cell lines (L1210, L1210FR), each probe (1 mM) in DMSO (15 μM) was injected directly into fresh cell suspensions to give a final concentration of 5 μM, and cells were incubated for similar time intervals. Following incubation, the cells were removed by treatment with trypsin as needed, washed twice with phosphate buffered solution (PBS), collected by centrifugation, and resuspended in PBS (150 μL) for subsequent confocal fluorescence microscopy imaging or flow cytometry analysis.

Confocal Fluorescence Microscopy (CFM) Imaging of the Treated Cells.

Cells treated as described above were resuspended in 150 μL of PBS after each experiment, and dropped onto an uncoated microslide with coverslip (MatTek Corp). CFM experiments were performed using a Zeiss LSM 510 META NLO two-photon laser scanning confocal microscope system, operating at a 488 nm excitation wavelength and at 527 ± 23 nm detecting emission wavelength using a 505-550 nm bandpass filter. Images were captured using

a C-Apochromat 63x/1.2 water (corr.) objective. Acquired data were analyzed using LSM 510 Meta software.

Flow Cytometry Fluorescent Measurements of the Cells.

Flow cytometry analysis of the cells treated with **6-6** was performed with a flow cytometer, FACSCalibur, operating at a 488 nm excitation wavelength and detecting 530 nm emission wavelengths with a 30 nm bandpass filter (515-545 nm range). Cells treated as described above were resuspended in 0.5 mL of PBS. Approximately 10,000 cells were counted for each experiment using *CellQuest 3.3* software (Becton Dickinson), and the distribution of FITC fluorescence was analyzed using *WinMDI 2.8* freeware (Joseph Trotter, Scripps Research Institute).

In Vitro Cytotoxicity Assays.

The cytotoxicities (IC_{50}, nM) of paclitaxel, SB-T-1214 and **6-4** were evaluated against various cancer cell lines by means of the standard quantitative colorimetric MTT assay.[28] The inhibitory activity of each compound is represented by the IC_{50} value, which is defined as the concentration required for inhibiting 50% of the cell growth. Cells were harvested, collected, and resuspended in 100 μL cell culture medium (RPMI-1640 or DMEM) at a concentrations ranging from 0.5-1.5 x 10^4 cells per well in a 96-well plate. For adhesive cell types, cells were allowed to descend to the bottom of the wells overnight, and appropriate fresh medium was added to each well upon removal of the old medium.

For the MTT assay of paclitaxel, SB-T-1214, and **6-4**, cells were resuspended in 200 μL medium with 8,000 to 10,000 cells per well of a 96-well plate and incubated at 37 °C for 24 h before drug treatment. In DMSO stock solutions, each drug or conjugate was diluted to a series of concentrations in cell culture medium to prepare test solutions. After removing the old medium, these test solutions were added to the wells in the 96-well plate to give the final concentrations ranging from 0.5 to 5,000 nM (100 μL), and the cells were subsequently cultured at 37 °C for 72 h. For the leukemia cell lines, cells were harvested, collected, and resuspended in the test solutions ranging from 0.5 to 5,000 nM (100 μL) at 0.5 to 0.8 x 10^4 cells per well in a 96-well plate and subsequently incubated at 37 °C for 72 h.

In a second series of experiments, cells were incubated with **6-4** at 37 °C for 24 h and the drug medium was removed. Then, treated cells were washed with PBS, and GSH-OEt (6 equivalents) in cell culture medium (200 μL) was added to the wells. These cells were incubated at 37 °C for an additional 48 h; i.e., the total incubation time was 72 h.

In a third series of experiments, cells were incubated with **6-4** at 37 °C for 24 h, and GSH-OEt (6 equivalents) in cell culture medium (100 μL) was directly added to the wells. These cells were incubated at 37 °C for an additional 48 h; i.e. the total incubation time was also 72 h.

For all experiments, after removing the test medium, fresh solution of MTT in PBS (40 μL of 0.5 mg MTT/mL) was added to the wells, and the cells were incubated at 37 °C for 3 h. The MTT solution was then removed, and the resulting insoluble violet formazan crystals were dissolved in 0.1 N HCl in isopropanol with 10% Triton X-100 (40 μL) to give a violet solution. The spectrophotometric absorbance measurement of each well in the 96-well plate was run at 570 nm using a Labsystems Multiskan Ascent microplate reader. The IC_{50} values and their standard errors were calculated from the viability-concentration curve using Four Parameter Logistic Model of *Sigmaplot*. The concentration of DMSO per well was ≤1% in all cases. Each experiment was run in triplicate.

§6.6.0 References

1. Zolot, R. S.; Basu, S.; Million, R. P. Antibody-drug conjugates. *Nature Rev. Drug Discov.* **2013,** 12, 259-260.
2. Ducry, L.; Stump, B. Antibody-drug conjugates: targeted drug delivery for cancer. *Bioconjug. Chem.* **2010,** 21, 5-13.
3. Alley, S. C.; Okeley, N. M.; Senter, P. D. Antibody drug conjugates: targeted drug delivery for cancer. *Curr. Opin. Chem. Biol.* **2010,** 14, 529-537.
4. Carter, P. J.; Senter, P. D. Antibody-drug conjugates for cancer therapy. *Cancer J.* **2008,** 14, 154-169.
5. Ojima, I.; Geng, X.; Wu, X.; Qu, C.; Borella, C. P.; Xie, H.; Wilhelm, S. D.; Leece, B. A.; Bartle, L. M.; Goldmacher, V. S.; Chari, R. V. Tumor-specific novel taxoid-monoclonal antibody conjugates. *J. Med. Chem.* **2002,** 45, 5620-5623.
6. Jaracz, S.; Chen, J.; Kuznetsova, L. V.; Ojima, I. Recent advances in tumor-targeting anticancer drug conjugates. *Bioorg. Med. Chem.* **2005,** 13, 5043-5054.
7. Vlahov, I. R.; Leamon, C. P. Engineering folate-drug conjugates to target cancer: from chemistry to clinic. *Bioconjug. Chem.* **2012,** 23, 1357-1369.
8. Leamon, C. P. Folate-targeted drug strategies for the treatment of cancer. *Curr. Opin. Invest. Drugs* **2008,** 9, 1277-1286.
9. Chen, S.; Zhao, X.; Chen, J.; Kuznetsova, L.; Wong, S. S.; Ojima, I. Mechanism-based tumor-targeting drug delivery system. Validation of efficient vitamin receptor-mediated endocytosis and drug release. *Bioconjug. Chem.* **2010,** 21, 979-987.
10. Kuznetsova, L.; Chen, J.; Sun, L.; Wu, X.; Pepe, A.; Veith, J. M.; Pera, P.; Bernacki, R. J.; Ojima, I. Syntheses and evaluation of novel fatty acid-second-generation taxoid conjugates as promising anticancer agents. *Bioorg. Med. Chem. Lett.* **2006,** 16, 974-977.
11. Bradley, M. O.; Webb, N. L.; Anthony, F. H. Tumor targeting by covalent conjugation of a natural fatty acid to paclitaxel. *Clin. Cancer Res.* **2001,** 7, 3229-3238.
12. Ojima, I. Guided molecular missiles for tumor-targeting chemotherapy--case studies using the second-generation taxoids as warheads. *Acc. Chem. Res.* **2008,** 41, 108-119.
13. Vineberg, J. G.; Zuniga, E. S.; Kamath, A.; Chen, Y. J.; Seitz, J. D.; Ojima, I. Design, Synthesis and Biological Evaluations of Tumor-Targeting Dual-Warhead Conjugates for a Taxoid-Camptothecin Combination Chemotherapy. *J. Med. Chem.* **2014,** 57, 5777-5791.
14. Miller, P. W.; Long, N. J.; Vilar, R.; Gee, A. D. Synthesis of 11C, 18F, 15O, and 13N radiolabels for positron emission tomography. *Angew. Chem. Int. Ed. Engl.* **2008,** 47, 8998-9033.
15. Valderrama, S.; Van Roekel, N.; Andersson, M.; Goodacre, C. J.; Munoz, C. A. A comparison of the marginal and internal adaptation of titanium and gold-platinum-palladium metal ceramic crowns. *Int J Prosthodont* **1995,** 8, 29-37.
16. Koehler, L.; Gagnon, K.; McQuarrie, S.; Wuest, F. Iodine-124: A promising positron emitter for organic PET chemistry. *Molecules* **2010,** 15, 2686-2718.
17. van Tilburg, E. W.; Franssen, E. J. F.; van der Hoeven, J. J. M.; van der Meij, M.; Elshove, D.; Lammertsma, A. A.; Windhorst, A. D. Radiosynthesis of [11C]docetaxel. *J. Labelled Comp. Radiopharm.* **2004,** 47, 763-777.
18. Seitz, J. D.; Vineberg, J. G.; Ojima, I. Synthesis of a next-generation taxoid by rapid methylation amenable for [11C]-labeling. *J. Org. Chem.*, To be submitted shortly.
19. Morita, S.; Otsubo, K.; Matsubara, J.; Ohtani, T.; Kawano, Y.; Ohmori, K.; Ohguro, K.; Uchida, M. Synthesis of possible metabolites of 1-cyclopropyl-1,4-dihydro-6-fluoro-5-methyl-7-

(3-methyl-1-piperazinyl)- 4-oxo-3-quinolinecarboxylic acid (Grepafloxacin, OPC-17116). *Chem Pharm Bull (Tokyo)* **1995,** 43, 2246-52.
20. Fowler, J. S.; Ido, T. Initial and subsequent approach for the synthesis of 18FDG. *Semin. Nucl. Med.* **2002,** 32, 6-12.
21. Marik, J.; Sutcliffe, J. L. Click for PET: rapid preparation of [18F]fluoropeptides using Cu(I) catalyzed 1,3-dipolar cycloaddition. *Tetrahedron Lett.* **2006,** 47, 6681-6684.
22. Shoup, T. M.; Fischman, A. J.; Jaywook, S.; Babich, J. W.; Strauss, H. W.; Elmaleh, D. R. Synthesis of fluorine-18-labeled biotin derivatives: biodistribution and infection localization. *J. Nucl. Med.* **1994,** 35, 1685-90.
23. Kudo, T.; Ueda, M.; Konishi, H.; Kawashima, H.; Kuge, Y.; Mukai, T.; Miyano, A.; Tanaka, S.; Kizaka-Kondoh, S.; Hiraoka, M.; Saji, H. PET imaging of hypoxia-inducible factor-1-active tumor cells with pretargeted oxygen-dependent degradable streptavidin and a novel 18F-labeled biotin derivative. *Mol. Imaging Biol.* **2011,** 13, 1003-10.
24. Kim, D. W.; Jeong, H. J.; Lim, S. T.; Sohn, M. H.; Katzenellenbogen, J. A.; Chi, D. Y. Facile nucleophilic fluorination reactions using tert-alcohols as a reaction medium: significantly enhanced reactivity of alkali metal fluorides and improved selectivity. *Journal of Organic Chemistry* **2008,** 73, 957-62.
25. Paulos, C. M.; Reddy, J. A.; Leamon, C. P.; Turk, M. J.; Low, P. S. Ligand binding and kinetics of folate receptor recycling in vivo: impact on receptor-mediated drug delivery. *Mol Pharmacol* **2004,** 66, 1406-14.
26. Shai, Y.; Kirk, K. L.; Channing, M. A.; Dunn, B. B.; Lesniak, M. A.; Eastman, R. C.; Finn, R. D.; Roth, J.; Jacobson, K. A. 18F-labeled insulin: a prosthetic group methodology for incorporation of a positron emitter into peptides and proteins. *Biochemistry* **1989,** 28, 4801-6.
27. Breyholz, H. J.; Wagner, S.; Faust, A.; Riemann, B.; Holtke, C.; Hermann, S.; Schober, O.; Schafers, M.; Kopka, K. Radiofluorinated pyrimidine-2,4,6-triones as molecular probes for noninvasive MMP-targeted imaging. *ChemMedChem.* **2010,** 5, 777-89.
28. Mosmann, T. Rapid colorimetric assay for cellular growth and survival: application to proliferation and cytotoxicity assays. *J. Immunol. Methods* **1983,** 65, 55-63.

Chapter 7

Development of Novel ^{11}C- and ^{18}F-labeled Radiotracers for PET Imaging

Chapter Contents

§7.1 Introduction

§7.1.1 Positron Emission Tomography

Positron emission tomography (PET) is a non-invasive molecular imaging technology that is used to study and visualize the physiology of living biological systems by the detection of positron-emitting radiopharmaceuticals.[1] Unlike other common imaging techniques, such as magnetic resonance imaging (MRI), X-rays, or ultrasound (US), which namely give structural information, PET and SPECT (single-photon emission computed tomography) imaging uniquely provides information on metabolic or molecular events that cannot be generated with techniques limited to determining organ structure.[1] Since many positron-emitters, such as ^{11}C, ^{13}N, and ^{15}O, are elements low in atomic mass and the main constituents of bioorganic molecules, these radionuclides can be incorporated directly into radiopharmaceuticals that are chemically indistinguishable from their non-radioactive counterparts.[1, 2]

Radiopharmaceuticals play an essential role in determining the pharmacokinetic properties of a drug or target compound. In early-stage drug development, PET can elucidate biodistribution patterns of a radiotracer *in vivo* with target binding, accumulation of the tracer, metabolism, and rate of clearance. Later on, PET can provide insight into mechanisms of action and aid in dose determination.[1]

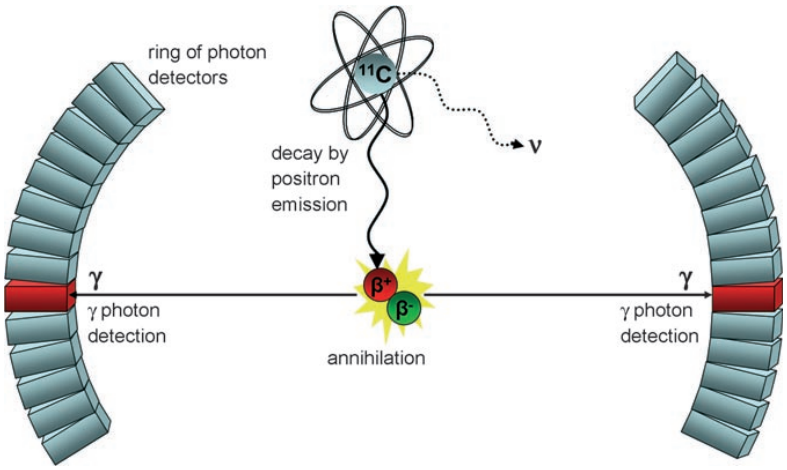

Figure 7.1. Representation of positron decay and annihilation that produces two 511 keV γ-rays. Reprinted from reference [1].

PET radiotracers are labeled with positron-emitting radionuclides, which decay by the emission of a positively charged particle, a positron.[2] Following emission from the nucleus, the positron travels a short distance, known as the positron range, in the surrounding tissue before it collides with an electron.[2] This collision of matter and antimatter, known as an annihilation, produces two gamma ray photons (γ) of 511 keV that are emitted simultaneously in opposite directions (180°) and are then detected by surrounding detectors (Figure 7.1).[1, 2] The summation of a large number of coincidence events provides the necessary information to reconstruct the sequence of annihilation events with spatial and temporal distribution of radioactivity, and hence biodistribution of a radiotracer, as a function of time.[2]

Shown in Table 7.1 are the most common positron-emitting radionuclides and their physical properties.

Table 7.1. Physical properties of commonly used positron-emitting radionuclides. Adapted from references [1, 2].

Radionuclide	Half-life, $t_{1/2}$ (min)	Nuclear Reaction	Target	Product	Decay Product	Theoretical Specific Activity (GBq/μmol)
^{11}C	20.4	$^{14}N(p,\alpha)^{11}C$	$N_2(+O_2)$ $N_2(+H_2)$	$[^{11}C]CO_2$ $[^{11}C]CH_4$	^{11}B	3.4 x 10^5
^{13}N	9.97	$^{16}O(p,\alpha)^{13}N$	H_2O H_2O+EtOH	$[^{13}N]NO_x$ $[^{13}N]NH_3$	^{13}C	7.0 x 10^5
^{15}O	2.04	$^{15}N(d,n)^{15}O$	$N_2(+O_2)$	$[^{15}O]O_2$	^{15}N	3.4 x 10^6
^{18}F	110	$^{18}O(p,n)^{18}F$ $^{20}Ne(d,\alpha)^{18}F$	$[^{18}O]H_2O$ $Ne(+F_2)$	$^{18}F^-$ $[^{18}F]F_2$	^{18}O	6.3 x 10^4

The relatively short half-lives of these radionuclides necessitates that the total synthesis time, including purification, analysis, and formulation, be kept as short as possible, usually within three physical half-lives from the end of bombardment of the target with a proton or deuteron beam in the cyclotron.[1, 2] Multistep syntheses may be employed for complex molecules, however these strategies aim to incorporate the radionuclide as late in the synthetic sequence as possible.[2] Furthermore, a large amount of unlabeled precursor in about 10^3–10^4-fold excess is typically used to drive incorporation of the radionuclide and increase radiochemical conversion.[2] Depending on the radionuclide, reaction times vary from one to thirty minutes, and reaction volumes are much smaller than traditional organic synthesis, ranging from 0.2 to 1 mL.

Over the past three decades, PET imaging has been employed in oncology to observe the accumulation and metabolism of certain PET probes within the tumor,[1, 3-5] in cardiology for myocardial perfusion imaging to diagnose coronary heart disease,[1, 6] in neurology for characterization of early-stage neurological disorders,[1, 7, 8] such as Parkinson's and Alzheimer's diseases, as well as in many other medical areas.

§7.2 Carbon-11

§7.2.1 Radiolabeling with Carbon-11

With a physical half-life of 20.4 min, carbon-11 is well suited for labeling compounds with short biological half-lives.[2] Since carbon is present in nearly all natural products and drug compounds, "hot" ^{11}C-labeled tracers will interact in living systems the same, both chemically and biologically, as their "cold" ^{13}C-incorporated equivalents.[1] Additionally, multiple PET studies can be performed repeatedly on the same subject in a given day, due to the short half-life of carbon-11.

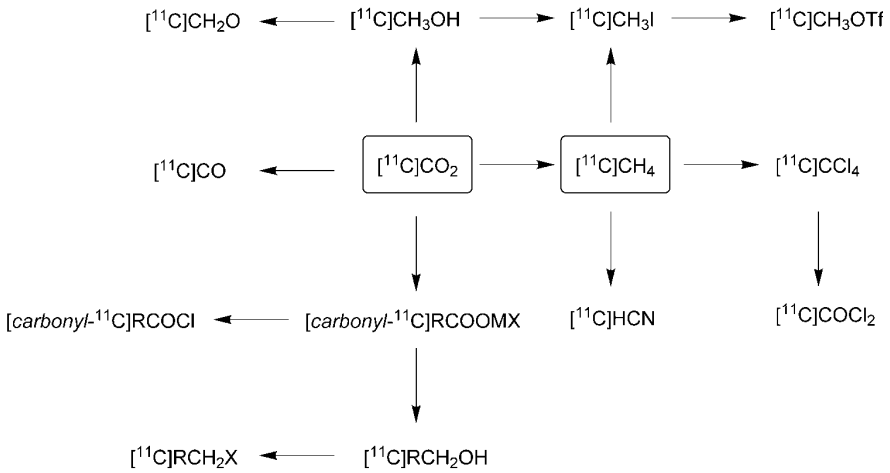

Figure 7.2. Chemical pathways to carbon-11 reagents. Reprinted from reference [1].

The most common method for production of carbon-11 is the bombardment of a nitrogen gas target in a cyclotron with a proton beam according to the $^{14}N(p,\alpha)^{11}C$ reaction.[9, 10] The two primary ^{11}C precursors are $[^{11}C]CO_2$ and $[^{11}C]CH_4$, both of which can be chemically converted to various other carbon-11 precursors, such as $[^{11}C]CO$ and $[^{11}C]CN$ (Figure 7.2).

Carbon-11 methylation leads to the incorporation of $[^{11}C]CH_3$ methyl group into a target compound, and many ^{11}C-methylation procedures have been previously reported.[2, 11] Amongst these methods, the most widely used methylating agent is $[^{11}C]$methyl iodide, which can be prepared by reducing $[^{11}C]CO_2$ using $LiAlH_4$, followed by reaction with hydroiodic acid,[12] or by the gas-solid iodination reaction of $[^{11}C]CH_4$ at high temperature.[1, 13, 14] Palladium(0)-mediated Stille-type coupling reactions have received the most attention for the introduction of $[^{11}C]$methyl groups into radiopharmaceuticals, and many studies on rapid palladium-mediated $[^{11}C]$methylation have been previously reported.[15-18]

§7.2.2 Radiolabeled Taxanes and [^{11}C]SB-T-1214

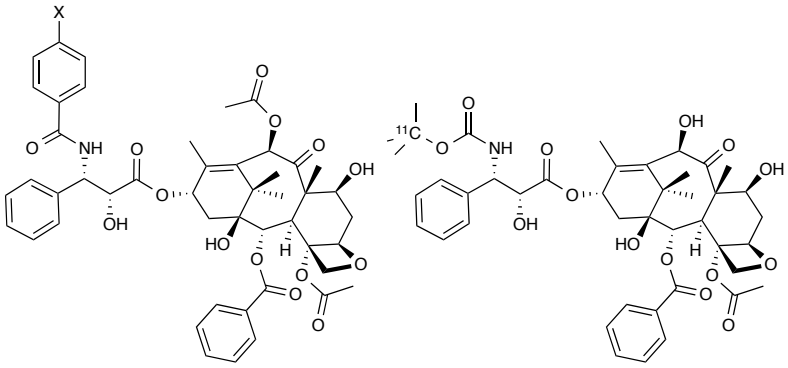

Figure 7.3. Radiolabeled taxanes under clinical development.

Several taxanes or taxoid derivatives, including paclitaxel and docetaxel, have been successfully radiolabeled with positron-emitting radionuclides such as ^{11}C, ^{18}F, ^{76}Br, and ^{124}I for PET imaging (Figure 7.3).[19, 20] Paclitaxel was modified at the 4-position of the C3'*N*-phenyl

group with fluorine, bromine, and iodine as radionuclides, though these installations required modifications to paclitaxel.[19] A PET tracer for docetaxel was developed in which the exact structure was retained with incorporation of carbon-11 in the C3'*N*-Boc group.[20]

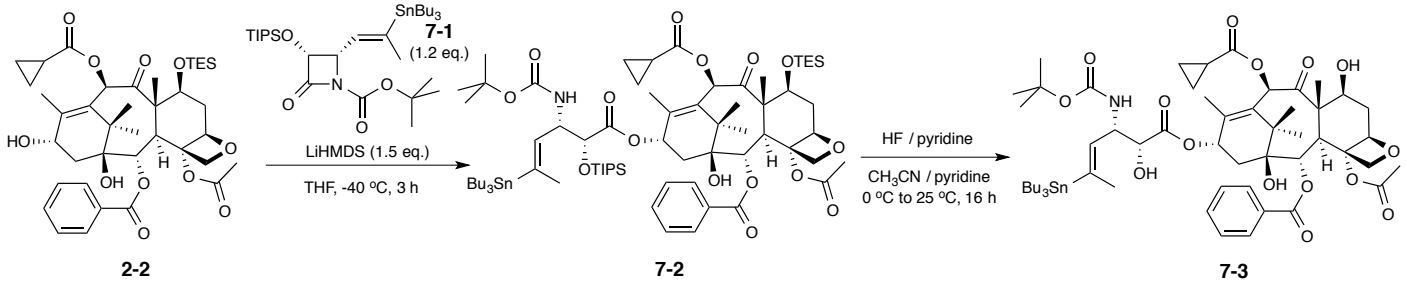

Scheme 7.1. Chemical synthesis of 3'-dephenyl-3'-(2-methyl-2-tributylstannyl-1-propenyl)-10-(cyclopropanecarbonyl)docetaxel (**7-3**). Adapted from references [21, 22].

A novel synthetic route towards the synthesis of SB-T-1214 that allows for incorporation of radionuclides via [^{11}C]CH_3I at the final step of chemical synthesis was developed by co-worker Dr. Joshua D. Seitz. Rapid methylation of novel vinylstannyl-taxoid (**7-3**), which was prepared through Ojima-Holton coupling of enantiopure β-lactam **7-1** to baccatin **2-2** and followed by HF-deprotection (Scheme 7.1), with CH_3I by Stille coupling gave SB-T-1214 in an efficient synthesis.[21, 22] Various reaction conditions for Stille coupling were screened.[22] However, SB-T-1214 was only obtained using CH_3I, tetrakis(triphenylphosphine)palladium(0) [$Pd(Ph_3P)_4$], and copper(I)-thiophene-2-carboxylate (CuTC). Formation of SB-T-1214 in a time frame permissible for radiolabeling with ^{11}C for PET imaging was verified by LC-MS with equimolar reagents, $CH_3I/Pd(PPh_3)_4$/CuTC (1:1:1).[21, 22]

However, since the radionuclide is typically used as the limiting reagent in radiosynthesis by 3-4 orders of magnitude compared to the substrate to be labeled, further optimization of methylation of **7-3** under these types of limiting conditions became necessary.

§7.2.3 Cold synthesis of SB-T-1214 via Stille Coupling

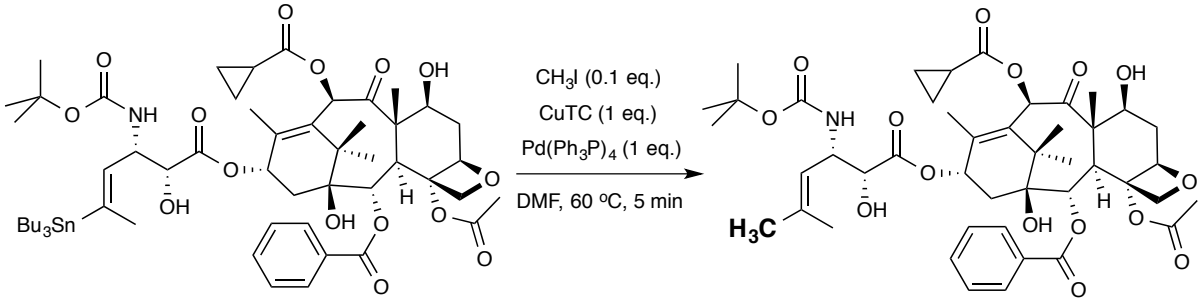

Scheme 7.2. Rapid methylation of **7-3** with CH_3I by Stille coupling to give SB-T-1214.

Conditions for "hot-like" radiosynthesis were optimized on the "cold" material with methyl iodide serving as the limiting reagent, shown in Scheme 7.2. The palladium(0) and copper reagents were used in excess, along with vinylstannyl-taxoid (**7-3**).

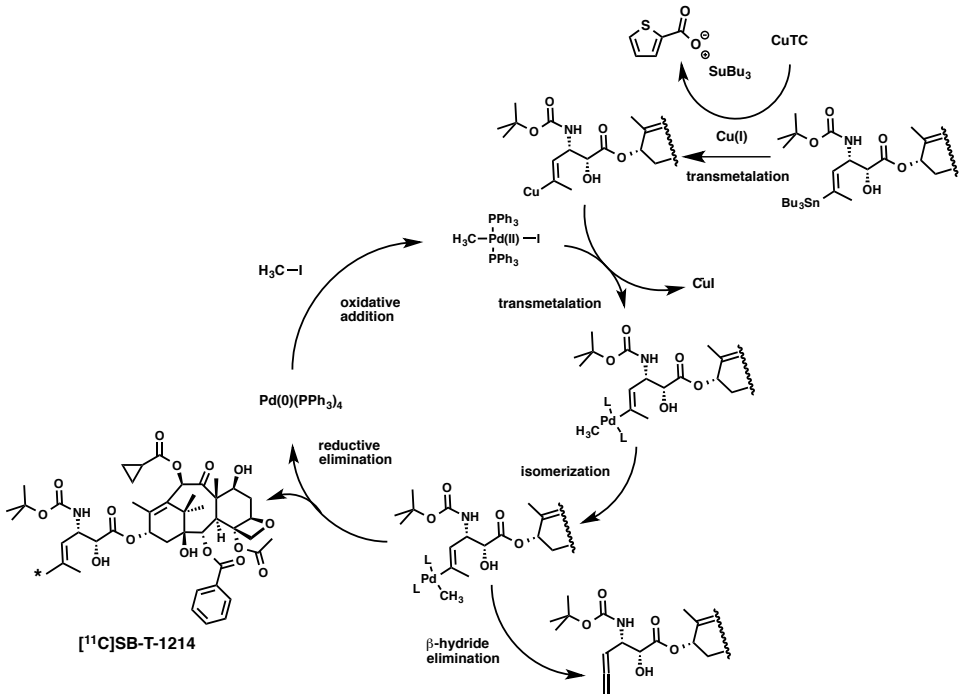

Figure 7.4. Proposed mechanism for palladium- and copper-cocatalyzed Stille coupling of CH_3I to vinylstannyl-taxoid (**7-3**). Adapted from reference [21].

Oxidative addition of the electrophilic methyl iodide to Pd(0) begins with preincubation of a solution of methyl iodide in DMF with a solution of $Pd(Ph_3P)_4$ in DMF.[23] Palladium-catalyzed Stille coupling reactions have been shown to be accelerated by copper(I) catalysts via vinylcuprates.[23-26] First, the vinylstannyl-taxoid (**7-3**) is preincubated with CuTC, and addition of the CH_3-Pd(II) species is followed by transmetallation of the methyl group from copper/tin to palladium and ends with reductive elimination of the CH_3-taxoid from palladium. This mechanism is illustrated in Figure 7.4.

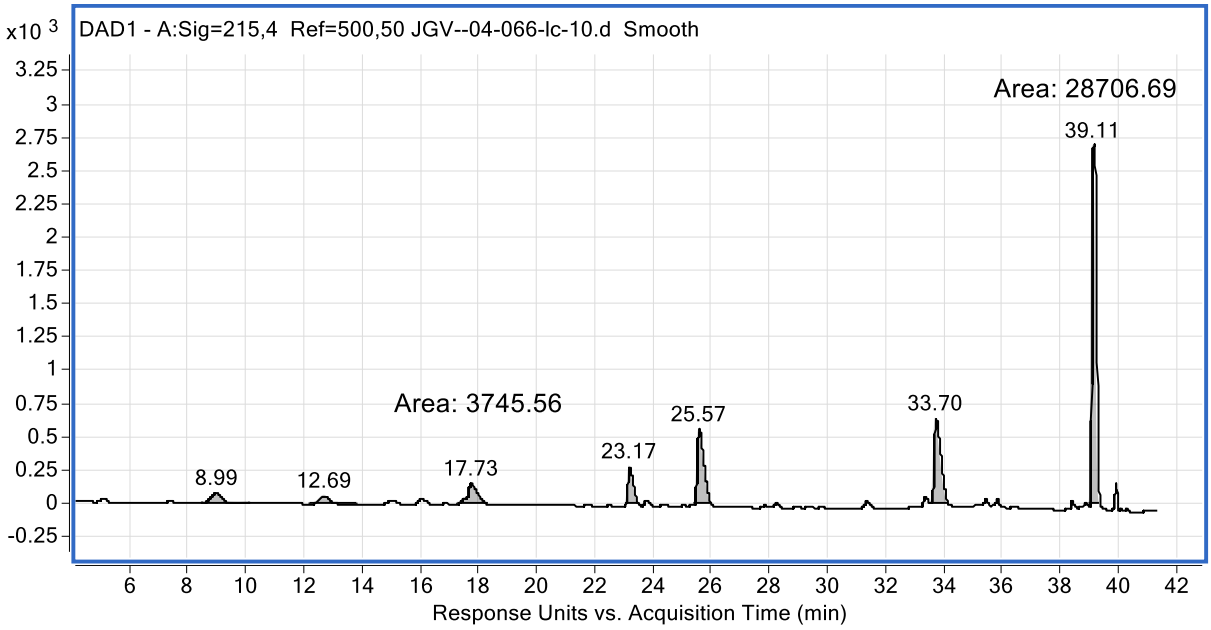

Figure 7.5. HPLC chromatogram (λ = 215 nm) for the Stille coupling of **7-3** with CH_3I as limiting reagent.

After five minutes, the reaction mixture was immediately analyzed by LCMS with the UV detector (λ) set to 215 and 254 nm. The HPLC chromatogram for the reaction mixture, with CH_3I serving as the limiting reagent, is shown in Figure 7.5. Standard SB-T-1214, prepared by Ojima-Holton coupling of isobutenyl-β-lactam (+)**1-6** and modified baccatin **2-2**, was analyzed by LCMS under the same conditions. The desired taxoid eluted at 17.73 min, which was confirmed by analysis of its corresponding mass spectrum (*m/z* 854) and the agreement of its retention time with the standard SB-T-1214 sample, shown in Figure 7.6.

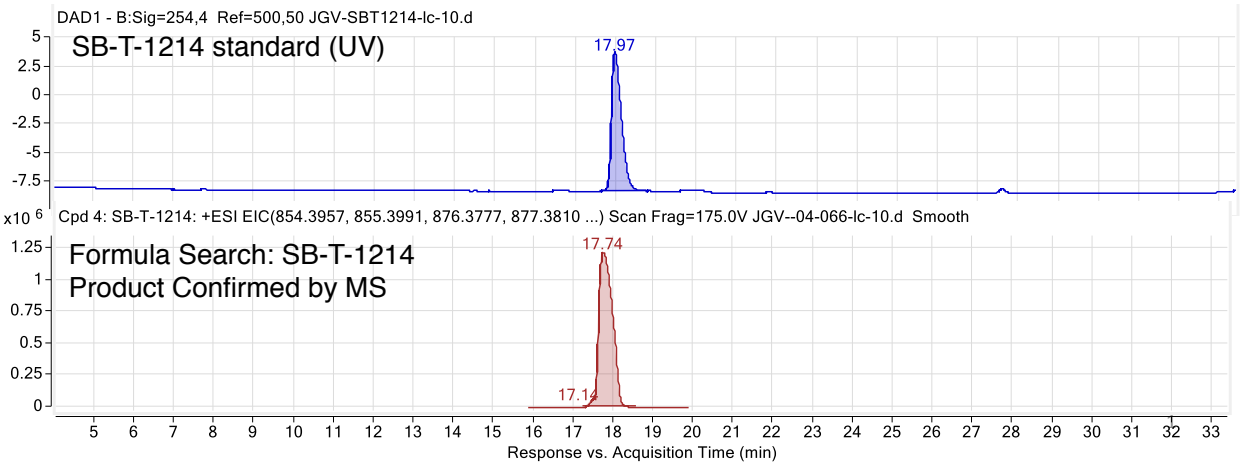

Figure 7.6. HPLC chromatogram (λ = 254 nm) of standard SB-T-1214 (*above*) and confirmed compound search for SB-T-1214 in Stille coupling reaction (*bottom*).

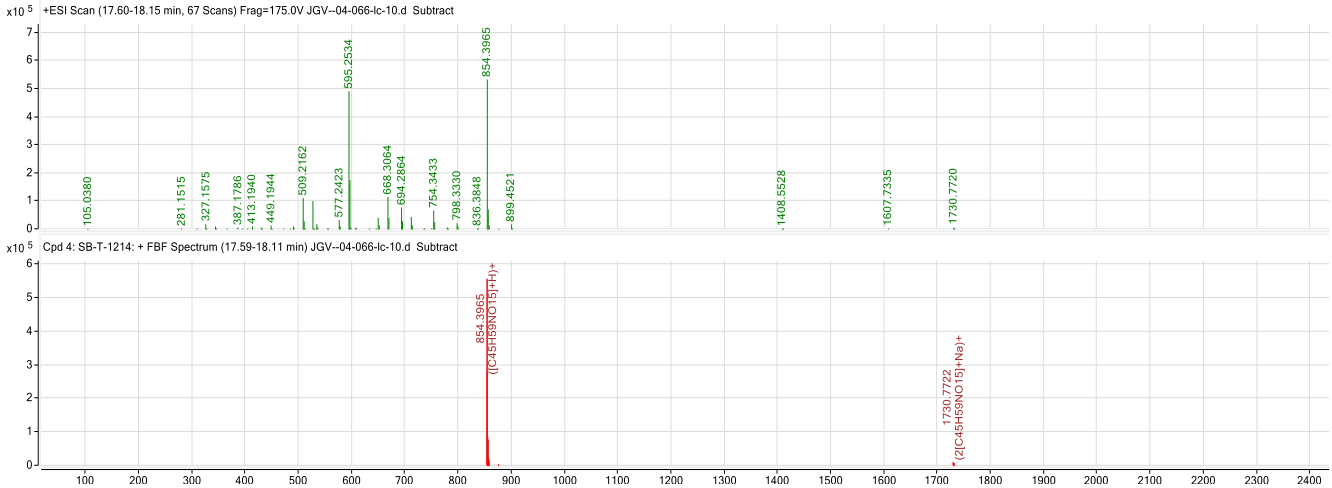

Figure 7.7. High-resolution mass spectrum of the eluted compound at 17. 7 min, with product confirmation for SB-T-1214 as $[M+H^+]$ and $[2M+Na^+]$ ions.

The excess vinylstannyl taxoid substrate (**7-3**) eluted at 39.11 min, which was confirmed by analysis and comparison of its mass spectrum with a standard sample (*m/z* 1130). Comparison of the integrated area under the product peak (17.73 min) and the vinylstannyl-taxoid (39.11 min) gave a ratio of 7.6:1, which is supported by the reaction conditions with CH_3I as the limiting reagent.

Three additional peaks contain signature *m/z* characteristics of taxoids and were likely derived from **7-3**. First, the peak at 23.17 min has a *m/z* of 966.3, which corresponds to the formation of a vinyliodotaxoid during the reaction, shown in Figure 7.5. Then, the peaks at 25.57 and 33.70 contain signature taxoid fragmentation patterns with a *m*/z of 595.3, which correspond to the allylic cation of the modified baccatin with fragmentation at the C13 side chain. However, further analysis will be required to identify the structures of these taxoid by products.

Along with the desired taxoid, SB-T-1214, at 17.7 min is a minor by-product (ca. 10%, according to TIC) corresponding to a C3'-allenyl taxoid (Figure 7.5). It has been proposed that the formation of this by-product can be attributed to β-hydride elimination following ligand dissociation during transmetallation and isomerization.[22] Though, the presence of this side-product should not interfere with a PET biodistribution study since the C3'-allenyl taxoid should not contain the radiolabeled methyl group, and, in addition, the mechanism of taxoid internalization is not limited by receptor-binding, so competitive binding will not be a limitation.

§7.3 Fluorine-18

§7.3.1 Radiolabeling with Fluorine-18

Amongst radionuclides, fluorine-18 possesses the most favorable physical properties for PET imaging, due to its optimal physical half-life ($t_{1/2}$ = 110 min), low positron energy, and ease of production.[27] Its optimal physical half-life allows for longer radiosynthesis, extended *in vivo* studies, and for multiple patients to receive radiotracer doses over the course of a single day.[1, 2] Its short positron linear range in tissue (2.3 mm) gives the highest resolution PET images of available positron emitters.[1]

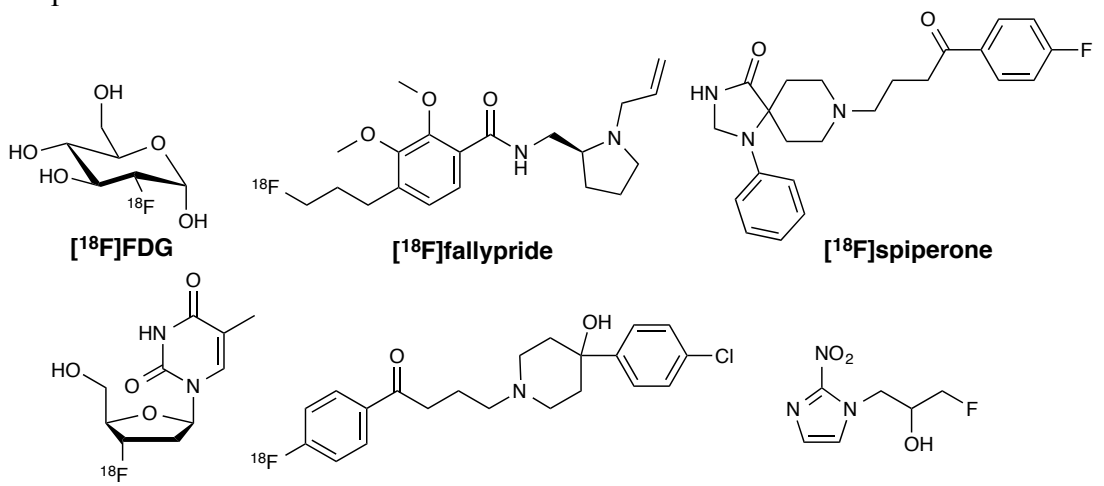

Figure 7.8. Examples of commonly employed ^{18}F PET radiotracers. Adapted from references [28-32].

Unlike carbon-11, fluorine-18 is well suited for labeling compounds with extended biological half-lives. However, there are two primary disadvantages of using fluorine-18 in labeling of PET radiotracers: (1) fluorine is not typically incorporated in biologically active molecules; and (2) the effects of incorporating fluorine as an unnatural radioligand makes it difficult to make direct comparisons between the fluorine-labeled radiotracer and the native non-fluorinated species.[1, 33] However, beneficial effects of substitution of hydrogen atoms with

fluorine atoms on the physical and biological properties of a molecule has led to an increase in the number of biologically active fluoroorganic drugs, shown in Figure 7.8.[1, 28-35]

The chemical methods for introduction of fluorine-18 into target molecules is limited compared to those available for carbon-11.[1] Fluorine-18 can be introduced by direct fluorination of the target of interest, by nucleophilic or electrophilic substitution reactions, or by fluorination of a prosthetic group in a multistep synthetic approach.[1] Nucleophilic $[^{18}F]F^-$ is typically produced by the nuclear reaction $^{18}O(p,n)^{18}F$ from $[^{18}O]H_2O$. After generation from a cyclotron, $^{18}F^-$ is trapped on an ion-exchange resin, allowing for recovery of $[^{18}O]H_2O$, and eluted from the resin with potassium carbonate in a water-acetonitrile solution to afford $[^{18}F]KF$ in aqueous solution.[1] The addition of a phase-transfer catalyst, such as kryptofix-222 (K_{222}), which forms a strong complex with the potassium cation and enhances the nucleophilicity of the fluoride anion in polar nonprotic solvents, followed by azeotropic distillation of water, has improved the reactivity of $^{18}F^-$ in nucleophilic substitution reactions.[1] Elution with tetrabutylammonium bicarbonate in a water-acetonitrile solution affords $[^{18}F]$TBAF as a nucleophilic radiofluorination reagent.[36]

§7.3.2 Radiotracer Vitamins and Drug Conjugates

Numerous radiolabeled vitamin derivatives of folic acid and biotin have been reported for development as PET and SPECT radiotracers.[37-39] Etarfolatide (^{99m}Tc-EC20), the most advanced folate-based imaging agent in the clinic, was designed as a companion imaging agent for folate-based SMDC vintafolide with ^{99m}Tc as the radionuclide.[39] A folic acid derivative, 3'-aza-2'-$[^{18}F]$fluorofolic acid, was designed as an $[^{18}F]$-labeled PET radiotracer and allowed for visualization of FR-positive tumors in mice with high image contrast and only minor accumulation in non-targeted tissue.[38] In addition, a biotin derivative, (4-$[^{18}F]$fluorobenzoyl)norbiotinamide, was developed to validate its ability to bind to streptavidin both *in vitro* and *in vivo*.[37] The chemical structures of these three imaging agents are illustrated in Figure 7.9.

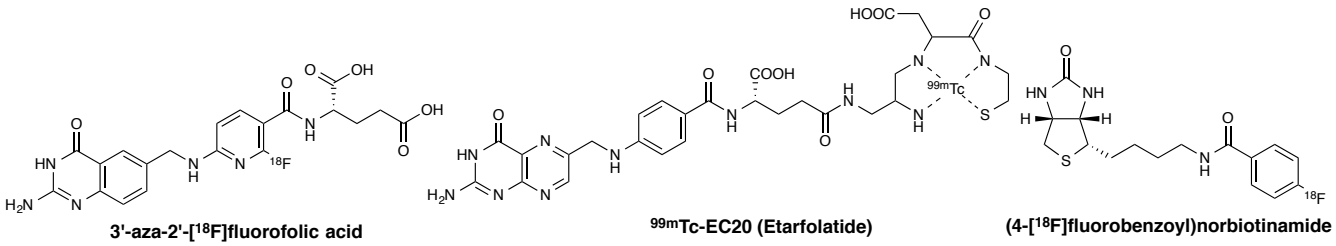

Figure 7.9. Chemical structures of radiolabeled vitamins designed for PET and SPECT imaging. Adapted from references [37-39].

However, while significant advances have been made in elucidating the biodistribution pattern of folic acid and its derivatives in FR-positive tumor-bearing mice, there is little information available regarding the biodistribution of biotin *in vivo* in BR-positive tumor-bearing mice. Thus, we designed a novel biotin derivative as a PET radiotracer with fluorine-18 as the radionuclide, shown in Figure 7.10, as a proof-of-concept for biotin as a tumor-targeting moiety in targeted oncology. During this development, however, the same compound was reported by Claesener et al.; but, it was employed to investigate the biotin-avidin non-covalent interaction, and the role of biotin as a tumor-targeting module in targeted oncology remained unclarified.

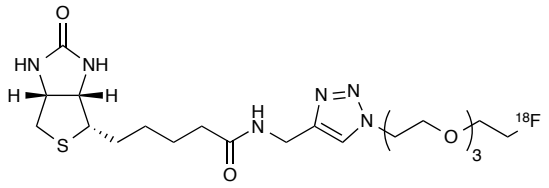

[^{18}F]4-20

Figure 7.10. Chemical structure of [^{18}F]biotin-PEG-F.

§7.3.3 Radiosynthesis of [^{18}F]Biotin-PEG-F

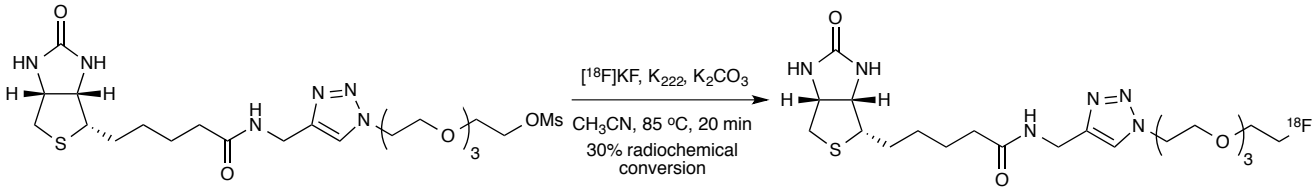

4-19 **[^{18}F]4-20**

Scheme 7.3. Radiosynthesis of [^{18}F]biotin-PEG-F ([^{18}F]**4-20**)

Optimization of reaction conditions for radiosynthesis and method development for purification and isolation of [^{18}F]biotin-PEG-F were performed at Brookhaven National Laboratory under the supervision of Dr. Joanna S. Fowler's group. No-carrier-added [^{18}F]F$^-$ was produced from [^{18}O]H_2O by the $^{18}O(p,n)^{18}F$ reaction, and received as an aqueous solution of [^{18}F]KF (4 mL) with specific activity of approximately 25 mCi. Azeotropic distillation of aliquots of the aqueous fluoride source (0.4 mL, 2-3 mCi) with K_2CO_3 (1 mg) and 4,7,13,16,21,24-hexaoxa-1,10-diazabicyclo[8.8.8]hexacosane (Kryptofix® 2.2.2) (6 mg) at 100 °C with acetonitrile gave [^{18}F]KF as a dried white solid. The precursor, in solution, was added directly to the reaction vial containing [^{18}F]KF, K_2CO_3, and K_{222}, and the vial was sealed and heated with vigorous stirring. The radiosynthesis is shown in Scheme 7.3.

Table 7.2. Fluorination of 4-19 with [^{18}F]KF under various reaction conditions.

Entry	Substrate **4-19** Mass	Solvent	Volume (μL)	T (°C)	Time (min)	Radiochemical Conversion
1	1.7 mg	CH_3CN	250	85	5	17.9 %
2	1.7 mg	CH_3CN	250	85	8	23.0 %
3	1.7 mg	CH_3CN	250	85	13	30.0 %
4	1.7 mg	CH_3CN	250	85	18	28.0 %
5	4.2 mg	CH_3CN	400	85	13	19.9 %
6	3.7 mg	CH_3CN	250	95	13	18.5 %
7	1.7 mg	CH_3CN	1000	85	13	18.5 %
8	2.0 mg	*t*-AmOH:DMSO (3:2)	250	85	13	12.0 %
9	2.0 mg	*t*-AmOH:DMSO (3:2)	250	105	13	7.9 %

After validation of product formation, reaction conditions, such as substrate mass, solvent, reaction volume, temperature, and time, were screened for optimization of radiochemical conversion, shown in Table 7.2. Reaction progress was monitored at 5, 8, 13, and 18 min by radiological TLC with a fixed substrate mass 1.7 mg (**4-19**) in CH_3CN (250 μL) at 85

°C (Entries 1-4), and the highest radiochemical conversion of [^{18}F]F$^-$ was observed after 13 minutes (Entry 3). The radio-TLC for fluorination of **4-19** for Entry 3 is shown in Figure 7.11, with the desired product appearing at a retention time (R_f) of 0.309 and the unreacted [^{18}F]F$^-$ on the baseline.

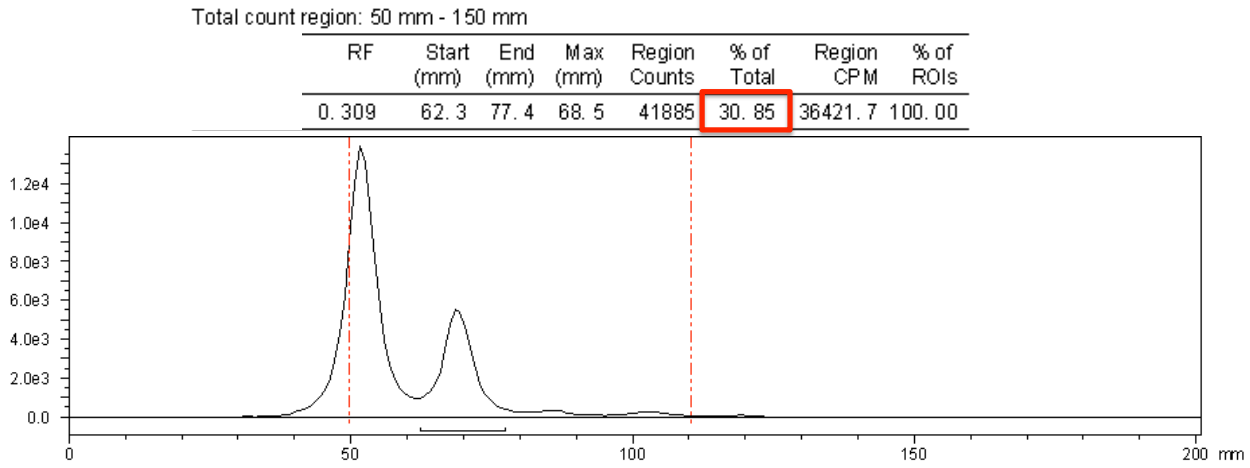

Figure 7.11. Thin-layer radiochromatogram (eluent: CH_2Cl_2/CH_3OH = 9:1) of fluorination of **4-19** with [^{18}F]KF indicating product formation at 0.309 (R_f) in 30% radiochemical conversion.

Increasing the starting material substrate mass (Entry 5) and temperature from 85 °C to 95 °C (Entry 6), and diluting the reaction volume to 1 mL (Entry 7) did not improve the radiochemical conversion. Furthermore, using *t*-AmOH and DMSO (3:2) as a reaction co-solvent at 85 °C and 105 °C lowered the radiochemical conversion. However, use of solely DMSO as the reaction medium and higher temperatures (>105 °C) may provide a higher radiochemical conversion of the fluoride source. Though, 30% radiochemical conversion is sufficient to provide enough radiotracer following purification and isolation for a live-animal PET study.

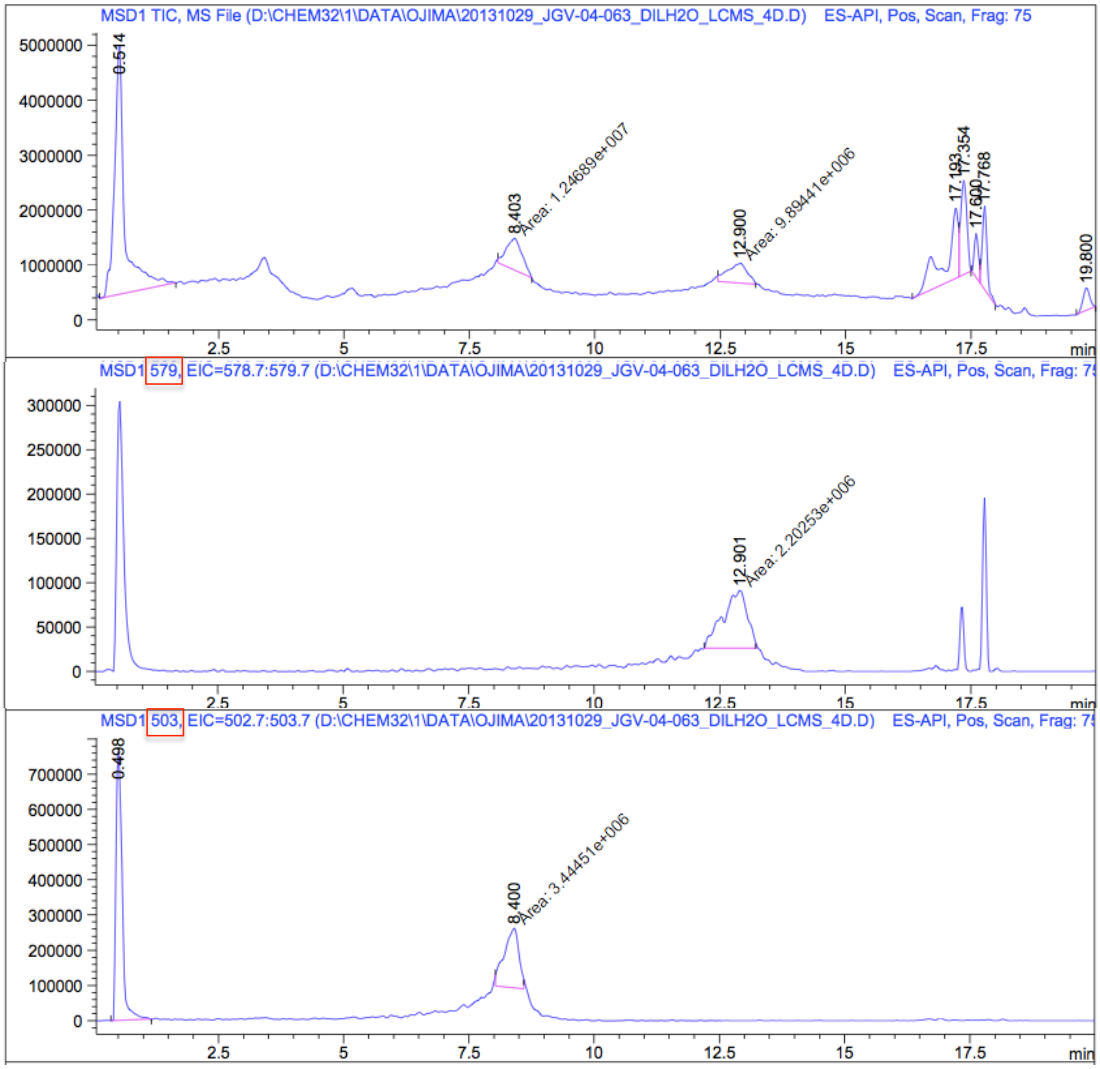

Figure 7.12. Optimized analytical HPLC trace for separation of starting material biotin precursor (**4-19**) at 12.9 min and the desired fluorinated biotin derivative (**4-20**) at 8.4 min.

Method development for purification and isolation of biotin-PEG-F was first carried out using LC-MS on the cold reaction mixture. The reaction mixture was composed of *tert*-amyl alcohol (150 µL) and DMSO (100 µL), and the mixture was diluted with water (1 mL) prior to injection. A 75 µL aliquot of the diluted reaction mixture was injected into a Luna PFP column (150 x 3 mm; 3 µm) with a flow rate of 1.0 mL/min of 10% CH_3CN in H_2O (isocratic). The molecular ion peaks [M+H$^+$] for both the starting material precursor **5-8** (*m/z* 579) and the product (*m/z* 503) were extracted from the LC-MS trace to determine product separation. As shown in Figure 7.12, over 4 minutes of separation between the precursor and product was observed under these conditions.

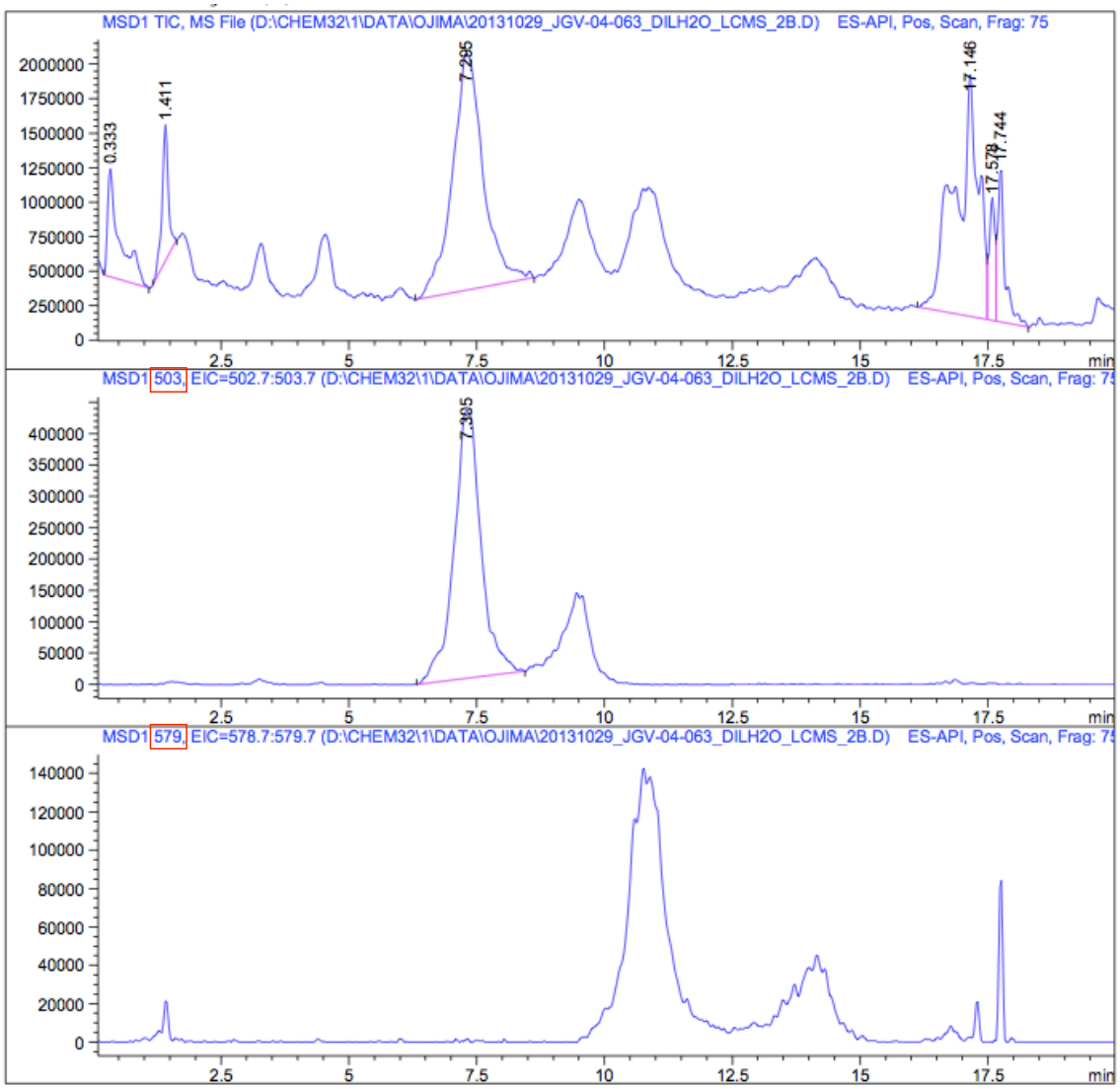

Figure 7.13. Demonstration of regioisomers from "click" reaction by analytical HPLC and LC-MS.

Interestingly, with only a 10 μL injection volume of the above-described reaction mixture under the same HPLC conditions, distinct separation of the regioisomers resulting from the "click" reaction was observed in the LC-MS trace for both the starting material and the product. The LC-MS traces for these conditions are shown in Figure 7.13.

The live-animal PET biodistribution study of [^{18}F]-biotin-PEG-F will be carried out in collaboration with Dr. Jacob Hooker at Massachusetts General Hospital, Athinoula A. Martinos Center for Biomedical Imaging, and Harvard Medical School. Tumor-bearing Swiss Webster athymic nude SCID mice bearing MX-1 tumor xenografts as well as healthy mice will be provided by Dr. Thomas Zimmerman at the Division of Laboratory Animal Resources at State University of New York at Stony Brook.

§7.3.4 Radiosynthesis of [^{18}F]F-PEG-N_3

[^{18}F]BLT-F was designed as a companion imaging agent for the biotin-linker-taxoid SMDC series. The radiosynthesis of tumor-targeting theranostic conjugate [^{18}F]BLT-F (**[^{18}F]6-4**) was performed over two steps: first, fluorination of an azide-bearing prosthetic with [^{18}F]F^- gave **[^{18}F]6-3**, followed by the "click" reaction of the azide with the acetylene of **5-8**. However, to remove excess mesylate prior to the "click" reaction, reaction optimization for radiosynthesis and method development for purification and isolation of **[^{18}F]6-3**. The fluorination reaction of PEG-mesylate precursor **4-16** is illustrated in Scheme 7.4.

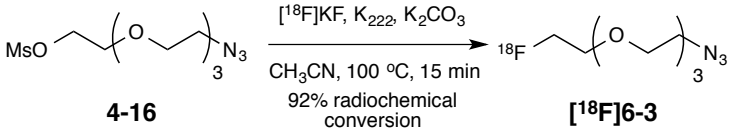

4-16 **[^{18}F]6-3**

Scheme 7.4. Chemical radiosynthesis of [^{18}F]F-PEG_3-N_3 (**[^{18}F]6-3**)

Treatment of precursor mesylate **4-16** with [^{18}F]KF, K_{222}, and K_2CO_3, dried by azeotropic distillation with CH_3CN, at 100 °C in CH_3CN for 15 min gave **[^{18}F]6-3** in excellent radiochemical conversion (92%). The radiological TLC for the above-described reaction is shown in Figure 7.14, with the product appearing with a retention time (R_f) of 0.853 and the unreacted [^{18}F]F^- (less than 3%) on the baseline.

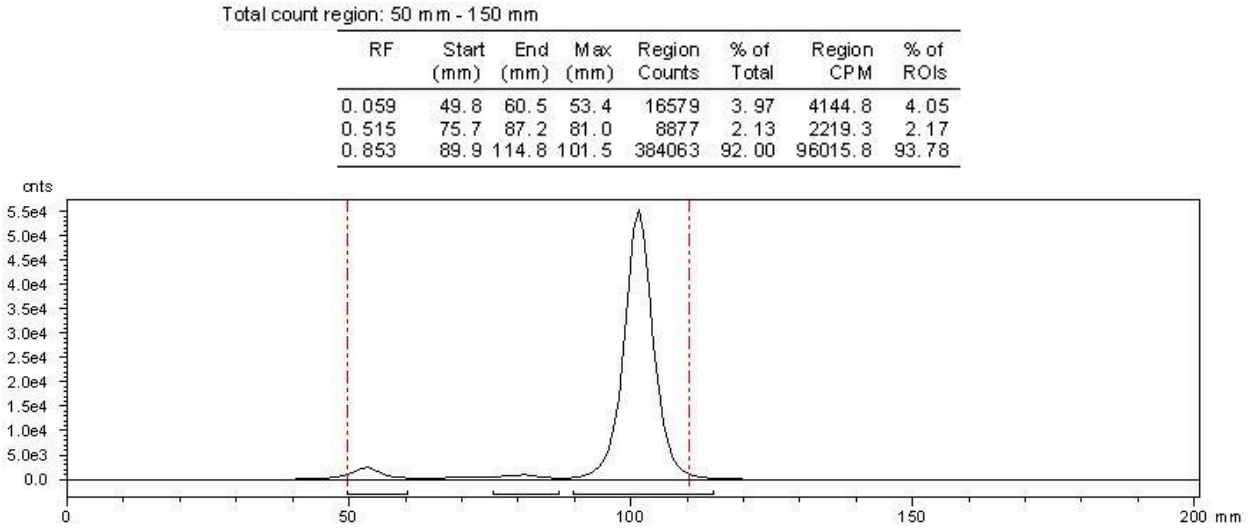

Figure 7.14. Thin-layer radiochromatogram (eluent: CH_2Cl_2/CH_3OH = 9:1) of fluorination of **4-16** with [^{18}F]KF indicating product formation at 0.853 (R_f) in 92% radiochemical conversion.

An analytical HPLC method was optimized for the purification of **[^{18}F]6-3**. Following completion of the reaction, the reaction mixture was diluted with water (1 mL), and 30 µL of the diluted mixture was injected directly into the HPLC instrument. The aliquot was injected onto a Nucleosil C18 column (250 x 4.6 mm; 5 µm) with a flow rate of 1.8 mL/min of 24% CH_3CN in H_2O (isocratic). The HPLC traces including UV channel (λ = 200 nm) and radioactivity channel for the fluorination of **4-16** are shown in Figure 7.15. The excess starting material precursor peak was detected on the UV channel at 12.1 min, which was confirmed against a standard precursor trace. Three other peaks were observed, eluting with the solvent front, at 2.0 and 3.9 minutes,

and these peaks can be attributed to excess K_{222}, possible non-radioactive side-product formation, or impurities. As expected, the major product peak was observed on the radioactive channel at 9.9 minutes. A very small amount of unreacted [^{18}F]KF was observed at 1.4 minutes. Thus, this analytical HPLC method was optimized with over 2 minutes of separation between the product (9.9 min) and the starting material precursor (12.1 min).

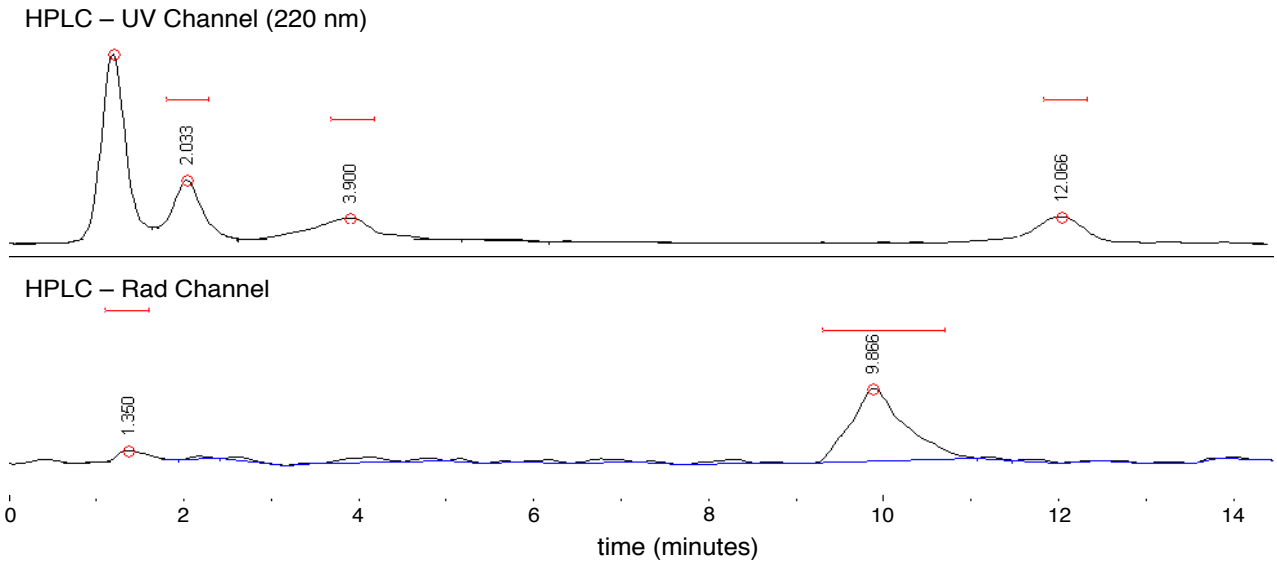

Figure 7.15. HPLC Chromatogram of radiosynthesis of **[^{18}F]6-3** on UV channel (λ = 220 nm; *top*) and radioactive channel (*bottom*).

§7.3.5 Radiosynthesis of [^{18}F]BLT-F Theranostic Conjugate via "Click"

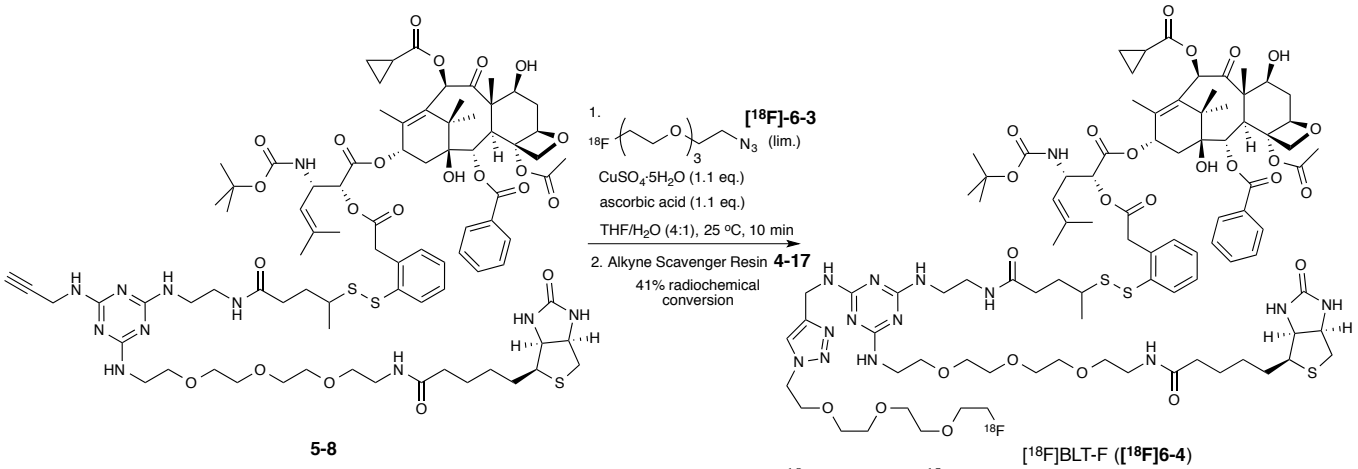

Scheme 7.5. Chemical radiosynthesis of [^{18}F]BLT-F (**[^{18}F]6-4**).

Fluorinated-PEG prosthetic **[^{18}F]6-3** was treated with acetylene drug conjugate precursor **5-8** in the presence of copper sulfate and ascorbic acid to give [^{18}F]BLT-F (**[^{18}F]6-4**). The reaction was allowed to progress for 10 minutes before alkyne scavenger resin **4-17** was added to consume excess unreacted precursor **5-8**. The radio-TLC trace is shown in Figure 7.16, with the product appearing with a retention time (R_f) of 0.529 and the unreacted **[^{18}F]6-3** appearing with

an R_f of 0.824. Some side product formation may account for the radioactivity detected at the baseline.

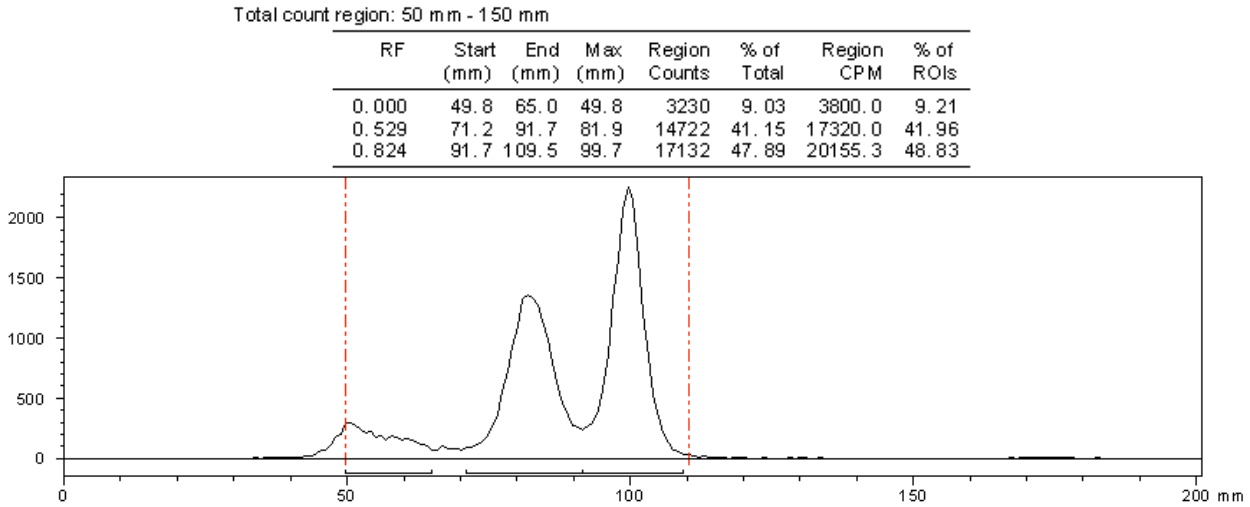

Figure 7.16. Thin-layer radiochromatogram (eluent: CH_2Cl_2/CH_3OH = 9:1) of the "click" reaction with **5-8** and **[^{18}F]6-3** indicating product formation at 0.853 (R_f) in 41% radiochemical conversion.

With over 40% conversion of the fluorinated prosthetic to [^{18}F]BLT-F, these conditions may be further optimized for increased radiochemical conversion by varying reaction duration, temperature, and concentration.

§7.4 Summary

Three novel PET radiotracers were designed for elucidation of the biodistribution profiles of SB-T-1214, a small molecule biotin derivative, and a larger biotin- and taxoid-based SMDC. Rapid methylation of a novel vinylstannyl-taxoid with methyl iodide as a limiting reagent gave SB-T-1214 as an isolatable product by HPLC. Product formation was confirmed by LC-MS with the expected *m/z* 854. Since SB-T-1214 has been previously shown to be more effective than paclitaxel or docetaxel in multidrug resistant tumor cell lines, this radiolabeled taxoid may demonstrate a unique biodistribution profile compared to the parent taxanes.

Furthermore, a small-molecule biotin derivative, [^{18}F]biotin-PEG-F, was developed to show the biodistribution pattern of biotin in tumor-bearing mice and validate its potential as a tumor-targeting module *in vivo*. Fluorination conditions were screened with [^{18}F]KF, K_{222}, and K_2CO_3 with varying solvents, temperatures, reaction duration, and concentrations. At 85 °C for 13 minute, 30% radiochemical conversion as observed. However, higher radiochemical conversion may be obtained at higher temperatures in DMSO. Following analytical HPLC method development, the starting material precursor and radiolabeled product were separated with greater than 4 minutes difference in retention times.

In addition, a theranostic conjugate, BLT-F, was developed as a companion imaging agent for the biotin-linker-taxoid SMDC series. Rapid fluorination of a prosthetic with [^{18}F]KF, K_{222}, and K_2CO_3 was achieved in 92% radiochemical yield, followed by "click" chemistry to introduce the radiolabeled prosthetic to a biotin- and taxoid-based drug delivery scaffold. Product formation was confirmed on radio-TLC, and current optimization of these reaction conditions is in progress.

Continuous development of these three radiotracers for [^{11}C]- and [^{18}F]-labeling is currently on going. Subsequent live-animal PET biodistribution studies on these three radiotracers in tumor-bearing mice will be performed and reported in due course.

§7.5 Experimental

§7.5.1 Caution

Taxoids have been identified as potent cytotoxic agents. Thus, all drugs and structurally related compounds and derivatives must be considered mutagens and potential reproductive hazards for both males and females. All appropriate precautions, such as the use of gloves, goggles, labware, and fume hood, must be taken while handling the compounds at all times. Exposure to radioactive materials has been identified as a potential health hazard for cancer and teratogenic and genetic mutations. Thus, all radioactive sources, compounds, and contaminated materials must be considered potential hazards, and all appropriate precautions, such as the use of gloves, goggles, labware, fume hood, shielding, and radioactive decontamination protocols must been taken while handling the compounds at all times.

§7.5.2 General Information

TLC was performed on Sorbent Technologies aluminum-backed Silica G TLC plates (Sorbent Technologies, 200 μm, 20 x 20 cm), and column chromatography was carried out on silica gel 60 (Merck, 230-400 mesh ASTM). Purity was determined with a Shimadzu L-2010A HPLC HT series HPLC assembly, using a Kinetex PFP column (4.6 mm x 100 mm, 2.6 μm) with a methanol-water or acetonitrile-water gradient solvent system. Low resolution mass spectrometry analysis was carried out on an Agilent LC-MSD at the Institute of Chemical Biology and Drug Discovery, Stony Brook, NY. High resolution mass spectrometry analysis was carried out on an Agilent LC-UV-TOF mass spectrometer at the Institute of Chemical Biology and Drug Discovery, Stony Brook, NY or at the Mass Spectrometry Laboratory, University of Illinois at Urbana-Champaign, Urbana, IL.

§7.5.3 Materials

The chemicals were purchased from Sigma-Aldrich, Fisher Scientific, and VWR International, and used as received or purified before use by standard methods. Tetrahydrofuran was freshly distilled from sodium and benzophenone. Dichloromethane was also distilled immediately prior to use under nitrogen from calcium hydride. 3'-dephenyl-3'-(2-methyl-2-tributylstannyl-1-propenyl)-10-(cyclopropanecarbonyl)docetaxel (**7-3**) was prepared by co-worker Dr. Joshua D. Seitz and used as received.[21, 22] An aqueous solution of [^{18}F]KF was produced by a cyclotron at Brookhaven National Laboratory and used immediately following receipt.

§7.5.4 Experimental Procedure

SB-T-1214 via Rapid Methylation (Cold Synthesis)

To a solution of tetrakis(triphenylphosphine)palladium(0) (1.0 mg, 0.886 μmol) in DMF (100 μL) was added a solution of methyl iodide (12.6 μg, 0.0886 μmol) in DMF (100 μL), and the solution was added to a suspension of copper(I)-thiophene-2-carboxylate (0.17 mg, 0.886 μmol) and 3'-dephenyl-3'-(2-methyl-2-tributylstannyl)-10-(cyclopropanecarbonyl)docetaxel (**7-3**) (1.0

mg, 0.886 μmol) in DMF (100 μL). The reaction mixture was heated to 60 °C and allowed to react for 5 min with stirring. The reaction was quenched with methanol (300 μL), and the reaction mixture was passed through a solid-phase extraction filter. The filtrate was analyzed by HPLC and LC-MS with a Kinetex PFP column (2.6 μm, 100 x 4.6 mm) and a flow rate of 1.0 mL/min with a gradient of 60→95% CH_3OH in H_2O from the 0–40 min period. HRMS (TOF) for $C_{45}H_{60}NO_{15}^+$ calcd: 854.3957. Found: 854.3965 (Δ = 0.9 ppm). Desired taxoid SB-T-1214 (**2-4**): t = 17.7 min.

[^{18}F]Biotin-PEG$_3$-F ([^{18}F]4-20):
No-carrier-added aqueous [^{18}F]fluoride was produced in a cyclotron by the $^{18}O(p,n)^{18}F$ reaction and received as an aqueous solution of [^{18}F]KF. A volume of [^{18}F]KF solution (0.3 mL, 1.355 mCi) was added to a reaction vial containing Kryptofix 2.2.2 (6.0 mg) and K_2CO_3 (2.1 mg). Azeotropic distillations were conducted with 200 μL aliquots CH_3CN (6 mL) at 100 °C under a gentle stream of argon until a white residue formed along the reaction vial. A solution of **4-19** (1.7 mg, 2.94 μmol) in CH_3CN (300 μL) was added to the reaction vial containing fluoride, and the mixture was sealed and stirred for 13 min at 85 °C in an oil bath. After venting of the system with a needle, the crude compound was dissolved in water (1 mL). Reaction progress was monitored by radio-TLC with CH_2Cl_2/CH_3OH (9:1) as eluent, and the desired product **[^{18}F]4-20** had an R_f of 0.309 with 30% radiochemical conversion. The crude compound was injected onto reverse-phase HPLC (LC-MS) for analysis with a Luna PFP column (5 μm, 250 x 4.6 mm) and a flow rate of 1.0 mL/min with 10% CH_3CN in H_2O (isocratic). The starting material precursor (**4-19**) was detected by TIC (*m/z* 579) and eluted with a retention time of 12.1 min. The product **[^{18}F]4-20** was detected by TIC (*m/z* 503) and eluted with a retention time of 9.9 min.

1-Azido-2-[2-[2-[2-[^{18}F]fluoroethoxy]ethoxy]ethoxy]ethane ([^{18}F]6-3):
No-carrier-added aqueous [^{18}F]fluoride was produced in a cyclotron by the $^{18}O(p,n)^{18}F$ reaction and received as an aqueous solution of [^{18}F]KF. A volume of [^{18}F]KF solution (0.3 mL, 868 mCi) was added to a reaction vial containing Kryptofix 2.2.2 (6.5 mg) and potassium carbonate (4.3 mg). Azeotropic distillations were conducted with 200 μL aliquots CH_3CN (6 mL) at 100 °C under a gentle stream of argon until a white residue formed along the reaction vial. A solution of **4-16** (1.7 mg, 5.72 μmol) in CH_3CN (350 μL) was added to the reaction vial containing fluoride, and the mixture was sealed and stirred for 20 min at 100 °C in an oil bath. After venting of the system with a needle and cooling to room temperature, the solvent was evaporated with a gentle stream of argon. The crude compound was dissolved in acetonitrile (1 mL). Reaction progress was monitored by radio-TLC with CH_2Cl_2/CH_3OH (9:1) as eluent, and the desired product **[^{18}F]6-3** had an R_f of 0.853 with 92% radiochemical conversion. The crude compound was injected onto reverse-phase HPLC for analysis with a Nucleosil C18 column (5 μm, 250 x 4.6 mm) and a flow rate of 1.8 mL/min with 24% CH_3CN in H_2O (isocratic). The starting material precursor (**4-16**) was detected by the UV channel at λ = 200 nm and eluted with a retention time of 12.1 min. The product was detected by the radioactive channel and eluted with a retention time of 9.9 min.

[^{18}F]BLT-F ([^{18}F]6-4):
To a solution of **5-8** (5 mg, 2.90 μmol) and ascorbic acid (4 mg, 22.7 μmol) in THF (0.4 mL) was added **[^{18}F]6-3** in THF (0.2 mL), followed by $CuSO_4 \cdot 5H_2O$ (4 mg, 16 μmol) in H_2O (0.15 mL), and the mixture was allowed to react for 10 min at 25 °C with stirring. Alkyne scavenger **4-17** (3

mg) was added to consume unreacted precursor **5-8**, and the reaction was quenched with CH_3CN (1 mL). Reaction progress was monitored by radio-TLC with CH_2Cl_2/CH_3OH (9:1) as eluent, and the desired product **[^{18}F]6-4** had an R_f of 0.521 with 41% radiochemical conversion. Subsequent reaction optimization under hot conditions and purification by reverse-phase HPLC is currently under development.

§7.6 References

1. Miller, P. W.; Long, N. J.; Vilar, R.; Gee, A. D. Synthesis of [11C], [18F], [15O], and [13N] radiolabels for positron emission tomography. *Angew. Chem. Int. Ed.* **2008,** 47, 8998-9033.
2. Ametamey, S. M.; Honer, M.; Schubiger, P. A. Molecular imaging with PET. *Chem. Rev.* **2008,** 108, 1501-1516.
3. Wood, K. A.; Hoskin, P. J.; Saunders, M. I. Positron emission tomography in oncology: A review. *Clin. Oncol.* **2007,** 19, 237-255.
4. Weber, W. A. Positron emission tomography as an imaging biomarker. *J. Clin. Oncol.* **2006,** 24, 3282-3292.
5. Oriuchi, N.; Higuchi, T.; Ishikita, T.; Miyakubo, M.; Hanaoka, H.; Ilda, Y.; Endo, K. Present role and future prospects of positron emission tomography in clinical oncology. *Cancer Sci.* **2006,** 97, 1291-1297.
6. Schwaiger, M.; Ziegler, S.; Nekolla, S. G. PET/CT: challenge for nuclear cardiology. *J. Nucl. Med.* **2005,** 46, 1664-1678.
7. Herholz, K.; Heiss, W. D. Positron emission tomography in clinical neurology. *Mol. Imaging Biol.* **2004,** 6, 239-269.
8. Wu, C. Y.; Pike, V. W.; Wang, Y. M. Amyloid imaging: From benchtop to bedside. *Curr. Top. Dev. Biol.* **2005,** 70, 171-213.
9. Wolf, A. P.; Redvantly, C. S. Carbon-11 and radiopharmaceuticals. *Appl. Radiat. Isot.* **1977,** 28, 29-48.
10. Ferreiri, R. A.; Wolf, A. P. The chemistry of positron emitting nucleogenic (hot) atoms with regard to preparation of labelled compounds of practical utility. *Radiochim. Acta* **1983,** 34, 69-84.
11. Bolton, R. Isotopic methylation. *J. Labelled Compd. Radiopharm.* **2001,** 44, 701-736.
12. Långström, B.; Antoni, G.; Gullberg, P.; Halldin, C.; Malmborg, P.; Nagren, K.; Rimland, A.; Svard, H. Synthesis of L-and D-[methyl-11C] methionine. *J. Nucl. Med.* **1987,** 28, 1037-1040.
13. Larsen, P.; Ulin, J.; Dahlstrom, K.; Jensen, M. Synthesis of [11C] iodomethane by iodination of [11C] methane. *Appl. Radiat. Isot.* **1997,** 48, 153-157.
14. Link, J. M.; Krohn, K. A.; Clark, J. C. Production of [11C] CH3I by single pass reaction of [11C] CH4 with I2. *Nucl. Med. Biol.* **1997,** 24, 93-97.
15. Hosoya, T.; Sumi, K.; Doi, H.; Wakao, M.; Suzuki, M. Rapid methylation on carbon frameworks useful for the synthesis of 11 CH 3-incorporated PET tracers: Pd (0)-mediated rapid coupling of methyl iodide with an alkenyltributylstannane leading to a 1-methylalkene. *Org. Biomol. Chem.* **2006,** 4, 410-415.
16. Hamill, T. G.; Krause, S.; Ryan, C.; Bonnefous, C.; Govek, S.; Seiders, T. J.; Cosford, N. D. P.; Roppe, J.; Kamenecka, T.; Patel, S.; Gibson, R. E.; Sanabria, S.; Riffel, K.; Eng, W. S.; King, C.; Yang, X. Q.; Green, M. D.; O'Malley, S. S.; Hargreaves, R.; Burns, H. D. Synthesis,

characterization, and first successful monkey imaging studies of metabotropic glutamate receptor subtype 5 (mGluR5) PET radiotracers. *Synapse* **2006,** 56, 205-216.
17. Andersson, Y.; Cheng, A.; Langstrom, B. Palladium-promoted coupling reactions of [11C]methyl iodide with organotin and organoboron compounds. *Acta Chem. Scand.* **1995,** 49, 683-688.
18. Koehler, L.; Gagnon, K.; McQuarrie, S.; Wuest, F. Iodine-124: A promising positron emitter for organic PET chemistry. *Molecules* **2010,** 15, 2686-2718.
19. Kiesewetter, D. O.; Jagoda, E. M.; Kao, C.-H. K.; Ma, Y.; Ravasi, L.; Shimoji, K.; Szajek, L. P.; Eckelman, W. C. Fluoro-, bromo-, and iodopaclitaxel derivatives: synthesis and biological evaluation. *Nucl. Med. Biol.* **2003,** 30, 11-24.
20. van Tilburg, E. W.; Franssen, E. J. F.; van der Hoeven, J. J. M.; van der Meij, M.; Elshove, D.; Lammertsma, A. A.; Windhorst, A. D. Radiosynthesis of [11C]docetaxel. *J. Labelled Comp. Radiopharm.* **2004,** 47, 763-777.
21. Seitz, J. D.; Vineberg, J. G.; Ojima, I. Synthesis of a next-generation taxoid by rapid methylation amenable for [11C]-labeling. *J. Org. Chem.*, To be submitted shortly.
22. Seitz, J. D. The design, synthesis and biological evaluation of novel taxoid anticancer agents and their tumor-targeted drug conjugates (Doctoral Dissertation). State University of New York at Stony Brook, 2013.
23. Morita, D. K.; Stille, J. K.; Norton, J. R. Methyl/phenyl exchange between palladium and a phosphine ligand. Consequences for catalytic coupling reactions. *J. Am. Chem. Soc.* **1995,** 117, 8576-8581.
24. Hinkle, R. J.; Poulter, G. T.; Stang, P. J. Palladium (II) and copper (I) cocatalyzed coupling of stereodefined alkenyl (phenyl) iodonium triflates and unsaturated tri-n-butylstannanes. *J. Am. Chem. Soc.* **1993,** 115, 11626-11627.
25. Liebeskind, L. S.; Fengl, R. W. 3-Stannylcyclobutenediones as nucleophilic cyclobutenedione equivalents. Synthesis of substituted cyclobutenediones and cyclobutenedione monoacetals and the beneficial effect of catalytic copper iodide on the Stille reactio. *J. Org. Chem.* **1990,** 55, 5359-5364.
26. Farina, V.; Kapadia, S.; Krishnan, B.; Wang, C.; Liebeskind, L. S. On the nature of the "copper effect" in the Stille cross-coupling. *J. Org. Chem.* **1994,** 59, 5905-5911.
27. Kim, D. W.; Choe, Y. S.; Chi, D. Y. A new nucleophilic fluorine-18 labeling method for aliphatic mesylates: Reaction in ionic liquids show tolerance for water. *Nucl. Med. Biol.* **2003,** 30, 345-350.
28. Been, L. B.; Suurmeijer, A. J.; Cobben, D. C.; Jager, P. L.; Hoekstra, H. J.; Elsinga, P. H. [18F]FLT-PET in oncology: current status and opportunities. *Eur. J. Nucl. Med. Mol. Imaging* **2004,** 31, 1659-1672.
29. Mukherjee, J.; Yang, Z. Y.; Das, M. K.; Brown, T. Fluorinated benzamide neuroleptics - III. Development of (S)-N-[(1-allyl-2-pyrrolidinyl)methyl]-5-(3-[18F]fluoropropyl)-2, 3-dimethoxybenzamide as an improved dopamine D-2 receptor tracer. *Nucl. Med. Biol.* **1995,** 22, 283-296.
30. Kilbourn, M. R.; Welch, M. J.; Dence, C. S.; Tewson, T. J.; Saji, H.; Maeda, M. Carrier-added and no-carrier-added syntheses of [18F]spiroperidol and [18F]haloperidol. *Int. J. Appl. Radiat. Isot.* **1984,** 35, 591-598.
31. Hamacher, K.; Hamkens, W. Remote controlled one-step production of 18F labeled butyrophenone neuroleptics exemplified by the synthesis of nca [18F] N-methylspiperone. *Appl. Radiat. Isot.* **1995,** 46, 911-916.

32. Grierson, J. R.; Link, J. M.; Mathis, C. A.; Rasey, J. S.; Krohn, K. A. A radiosynthesis of fluorine-18 fluoromisonidazole. *J. Nucl. Med.* **1989,** 30, 343-350.
33. Park, B. K.; Kitteringham, N. R.; O'Neill, P. M. Metabolism of fluorine-containing drugs. *Annu. Rev. Pharmacol. Toxicol.* **2001,** 41, 443-470.
34. Bohm, H. J.; Banner, D.; Bendels, S.; Kansy, M.; Kuhn, B.; Muller, K.; Obst-Sander, U.; Stahl, M. Fluorine in medicinal chemistry. *ChemBioChem* **2004,** 5, 637-643.
35. Bégué, J.; Bonnet-Delpon, D. Recent advances (1995-2005) in fluorinated pharmaceuticals based on natural products. *J. Fluor. Chem.* **2006,** 127, 992-1012.
36. Claesener, M.; Breyholz, H. J.; Hermann, S.; Faust, A.; Wagner, S.; Schober, O.; Schafers, M.; Kopka, K. Efficient synthesis of a fluorine-18 labeled biotin derivative. *Nucl. Med. Biol.* **2012,** 39, 1189-1194.
37. Kudo, T.; Ueda, M.; Konishi, H.; Kawashima, H.; Kuge, Y.; Mukai, T.; Miyano, A.; Tanaka, S.; Kizaka-Kondoh, S.; Hiraoka, M.; Saji, H. PET imaging of hypoxia-inducible factor-1-active tumor cells with pretargeted oxygen-dependent degradable streptavidin and a novel 18F-labeled biotin derivative. *Mol. Imaging Biol.* **2011,** 13, 1003-1010.
38. Betzel, T.; Muller, C.; Groehn, V.; Muller, A.; Reber, J.; Fischer, C. R.; Kramer, S. D.; Schibli, R.; Ametamey, S. M. Radiosynthesis and preclinical evaluation of 3'-Aza-2'-[(18)F]fluorofolic acid: a novel PET radiotracer for folate receptor targeting. *Bioconjug. Chem.* **2013,** 24, 205-214.
39. Morris, R. T.; Joyrich, R. N.; Naumann, R. W.; Shah, N. P.; Maurer, A. H.; Strauss, H. W.; Uszler, J. M.; Symanowski, J. T.; Ellis, P. R.; Harb, W. A. Phase II study of treatment of advanced ovarian cancer with folate-receptor-targeted therapeutic (vintafolide) and companion SPECT-based imaging agent (99mTc-etarfolatide). *Ann. Oncol.* **2014,** 25, 852-858.

Chapter 8

Folate-Linker-Taxoid Tumor-targeting Drug Conjugates

Chapter Contents

§8.1 Introduction

§8.1.1 Folic Acid: A B-Class Vitamin

Folic acid (vitamin B_9 or vitamin M) is a B-class vitamin that is produced synthetically and obtained by mammals externally through the diet.[1] While oxidized folates, such as folic acid, are not biologically active, once reduced in the liver following intestinal absorption and metabolism, reduced forms of the vitamin carry out biological functions such as single-carbon methylation reactions and *de novo* synthesis of nucleotide bases.[2] The various coenzymes and derivatives of folic acid play a role in DNA synthesis, repair, and methylation, and serve as cofactors in numerous other biochemical reactions, such as the interconversion of serine and glycine, and histidine catabolism.[1]

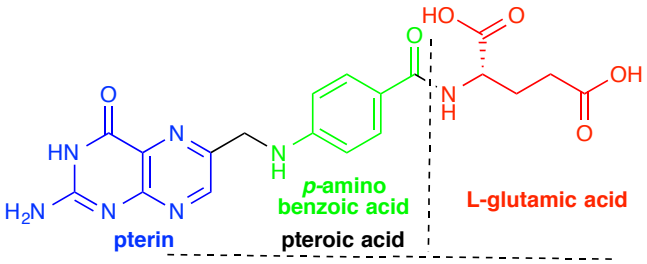

Folic Acid

Figure 8.1. Chemical structure of folic acid. Adapted from reference [2].

Folic acid consists of a pteroyl group, comprised of a pterin moiety connected to *p*-aminobenzoic acid, and a chiral side chain of L-glutamic acid. The chemical structure of folic acid and its components are illustrated in Figure 8.1.

§8.1.2 The Folate Receptor: A Tumor-Specific Biomarker

Folic acid and its reduced derivatives are internalized into cells via three different pathways: (1) receptor-mediated endocytosis via the folate receptor (FR); (2) anion transport via the reduced folate carrier that can shuttle folate molecules directly into the cell; and (3) via the proton-coupled folate transporter.[2]

Folic acid has shown a remarkably high binding affinity ($K_d \sim 10^{-10}$ M) for the alpha isoform of the folate receptor (α-FR), a glycosylphosphatidylinositol-linked membrane protein that binds to folic acid and folate-tagged ligands and internalizes them *via* receptor-mediated endocytosis through a nonharmful endosomal pathway that is recycling, nondegradative, and nonlysosomal.[2-4] Folate, when attached via its γ-carboxylate to low- or high-molecular weight therapeutic or imaging agents, retains its ability to bind to the α-folate receptor without reduced affinity and enter the cell by RME; the number of molecules internalized is large, over 10^6 per hour.[4] In addition, folate and its reduced counterparts are stable during storage, non-immunogenic, and do not interfere with extravasation and intracellular division.[4] The folate-receptor mediated endocytosis of FA-based SMDCs is shown in Figure 8.2.

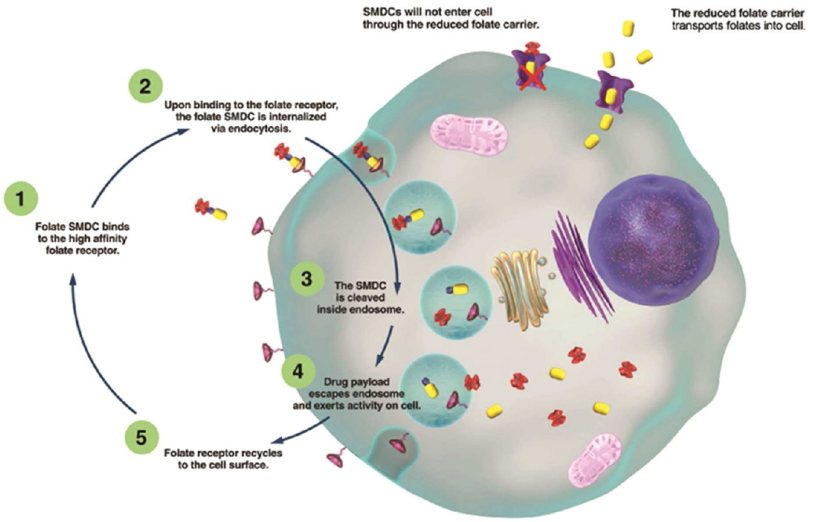

Figure 8.2. Tumor cellular uptake of a FA-based SMDC by FR-mediated endocytosis. Reprinted from reference [2].

The α-folate receptor is overexpressed on approximately 40% of human cancers in a wide variety of tumors,[5] such as breast, kidney, ovary, colon, brain, and hematologic malignancies, yet absent in most normal and healthy tissues.[2, 6-10] The concentration of folic acid in human serum and extracellular fluids is very low (approximately 2×10^{-8} M), and so expression of α-FR enables cancer cells to compete more aggressively for the vitamin.[11] Uptake of folates into virtually all cells of the body is mediated by either the reduced folate carrier,[12] or the proton coupled folate transporter.[5, 13] However, folate-based small-molecule drug conjugates (SMDCs) are not substrates of either the reduced folate carrier or the proton-coupled folate transporter, and thus internalization of these drug conjugates in FR-negative normal cells does not occur.[14]

In addition to its overexpression on the tumor cell surface in malignant cells, the α-FR is also present on the apical membrane of proximal tubules in the kidney, which recovers folate from urine filtered through the glomeruli and recycles it to the blood stream.[6] However, the pathway for the trafficking of folates in the kidneys differs from RME in that the folates undergo a receptor-mediated transcytosis in the proximal tubule cells in lysosome-like compartments.[6, 15] Despite accumulation in the kidney, renal toxicities are not typically observed in preclinical and clinical studies of folate-targeted drugs.[16-18] Uptake of folate in the kidneys is characterized by a rapid luminal entry into proximal tubules followed by a slow cytoplasmic transport, though folate is not stored in high concentrations within the PT cell cytoplasm.[6, 19] Most folate or folate conjugate initially accumulates within a lysosomal compartment, but is soon transferred from the apical to the basolateral domain via a transcytotic pathway, and the majority of folate undergoes FR-mediated transtubular transport from the lumen back to the bloodstream largely intact.[6]

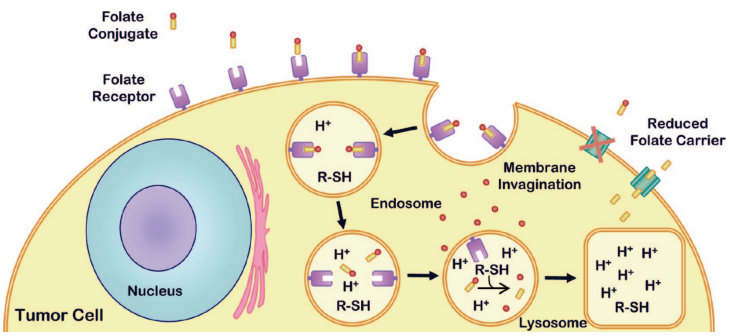

Figure 8.3. FR-mediated endocytosis of a folic acid drug conjugate. Reprinted from reference [20].

As a low molecular weight ligand that circumvents many of the limitations associated with antibody-mediated carriers and other macromolecular delivery molecules, folic acid has become widely recognized as a tumor-targeting module to deliver molecular payloads ranging from small radionuclides to large DNA and liposomal constructs successfully to cancer cells *via* the α-folate receptor.[2] Oxidized folates, which include FA-mediated SMDCs, display the highest affinity for the α-FR and, once internalized across the cell membrane, become exposed to a mildly acidic endosomal microenvironment, endogenous thiols such as glutathione (GSH), and specific enzymatic proteases.[2, 21, 22] Changes in the endosome result in the detachment of folic acid from the drug payload as the vitamin recycles back outside the cell membrane.[2] Folate receptor-targeted disulfide-linked drugs typically (1) remain intact in blood circulation for at least 30 min, (2) rapidly localize to FR on the apical membrane of the proximal tubule cells, (3) undergo partial but incomplete reduction during trafficking in PTs, (4) are reduced during prolonged circulation outside of the kidney, and (5) eventually are excreted through the kidneys.[6] The internalization of FA-based SMDCs and subsequent drug release via disulfide reduction is illustrated in Figure 8.3.

§8.1.3 Folate-based Drug Conjugates in Clinical Development

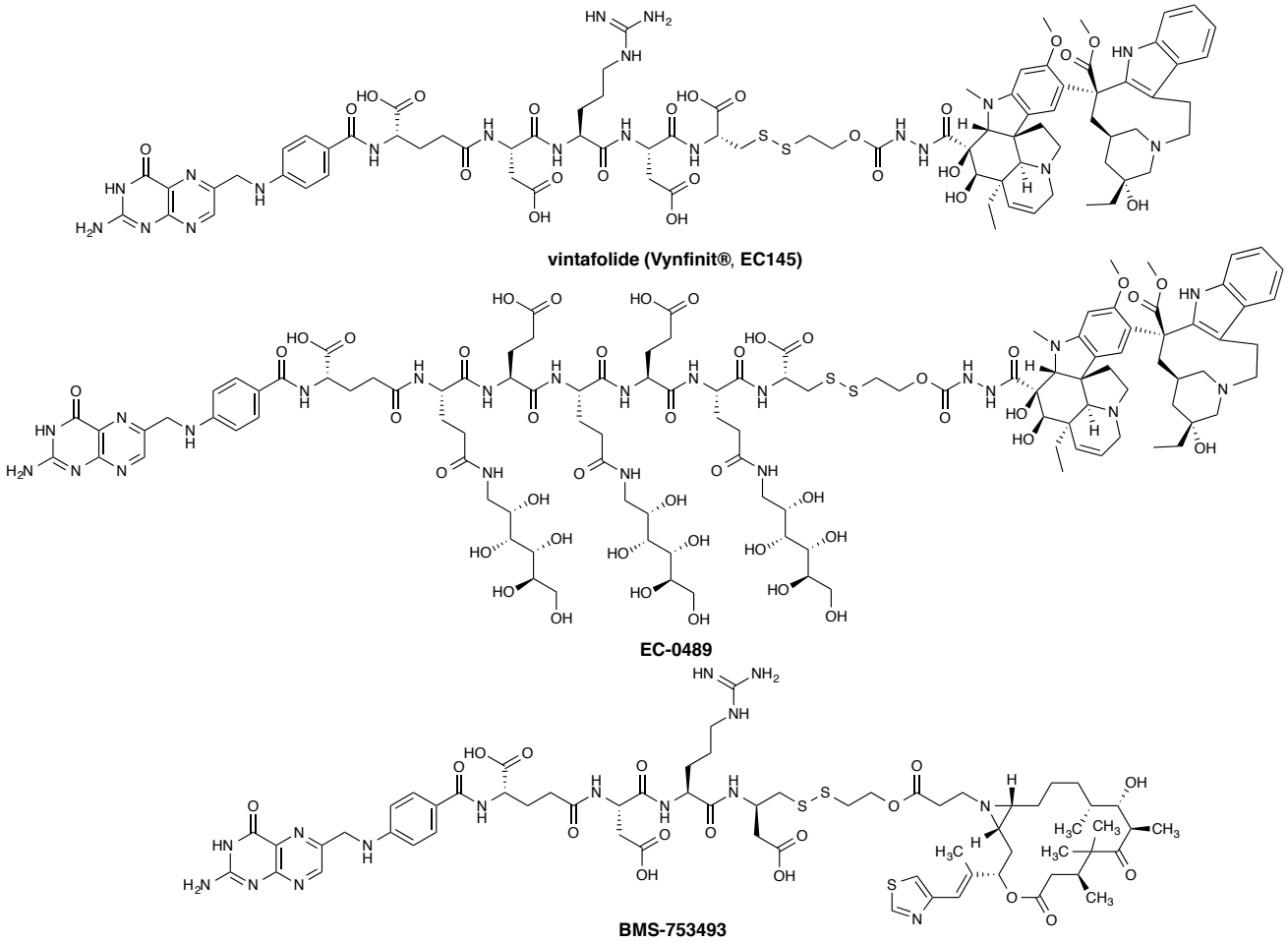

Figure 8.4. Chemical structures of folate-based SMDCs under development.

Several folate-based SMDCs have been or are currently under evaluation in clinical trials, shown in Figure 8.4.[2] Vintafolide (Vynfinit®), developed by Endocyte and licensed to Merck in 2012 for development, manufacturing, and commercialization for $120M and up to $1B in milestone incentives, had received conditional regulatory approval in the European Union (EU) for treatment of platinum-resistant ovarian cancer in combination with liposomal doxorubicin (Doxil).[23] Vintafolide is a FR targeting conjugate of desacetylvinblastine monohydrazide connected via a hydrophilic peptide spacer and a reductively labile disulfide linker.[24] However, in May 2014, Merck halted its Phase III clinical study in U.S. for treatment of the same indication due to futility, and the conditional marketing authorization in the EU was subsequently withdrawn.[25, 26] As of June 2014, vintafolide still remains in Phase IIb clinical trials in combination with docetaxel for treatment of non-small cell lung cancer (NSCLC). A modified derivative of vintafolide, EC0489, was also developed by Endocyte as a folate-desacetylvinblastine monohydrazide conjugate with saccharopeptidic modifications and is currently in Phase I clinical trials for refractory or advanced metastatic cancers.[27] As discussed in Chapter 5, EC0225 was developed as a multi-drug folate conjugate of desacetylvinblastine monohydrazide and mitomycin C and has advanced to Phase I clinical trials for the treatment of refractory or metastatic solid tumors.[28] Epofolate (BMS-753493), a folate conjugate of epothilone A, was developed by Endocyte and Bristol-Myers Squibb and is currently in Phase II clinical trials for treatment of advanced cancers.[29] EC1456 (folate tubulysin), also developed by Endocyte, is a folate conjugate of tubulysin monohydrazide that is currently in Phase I clinical trials.

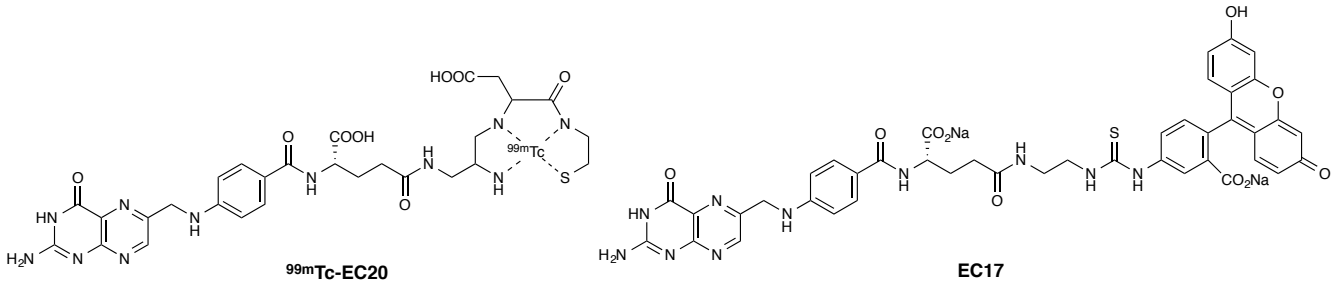

Figure 8.5. Chemical structures of folate-based radiopharmaceuticals and theranostics under development.

Additionally, a number of folate-based radiopharmaceuticals have been developed and evaluated both in preclinical and clinical trials as diagnostic tools for positron emission tomography (PET) and single photon emission tomography (SPECT) of FR-positive cancers, shown in Figure 8.5.[30] Etarfolatide (Folcepri®, ^{99m}Tc-EC20), developed by Endocyte, is a non-invasive folate-targeted molecular imaging agent designed to identify tumors that express folate receptors that may respond to folate-targeted therapy and is being co-developed as the companion imaging agent to vintafolide and EC1456. Etarfolatide had received conditional regulatory approval in the European Union as a companion diagnostic for vintafolide, but the conditional marketing authorization for etarfolatide was withdrawn along with vintafolide in Europe; etarfolatide remains in Phase III clinical trials in the U.S. for FR-positive cancers.[26] EC17 (folate-fluorescein) was also developed by Endocyte as a theranostic targeted hapten and advanced to a Phase II study for the treatment of kidney cancer.[5]

§8.1.4 Taxol-Folic Acid Conjugates

A series of Taxol derivatives covalently tethered at C2' and C7 to folate and glutamates were synthesized and evaluated as prodrugs which release Taxol via hydrolytic cleavage of their α-alkoxy and α-amino esters.[4] However, the most promising of these conjugates, Taxol-7-PEG-Folate, while shown to increase the lifespan in M109 tumor-bearing mice, was less effective than Taxol itself.[4] The most promising of these folate-Taxol conjugates is illustrated in Figure 8.6.

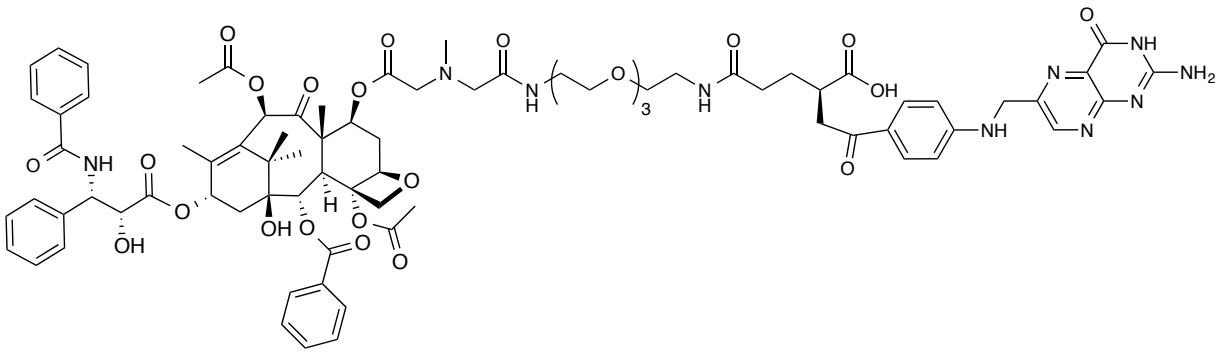

Figure 8.6. Chemical structure of Taxol-folate conjugate. Adapted from reference [4].

Despite the improvement over Taxol in aqueous solubility of the Taxol-folate conjugates, the low water solubility may have prevented the administration of a more effective higher dose in the *in vivo* preclinical studies. Additionally, a more efficient drug release mechanism, rather than through a hydrolytic ester linkage, may be accomplished with an improved linker system, since hydrolysis of the ester linkage was slowed under mildly acidic conditions like those in the endosome.[4] With these considerations in hand, a next-generation folate-dipeptide-PEG-(SS-linker)-taxoid conjugate was designed and synthesized for biological evaluation.

§8.2 Folate-Linker-Taxoid Drug Conjugates

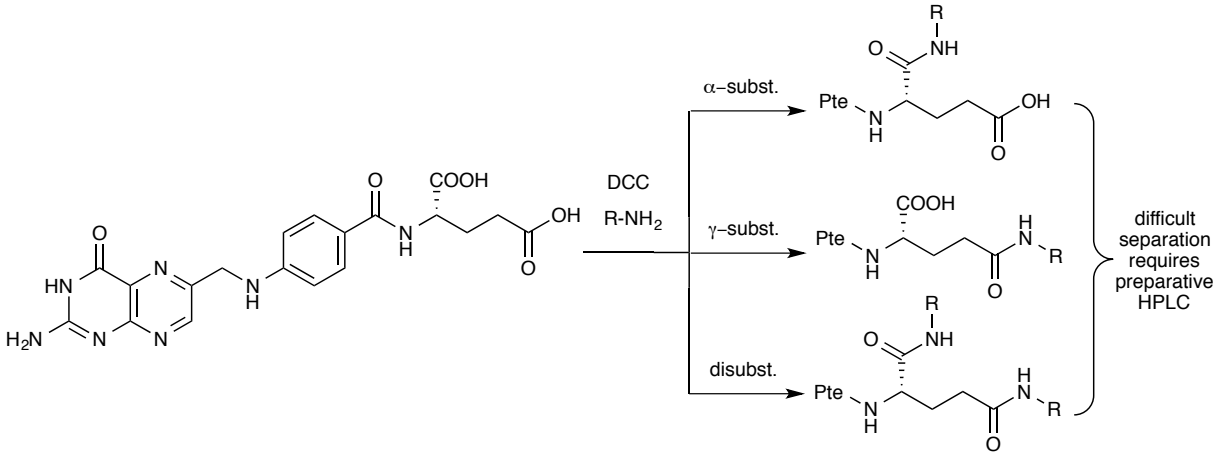

Scheme 8.1. Functionalization of folic acid by DCC coupling.

Folic acid has attracted considerable attention as a tumor-targeting module in small-molecule drug conjugates. However, a major challenge in drug design surrounds the synthetic aspects of folate SMDC preparation. Treatment of folic acid with a coupling reagent, such as DCC, results in a mixture of the inactive α-conjugate, the active γ-conjugate, with the bis-

functionalized derivative and sometimes recovered folic acid (Scheme 8.1); and separation of these mixtures is typically tedious and difficult.[31] Regiospecific functionalization of folic acid at the γ-carboxylate of glutamic acid can be accomplished through coupling of modified glutamates with pteroyl azide or carboxlic acid derivatives.[31]

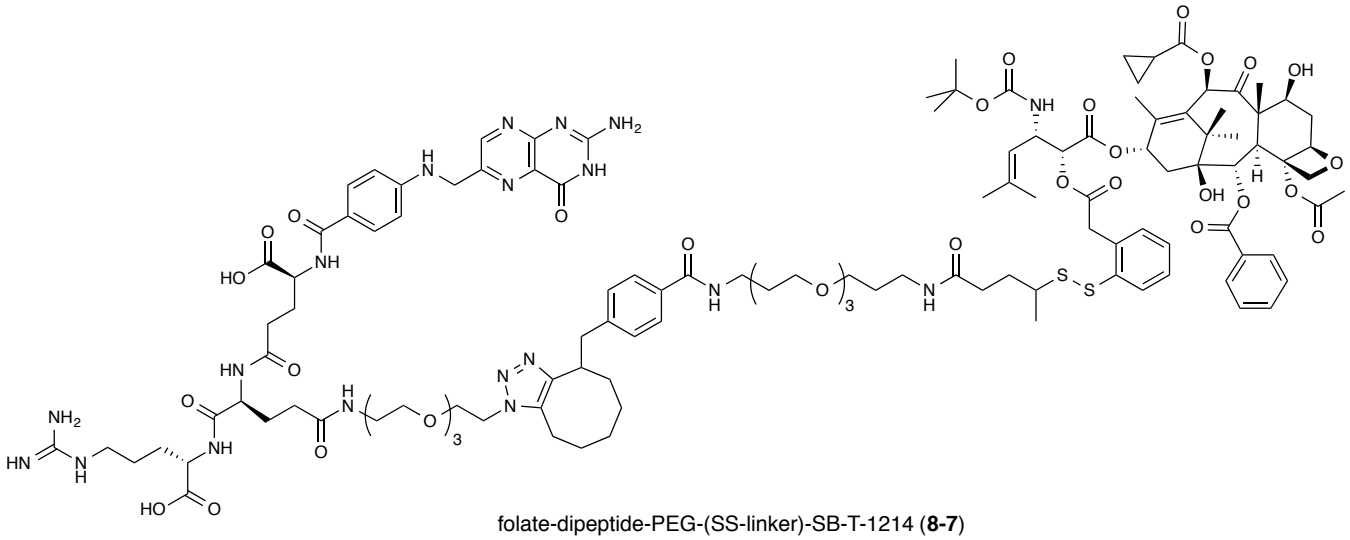

folate-dipeptide-PEG-(SS-linker)-SB-T-1214 (**8-7**)

Figure 8.7. Chemical structure of folate-dipeptide-PEG-(SS-linker)-taxoid (**8-7**).

Folate-based conjugate of SB-T-1214 (**8-7**), illustrated in Scheme 8.7 and first synthesized by former group member Dr. Joshua D. Seitz, was designed to possess improved solubility and be constructed from two smaller units using bioorthogonal copper-free "click" chemistry. The folate targeting moiety was regiospecifically modified at its γ-carboxylate with a PEGylated zwitterionic dipeptide spacer to improve aqueous solubility. Incorporation of charged amino acid residues, such as Asp and Glu, has been shown to suppress the passive diffusion of tumor-targeted SMDCs across the lipophilic cell membrane, thereby decreasing undesired delivery to non-cancerous cells.[28] With a finite number of FRs on the surface of a given tumor cell, on the order of 1–10 million copies per cell, and a recycling rate of 8–12 hours, there is both a lag time and limit to the intracellular drug concentration that can be achieved; and cytotoxic agents with IC_{50} values in the low nM range have been found to be ideal candidates for folate-based drug delivery.[2, 32] Thus, SB-T-1214 was selected as the cytotoxic agent and connected to a PEGylated self-immolative disulfide linker and cyclooctyne terminus for alkyne-azide cycloaddition. Unlike previously designed folate-based conjugates, such as vintafolide and EC0489, in which the active agent desacetylvinblastine hydrazide is released in modified form, intracellular disulfide reduction of **8-7** through thiolactonization releases SB-T-1214 in its active and unmodified form.

§8.2.1 Synthesis of Pteroyl Azide

Regiospecific functionalization of folic acid can be accomplished through a retrosynthetic approach beginning with commercially available and inexpensive folic acid. First, the glutamate side-chain is cyclized to afford a pyrofolic acid derivative, which can be converted to the highly versatile pteroyl azide in an efficient and inexpensive synthesis.

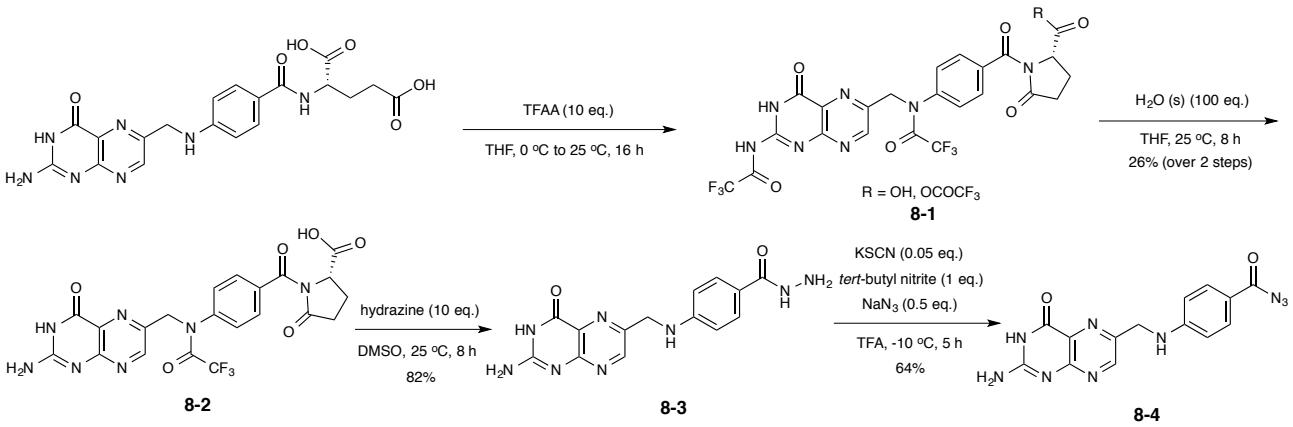

Scheme 8.2. Synthesis of pteroyl azide (**8-4**).

Folic acid was treated with excess trifluoroacetic anhydride at 0 °C to produce $N^{2,10}$-bis(trifluoroacetyl)pyrofolic acid (**8-1**), which was obtained as a mixture of the diacylated anhydride and diacylated carboxylic acid in a 1:4 ratio according to ^{19}F NMR analysis. Stirring of **8-1** with ice water hydrolyzed the N^{2}-trifluoroacetyl substituent as well as any existing anhydride present to give N^{10}-(trifluoroacetyl)pyrofolic acid (**8-2**) as a single compound. Addition of hydrazine to **8-2** cleaved both the N^{10}-trifluoroacetyl substituent and the cyclic glutamate to give pteroyl hydrazide (**8-3**) in good yield (82%) as well as pyroglutamic acid, which was removed by washing with methanol and diethyl ether. Then, treatment of **8-3** with one equivalent of *tert*-butyl nitrite with 5 mol% potassium thiocyanate gave pteroyl azide **8-4** in modest yield (64%), along with N^{10}-nitrosopteroyl azide, which was converted to **8-4** with the addition of sodium azide. The synthesis of pteroyl azide **8-4** shown in Scheme 8.2.

§8.2.2 Synthesis of Folate-Linker-Taxoid

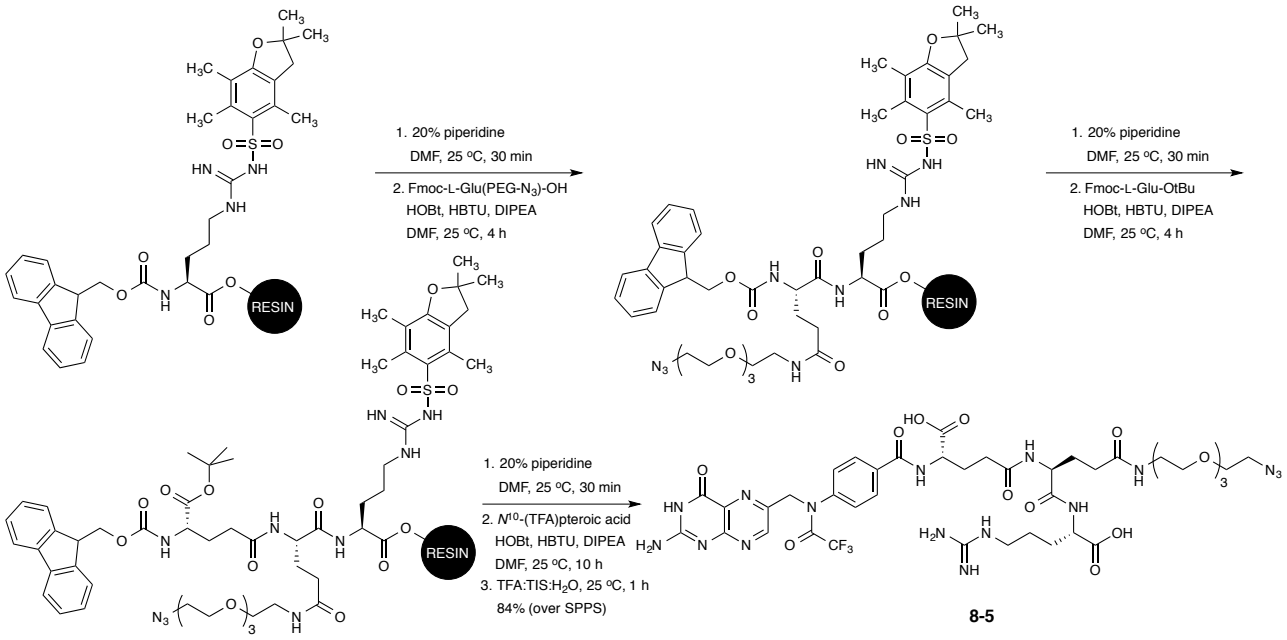

Scheme 8.3. Synthesis of folate-dipeptide-PEG-N_3 (**8-5**).

Regiospecific preparation of folate-γ-dipeptide-PEG-N_3 (**8-5**) was achieved using solid-phase peptide synthesis (SPPS). Starting with Fmoc-Arg(Pbf)-Wang resin, the Fmoc group was first deprotected with piperidine, and the corresponding amine was coupled to Fmoc-Glu(PEG-N_3)-OH in the presence of HOBt, HBTU, and DIPEA. After another Fmoc deprotection, Fmoc-Glu-O*t*Bu was coupled to the resin-bound amine under the same peptide coupling conditions to give the tripeptide intermediate. Following one more Fmoc deprotection, N^{10}-(trifluoroacetyl)pteroic acid was coupled to the resin-bound amine to give the protected folate-dipeptide. Subsequent cleavage from the resin and esterolysis of the *tert*-butyl ester with TFA gave **8-5** in a single step. PEGylated N^{10}-folate-dipeptide **8-5** was isolated in good yield (84%). The SPPS of **8-5** is illustrated in Scheme 8.3.

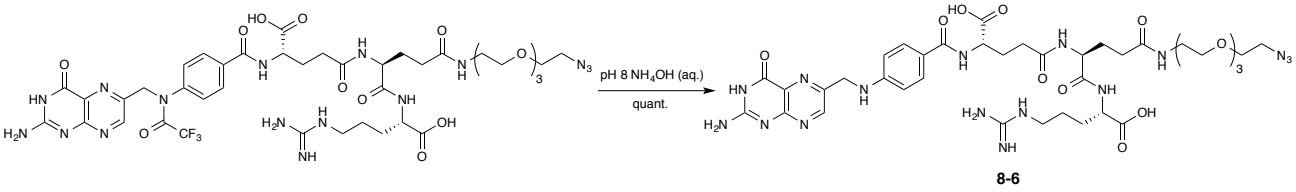

Scheme 8.4. Deprotection of N^{10}-TFA group under mild basic conditions.

Basic hydrolysis of the N^{10}-TFA group of **8-5** with aqueous ammonium hydroxide (pH 8) afforded **8-6** in quantitative yield, shown in Scheme 8.4. Reaction progress was monitored by mass spectrometry. Following completion of the reaction, the aqueous basic solution was removed by lyophilization.

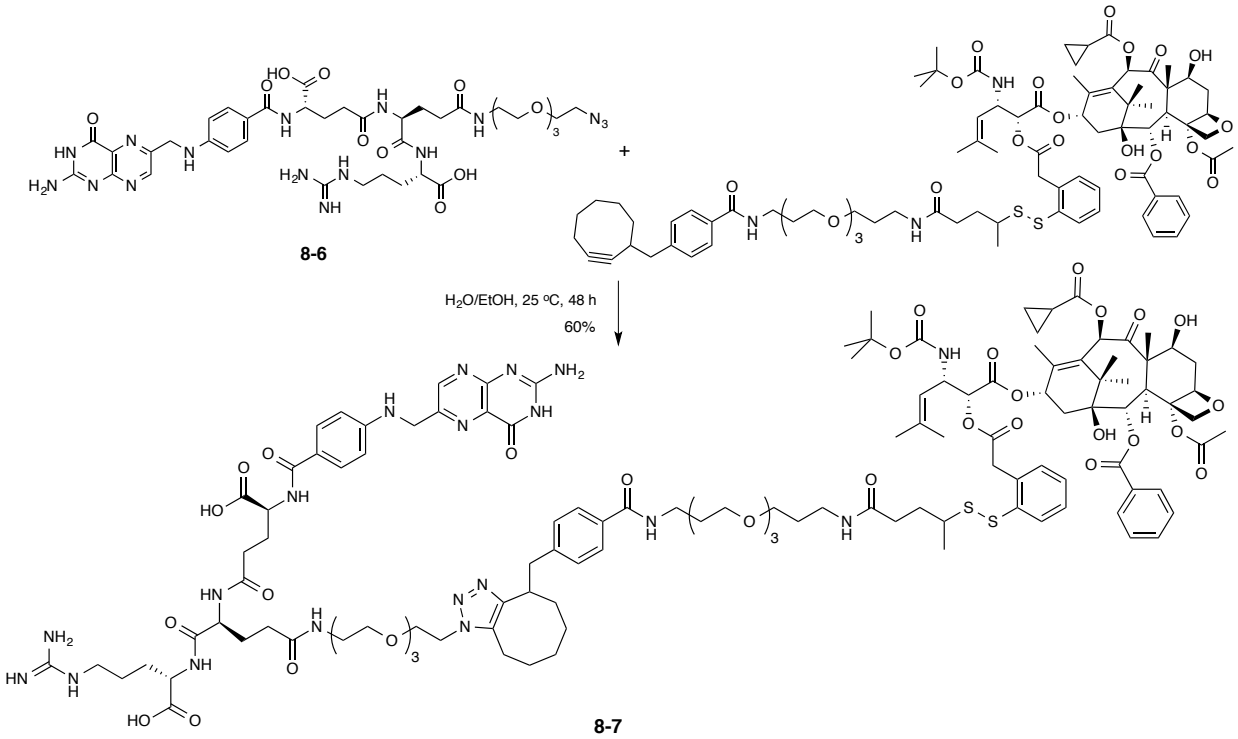

Scheme 8.5. Synthesis of folate-dipeptide-PEG-(SS-linker)-SB-T-1214 (**8-7**).

SB-T-1214-(SS-linker)-PEG-cyclooctyne was designed by Dr. Joshua D. Seitz and prepared by Evan Herlihy under the his guidance. Equimolar amounts of SB-T-1214-(SS-linker)-PEG-cyclooctyne and **8-6** were combined in ethanol:water (1:1), and reaction progress was monitored by mass spectrometry. The product, folate-dipeptide-PEG-(SS-linker)-SB-T-1214 (**8-7**), precipitated out of solution during the reaction and was isolated by centrifugation and filtration in modest yield (40%). Both regioisomers, if present, were treated as a single compound; however, the presence of regioisomers was could not be confirmed by analytical techniques such as ^{1}H NMR and MS. The synthesis is illustrated in Scheme 8.5.

§8.3 Biological Evaluation of Folate-Linker-Taxoid In Vitro

The potency and efficacy of folate-dipeptide-PEG-(SS-linker)-SB-T-1214 (**8-7**) were evaluated *in vitro* against various FR+ and FR- cell lines. The cytotoxicity assays of **8-7** against ID8 (FR^{+++}), MX-1 (FR^{++}), L1210FR (FR^{++}), MCF-7 (FR^{+}), and WI-38 (FR^{-}) were performed by MTT method.[33] As controls for comparison, paclitaxel and parent taxoid SB-T-1214 were evaluated as well. The results for 72 h drug incubation without supplemental GSH-OEt are given in Table 8.1.

Table 8.1. Cytotoxicities (IC_{50}, nM) of paclitaxel, SB-T-1214, and folate-dipeptide-PEG-(SS-linker)-SB-T-1214 on various FR+ cancer cell lines.

Entry	Compound	ID8[a]	MX-1[b]	L1210FR[c]	MCF-7[d]	WI-38[e]
1[f]	paclitaxel	13.8 ± 2.7	4.07 ± 0.8	55.8 ± 10.1	6.25 ± 0.8	71.2 ± 8.1
2[f]	SB-T-1214	2.82 ± 0.7	2.66 ± 0.1	1.13 ± 0.3	1.01 ± 0.40	6.25 ± 0.5
3[f]	**8-7**	2.52 ± 1.5	7.54 ± 1.9	11.1 ± 4.0	12.0 ± 0.9	>5000

[a]Murine ovarian carcinoma cell line (FR+++); [b]Human breast carcinoma cell line (FR++); [c]Murine lymphocytic leukemia cell line (FR++); [d]Human breast carcinoma cell line (FR+); [e]Human lung fibroblast cell line (FR-); [f]Cells were incubated with a drug or conjugate at 37 °C for 72 h;

As anticipated, SB-T-1214 was found to be highly potent against all cell lines tested with IC_{50} values ranging from 1–6 nM. Folate conjugate **8-7** demonstrated equally high potency against FR^{+++} ovarian cancer cell line ID8 (IC_{50} 2.52 nM) as the parent taxoid, indicating rapid internalization and efficient drug release, and high potency against FR^{++} leukemia cell line L1210FR (IC_{50} 11.1 nM), although slightly less than the parent taxoid. However, against FR^{-} normal lung fibroblast cell line WI38, the folate conjugate was virtually non-toxic (IC_{50} > 5μM). The difference in cytotoxicity of **8-7** against FR-positive and FR-negative cell lines was of at least three orders of magnitude. These results indicate that this folate-based conjugate design vastly reduces non-specific internalization.

§8.4 Dual-vitamin Tumor-targeting Drug Conjugates

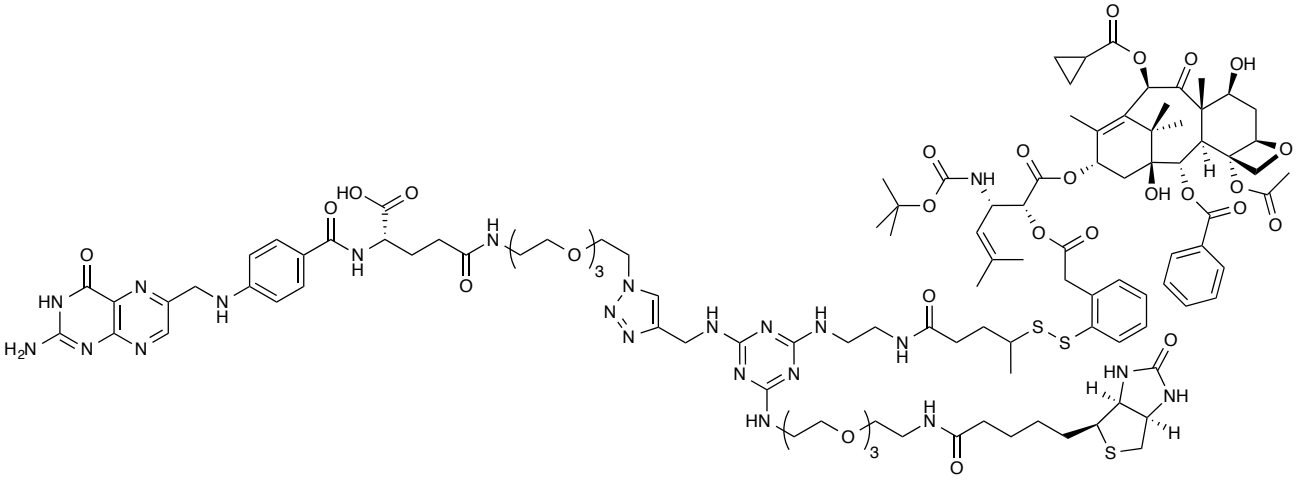

Figure 8.8. Chemical structure of dual-vitamin conjugate of folic acid and biotin with SB-T-1214 as the warhead (**8-18**).

A dual-vitamin conjugate of SB-T-1214 with both folate and biotin as tumor-targeting modules (**8-18**) was synthesized based on the same TTDDS as double-warhead conjugates DW-1 (**5-9**) and DW-2 (**5-12**) and theranostic conjugate **6-4**. The taxoid was connected to a self-immolative disulfide linker for glutathione-triggered intracellular drug release, and both the folic acid and biotin moieties were connected to a 1,3,5-triazine splitter by PEG spacers to promote

water solubility. The chemical structure of dual-vitamin conjugate (**8-18**) is illustrated in Figure 8.8.

However, the initial route towards a dual-vitamin tumor-targeting drug conjugate involved the reaction of a cysteine thiol with a benzyl bromide to install the second vitamin module. Both synthetic routes are discussed below in the following Sections.

§8.4.1 First Route Towards Dual-vitamin Tumor-targeting Drug Conjugate

The first synthetic route towards a dual-vitamin tumor-targeting drug conjugate required the preparation of a folate-dipeptide-PEG-N_3 component containing a cysteine residue. As discussed earlier in Chapter 4, biotin-PEG-Bn-Br (**4-12**) was synthesized and employed in this route for site-specific reactivity with the cysteine thiol. Though orthogonal "click" chemistry, an alkyne-bearing prodrug of SB-T-1214 would be introduced at the azido functional group.

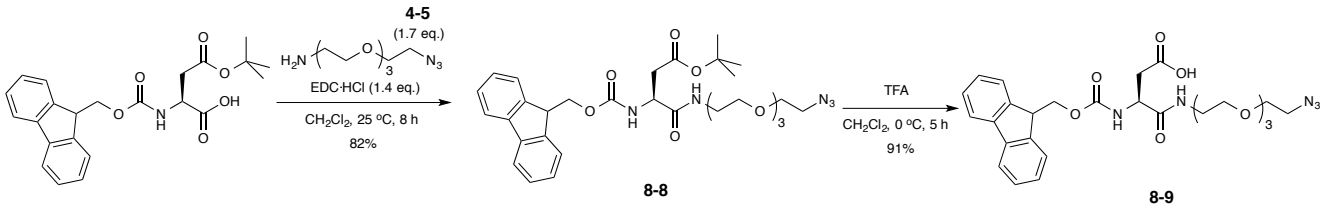

Scheme 8.6. Synthesis of Fmoc-Asp-PEG-N_3 (**8-9**).

Coupling of Fmoc-Asp(O*t*Bu)-OH to **4-5** in the presence of EDC·HCl afforded **8-8** in good yield (82%), and the corresponding *tert*-butyl ester was removed by trifluoroacetic acid to afford **8-9** in excellent yield (91%). The synthesis of Fmoc-Asp-PEG-N_3 is shown in Scheme 8.6.

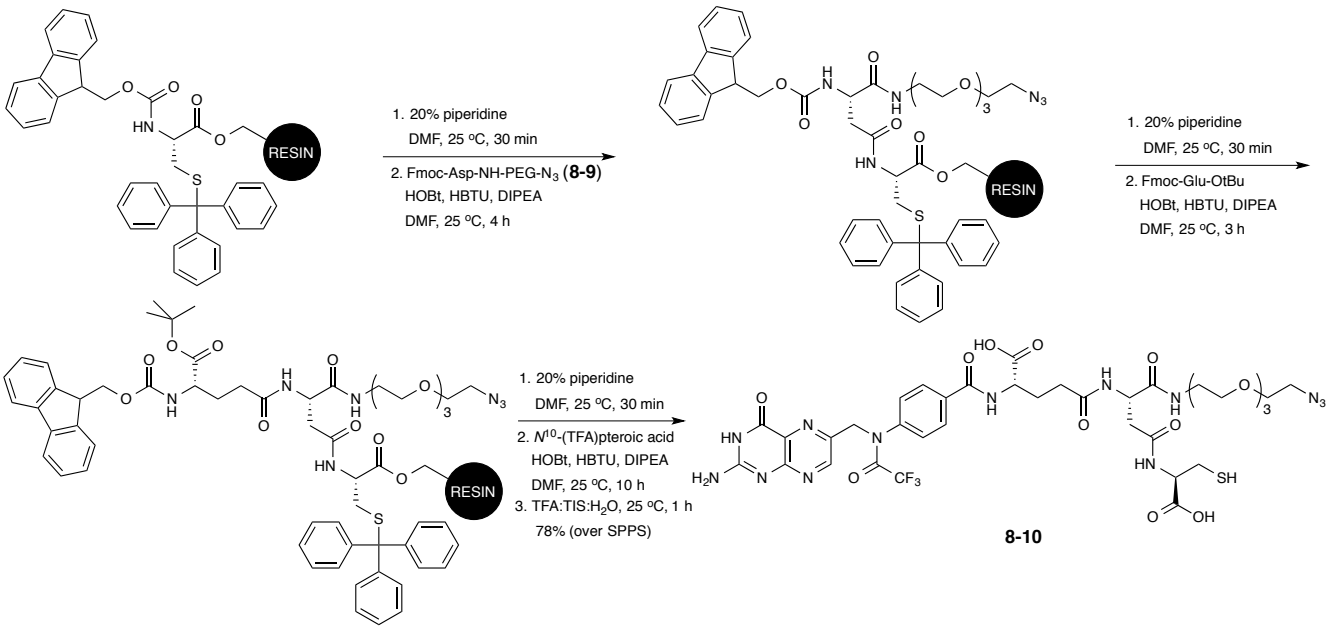

Scheme 8.7. Solid-phase peptide synthesis (SPPS) of folate-Asp(Cys)-PEG-N_3 (**8-10**).

Beginning with Fmoc-Cys(Trt)-Wang resin, the Fmoc group was first deprotected with piperidine, and the corresponding amine was coupled to **8-9** in the presence of HOBt, HBTU,

and DIPEA. After another Fmoc deprotection, coupling of Fmoc-Glu-O*t*Bu to the resin-bound amine under the same peptide coupling conditions gave the tripeptide intermediate. Following one more Fmoc deprotection, coupling of N^{10}-(TFA)pteroic acid to the resin-bound amine under the same peptide coupling conditions gave the protected resin-bound folate-dipeptide. Subsequent cleavage from the resin and esteroylsis of the *tert*-butyl ester with TFA gave **8-10** in a single step. PEGylated N^{10}-folate-Asp(Cys)-PEG-N_3 **8-10** was isolated in good yield (78%). The SPPS of **8-10** is illustrated in Scheme 8.7.

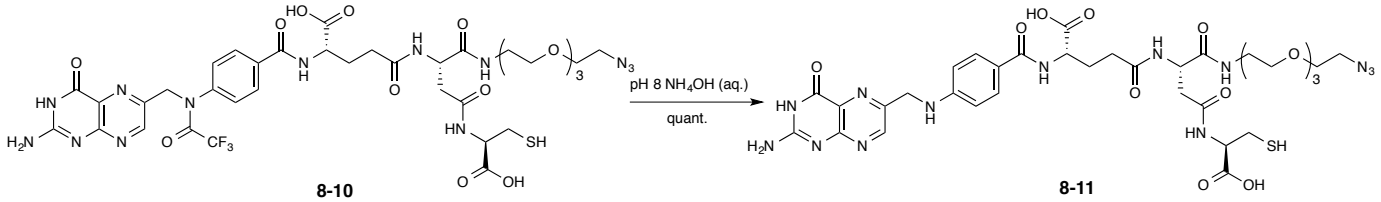

Scheme 8.8. Deprotection of N^{10}-TFA group under mild basic conditions.

Basic hydrolysis of the N^{10}-TFA group of **8-10** with aqueous ammonium hydroxide (pH 8) afforded **8-11** in quantitative yield, shown in Scheme 8.8. Reaction progress was monitored by mass spectrometry. Following completion of the reaction, the aqueous basic solution was removed by lyophilization.

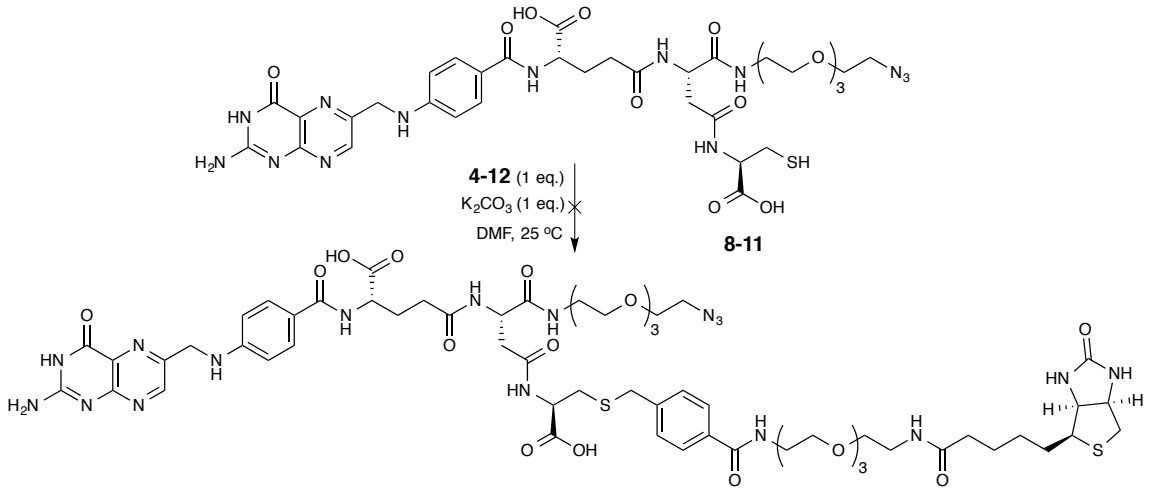

Scheme 8.9. Unsuccessful coupling reaction of folate-Arg(Cys)-PEG-N_3 (**8-11**) with biotin-PEG-Bn-Br (**4-12**).

The coupling reaction of **8-11** and biotin-PEG-Bn-Br (**4-12**) in the presence of K_2CO_3 did not afford the desired dual-vitamin scaffold, shown in Scheme 8.9. Reaction progress was monitored by mass spectrometry, which indicated degradation of starting materials as indicated by the loss of the $[M+H]^+$ ions for each. No relevant product was observed or isolated, and this synthetic route was subsequently abandoned. Thus, an alternate route towards the synthesis of a dual-vitamin drug conjugate was explored.

§8.4.2 Second Route Towards Dual-vitamin Tumor-targeting Drug Conjugate

Synthesis of dual-vitamin conjugate DV-1 (**8-18**) was carried out following the preparation of two components: (a) regiospecific folate-γ-PEG-N_3 (**8-17**), (b) tumor-targeted

drug delivery platform bearing biotin as the TTM and SB-T-1214 as the cytotoxic agent via 1,3,5-triazine splitter with a propargylamino arm.

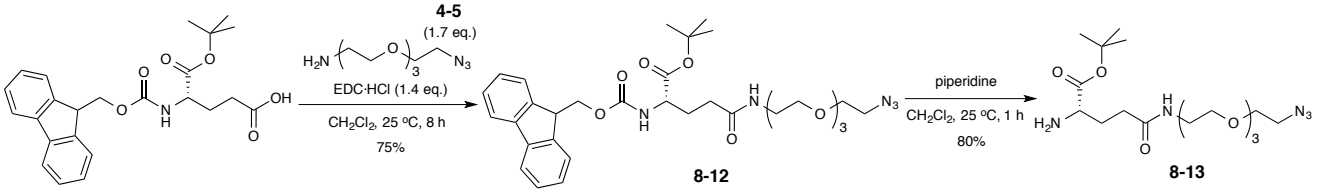

Scheme 8.10. Synthesis of Fmoc-Glu(PEG-N_3)-OH (**8-13**).

First, coupling of the γ-carboxylate of commercially available *N*-Fmoc-Glu-O*t*Bu to **4-5** in the presence of EDC·HCl gave **8-12** in good yield (75%). Deprotection of the Fmoc group of **8-12** with piperidine afforded **8-13** in very good yield (80%), shown in Scheme 8.10. Modified glutamate **8-13** was used in the regiospecific synthesis of γ-functionalized folate derivative **8-17**.

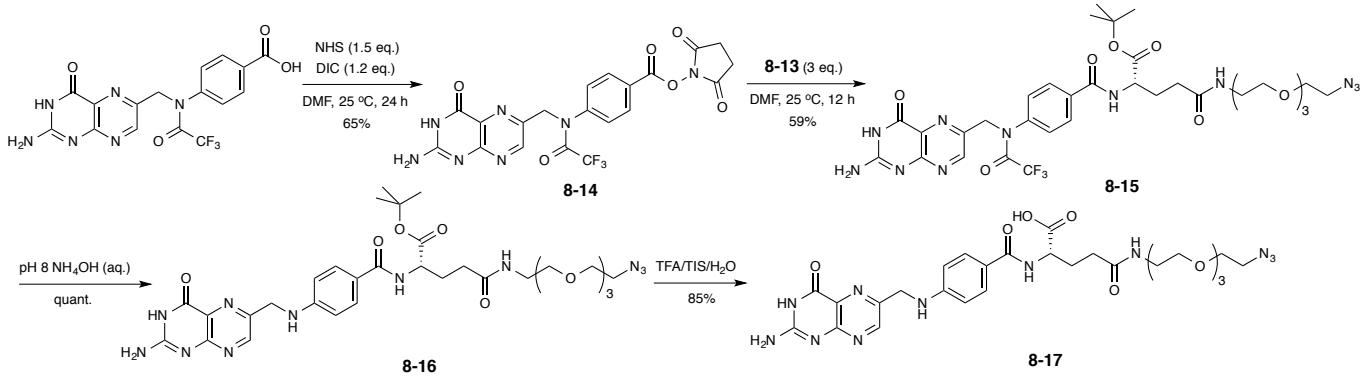

Scheme 8.11. Synthesis of folate-γ-PEG-N_3 (**8-17**).

N^{10}-(trifluoroacetyl)pteroic acid was activated with NHS in the presence of DIC to give **8-14** in good yield (65%), and the corresponding succinimide ester was coupled to **8-13** in DMF to afford protected folate derivative **8-15** in modest yield (59%). The product was purified with ample washing with ethyl acetate, dichloromethane, and diethyl ether to remove excess reagents, such as HOSu and DIC/DIU. Basic hydrolysis of the N^{10}-trifluoroacetyl group with aqueous ammonium hydroxide (pH 8) followed by esterolysis of the *tert*-butyl ester with trifluoroacetic acid afforded regiospecific folate-γ-PEG-N_3 (**8-17**) in excellent yield (85% over 2 steps), shown in Scheme 8.11.

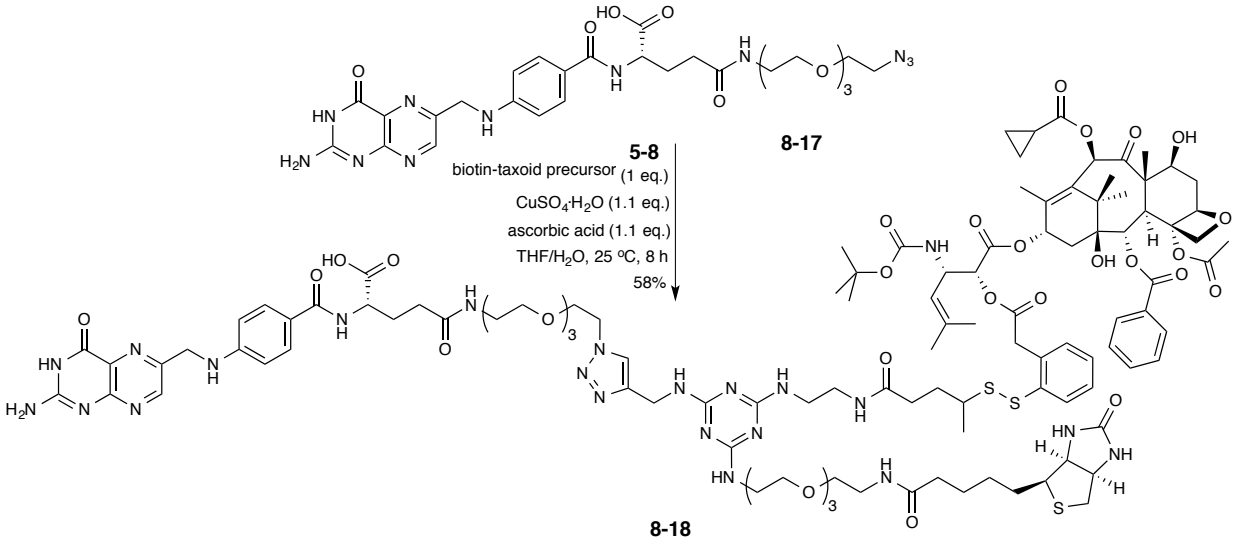

Scheme 8.12. Synthesis of double-vitamin conjugate of SB-T-1214 (**8-18**).

Biotin-taxoid precursor **5-8** was subjected to a "click" reaction with azide **8-17** in the presence of copper(II) sulfate and ascorbic acid to give double-vitamin conjugate DV-1 (**8-18**) in modest yield (58%), shown in Scheme 8.12. Reaction progress was monitored by mass spectrometry. Purification of the product by washing with methanol, water, dichloromethane, and diethyl ether gave **8-18** as an orange solid. Both regioisomers, if present, were treated as a single compound; however, the presence of regioisomers was not detected by ^{1}H NMR and a more thorough analysis will be necessary to detect the presence of regioisomers.

§8.5 Biological Evaluation of Double-vitamin Drug Conjugate

The potency and efficacy of dual-vitamin conjugate (**8-18**) were evaluated *in vitro* against various FR+. The cytotoxicity assays of **8-18** against MX-1 (FR^{++}) and MCF-7 (FR^{+}) were performed by MTT method.[33] As controls for comparison, parent taxoid SB-T-1214 was evaluated as well. The results for 72 h drug incubation without supplemental GSH-OEt are given in Table 8.2.

Table 8.2. Cytotoxicities (IC_{50}, nM) of SB-T-1214 and double-vitamin conjugate **8-18** on various FR+ cancer cell lines.

Entry	Compound	MX-1[a]	MCF-7[b]	WI-38[c]
1[d]	SB-T-1214	2.66 ± 0.16	1.01 ± 0.40	6.25 ± 0.50
2[d]	**8-18**	2.84 ± 0.11	15.90 ± 0.59	pending

[a]Human breast carcinoma cell line (FR^{++}/BR^{+++}); [b]Human lung fibroblast cell line (FR^{+}/BR^{++}); [c]Human lung fibroblast (FR-/BR-); [d]Cells were incubated with a drug or conjugate at 37 °C for 72 h.

Dual-vitamin conjugate of folate and biotin (**8-18**) demonstrated equally high potency against FR^{++}/BR^{+++} human breast carcinoma cell line MX-1 (IC_{50} 2.84 nM) as the parent taxoid, indicating rapid internalization and efficient drug release. Compared with folate-linker-taxoid conjugate (**8-7**) against MX-1 (IC_{50} 7.54 nM), the dual-targeting conjugate exhibited a two to three fold increase in potency with the additional biotin-targeting module. Furthermore, **8-18** displayed high potency, against FR^{+}/BR^{++} human breast carcinoma cell line MCF-7 (IC_{50} 15.9 nM), and slightly less than the parent taxoid.

§8.6.0 Summary

The folate receptor has shown considerable promise as a therapeutic target in targeted drug delivery and has been widely recognized as a tumor-specific biomarker. Because of its small size, low cost, synthetic versatility, and lack of immunogenicity, folic acid is an attractive candidate for receptor-mediated delivery of highly potent cytotoxic agents. Folate-based small-molecule drug conjugates (SMDCs) have demonstrated excellent target specificity for the α-folate receptor and numerous drug conjugates and imaging agents have emerged in clinical trials with positive results.

However, a recent Phase III clinical trial of vintafolide, the most advanced folate-based SMDC, for treatment of platinum-resistant ovarian cancer was recently halted in Phase III due to futility, and conditional approval for marketing of the conjugate and its corresponding imaging diagnostic in the EU was subsequently withdrawn. While significant advances in folate-based conjugates have been made, this news clearly underscores the need for improvements in design of the tumor-targeted drug delivery system.

A novel folate-based drug conjugate of next-generation taxoid SB-T-1214 was designed and synthesized using a combination of solid-phase peptide synthesis with synthetically modified amino acids and copper-free “click” chemistry. The folate-linker-taxoid conjugate contains two polyethylene glycol spacers along with a zwitterionic dipeptide spacer to promote aqueous solubility and promote tumor-specific uptake, and a mechanism-based self-immolative disulfide linker for site-specific prodrug activation. The conjugate was evaluated *in vitro* against a series of FR-positive cancer cell lines, and excellent target-specificity was observed for the FR. When administered to FR-negative cells, the folate conjugate was virtually non-toxic.

In addition, a novel dual-vitamin tumor-targeting drug conjugate of SB-T-1214 with folate and biotin as dual tumor-targeting modules was designed and synthesized using a PEGylated 1,3,5-triazine splitter as the drug delivery scaffold. The dual-targeting drug conjugate was evaluated *in vitro* against cancer cell lines that overexpress both the folate and biotin receptors, and the conjugate demonstrated excellent specificity for the FR whereas it was similarly virtually non-toxic against FR-/BR- normal cells. In particular, the conjugate demonstrate equipotent activity compared to the free taxoid against human breast carcinoma cell line, MX-1. The biological evaluation *in vitro* of the taxoid-based drug conjugates, folate-linker-taxoid and the dual-vitamin conjugate of folate and biotin, yielded positive results for these conjugates as therapeutic candidates, and preclinical studies against FR+ tumor-bearing mice will be carried out in due course.

§8.7.0 Experimental

§8.7.1 Caution

Taxoids have been identified as potent cytotoxic agents. Thus, all drugs and structurally related compounds and derivatives must be considered mutagens and potential reproductive hazards for both males and females. All appropriate precautions, such as the use of gloves, goggles, labware, and fume hood, must be taken while handling the compounds at all times.

§8.7.2 General Information

^{1}H, ^{13}C, and ^{19}F NMR spectra were measured on a Varian 300 MHz NMR spectrometer or Bruker 300, 400, 500, or 700 MHz NMR spectrometer. Hexafluorobenzene was used as an external reference for ^{19}F NMR analysis. Melting points were measured on a Thomas-Hoover capillary melting point apparatus and are uncorrected. TLC was performed on Sorbent Technologies aluminum-backed Silica G TLC plates (Sorbent Technologies, 200 μm, 20 x 20 cm), and column chromatography was carried out on silica gel 60 (Merck, 230-400 mesh ASTM). High resolution mass spectrometry analysis was carried out on an Agilent LC-UV-TOF mass spectrometer at the Institute of Chemical Biology and Drug Discovery, Stony Brook, NY or at the Mass Spectrometry Laboratory, University of Illinois at Urbana-Champaign, Urbana, IL.

§8.7.3 Materials

The chemicals were purchased from Sigma-Aldrich, Fisher Scientific, and VWR International, and used as received or purified before use by standard methods. Tetrahydrofuran was freshly distilled from sodium and benzophenone. Dichloromethane was also distilled immediately prior to use under nitrogen from calcium hydride. 3-(4,5-Dimethylthiazol-2-yl)-2,5-diphenyltetrazolium bromide (MTT) was obtained from Sigma Chemical Co. Biological materials including RPMI-1640 (folate-free) cell culture medium, fetal bovine serum, PenStrep, and TrypLE were obtained from Gibco and VWR International, and used as received for cell-based assays.

§8.7.4 Experimental Procedure

$N^{2,10}$-Bis(trifluoroacetyl)pyrofolic Acid/Anhydride [8-1]:[31]

To a cooled solution of folic acid (5.0 g, 11.33 mmol) in THF (50 mL) was added trifluoroacetic anhydride (12.8 mL, 90.2 mmol) over 20 min, and the mixture was allowed to warm from 0 °C to room temperature and react for 16 h with stirring. Reaction progress was monitored by mass spectrometry. The reaction mixture was concentrated *in vacuo* to give a red oil, which was slowly added to 2-propanol (50 mL) to afford a yellow precipitate. The solid was removed by filtration, washed with Et_2O (3 x 100 mL), and collected to give **8-1** (1.593 g, 23%) as a yellow solid; contains trace Et_2O and IPA; ^{1}H NMR (300 MHz, DMSO-d_6) δ 2.55-2.65 (m, 4H), 4.78 (m, 1H), 5.21 (s, 2H), 7.69 (m, 4H), 8.77 (s, 1H); ^{13}C NMR (125 MHz, DMSO-d_6) δ 21.85, 31.70, 54.33, 58.91, 113.07, 115.37, 117.68, 1119.99, 128.55, 130.28, 135.24, 142.41, 146.17, 153.71, 156.29, 159.03, 159.31, 159.60, 159.88, 160.43, 169.31, 172.82, 174.66; ^{19}F NMR (376 MHz, DMSO-d_6) δ -66.66 (s, 3F), -75.19 (s, 3F), 80.91 (m, 3F), ratio: 0.8:1.0:0.1. All data are in agreement with literature values.[31]

N^{10}-(Trifluoroacetyl)pyrofolic Acid [8-2]:[31]

To a solution of **8-1** (1.593 g, 2.607 mmol) in THF was added H_2O (s) (4.0 g, 0.222 mol), and the mixture was allowed to react for 8 h at room temperature with stirring. Reaction progress was monitored by mass spectrometry. The reaction mixture was added dropwise to Et_2O (500 mL) to give a yellow precipitate. The solid was removed by filtration, washed with Et_2O (3 x 100 mL), and collected to give **8-2** (1.500 g, 26% over 2 steps) as a yellow solid; ^{1}H NMR (500 MHz, DMSO-d_6) δ 2.45-2.55 (m, 4H), 4.61 (m, 1H), 5.13 (s, 2H), 7.62 (m, 4H), 8.65 (s, 1H); ^{13}C NMR (125 MHz, DMSO-d_6) δ 21.80, 31.68, 54.30, 59.92, 113.08, 115.38, 117.67, 119.96, 128.54, 130.25, 135.18, 142.36, 144.90, 146.62, 149.70, 154.35, 156.28, 161.30, 169.35, 172.89, 174.73, 176.10; ^{19}F NMR (282 MHz, DMSO-d_6) δ -66.63. All data are in agreement with literature values.[31]

Pteroyl Hydrazide [8-3]:[31]

To a solution of **8-2** (1.500 g, 2.89 mmol) in DMSO in a room temperature water bath was added hydrazine (1.0 mL, 31.3 mmol), and the mixture was allowed to react for 8 h at room temperature with stirring. The reaction mixture was added dropwise to CH_3OH (500 mL) to give a yellow solid. The precipitate was removed by filtration, washed with CH_3OH (3 x 100 mL) and Et_2O (3 x 100 mL), and collected to give **8-3** (0.772 g, 82%) as a yellow solid; ^{1}H NMR (300 MHz, DMSO-d_6) δ 4.46 (d, J = 5.4 Hz, 2H), 6.61 (d, J = 8.7 Hz, 2H), 7.16 (bs, 2H), 7.59 (d, J = 8.7 Hz, 2H), 8.63 (s, 1H); HRMS (TOF) for $C_{14}H_{15}N_8O_2^+$ calcd: 327.1312. Found: 327.1318 (Δ = 1.8 ppm). All data are in agreement with literature values.[31]

Pteroyl Azide [8-4]:[31]

To a cooled solution of **8-3** (0.772 g, 2.368 mmol) and potassium thiocyanate (0.012 g, 0.118 mmol) in trifluoroacetic acid (20 mL) at -10 °C was added neat *tert*-butyl nitrite (0.28 mL, 2.368 mmol), and the mixture was allowed to react for 5 h at -10 °C with stirring. Reaction progress was monitored by mass spectrometry. Next, the reaction was allowed to warm to room temperature, and NaN_3 (0.077 g, 1.184 mmol) was added to convert any N^{10}-nitrosopteroyl azide to **8-4**. The reaction mixture was filtered over celite to remove trace solid residue. Slow addition of 2-propanol (25 mL) to the stirred filtrate afforded an orange solid, which was removed by filtration and washed thoroughly with H_2O (3 x 50 mL), CH_3CN (3 x 30 mL), and Et_2O (3 x 20 mL) to give **8-4** (0.510 g, 64%), as an orange solid; ^{1}H NMR (300 MHz, DMSO-d_6) δ 4.57 (s, 2H), 6.70 (d, J = 8.4 Hz, 2H), 7.69 (d, J = 8.7 Hz, 2H), 8.70 (s, 1H). All data are in agreement with literature values.[31]

N^{10}-TFA-Folate-Glu(Arg)-PEG-N_3 [8-5]:

In a peptide synthesis vessel, Fmoc-Arg(Pbf) Wang resin (0.098 g, 0.049 mmol) was loaded and allowed to swell in DMF (1 mL), and the beads were shaken for 30 min and subsequently washed with DMF (3 x 1 mL). To the vessel was added 20% piperidine in DMF (1 mL), and the vessel was subsequently shaken for 30 min. After 30 min, the piperidine solution was removed, and the beads were washed with DMF (3 x 1 mL).

To vessel were then introduced Fmoc-Glu-NH-PEG_3-N_3 (0.049 g, 0.122 mmol), HOBt (0.017 g, 0.122 mmol), HBTU (0.046 g, 0.122 mmol), and DIPEA (63 μL, 0.366 mmol) in DMF (1 mL), and the reaction vessel was shaken for 4 h. Kaiser tests were performed to assess reaction completion. After 4 h, the amino acid solution was removed, and the beads were washed with

DMF (3 x 1 mL). Fmoc deprotection was carried out using 20% piperidine in DMF (1 mL) for 30 min. The piperidine solution was removed, and the beads were washed with DMF (3 x 1 mL). To vessel were then introduced Fmoc-Glu-O*t*Bu (0.052 g, 0.122 mmol), HOBt (0.017 g, 0.122 mmol), HBTU (0.046 g, 0.122 mmol), and DIPEA (63 μL, 0.366 mmol) in DMF (1 mL), and the reaction vessel was shaken for 4 h. Kaiser tests were performed to assess reaction completion. After 4 h, the amino acid solution was removed, and the beads were washed with DMF (3 x 1 mL). Fmoc deprotection was carried out using 20% piperidine in DMF (1 mL) for 30 min. The piperidine solution was removed, and the beads were washed with DMF (3 x 1 mL).
To vessel were then introduced N^{10}-(trifluoroacetyl)pteroic acid (0.050 g, 0.122 mmol), HOBt (0.017 g, 0.122 mmol), HBTU (0.046 g, 0.122 mmol), and DIPEA (63 μL, 0.366 mmol) in DMF (1 mL), and the reaction vessel was shaken for 10 h. Kaiser tests were performed to assess reaction completion. After 8 h, the amino acid solution was removed, and the beads were washed with DMF (3 x 1 mL).
To the vessel was introduced a 95/2.5/2.5 solution of TFA/TIS/H_2O (5 mL), and the vessel was shaken for 1 h. After 1 h, the resulting orange solution was collected, and the beads were washed with a TFA/TIS/H_2O (95/2.5/2.5) solution. The solution was concentrated *in vacuo* to give an orange oil, which was triturated with Et_2O (2 mL) to give a pale yellow solid. The yellow solid was dissolved in H_2O (5 mL), and the Et_2O layer was removed. The aqueous layer was lyophilized to give **8-5** (0.042 g, 84%) as a yellow solid; ^{1}H NMR (500 MHz, DMSO-d_6) δ 1.53 (m, 2H), 1.64 (m, 2H), 1.77 (m, 1H), 1.92 (m, 2H), 2.15 (m, 3H), 2.31 (m, 2H), 3.14 (m, 2H), 3.21 (m, 2H), 3.41 (t, J = 4.4 Hz, 4H), 3.56 (m, 8H), 3.62 (t, J = 4.7 Hz, 2H), 4.20 (m, 1H), 4.30 (m, 1H), 4.38 (m, 1H), 7.53 (m, 1H), 7.68 (d, J = 8.2 Hz, 2H), 7.95 (d, J = 8.4 Hz, 2H), 8.06 (d, J = 8.3 Hz, 1H), 8.25 (d, J = 8.3 Hz, 1H), 8.69 (s, 1H), 8.76 (d, J = 7.5 Hz, 1H); ^{13}C NMR (125 MHz, DMSO-d_6) δ 22.83, 25.62, 26.27, 26.90, 28.50, 28.67, 28.77, 32.12, 32.25, 34.84, 50.44, 51.91, 52.37, 52.67, 54.30, 69.53, 69.71, 70.00, 70.13, 70.20, 70.23, 128.59, 128.96, 129.17, 134.96, 142.05, 145.10, 149.72, 154.23, 154.23, 157.08, 161.01, 166.21, 171.85, 172.13, 173.77, 173.81, 174.03, 174.29; ^{19}F NMR (282 MHz, DMSO-d_6) δ -66.58 (s, 3F); HRMS for $C_{40}H_{54}F_3N_{16}O_{13}^+$ calcd: 1023.4003. Found: 1023.3997. (Δ = -0.6 ppm)

Folate-(SS-Linker)-PEG-Taxoid [8-7]:
A solution of **8-5** (0.035 g, 0.034 mmol) in pH 8 NH_4OH (aq.) (1.5 mL) was allowed to react for 1 h at room temperature with stirring. Reaction progress was monitored by mass spectrometry. The aqueous solution was lyophilized to give **8-6** (0.032 g, quant.) as a yellow solid. The product was taken directly to the subsequent step without further purification. To a solution of **8-7** (0.012 g, 13.0 μmol) in H_2O (1 mL) was added SB-T-1214-(SS-linker)-PEG-cyclooctyne (0.020 g, 13.0 μmol) in EtOH (1 mL), and the mixture was stirred for 48 h at 25 °C with stirring. After 48 h, a yellow solid precipitated out of solution, and the solid was collected following several rounds of centrifugation, removal of the supernatant, and thorough washing with EtOH/H_2O (1:1) (3 x 3 mL) and Et_2O (3 x 3 mL) to give **8-7** (19.4 mg, 60%) as a yellow solid; ^{1}H NMR (500 MHz, DMSO-d_6) δ 0.92 (m, 2H), 1.00 (m, 4H), 1.08 (s, 3H), 1.10 (s, 3H), 1.22 (d, J = 6.8 Hz, 3H), 1.27 (s, 2H), 1.42 (s, 9H), 1.55 (s, 3H), 1.61 (m, 1H), 1.62 (s, 6H), 1.69 (m, 2H), 1.74 (s, 3H), 1.83 (s, 3H), 1.87 (m, 1H), 2.02 (m, 2H), 2.11 (m, 3H), 2.18 (t, J = 7.4 Hz, 2H), 2.24 (m, 2H), 2.37 (s, 3H), 2.69 (m, 1H), 2.93 (m, 1H), 3.08 (m, 4H), 3.20 (m, 4H), 3.47 (m, 12H), 3.54 (m, 12H), 3.71 (d, J = 6.8 Hz, 2H), 3.78 (m, 2H), 4.00 (s, 2H), 4.14 (m, 2H), 4.15 (m, 1H), 4.26 (m, 1H), 4.40 (m, 1H), 4.51 (s, 2H), 4.75 (m, 1H), 4.85 (d, J = 7.8 Hz, 1H), 4.96 (s, 2H), 5.00 (m, 1H), 5.19 (m, 1H), 5.21 (d, J = 7.0, 1H), 6.03 (m, 1H), 6.35 (s, 1H), 6.67 (d, J = 7.0 Hz, 2H),

6.97 (m, 2H), 7.34 (m, 6H), 7.40 (t, J = 7.8 Hz, 2H), 7.57 (t, J = 7.6, 2H), 7.62 (d, J = 7.6 Hz, 2H), 7.72 (m, 5H), 7.77 (t, J = 7.3 Hz, 2H), 7.84 (m, 1H), 7.91 (m, 1H), 8.04 (d, J = 7.8 Hz, 2H), 8.06 (m, 1H), 8.37 (m, 1H), 8.67 (s, 1H); ^{13}C NMR (125 MHz, DMSO-d_6) δ 8.76, 8.84, 10.24, 13.15, 14.21, 14.24, 18.36, 20.37, 20.48, 21.51, 21.91, 22.99, 24.80, 25.96, 26.08, 26.81, 28.65, 29.80, 29.88, 31.28, 31.64, 32.06, 32.39, 32.94, 33.06, 35.23, 35.89, 36.26, 36.31, 36.40, 37.05, 37.09, 38.27, 38.30, 38.94, 43.49, 45.97, 46.11, 46.40, 46.69, 47.42, 47.69, 49.74, 52.45, 53.03, 53.49, 57.95, 68.52, 68.76, 69.52, 69.82, 70.03, 70.14, 70.25, 70.88, 71.02, 74.99, 75.78, 77.21, 78.59, 80.87, 84.06, 111.67, 111.75, 120.72, 121.90, 122.44, 127.39, 127.47, 127.90, 128.40, 128.84, 129.12, 129.36, 129.45, 129.54, 129.99, 130.40, 131.65, 132.63, 132.94, 132.96, 133.30, 133.33, 133.80, 133.89, 134.57, 136.45, 137.31, 137.36, 139.99, 144.87, 145.55, 148.96, 149.05, 151.02, 151.20, 155.40, 157.58, 165.60, 166.58, 169.27, 170.07, 170.67, 171.64, 172.16, 172.65, 203.03; HRMS (TOF) for $C_{122}H_{167}N_{19}O_{33}S_2^{2+}$ calcd: 1245.0702. Found: 1245.0673 (Δ = -2.3 ppm).

***N*-Fmoc-L-Asp(O*t*-Bu)-NH-PEG-N$_3$ [8-8]:**
To a solution of Fmoc-L-aspartic acid(O*t*-Bu)-OH (1.028 g, 2.520 mmol) and EDC·HCl (0.671 g, 3.500 mmol) in CH_2Cl_2 (25 mL) was added **4-5** (0.934 g, 4.284 mmol) in CH_2Cl_2 (2 mL), and the mixture was allowed to react for 8 h at room temperature with stirring. The reaction was diluted with H_2O (20 mL), and the mixture was extracted with CH_2Cl_2 (3 x 15 mL). The combined organic layers were dried over $MgSO_4$ and concentrated *in vacuo* to give a yellow oil. Purification of the crude product by column chromatography on silica gel with hexanes/ethyl acetate (1:6) as eluent gave **8-8** (1.355 g, 82%) as a waxy, colorless solid; R_f = 0.8 (hexanes/ethyl acetate: 5/95); ^{1}H NMR (500 MHz, $CDCl_3$) δ 1.45 (s, 9H), 2.62 (dd, J = 6.3 Hz, 16.7 Hz, 1H), 2.87 (dd, J = 4.6, 16.7 Hz, 1H), 3.36 (t, J = 5.0 Hz, 2H), 3.46 (m, 2H), 3.54 (t, J = 5.0 Hz, 2H), 3.63 (m, 10H), 4.22 (t, J = 7.0 Hz, 1H), 4.41 (m, 2H), 4.52 (m, 1H), 5.97 (d, J = 8.5 Hz, 1H), 6.86 (bt, 1H), 7.31 (t, J = 7.4 Hz, 2H), 7.40 (t, J = 7.5 Hz, 2H), 7.59 (d, J = 7.4 Hz, 2H), 7.76 (d, J = 7.4 Hz, 2H); ^{13}C NMR (125 MHz, $CDCl_3$) δ 28.07, 37.73, 39.53, 47.16, 50.66, 51.30, 67.18, 69.63, 70.01, 70.37, 70.58, 70.61, 70.69, 81.75, 120.06, 125.08, 127.13, 127.81, 141.33, 143.74, 156.03, 170.44, 170.97; HRMS for $C_{31}H_{42}N_5O_8^+$ calcd: 612.3028. Found: 612.3025 (Δ = -0.5 ppm).

***N*-Fmoc-L-Asp-NH-PEG-N$_3$ [8-9]:**
To a cooled solution of **8-8** (0.616 g, 1.008 mmol) in CH_2Cl_2 (17 mL) was added trifluoroacetic acid (4 mL), and the mixture was allowed to react for 5 h at 0 °C with stirring. The reaction was diluted with CH_2Cl_2 (10 mL), and the mixture was washed with H_2O (3 x 20 mL). The organic layer was dried over $MgSO_4$ and concentrated *in vacuo* to give **8-9** (0.509 g, 91%) as a waxy, colorless solid; ^{1}H NMR (500 MHz, $CDCl_3$) δ 2.64 (dd, J = 9.0, 16.0 Hz, 1H), 3.06 (dd, J = 4.0, 16.0 Hz, 1H), 3.35 (m, 1H), 3.41 (t, J = 5.0 Hz, 2H), 3.49 (m, 1H), 3.55 (m, 1H), 3.60-3.72 (m, 12 H), 4.24 (t, J = 6.5 Hz, 1H), 4.43 (d, J = 7.0 Hz, 2H), 4.63 (m, 1H), 6.07 (d, J = 8.0 Hz, 1H), 6.89 (m, 1H), 7.34 (t, J = 7.5 Hz, 2H), 7.43 (t, J = 7.5 Hz, 2H), 7.63 (d, J = 7.0 Hz, 2H), 7.79 (d, J = 7.5 Hz, 2H); ^{13}C NMR (125 MHz, $CDCl_3$) δ 37.97, 39.47, 47.13, 50.60, 51.29, 53.46, 67.15, 69.43, 69.88, 70.04, 70.33, 70.39, 70.96, 120.03, 125.09, 125.12, 127.12, 127.77, 141.31, 143.72, 155.70, 170.40, 172.53; HRMS for $C_{27}H_{34}N_5O_8^+$ calcd: 556.2402. Found: 556.2398 (Δ = -0.7 ppm).

N^{10}-TFA-Folate-Asp(Cys)-NH-PEG$_3$-N$_3$ [8-10]:
In a peptide synthesis vessel, Fmoc-Cys(Trt) Wang resin (0.200 g, 0.126 mmol) was loaded and allowed to swell in DMF (3 mL), and the beads were shaken for 30 min and subsequently washed with DMF (3 x 3 mL). To the vessel was added 20% piperidine in DMF (3 mL), and the vessel was then shaken for 30 min. After 30 min, the piperidine solution was removed, and the beads were washed with DMF (3 x 3 mL).
To vessel were then introduced **8-9** (0.175 g, 0.315 mmol), HOBt (0.042 g, 0.315 mmol), HBTU (0.119 g, 0.315 mmol), and DIPEA (220 μL, 1.26 mmol) in DMF (3 mL), and the reaction vessel was shaken for 4 h. Kaiser tests were performed to assess reaction completion. After 4 h, the amino acid solution was removed, and the beads were washed with DMF (3 x 3 mL). Fmoc deprotection was carried out using 20% piperidine in DMF (3 mL) for 30 min. The piperidine solution was removed, and the beads were again washed with DMF (3 x 3 mL).
To the vessel were introduced Fmoc-Glu-OtBu (0.134 mmol, 0.315 mmol), HOBt (0.042 g, 0.315 mmol), HBTU (0.119 g, 0.315 mmol), and DIPEA (220 μL, 1.26 mmol) in DMF (3 mL), and the reaction vessel was shaken for 3 h. Kaiser tests were performed to assess reaction completion. After 3 h, the amino acid solution was removed, and the beads were washed with DMF (3 x 3 mL). Fmoc deprotection was carried out using 20% piperidine in DMF (3 mL) for 30 min. The piperidine solution was removed, and the beads were washed with DMF (3 x 3 mL).
To the vessel were introduced N^{10}-(trifluoroacetyl)pteroic acid (0.128 mg, 0.315 mmol), HOBt (0.042 g, 0.315 mmol), HBTU (0.119 g, 0.315 mmol), and DIPEA (220 μL, 1.26 mmol) in DMF (3 mL), and the reaction vessel was shaken for 8 h. Kaiser tests were performed to assess reaction completion. After 8 h, the amino acid solution was removed, and the beads were washed with DMF (3 x 3 mL).
To the vessel was introduced a 95/2.5/2.5 solution of TFA/TIS/H_2O (10 mL), and the vessel was shaken for 1 h. After 1 h, the resulting orange solution was collected, and the beads were washed with a TFA:TIS:H_2O (95:2.5:2.5) solution. The solution was concentrated *in vacuo* to give an orange oil, which was triturated with Et_2O (2 mL) to give a pale yellow solid. The yellow solid was dissolved in H_2O (5 mL), and the Et_2O layer was removed. The aqueous layer was lyophilized to give **8-10** (0.094 g, 78%) as a yellow solid; ^{1}H NMR (500 MHz, DMSO-d_6) δ 1.96 (m, 1H), 2.11 (m, 1H), 2.29 (m, 2H), 2.84 (m, 1H), 3.21 (m, 2H), 3.41-3.57 (m, 14H), 3.62 (t, J = 4.9 Hz, 2H), 4.37 (m, 1H), 4.44 (m, 1H), 4.57 (m, 1H), 5.17 (s, 2H), 6.71 (d, J = 8.3 Hz, 1H), 7.11 (d, J = 8.3 Hz, 1H), 7.67 (d, J = 8.0 Hz, 2H), 7.95 (d, J = 8.0 Hz, 2H), 8.06 (d, J = 8.3 Hz, 1H), 8.19 (d, J = 8.3 Hz, 1H), 8.69 (s, 1H), 8.83 (d, J = 7.5 Hz, 1H); ^{13}C NMR (125 MHz, DMSO-d_6) δ 15.65, 26.11, 26.82, 31.24, 32.38, 36.26, 50.43, 52.86, 54.28, 54.79, 65.40, 69.25, 69.71, 70.04, 70.13, 70.21, 70.25, 115.57, 117.45, 128.60, 128.92, 129.16, 129.51, 130.45, 134.94, 142.02, 145.07, 149.73, 154.23, 155.95, 156.23, 156.72, 161.03, 162.78, 166.02, 171.98, 172.02, 173.77; ^{19}F NMR (376 MHz, DMSO-d_6) δ -66.06; HRMS for $C_{36}H_{44}F_3N_{13}O_{13}S$ calcd: 956.2927. Found: 956.2924 (Δ = -0.3 ppm).

Folate-Asp(Cys)-NH-PEG$_3$-N$_3$ [8-11]:
A solution of **8-10** (0.083 g, 0.087 mmol) in pH 8 NH_4OH (aq.) (2 mL) was allowed to react for 1 h at room temperature with stirring. Reaction progress was monitored by mass spectrometry. The aqueous solution was lyophilized to give **8-11** (0.075 g, quant.) as a yellow solid; ^{1}H NMR (500 MHz, DMSO-d_6) δ 1.20 (m, 1H), 1.42 (m, 1H), 1.91 (m, 2H), 2.22 (m, 2H), 2.37 (d, J = 7.2 Hz, 1H), 3.48 (m, 24 H), 4.19 (s, 1H), 4.25 (s, 1H), 4.48 (s, 1H), 6.64 (d, J = 7.6 Hz, 2H), 6.94

(bs, 1H), 7.63 (d, J = 7.6 Hz, 2H), 8.64 (s, 1H); HRMS for $C_{34}H_{46}N_{13}O_{12}S^+$ calcd: 860.3104. Found: 860.3100 (Δ = -0.5 ppm).

N-Fmoc-L-glutamic acid(PEG-N_3)-α-*tert*-butyl ester [8-12]:
To a solution of N-Fmoc-L-glutamic acid *tert*-butyl ester (0.200 g, 0.471 mmol) and EDC·HCl (0.108 g, 0.565 mmol) in CH_2Cl_2 (10 mL) was added **4-5** (0.154 g, 0.706 mmol), and the mixture was allowed to react for 13 h at room temperature with stirring. The reaction was diluted with CH_2Cl_2 (3 x 10 mL), and the mixture was washed with H_2O (3 x 20 mL). The combined organic layers were dried over $MgSO_4$ and concentrated *in vacuo* to give a yellow oil. Purification of the crude product by column chromatography on silica with hexanes/ethyl acetate (1:19) as eluent gave **8-12** (0.221 g, 75%) as a colorless oil; R_f = 0.85 (100% ethyl acetate); ^{1}H NMR (500 MHz, $CDCl_3$) δ 1.50 (s, 9H), 1.99 (m, 1H), 2.25 (m, 3H), 3.37 (t, J = 5.1 Hz, 2H), 3.46 (m, 2H), 3.56 (t, J = 4.8 Hz, 2H), 3.64 (m, 10H), 4.24 (m, 2H), 4.40 (m, 2H), 5.70 (d, J = 7.5 Hz, 1H), 6.35 (bs, 1H), 7.33 (t, J = 7.0 Hz, 2H), 7.42 (t, J = 7.5 Hz, 2H), 7.62 (d, J = 7.8 Hz, 2H), 7.77 (d, J = 7.5 Hz, 2H); ^{13}C NMR (125 MHz, $CDCl_3$) δ 28.02, 28.73, 32.51, 39.33, 47.20, 50.66, 54.13, 61.78, 69.96, 69.80, 70.00, 70.25, 70.52, 70.61, 70.65, 72.50, 82.40, 119.99, 125.18, 127.10, 127.73, 141.32, 143.75, 143.97, 156.27, 171.19, 172.05; HRMS (TOF) for $C_{32}H_{44}N_5O_8^+$ calcd: 626.3184. Found: 626.3189 (Δ = 0.8 ppm).

L-Glutamic acid(PEG$_3$-N_3)-α-*tert*-butyl ester [8-13]:
To a solution of **8-12** (0.100 g, 0.159 mmol) in CH_2Cl_2 (3 mL) was added piperidine (0.4 mL, 4.056 mmol), and the mixture was allowed to react for 1 h at room temperature with stirring. The reaction was diluted with CH_2Cl_2 (10 mL), and the mixture was washed with H_2O (3 x 20 mL). The combined organic layers were dried over $MgSO_4$ and concentrated *in vacuo* to give a yellow oil. The oil was triturated with hexanes to remove the dibenzofulvene-piperidine adduct and give **8-13** (0.051 g, 80%) as a colorless oil; R_f = 0.15 (100% ethyl acetate); ^{1}H NMR (500 MHz, $CDCl_3$) δ 1.49 (s, 9H), 1.80 (m, 1H), 2.14 (m, 1H), 2.37 (m, 2H), 3.14 (t, J = 6.0 Hz, 1H), 3.35 (m, 1H), 3.43 (t, J = 6.0 Hz, 2H), 3.58 (t, J = 6.0 Hz, 2H), 3.70 (m, 12H); 6.65 (bs, 1H); ^{13}C NMR (125 MHz, $CDCl_3$) δ 28.06, 30.39, 32.90, 39.20, 50.69, 54.35, 69.92, 70.04, 70.24, 70.57, 70.66, 70.70, 81.28, 172.58, 175.07; HRMS (TOF) for $C_{17}H_{34}N_5O_6^+$ calcd: 404.2504. Found: 404.2509. (Δ = 1.2 ppm).

N^{10}-(Trifluoroacetyl)folate-γ-(PEG-N_3)-α-*tert*-butyl ester [8-15]:
To a solution of N^{10}-(trifluoroacetyl)pteroic acid (25 mg, 61.3 μmol) and HOSu (10.6 mg, 91.9 μmol) in DMF (1.5 mL) was added DIC (12 μL, 73.6 μmol), and the mixture was allowed to react for 24 h at room temperature with stirring. Reaction progress was monitored by mass spectrometry. The reaction was diluted with H_2O (3 mL), and the mixture was lyophilized to afford a yellow solid, which was the washed with Et_2O (3 x 5 mL), ethyl acetate (3 x 5 mL), and CH_2Cl_2 (3 x 5 mL) to give **8-14** (20 mg, 65%) as a yellow solid. HRMS for $C_{20}H_{15}F_3N_7O_6^+$ calcd: 506.1030. Found: 506.1031 (Δ = 0.2 ppm). The product was taken directly to the next step without additional purification. A solution of **8-14** (20 mg, 39.6 μmol) and **8-13** (47 mg, 0.116 mmol) in DMF (1.5 mL) was allowed to react for 12 h at room temperature with stirring. Reaction progress was monitored by mass spectrometry. The reaction mixture was diluted with H_2O (5 mL) and lyophilized to afford a yellow solid, which was then washed with Et_2O (3 x 5 mL), ethyl acetate (3 x 5 mL), and CH_2Cl_2 (3 x 5 mL) to give **8-15** (18.6 mg, 59%) as a yellow

solid; MS (ESI) *m/z* for $C_{33}H_{43}F_3N_{11}O_9^+$ calcd: 794.3. Found: 794.3. The product was taken directly to the subsequent step without further purification.

Folate-γ-(PEG-N_3)-α-*tert*-butyl ester [8-16]:[34]
A solution of **8-15** (18 mg, 22.7 μmol) in pH 8 NH_4OH (aq.) (1 mL) was allowed to react for 2 h at room temperature with stirring. Reaction progress was monitored by mass spectrometry. The aqueous solution was lyophilized to give **8-16** (15.8 mg, quant.) as a yellow solid; HRMS (TOF) for $C_{31}H_{44}N_{11}O_8^+$ calcd: 698.3369. Found: 698.3412 (Δ = 6.2 ppm). The product was taken directly to the subsequent step without further purification. All data are in agreement with literature values.[34]

Folate-γ-(PEG-N_3)-OH [8-17]:[34]
(JGV-04-076)
A solution of **8-16** (15 mg, 21.5 μmol) in a 95/2.5/2.5 solution of TFA/TIS/H_2O (2 mL), and the reaction mixture was allowed to react for 1 h at room temperature with stirring. Reaction progress was monitored by mass spectrometry. The reaction mixture was diluted with H_2O (5 mL) and lyophilized to afford a yellow solid, which was then washed with Et_2O (3 x 5 mL), ethyl acetate (3 x 5 mL), and CH_2Cl_2 (3 x 5 mL) to give **8-17** (12 mg, 85%) as a yellow solid; HRMS (TOF) for $C_{27}H_{36}N_{11}O_8^+$ calcd: 642.2743. Found: 642.2749 (Δ = 0.9 ppm). All data are in agreement with literature values.[34]

Dual-targeting Biotin-Folate Taxoid Conjugate [8-18]:
To a solution of **5-8** (32 mg, 20.3 μmol), **8-17** (13 mg, 18.7 μmol), and ascorbic acid (3.5 mg, 20.6 μmol) in DMSO (0.8 mL) was added $CuSO_4 \cdot 5H_2O$ (5 mg, 20.6 μmol) in H_2O (1:1) (0.2 mL), and the mixture was stirred for 8 h at room temperature with stirring. The reaction was diluted with H_2O (5 mL), and the mixture was lyophilized to afford a brown solid, which was then washed with Et_2O (3 x 5 mL), THF (3 x 5 mL), and H_2O (3 x 5 mL) to give a yellow solid. The solid was suspended in H_2O (5 mL) and lyophilized to give **8-18** (26 mg, 58%) as a yellow solid; ^{1}H NMR (400 MHz, DMSO-d_6) δ 0.88 (m, 3H), 0.97 (m, 3H), 1.04 (s, 3H), 1.06 (s, 3H), 1.19 (d, *J* = 6.8 Hz, 3H), 1.30 (m, 3H), 1.39 (s, 9H), 1.47 (m, 4H), 1.51 (s, 3H), 1.59 (s, 3H), 1.63 (m, 2H), 1.71 (s, 3H), 1.80 (s, 3H), 1.83 (m, 1H), 2.06 (m, 2H), 2.20 (m, 3H), 2.32 (s, 3H), 2.34 (m, 1H), 2.58 (d, *J* = 12.7 Hz, 1H), 2.81 (dd, *J* = 5.0, 12.7 Hz, 1H), 3.11 (m, 1H), 3.18 (m, 4H), 3.49 (m, 24H), 3.67 (m, 3H), 3.77 (m, 1H), 3.98 (m, 1H), 4.05 (s, 2H), 4.13 (m, 2H), 4.32 (m, 2H), 4.46 (m, 2H), 4.71 (m, 2H), 4.81 (d, *J* = 7.9 Hz, 1H), 4.91 (s, 2H), 4.94 (m, 1H), 5.14 (m, 2H), 5.48 (d, *J* = 7.0 Hz, 1H) 5.99 (m, 1H), 6.31 (s, 1H), 6.36 (m, 1H), 6.62 (m, 1H), 6.89 (m, 1H), 7.31 (m, 3iH), 7.37 (t, *J* = 7.5 Hz, 1H) 7.54 (t, *J* = 7.5 Hz, 2H), 7.67 (t, *J* = 7.2 Hz, 2H), 7.74 (d, *J* = 7.2 Hz, 1H), 7.81 (m, 1H), 7.86 (m, 1H), 7.96 (s, 1H), 8.01 (d, *J* = 7.6 Hz, 2H), 8.66 (m, 1H), 11.45 (bs, 1H); ^{13}C NMR (175 MHz, DMSO-d_6) δ 8.73, 8.82, 10.22, 13.14, 14.19, 14.22, 18.34, 20.50, 20.53, 21.88, 22.97, 25.72, 25.94, 26.80, 28.50, 28.64, 31.23, 31.56, 32.47, 33.05, 35.41, 35.56, 36.24, 37.00, 38.35, 38.87, 43.48, 46.03, 46.69, 49.73, 55.88, 57.97, 59.66, 61.50, 69.60, 70.00, 70.06, 70.19, 70.90, 74.99, 75.77, 77.21, 78.59, 80.88, 84.05, 111.64, 120.70, 127.91, 128.82, 129.10, 129.52, 129.98, 130.39, 131.61, 133.33, 133.86, 136.46, 137.34, 139.98, 155.39, 162.76, 163.17, 165.59, 169.25, 170.06, 170.61, 172.65, 203.00; HRMS (TOF) for $C_{111}H_{151}N_{22}O_{30}S_3^+$ calcd: 2368.0123. Found: 2367.9927 (Δ = -8.3 ppm).

Cell Culture.

All cell lines were obtained from ATCC unless otherwise noted. Cells were cultured in RPMI-1640 cell culture medium (Gibco) in the absence of folic acid, supplemented with 10% (v/v) heat-inactivated fetal bovine serum (FBS) and 1% (v/v) penicillin and streptomycin (PenStrep) at 37 °C in a humidified atmosphere with 5% CO_2. Murine leukemia cell line L1210FR (a gift from Dr. Gregory Russell-Jones, Access Pharmaceuticals Pty Ltd., Australia) was grown as a suspension in supplemented RPMI-1640. Human breast carcinoma, MX-1 and MCF-7, murine ovarian carcinoma, ID8, and normal lung fibroblast, WI-38, cell lines were cultured as monolayers on 100 mm tissue culture dishes in a supplemented RPMI-1640 cell culture medium. Cells were harvested, collected by centrifugation at 850 rpm for 5 min, and resuspended in fresh culture medium. Cell cultures were routinely divided by treatment with trypsin (TrypLE, Gibco) as needed every 2-4 days and collected by centrifugation at 850 rpm for 5 min, and resuspended in fresh cell culture medium, containing varying cell densities for subsequent biological experiments and analysis.

In Vitro Cytotoxicity Assays.

The cytotoxicities (IC_{50}, nM) of paclitaxel, SB-T-1214, folate-dipeptide-PEG-(SS-linker)-SB-T-1214 (**8-7**), and dual-vitamin conjugate DV-1 (**8-18**) were evaluated against various cancer cell lines by means of the standard quantitative colorimetric MTT assay.[33] The inhibitory activity of each compound is represented by the IC_{50} value, which is defined as the concentration required for inhibiting 50% of the cell growth. Cells were harvested, collected, and resuspended in 100 μL cell culture medium (RPMI-1640, folate-free) at a concentrations ranging from 0.5-1.5 x 10^4 cells per well in a 96-well plate. For adhesive cell types, cells were allowed to descend to the bottom of the wells overnight, and appropriate fresh medium was added to each well upon removal of the old medium.

For the MTT assay of paclitaxel, SB-T-1214, **8-7**, and **8-18**, cells were resuspended in 200 μL medium with 8,000 to 10,000 cells per well of a 96-well plate and incubated at 37 °C for 24 h before drug treatment. In DMSO stock solutions, each drug or conjugate was diluted to a series of concentrations in cell culture medium to prepare test solutions. After removing the old medium, these test solutions were added to the wells in the 96-well plate to give the final concentrations ranging from 0.5 to 5,000 nM (100 μL), and the cells were subsequently cultured at 37 °C for 48 of 72 h. For the leukemia cell lines, cells were harvested, collected, and resuspended in the test solutions ranging from 0.5 to 5,000 nM (100 μL) at 0.5 to 0.8 x 10^4 cells per well in a 96-well plate and subsequently incubated at 37 °C for 48 or 72 h.

In another experiment, cells were incubated with **8-7** at 37 °C for 24 h, and GSH (6 equivalents) in cell culture medium (100 μL) was directly added to the wells. These cells were incubated at 37 °C for an additional 48 h; i.e. the total incubation time was also 72 h.

In a separate set of experiments, cells were incubated with [10 μM] folic acid, [10 μM] biotin, or [10 μM] folic acid and [10 μM] biotin for 24 h. Following removal of the vitamin-fortified media and ample washing with PBS, the cells were incubated with **8-7** or **8-18** at 37 °C for an additional 48 h; i.e., the total incubation time was 72 h.

For all experiments, after removing the test medium, fresh solution of MTT in PBS (40 μL of 0.5 mg MTT/mL) was added to the wells, and the cells were incubated at 37 °C for 3 h. The MTT solution was then removed, and the resulting insoluble violet formazan crystals were dissolved in 0.1 N HCl in isopropanol with 10% Triton X-100 (40 μL) to give a violet solution. The spectrophotometric absorbance measurement of each well in the 96-well plate was run at

570 nm using a Labsystems Multiskan Ascent microplate reader. The IC_{50} values and their standard errors were calculated from the viability-concentration curve using Four Parameter Logistic Model of *Sigmaplot*. The concentration of DMSO per well was ≤1% in all cases. Each experiment was run in triplicate.

§8.8.0 References

1. Lucock, M. Folic acid: nutritional biochemistry, molecular biology, and role in disease processes. *Mol Genet Metab.* **2000,** 71, 121-138.
2. Vlahov, I. R.; Leamon, C. P. Engineering folate-drug conjugates to target cancer: from chemistry to clinic. *Bioconjug. Chem.* **2012,** 23, 1357-1369.
3. Leamon, C. P. Folate-targeted drug strategies for the treatment of cancer. *Curr. Opin. Invest. Drugs* **2008,** 9, 1277-1286.
4. Lee, J. W.; Lu, J. Y.; Low, P. S.; Fuchs, P. L. Synthesis and evaluation of taxol-folic acid conjugates as targeted antineoplastics. *Bioorg. Med. Chem.* **2002,** 10, 2397-2414.
5. Low, P. S.; Kularatne, S. A. Folate-targeted therapeutic and imaging agents for cancer. *Curr. Opin. Chem. Biol.* **2009,** 13, 256-262.
6. Yang, J. J.; Kularatne, S. A.; Chen, X.; Low, P. S.; Wang, E. Characterization of in vivo disulfide-reduction mediated drug release in mouse kidneys. *Mol. Pharm.* **2012,** 9, 310-317.
7. Bueno, R.; Appasani, K.; Mercer, H.; Lester, S.; Sugarbaker, D. The alpha folate receptor is highly activated in malignant pleural mesothelioma. *J. Thorac. Cardiovasc. Surg.* **2001,** 121, 225-233.
8. Parker, N.; Turk, M. J.; Westrick, E.; Lewis, J. D.; Low, P. S.; Leamon, C. P. Folate receptor expression in carcinomas and normal tissues determined by a quantitative radioligand binding assay. *Anal. Biochem.* **2005,** 338, 284-293.
9. Ross, J. F.; Chaudhuri, P. K.; Ratnam, M. Differential regulation of folate receptor isoforms in normal and malignant tissues in vivo and in established cell lines. Physiologic and clinical implications. *Cancer* **1994,** 73, 2432-2443.
10. Weitman, S. D.; Lark, R. H.; Coney, L. R.; Fort, D. W.; Frasca, V.; Zurawski, V. R., Jr.; Kamen, B. A. Distribution of the folate receptor GP38 in normal and malignant cell lines and tissues. *Cancer Res.* **1992,** 52, 3396-4401.
11. Salazar, M. D.; Ratnam, M. The folate receptor: what does it promise in tissue-targeted therapeutics? *Cancer Metast Rev* **2007,** 26, 141-152.
12. Matherly, L. H.; Hou, Z.; Deng, Y. Human reduced folate carrier translation of basic biology to cancer etiology and therapy. *Cancer Metast Rev* **2007,** 26, 111-128.
13. Zhao, R.; Min, S. H.; Wang, Y.; Campanella, E.; Low, P. S.; Goldman, I. D. A role for the proton-coupled folate transporter (PCFT-SLC46A1) in folate receptor-mediated endocytosis. *J. Biol. Chem.* **2009,** 284, 4267-4274.
14. Leamon, C. P.; Jackman, A. L. Exploitation of the folate receptor in the management of cancer and inflammatory disease. In *Vitamins and Hormones*, Litwack, G., Ed. 2008; pp 203-233.
15. Sandoval, R. M.; Kennedy, M. D.; Low, P. S.; Molitoris, B. A.; microscopy, U. a. t. o. f. c. o. f. a. i. t. k. d. u. i. t.-p. Uptake and trafficking of fluorescent conjugate of folic acid in tact kidney determined using intravital two-photon microscopy. *Am. J. Physiol.* **2004,** 2, C517-526.
16. Leamon, C. P.; Reddy, J. A.; Vlahov, I.; Westrick, E.; Parker, N.; Nicoson, J. S.; Vetzel, M. Comparative preclinical activity of the folate-targeted Vinca alkaloid conjugates EC140 and EC145. *Int. J. Cancer* **2007,** 121, 1585-1592.

17. Leamon, C. P.; Reddy, J. A.; Vetzel, M.; Dorton, R.; Westrick, E.; Parker, N.; Wang, Y.; Vlahov, I. Folate targeting enables durable and specific antitumor responses from a therapeutically null tubulysin B analogue. *Cancer Res.* **2008,** 68, 9839-9844.
18. Leamon, C. P.; Reddy, J. A.; Vlahov, I.; Westrick, E.; Dawson, A.; Dorton, R.; Vetzel, M.; Santhapuram, H. K.; Wang, Y. Preclinical antitumor activity of a novel folate-targeted dual drug conjugate. *Mol. Pharm.* **2007,** 4, 659-667.
19. Selhub, J.; Emmanouel, D.; Stavropoulos, T.; Arnold, R. Renal folate absorption and the kidney folate binding protein. I. Urinary clearance studies. *Am. J. Physiol.* **1987,** 252, F750-756.
20. Low, P. S.; Henne, W. A.; Doorneweerd, D. D. Discovery and development of folic-acid-based receptor targeting for imaging and therapy of cancer and inflammatory diseases. *Acc. Chem. Res.* **2008,** 41, 120-129.
21. Westerhof, G. R.; Schornagel, J. H.; Kathmann, I.; Jackman, A. L.; Rosowsky, A.; Forsch, R. A.; Hynes, J. B.; Boyle, F. T.; Peters, G. J.; Pinedo, H. M.; et al. Carrier- and receptor-mediated transport of folate antagonists targeting folate-dependent enzymes: correlates of molecular-structure and biological activity. *Mol. Pharm.* **1995,** 48, 459-71.
22. Leamon, C. P.; You, F.; Santhapuram, H. K.; Fan, M.; Vlahov, I. R. Properties influencing the relative binding affinity of pteroate derivatives and drug conjugates thereof to the folate receptor. *Pharm Res.* **2009,** 26, 1315-23.
23. Loftus, P. Merck to pay up to $1 billion for cancer drug. *The Wall Street Journal,* April 16, 2012.
24. Vlahov, I. R.; Santhapuram, H. K.; Kleindl, P. J.; Howard, S. J.; Stanford, K. M.; Leamon, C. P. Design and regioselective synthesis of a new generation of targeted chemotherapeutics. Part 1: EC145, a folic acid conjugate of desacetylvinblastine monohydrazide. *Bioorg. Med. Chem. Lett.* **2006,** 16, 5093-5096.
25. Merck; (2014). Merck and Endocyte announce independent DSMB recommends Vintafolide PROCEED phase 3 trial be stopped for futility following interim analysis [Press Release]. Retrieved from http://www.mercknewsroom.com/news-release/oncology-newsroom/merck-and-endocyte-announce-independent-dsmb-recommends-vintafolide-p.
26. Endocyte; (2014). Merck and Endocyte announce withdrawal of conditional marketing authorization applications for Vintafolide and companion imaging components, Etarfolide and intravenous (IV) folic acid in Europe [Press Release]. Retrieved from http://investor.endocyte.com/releasedetail.cfm?releaseid=848856.
27. Leamon, C. P.; Reddy, J. A.; Klein, P. J.; Vlahov, I. R.; Dorton, R.; Bloomfield, A.; Nelson, M.; Westrick, E.; Parker, N.; Bruna, K.; Vetzel, M.; Gehrke, M.; Nicoson, J. S.; Messmann, R. A.; LoRusso, P. M.; Sausville, E. A. Reducing undesirable hepatic clearance of a tumor-targeted vinca alkaloid via novel saccharopeptidic modifications. *J. Pharmacol. Exp. Ther.* **2011,** 336, 336-343.
28. Vlahov, I. R.; Santhapuram, H. K.; Wang, Y.; Kleindl, P. J.; You, F.; Howard, S. J.; Westrick, E.; Reddy, J. A.; Leamon, C. P. An assembly concept for the consecutive introduction of unsymmetrical disulfide bonds: synthesis of a releasable multidrug conjugate of folic acid. *J. Org. Chem.* **2007,** 72, 5968-5972.
29. Covello, K.; Flefleh, C.; Menard, K.; Wiebesiek, A.; McGlinchey, K.; Wen, M.; Westhouse, R.; Reddy, J.; Vlahov, I.; Hunt, J.; Rose, W.; Leamon, C.; Vite, G.; Lee, F. (April 12-16, 2008). Preclinical pharmacology of epothilone-folate conjugate BMS-753493, a tumor-targeting agent selected for clinical development. *Proceedings of the 99th Annual Meeting of AARC.*, San Diego, CA. Abstract #2326.

30. Fischer, C. R.; Muller, C.; Reber, J.; Muller, A.; Kramer, S. D.; Ametamey, S. M.; Schibli, R. [18F]fluoro-deoxy-glucose folate: a novel PET radiotracer with improved in vivo properties for folate receptor targeting. *Bioconjug. Chem.* **2012,** 23, 805-813.
31. Luo, J.; Smith, M. D.; Lantrip, D. A.; Wang, S.; Fuchs, P. L. Efficient Syntheses of Pyrofolic Acid and Pteroyl Azide, Reagents for the Production of Carboxyl-Differentiated Derivatives of Folic Acid. *J. Am. Chem. Soc.* **1997,** 119, 10004-10013.
32. Paulos, C. M.; Reddy, J. A.; Leamon, C. P.; Turk, M. J.; Low, P. S. Ligand binding and kinetics of folate receptor recycling in vivo: impact on receptor-mediated drug delivery. *Mol. Pharm.* **2004,** 66, 1406-1414.
33. Mosmann, T. Rapid colorimetric assay for cellular growth and survival: application to proliferation and cytotoxicity assays. *J. Immunol. Methods* **1983,** 65, 55-63.
34. Willibald, J.; Harder, J.; Sparrer, K.; Conzelmann, K. K.; Carell, T. Click-modified anandamide siRNA enables delivery and gene silencing in neuronal and immune cells. *J. Am. Chem. Soc.* **2012,** 134, 12330-12333.

References

References for Chapter 1:

1. Drawz, S. M.; Bonomo, R. A. Three decades of beta-lactamase inhibitors. *Clin. Microbiol. Rev.* **2010,** 23, 160-201.
2. Ojima, I. Recent advances in the β-Lactam Synthon Method. *Acc. Chem. Res.* **1995,** 28, 383-389.
3. Kamath, A.; Ojima, I. Advances in the chemistry of beta-lactam and its medicinal applications. *Tetrahedron* **2012,** 68, 10640-10664.
4. Palomo, C.; Aizpurua, J. M.; Ganboa, I.; Oiarbide, M. From beta-lactams to alpha- and beta-amino acid derived peptides. *Amino Acids* **1999,** 16, 321-343.
5. Del Buttero, P.; Molteni, G.; Roncoroni, M. Reductive ring opening of 2-azetidinones promoted by sodium borohydride. *Tetrahedron Lett.* **2006,** 47, 2209-2211.
6. Alcaide, B.; Martin-Cantalejo, Y.; Rodriguez-Lopez, J.; Sierra, M. New reactivity patterns of the beta-lactam ring: tandem C3-C4 bond breakage-rearrangement of 4-acyl- or 4-imino-3,3-dimethoxy-2-azetidinones promoted by stannous chloride (SnCl2-2H2O). *J. Org. Chem.* **1993,** 58, 4767-4770.
7. Staudinger, H. Justus Liebigs Ann. Chem. *Liebigs Ann. Chem.* **1907,** 356, 51.
8. Ojima, I.; Habus, I. Asymmetric synthesis of β-lactams by chiral ester enolate-imine condensation. *Tetrahedron Lett.* **1990,** 31, 4289-4292.
9. Ojima, I.; Habus, I.; Zhao, M.; Zucco, M.; Park, Y. H.; Sun, C. M.; Brigaud, T. New and efficient approaches to the semisynthesis of Taxol and its C-13 side chain analogs by means of β-lactam Synthon Method. *Tetrahedron* **1992,** 48, 6985-7012.
10. Ojima, I.; Slater, J. C.; Michaud, E.; Kuduk, S. D.; Bounaud, P. Y.; Vrignaud, P.; Bissery, M. C.; Veith, J. M.; Pera, P.; Bernacki, R. J. Syntheses and structure-activity relationships of the second-generation antitumor taxoids: exceptional activity against drug-resistant cancer cells. *J. Med. Chem.* **1996,** 39, 3889-3896.
11. Lopez, R.; Sordo, T. L.; Sordo, J. A.; Gonzalez, J. Torquoelectronic effect in the control of stereoselectivity of ketene-imine cycloaddition reactions. *J. Org. Chem.* **1993,** 58, 7036-7037.
12. Jiao, L.; Liang, Y.; Xu, J. Origin of the relative stereoselectivity of the beta-lactam formation in the Staudinger reaction. *J. Am. Chem. Soc.* **2006,** 128, 6060-6069.
13. Palomo, C.; Aizpurua, J. M.; Ganboa, I.; Oiarbide, M. Asymmetric synthesis of β-Lactams by Staudinger Ketene-Imine Cycloaddition Reaction. *Eur. J. Org. Chem.* **1999,** 12, 3223-3235.
14. Lee, E. C.; Hodous, B. L.; Bergin, E.; Shih, C.; Fu, G. C. Catalytic asymmetric Staudinger reactions to form beta-lactams: an unanticipated dependence of diastereoselectivity on the choice of the nitrogen substituent. *J. Am. Chem. Soc.* **2005,** 127, 11586-11587.
15. Brieva, R.; Crich, J. Z.; Sih, C. Chemoenzymatic synthesis of the C-13 side chain of Taxol: Optically-active 3-hydroxy-4-phenyl β-lactam derivatives. *J. Org. Chem.* **1993,** 58, 1068-1075.
16. Whitesell, J. K.; Chen, H.-H.; Lawrence, R. M. trans-2-Phenylcyclohexanol: A powerful and readily available chiral auxiliary. *J. Org. Chem.* **1985,** 50, 4663.
17. Brimble, M. A.; Lee, C. K. Y. Asymmetric azo-ene reactions using the chiral azo-enophile di-(-)-(1R, 2S)-2-phenyl-1-cyclohexyl diazenedicarboxylate. *Tetrahedron: Asymmetry* **1998,** 9, 873-884.

18. Denmark, S. E.; Hurd, A. R.; Sacha, H. J. Tandem [4+2]/[3+2] cycloadditions of nitroalkenes. 13. The synthesis of (-)-detoxinine. *J. Org. Chem.* **1997,** 62, 1668-1674.
19. De Azevedo, M. B. M.; Murta, M. M.; Greene, A. E. Novel, enantioselective lactone construction. First synthesis of methylenolactocin, antitumor antibiotic from Penicillium sp. *J. Org. Chem.* **1992,** 57, 4567-4569.
20. Castro, J.; Moyano, A.; Pericas, M. A.; Riera, A.; Greene, A. E.; Alvarez-Larena, A.; Piniella, J. F. Asymmetric Approach to (+)-beta-Cuparenone by Intramolecular Pauson-Khand Reaction. *J. Org. Chem.* **1996,** 61, 9016-9020.
21. Chassaing, C.; Haudrechy, A.; Langois, Y. Asymmetric palladium annulation: formal synthesis of (+)-huperzine A. *Tetrahedron Lett.* **1999,** 40, 8805-8809.
22. Shankar, B. B.; Kirkup, M. P.; McCombie, S. W.; Clader, J. W.; Ganguly, A. K. Synthesis of an optically pure 3-unsubstituted β-lactam using an asymmetric Reformatsky reaction and its conversion to cholesterol absorption inhibitors. *Tetrahedron Lett.* **1996,** 37, 4095-4098.
23. Carpenter, B. E.; Hunt, I. R.; Keay, B. R. A short efficient preparation of (+) and (−)-trans-2-phenylcyclohexanol. *Tetrahedron: Asymmetry* **1996,** 7, 3107-3108.
24. King, S. B.; Sharpless, K. B. An efficient synthesis of enantiomerically pure trans-2-phenylcyclohexanol. *Tetrahedron Lett.* **1994,** 35, 5611-5612.
25. Kuznetsova, L. U., I.M.; Pepe, A.; Zanardi, I.; Wu, X.; Ojima, I. Trifluoromethyl- and difluoromethyl-β-lactams as useful building blocks for the synthesis of fluorinated amino acids, dipeptides, and fluoro-taxoids. *J. Fluor. Chem.* **2004,** 125, 487-500.
26. Ojima, I.; Fumero-Oderda, C. L.; Kuduk, S. D.; Ma, Z.; Kirikae, F.; Kirikae, T. Structure-activity relationship study of taxoids for their ability to activate murine macrophages as well as inhibit the growth of macrophage-like cells. *Bioorg. Med. Chem.* **2003,** 11, 2867-2888.
27. Kuznetsova, L. V.; Pepe, A.; Ungureanu, I. M.; Pera, P.; Bernacki, R. J.; Ojima, I. Syntheses and Structure-Activity Relationships of Novel 3'-Difluoromethyl and 3'-Trifluoromethyl-Taxoids. *J. Fluor. Chem.* **2008,** 129, 817-828.
28. Gonzalez, J. A., C.; Truesdale, L. Synthesis of (+)-(1S,2R)- and (-)-(1R,2S)-trans-2-phenylcyclohexanol via Sharpless Asymmetric Dihydroxylation (AD). *Org. Synth.* **2002,** 79, 93.
29. Brenner, S.; Goelet, P.; Millward, S. W.; Stackhouse, J. Drug conjugates and methods of designing the same. *US Patent No. WO2001013958 A2* **2000**.
30. Hongwu, Y.; Ballard, C. E.; Boyle, P. D.; Wang, B. An inexpensive carbohydrate derivative used as a chiral auxiliary in the synthesis of α-hydroxy carboxylic acids. *Tetrahedron* **2002,** 58, 7663-7679.
31. Batchelor, M. J.; Bebbington, D.; Bemis, G.; Fridman, W.; Gillespie, R. J.; Golec, J.; Gu, Y.; Lauffer, D. J.; Livingston, D.; Matharu, S. Inhibitors of interleukin-1β converting enzyme. *US Patent No. WO9722619 A2* **1997**.
32. Macrae, M. X.; Blake, S.; Mayer, M.; Yang, J. Nanoscale ionic diodes with tunable and switchable rectifying behavior. *J. Am. Chem. Soc.* **2010,** 132, 1766-1767.
33. Kuznetsova, L.; Sun, L.; Chen, J.; Zhao, X.; Seitz, J.; Das, M.; Li, Y.; Veith, J. M.; Pera, P.; Bernacki, R. J.; Xia, S.; Horwitz, S. B.; Ojima, I. Synthesis and Biological Evaluation of Novel 3'-Difluorovinyl Taxoids. *J. Fluor. Chem.* **2012,** 143, 177-188.

References for Chapter 2:

1. Cancer Statistics 2013: A Presentation from the American Cancer Society, ©2013. American Cancer Society, Inc.
2. *American Cancer Society. Cancer Facts & Figures 2013*; Atlanta: American Cancer Society, 2013.
3. Heron, M. Deaths: leading causes for 2009. *Natl. Vital Stat. Rep.* **2012,** 61, 1-95.
4. Wani, M. C.; Taylor, H. L.; Wall, M. E.; Coggon, P.; McPhail, A. T. Plant antitumor agents. VI. The isolation and structure of taxol, a novel antileukemic and antitumor agent from Taxus brevifolia. *J. Am. Chem. Soc.* **1971,** 93, 2325-2327.
5. Cragg, G. M.; Kingston, D. G. I.; Newman, D. J. *Anticancer agents from natural products*. CRC Press: 2011.
6. Weiss, R. B.; Donehower, R. C.; Wiernik, P. H.; Ohnuma, T.; Gralla, R. J.; Trump, D. L.; Baker, J. R., Jr.; Van Echo, D. A.; Von Hoff, D. D.; Leyland-Jones, B. Hypersensitivity reactions from taxol. *J. Clin. Oncol.* **1990,** 8, 1263-1268.
7. McGuire, W. P.; Rowinsky, E. K.; Rosenshein, N. B.; Grumbine, F. C.; Ettinger, D. S.; Armstrong, D. K.; Donehower, R. C. Taxol: a unique antineoplastic agent with significant activity in advanced ovarian epithelial neoplasms. *Ann. Intern. Med.* **1989,** 111, 273-279.
8. Holmes, F. A.; Walters, R. S.; Theriault, R. L.; Forman, A. D.; Newton, L. K.; Raber, M. N.; Buzdar, A. U.; Frye, D. K.; Hortobagyi, G. N. Phase II trial of taxol, an active drug in the treatment of metastatic breast cancer. *J. Natl. Cancer Inst.* **1991,** 83, 1797-1805.
9. Schiff, P. B.; Fant, J.; Horwitz, S. B. Promotion of microtubule assembly in vitro by taxol. *Nature* **1979,** 277, 665-667.
10. Zhao, X. Design, synthesis and biological evaluation of novel taxane-based anticancer agents and their applications to tumor-targeting drug delivery systems (Doctoral Dissertation). State University of New York at Stony Brook, 2009.
11. Haldar, S.; Chintapalli, J.; Croce, C. M. Taxol induces bcl-2 phosphorylation and death of prostate cancer cells. *Cancer Res.* **1996,** 56, 1253-1255.
12. Blagosklonny, M. V.; Giannakakou, P.; el-Deiry, W. S.; Kingston, D. G.; Higgs, P. I.; Neckers, L.; Fojo, T. Raf-1/bcl-2 phosphorylation: a step from microtubule damage to cell death. *Cancer Res.* **1997,** 57, 130-135.
13. Rodi, D. J.; Janes, R. W.; Sanganee, H. J.; Holton, R. A.; Wallace, B. A.; Makowski, L. Screening of a library of phage-displayed peptides identifies human bcl-2 as a taxol-binding protein. *J. Mol. Biol.* **1999,** 285, 197-203.
14. Bissery, M. C.; Nohynek, G.; Sanderink, G. J.; Lavelle, F. Docetaxel (Taxotere): a review of preclinical and clinical experience. Part I: Preclinical experience. *Anti-cancer Drugs* **1995,** 6, 339-355.
15. Gueritte, F. General and recent aspects of the chemistry and structure-activity relationships of taxoids. *Curr. Pharm. Des.* **2001,** 7, 1229-1249.
16. FDA; (2014). FDA approves new treatment for advanced head and neck cancer [Press Release]. Retrieved from http://www.fda.gov/NewsEvents/Newsroom/PressAnnouncements/2006/ucm108771.htm.
17. Galsky, M. D.; Dritselis, A.; Kirkpatrick, P.; Oh, W. K. Cabazitaxel. *Nat. Rev. Drug Discov.* **2010,** 9, 677-678.

18. Pivot, X.; Koralewski, P.; Hidalgo, J. L.; Chan, A.; Goncalves, A.; Schwartsmann, G.; Assadourian, S.; Lotz, J. P. A multicenter phase II study of XRP6258 administered as a 1-h i.v. infusion every 3 weeks in taxane-resistant metastatic breast cancer patients. *Ann. Oncol.* **2008,** 19, 1547-1552.
19. Chase, M. Cancer drug may save many human lives - at a cost of rare trees. *Wall Street J.* 1991, p A8.
20. Holton, R. A.; Somoza, C.; Kim, B. K.; Liang, F.; Biediger, R. J.; Boatman, P. D.; Shindo, M.; Smith, C. C.; Kim, S. First total synthesis of taxol: 1. Functionalization of the B-ring. *J. Am. Chem. Soc.* **1994,** 116, 1597-1598.
21. Nicolaou, K. C.; Yang, Z.; Liu, J. J.; Ueno, H.; Nantermet, P. G.; Guy, R. K.; Claiborne, C. F.; Renaud, J.; Couladouros, E. A.; Paulvannan, K.; et al. Total synthesis of taxol. *Nature* **1994,** 367, 630-634.
22. Danishefsky, S.; Masters, J.; Young, W.; Link, J.; Snyder, L.; Magee, T.; Jung, D.; Isaacs, R.; Bornmann, W.; Alaimo, C.; Coburn, C.; Grandi, M. Total synthesis of Baccatin III and Taxol. *J. Am. Chem. Soc.* **1996,** 118, 2843-2859.
23. Wender, P. A.; Badham, N.; Conway, S.; Floreancig, P.; Glass, T.; Granicher, C.; Houze, J. B.; Janichen, J.; Lee, D.; Marquess, D.; McGrane, P. L.; Meng, W.; Muccairo, T. P.; Muhlebach, M.; Natchus, M. G.; Paulsen, H.; Rawlins, D. B.; Satkofsky, J.; Shuker, A. J.; Sutton, J. C.; Taylor, R. E.; Tomooka, K. The Pinene Path to Taxanes. 5. Stereocontrolled synthesis of a versatile taxane precursor. *J. Am. Chem. Soc.* **1997,** 119, 2755-2756.
24. Morihira, K.; Hara, R.; Kawahara, S.; Nishimori, T.; Kashima, H.; Nakamura, N.; Kusama, H.; Kuwajima, I. Enantioselective total synthesis of taxol. *J. Am. Chem. Soc.* **1998,** 120, 12980-12981.
25. Mukaiyama, T.; Shiina, I.; Iwadare, H.; Saitoh, M.; Nishimura, T.; Ohkawa, N.; Sakoh, H.; Nishimura, K.; Tani, Y.; Hsagawa, M.; Yamada, K.; Saitoh, K. Asymmetric total synthesis of taxol. *Chem. Eur. J.* **1999,** 5, 121-161.
26. Doi, T.; Fuse, S.; Miyamoto, S.; Nakai, K.; Sasuga, D.; Takahashi, T. A formal total synthesis of taxol aided by an automated synthesizer. *Chem. Asian J.* **2006,** 1, 370-383.
27. Denis, J.; Greene, A. A highly efficient, practical approach to natural Taxol. *J. Am. Chem. Soc.* **1988,** 110, 5917-5919.
28. Ojima, I.; Habus, I.; Zhao, M.; Zucco, M.; Park, Y. H.; Sun, C. M.; Brigaud, T. New and efficient approaches to the semisynthesis of Taxol and its C-13 side chain analogs by means of β-lactam Synthon Method. *Tetrahedron* **1992,** 48, 6985-7012.
29. Ojima, I.; Chen, J.; Sun, L.; Borella, C. P.; Wang, T.; Miller, M. L.; Lin, S.; Geng, X.; Kuznetsova, L.; Qu, C.; Gallager, D.; Zhao, X.; Zanardi, I.; Xia, S.; Horwitz, S. B.; Mallen-St Clair, J.; Guerriero, J. L.; Bar-Sagi, D.; Veith, J. M.; Pera, P.; Bernacki, R. J. Design, synthesis, and biological evaluation of new-generation taxoids. *J. Med. Chem.* **2008,** 51, 3203-3221.
30. Neidigh, K. A.; Gharpure, M. M.; Rimoldi, J. M.; Kingston, D. G. I.; Jiang, Y. Q.; Hamel, E. Synthesis and biological evaluation of 4-deacetylpaclitaxel. *Tetrahedron Lett.* **1994,** 35, 6839-6842.
31. du Bois, A.; Jung, B.; Loehr, A.; Schaller-Kranz, T.; Cohen, M.; Frickhofen, N. A phase I and pharmacokinetic study of novel taxane BMS-188797 and cisplatin in patients with advanced solid tumors. *Br. J. Cancer* **2006,** 94, 79-84.
32. Bröeker, L. E.; de Vos, F. Y. F. L.; van Groeningen, C. J.; Kuenen, B. C.; Gall, H. E.; Woo, M. H.; Voi, M.; Gietema, J. A.; de Vries, E. G. E.; Gianccone, G. Phase I trial with BMS-

275183, a novel oral taxane with promising antitumor activity. *Clin. Cancer Res.* **2006,** 12, 1760-1767.
33. Doggrell, S. A. Clinical trials in restenosis with 7-hexanoyltaxol and paclitaxel-eluting stents. *Expert Rev. Cardiovasc. Ther.* **2004,** 2, 745-752.
34. Altstadt, T. J.; Fairchild, C. R.; Golik, J.; Johnston, K. A.; Kadow, J. F.; Lee, F. Y.; Long, B. H.; Rose, W. C.; Vyas, D. M.; Wong, H.; Wu, M. J.; Wittman, M. D. Synthesis and antitumor activity of novel C-7 paclitaxel ethers: discovery of BMS-184476. *J. Med. Chem.* **2001,** 44, 4577-4583.
35. Ryu, B. Y.; Sohn, J. S.; Hess, M.; Choi, S. K.; Choi, J. K.; Jo, B. W. Synthesis and anti-cancer efficacy of rapid hydrolysed water-soluble paclitaxel pro-drugs. *J. Biomater. Sci. Polym. Ed.* **2008,** 19, 311-324.
36. Chen, S.-H.; Fairchild, C.; Mamber, S. W.; Farina, V. Taxol structure-activity relationships: Synthesis and biological evaluation of 10-deoxytaxol. *J. Org. Chem.* **1993,** 58, 2927-2928.
37. Lyseng-Williamson, K. A.; Fenton, C. Docetaxel. *Drugs* **2005,** 65, 2513-2531.
38. Attard, G.; Greystoke, A.; Kaye, S.; De Bono, J. Update on tubulin-binding agents. *Pathol. Biol. (Paris)* **2006,** 54, 72-84.
39. Ojima, I. Use of fluorine in the medicinal chemistry and chemical biology of bioactive compounds--a case study on fluorinated taxane anticancer agents. *ChemBioChem* **2004,** 5, 628-635.
40. Ojima, I.; Kumar, K.; Awasthi, D.; Vineberg, J. G. Drug discovery targeting cell division proteins, microtubules and FtsZ. *Bioorg. Med. Chem.* **2014,** 2014.02.036 [Epub ahead of print] (March 5, 2014).
41. Kingston, D. G.; Chordia, M. D.; Jagtap, P. G.; Liang, J.; Shen, Y. C.; Long, B. H.; Fairchild, C. R.; Johnston, K. A. Synthesis and Biological Evaluation of 1-Deoxypaclitaxel Analogues. *J. Org. Chem.* **1999,** 64, 1814-1822.
42. Geney, R.; Chen, J.; Ojima, I. Recent advances in the new generation taxane anticancer agents. *Med. Chem.* **2005,** 1, 125-139.
43. Beer, M.; Lenaz, L.; Amadori, D. Phase II study of ortataxel in taxane-resistant breast cancer. *J. Clin. Oncol.* **2008,** 26, 1066.
44. Wind, N. S.; Holen, I. Multidrug resistance in breast cancer: from in vitro models to clinical studies. *Int. J. Breast Cancer* **2011,** 2011, 1-12.
45. Goldstein, L. J. MDR1 gene expression in solid tumours. *Eur. J. Cancer* **1996,** 32A, 1039-1050.
46. Mechetner, E.; Kyshtoobayeva, A.; Zonis, S.; Kim, H.; Stroup, R.; Garcia, R.; Parker, R. J.; Fruehauf, J. P. Levels of multidrug resistance (MDR1) P-glycoprotein expression by human breast cancer correlate with in vitro resistance to taxol and doxorubicin. *Clin. Cancer Res.* **1998,** 4, 389-398.
47. Riordan, J. R.; Deuchars, K.; Kartner, N.; Alon, N.; Trent, J.; Ling, V. Amplification of P-glycoprotein genes in multidrug-resistant mammalian cell lines. *Nature* **1985,** 316, 817-819.
48. Ojima, I.; Zuniga, E. S.; Berger, W. T.; Seitz, J. D. Tumor-targeting drug delivery of new-generation taxoids. *Future Med. Chem.* **2012,** 4, 33-50.
49. Ojima, I.; Slater, J. C.; Michaud, E.; Kuduk, S. D.; Bounaud, P. Y.; Vrignaud, P.; Bissery, M. C.; Veith, J. M.; Pera, P.; Bernacki, R. J. Syntheses and structure-activity relationships of the second-generation antitumor taxoids: exceptional activity against drug-resistant cancer cells. *J. Med. Chem.* **1996,** 39, 3889-3896.

50. Giannakakou, P.; Sackett, D. L.; Kang, Y.-K.; Zhan, Z.; Buters, J. T. M.; Fojo, T.; Poruchynsky, M. S. Paclitaxel-resistant human ovarian cancer cells have mutant β-tubulins that exhibit impaired paclitaxel-driven polymerization. *J. Biol. Chem.* **1997,** 272, 17118-17125.
51. Kovar, J.; Ehrlichova, M.; Smejkalova, B.; Zanardi, I.; Ojima, I.; Gut, I. Comparison of cell death-inducing effect of novel taxane SB-T-1216 and paclitaxel in breast cancer cells. *Anticancer Res.* **2009,** 29, 2951-2960.
52. Ojima, I.; Inoue, T.; Chakravarty, S. Enantiopure fluorine-containing taxoids: potent anticancer agents and versatile probes for biomedical problems. *J. Fluor. Chem.* **1999,** 97, 3-10.
53. Sun, L.; Simmerling, C.; Ojima, I. Recent advances in the study of the bioactive conformation of taxol. *ChemMedChem* **2009,** 4, 719-731.
54. Gut, I.; Ojima, I.; Vaclavikova, R.; Simek, P.; Horsky, S.; Linhart, I.; Soucek, P.; Kondrova, E.; Kuznetsova, L. V.; Chen, J. Metabolism of new-generation taxanes in human, pig, minipig and rat liver microsomes. *Xenobiotica* **2006,** 36, 772-792.
55. Marre, F.; Sanderink, G. J.; de Sousa, G.; Gaillard, C.; Martinet, M.; Rahmani, R. Hepatic biotransformation of docetaxel (Taxotere) in vitro: involvement of the CYP3A subfamily in humans. *Cancer Res.* **1996,** 56, 1296-1302.
56. Monsarrat, B.; Mariel, E.; Cros, S.; Gares, M.; Guenard, D.; Gueritte-Voegelein, F.; Wright, M. Taxol metabolism. Isolation and identification of three major metabolites of taxol in rat bile. *Drug Metab. Dispos.* **1990,** 18, 895-901.
57. Kuznetsova, L.; Sun, L.; Chen, J.; Zhao, X.; Seitz, J.; Das, M.; Li, Y.; Veith, J. M.; Pera, P.; Bernacki, R. J.; Xia, S.; Horwitz, S. B.; Ojima, I. Synthesis and Biological Evaluation of Novel 3'-Difluorovinyl Taxoids. *J. Fluor. Chem.* **2012,** 143, 177-188.
58. Voborilova, J.; Nemcoa-Furstova, V.; Neubauerova, J.; Ojima, I.; Zanardi, I.; Gut, I.; Kovar, J. Cell death induced by novel fluorinated taxanes in drug-sensitive and drug-resistant cancer cells. *Invest. New Drugs* **2011,** 29, 411-423.
59. Ojima, I.; Das, M. Recent advances in the chemistry and biology of new generation taxoids. *J. Nat. Prod.* **2009,** 72, 554-565.
60. Ojima, I. Tumor-targeting drug delivery of chemotherapeutic agents. *Pure Appl. Chem.* **2011,** 83, 1685-1698.
61. Seitz, J. D.; Vineberg, J. G.; Wei, L.; Khan, J. F.; Lichtenthal, B.; Feng, C.-F.; Ojima, I. Design, synthesis, and application of fluorine-labeled taxoids as 19F NMR probes for the metabolic stability assessment of tumor-targeted drug delivery systems. *J. Fluor. Chem.* **2014**, Submitted.
62. Mosmann, T. Rapid colorimetric assay for cellular growth and survival: application to proliferation and cytotoxicity assays. *J. Immunol. Methods* **1983,** 65, 55-63.
63. Chen, S.; Zhao, X.; Chen, J.; Kuznetsova, L.; Wong, S. S.; Ojima, I. Mechanism-based tumor-targeting drug delivery system. Validation of efficient vitamin receptor-mediated endocytosis and drug release. *Bioconjug. Chem.* **2010,** 21, 979-987.
64. Li, X.; Barasoain, I.; Matesnz, R.; Diaz, J. F.; Fang, W.-S. Synthesis and biological activities of high affinity taxane-based fluorescent probes. *Bioorg. Med. Chem. Lett.* **2009,** 19, 751-754.
65. Kuznetsova, L. U., I.M.; Pepe, A.; Zanardi, I.; Wu, X.; Ojima, I. Trifluoromethyl- and difluoromethyl-β-lactams as useful building blocks for the synthesis of fluorinated amino acids, dipeptides, and fluoro-taxoids. *J. Fluor. Chem.* **2004,** 125, 487-500.

66. Mangatal, L.; Adeline, M.; Guenard, D.; Gueritte-Voegelein, F.; Potier, P. Application of the vicinal oxyamination reaction with asymmetric induction to the hemisynthesis of Taxol and analogues. *Tetrahedron* **1989,** 45, 4177-4190.

References for Chapter 3:

1. Ferrara, N.; Kerbel, R. S. Angiogenesis as a therapeutic target. *Nature* **2005,** 438, 967-974.
2. Le, X. F.; Pruefer, F.; Bast, R. C., Jr. HER2-targeting antibodies modulate the cyclin-dependent kinase inhibitor p27Kip1 via multiple signaling pathways. *Cell Cycle* **2005,** 4, 87-95.
3. Goldman, J. M.; Melo, J. V. Chronic myeloid leukemia--advances in biology and new approaches to treatment. *N. Engl. J. Med.* **2003,** 349, 1451-1464.
4. Ojima, I. Guided molecular missiles for tumor-targeting chemotherapy--case studies using the second-generation taxoids as warheads. *Acc. Chem. Res.* **2008,** 41, 108-119.
5. Colquhoun, A.; Miyake, J. A.; Benadiba, M. Fatty acids, eicosanoids, and cancer. *Nutr. Thera. Metabol.* **2009,** 27, 105-112.
6. Schonberg, S. A.; Lundemo, A. G.; Fladvad, T.; Holmgren, K.; Bremseth, H.; Nilsen, A.; Gederaas, O.; Tvedt, K. E.; Egeberg, K. W.; Krokan, H. E. Closely related colon cancer cell lines display different sensitivity to polyunsaturated fatty acids, accumulate different lipid classes and downregulate sterol regulatory element-binding protein 1. *FEBS J.* **2006,** 273, 2749-2765.
7. Lauritzen, L.; Hansen, H. S.; Jorgensen, M. H.; Michaelsen, K. F. The essentiality of long chain n-3 fatty acids in relation to development and function of the brain and retina. *Prog. Lipid Res.* **2001,** 40, 1-94.
8. Schonberg, S. A.; Rudra, P. K.; Noding, R.; Skorpen, F.; Bjerve, K. S.; Krokan, H. E. Evidence that changes in Se-glutathione peroxidase levels affect the sensitivity of human tumour cell lines to n-3 fatty acids. *Carcinogenesis* **1997,** 18, 1897-904.
9. Seitz, J. D. Drug Conjugates with Polyunsaturated Fatty Acids. In *Drug Deliver in Oncology: From Basic Research to Cancer Therapy*, First ed.; Kratz, F., Ed. Wiley-VCH Verlag GmbH & Co. KGaA: Germany, 2012; Vol. 3, pp 1323-1357.
10. Grammatikos, S.; Subbaiah, P.; Victor, T.; Miller, W. n-3 and n-6 fatty acid processing and growth effects in neoplastic and non-cancerous human mammary epithelial cell lines. *Brit. J. Cancer* **1994,** 70, 219-227.
11. Bradley, M. O.; Swindell, C. S.; Anthony, F. H.; Witman, P. A.; Devanesan, P.; Webb, N. L.; Baker, S. D.; Wolff, A. C.; Donehower, R. C. Tumor targeting by conjugation of DHA to paclitaxel. *J. Control. Release* **2001,** 74, 233-236.
12. Mellado, W.; Magri, N. F.; Kingston, D. G.; Garcia-Arenas, R.; Orr, G. A.; Horwitz, S. B. Preparation and biological activity of taxol acetates. *Biochem. Biophys. Res. Commun.* **1984,** 124, 329-336.
13. Bedikian, A. Y.; DeConti, R. C.; Conry, R.; Agarwala, S.; Papadopoulos, N.; Kim, K. B.; Ernstoff, M. Phase 3 study of docosahexaenoic acid-paclitaxel versus dacarbazine in patients with metastatic malignant melanoma. *Ann. Oncol.* **2010,** 22, 787-793.
14. Bradley, M. O.; Webb, N. L.; Anthony, F. H.; Devanesan, P.; Witman, P. A.; Hemamalini, S.; Chander, M. C.; Baker, S. D.; He, L.; Horwitz, S. B.; Swindell, C. S. Tumor targeting by covalent conjugation of a natural fatty acid to paclitaxel. *Clin. Cancer Res.* **2001,** 7, 3229-3238.

15. Kuznetsova, L.; Chen, J.; Sun, L.; Wu, X.; Pepe, A.; Veith, J. M.; Pera, P.; Bernacki, R. J.; Ojima, I. Syntheses and evaluation of novel fatty acid-second-generation taxoid conjugates as promising anticancer agents. *Bioorg. Med. Chem. Lett.* **2006,** 16, 974-977.
16. Seitz, J. D.; Vineberg, J. G.; Ojima, I. Synthesis of a next-generation taxoid by rapid methylation amenable for [11C]-labeling. *J. Org. Chem.*, To be submitted shortly.
17. Warnecke, A. Site-Specific Prodrug Activation and the Concept of Self-Immolation. In *Drug Delivery in Oncology: From Basic Research to Cancer Therapy*, 1 ed.; Kratz, F., Ed. Wiley-VCH Verlag GmbH & Co. KGaA: Germany, 2012; Vol. 2, pp 553-589.
18. Zheng, Z. B.; Zhu, G.; Tak, H.; Joseph, E.; Eiseman, J. L.; Creighton, D. J. N-(2-hydroxypropyl)methacrylamide copolymers of a glutathione (GSH)-activated glyoxalase i inhibitor and DNA alkylating agent: synthesis, reaction kinetics with GSH, and in vitro antitumor activities. *Bioconjug. Chem.* **2005,** 16, 598-607.
19. Ojima, I.; Geng, X.; Wu, X.; Qu, C.; Borella, C. P.; Xie, H.; Wilhelm, S. D.; Leece, B. A.; Bartle, L. M.; Goldmacher, V. S.; Chari, R. V. Tumor-specific novel taxoid-monoclonal antibody conjugates. *J. Med. Chem.* **2002,** 45, 5620-5623.
20. Jaracz, S.; Chen, J.; Kuznetsova, L. V.; Ojima, I. Recent advances in tumor-targeting anticancer drug conjugates. *Bioorg. Med. Chem.* **2005,** 13, 5043-5054.
21. Chen, J.; Chen, S.; Zhao, X.; Kuznetsova, L. V.; Wong, S. S.; Ojima, I. Functionalized single-walled carbon nanotubes as rationally designed vehicles for tumor-targeted drug delivery. *J. Am. Chem. Soc.* **2008,** 130, 16778-16785.
22. Ojima, I. Use of fluorine in the medicinal chemistry and chemical biology of bioactive compounds--a case study on fluorinated taxane anticancer agents. *ChemBioChem* **2004,** 5, 628-635.
23. Wolf, W.; Albright, M. J.; Silver, M. S.; Weber, H.; Reichardt, U.; Sauer, R. Fluorine-19 NMR spectroscopic studies of the metabolism of 5-fluorouracil in the liver of patients undergoing chemotherapy. *Magn. Reson. Imaging* **1987,** 5, 165-169.
24. Gerig, J. T. Fluorine nuclear magnetic resonance of fluorinated ligands. *Methods Enzymol.* **1989,** 177, 3-23.
25. Dalvit, C.; Ardini, E.; Flocco, M.; Fogliatto, G. P.; Mongelli, N.; Veronesi, M. A general NMR method for rapid, efficient, and reliable biochemical screening. *J. Am. Chem. Soc.* **2003,** 125, 14620-14625.
26. Marek, P.; Yirmiya, R.; Liebeskind, J. C. Genetic influences on brain stimulation-produced analgesia in mice: II. Correlation with brain opiate receptor concentration. *Brain Res* **1990,** 507, 155-7.
27. Liebeskind, L. S.; Fengl, R. W. 3-Stannylcyclobutenediones as nucleophilic cyclobutenedione equivalents. Synthesis of substituted cyclobutenediones and cyclobutenedione monoacetals and the beneficial effect of catalytic copper iodide on the Stille reaction. *J. Org. Chem.* **1990,** 55, 5359-5364.
28. Seitz, J. D.; Vineberg, J. G.; Wei, L.; Khan, J. F.; Lichtenthal, B.; Feng, C.-F.; Ojima, I. Design, synthesis, and application of fluorine-labeled taxoids as 19F NMR probes for the metabolic stability assessment of tumor-targeted drug delivery systems. *J. Fluor. Chem.* **2014**, Submitted.
29. Appenzeller-Herzog, C. Glutathione- and non-glutathione-based oxidant control in the endoplasmic reticulum. *J. Cell. Sci.* **2011,** 124, 847-855.
30. Shaabani, A. Potassium Permanganate Oxidation of Organic Compounds. *Synth. Commun.* **2005,** 35, 571-580.

31. Bordwell, F. G. Heterocyclic Aromatic Anions with 4n+2 pi Electrons. *J. Org. Chem.* **1991,** 56, 4218-4223.
32. Chen, S.; Zhao, X.; Chen, J.; Kuznetsova, L.; Wong, S. S.; Ojima, I. Mechanism-based tumor-targeting drug delivery system. Validation of efficient vitamin receptor-mediated endocytosis and drug release. *Bioconjug. Chem.* **2010,** 21, 979-987.
33. Widdison, W. C.; Wilhelm, S. D.; Cavanagh, E. E.; Whiteman, K. R.; Leece, B. A.; Kovtun, Y.; Goldmacher, V. S.; Xie, H.; Steeves, R. M.; Lutz, R. J.; Zhao, R.; Wang, L.; Blattler, W. A.; Chari, R. V. Semisynthetic maytansine analogues for the targeted treatment of cancer. *J. Med. Chem.* **2006,** 49, 4392-4408.
34. Banerjee, P. S.; Zuniga, E. S.; Ojima, I.; Carrico, I. S. Targeted and armed oncolytic adenovirus via chemoselective modification. *Bioorg. Med. Chem. Lett.* **2011,** 21, 4985-4988.
35. Vineberg, J. G.; Zuniga, E. S.; Kamath, A.; Chen, Y. J.; Seitz, J. D.; Ojima, I. Design, Synthesis and Biological Evaluations of Tumor-Targeting Dual-Warhead Conjugates for a Taxoid-Camptothecin Combination Chemotherapy. *J. Med. Chem.* **2014,** 57, 5777-5791.

References for Chapter 4:

1. Sauberlich, H. E. Bioavailability of vitamins. *Prog. Food Nutr. Sci.* **1985,** 9, 1-33.
2. Zempleni, J.; Wijeratne, S. S.; Hassan, Y. I. Biotin. *Biofactors* **2009,** 35, 36-46.
3. Leamon, C. P. Folate-targeted drug strategies for the treatment of cancer. *Curr. Opin. Invest. Drugs* **2008,** 9, 1277-1286.
4. Russell-Jones, G.; McTavish, K.; McEwan, J.; Rice, J.; Nowotnik, D. Vitamin-mediated targeting as a potential mechanism to increase drug uptake by tumours. *J. Inorg. Biochem.* **2004,** 98, 1625-1633.
5. Lu, Y.; Low, P. S. Folate-mediated delivery of macromolecular anticancer therapeutic agents. *Adv. Drug Deliv. Rev.* **2002,** 54, 675-693.
6. Chen, S.; Zhao, X.; Chen, J.; Kuznetsova, L.; Wong, S. S.; Ojima, I. Mechanism-based tumor-targeting drug delivery system. Validation of efficient vitamin receptor-mediated endocytosis and drug release. *Bioconjug. Chem.* **2010,** 21, 979-987.
7. Chen, J.; Chen, S.; Zhao, X.; Kuznetsova, L. V.; Wong, S. S.; Ojima, I. Functionalized single-walled carbon nanotubes as rationally designed vehicles for tumor-targeted drug delivery. *J. Am. Chem. Soc.* **2008,** 130, 16778-16785.
8. Ojima, I. Guided molecular missiles for tumor-targeting chemotherapy--case studies using the second-generation taxoids as warheads. *Acc. Chem. Res.* **2008,** 41, 108-119.
9. Ojima, I.; Zuniga, E. S.; Berger, W. T.; Seitz, J. D. Tumor-targeting drug delivery of new-generation taxoids. *Future Med. Chem.* **2012,** 4, 33-50.
10. Leamon, C. P.; Reddy, J. A.; Klein, P. J.; Vlahov, I. R.; Dorton, R.; Bloomfield, A.; Nelson, M.; Westrick, E.; Parker, N.; Bruna, K.; Vetzel, M.; Gehrke, M.; Nicoson, J. S.; Messmann, R. A.; LoRusso, P. M.; Sausville, E. A. Reducing undesirable hepatic clearance of a tumor-targeted vinca alkaloid via novel saccharopeptidic modifications. *J. Pharmacol. Exp. Ther.* **2011,** 336, 336-343.
11. Vlahov, I. R.; Santhapuram, H. K.; Wang, Y.; Kleindl, P. J.; You, F.; Howard, S. J.; Westrick, E.; Reddy, J. A.; Leamon, C. P. An assembly concept for the consecutive introduction of unsymmetrical disulfide bonds: synthesis of a releasable multidrug conjugate of folic acid. *J. Org. Chem.* **2007,** 72, 5968-5972.

12. Fischer, C. R.; Muller, C.; Reber, J.; Muller, A.; Kramer, S. D.; Ametamey, S. M.; Schibli, R. [18F]fluoro-deoxy-glucose folate: a novel PET radiotracer with improved in vivo properties for folate receptor targeting. *Bioconjug. Chem.* **2012,** 23, 805-813.
13. Zempleni, J. Uptake, localization, and noncarboxylase roles of biotin. *Annu. Rev. Nutr.* **2005,** 25, 175-196.
14. McMahon, R. J. Biotin in metabolism and molecular biology. *Annu. Rev. Nutr.* **2002,** 22, 221-239.
15. Prasad, P. D.; Wang, H.; Kekuda, R.; Fujita, T.; Fei, Y. J.; Devoe, L. D.; Leibach, F. H.; Ganapathy, V. Cloning and functional expression of a cDNA encoding a mammalian sodium-dependent vitamin transporter mediating the uptake of pantothenate, biotin, and lipoate. *J. Biol. Chem.* **1998,** 273, 7501-7506.
16. Luo, S.; Kansara, V. S.; Zhu, X.; Mandava, N. K.; Pal, D.; Mitra, A. K. Functional characterization of sodium-dependent multivitamin transporter in MDCK-MDR1 cells and its utilization as a target for drug delivery. *Mol. Pharmacol.* **2006,** 3, 329-339.
17. Widdison, W. C.; Wilhelm, S. D.; Cavanagh, E. E.; Whiteman, K. R.; Leece, B. A.; Kovtun, Y.; Goldmacher, V. S.; Xie, H.; Steeves, R. M.; Lutz, R. J.; Zhao, R.; Wang, L.; Blattler, W. A.; Chari, R. V. Semisynthetic maytansine analogues for the targeted treatment of cancer. *J. Med. Chem.* **2006,** 49, 4392-4408.
18. Harris, J. M.; Chess, R. B. Effect of pegylation on pharmaceuticals. *Nat. Rev. Drug Discov.* **2003,** 2, 214-221.
19. Cheng, T. L.; Chuang, K. H.; Chen, B. M.; Roffler, S. R. Analytical Measurement of PEGylated Molecules. *Bioconjug. Chem.* **2012,** 23, 881-889.
20. Veronese, F. M.; Pasut, G. PEGylation, successful approach to drug delivery. *Drug Discov. Today* **2005,** 10, 1451-1458.
21. Vlashi, E.; Kelderhouse, L. E.; Sturgis, J. E.; Low, P. S. Effect of folate-targeted nanoparticle size on their rates of penetration into solid tumors. *ACS Nano* **2013,** 7, 8573-8582.
22. Schwabacher, A. W.; Lane, J. W.; Schiesher, M. W.; Leigh, K. M.; Johnson, C. W. Desymmetrization reactions: Efficient preparation of unsymmetrically substituted linker molecules. *J. Org. Chem.* **1998,** 63, 1727-1729.
23. Vineberg, J. G.; Zuniga, E. S.; Kamath, A.; Chen, Y. J.; Seitz, J. D.; Ojima, I. Design, Synthesis and Biological Evaluations of Tumor-Targeting Dual-Warhead Conjugates for a Taxoid-Camptothecin Combination Chemotherapy. *J. Med. Chem.* **2014,** 57, 5777-5791.
24. Mosmann, T. Rapid colorimetric assay for cellular growth and survival: application to proliferation and cytotoxicity assays. *J. Immunol. Methods* **1983,** 65, 55-63.
25. Seitz, J. D.; Vineberg, J. G.; Ojima, I. Synthesis of a next-generation taxoid by rapid methylation amenable for [11C]-labeling. *J. Org. Chem.*, To be submitted shortly.
26. Claesener, M.; Breyholz, H. J.; Hermann, S.; Faust, A.; Wagner, S.; Schober, O.; Schafers, M.; Kopka, K. Efficient synthesis of a fluorine-18 labeled biotin derivative. *Nucl. Med. Biol.* **2012,** 39, 1189-1194.
27. Zhang, D.; Macinkovic, I.; Devarie-Baez, N. O.; Pan, J.; Park, C. M.; Carroll, K. S.; Filipovic, M. R.; Xian, M. Detection of protein S-sulfhydration by a tag-switch technique. *Angew. Chem. Int. Ed.* **2014,** 53, 575-581.
28. Wilchek, M.; Bayer, E. A. Biotin-containing reagents. *Methods Enzymol.* **1990,** 184, 123-138.
29. Fusz, S.; Srivatsan, S. G.; Ackermann, D.; Famulok, M. Photocleavable initiator nucleotide substrates for an aldolase ribozyme. *J. Org. Chem.* **2008,** 73, 5069-5077.

30. Borcard, F.; Godinat, A.; Staedler, D.; Blanco, H. C.; Dumont, A. L.; Chapuis-Bernasconi, C.; Scaletta, C.; Applegate, L. A.; Juillerat, F. K.; Gonzenbach, U. T.; Gerber-Lemaire, S.; Juillerat-Jeanneret, L. Covalent cell surface functionalization of human fetal osteoblasts for tissue engineering. *Bioconjug. Chem.* **2011,** 22, 1422-1432.
31. Li, J. L.; Wang, Y. X.; Tian, H. B.; Zhou, W.; Zhang, X. L.; Lin, Y. W.; Yin, D. Z. An improved radiochemical synthesis of N-succinimidyl 4-F-18-(fluoromethyl)benzoate and the labeling of IgG. *J. Radioanal. Nucl. Chem.* **2002,** 254, 415-419.
32. Luo, Z.; Ding, X.; Hu, Y.; Wu, S.; Xiang, Y.; Zeng, Y.; Zhang, B.; Yan, H.; Zhang, H.; Zhu, L.; Liu, J.; Li, J.; Cai, K.; Zhao, Y. Engineering a hollow nanocontainer platform with multifunctional molecular machines for tumor-targeted therapy in vitro and in vivo. *ACS Nano* **2013,** 7, 10271-10284.
33. Sachin, K.; Jadhav, V. H.; Kim, E. M.; Kim, H. L.; Lee, S. B.; Jeong, H. J.; Lim, S. T.; Sohn, M. H.; Kim, D. W. F-18 labeling protocol of peptides based on chemically orthogonal strain-promoted cycloaddition under physiologically friendly reaction conditions. *Bioconjug. Chem.* **2012,** 23, 1680-1686.
34. Rong, L.; Liu, L. H.; Chen, S.; Cheng, H.; Chen, C. S.; Li, Z. Y.; Qin, S. Y.; Zhang, X. Z. A coumarin derivative as a fluorogenic glycoproteomic probe for biological imaging. *Chem. Commun.* **2014,** 50, 667-669.

References for Chapter 5:

1. Lay, H. N.; Ekert, H.; Colebatch, J. H. Combination chemotherapy for children with acute lymphocytic leukemia who fail to respond to standard remission-induction therapy. *Cancer* **1975,** 36, 1220-1222.
2. Devita, V. T., Jr.; Serpick, A. A.; Carbone, P. P. Combination chemotherapy in the treatment of advanced Hodgkin's disease. *Ann. Intern. Med.* **1970,** 73, 881-895.
3. Rocha Lima, C.; Catapano, C. V.; Pacheco, D.; Sherman, C.; Oakhill, G.; Chaudhry, M.; Freeman, K. D.; Green, M. R. A phase I study of sequential administration of escalating doses of intravenous paclitaxel, oral topotecan, and fixed-dose oral etoposide in patients with solid tumors. *Cancer* **2004,** 100, 2671-2679.
4. Jensen, P. B.; Holm, B.; Sorensen, M.; Christensen, I. J.; Sehested, M. In vitro cross-resistance and collateral sensitivity in seven resistant small-cell lung cancer cell lines: preclinical identification of suitable drug partners to taxotere, taxol, topotecan and gemcitabin. *Br. J. Cancer* **1997,** 75, 869-877.
5. Zimmermann, G. R.; Lehar, J.; Keith, C. T. Multi-target therapeutics: when the whole is greater than the sum of the parts. *Drug. Discov. Today* **2007,** 12, 34-42.
6. Bahadori, H. R.; Green, M. R.; Catapano, C. V. Synergistic interaction between topotecan and microtubule-interfering agents. *Cancer Chemother. Pharmacol.* **2001,** 48, 188-196.
7. Whitacre, C. M.; Zborowska, E.; Gordon, N. H.; Mackay, W.; Berger, N. A. Topotecan increases topoisomerase IIalpha levels and sensitivity to treatment with etoposide in schedule-dependent process. *Cancer Res.* **1997,** 57, 1425-1428.
8. Murren, J. R.; Peccerillo, K.; DiStasio, S. A.; Li, X.; Leffert, J. J.; Pizzorno, G.; Burtness, B. A.; McKeon, A.; Cheng, Y. Dose escalation and pharmacokinetic study of irinotecan in combination with paclitaxel in patients with advanced cancer. *Cancer Chemother. Pharmacol.* **2000,** 46, 43-50.

9. Kaufmann, S. H.; Peereboom, D.; Buckwalter, C. A.; Svingen, P. A.; Grochow, L. B.; Donehower, R. C.; Rowinsky, E. K. Cytotoxic effects of topotecan combined with various anticancer agents in human cancer cell lines. *J. Natl. Cancer Inst.* **1996,** 88, 734-741.
10. Hsiang, Y. H.; Lihou, M. G.; Liu, L. F. Arrest of replication forks by drug-stabilized topoisomerase I-DNA cleavable complexes as a mechanism of cell killing by camptothecin. *Cancer Res.* **1989,** 49, 5077-5082.
11. Slichenmyer, W. J.; Rowinsky, E. K.; Donehower, R. C.; Kaufmann, S. H. The current status of camptothecin analogues as antitumor agents. *J. Natl. Cancer Inst.* **1993,** 85, 271-291.
12. Rothenberg, M. L. Topoisomerase I inhibitors: review and update. *Ann. Oncol.* **1997,** 8, 837-855.
13. Li, L. H.; Fraser, T. J.; Olin, E. J.; Bhuyan, B. K. Action of camptothecin on mammalian cells in culture. *Cancer Res.* **1972,** 32, 2643-2650.
14. Horwitz, S. B.; Horwitz, M. S. Effects of camptothecin on the breakage and repair of DNA during the cell cycle. *Cancer Res.* **1973,** 33, 2834-2836.
15. Rapisarda, A.; Uranchimeg, B.; Scudiero, D. A.; Selby, M.; Sausville, E. A.; Shoemaker, R. H.; Melillo, G. Identification of small molecule inhibitors of hypoxia-inducible factor 1 transcriptional activation pathway. *Cancer Res.* **2002,** 62, 4316-4324.
16. Rapisarda, A.; Uranchimeg, B.; Sordet, O.; Pommier, Y.; Shoemaker, R. H.; Melillo, G. Topoisomerase I-mediated inhibition of hypoxia-inducible factor 1: mechanism and therapeutic implications. *Cancer Res.* **2004,** 64, 1475-1482.
17. Robati, M.; Holtz, D.; Dunton, C. J. A review of topotecan in combination chemotherapy for advanced cervical cancer. *Ther. Clin. Risk Manag.* **2008,** 4, 213-218.
18. Marxsen, J. H.; Schmitt, O.; Metzen, E.; Jelkmann, W.; Hellwig-Burgel, T. Vascular endothelial growth factor gene expression in the human breast cancer cell line MX-1 is controlled by O2 availability in vitro and in vivo. *Ann. Anat.* **2001,** 183, 243-249.
19. Debernardis, D.; Cimoli, G.; Parodi, S.; Russo, P. Interactions between taxol and camptothecin. *Anticancer Drugs* **1996,** 7, 531-4.
20. Madden, T.; Newman, R. A.; Antoun, G.; Johansen, M. J.; Ali-Osman, F. Low-level taxane exposure increases the activity of topoisomerase I targeted agents. *Proc. Am. Assoc. Cancer Res.* **1998,** 39, 527.
21. Bissery, M. C.; Vrignaud, P.; Lavelle, F. In vivo evaluation of the docetaxel-irinotecan combination. *Proc. Am. Assoc. Cancer Res.* **1996,** 37, 378.
22. Chou, T. C.; Motzer, R. J.; Tong, Y.; Bosl, G. J. Computerized quantitation of synergism and antagonism of taxol, topotecan, and cisplatin against human teratocarcinoma cell growth: a rational approach to clinical protocol design. *J. Natl. Cancer Inst.* **1994,** 86, 1517-1524.
23. Pei, X. H.; Nakanishi, Y.; Takayama, K.; Bai, F.; Kawasaki, M.; Tsuruta, N.; Mizuno, K.; Hara, N. Effect of CPT-11 in combination with other anticancer agents in lung cancer cells. *Anticancer Drugs* **1997,** 8, 231-237.
24. Brangi, M.; Litman, T.; Ciotti, M.; Nishiyama, K.; Kohlhagen, G.; Takimoto, C.; Robey, R.; Pommier, Y.; Fojo, T.; Bates, S. E. Camptothecin resistance: role of the ATP-binding cassette (ABC), mitoxantrone-resistance half-transporter (MXR), and potential for glucuronidation in MXR-expressing cells. *Cancer Res.* **1999,** 59, 5938-5946.
25. Hoki, Y.; Fujimori, A.; Pommier, Y. Differential cytotoxicity of clinically important camptothecin derivatives in P-glycoprotein-overexpressing cell lines. *Cancer Chemother. Pharmacol.* **1997,** 40, 433-438.

26. Takahashi, T.; Fujiwara, Y.; Yamakido, M.; Katoh, O.; Watanabe, H.; Mackenzie, P. I. The role of glucuronidation in 7-ethyl-10-hydroxycamptothecin resistance in vitro. *Cancer Sci.* **1997,** 88, 1211-1217.
27. Ojima, I.; Slater, J. C.; Michaud, E.; Kuduk, S. D.; Bounaud, P. Y.; Vrignaud, P.; Bissery, M. C.; Veith, J. M.; Pera, P.; Bernacki, R. J. Syntheses and structure-activity relationships of the second-generation antitumor taxoids: exceptional activity against drug-resistant cancer cells. *J. Med. Chem.* **1996,** 39, 3889-3896.
28. Ojima, I.; Slater, J. C.; Kuduk, S. D.; Takeuchi, C. S.; Gimi, R. H.; Sun, C. M.; Park, Y. H.; Pera, P.; Veith, J. M.; Bernacki, R. J. Syntheses and structure-activity relationships of taxoids derived from 14 beta-hydroxy-10-deacetylbaccatin III. *J. Med. Chem.* **1997,** 40, 267-278.
29. Ojima, I.; Wang, T.; Miller, M. L.; Lin, S.; Borella, C.; Geng, X.; Pera, P.; Bernacki, R. J. Syntheses and structure-activity relationships of new second-generation taxoids. *Bioorg. Med. Chem. Lett.* **1999,** 9, 3423-3428.
30. Ojima, I.; Das, M. Recent advances in the chemistry and biology of new generation taxoids. *J. Nat. Prod.* **2009,** 72, 554-565.
31. Vineberg, J. G.; Zuniga, E. S.; Kamath, A.; Chen, Y. J.; Seitz, J. D.; Ojima, I. Design, Synthesis and Biological Evaluations of Tumor-Targeting Dual-Warhead Conjugates for a Taxoid-Camptothecin Combination Chemotherapy. *J. Med. Chem.* **2014,** 57, 5777-5791.
32. Pouillart, P.; Weiner, R.; Schwarzenberg, L.; Misset, J. L.; Oldham, R.; Amiel, J. L.; Mathe, G. Combination chemotherapy based on a model of cell recruitment by partial synchronization. *Med. Pediatr. Oncol.* **1975,** 1, 123-134.
33. Vlahov, I. R.; Santhapuram, H. K.; Wang, Y.; Kleindl, P. J.; You, F.; Howard, S. J.; Westrick, E.; Reddy, J. A.; Leamon, C. P. An assembly concept for the consecutive introduction of unsymmetrical disulfide bonds: synthesis of a releasable multidrug conjugate of folic acid. *J. Org. Chem.* **2007,** 72, 5968-5972.
34. Mosmann, T. Rapid colorimetric assay for cellular growth and survival: application to proliferation and cytotoxicity assays. *J. Immunol. Methods* **1983,** 65, 55-63.
35. Burke, T. G.; Mishra, A. K.; Wani, M. C.; Wall, M. E. Lipid bilayer partitioning and stability of camptothecin drugs. *Biochemistry* **1993,** 32, 5352-5364.
36. Mistry, S. N.; Baker, J. G.; Fischer, P. M.; Hill, S. J.; Gardiner, S. M.; Kellam, B. Synthesis and in vitro and in vivo characterization of highly beta1-selective beta-adrenoceptor partial agonists. *J. Med. Chem.* **2013,** 56, 3852-3865.

References for Chapter 6:

1. Zolot, R. S.; Basu, S.; Million, R. P. Antibody-drug conjugates. *Nature Rev. Drug Discov.* **2013,** 12, 259-260.
2. Ducry, L.; Stump, B. Antibody-drug conjugates: targeted drug delivery for cancer. *Bioconjug. Chem.* **2010,** 21, 5-13.
3. Alley, S. C.; Okeley, N. M.; Senter, P. D. Antibody drug conjugates: targeted drug delivery for cancer. *Curr. Opin. Chem. Biol.* **2010,** 14, 529-537.
4. Carter, P. J.; Senter, P. D. Antibody-drug conjugates for cancer therapy. *Cancer J.* **2008,** 14, 154-169.

5. Ojima, I.; Geng, X.; Wu, X.; Qu, C.; Borella, C. P.; Xie, H.; Wilhelm, S. D.; Leece, B. A.; Bartle, L. M.; Goldmacher, V. S.; Chari, R. V. Tumor-specific novel taxoid-monoclonal antibody conjugates. *J. Med. Chem.* **2002,** 45, 5620-5623.
6. Jaracz, S.; Chen, J.; Kuznetsova, L. V.; Ojima, I. Recent advances in tumor-targeting anticancer drug conjugates. *Bioorg. Med. Chem.* **2005,** 13, 5043-5054.
7. Vlahov, I. R.; Leamon, C. P. Engineering folate-drug conjugates to target cancer: from chemistry to clinic. *Bioconjug. Chem.* **2012,** 23, 1357-1369.
8. Leamon, C. P. Folate-targeted drug strategies for the treatment of cancer. *Curr. Opin. Invest. Drugs* **2008,** 9, 1277-1286.
9. Chen, S.; Zhao, X.; Chen, J.; Kuznetsova, L.; Wong, S. S.; Ojima, I. Mechanism-based tumor-targeting drug delivery system. Validation of efficient vitamin receptor-mediated endocytosis and drug release. *Bioconjug. Chem.* **2010,** 21, 979-987.
10. Kuznetsova, L.; Chen, J.; Sun, L.; Wu, X.; Pepe, A.; Veith, J. M.; Pera, P.; Bernacki, R. J.; Ojima, I. Syntheses and evaluation of novel fatty acid-second-generation taxoid conjugates as promising anticancer agents. *Bioorg. Med. Chem. Lett.* **2006,** 16, 974-977.
11. Bradley, M. O.; Webb, N. L.; Anthony, F. H. Tumor targeting by covalent conjugation of a natural fatty acid to paclitaxel. *Clin. Cancer Res.* **2001,** 7, 3229-3238.
12. Ojima, I. Guided molecular missiles for tumor-targeting chemotherapy--case studies using the second-generation taxoids as warheads. *Acc. Chem. Res.* **2008,** 41, 108-119.
13. Vineberg, J. G.; Zuniga, E. S.; Kamath, A.; Chen, Y. J.; Seitz, J. D.; Ojima, I. Design, Synthesis and Biological Evaluations of Tumor-Targeting Dual-Warhead Conjugates for a Taxoid-Camptothecin Combination Chemotherapy. *J. Med. Chem.* **2014,** 57, 5777-5791.
14. Miller, P. W.; Long, N. J.; Vilar, R.; Gee, A. D. Synthesis of 11C, 18F, 15O, and 13N radiolabels for positron emission tomography. *Angew. Chem. Int. Ed. Engl.* **2008,** 47, 8998-9033.
15. Valderrama, S.; Van Roekel, N.; Andersson, M.; Goodacre, C. J.; Munoz, C. A. A comparison of the marginal and internal adaptation of titanium and gold-platinum-palladium metal ceramic crowns. *Int J Prosthodont* **1995,** 8, 29-37.
16. Koehler, L.; Gagnon, K.; McQuarrie, S.; Wuest, F. Iodine-124: A promising positron emitter for organic PET chemistry. *Molecules* **2010,** 15, 2686-2718.
17. van Tilburg, E. W.; Franssen, E. J. F.; van der Hoeven, J. J. M.; van der Meij, M.; Elshove, D.; Lammertsma, A. A.; Windhorst, A. D. Radiosynthesis of [11C]docetaxel. *J. Labelled Comp. Radiopharm.* **2004,** 47, 763-777.
18. Seitz, J. D.; Vineberg, J. G.; Ojima, I. Synthesis of a next-generation taxoid by rapid methylation amenable for [11C]-labeling. *J. Org. Chem.*, To be submitted shortly.
19. Morita, S.; Otsubo, K.; Matsubara, J.; Ohtani, T.; Kawano, Y.; Ohmori, K.; Ohguro, K.; Uchida, M. Synthesis of possible metabolites of 1-cyclopropyl-1,4-dihydro-6-fluoro-5-methyl-7-(3-methyl-1-piperazinyl)- 4-oxo-3-quinolinecarboxylic acid (Grepafloxacin, OPC-17116). *Chem Pharm Bull (Tokyo)* **1995,** 43, 2246-52.
20. Fowler, J. S.; Ido, T. Initial and subsequent approach for the synthesis of 18FDG. *Semin. Nucl. Med.* **2002,** 32, 6-12.
21. Marik, J.; Sutcliffe, J. L. Click for PET: rapid preparation of [18F]fluoropeptides using Cu(I) catalyzed 1,3-dipolar cycloaddition. *Tetrahedron Lett.* **2006,** 47, 6681-6684.
22. Shoup, T. M.; Fischman, A. J.; Jaywook, S.; Babich, J. W.; Strauss, H. W.; Elmaleh, D. R. Synthesis of fluorine-18-labeled biotin derivatives: biodistribution and infection localization. *J. Nucl. Med.* **1994,** 35, 1685-90.

23. Kudo, T.; Ueda, M.; Konishi, H.; Kawashima, H.; Kuge, Y.; Mukai, T.; Miyano, A.; Tanaka, S.; Kizaka-Kondoh, S.; Hiraoka, M.; Saji, H. PET imaging of hypoxia-inducible factor-1-active tumor cells with pretargeted oxygen-dependent degradable streptavidin and a novel 18F-labeled biotin derivative. *Mol. Imaging Biol.* **2011,** 13, 1003-10.
24. Kim, D. W.; Jeong, H. J.; Lim, S. T.; Sohn, M. H.; Katzenellenbogen, J. A.; Chi, D. Y. Facile nucleophilic fluorination reactions using tert-alcohols as a reaction medium: significantly enhanced reactivity of alkali metal fluorides and improved selectivity. *Journal of Organic Chemistry* **2008,** 73, 957-62.
25. Paulos, C. M.; Reddy, J. A.; Leamon, C. P.; Turk, M. J.; Low, P. S. Ligand binding and kinetics of folate receptor recycling in vivo: impact on receptor-mediated drug delivery. *Mol Pharmacol* **2004,** 66, 1406-14.
26. Shai, Y.; Kirk, K. L.; Channing, M. A.; Dunn, B. B.; Lesniak, M. A.; Eastman, R. C.; Finn, R. D.; Roth, J.; Jacobson, K. A. 18F-labeled insulin: a prosthetic group methodology for incorporation of a positron emitter into peptides and proteins. *Biochemistry* **1989,** 28, 4801-6.
27. Breyholz, H. J.; Wagner, S.; Faust, A.; Riemann, B.; Holtke, C.; Hermann, S.; Schober, O.; Schafers, M.; Kopka, K. Radiofluorinated pyrimidine-2,4,6-triones as molecular probes for noninvasive MMP-targeted imaging. *ChemMedChem.* **2010,** 5, 777-89.
28. Mosmann, T. Rapid colorimetric assay for cellular growth and survival: application to proliferation and cytotoxicity assays. *J. Immunol. Methods* **1983,** 65, 55-63.

References for Chapter 7:

1. Miller, P. W.; Long, N. J.; Vilar, R.; Gee, A. D. Synthesis of [11C], [18F], [15O], and [13N] radiolabels for positron emission tomography. *Angew. Chem. Int. Ed.* **2008,** 47, 8998-9033.
2. Ametamey, S. M.; Honer, M.; Schubiger, P. A. Molecular imaging with PET. *Chem. Rev.* **2008,** 108, 1501-1516.
3. Wood, K. A.; Hoskin, P. J.; Saunders, M. I. Positron emission tomography in oncology: A review. *Clin. Oncol.* **2007,** 19, 237-255.
4. Weber, W. A. Positron emission tomography as an imaging biomarker. *J. Clin. Oncol.* **2006,** 24, 3282-3292.
5. Oriuchi, N.; Higuchi, T.; Ishikita, T.; Miyakubo, M.; Hanaoka, H.; Ilda, Y.; Endo, K. Present role and future prospects of positron emission tomography in clinical oncology. *Cancer Sci.* **2006,** 97, 1291-1297.
6. Schwaiger, M.; Ziegler, S.; Nekolla, S. G. PET/CT: challenge for nuclear cardiology. *J. Nucl. Med.* **2005,** 46, 1664-1678.
7. Herholz, K.; Heiss, W. D. Positron emission tomography in clinical neurology. *Mol. Imaging Biol.* **2004,** 6, 239-269.
8. Wu, C. Y.; Pike, V. W.; Wang, Y. M. Amyloid imaging: From benchtop to bedside. *Curr. Top. Dev. Biol.* **2005,** 70, 171-213.
9. Wolf, A. P.; Redvantly, C. S. Carbon-11 and radiopharmaceuticals. *Appl. Radiat. Isot.* **1977,** 28, 29-48.
10. Ferreiri, R. A.; Wolf, A. P. The chemistry of positron emitting nucleogenic (hot) atoms with regard to preparation of labelled compounds of practical utility. *Radiochim. Acta* **1983,** 34, 69-84.
11. Bolton, R. Isotopic methylation. *J. Labelled Compd. Radiopharm.* **2001,** 44, 701-736.

12. Långström, B.; Antoni, G.; Gullberg, P.; Halldin, C.; Malmborg, P.; Nagren, K.; Rimland, A.; Svard, H. Synthesis of L-and D-[methyl-11C] methionine. *J. Nucl. Med.* **1987,** 28, 1037-1040.
13. Larsen, P.; Ulin, J.; Dahlstrom, K.; Jensen, M. Synthesis of [11C] iodomethane by iodination of [11C] methane. *Appl. Radiat. Isot.* **1997,** 48, 153-157.
14. Link, J. M.; Krohn, K. A.; Clark, J. C. Production of [11C] CH3I by single pass reaction of [11C] CH4 with I2. *Nucl. Med. Biol.* **1997,** 24, 93-97.
15. Hosoya, T.; Sumi, K.; Doi, H.; Wakao, M.; Suzuki, M. Rapid methylation on carbon frameworks useful for the synthesis of 11 CH 3-incorporated PET tracers: Pd (0)-mediated rapid coupling of methyl iodide with an alkenyltributylstannane leading to a 1-methylalkene. *Org. Biomol. Chem.* **2006,** 4, 410-415.
16. Hamill, T. G.; Krause, S.; Ryan, C.; Bonnefous, C.; Govek, S.; Seiders, T. J.; Cosford, N. D. P.; Roppe, J.; Kamenecka, T.; Patel, S.; Gibson, R. E.; Sanabria, S.; Riffel, K.; Eng, W. S.; King, C.; Yang, X. Q.; Green, M. D.; O'Malley, S. S.; Hargreaves, R.; Burns, H. D. Synthesis, characterization, and first successful monkey imaging studies of metabotropic glutamate receptor subtype 5 (mGluR5) PET radiotracers. *Synapse* **2006,** 56, 205-216.
17. Andersson, Y.; Cheng, A.; Langstrom, B. Palladium-promoted coupling reactions of [11C]methyl iodide with organotin and organoboron compounds. *Acta Chem. Scand.* **1995,** 49, 683-688.
18. Koehler, L.; Gagnon, K.; McQuarrie, S.; Wuest, F. Iodine-124: A promising positron emitter for organic PET chemistry. *Molecules* **2010,** 15, 2686-2718.
19. Kiesewetter, D. O.; Jagoda, E. M.; Kao, C.-H. K.; Ma, Y.; Ravasi, L.; Shimoji, K.; Szajek, L. P.; Eckelman, W. C. Fluoro-, bromo-, and iodopaclitaxel derivatives: synthesis and biological evaluation. *Nucl. Med. Biol.* **2003,** 30, 11-24.
20. van Tilburg, E. W.; Franssen, E. J. F.; van der Hoeven, J. J. M.; van der Meij, M.; Elshove, D.; Lammertsma, A. A.; Windhorst, A. D. Radiosynthesis of [11C]docetaxel. *J. Labelled Comp. Radiopharm.* **2004,** 47, 763-777.
21. Seitz, J. D.; Vineberg, J. G.; Ojima, I. Synthesis of a next-generation taxoid by rapid methylation amenable for [11C]-labeling. *J. Org. Chem.*, To be submitted shortly.
22. Seitz, J. D. The design, synthesis and biological evaluation of novel taxoid anticancer agents and their tumor-targeted drug conjugates (Doctoral Dissertation). State University of New York at Stony Brook, 2013.
23. Morita, D. K.; Stille, J. K.; Norton, J. R. Methyl/phenyl exchange between palladium and a phosphine ligand. Consequences for catalytic coupling reactions. *J. Am. Chem. Soc.* **1995,** 117, 8576-8581.
24. Hinkle, R. J.; Poulter, G. T.; Stang, P. J. Palladium (II) and copper (I) cocatalyzed coupling of stereodefined alkenyl (phenyl) iodonium triflates and unsaturated tri-n-butylstannanes. *J. Am. Chem. Soc.* **1993,** 115, 11626-11627.
25. Liebeskind, L. S.; Fengl, R. W. 3-Stannylcyclobutenediones as nucleophilic cyclobutenedione equivalents. Synthesis of substituted cyclobutenediones and cyclobutenedione monoacetals and the beneficial effect of catalytic copper iodide on the Stille reactio. *J. Org. Chem.* **1990,** 55, 5359-5364.
26. Farina, V.; Kapadia, S.; Krishnan, B.; Wang, C.; Liebeskind, L. S. On the nature of the "copper effect" in the Stille cross-coupling. *J. Org. Chem.* **1994,** 59, 5905-5911.

27. Kim, D. W.; Choe, Y. S.; Chi, D. Y. A new nucleophilic fluorine-18 labeling method for aliphatic mesylates: Reaction in ionic liquids show tolerance for water. *Nucl. Med. Biol.* **2003,** 30, 345-350.
28. Been, L. B.; Suurmeijer, A. J.; Cobben, D. C.; Jager, P. L.; Hoekstra, H. J.; Elsinga, P. H. [18F]FLT-PET in oncology: current status and opportunities. *Eur. J. Nucl. Med. Mol. Imaging* **2004,** 31, 1659-1672.
29. Mukherjee, J.; Yang, Z. Y.; Das, M. K.; Brown, T. Fluorinated benzamide neuroleptics - III. Development of (S)-N-[(1-allyl-2-pyrrolidinyl)methyl]-5-(3-[18F]fluoropropyl)-2, 3-dimethoxybenzamide as an improved dopamine D-2 receptor tracer. *Nucl. Med. Biol.* **1995,** 22, 283-296.
30. Kilbourn, M. R.; Welch, M. J.; Dence, C. S.; Tewson, T. J.; Saji, H.; Maeda, M. Carrier-added and no-carrier-added syntheses of [18F]spiroperidol and [18F]haloperidol. *Int. J. Appl. Radiat. Isot.* **1984,** 35, 591-598.
31. Hamacher, K.; Hamkens, W. Remote controlled one-step production of 18F labeled butyrophenone neuroleptics exemplified by the synthesis of nca [18F] N-methylspiperone. *Appl. Radiat. Isot.* **1995,** 46, 911-916.
32. Grierson, J. R.; Link, J. M.; Mathis, C. A.; Rasey, J. S.; Krohn, K. A. A radiosynthesis of fluorine-18 fluoromisonidazole. *J. Nucl. Med.* **1989,** 30, 343-350.
33. Park, B. K.; Kitteringham, N. R.; O'Neill, P. M. Metabolism of fluorine-containing drugs. *Annu. Rev. Pharmacol. Toxicol.* **2001,** 41, 443-470.
34. Bohm, H. J.; Banner, D.; Bendels, S.; Kansy, M.; Kuhn, B.; Muller, K.; Obst-Sander, U.; Stahl, M. Fluorine in medicinal chemistry. *ChemBioChem* **2004,** 5, 637-643.
35. Bégué, J.; Bonnet-Delpon, D. Recent advances (1995-2005) in fluorinated pharmaceuticals based on natural products. *J. Fluor. Chem.* **2006,** 127, 992-1012.
36. Claesener, M.; Breyholz, H. J.; Hermann, S.; Faust, A.; Wagner, S.; Schober, O.; Schafers, M.; Kopka, K. Efficient synthesis of a fluorine-18 labeled biotin derivative. *Nucl. Med. Biol.* **2012,** 39, 1189-1194.
37. Kudo, T.; Ueda, M.; Konishi, H.; Kawashima, H.; Kuge, Y.; Mukai, T.; Miyano, A.; Tanaka, S.; Kizaka-Kondoh, S.; Hiraoka, M.; Saji, H. PET imaging of hypoxia-inducible factor-1-active tumor cells with pretargeted oxygen-dependent degradable streptavidin and a novel 18F-labeled biotin derivative. *Mol. Imaging Biol.* **2011,** 13, 1003-1010.
38. Betzel, T.; Muller, C.; Groehn, V.; Muller, A.; Reber, J.; Fischer, C. R.; Kramer, S. D.; Schibli, R.; Ametamey, S. M. Radiosynthesis and preclinical evaluation of 3'-Aza-2'-[(18)F]fluorofolic acid: a novel PET radiotracer for folate receptor targeting. *Bioconjug. Chem.* **2013,** 24, 205-214.
39. Morris, R. T.; Joyrich, R. N.; Naumann, R. W.; Shah, N. P.; Maurer, A. H.; Strauss, H. W.; Uszler, J. M.; Symanowski, J. T.; Ellis, P. R.; Harb, W. A. Phase II study of treatment of advanced ovarian cancer with folate-receptor-targeted therapeutic (vintafolide) and companion SPECT-based imaging agent (99mTc-etarfolatide). *Ann. Oncol.* **2014,** 25, 852-858.

References for Chapter 8:

1. Lucock, M. Folic acid: nutritional biochemistry, molecular biology, and role in disease processes. *Mol Genet Metab.* **2000,** 71, 121-138.

2. Vlahov, I. R.; Leamon, C. P. Engineering folate-drug conjugates to target cancer: from chemistry to clinic. *Bioconjug. Chem.* **2012,** 23, 1357-1369.
3. Leamon, C. P. Folate-targeted drug strategies for the treatment of cancer. *Curr. Opin. Invest. Drugs* **2008,** 9, 1277-1286.
4. Lee, J. W.; Lu, J. Y.; Low, P. S.; Fuchs, P. L. Synthesis and evaluation of taxol-folic acid conjugates as targeted antineoplastics. *Bioorg. Med. Chem.* **2002,** 10, 2397-2414.
5. Low, P. S.; Kularatne, S. A. Folate-targeted therapeutic and imaging agents for cancer. *Curr. Opin. Chem. Biol.* **2009,** 13, 256-262.
6. Yang, J. J.; Kularatne, S. A.; Chen, X.; Low, P. S.; Wang, E. Characterization of in vivo disulfide-reduction mediated drug release in mouse kidneys. *Mol. Pharm.* **2012,** 9, 310-317.
7. Bueno, R.; Appasani, K.; Mercer, H.; Lester, S.; Sugarbaker, D. The alpha folate receptor is highly activated in malignant pleural mesothelioma. *J. Thorac. Cardiovasc. Surg.* **2001,** 121, 225-233.
8. Parker, N.; Turk, M. J.; Westrick, E.; Lewis, J. D.; Low, P. S.; Leamon, C. P. Folate receptor expression in carcinomas and normal tissues determined by a quantitative radioligand binding assay. *Anal. Biochem.* **2005,** 338, 284-293.
9. Ross, J. F.; Chaudhuri, P. K.; Ratnam, M. Differential regulation of folate receptor isoforms in normal and malignant tissues in vivo and in established cell lines. Physiologic and clinical implications. *Cancer* **1994,** 73, 2432-2443.
10. Weitman, S. D.; Lark, R. H.; Coney, L. R.; Fort, D. W.; Frasca, V.; Zurawski, V. R., Jr.; Kamen, B. A. Distribution of the folate receptor GP38 in normal and malignant cell lines and tissues. *Cancer Res.* **1992,** 52, 3396-4401.
11. Salazar, M. D.; Ratnam, M. The folate receptor: what does it promise in tissue-targeted therapeutics? *Cancer Metast Rev* **2007,** 26, 141-152.
12. Matherly, L. H.; Hou, Z.; Deng, Y. Human reduced folate carrier translation of basic biology to cancer etiology and therapy. *Cancer Metast Rev* **2007,** 26, 111-128.
13. Zhao, R.; Min, S. H.; Wang, Y.; Campanella, E.; Low, P. S.; Goldman, I. D. A role for the proton-coupled folate transporter (PCFT-SLC46A1) in folate receptor-mediated endocytosis. *J. Biol. Chem.* **2009,** 284, 4267-4274.
14. Leamon, C. P.; Jackman, A. L. Exploitation of the folate receptor in the management of cancer and inflammatory disease. In *Vitamins and Hormones*, Litwack, G., Ed. 2008; pp 203-233.
15. Sandoval, R. M.; Kennedy, M. D.; Low, P. S.; Molitoris, B. A.; microscopy, U. a. t. o. f. c. o. f. a. i. t. k. d. u. i. t.-p. Uptake and trafficking of fluorescent conjugate of folic acid in tact kidney determined using intravital two-photon microscopy. *Am. J. Physiol.* **2004,** 2, C517-526.
16. Leamon, C. P.; Reddy, J. A.; Vlahov, I.; Westrick, E.; Parker, N.; Nicoson, J. S.; Vetzel, M. Comparative preclinical activity of the folate-targeted Vinca alkaloid conjugates EC140 and EC145. *Int. J. Cancer* **2007,** 121, 1585-1592.
17. Leamon, C. P.; Reddy, J. A.; Vetzel, M.; Dorton, R.; Westrick, E.; Parker, N.; Wang, Y.; Vlahov, I. Folate targeting enables durable and specific antitumor responses from a therapeutically null tubulysin B analogue. *Cancer Res.* **2008,** 68, 9839-9844.
18. Leamon, C. P.; Reddy, J. A.; Vlahov, I.; Westrick, E.; Dawson, A.; Dorton, R.; Vetzel, M.; Santhapuram, H. K.; Wang, Y. Preclinical antitumor activity of a novel folate-targeted dual drug conjugate. *Mol. Pharm.* **2007,** 4, 659-667.
19. Selhub, J.; Emmanouel, D.; Stavropoulos, T.; Arnold, R. Renal folate absorption and the kidney folate binding protein. I. Urinary clearance studies. *Am. J. Physiol.* **1987,** 252, F750-756.

20. Low, P. S.; Henne, W. A.; Doorneweerd, D. D. Discovery and development of folic-acid-based receptor targeting for imaging and therapy of cancer and inflammatory diseases. *Acc. Chem. Res.* **2008,** 41, 120-129.
21. Westerhof, G. R.; Schornagel, J. H.; Kathmann, I.; Jackman, A. L.; Rosowsky, A.; Forsch, R. A.; Hynes, J. B.; Boyle, F. T.; Peters, G. J.; Pinedo, H. M.; et al. Carrier- and receptor-mediated transport of folate antagonists targeting folate-dependent enzymes: correlates of molecular-structure and biological activity. *Mol. Pharm.* **1995,** 48, 459-71.
22. Leamon, C. P.; You, F.; Santhapuram, H. K.; Fan, M.; Vlahov, I. R. Properties influencing the relative binding affinity of pteroate derivatives and drug conjugates thereof to the folate receptor. *Pharm Res.* **2009,** 26, 1315-23.
23. Loftus, P. Merck to pay up to $1 billion for cancer drug. *The Wall Street Journal,* April 16, 2012.
24. Vlahov, I. R.; Santhapuram, H. K.; Kleindl, P. J.; Howard, S. J.; Stanford, K. M.; Leamon, C. P. Design and regioselective synthesis of a new generation of targeted chemotherapeutics. Part 1: EC145, a folic acid conjugate of desacetylvinblastine monohydrazide. *Bioorg. Med. Chem. Lett.* **2006,** 16, 5093-5096.
25. Merck; (2014). Merck and Endocyte announce independent DSMB recommends Vintafolide PROCEED phase 3 trial be stopped for futility following interim analysis [Press Release]. Retrieved from http://www.mercknewsroom.com/news-release/oncology-newsroom/merck-and-endocyte-announce-independent-dsmb-recommends-vintafolide-p.
26. Endocyte; (2014). Merck and Endocyte announce withdrawal of conditional marketing authorization applications for Vintafolide and companion imaging components, Etarfolide and intravenous (IV) folic acid in Europe [Press Release]. Retrieved from http://investor.endocyte.com/releasedetail.cfm?releaseid=848856.
27. Leamon, C. P.; Reddy, J. A.; Klein, P. J.; Vlahov, I. R.; Dorton, R.; Bloomfield, A.; Nelson, M.; Westrick, E.; Parker, N.; Bruna, K.; Vetzel, M.; Gehrke, M.; Nicoson, J. S.; Messmann, R. A.; LoRusso, P. M.; Sausville, E. A. Reducing undesirable hepatic clearance of a tumor-targeted vinca alkaloid via novel saccharopeptidic modifications. *J. Pharmacol. Exp. Ther.* **2011,** 336, 336-343.
28. Vlahov, I. R.; Santhapuram, H. K.; Wang, Y.; Kleindl, P. J.; You, F.; Howard, S. J.; Westrick, E.; Reddy, J. A.; Leamon, C. P. An assembly concept for the consecutive introduction of unsymmetrical disulfide bonds: synthesis of a releasable multidrug conjugate of folic acid. *J. Org. Chem.* **2007,** 72, 5968-5972.
29. Covello, K.; Flefleh, C.; Menard, K.; Wiebesiek, A.; McGlinchey, K.; Wen, M.; Westhouse, R.; Reddy, J.; Vlahov, I.; Hunt, J.; Rose, W.; Leamon, C.; Vite, G.; Lee, F. (April 12-16, 2008). Preclinical pharmacology of epothilone-folate conjugate BMS-753493, a tumor-targeting agent selected for clinical development. *Proceedings of the 99th Annual Meeting of AARC.*, San Diego, CA. Abstract #2326.
30. Fischer, C. R.; Muller, C.; Reber, J.; Muller, A.; Kramer, S. D.; Ametamey, S. M.; Schibli, R. [18F]fluoro-deoxy-glucose folate: a novel PET radiotracer with improved in vivo properties for folate receptor targeting. *Bioconjug. Chem.* **2012,** 23, 805-813.
31. Luo, J.; Smith, M. D.; Lantrip, D. A.; Wang, S.; Fuchs, P. L. Efficient Syntheses of Pyrofolic Acid and Pteroyl Azide, Reagents for the Production of Carboxyl-Differentiated Derivatives of Folic Acid. *J. Am. Chem. Soc.* **1997,** 119, 10004-10013.

32. Paulos, C. M.; Reddy, J. A.; Leamon, C. P.; Turk, M. J.; Low, P. S. Ligand binding and kinetics of folate receptor recycling in vivo: impact on receptor-mediated drug delivery. *Mol. Pharm.* **2004,** 66, 1406-1414.
33. Mosmann, T. Rapid colorimetric assay for cellular growth and survival: application to proliferation and cytotoxicity assays. *J. Immunol. Methods* **1983,** 65, 55-63.
34. Willibald, J.; Harder, J.; Sparrer, K.; Conzelmann, K. K.; Carell, T. Click-modified anandamide siRNA enables delivery and gene silencing in neuronal and immune cells. *J. Am. Chem. Soc.* **2012,** 134, 12330-12333.

Appendix Chapter 1

Compound Name: JGV-01-040
Processed by: Jacob Vineberg
Pulse Sequence: s2pul
Spectrometer Freq.: 300.07 MHz
Solvent: $CDCl_3$
Temperature: 298.15 K
Spectral Width: 15.00 ppm
Number of Scans: 16
Relaxation Delay: 1.000 s

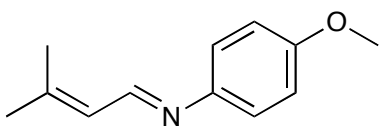

Imine 1-1

Compound Name: JGV-01-008b
Processed by: Jacob Vineberg
Pulse Sequence: s2pul
Spectrometer Freq.: 300.07 MHz
Solvent: $CDCl_3$
Temperature: 298.15 K
Spectral Width: 15.00 ppm
Number of Scans: 80
Relaxation Delay: 1.000 s

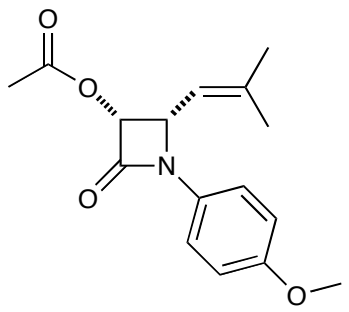

β-Lactam (±)1-2

Compound Name: JGV-01-011a
Processed by: Jacob Vineberg
Pulse Sequence: s2pul
Spectrometer Freq.: 300.07 MHz
Solvent: $CDCl_3$
Temperature: 298.15 K
Spectral Width: 15.00 ppm
Number of Scans: 16
Relaxation Delay: 1.000 s

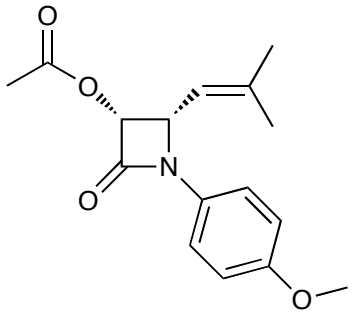

β-Lactam (+)1-2

Compound Name: JGV-01-018
Processed by: Jacob Vineberg
Pulse Sequence: s2pul
Spectrometer Freq.: 300.07 MHz
Solvent: $CDCl_3$
Temperature: 298.15 K
Spectral Width: 15.00 ppm
Number of Scans: 16
Relaxation Delay: 1.000 s

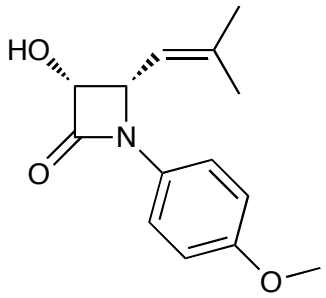

β-Lactam (+)1-3

Compound Name: JGV-01-044
Processed by: Jacob Vineberg
Pulse Sequence: s2pul
Spectrometer Freq.: 300.07 MHz
Solvent: $CDCl_3$
Temperature: 298.15 K
Spectral Width: 15.00 ppm
Number of Scans: 16
Relaxation Delay: 1.000 s

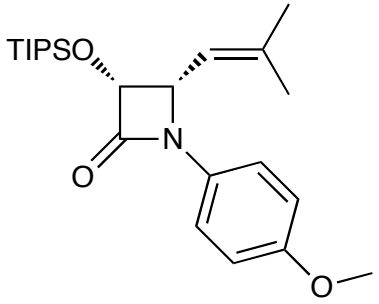

β-Lactam (+)1-4

Compound Name: JGV-01-022
Processed by: Jacob Vineberg
Pulse Sequence: s2pul
Spectrometer Freq.: 300.07 MHz
Solvent: $CDCl_3$
Temperature: 298.15 K
Spectral Width: 15.00 ppm
Number of Scans: 16
Relaxation Delay: 1.000 s

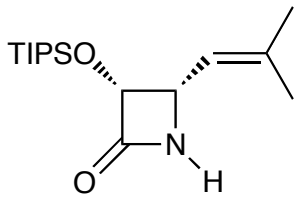

β-Lactam (+)1-5

Compound Name: JGV-01-024
Processed by: Jacob Vineberg
Pulse Sequence: zg30
Spectrometer Freq.: 499.89 MHz
Solvent: $CDCl_3$
Temperature: 298.15 K
Spectral Width: 20.00 ppm
Number of Scans: 8
Relaxation Delay: 1.000 s

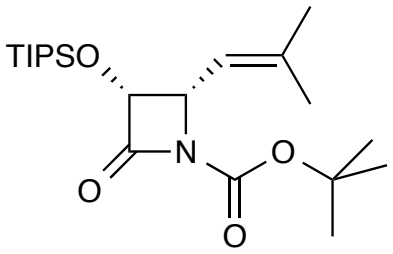

β-Lactam (+)1-6

Compound Name: JGV-01-014
Processed by: Jacob Vineberg
Pulse Sequence: s2pul
Spectrometer Freq.: 300.07 MHz
Solvent: $CDCl_3$
Temperature: 298.15 K
Spectral Width: 15.00 ppm
Number of Scans: 16
Relaxation Delay: 1.000 s

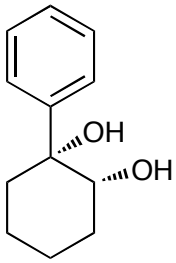

Compound 1-7

Compound Name: JGV-01-016
Processed by: Jacob Vineberg
Pulse Sequence: zg30
Spectrometer Freq.: 300.18 MHz
Solvent: $CDCl_3$
Temperature: 293.57 K
Spectral Width: 20.33 ppm
Number of Scans: 39
Relaxation Delay: 1.000 s

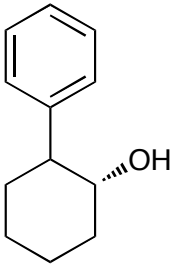

Compound 1-8
Chiral Auxiliary

Compound Name: JGV-01-025
Processed by: Jacob Vineberg
Pulse Sequence: s2pul
Spectrometer Freq.: 300.07 MHz
Solvent: $CDCl_3$
Temperature: 298.15 K
Spectral Width: 15.00 ppm
Number of Scans: 16
Relaxation Delay: 1.000 s

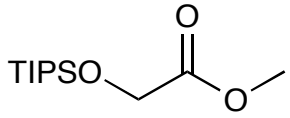

Compound 1-9

Compound Name: JGV-01-026
Processed by: Jacob Vineberg
Pulse Sequence: s2pul
Spectrometer Freq.: 300.07 MHz
Solvent: $CDCl_3$
Temperature: 298.15 K
Spectral Width: 15.00 ppm
Number of Scans: 16
Relaxation Delay: 1.000 s

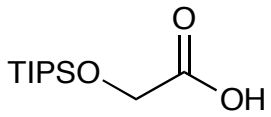

Compound 1-10

Compound Name: JGV-04-001
Processed by: Jacob Vineberg
Pulse Sequence: zg30
Spectrometer Freq.: 499.89 MHz
Solvent: $CDCl_3$
Temperature: 298.14 K
Spectral Width: 20.00 ppm
Number of Scans: 56
Relaxation Delay: 1.000 s

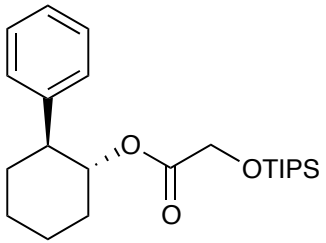

Compound 1-12
Chiral Ester

Compound Name: JGV-03-048
Processed by: Jacob Vineberg
Pulse Sequence: s2pul
Spectrometer Freq.: 300.07 MHz
Solvent: $CDCl_3$
Temperature: 298.15 K
Spectral Width: 15.00 ppm
Number of Scans: 16
Relaxation Delay: 1.000 s

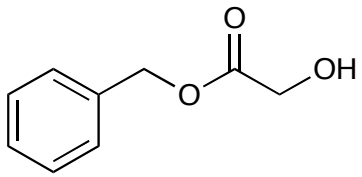

Compound 1-13

Compound Name: JGV-03-049
Processed by: Jacob Vineberg
Pulse Sequence: zg30
Spectrometer Freq.: 499.89 MHz
Solvent: $CDCl_3$
Temperature: 298.15 K
Spectral Width: 20.00 ppm
Number of Scans: 24
Relaxation Delay: 1.000 s

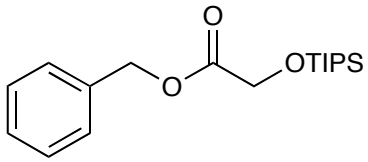

Compound 1-14

Compound Name: JGV-03-051
Processed by: Jacob Vineberg
Pulse Sequence: zg30
Spectrometer Freq.: 399.83 MHz
Solvent: $CDCl_3$
Temperature: 298.14 K
Spectral Width: 20.57 ppm
Number of Scans: 15
Relaxation Delay: 1.000 s

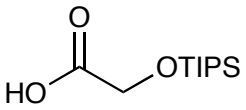

Compound 1-15

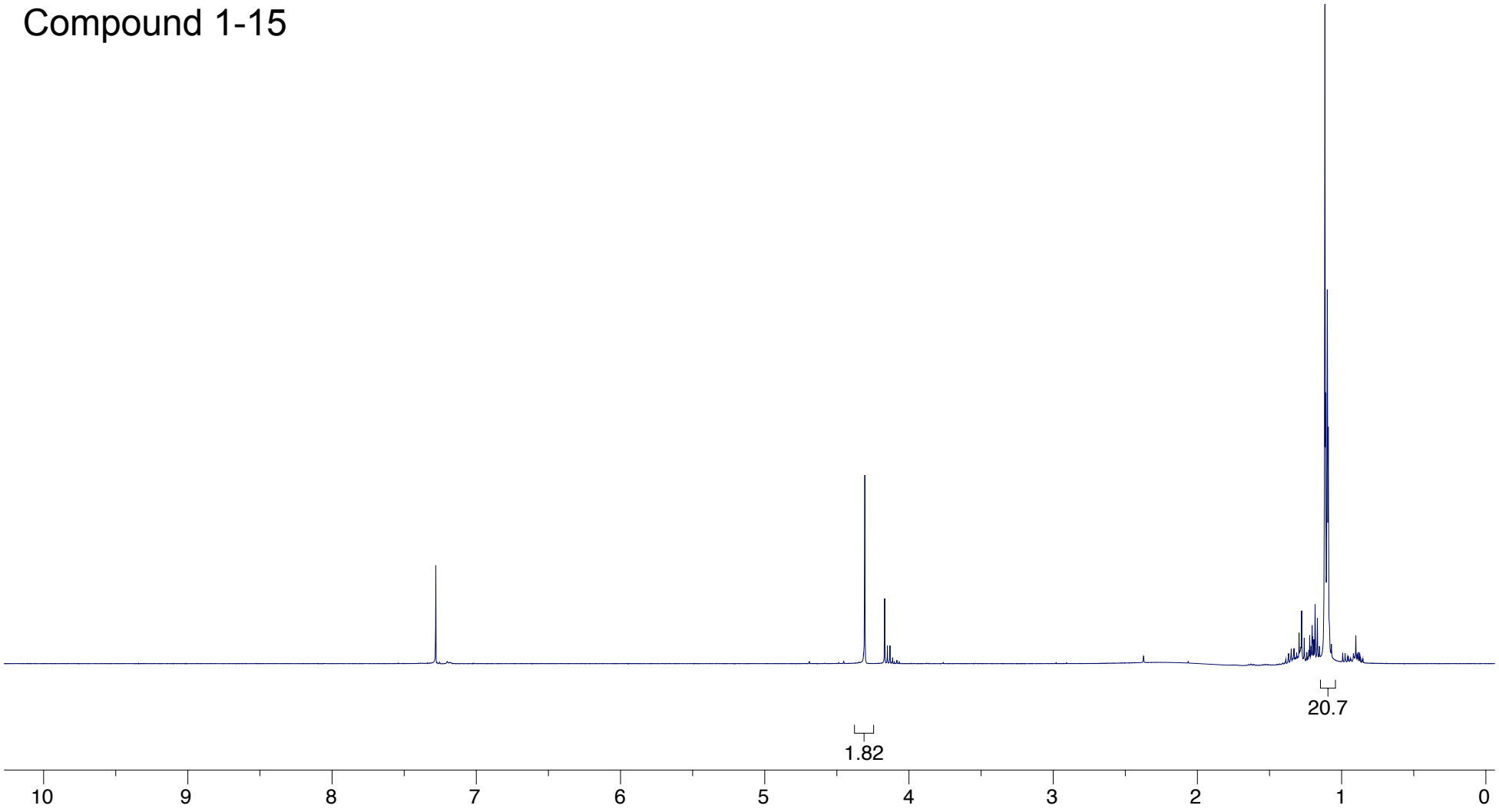

Compound Name: JGV-03-052
Processed by: Jacob Vineberg
Pulse Sequence: s2pul
Spectrometer Freq.: 300.07 MHz
Solvent: $CDCl_3$
Temperature: 298.15 K
Spectral Width: 15.00 ppm
Number of Scans: 24
Relaxation Delay: 1.000 s

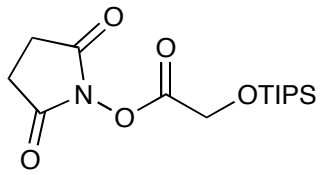

Compound 1-16

Compound Name: JGV-01-104
Processed by: Jacob Vineberg
Pulse Sequence: s2pul
Spectrometer Freq.: 599.72 MHz
Solvent: $CDCl_3$
Temperature: 298.15 K
Spectral Width: 13.34 ppm
Number of Scans: 25
Relaxation Delay: 1.000 s

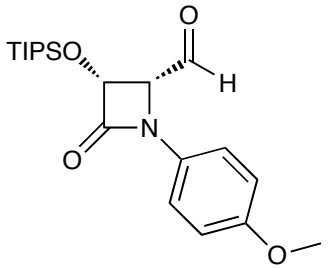

β-Lactam (+)1-17

Compound Name: JGV-01-102
Processed by: Jacob Vineberg
Pulse Sequence: s2pul
Spectrometer Freq.: 300.07 MHz
Solvent: $CDCl_3$
Temperature: 298.15 K
Spectral Width: 15.00 ppm
Number of Scans: 25
Relaxation Delay: 1.000 s

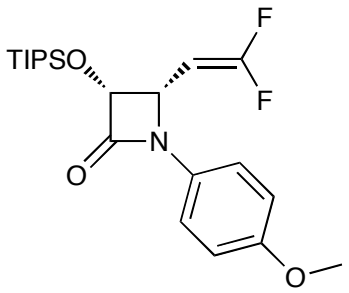

β-Lactam (+)1-18

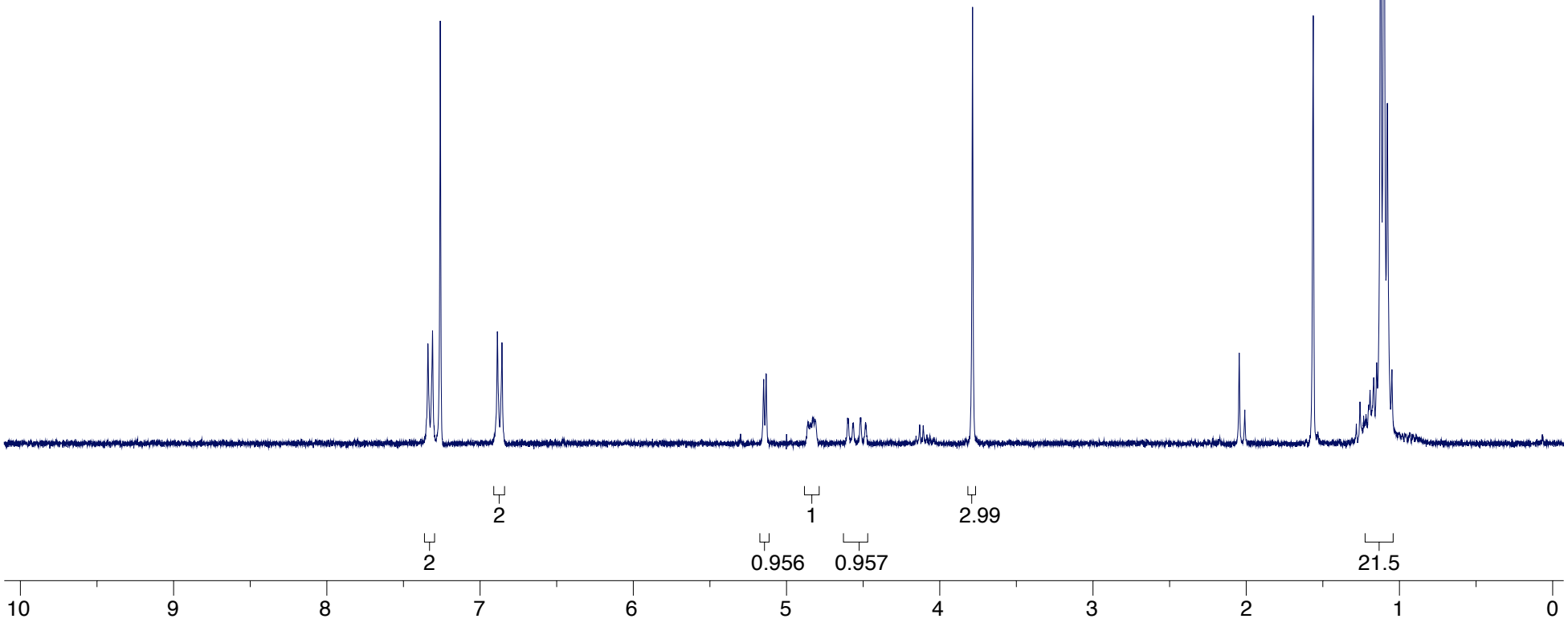

Compound Name: JGV-01-108
Processed by: Jacob Vineberg
Pulse Sequence: s2pul
Spectrometer Freq.: 599.72 MHz
Solvent: $CDCl_3$
Temperature: 298.15 K
Spectral Width: 13.34 ppm
Number of Scans: 25
Relaxation Delay: 1.000 s

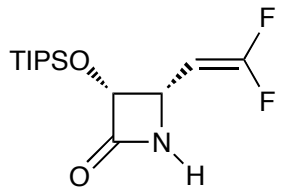

β-Lactam (+)1-19

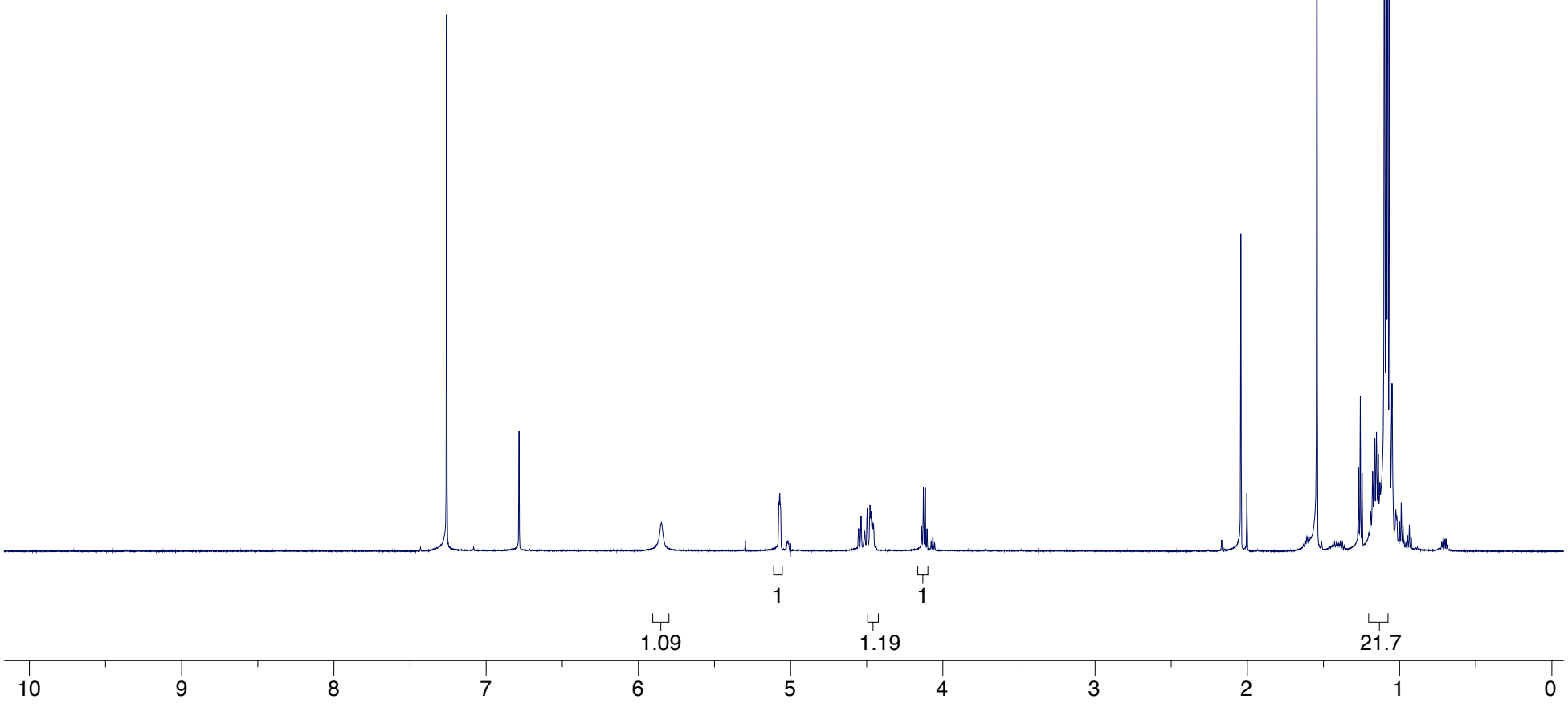

Compound Name: JGV-01-110
Processed by: Jacob Vineberg
Pulse Sequence: s2pul
Spectrometer Freq.: 599.72 MHz
Solvent: $CDCl_3$
Temperature: 298.15 K
Spectral Width: 13.34 ppm
Number of Scans: 25
Relaxation Delay: 1.000 s

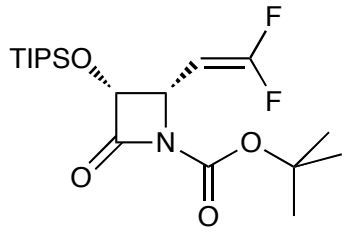

β-Lactam (+)1-20
Difluorovinyl β-lactam

Appendix Chapter 2

Compound Name: JGV-01-031
Processed by: Jacob Vineberg
Pulse Sequence: s2pul
Spectrometer Freq.: 300.07 MHz
Solvent: $CDCl_3$
Temperature: 298.15 K
Spectral Width: 15.00 ppm
Number of Scans: 16
Relaxation Delay: 1.000 s

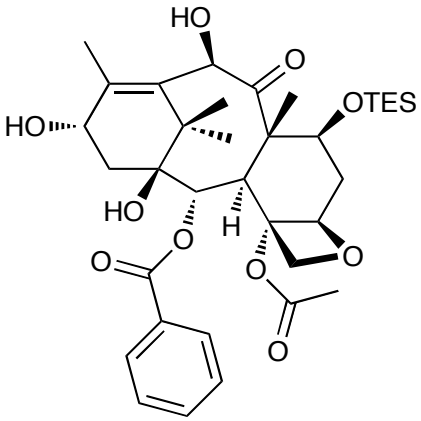

Compound 2-1

Compound Name: JGV-01-039
Processed by: Jacob Vineberg
Pulse Sequence: s2pul
Spectrometer Freq.: 300.07 MHz
Solvent: $CDCl_3$
Temperature: 298.15 K
Spectral Width: 15.00 ppm
Number of Scans: 16
Relaxation Delay: 1.000 s

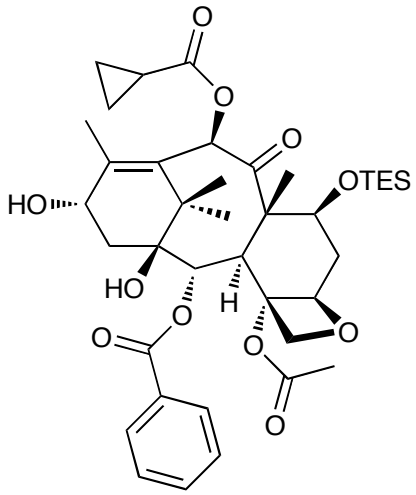

Compound 2-2

Compound Name: JGV-01-050a
Processed by: Jacob Vineberg
Pulse Sequence: s2pul
Spectrometer Freq.: 300.07 MHz
Solvent: $CDCl_3$
Temperature: 298.15 K
Spectral Width: 15.00 ppm
Number of Scans: 16
Relaxation Delay: 1.000 s

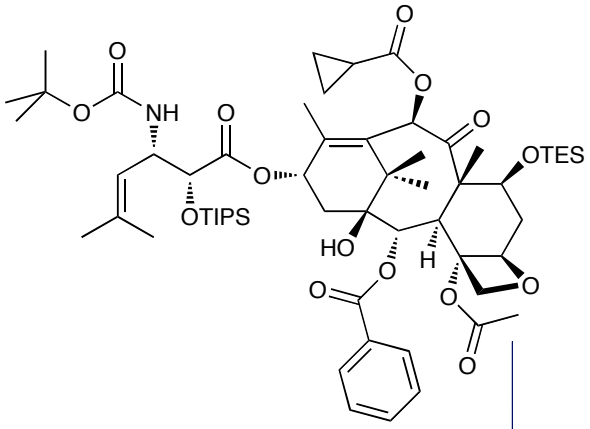

Compound 2-3

Compound Name: JGV-01-053
Processed by: Jacob Vineberg
Pulse Sequence: s2pul
Spectrometer Freq.: 300.07 MHz
Solvent: $CDCl_3$
Temperature: 298.15 K
Spectral Width: 15.00 ppm
Number of Scans: 50
Relaxation Delay: 1.000 s

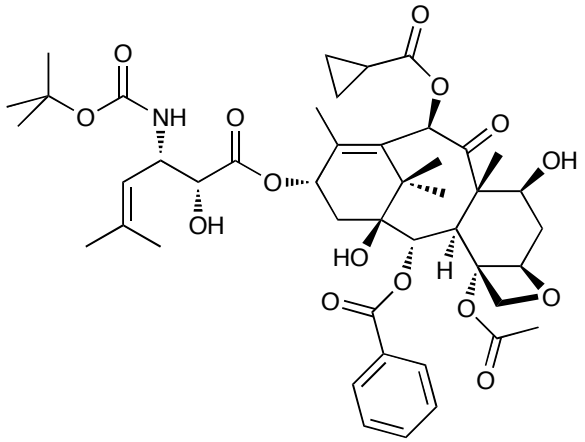

Taxoid 2-4 (SB-T-1214)

Compound Name: JGV-01-053-^{13}C
Processed by: Jacob Vineberg
Pulse Sequence: s2pul
Spectrometer Freq.: 100.55 MHz
Solvent: $CDCl_3$
Temperature: 298.15 K
Spectral Width: 248.64 ppm
Number of Scans: 50000
Relaxation Delay: 1.000 s

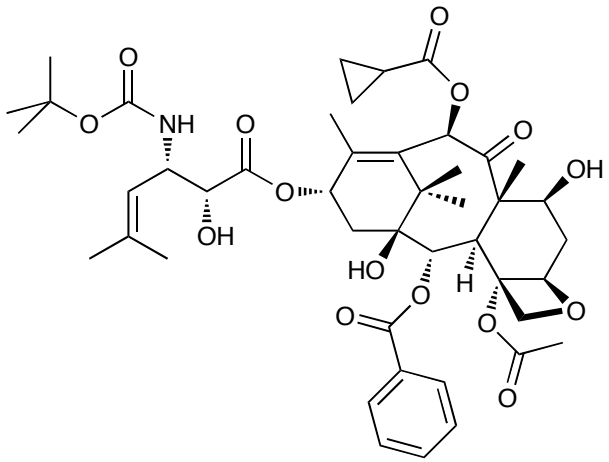

Taxoid 2-4 (SB-T-1214)

Compound Name: JGV-01-114
Processed by: Jacob Vineberg
Pulse Sequence: s2pul
Spectrometer Freq.: 599.72 MHz
Solvent: $CDCl_3$
Temperature: 298.15 K
Spectral Width: 13.34 ppm
Number of Scans: 25
Relaxation Delay: 1.000 s

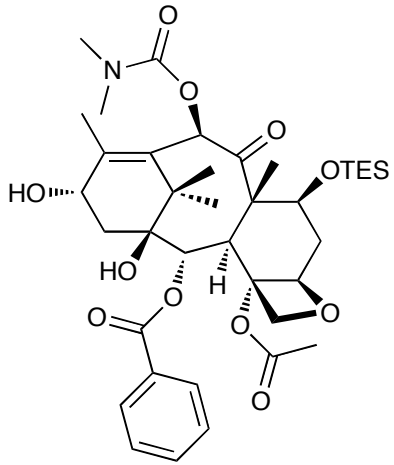

Compound 2-5

Compound Name: JGV-02-006
Processed by: Jacob Vineberg
Pulse Sequence: s2pul
Spectrometer Freq.: 300.07 MHz
Solvent: $CDCl_3$
Temperature: 298.15 K
Spectral Width: 15.00 ppm
Number of Scans: 100
Relaxation Delay: 1.000 s

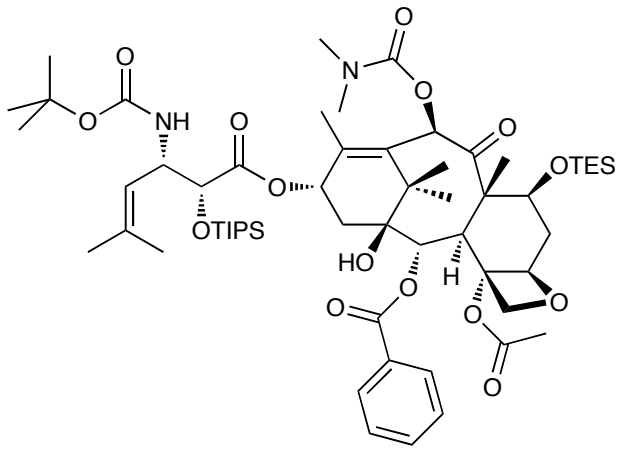

Compound 2-6

Compound Name: JGV-02-008
Processed by: Jacob Vineberg
Pulse Sequence: s2pul
Spectrometer Freq.: 499.90 MHz
Solvent: $CDCl_3$
Temperature: 298.15 K
Spectral Width: 16.00 ppm
Number of Scans: 200
Relaxation Delay: 1.000 s

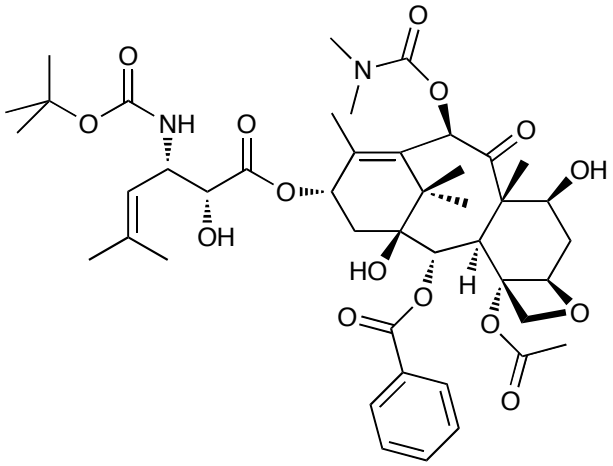

Taxoid 2-7 (SB-T-1216)

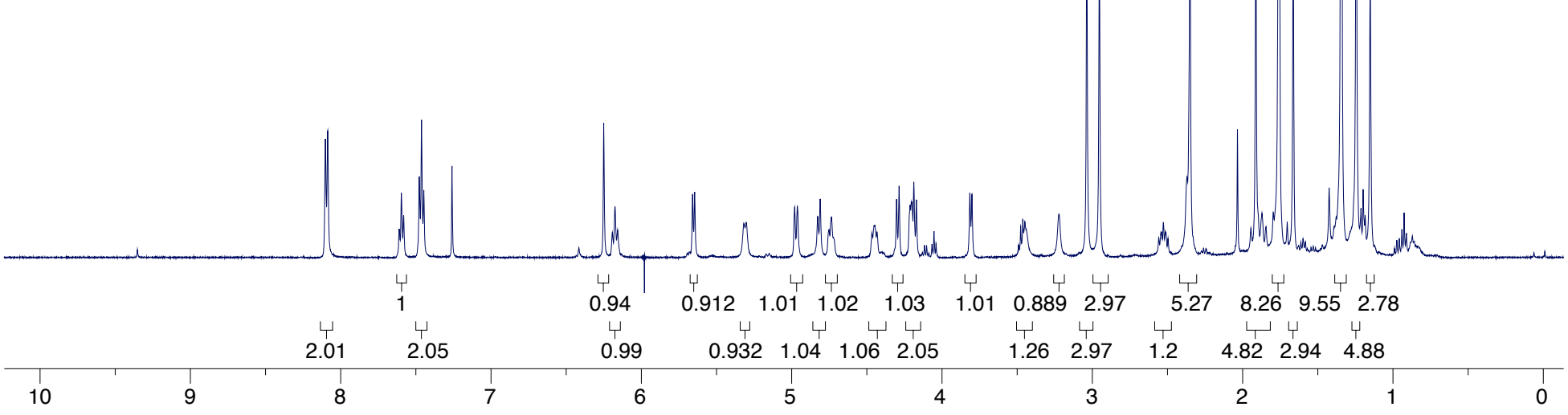

Compound Name: JGV-01-116
Processed by: Jacob Vineberg
Pulse Sequence: s2pul
Spectrometer Freq.: 599.72 MHz
Solvent: $CDCl_3$
Temperature: 298.15 K
Spectral Width: 13.34 ppm
Number of Scans: 35
Relaxation Delay: 1.000 s

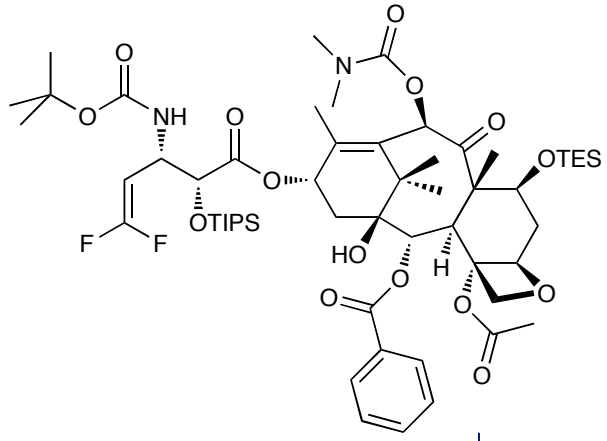

Compound 2-8

Compound Name: JGV-01-118
Processed by: Jacob Vineberg
Pulse Sequence: s2pul
Spectrometer Freq.: 599.72 MHz
Solvent: $CDCl_3$
Temperature: 298.15 K
Spectral Width: 13.34 ppm
Number of Scans: 35
Relaxation Delay: 1.000 s

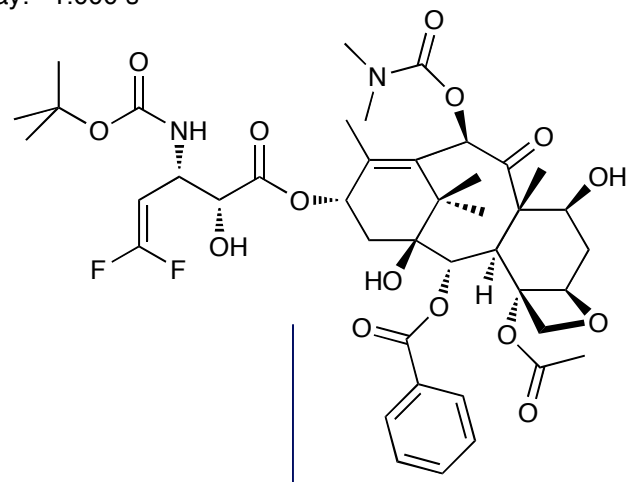

Taxoid 2-9 (SB-T-12854)

Compound Name: JGV-01-057c
Processed by: Jacob Vineberg
Pulse Sequence: s2pul
Spectrometer Freq.: 399.83 MHz
Solvent: $CDCl_3$
Temperature: 298.15 K
Spectral Width: 15.01 ppm
Number of Scans: 20
Relaxation Delay: 1.000 s

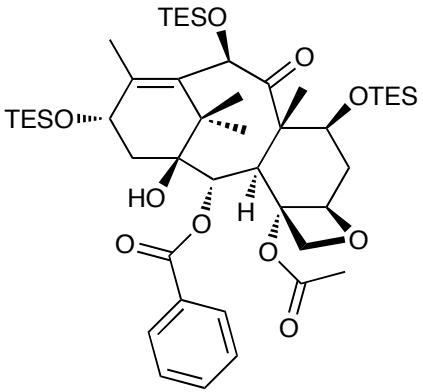

Compound 2-10

Compound Name: JGV-01-061a
Processed by: Jacob Vineberg
Pulse Sequence: s2pul
Spectrometer Freq.: 300.07 MHz
Solvent: $CDCl_3$
Temperature: 298.15 K
Spectral Width: 15.00 ppm
Number of Scans: 16
Relaxation Delay: 1.000 s

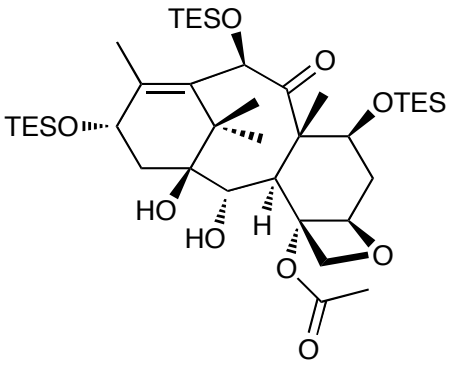

Compound 2-11

Compound Name: JGV-01-063
Processed by: Jacob Vineberg
Pulse Sequence: s2pul
Spectrometer Freq.: 599.72 MHz
Solvent: $CDCl_3$
Temperature: 298.15 K
Spectral Width: 13.34 ppm
Number of Scans: 25
Relaxation Delay: 1.000 s

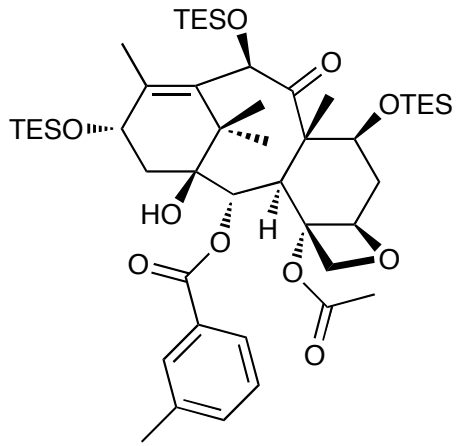

Compound 2-12

Compound Name: JGV-01-073
Processed by: Jacob Vineberg
Pulse Sequence: s2pul
Spectrometer Freq.: 599.72 MHz
Solvent: $CDCl_3$
Temperature: 298.15 K
Spectral Width: 13.34 ppm
Number of Scans: 30
Relaxation Delay: 1.000 s

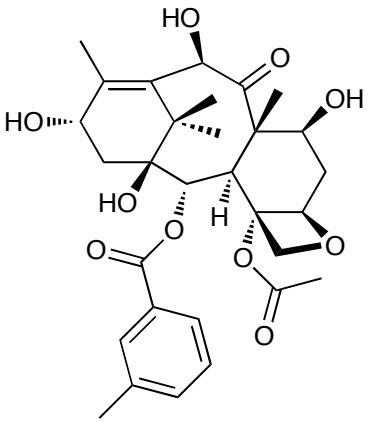

Compound 2-13

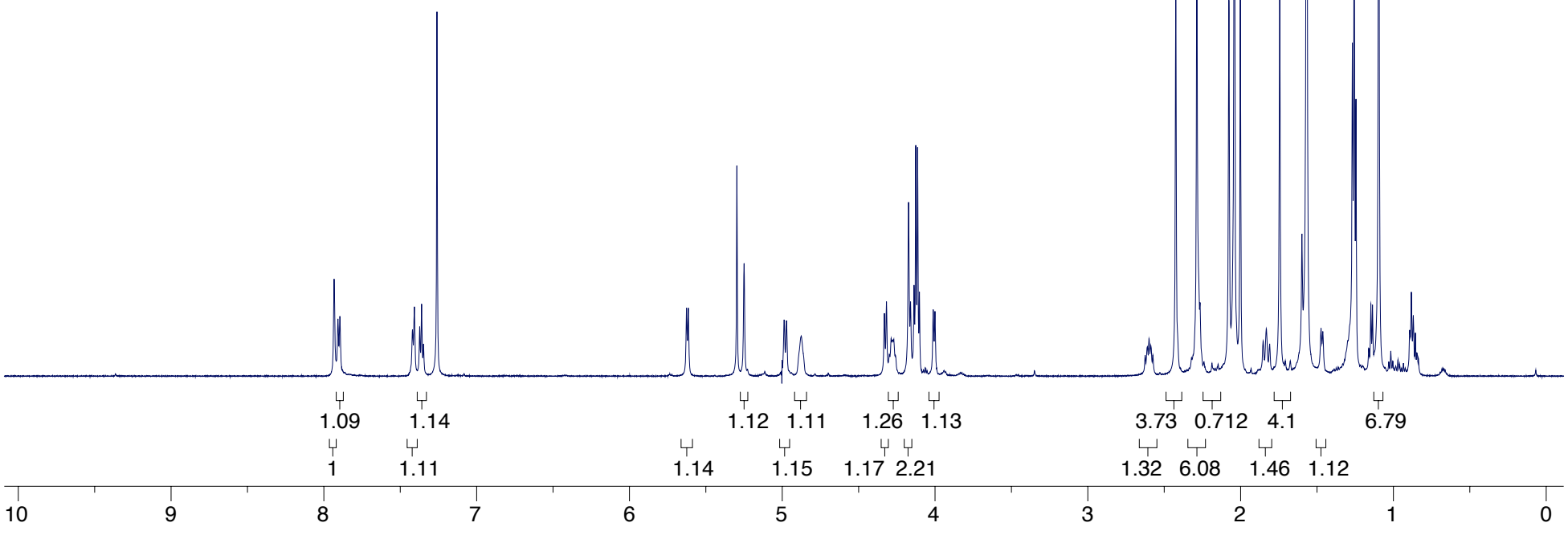

Compound Name: JGV-01-075
Processed by: Jacob Vineberg
Pulse Sequence: s2pul
Spectrometer Freq.: 599.72 MHz
Solvent: $CDCl_3$
Temperature: 298.15 K
Spectral Width: 13.34 ppm
Number of Scans: 25
Relaxation Delay: 1.000 s

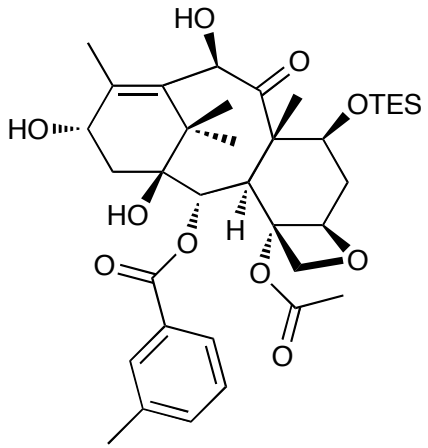

Compound 2-14

Compound Name: JGV-01-096
Processed by: Jacob Vineberg
Pulse Sequence: s2pul
Spectrometer Freq.: 599.72 MHz
Solvent: $CDCl_3$
Temperature: 298.15 K
Spectral Width: 13.34 ppm
Number of Scans: 25
Relaxation Delay: 1.000 s

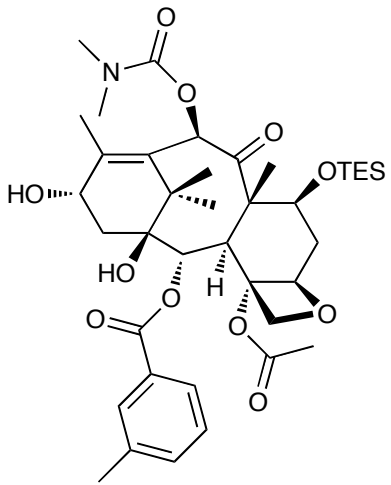

Compound 2-15

Compound Name: JGV-01-098
Processed by: Jacob Vineberg
Pulse Sequence: s2pul
Spectrometer Freq.: 599.72 MHz
Solvent: $CDCl_3$
Temperature: 298.15 K
Spectral Width: 13.34 ppm
Number of Scans: 30
Relaxation Delay: 1.000 s

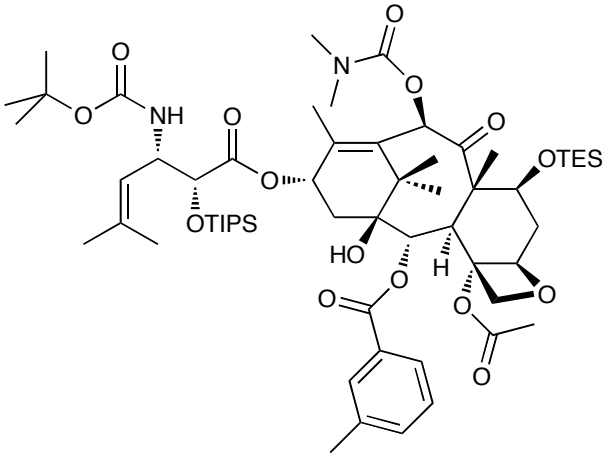

Compound 2-16

Compound Name: JGV-01-100
Processed by: Jacob Vineberg
Pulse Sequence: zg30
Spectrometer Freq.: 300.18 MHz
Solvent: $CDCl_3$
Temperature: 293.57 K
Spectral Width: 20.33 ppm
Number of Scans: 31
Relaxation Delay: 1.000 s

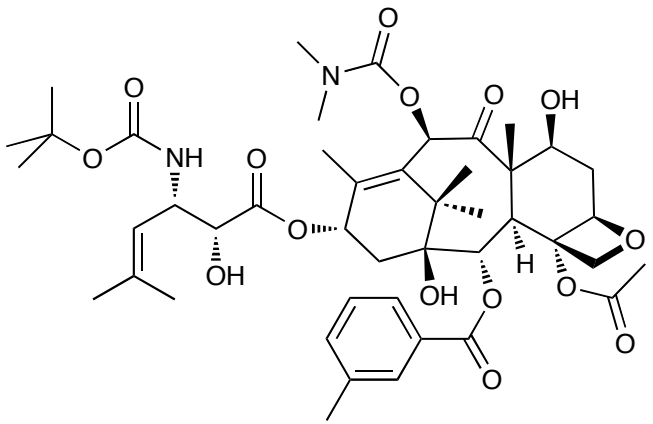

Taxoid 2-17 (SB-T-121602)

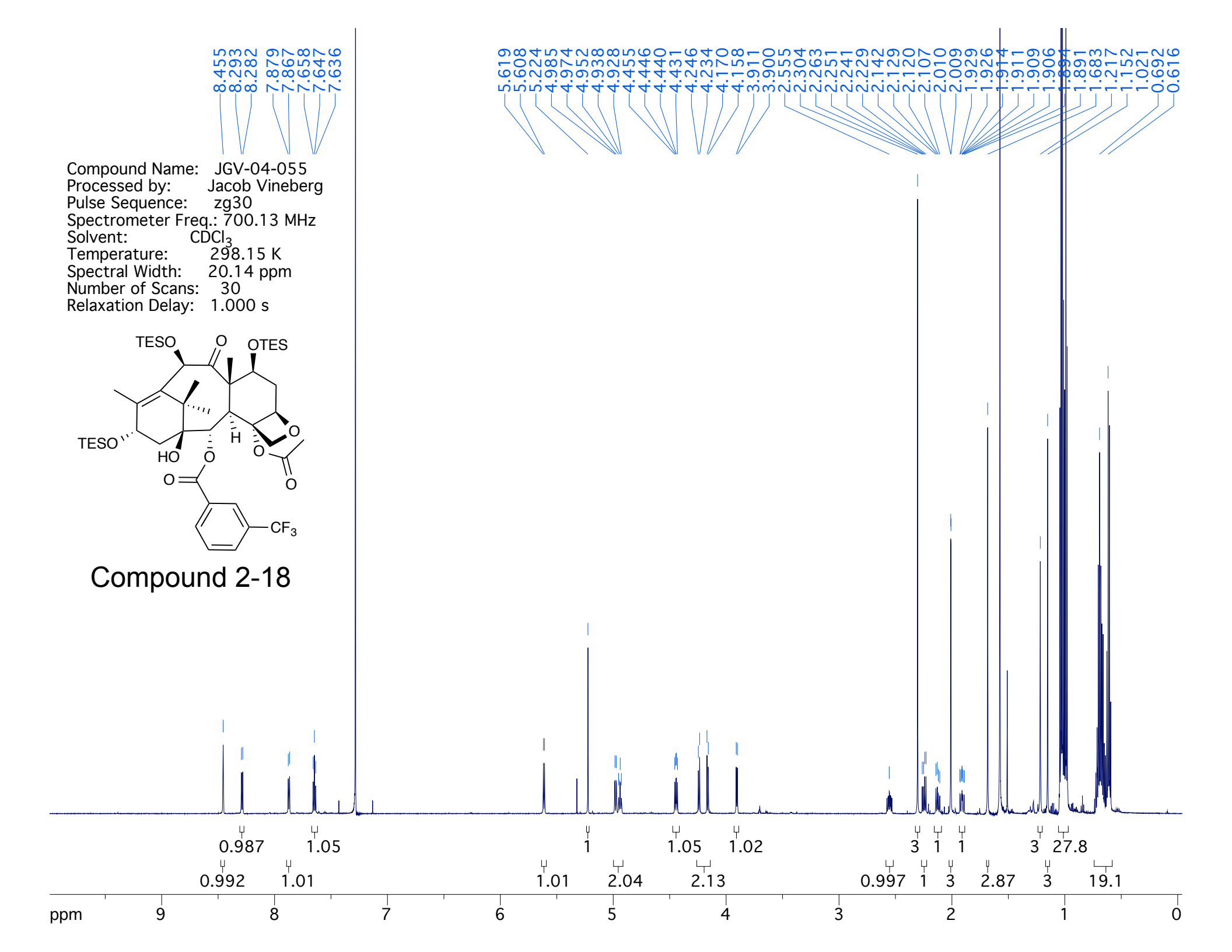
8.455
8.293
8.282
7.879
7.867
7.658
7.647
7.636
5.619
5.608
5.224
4.985
4.974
4.952
4.938
4.928
4.455
4.446
4.440
4.431
4.246
4.234
4.170
4.158
3.911
3.900
2.555
2.304
2.263
2.251
2.241
2.229
2.142
2.129
2.120
2.107
2.010
2.009
1.929
1.926
1.914
1.911
1.909
1.906
1.894
1.891
1.683
1.217
1.152
1.021
0.692
0.616
Compound Name: JGV-04-055
Processed by: Jacob Vineberg
Pulse Sequence: zg30
Spectrometer Freq.: 700.13 MHz
Solvent: $CDCl_3$
Temperature: 298.15 K
Spectral Width: 20.14 ppm
Number of Scans: 30
Relaxation Delay: 1.000 s
TESO
O
OTES
TESO
HO
O
H
O
O
O
O
O
CF_3
Compound 2-18
0.987
1.05
1
1.05
1.02
3
1
1
3
27.8
0.992
1.01
1.01
2.04
2.13
0.997
1
3
2.87
3
19.1
ppm
9
8
7
6
5
4
3
2
1
0

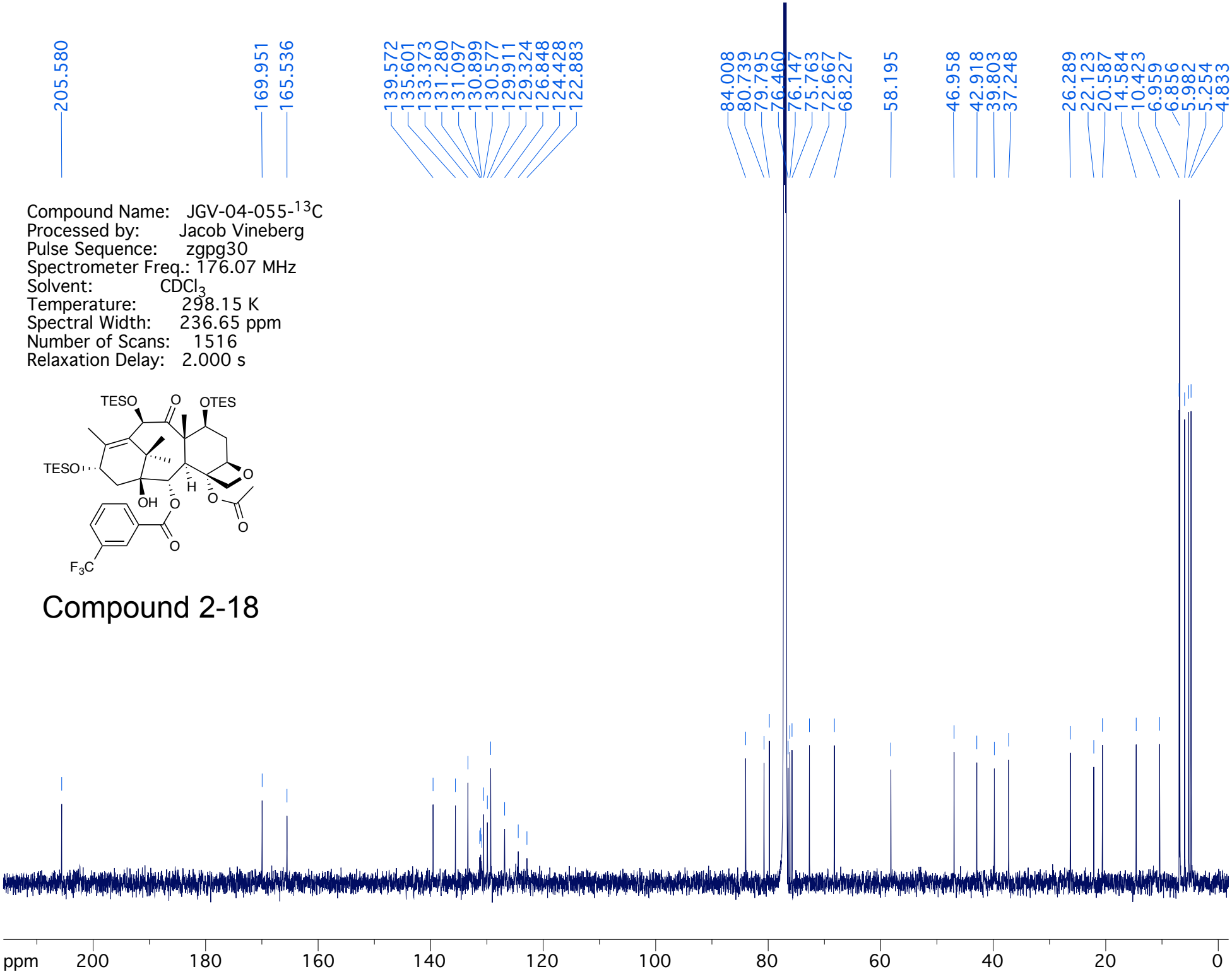
205.580
169.951
165.536
139.572
135.601
133.373
131.280
131.097
130.899
130.577
129.911
129.324
126.848
124.428
122.883
84.008
80.739
79.795
76.460
76.147
75.763
72.667
68.227
58.195
46.958
42.918
39.803
37.248
26.289
22.123
20.587
14.584
10.423
6.959
6.856
5.982
5.254
4.833
Compound Name: JGV-04-055-13C
Processed by: Jacob Vineberg
Pulse Sequence: zgpg30
Spectrometer Freq.: 176.07 MHz
Solvent: CDCl3
Temperature: 298.15 K
Spectral Width: 236.65 ppm
Number of Scans: 1516
Relaxation Delay: 2.000 s
TESO
O
OTES
TESO
H
OH
O
O
O
O
O
O
F3C
Compound 2-18
ppm
200
180
160
140
120
100
80
60
40
20
0

Compound Name: JGV-04-055-^{19}F
Processed by: Jacob Vineberg
Pulse Sequence: zgflqn
Spectrometer Freq.: 376.18 MHz
Solvent: $CDCl_3$
Temperature: 298.15 K
Spectral Width: 237.35 ppm
Number of Scans: 23
Relaxation Delay: 1.000 s

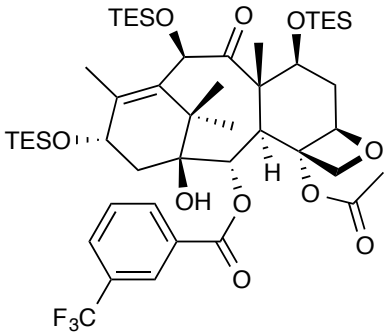

Compound 2-18

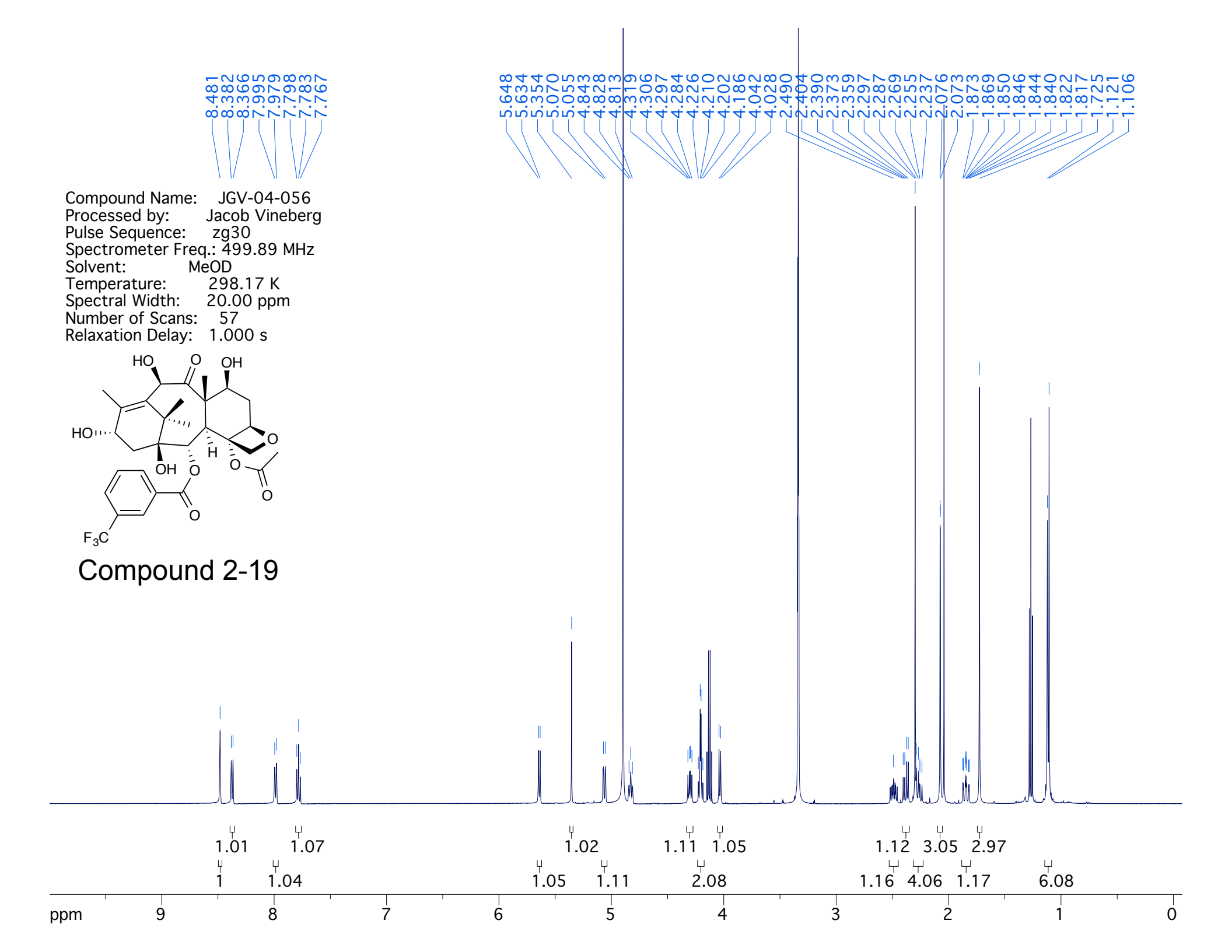
8.481
8.382
8.366
7.995
7.979
7.798
7.783
7.767
5.648
5.634
5.354
5.070
5.055
4.843
4.828
4.813
4.319
4.306
4.297
4.284
4.226
4.210
4.202
4.186
4.042
4.028
2.490
2.404
2.390
2.373
2.359
2.297
2.287
2.269
2.255
2.237
2.076
2.073
1.873
1.869
1.850
1.846
1.844
1.840
1.822
1.817
1.725
1.121
1.106
Compound Name: JGV-04-056
Processed by: Jacob Vineberg
Pulse Sequence: zg30
Spectrometer Freq.: 499.89 MHz
Solvent: MeOD
Temperature: 298.17 K
Spectral Width: 20.00 ppm
Number of Scans: 57
Relaxation Delay: 1.000 s
HO
O
OH
HO
H
O
OH
O
O
O
O
F3C
Compound 2-19
1.01
1.07
1.02
1.11
1.05
1.12
3.05
2.97
1
1.04
1.05
1.11
2.08
1.16
4.06
1.17
6.08
ppm
9
8
7
6
5
4
3
2
1
0

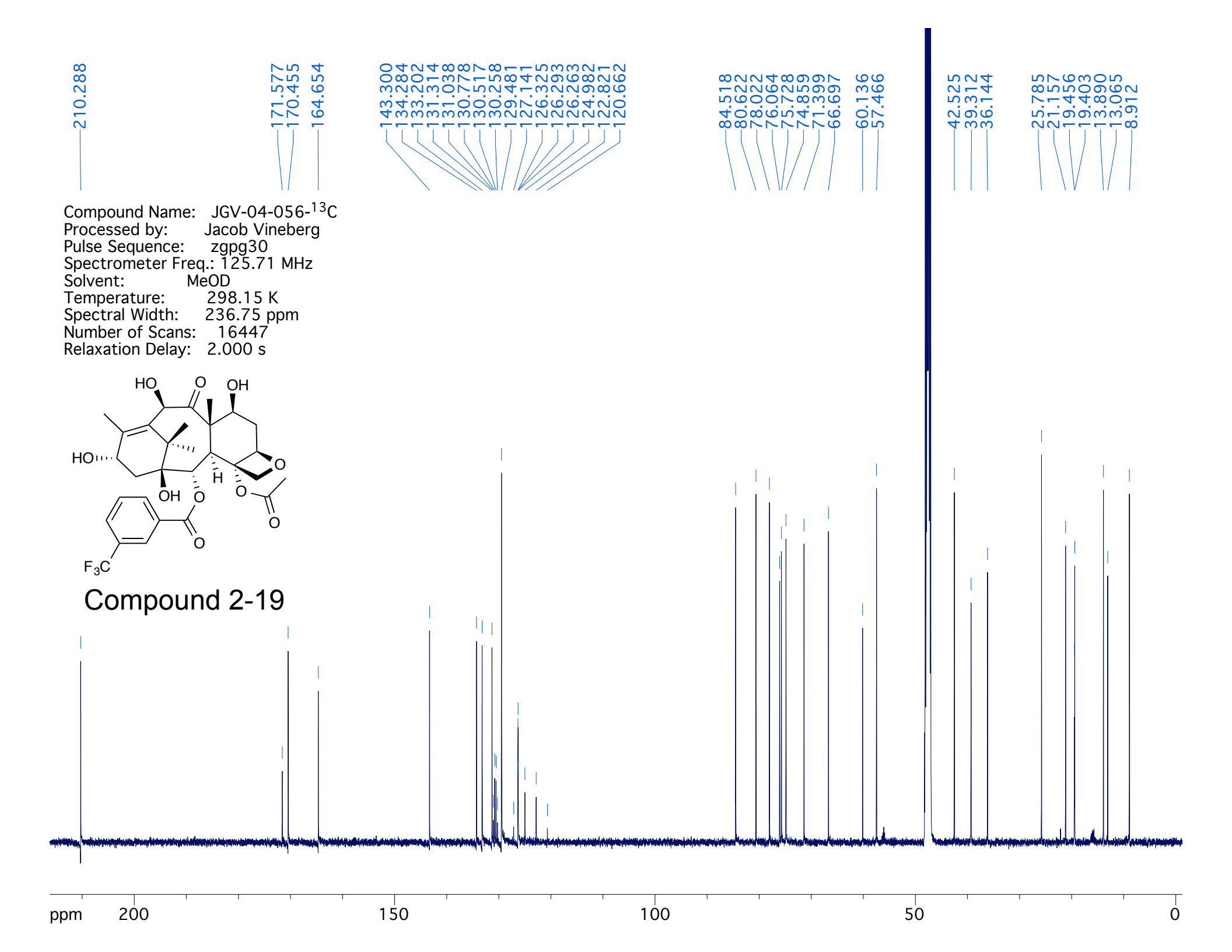
210.288
171.577
170.455
164.654
143.300
134.284
133.202
131.314
131.038
130.778
130.517
130.258
129.481
127.141
126.325
126.293
126.263
124.982
122.821
120.662
84.518
80.622
78.022
76.064
75.728
74.859
71.399
66.697
60.136
57.466
42.525
39.312
36.144
25.785
21.157
19.456
19.403
13.890
13.065
8.912
Compound Name: JGV-04-056-13C
Processed by: Jacob Vineberg
Pulse Sequence: zgpg30
Spectrometer Freq.: 125.71 MHz
Solvent: MeOD
Temperature: 298.15 K
Spectral Width: 236.75 ppm
Number of Scans: 16447
Relaxation Delay: 2.000 s
HO
O
OH
HO
H
O
OH
O
O
O
O
F3C
Compound 2-19
ppm
200
150
100
50
0

Compound Name: JGV-04-056-^{19}F
Processed by: Jacob Vineberg
Pulse Sequence: zgflqn
Spectrometer Freq.: 376.18 MHz
Solvent: $CDCl_3$
Temperature: 298.15 K
Spectral Width: 237.35 ppm
Number of Scans: 19
Relaxation Delay: 1.000 s

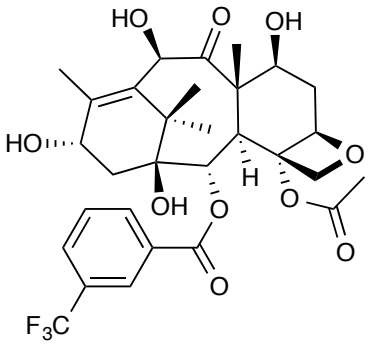

Compound 2-19

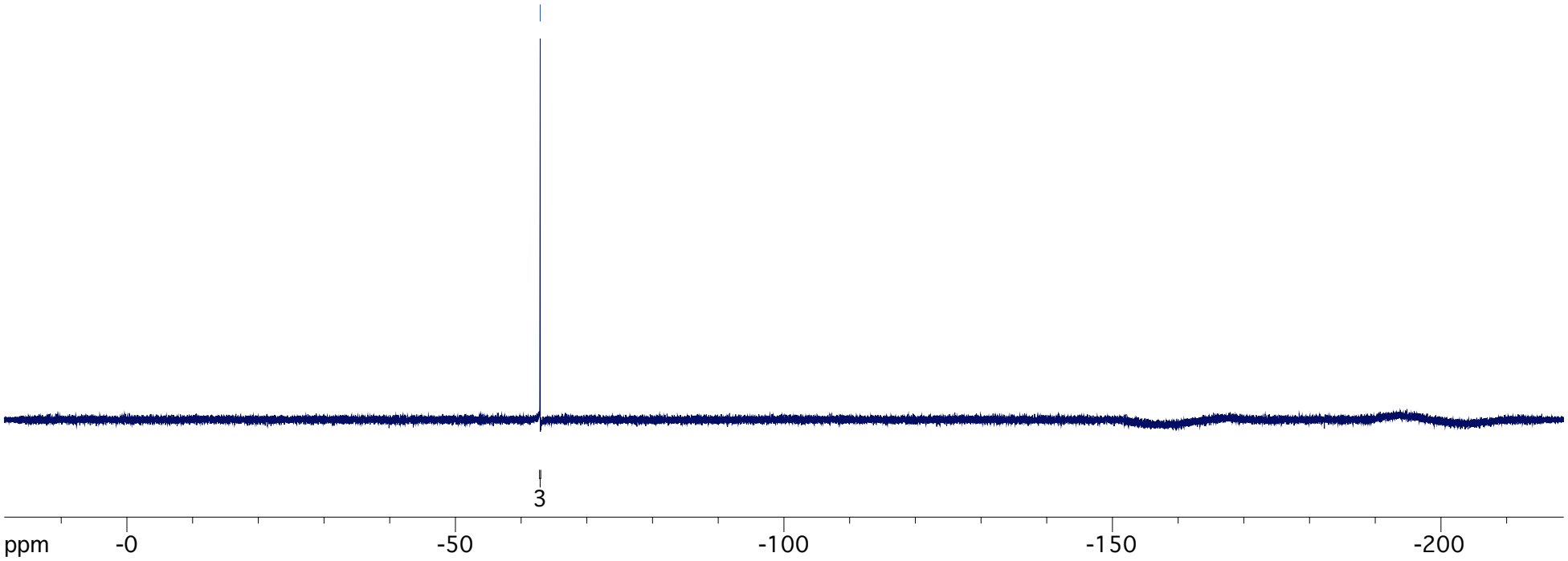

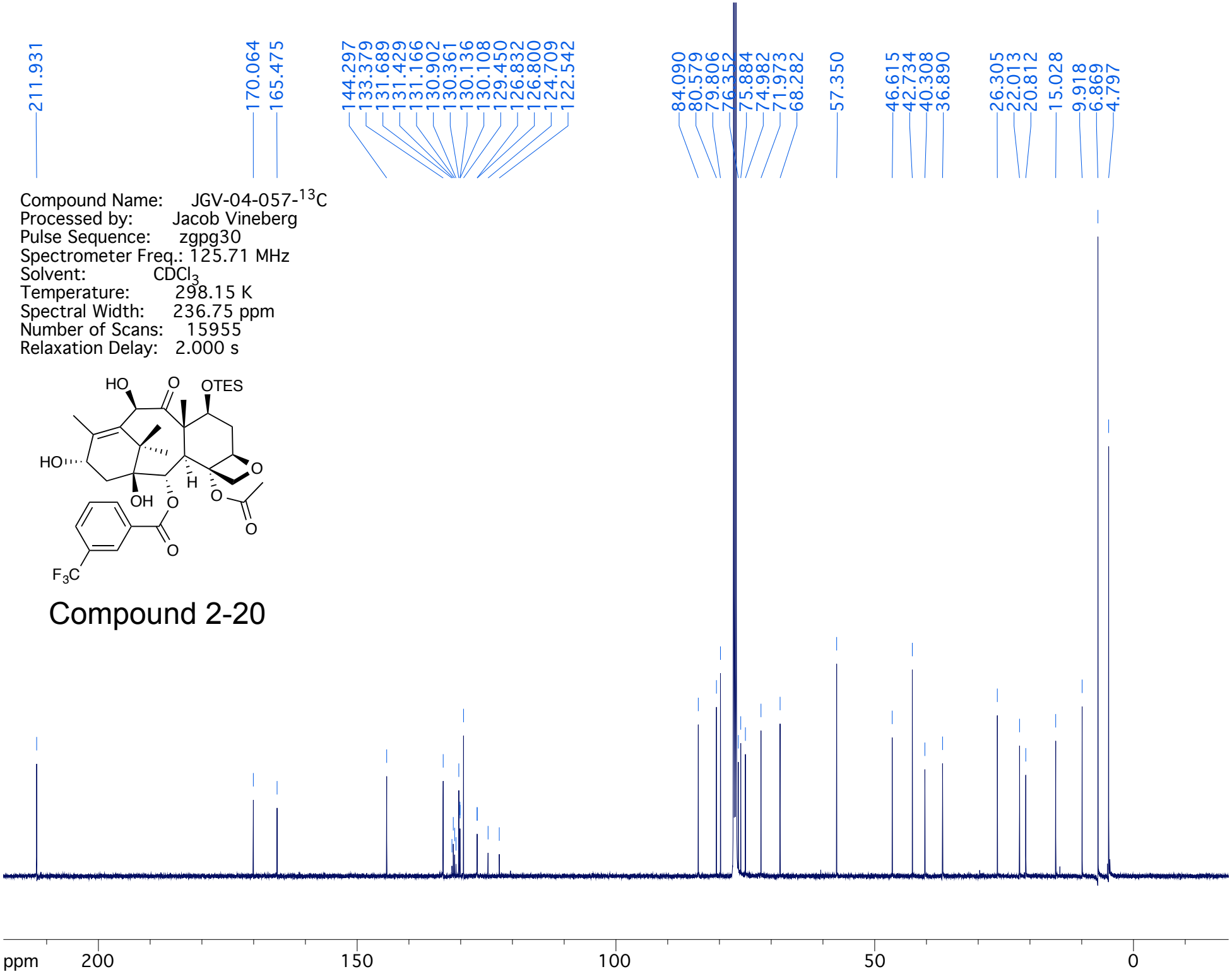
211.931
170.064
165.475
144.297
133.379
131.689
131.429
131.166
130.902
130.361
130.136
130.108
129.450
126.832
126.800
124.709
122.542
84.090
80.579
79.806
76.352
75.884
74.982
71.973
68.282
57.350
46.615
42.734
40.308
36.890
26.305
22.013
20.812
15.028
9.918
6.869
4.797
Compound Name: JGV-04-057-13C
Processed by: Jacob Vineberg
Pulse Sequence: zgpg30
Spectrometer Freq.: 125.71 MHz
Solvent: CDCl3
Temperature: 298.15 K
Spectral Width: 236.75 ppm
Number of Scans: 15955
Relaxation Delay: 2.000 s
HO
O
OTES
HO
H
O
OH
O
O
O
O
F3C
Compound 2-20
ppm
200
150
100
50
0

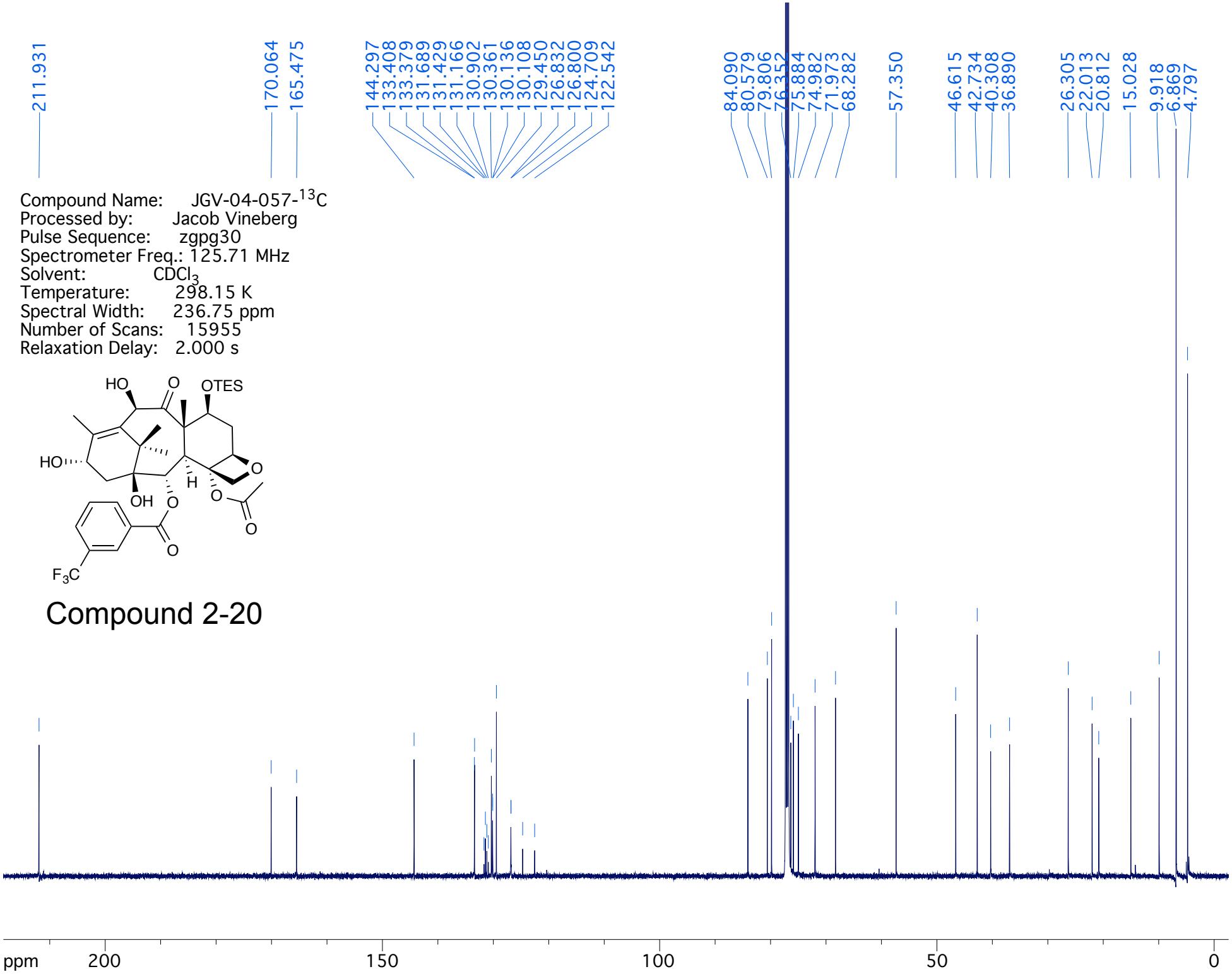
211.931
170.064
165.475
144.297
133.408
133.379
131.689
131.429
131.166
130.902
130.361
130.136
130.108
129.450
126.832
126.800
124.709
122.542
84.090
80.579
79.806
76.352
75.884
74.982
71.973
68.282
57.350
46.615
42.734
40.308
36.890
26.305
22.013
20.812
15.028
9.918
6.869
4.797
Compound Name: JGV-04-057-13C
Processed by: Jacob Vineberg
Pulse Sequence: zgpg30
Spectrometer Freq.: 125.71 MHz
Solvent: CDCl3
Temperature: 298.15 K
Spectral Width: 236.75 ppm
Number of Scans: 15955
Relaxation Delay: 2.000 s
HO
O
OTES
HO
H
O
OH
O
O
O
O
F3C
Compound 2-20
ppm
200
150
100
50
0

Compound Name: JGV-04-057-^{19}F
Processed by: Jacob Vineberg
Pulse Sequence: zgflqn
Spectrometer Freq.: 376.18 MHz
Solvent: $CDCl_3$
Temperature: 298.15 K
Spectral Width: 237.35 ppm
Number of Scans: 79
Relaxation Delay: 1.000 s

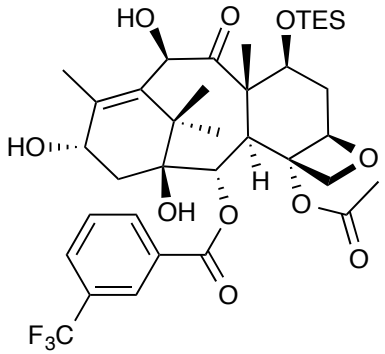

Compound 2-20

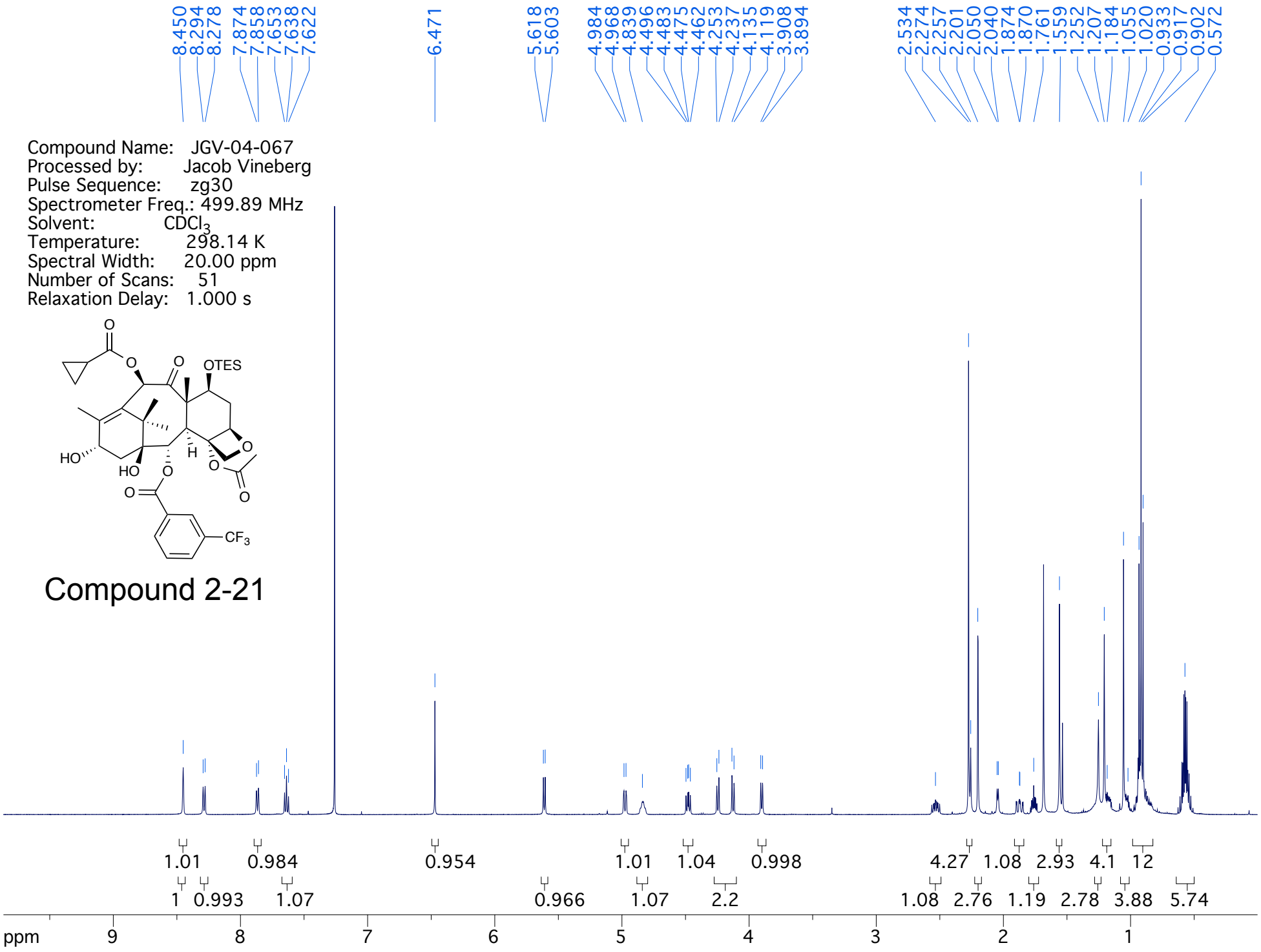
8.450
8.294
8.278
7.874
7.858
7.653
7.638
7.622
6.471
5.618
5.603
4.984
4.968
4.839
4.496
4.483
4.475
4.462
4.253
4.237
4.135
4.119
3.908
3.894
2.534
2.274
2.257
2.201
2.050
2.040
1.874
1.870
1.761
1.559
1.252
1.207
1.184
1.055
1.020
0.933
0.917
0.902
0.572
Compound Name: JGV-04-067
Processed by: Jacob Vineberg
Pulse Sequence: zg30
Spectrometer Freq.: 499.89 MHz
Solvent: CDCl3
Temperature: 298.14 K
Spectral Width: 20.00 ppm
Number of Scans: 51
Relaxation Delay: 1.000 s
OTES
HO
HO
H
CF3
Compound 2-21
1.01
0.984
0.954
1.01
1.04
0.998
4.27
1.08
2.93
4.1
12
1
0.993
1.07
0.966
1.07
2.2
1.08
2.76
1.19
2.78
3.88
5.74
ppm
9
8
7
6
5
4
3
2
1

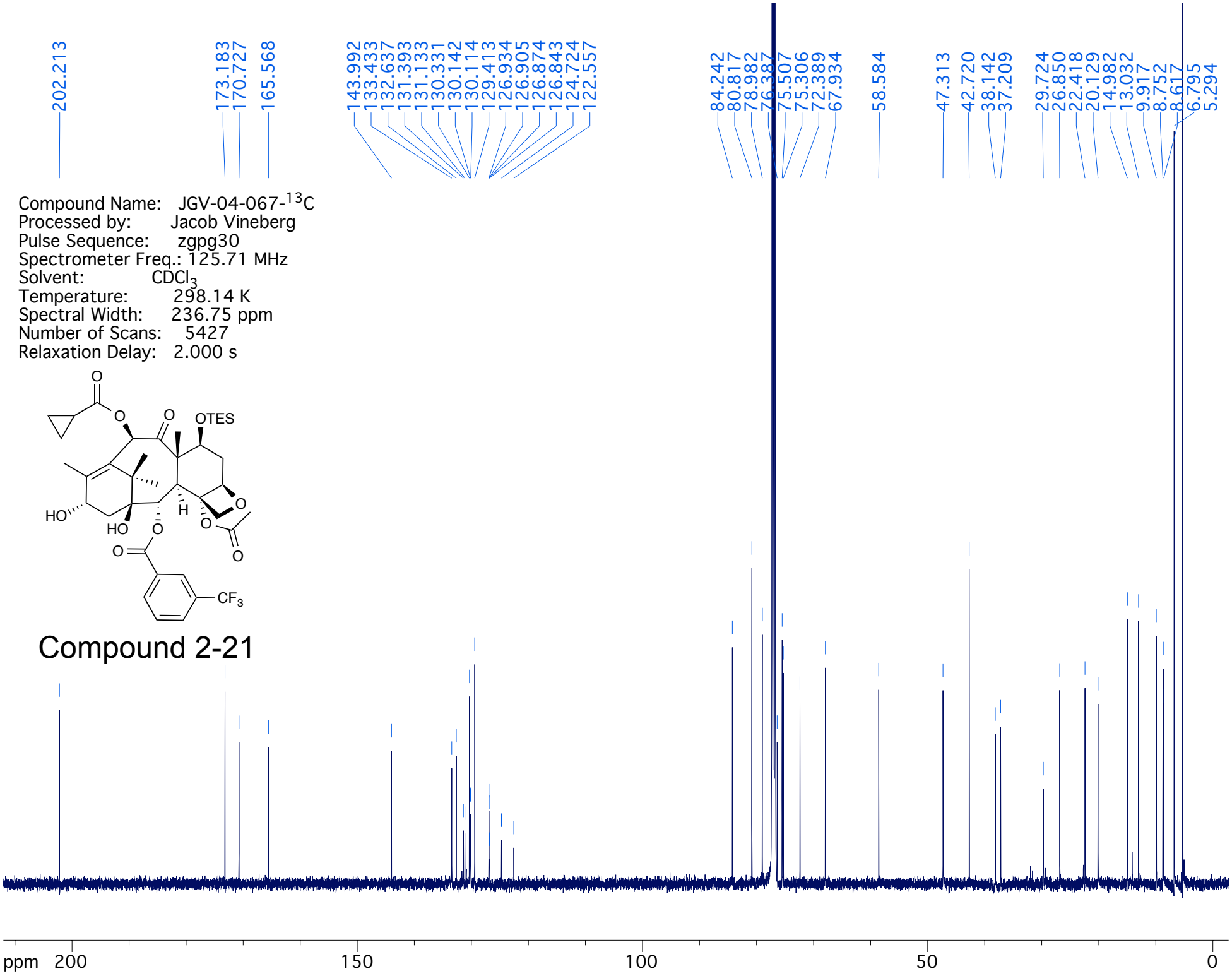

Compound Name: JGV-04-067-^{13}C
Processed by: Jacob Vineberg
Pulse Sequence: zgpg30
Spectrometer Freq.: 125.71 MHz
Solvent: $CDCl_3$
Temperature: 298.14 K
Spectral Width: 236.75 ppm
Number of Scans: 5427
Relaxation Delay: 2.000 s

Compound 2-21

Compound Name: JGV-04-067-^{19}F
Processed by: Jacob Vineberg
Pulse Sequence: zgflqn
Spectrometer Freq.: 376.18 MHz
Solvent: $CDCl_3$
Temperature: 298.15 K
Spectral Width: 237.35 ppm
Number of Scans: 13
Relaxation Delay: 1.000 s

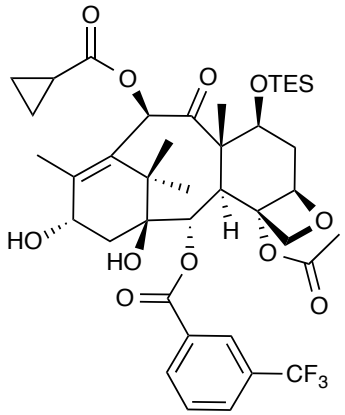

Compound 2-21

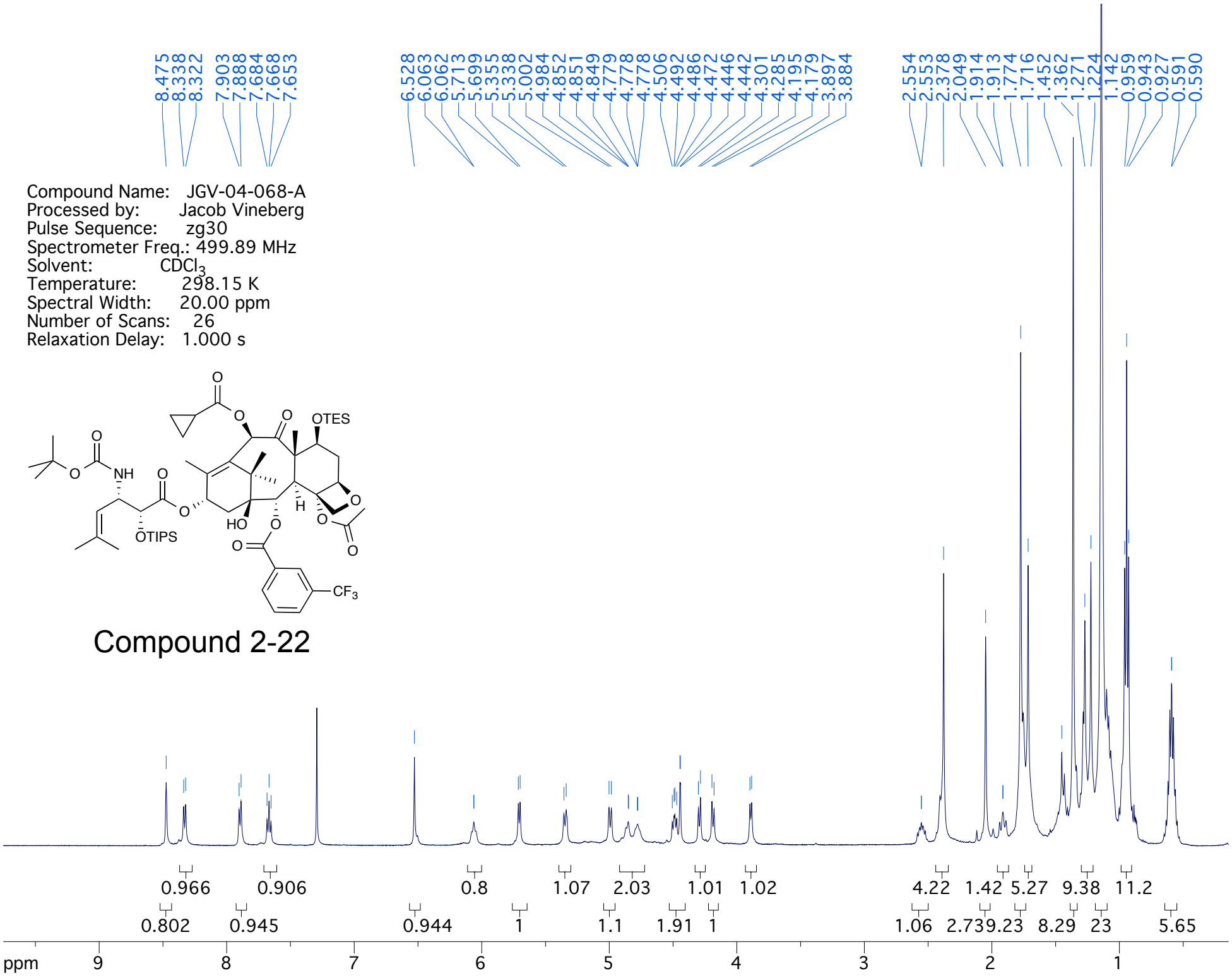
8.475
8.338
8.322
7.903
7.888
7.684
7.668
7.653
6.528
6.063
6.062
5.713
5.699
5.355
5.338
5.002
4.984
4.852
4.851
4.849
4.779
4.778
4.778
4.506
4.492
4.486
4.472
4.446
4.442
4.301
4.285
4.195
4.179
3.897
3.884
2.554
2.553
2.378
2.049
1.914
1.913
1.774
1.716
1.452
1.362
1.271
1.224
1.142
0.959
0.943
0.927
0.591
0.590
Compound Name: JGV-04-068-A
Processed by: Jacob Vineberg
Pulse Sequence: zg30
Spectrometer Freq.: 499.89 MHz
Solvent: CDCl3
Temperature: 298.15 K
Spectral Width: 20.00 ppm
Number of Scans: 26
Relaxation Delay: 1.000 s
OTES
NH
OTIPS
HO
H
CF3
Compound 2-22
0.966
0.906
0.8
1.07
2.03
1.01
1.02
4.22
1.42
5.27
9.38
11.2
0.802
0.945
0.944
1
1.1
1.91
1
1.06
2.73
9.23
8.29
23
5.65
ppm
9
8
7
6
5
4
3
2
1

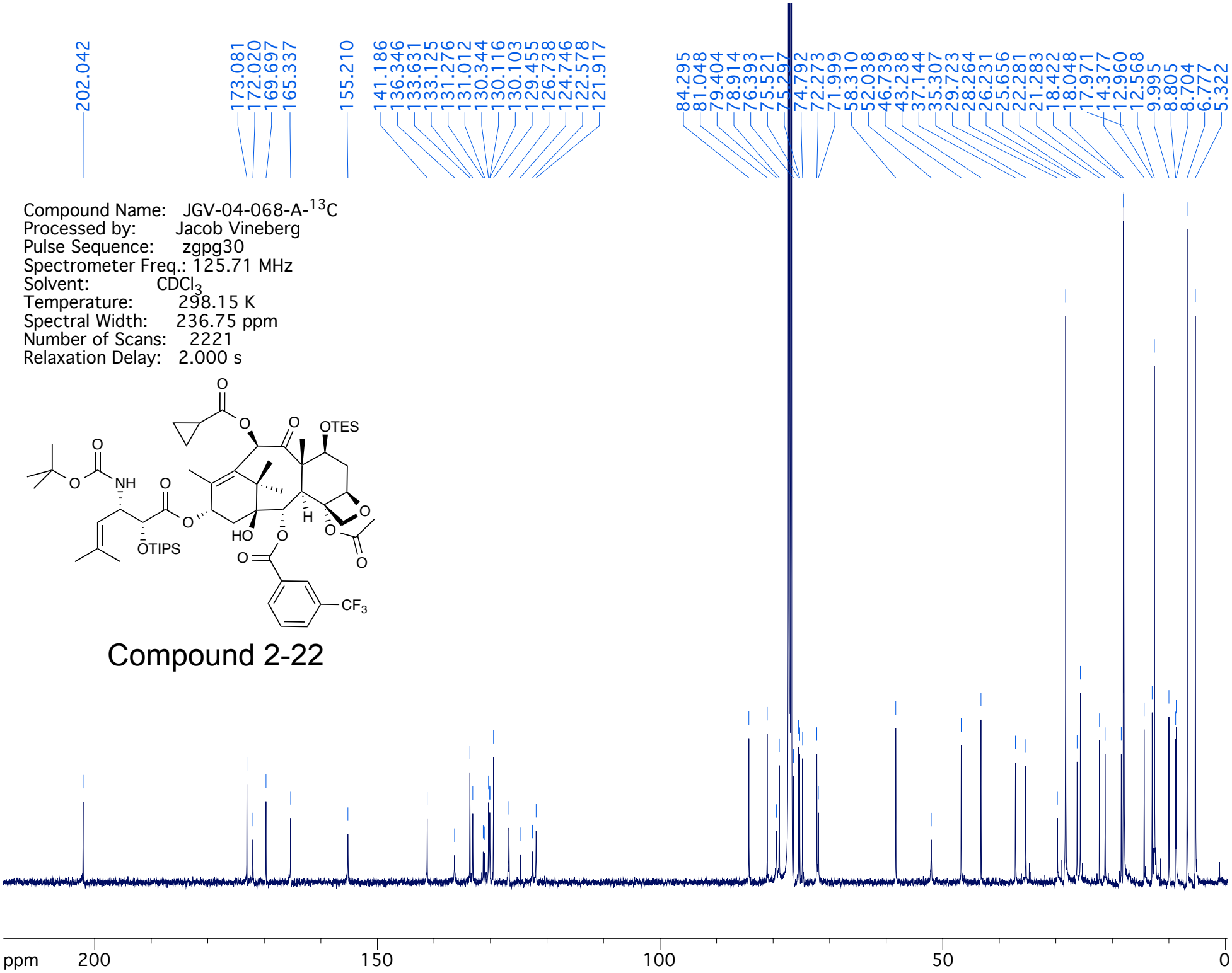
202.042
173.081
172.020
169.697
165.337
155.210
141.186
136.346
133.631
133.125
131.276
131.012
130.344
130.116
130.103
129.455
126.738
124.746
122.578
121.917
84.295
81.048
79.404
78.914
76.393
75.521
75.297
74.792
72.273
71.999
58.310
52.038
46.739
43.238
37.144
35.307
29.723
28.264
26.231
25.656
22.281
21.283
18.422
18.048
17.971
14.377
12.960
12.568
9.995
8.805
8.704
6.777
5.322
Compound Name: JGV-04-068-A-13C
Processed by: Jacob Vineberg
Pulse Sequence: zgpg30
Spectrometer Freq.: 125.71 MHz
Solvent: CDCl3
Temperature: 298.15 K
Spectral Width: 236.75 ppm
Number of Scans: 2221
Relaxation Delay: 2.000 s
OTES
NH
OTIPS
HO
H
CF3
Compound 2-22
ppm
200
150
100
50
0

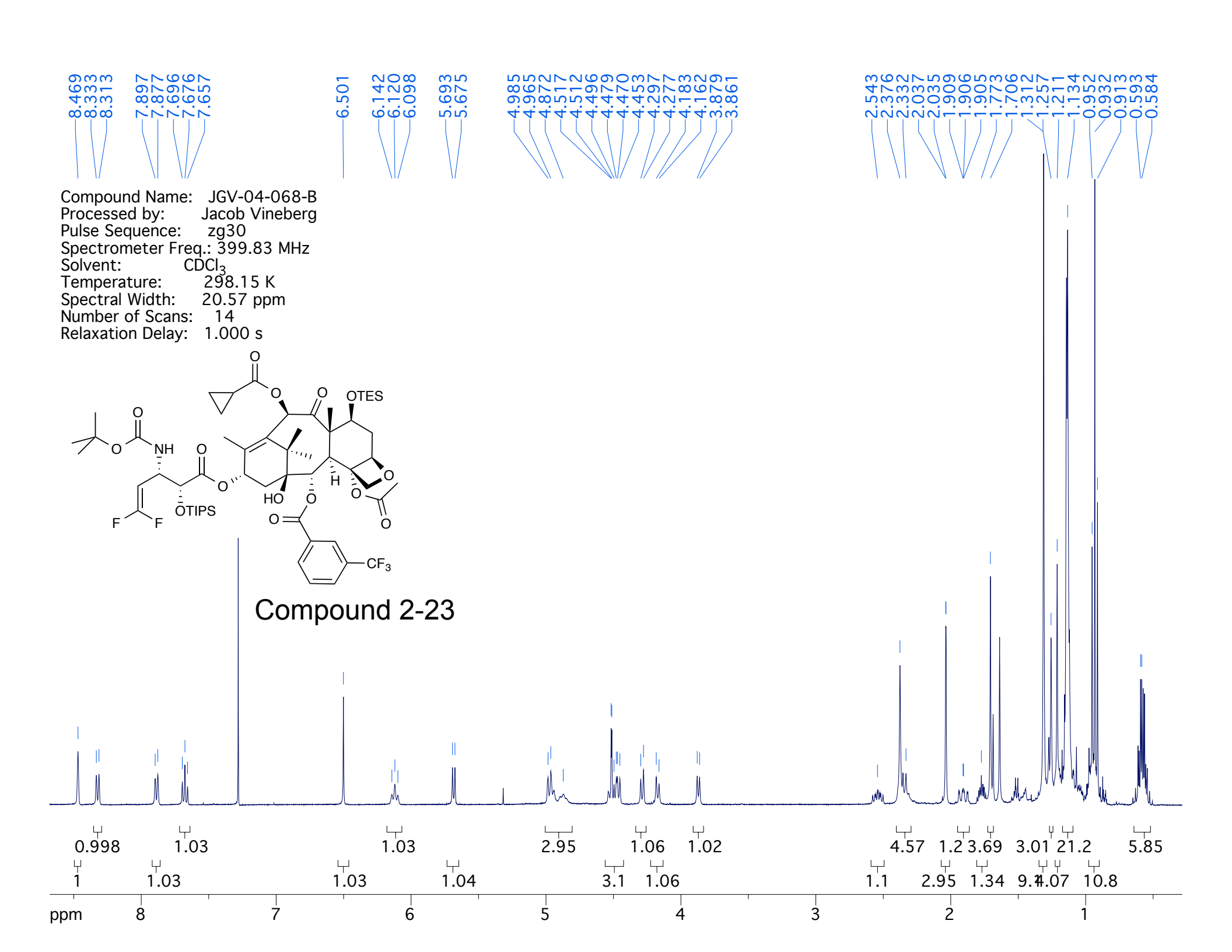
8.469
8.333
8.313
7.897
7.877
7.696
7.676
7.657
6.501
6.142
6.120
6.098
5.693
5.675
4.985
4.965
4.872
4.517
4.512
4.496
4.479
4.470
4.453
4.297
4.277
4.183
4.162
3.879
3.861
2.543
2.376
2.332
2.037
2.035
1.909
1.906
1.905
1.773
1.706
1.312
1.257
1.211
1.134
0.952
0.932
0.913
0.593
0.584
Compound Name: JGV-04-068-B
Processed by: Jacob Vineberg
Pulse Sequence: zg30
Spectrometer Freq.: 399.83 MHz
Solvent: CDCl3
Temperature: 298.15 K
Spectral Width: 20.57 ppm
Number of Scans: 14
Relaxation Delay: 1.000 s
OTES
NH
OTIPS
HO
H
F
F
CF3
Compound 2-23
0.998
1.03
1.03
2.95
1.06
1.02
4.57
1.2
3.69
3.01
21.2
5.85
1
1.03
1.03
1.04
3.1
1.06
1.1
2.95
1.34
9.4
4.07
10.8
ppm
8
7
6
5
4
3
2
1

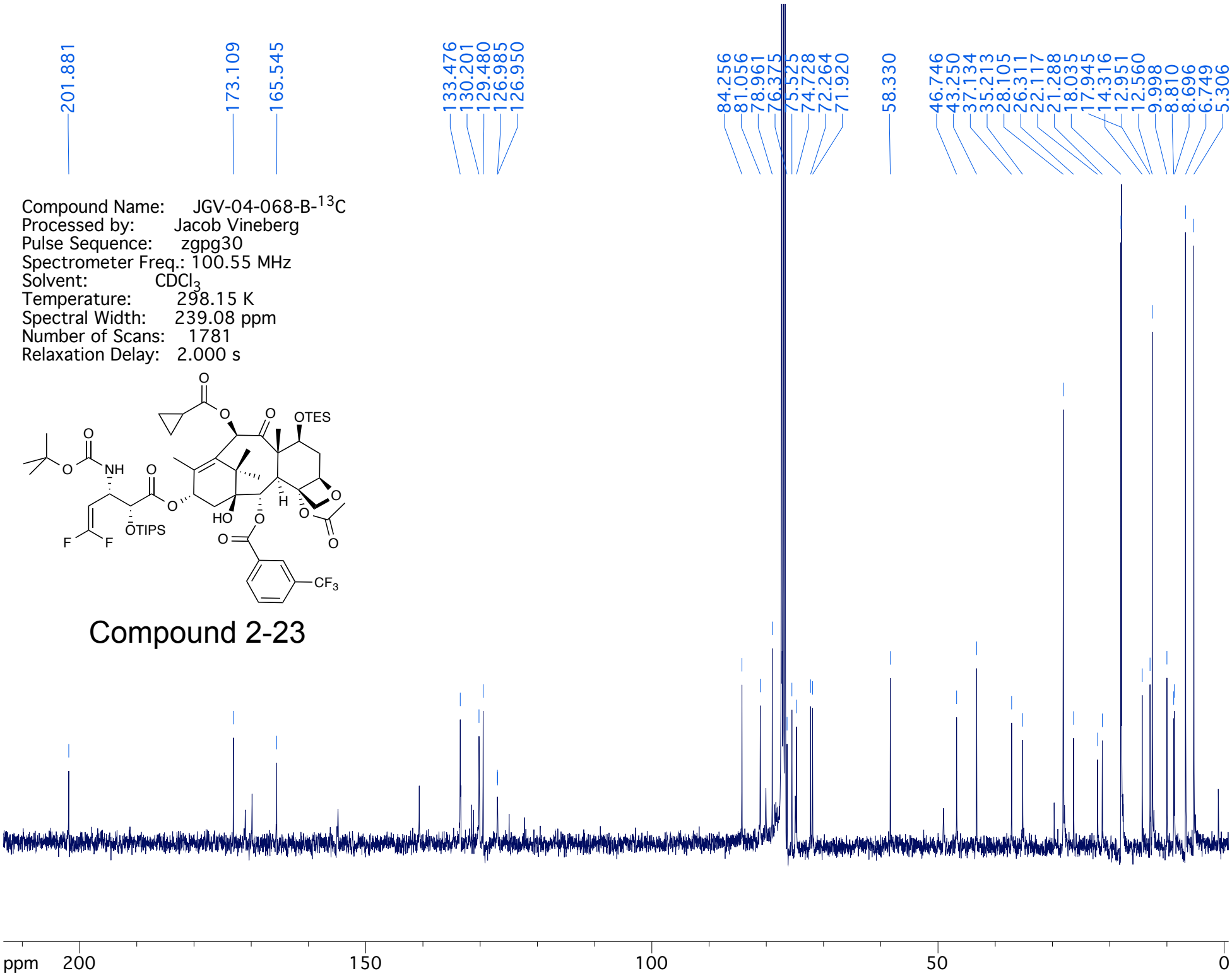
201.881
173.109
165.545
133.476
130.201
129.480
126.985
126.950
84.256
81.056
78.961
76.375
75.525
74.728
72.264
71.920
58.330
46.746
43.250
37.134
35.213
28.105
26.311
22.117
21.288
18.035
17.945
14.316
12.951
12.560
9.998
8.810
8.696
6.749
5.306
Compound Name: JGV-04-068-B-13C
Processed by: Jacob Vineberg
Pulse Sequence: zgpg30
Spectrometer Freq.: 100.55 MHz
Solvent: CDCl3
Temperature: 298.15 K
Spectral Width: 239.08 ppm
Number of Scans: 1781
Relaxation Delay: 2.000 s
OTES
NH
OTIPS
HO
H
F
F
CF3
Compound 2-23
ppm
200
150
100
50
0

Compound Name: JGV-04-068-B-^{19}F
Processed by: Jacob Vineberg
Pulse Sequence: zgflqn
Spectrometer Freq.: 376.18 MHz
Solvent: $CDCl_3$
Temperature: 298.15 K
Spectral Width: 237.35 ppm
Number of Scans: 40
Relaxation Delay: 1.000 s

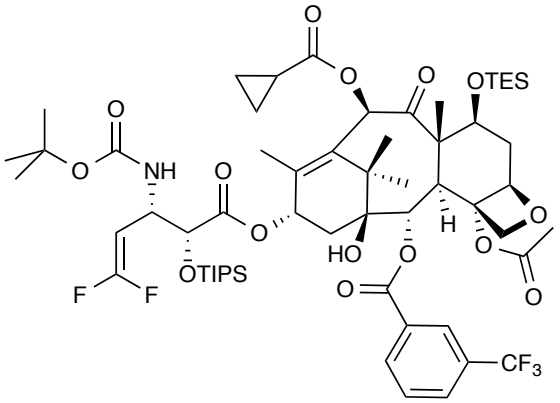

Compound 2-23

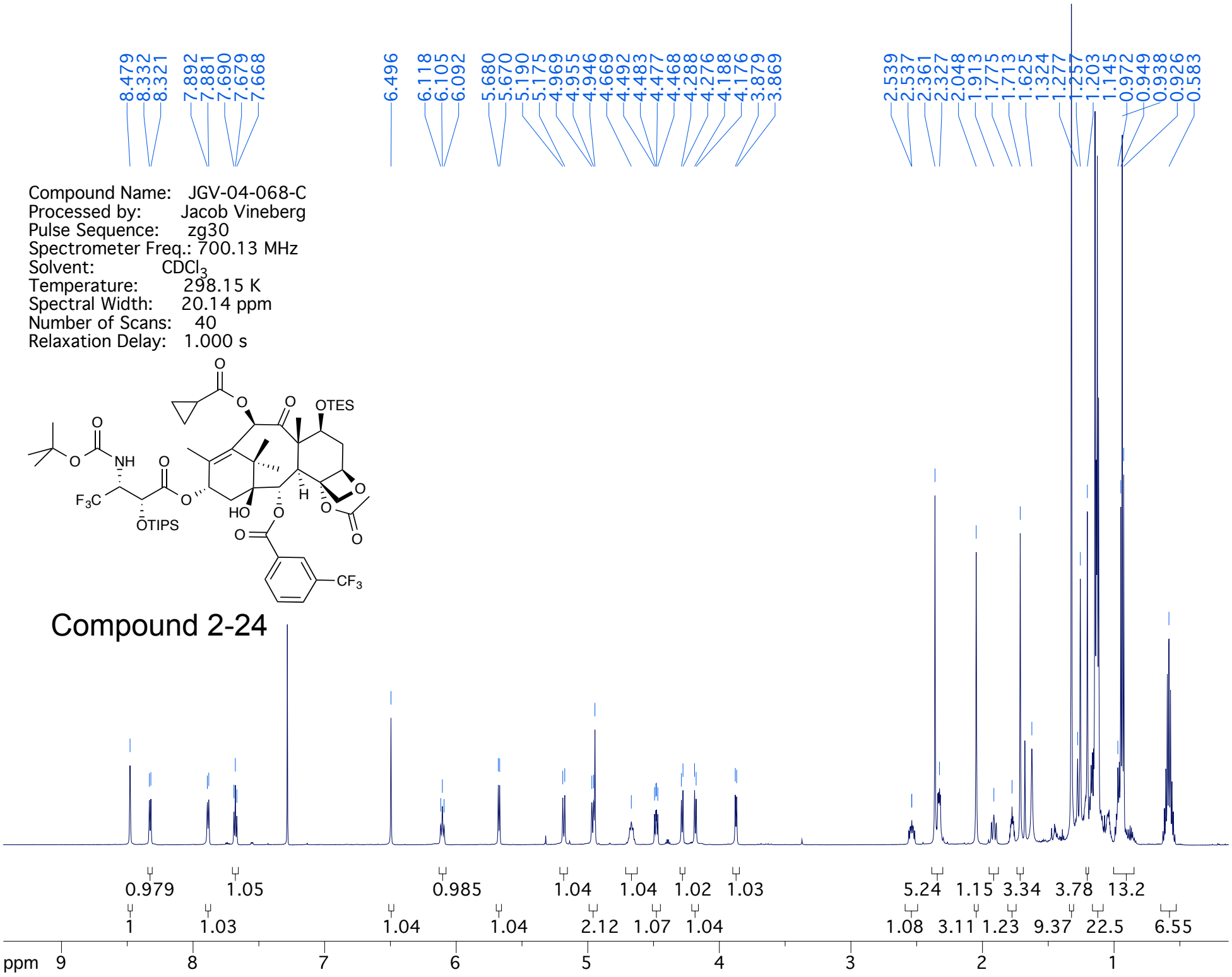
8.479
8.332
8.321
7.892
7.881
7.690
7.679
7.668
6.496
6.118
6.105
6.092
5.680
5.670
5.190
5.175
4.969
4.955
4.946
4.669
4.492
4.483
4.477
4.468
4.288
4.276
4.188
4.176
3.879
3.869
2.539
2.537
2.361
2.327
2.048
1.913
1.775
1.713
1.625
1.324
1.277
1.257
1.203
1.145
0.972
0.949
0.938
0.926
0.583
Compound Name: JGV-04-068-C
Processed by: Jacob Vineberg
Pulse Sequence: zg30
Spectrometer Freq.: 700.13 MHz
Solvent: CDCl3
Temperature: 298.15 K
Spectral Width: 20.14 ppm
Number of Scans: 40
Relaxation Delay: 1.000 s
OTES
NH
F3C
OTIPS
HO
H
CF3
Compound 2-24
0.979
1.05
0.985
1.04
1.04
1.02
1.03
5.24
1.15
3.34
3.78
13.2
1
1.03
1.04
1.04
2.12
1.07
1.04
1.08
3.11
1.23
9.37
22.5
6.55
ppm
9
8
7
6
5
4
3
2
1

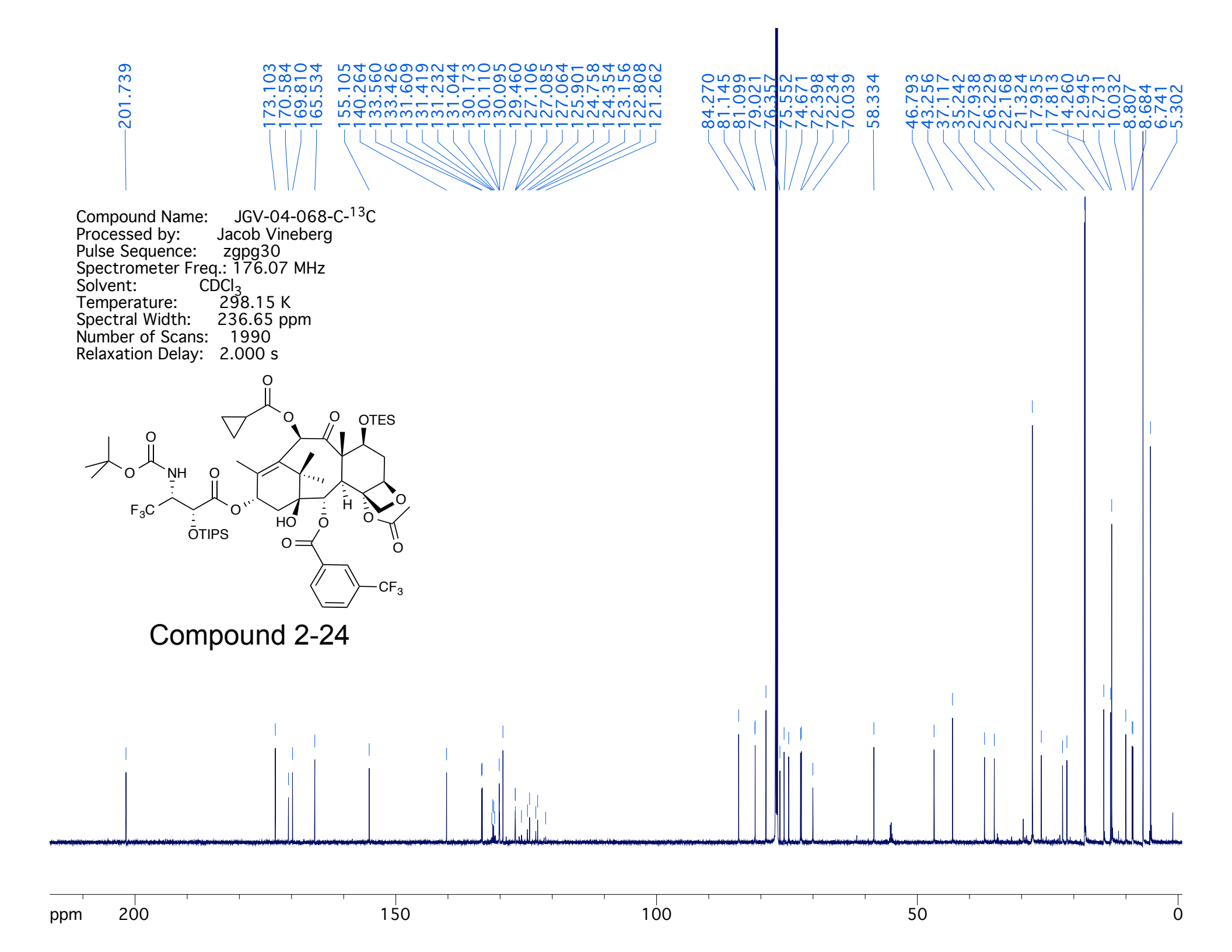
201.739
173.103
170.584
169.810
165.534
155.105
140.264
133.560
133.426
131.609
131.419
131.232
131.044
130.173
130.110
130.095
129.460
127.106
127.085
127.064
125.901
124.758
124.354
123.156
122.808
121.262
84.270
81.145
81.099
79.021
76.357
75.552
74.671
72.398
72.234
70.039
58.334
46.793
43.256
37.117
35.242
27.938
26.229
22.168
21.324
17.935
17.813
14.260
12.945
12.731
10.032
8.807
8.684
6.741
5.302
Compound Name: JGV-04-068-C-13C
Processed by: Jacob Vineberg
Pulse Sequence: zgpg30
Spectrometer Freq.: 176.07 MHz
Solvent: CDCl3
Temperature: 298.15 K
Spectral Width: 236.65 ppm
Number of Scans: 1990
Relaxation Delay: 2.000 s
OTES
NH
F3C
OTIPS
HO
H
CF3
Compound 2-24
ppm
200
150
100
50
0

Compound Name: JGV-04-068-C-^{19}F
Processed by: Jacob Vineberg
Pulse Sequence: zgflqn
Spectrometer Freq.: 376.18 MHz
Solvent: $CDCl_3$
Temperature: 298.15 K
Spectral Width: 237.35 ppm
Number of Scans: 28
Relaxation Delay: 1.000 s

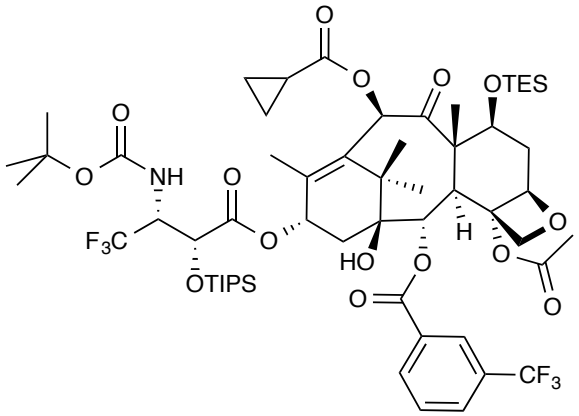

Compound 2-24

Compound Name: JGV-04-071
Processed by: Jacob Vineberg
Pulse Sequence: zg30
Spectrometer Freq.: 499.89 MHz
Solvent: $CDCl_3$
Temperature: 298.15 K
Spectral Width: 20.00 ppm
Number of Scans: 25
Relaxation Delay: 1.000 s

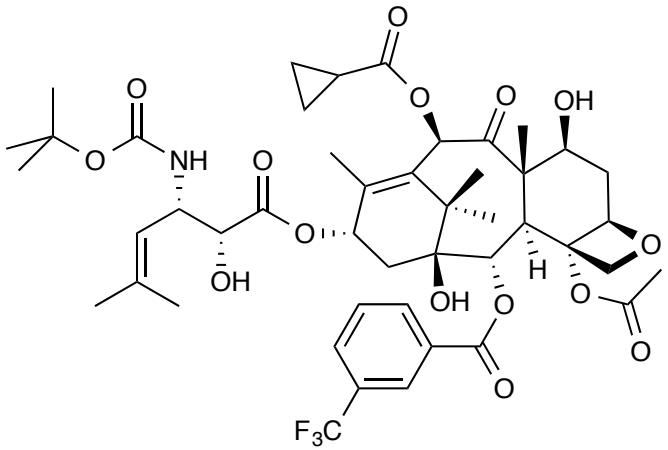

Compound 2-25 (SB-T-121406)

Compound Name: JGV-04-071-^{13}C
Processed by: Jacob Vineberg
Pulse Sequence: zgpg30
Spectrometer Freq.: 125.71 MHz
Solvent: $CDCl_3$
Temperature: 298.15 K
Spectral Width: 236.75 ppm
Number of Scans: 692
Relaxation Delay: 2.000 s

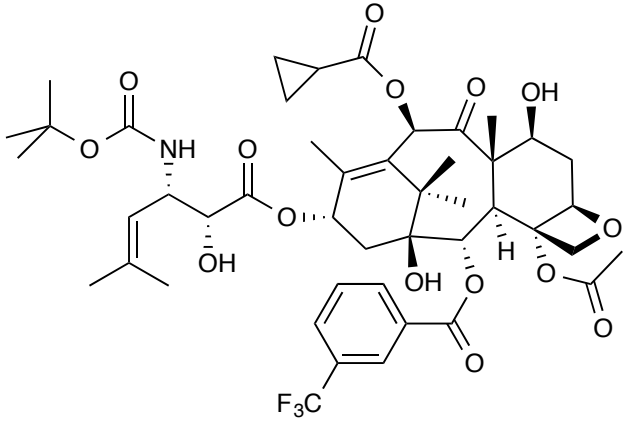

Compound 2-25 (SB-T-121406)

Compound Name: JGV-04-071-^{19}F
Processed by: Jacob Vineberg
Pulse Sequence: zgflqn
Spectrometer Freq.: 376.18 MHz
Solvent: $CDCl_3$
Temperature: 298.15 K
Spectral Width: 237.35 ppm
Number of Scans: 25
Relaxation Delay: 1.000 s

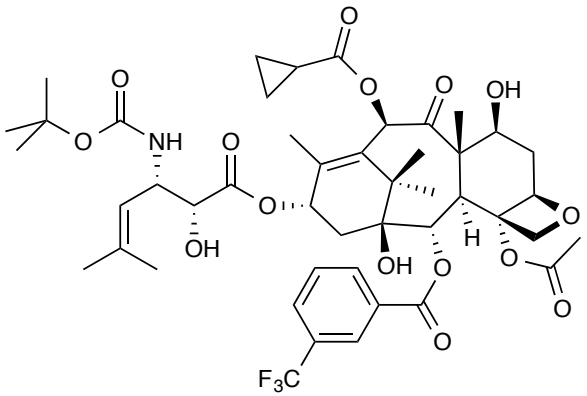

Taxoid 2-25 (SB-T-121406)

Compound Name: JGV-04-072
Processed by: Jacob Vineberg
Pulse Sequence: zg30
Spectrometer Freq.: 499.89 MHz
Solvent: $CDCl_3$
Temperature: 298.15 K
Spectral Width: 20.00 ppm
Number of Scans: 17
Relaxation Delay: 1.000 s

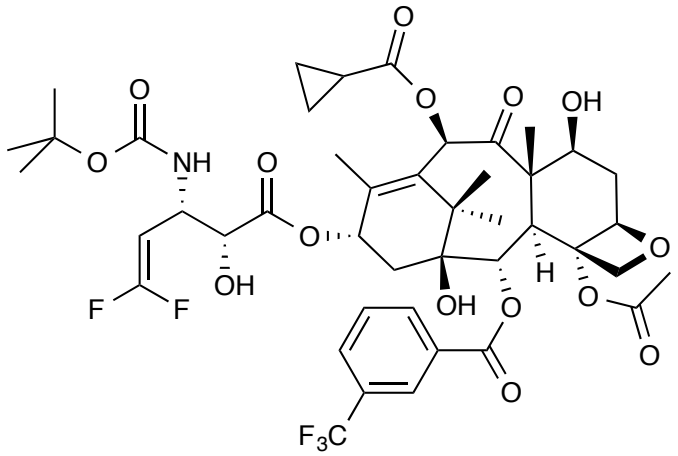

Taxoid 2-26 (SB-T-12852-6)

Comound Name: JGV-04-072-^{13}C
Processed by: Jacob Vineberg
Pulse Sequence: zgpg30
Spectrometer Freq.: 125.71 MHz
Solvent: $CDCl_3$
Temperature: 298.15 K
Spectral Width: 236.75 ppm
Number of Scans: 19768
Relaxation Delay: 2.000 s

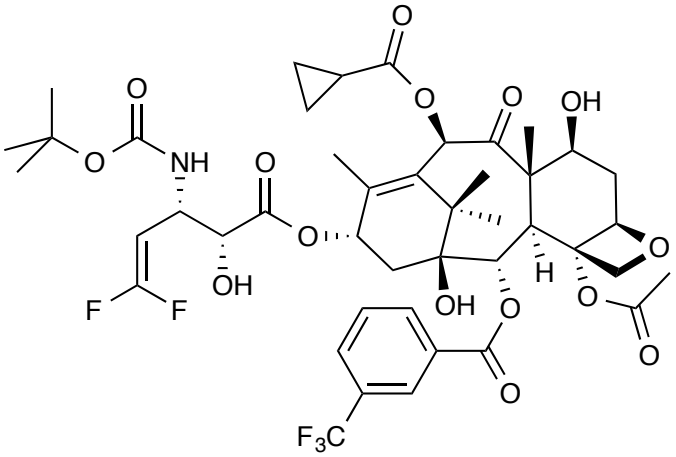

Taxoid 2-26 (SB-T-12852-6)

Compound Name: JGV-04-072-^{19}F
Processed by: Jacob Vineberg
Pulse Sequence: zgflqn
Spectrometer Freq.: 376.18 MHz
Solvent: $CDCl_3$
Temperature: 298.15 K
Spectral Width: 237.35 ppm
Number of Scans: 16
Relaxation Delay: 1.000 s

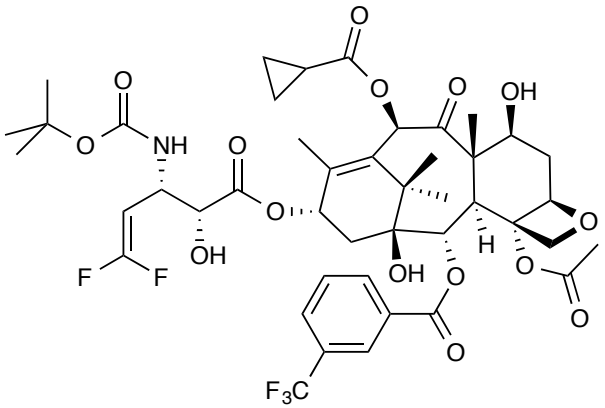

Taxoid 2-26 (SB-T-12852-6)

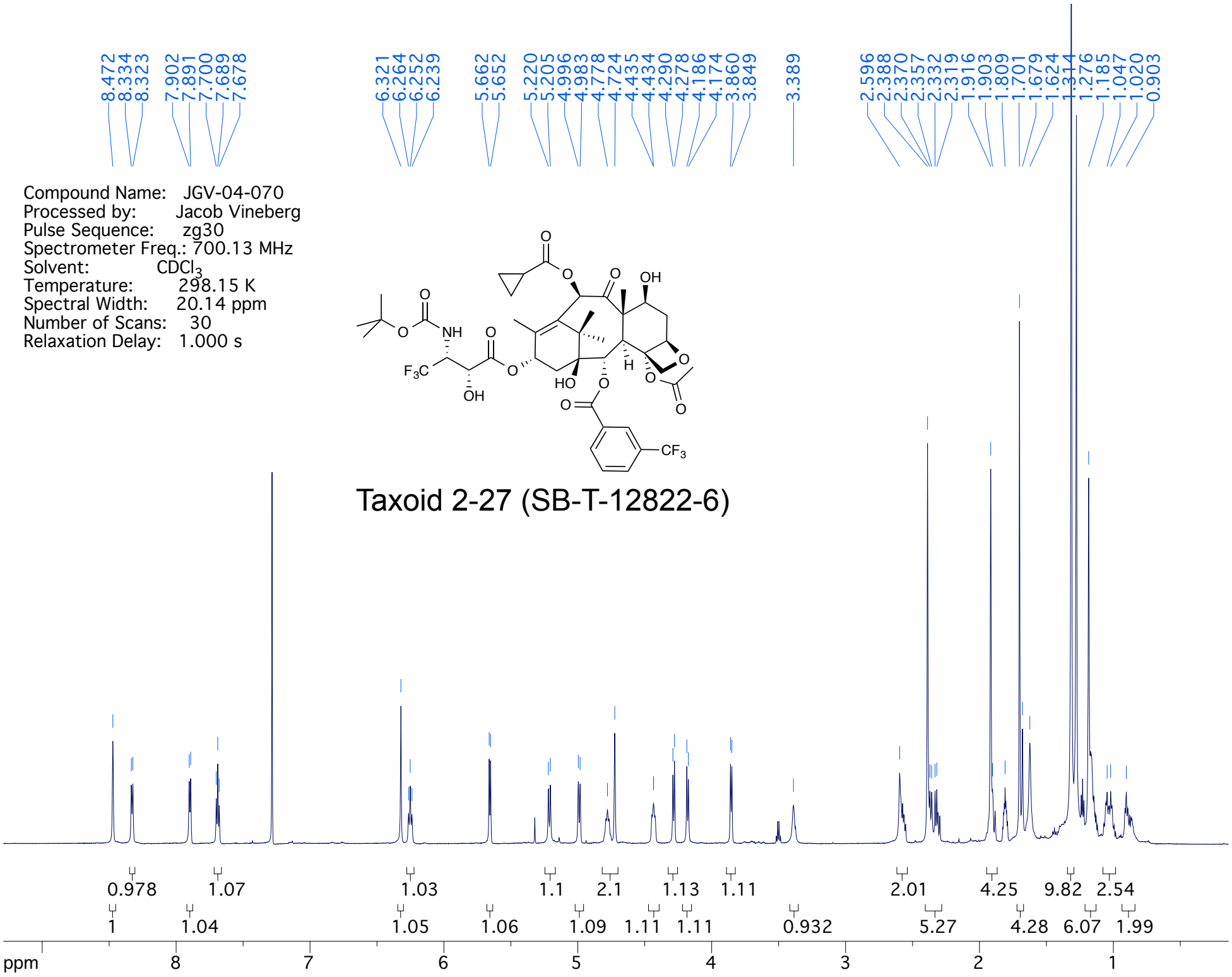
8.472
8.334
8.323
7.902
7.891
7.700
7.689
7.678
6.321
6.264
6.252
6.239
5.662
5.652
5.220
5.205
4.996
4.983
4.778
4.724
4.435
4.434
4.290
4.278
4.186
4.174
3.860
3.849
3.389
2.596
2.388
2.370
2.357
2.332
2.319
1.916
1.903
1.809
1.701
1.679
1.624
1.314
1.276
1.185
1.047
1.020
0.903
Compound Name: JGV-04-070
Processed by: Jacob Vineberg
Pulse Sequence: zg30
Spectrometer Freq.: 700.13 MHz
Solvent: CDCl3
Temperature: 298.15 K
Spectral Width: 20.14 ppm
Number of Scans: 30
Relaxation Delay: 1.000 s
Taxoid 2-27 (SB-T-12822-6)
0.978
1.07
1.03
1.1
2.1
1.13
1.11
2.01
4.25
9.82
2.54
1
1.04
1.05
1.06
1.09
1.11
1.11
0.932
5.27
4.28
6.07
1.99
ppm
8
7
6
5
4
3
2
1

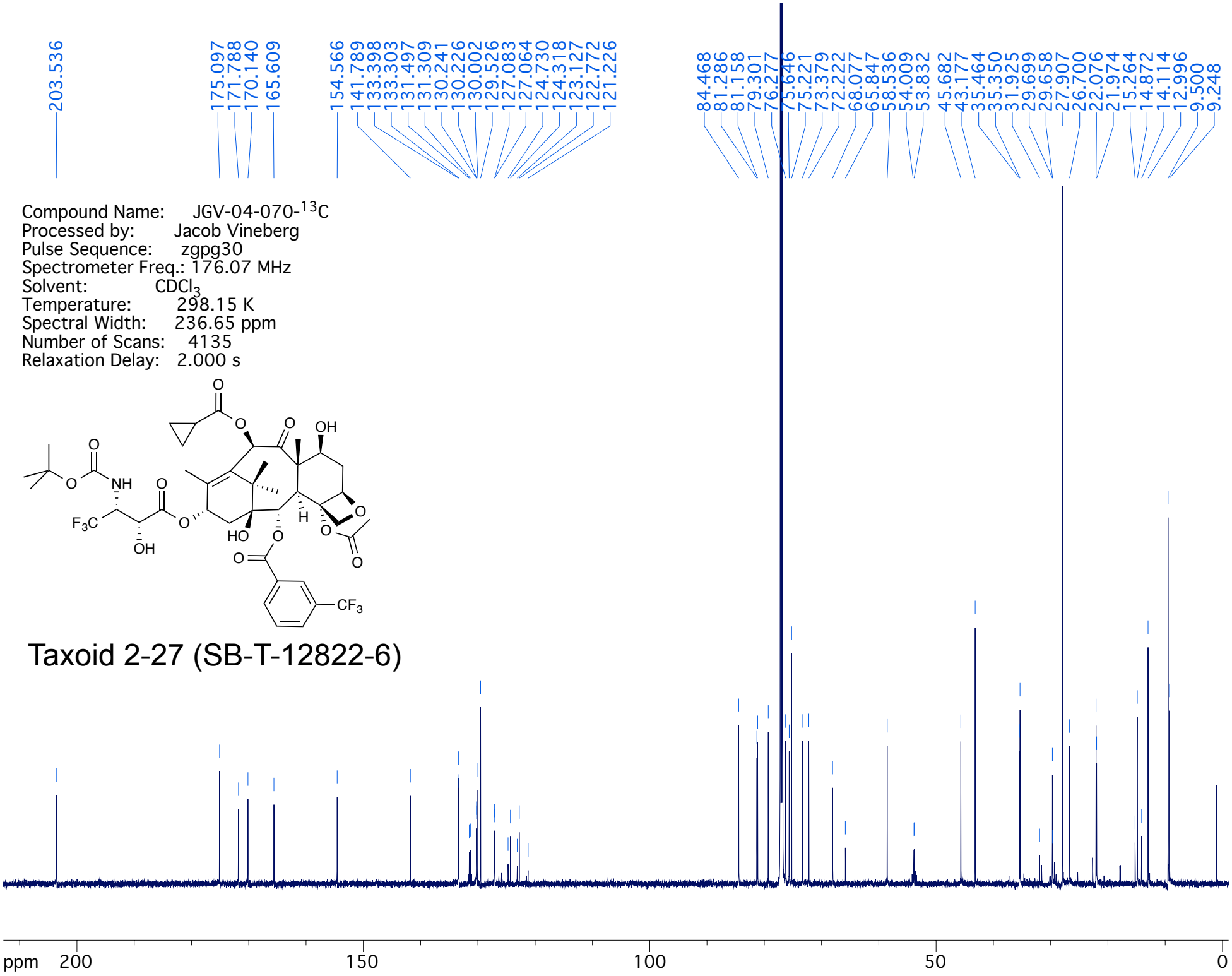
203.536
175.097
171.788
170.140
165.609
154.566
141.789
133.398
133.303
131.497
131.309
130.241
130.226
130.002
129.526
127.083
127.064
124.730
124.318
123.127
122.772
121.226
84.468
81.286
81.158
79.301
76.277
75.646
75.221
73.379
72.222
68.077
65.847
58.536
54.009
53.832
45.682
43.177
35.464
35.350
31.925
29.699
29.658
27.907
26.700
22.076
21.974
15.264
14.872
14.114
12.996
9.500
9.248
Compound Name: JGV-04-070-13C
Processed by: Jacob Vineberg
Pulse Sequence: zgpg30
Spectrometer Freq.: 176.07 MHz
Solvent: CDCl3
Temperature: 298.15 K
Spectral Width: 236.65 ppm
Number of Scans: 4135
Relaxation Delay: 2.000 s
Taxoid 2-27 (SB-T-12822-6)
ppm
200
150
100
50
0

Compound Name: JGV-04-090
Processed by: Jacob Vineberg
Pulse Sequence: zg30
Spectrometer Freq.: 399.83 MHz
Solvent: $CDCl_3$
Temperature: 298.15 K
Spectral Width: 20.57 ppm
Number of Scans: 50
Relaxation Delay: 1.000 s

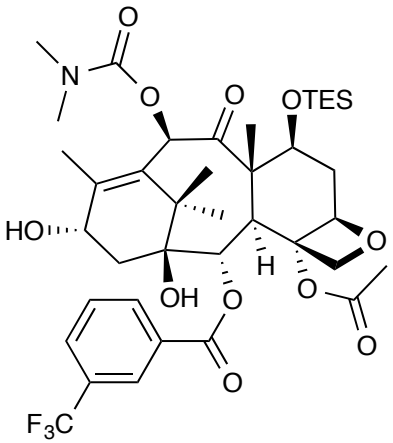

Compound 2-28

Compound Name: JGV-04-090-^{19}F
Processed by: Jacob Vineberg
Pulse Sequence: zgpg30
Spectrometer Freq.: 176.07 MHz
Solvent: $CDCl_3$
Temperature: 298.15 K
Spectral Width: 236.65 ppm
Number of Scans: 1312
Relaxation Delay: 2.000 s

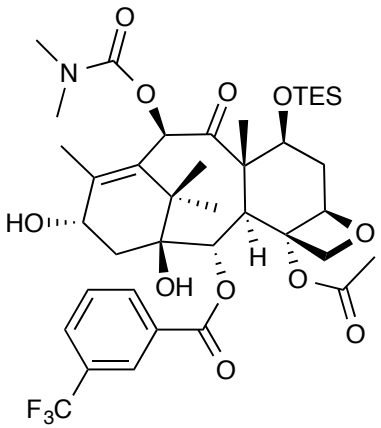

Compound 2-28

Compound Name: JGV-04-079
Processed by: Jacob Vineberg
Pulse Sequence: zg30
Spectrometer Freq.: 700.13 MHz
Solvent: $CDCl_3$
Temperature: 298.15 K
Spectral Width: 20.14 ppm
Number of Scans: 100
Relaxation Delay: 1.000 s

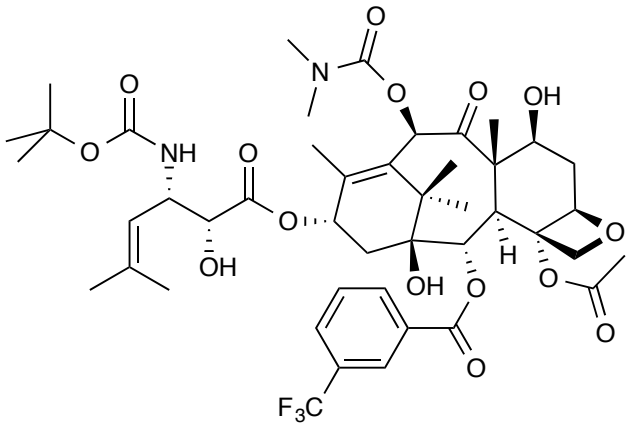

Taxoid 2-30 (SB-T-121606)

Compound Name: JGV-04-079-^{13}C
Processed by: Jacob Vineberg
Pulse Sequence: zgpg30
Spectrometer Freq.: 176.07 MHz
Solvent: $CDCl_3$
Temperature: 298.15 K
Spectral Width: 236.65 ppm
Number of Scans: 1312
Relaxation Delay: 2.000 s

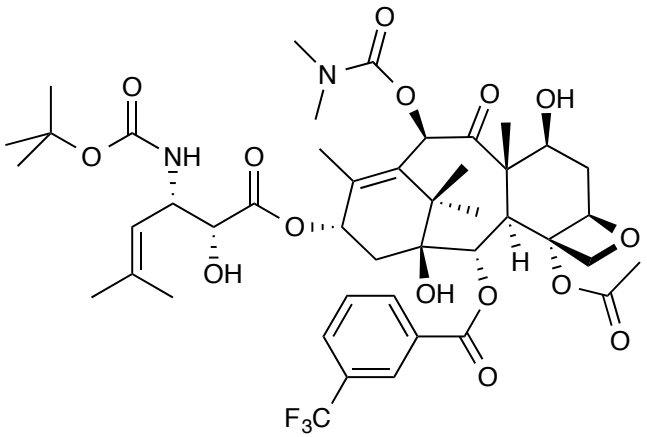

Taxoid 2-30 (SB-T-121606)

Compound Name: JGV-03-108
Processed by: Jacob Vineberg
Pulse Sequence: zg30
Spectrometer Freq.: 499.89 MHz
Solvent: $CDCl_3$
Temperature: 298.14 K
Spectral Width: 20.00 ppm
Number of Scans: 32
Relaxation Delay: 1.000 s

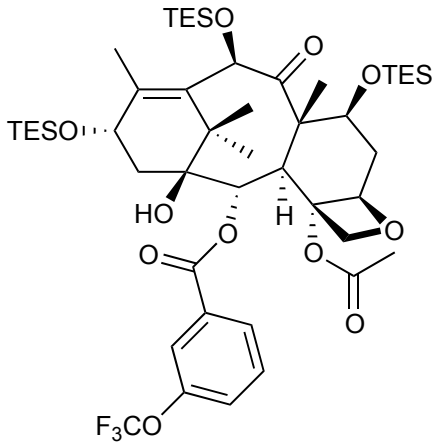

Compound 2-31

Compound Name: JGV-03-108-^{13}C
Processed by: Jacob Vineberg
Pulse Sequence: zgpg30
Spectrometer Freq.: 125.71 MHz
Solvent: $CDCl_3$
Temperature: 298.15 K
Spectral Width: 236.75 ppm
Number of Scans: 401
Relaxation Delay: 2.000 s

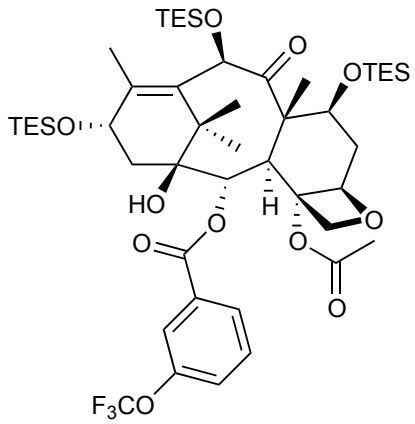

Compound 2-31

Compound Name: JGV-03-109
Processed by: Jacob Vineberg
Pulse Sequence: zg30
Spectrometer Freq.: 499.89 MHz
Solvent: DMSO
Temperature: 298.15 K
Spectral Width: 20.00 ppm
Number of Scans: 30
Relaxation Delay: 1.000 s

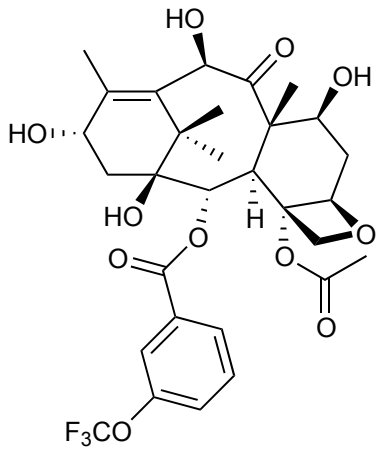

Compound 2-32

Compound Name: JGV-03-109-^{13}C
Processed by: Jacob Vineberg
Pulse Sequence: zgpg30
Spectrometer Freq.: 125.71 MHz
Solvent: DMSO
Temperature: 298.15 K
Spectral Width: 236.75 ppm
Number of Scans: 356
Relaxation Delay: 2.000 s

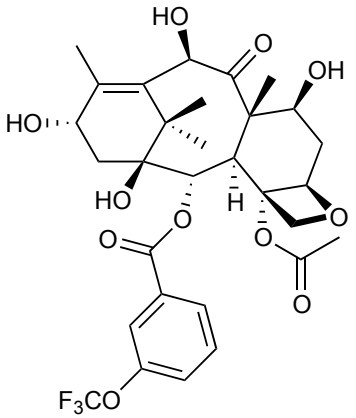

Compound 2-32

Compound Name: JGV-03-109-^{19}F
Processed by: Jacob Vineberg
Pulse Sequence: zgfhigqn.2
Spectrometer Freq.: 376.18 MHz
Solvent: DMSO
Temperature: 298.18 K
Spectral Width: 237.35 ppm
Number of Scans: 34
Relaxation Delay: 1.000 s

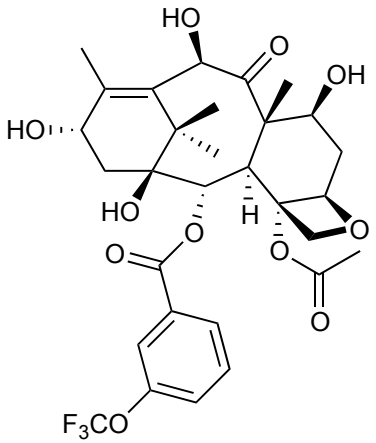

Compound 2-32

Compound Name: JGV-03-110
Processed by: Jacob Vineberg
Pulse Sequence: zg30
Spectrometer Freq.: 499.89 MHz
Solvent: $CDCl_3$
Temperature: 298.14 K
Spectral Width: 20.00 ppm
Number of Scans: 23
Relaxation Delay: 1.000 s

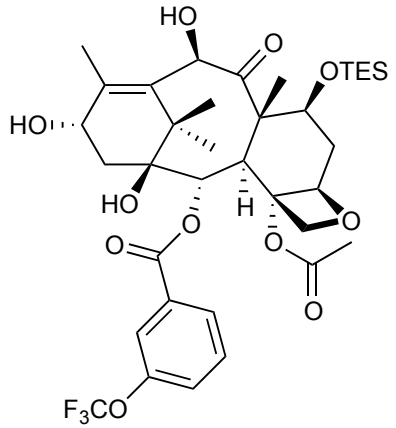

Compound 2-33

Compound Name: JGV-03-110-^{13}C
Processed by: Jacob Vineberg
Pulse Sequence: zgpg30
Spectrometer Freq.: 125.71 MHz
Solvent: $CDCl_3$
Temperature: 298.15 K
Spectral Width: 236.75 ppm
Number of Scans: 2579
Relaxation Delay: 2.000 s

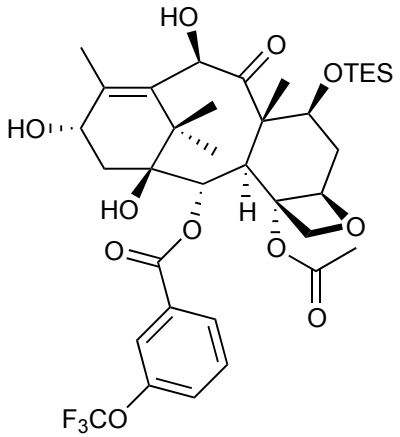

Compound 2-33

Compound Name: JGV-03-110-^{19}F
Processed by: Jacob Vineberg
Pulse Sequence: zgfhigqn.2
Spectrometer Freq.: 376.18 MHz
Solvent: $CDCl_3$
Temperature: 298.19 K
Spectral Width: 237.35 ppm
Number of Scans: 34
Relaxation Delay: 1.000 s

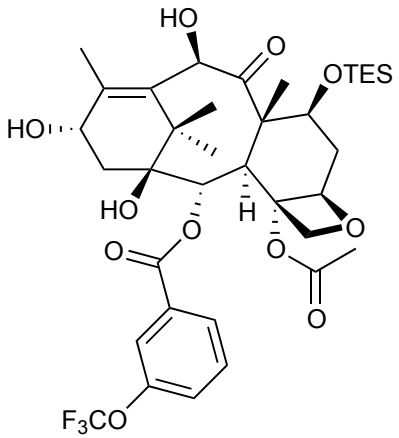

Compound 2-33

Compound Name: JGV-03-111
Processed by: Jacob Vineberg
Pulse Sequence: zg30
Spectrometer Freq.: 499.89 MHz
Solvent: $CDCl_3$
Temperature: 298.14 K
Spectral Width: 20.00 ppm
Number of Scans: 25
Relaxation Delay: 1.000 s

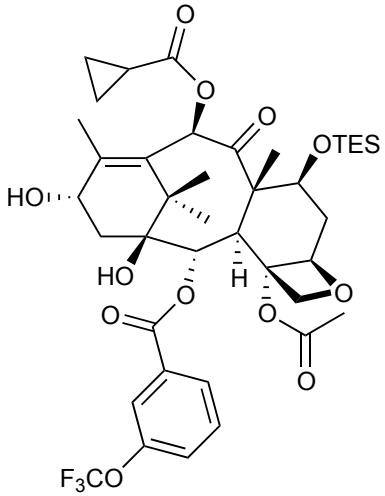

Compound 2-34

Compound Name: JGV-03-111-^{13}C
Processed by: Jacob Vineberg
Pulse Sequence: zgpg30
Spectrometer Freq.: 125.71 MHz
Solvent: $CDCl_3$
Temperature: 298.15 K
Spectral Width: 236.75 ppm
Number of Scans: 3852
Relaxation Delay: 2.000 s

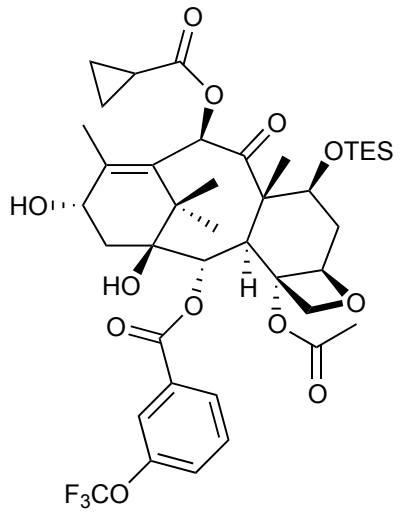

Compound 2-34

Compound Name: JGV-03-111-^{19}F
Processed by: Jacob Vineberg
Pulse Sequence: zgfhigqn.2
Spectrometer Freq.: 376.18 MHz
Solvent: $CDCl_3$
Temperature: 298.20 K
Spectral Width: 237.35 ppm
Number of Scans: 58
Relaxation Delay: 1.000 s

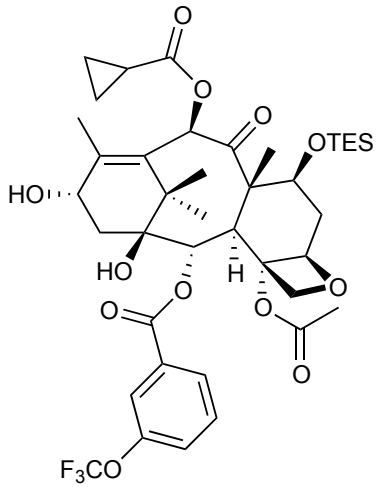

Compound 2-34

Compound Name: JGV-03-112
Processed by: Jacob Vineberg
Pulse Sequence: zg30
Spectrometer Freq.: 499.89 MHz
Solvent: $CDCl_3$
Temperature: 298.15 K
Spectral Width: 20.00 ppm
Number of Scans: 19
Relaxation Delay: 1.000 s

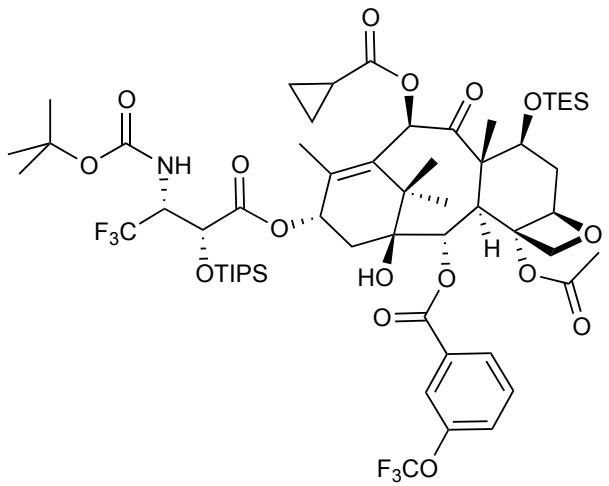

Compound 2-35

Compound Name: JGV-03-112-^{13}C
Processed by: Jacob Vineberg
Pulse Sequence: zgpg30
Spectrometer Freq.: 125.71 MHz
Solvent: $CDCl_3$
Temperature: 298.15 K
Spectral Width: 236.75 ppm
Number of Scans: 1233
Relaxation Delay: 2.000 s

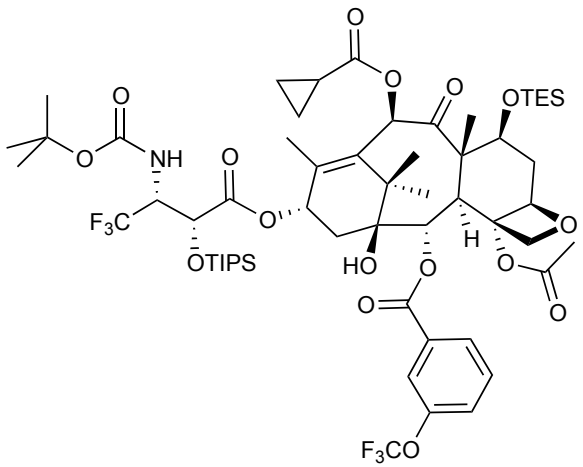

Compound 2-35

Compound Name: JGV-03-112-^{19}F
Processed by: Jacob Vineberg
Pulse Sequence: zgfhigqn.2
Spectrometer Freq.: 376.18 MHz
Solvent: $CDCl_3$
Temperature: 298.19 K
Spectral Width: 237.35 ppm
Number of Scans: 24
Relaxation Delay: 1.000 s

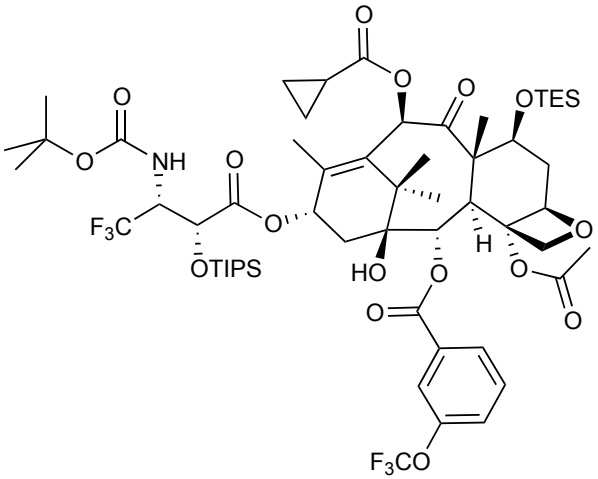

Compound 2-35

Compound Name: JGV-03-113
Processed by: Jacob Vineberg
Pulse Sequence: zg30
Spectrometer Freq.: 499.89 MHz
Solvent: $CDCl_3$
Temperature: 298.14 K
Spectral Width: 20.00 ppm
Number of Scans: 37
Relaxation Delay: 1.000 s

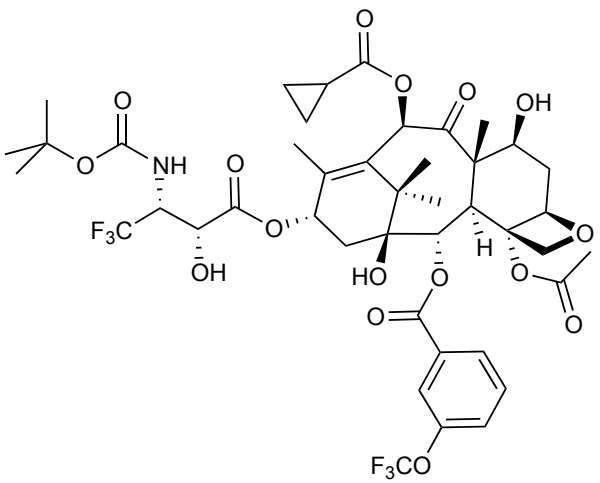

Taxoid 2-36 (SB-T-12822-5)

Compound Name: JGV-03-113-^{13}C
Processed by: Jacob Vineberg
Pulse Sequence: zgpg30
Spectrometer Freq.: 125.71 MHz
Solvent: $CDCl_3$
Temperature: 298.15 K
Spectral Width: 236.75 ppm
Number of Scans: 1002
Relaxation Delay: 2.000 s

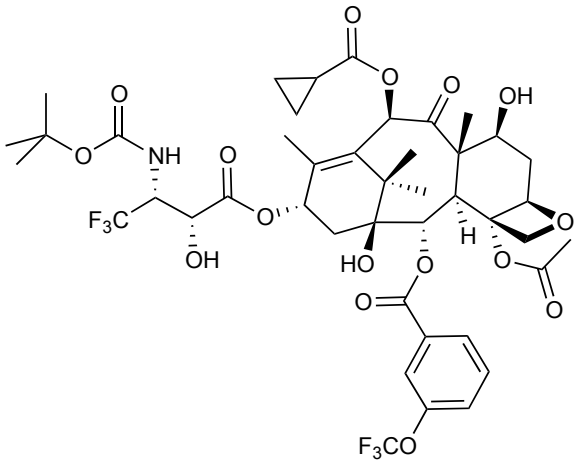

Taxoid 2-36 (SB-T-12822-5)

Compound Name: JGV-03-113-^{19}F
Processed by: Jacob Vineberg
Pulse Sequence: zg
Spectrometer Freq.: 470.34 MHz
Solvent: $CDCl_3$
Temperature: 298.15 K
Spectral Width: 29.97 ppm
Number of Scans: 1
Relaxation Delay: 5.000 s

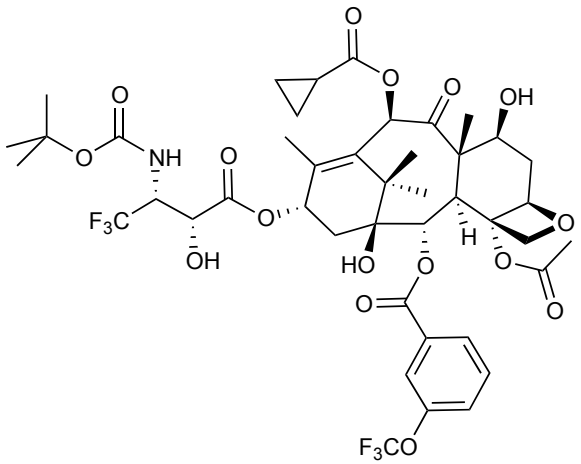

Taxoid 2-36 (SB-T-12822-5)

Compound Name: JGV-03-001
Processed by: Jacob Vineberg
Pulse Sequence: s2pul
Spectrometer Freq.: 300.07 MHz
Solvent: $CDCl_3$
Temperature: 298.15 K
Spectral Width: 15.00 ppm
Number of Scans: 100
Relaxation Delay: 1.000 s

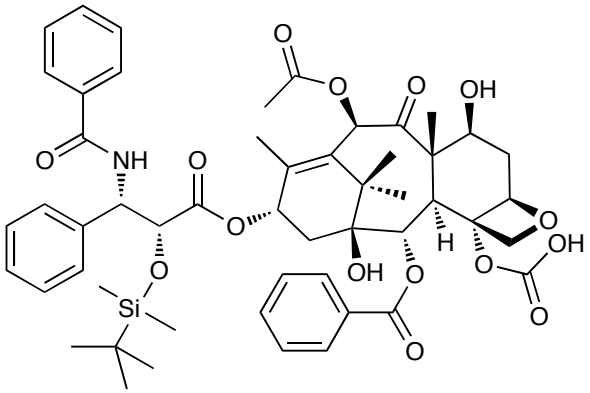

Compound 2-37

Compound Name: JGV-03-002
Processed by: Jacob Vineberg
Pulse Sequence: zg30
Spectrometer Freq.: 499.89 MHz
Solvent: $CDCl_3$
Temperature: 298.15 K
Spectral Width: 20.00 ppm
Number of Scans: 49
Relaxation Delay: 1.000 s

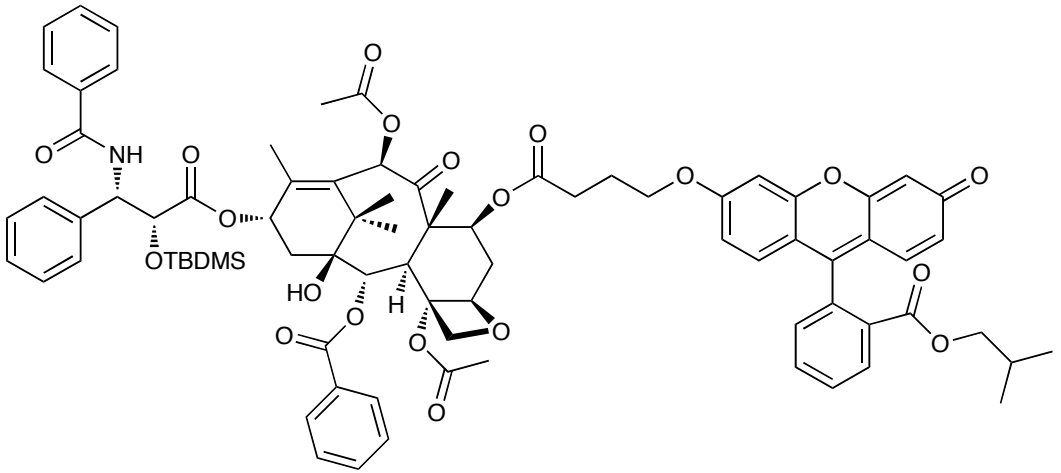

Compound 2-38

Compound Name: JGV-03-002-^{13}C
Processed by: Jacob Vineberg
Pulse Sequence: zgpg30
Spectrometer Freq.: 125.71 MHz
Solvent: $CDCl_3$
Temperature: 298.15 K
Spectral Width: 236.75 ppm
Number of Scans: 2137
Relaxation Delay: 2.000 s

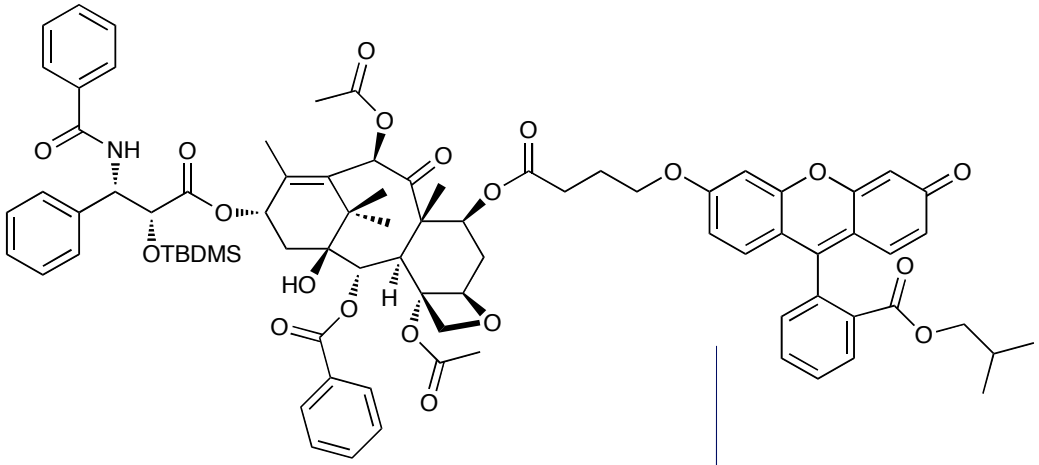

Compound 2-38

Compound Name: JGV-03-003
Processed by: Jacob Vineberg
Pulse Sequence: zg30
Spectrometer Freq.: 499.89 MHz
Solvent: $CDCl_3$
Temperature: 298.15 K
Spectral Width: 20.00 ppm
Number of Scans: 84
Relaxation Delay: 1.000 s

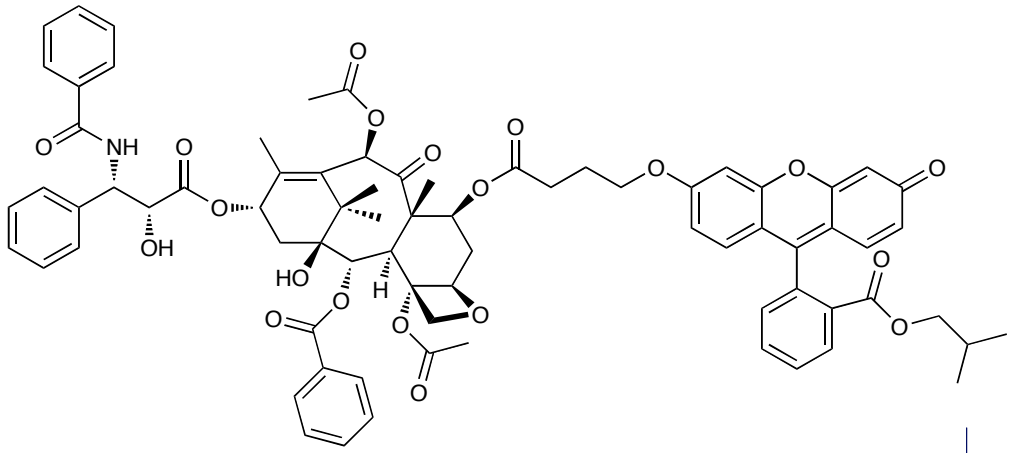

Conjugate 2-39 (Taxol-7-Fluorescein)

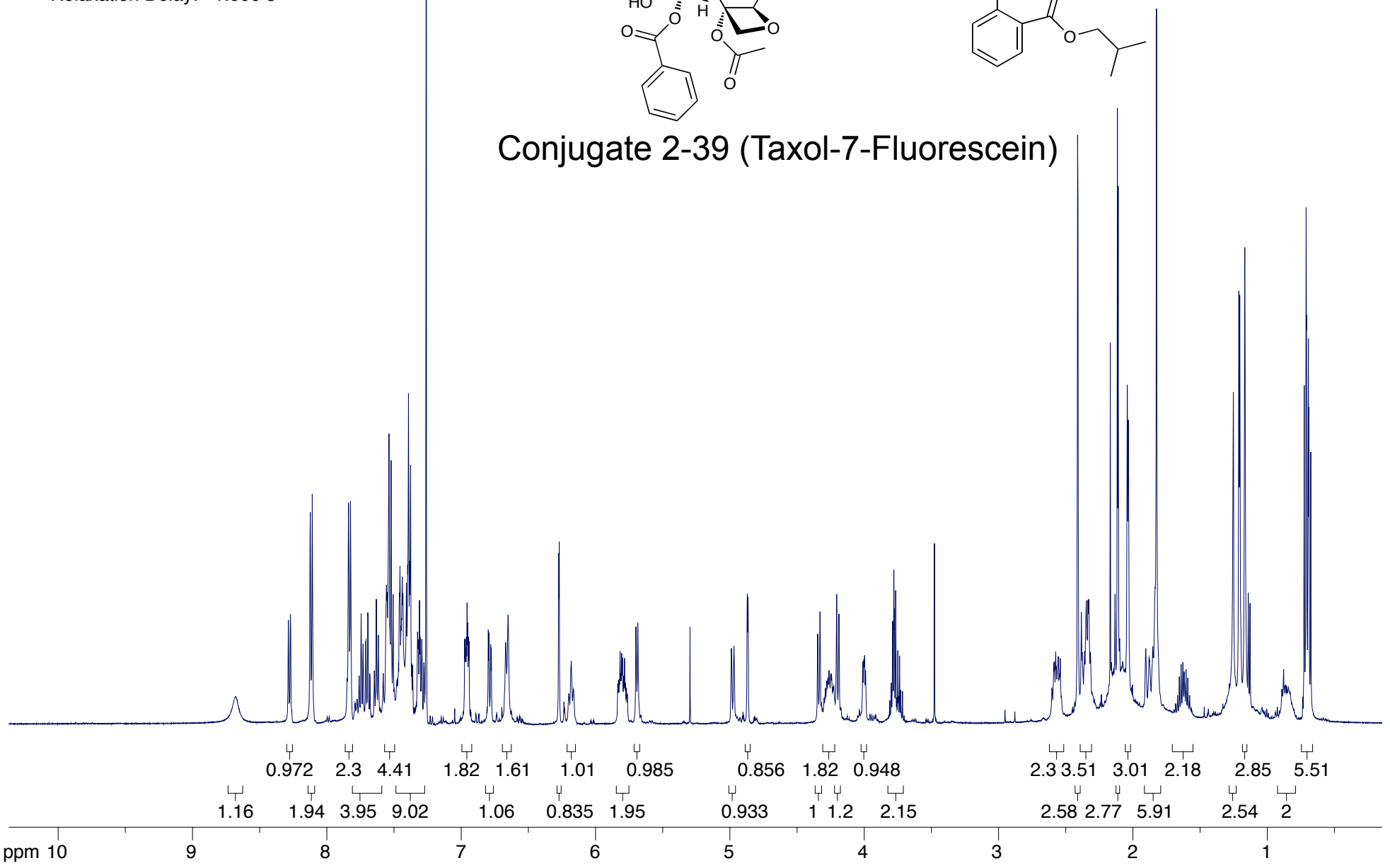

Compound Name: JGV-03-003-^{13}C
Processed by: Jacob Vineberg
Pulse Sequence: zgpg30
Spectrometer Freq.: 125.71 MHz
Solvent: $CDCl_3$
Temperature: 298.15 K
Spectral Width: 236.75 ppm
Number of Scans: 4256
Relaxation Delay: 2.000 s

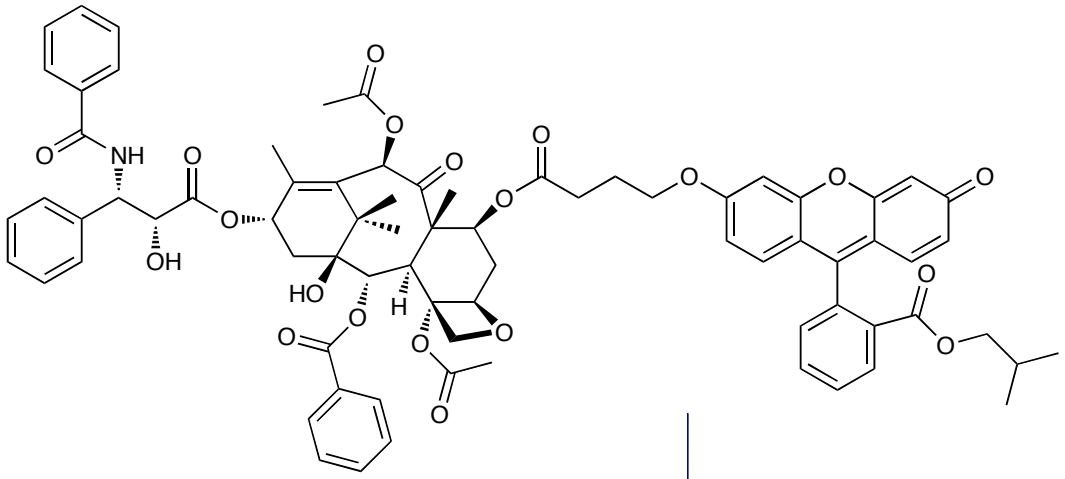

Conjugate 2-39
(Taxol-7-Fluorescein)

Appendix Chapter 3

Compound Name: JGV-01-154
Processed by: Jacob Vineberg
Pulse Sequence: zg30
Spectrometer Freq.: 300.18 MHz
Solvent: $CDCl_3$
Temperature: 293.57 K
Spectral Width: 20.33 ppm
Number of Scans: 52
Relaxation Delay: 1.000 s

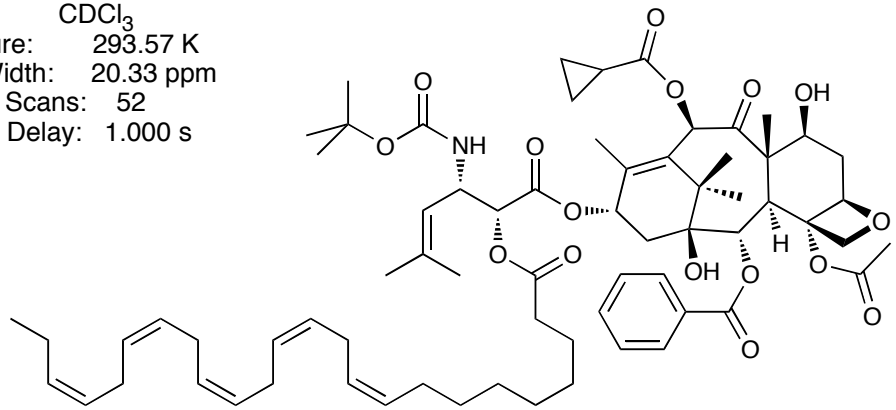

Conjugate 3-1 (LNA-SB-T-1214)

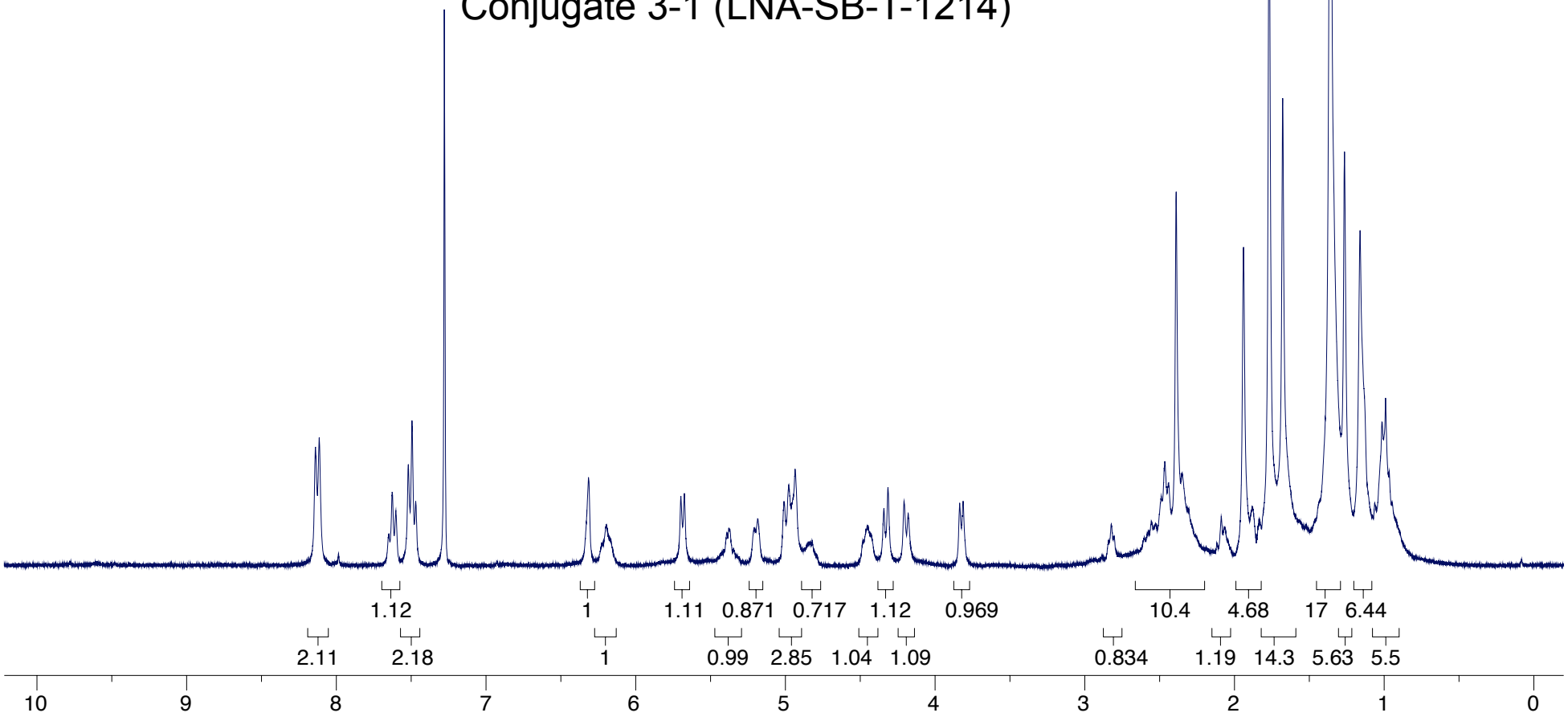

Compound Name: JGV-01-156
Processed by: Jacob Vineberg
Pulse Sequence: s2pul
Spectrometer Freq.: 599.72 MHz
Solvent: $CDCl_3$
Temperature: 298.15 K
Spectral Width: 13.34 ppm
Number of Scans: 50
Relaxation Delay: 1.000 s

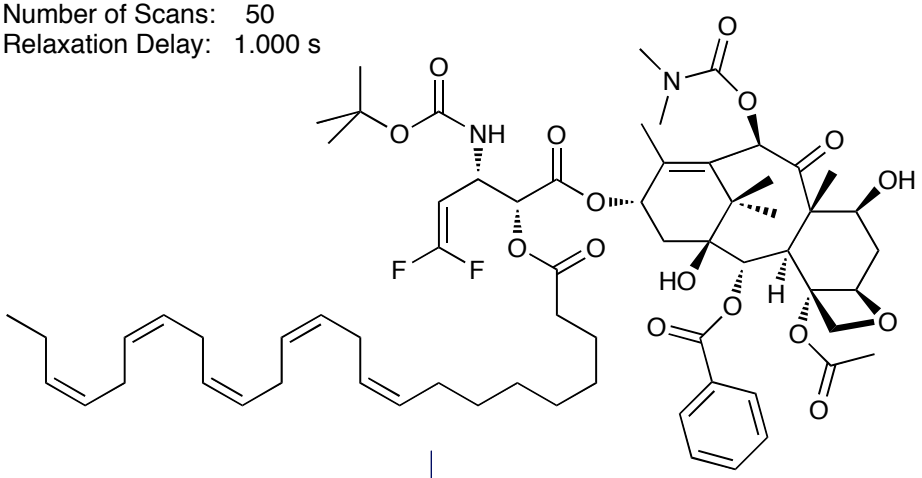

Conjugate 3-2 (LNA-SB-T-12854)

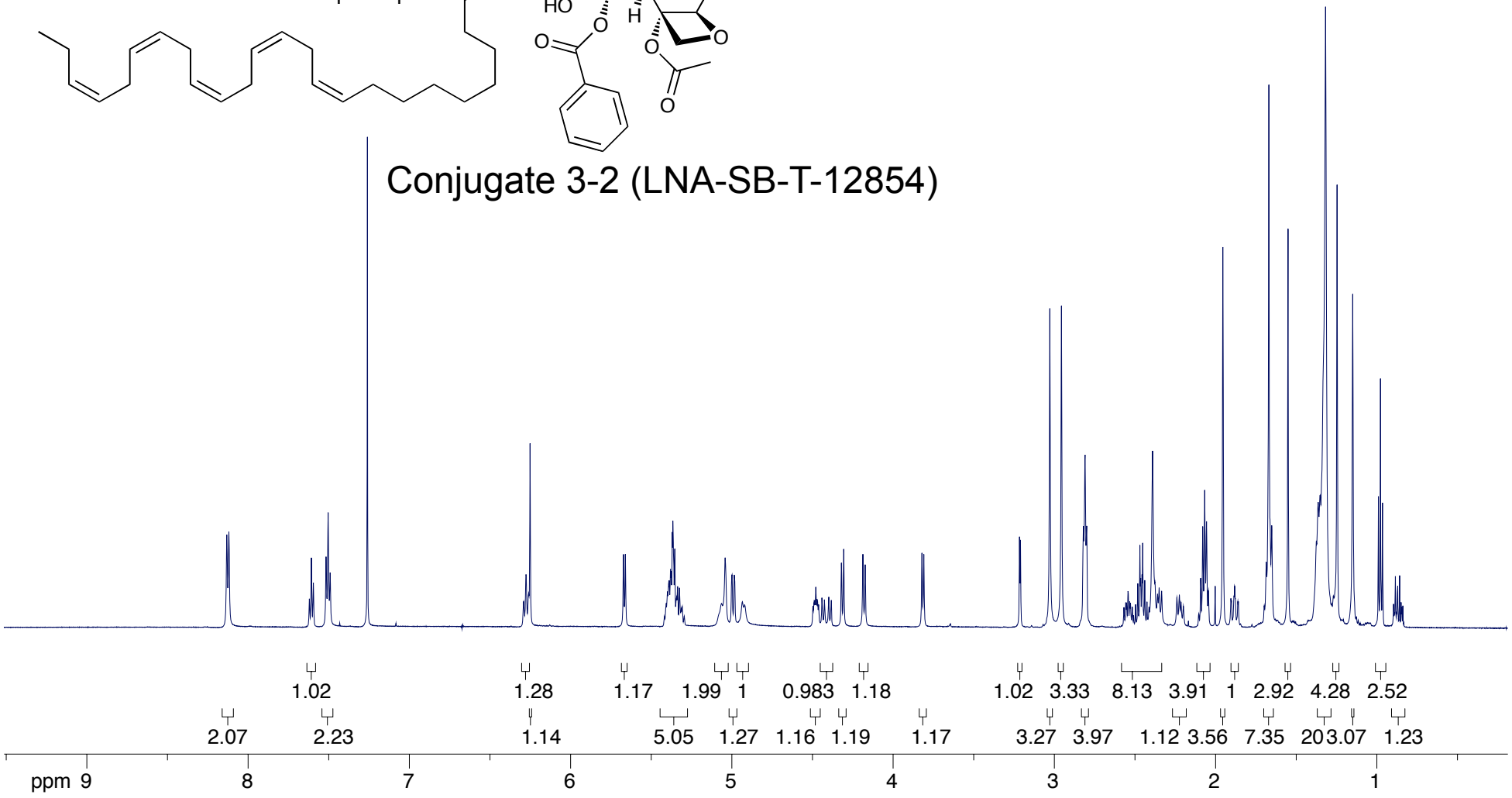

Compound Name: JGV-01-156-^{13}C
Processed by: Jacob Vineberg
Pulse Sequence: s2pul
Spectrometer Freq.: 100.55 MHz
Solvent: $CDCl_3$
Temperature: 298.15 K
Spectral Width: 248.64 ppm
Number of Scans: 85000
Relaxation Delay: 1.000 s

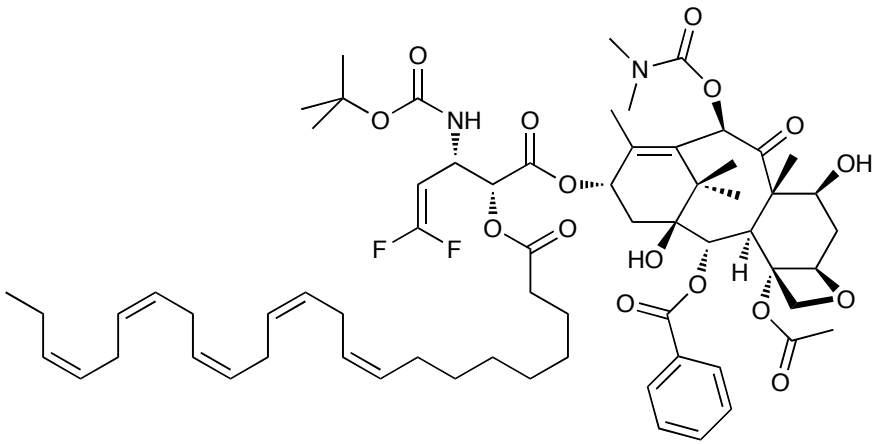

Conjugate 3-2 (LNA-SB-T-12854)

Compound Name: JGV-01-156-^{19}F
Processed by: Jacob Vineberg
Pulse Sequence: s2pul
Spectrometer Freq.: 282.32 MHz
Solvent: $CDCl_3$
Temperature: 298.15 K
Spectral Width: 212.52 ppm
Number of Scans: 1000
Relaxation Delay: 1.000 s

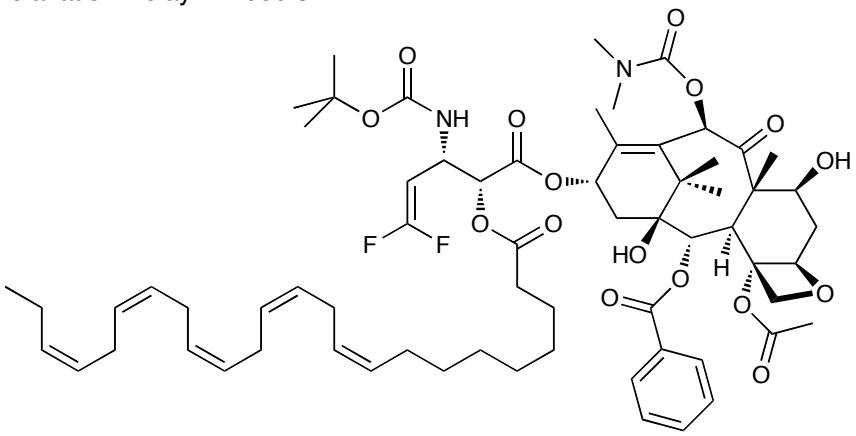

Conjugate 3-2 (LNA-SB-T-12854)

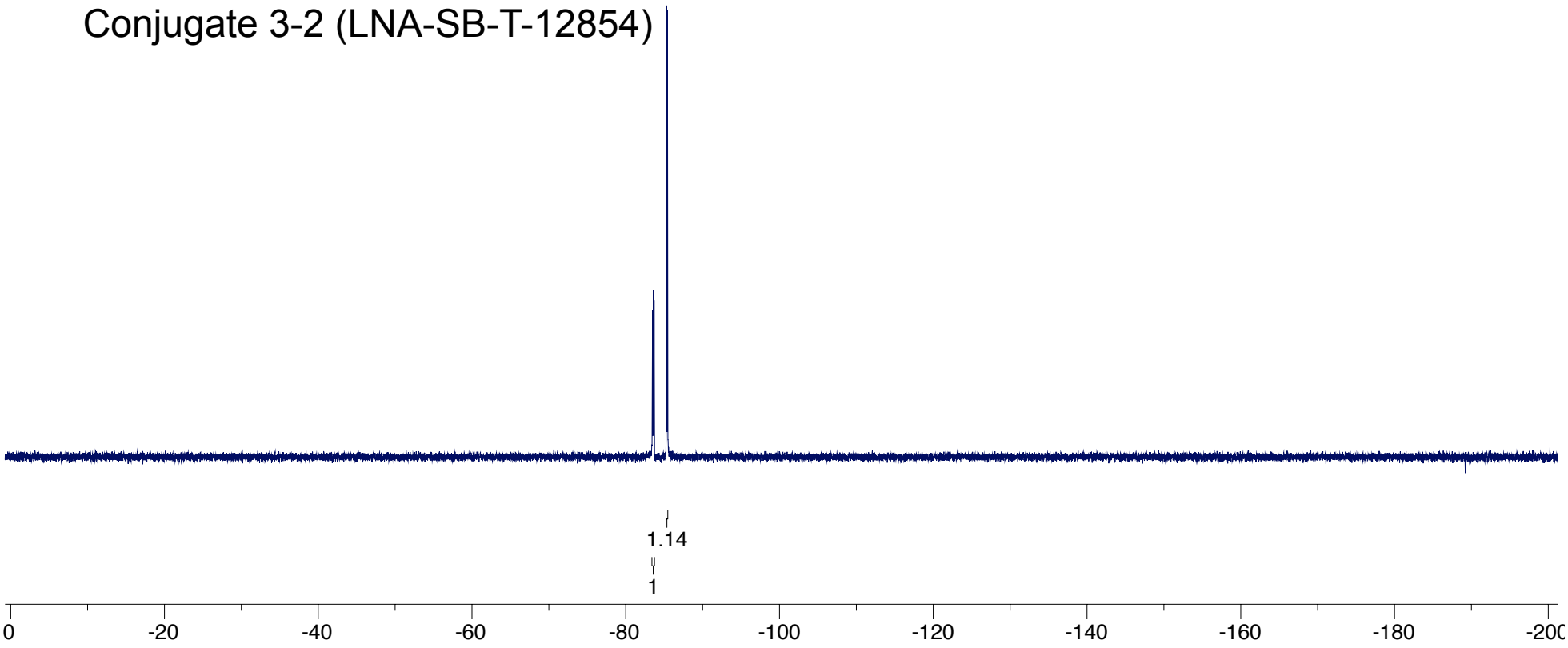

Compound Name: JGV-04-004
Processed by: Jacob Vineberg
Pulse Sequence: zg30
Spectrometer Freq.: 300.18 MHz
Solvent: $CDCl_3$
Temperature: 293.93 K
Spectral Width: 20.33 ppm
Number of Scans: 17
Relaxation Delay: 1.000 s

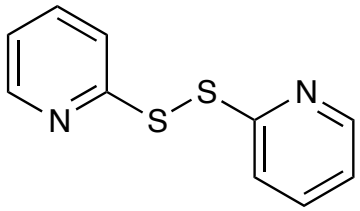

Compound 3-3

Compound Name: JGV-01-145
Processed by: Jacob Vineberg
Pulse Sequence: s2pul
Spectrometer Freq.: 599.72 MHz
Solvent: $CDCl_3$
Temperature: 298.15 K
Spectral Width: 13.34 ppm
Number of Scans: 35
Relaxation Delay: 1.000 s

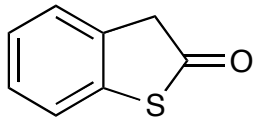

Compound 3-4

Compound Name: JGV-01-147b
Processed by: Jacob Vineberg
Pulse Sequence: s2pul
Spectrometer Freq.: 599.72 MHz
Solvent: $CDCl_3$
Temperature: 298.15 K
Spectral Width: 13.34 ppm
Number of Scans: 25
Relaxation Delay: 1.000 s

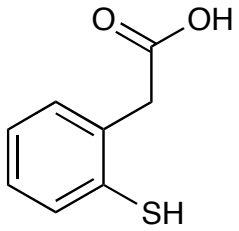

Compound 3-5

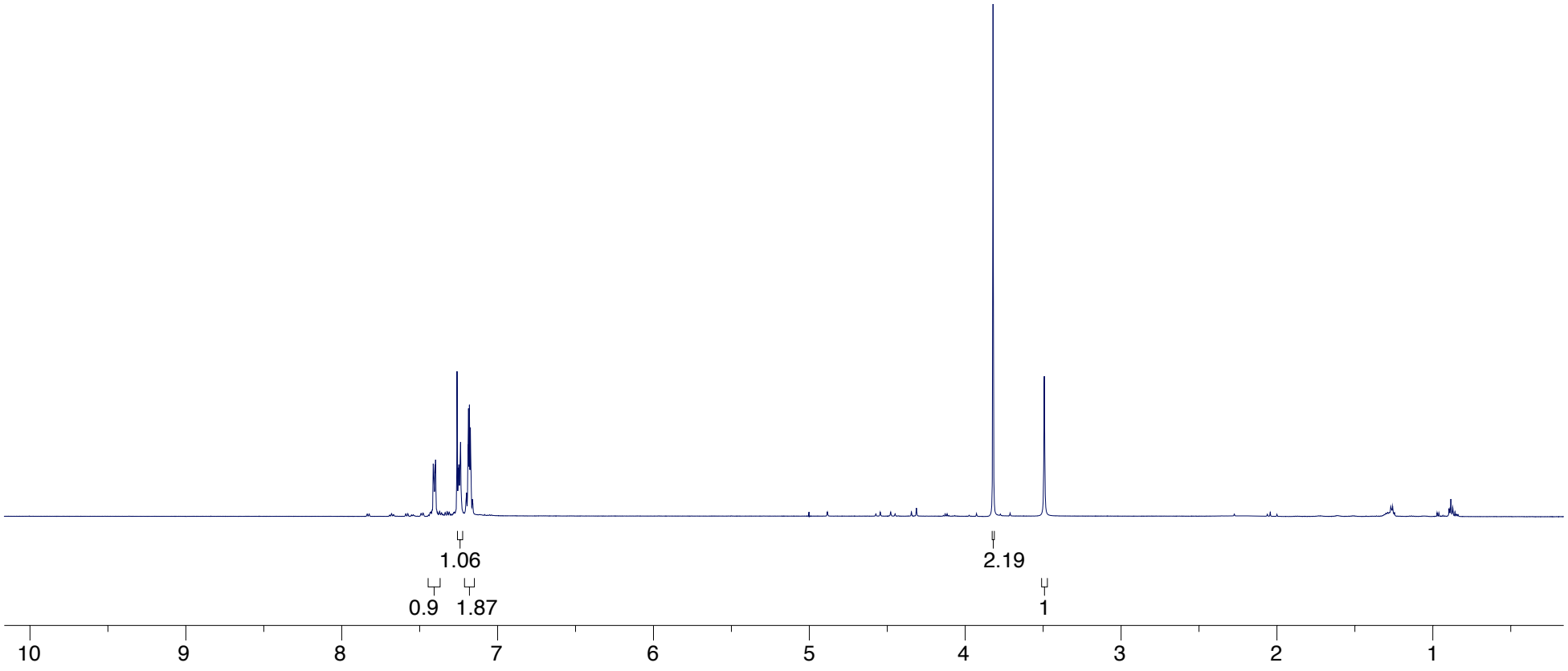

Compound Name: JGV-04-009
Processed by: Jacob Vineberg
Pulse Sequence: zg30
Spectrometer Freq.: 499.89 MHz
Solvent: $CDCl_3$
Temperature: 298.14 K
Spectral Width: 20.00 ppm
Number of Scans: 16
Relaxation Delay: 1.000 s

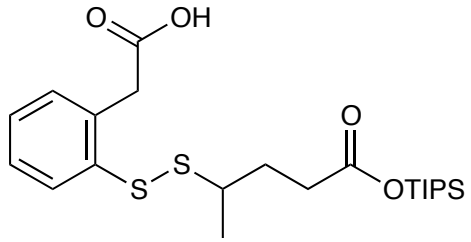

Compound 3-10

Compound Name: JGV-04-009-^{13}C
Processed by: Jacob Vineberg
Pulse Sequence: zgpg30
Spectrometer Freq.: 125.71 MHz
Solvent: $CDCl_3$
Temperature: 298.15 K
Spectral Width: 236.75 ppm
Number of Scans: 1489
Relaxation Delay: 2.000 s

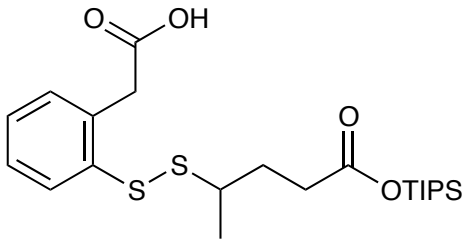

Compound 3-10

Compound Name: JGV-03-038
Processed by: Jacob Vineberg
Pulse Sequence: zg30
Spectrometer Freq.: 399.83 MHz
Solvent: $CDCl_3$
Temperature: 298.15 K
Spectral Width: 20.57 ppm
Number of Scans: 41
Relaxation Delay: 1.000 s

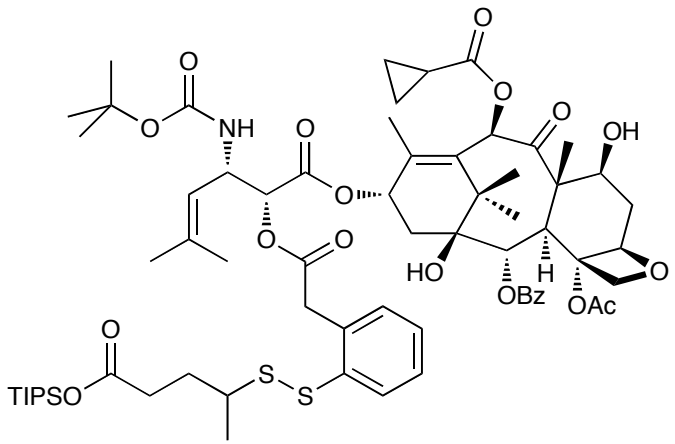

Compound 3-11

Compound Name: JGV-03-043
Processed by: Jacob Vineberg
Pulse Sequence: zg30
Spectrometer Freq.: 499.89 MHz
Solvent: $CDCl_3$
Temperature: 298.14 K
Spectral Width: 20.00 ppm
Number of Scans: 50
Relaxation Delay: 1.000 s

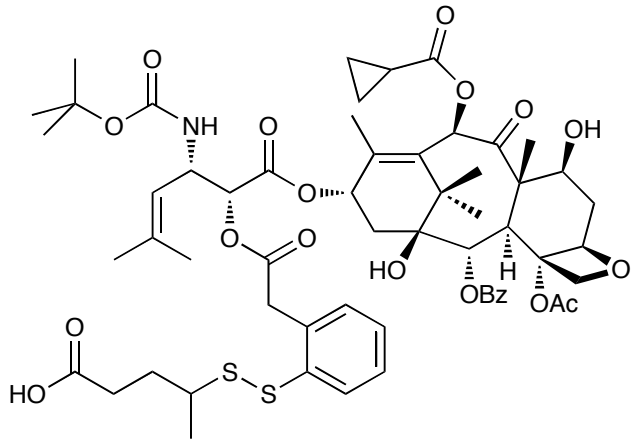

Compound 3-12

Compound Name: JGV-02-031b
Processed by: Jacob Vineberg
Pulse Sequence: s2pul
Spectrometer Freq.: 499.90 MHz
Solvent: $CDCl_3$
Temperature: 298.15 K
Spectral Width: 16.00 ppm
Number of Scans: 500
Relaxation Delay: 1.000 s

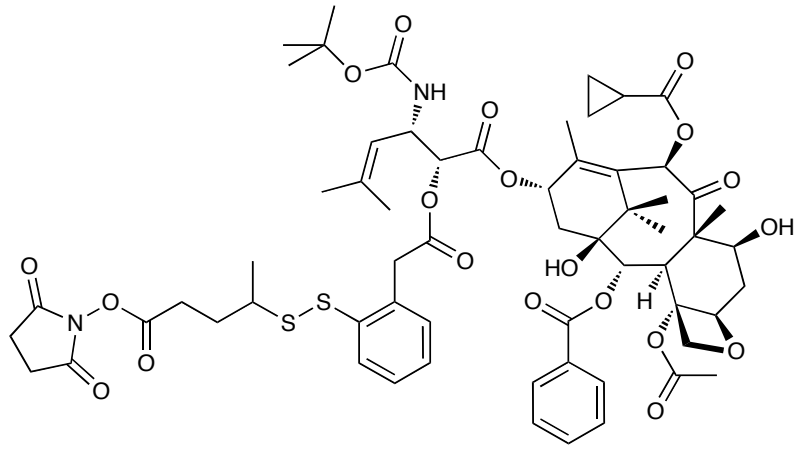

Compound 3-13

Compound Name: JGV-02-044-^{13}C
Processed by: Jacob Vineberg
Pulse Sequence: zgpg30
Spectrometer Freq.: 125.71 MHz
Solvent: $CDCl_3$
Temperature: 298.20 K
Spectral Width: 236.75 ppm
Number of Scans: 2173
Relaxation Delay: 2.000 s

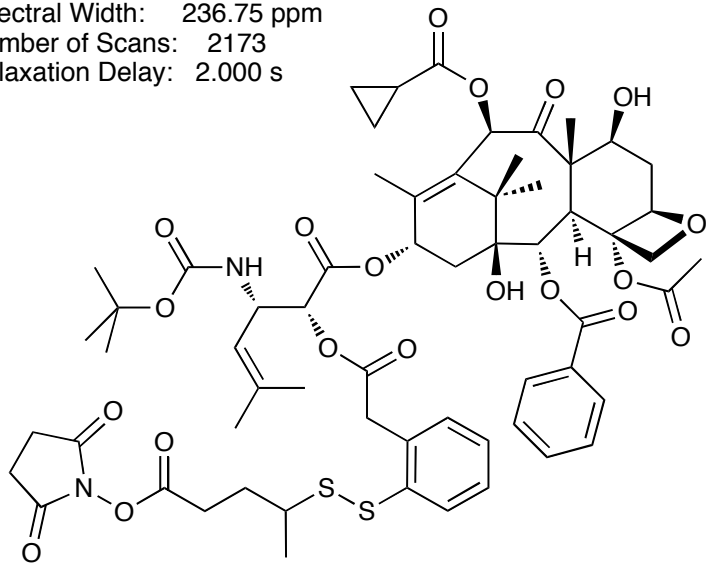

Compound 3-13

Compound Name: JGV-04-015
Processed by: Jacob Vineberg
Pulse Sequence: zg30
Spectrometer Freq.: 300.18 MHz
Solvent: $CDCl_3$
Temperature: 294.05 K
Spectral Width: 20.33 ppm
Number of Scans: 38
Relaxation Delay: 1.000 s

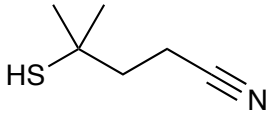

Compound 3-14

Compound Name: JGV-04-016
Processed by: Jacob Vineberg
Pulse Sequence: zg30
Spectrometer Freq.: 300.18 MHz
Solvent: $CDCl_3$
Temperature: 293.69 K
Spectral Width: 20.33 ppm
Number of Scans: 29
Relaxation Delay: 1.000 s

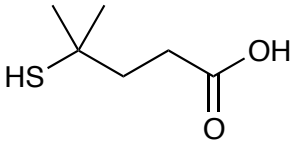

Compound 3-15

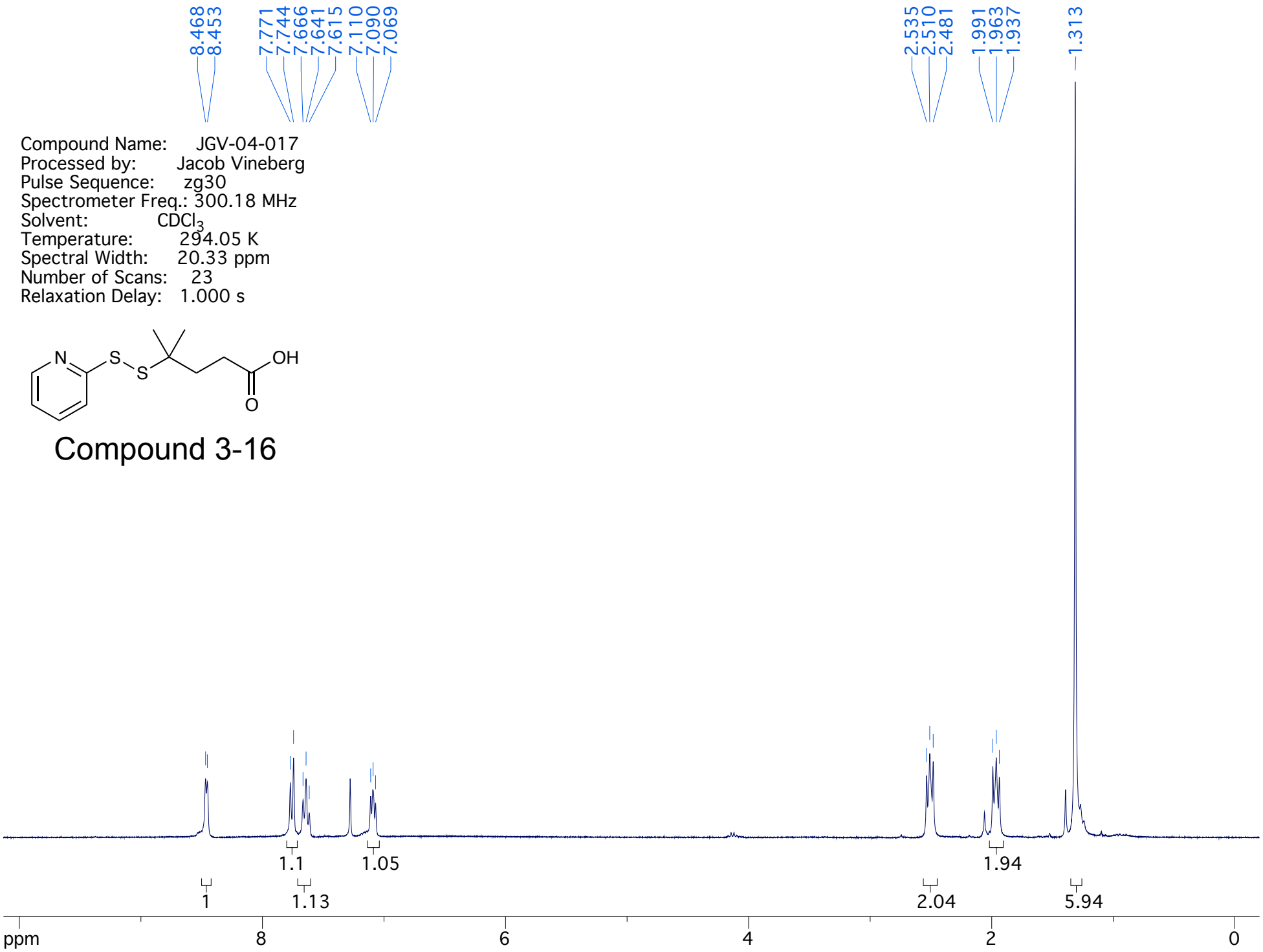
8.468
8.453
7.771
7.744
7.666
7.641
7.615
7.110
7.090
7.069
2.535
2.510
2.481
1.991
1.963
1.937
1.313
Compound Name: JGV-04-017
Processed by: Jacob Vineberg
Pulse Sequence: zg30
Spectrometer Freq.: 300.18 MHz
Solvent: $CDCl_3$
Temperature: 294.05 K
Spectral Width: 20.33 ppm
Number of Scans: 23
Relaxation Delay: 1.000 s
N
S
S
OH
O
Compound 3-16
1.1
1.05
1.94
1
1.13
2.04
5.94
ppm
8
6
4
2
0

Compound Name: JGV-04-017-^{13}C
Processed by: Jacob Vineberg
Pulse Sequence: zgpg30
Spectrometer Freq.: 75.49 MHz
Solvent: $CDCl_3$
Temperature: 294.41 K
Spectral Width: 323.42 ppm
Number of Scans: 839
Relaxation Delay: 2.000 s

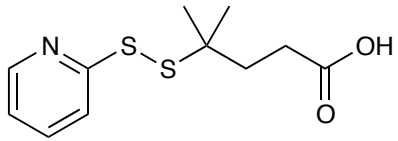

Compound 3-16

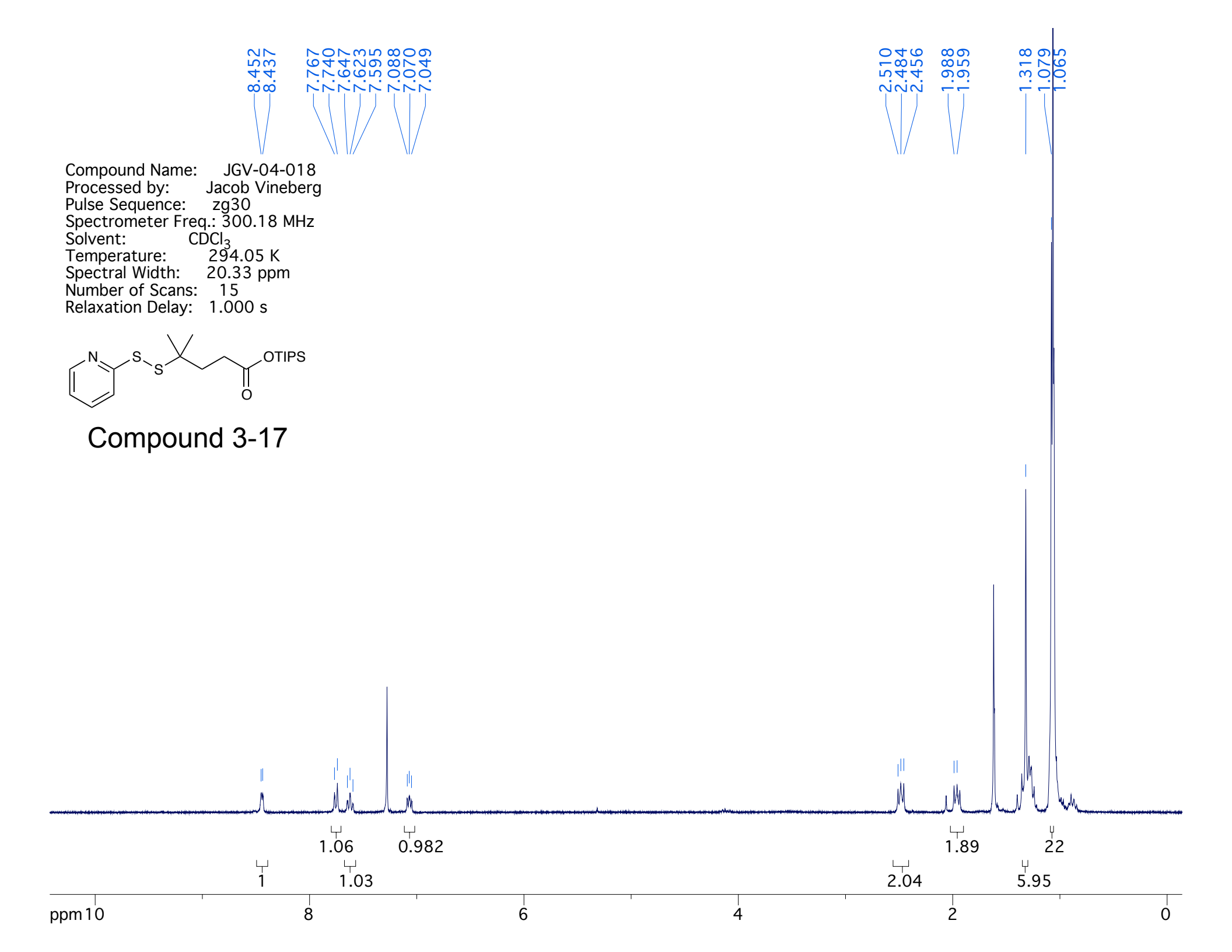
8.452
8.437
7.767
7.740
7.647
7.623
7.595
7.088
7.070
7.049
2.510
2.484
2.456
1.988
1.959
1.318
1.079
1.065
Compound Name: JGV-04-018
Processed by: Jacob Vineberg
Pulse Sequence: zg30
Spectrometer Freq.: 300.18 MHz
Solvent: CDCl3
Temperature: 294.05 K
Spectral Width: 20.33 ppm
Number of Scans: 15
Relaxation Delay: 1.000 s
N
S
S
OTIPS
O
Compound 3-17
1.06
0.982
1.89
22
1
1.03
2.04
5.95
ppm
10
8
6
4
2
0

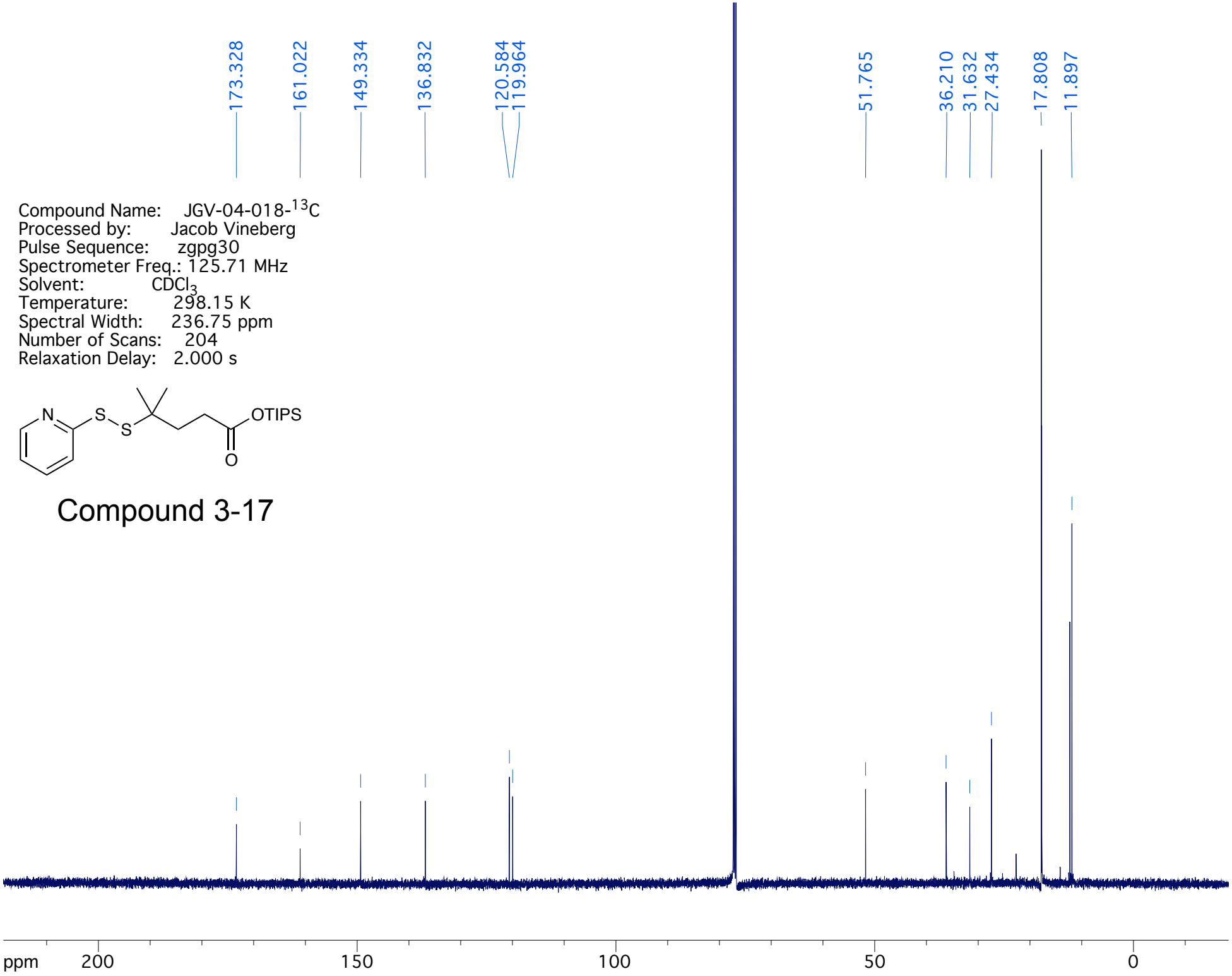
173.328
161.022
149.334
136.832
120.584
119.964
51.765
36.210
31.632
27.434
17.808
11.897
Compound Name: JGV-04-018-13C
Processed by: Jacob Vineberg
Pulse Sequence: zgpg30
Spectrometer Freq.: 125.71 MHz
Solvent: CDCl3
Temperature: 298.15 K
Spectral Width: 236.75 ppm
Number of Scans: 204
Relaxation Delay: 2.000 s
N
S
S
OTIPS
O
Compound 3-17
ppm
200
150
100
50
0

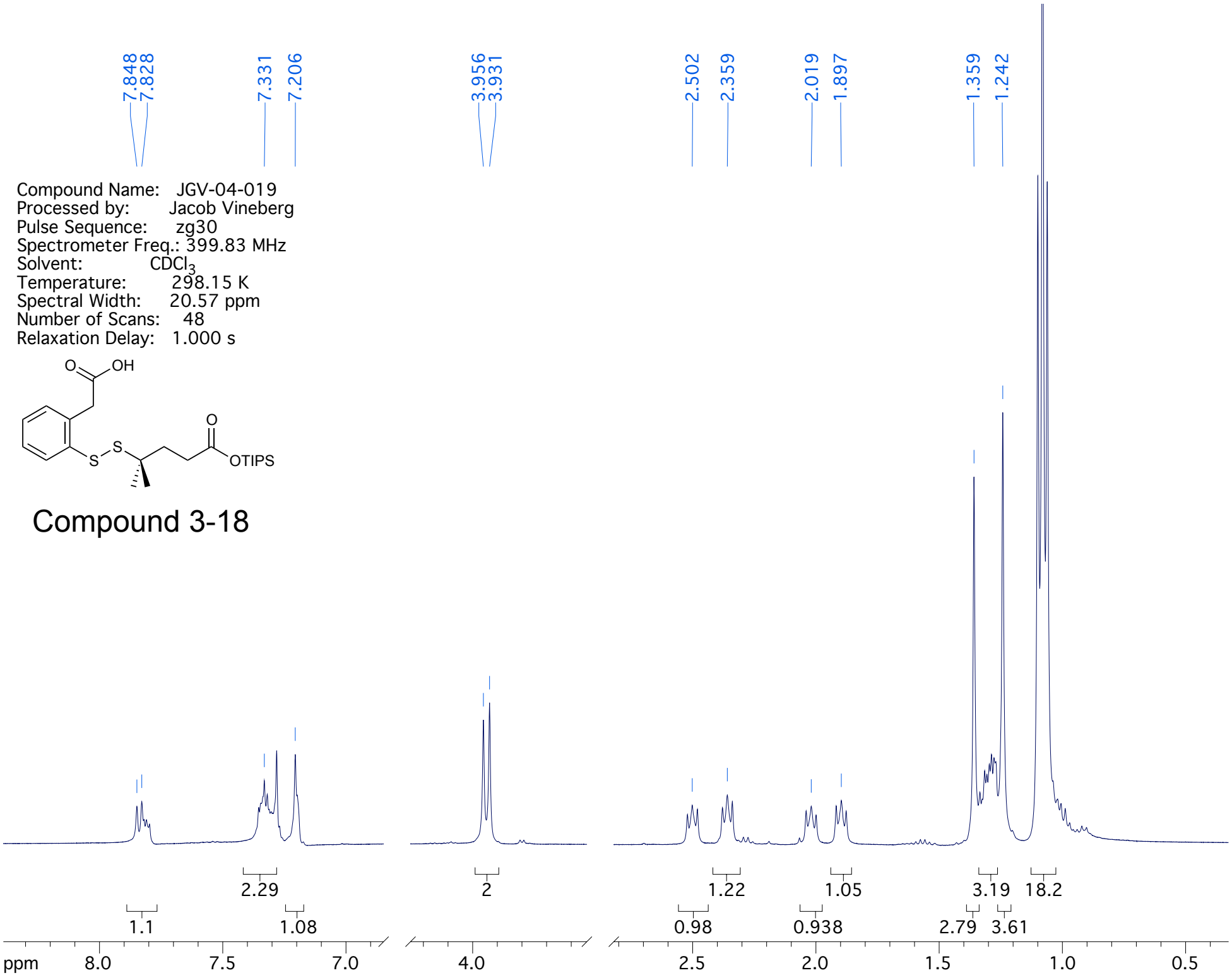
7.848
7.828
7.331
7.206
3.956
3.931
2.502
2.359
2.019
1.897
1.359
1.242
Compound Name: JGV-04-019
Processed by: Jacob Vineberg
Pulse Sequence: zg30
Spectrometer Freq.: 399.83 MHz
Solvent: CDCl3
Temperature: 298.15 K
Spectral Width: 20.57 ppm
Number of Scans: 48
Relaxation Delay: 1.000 s
O
OH
O
S
S
OTIPS
Compound 3-18
2.29
1.1
1.08
2
1.22
0.98
1.05
0.938
3.19
2.79
3.61
18.2
ppm
8.0
7.5
7.0
4.0
2.5
2.0
1.5
1.0
0.5

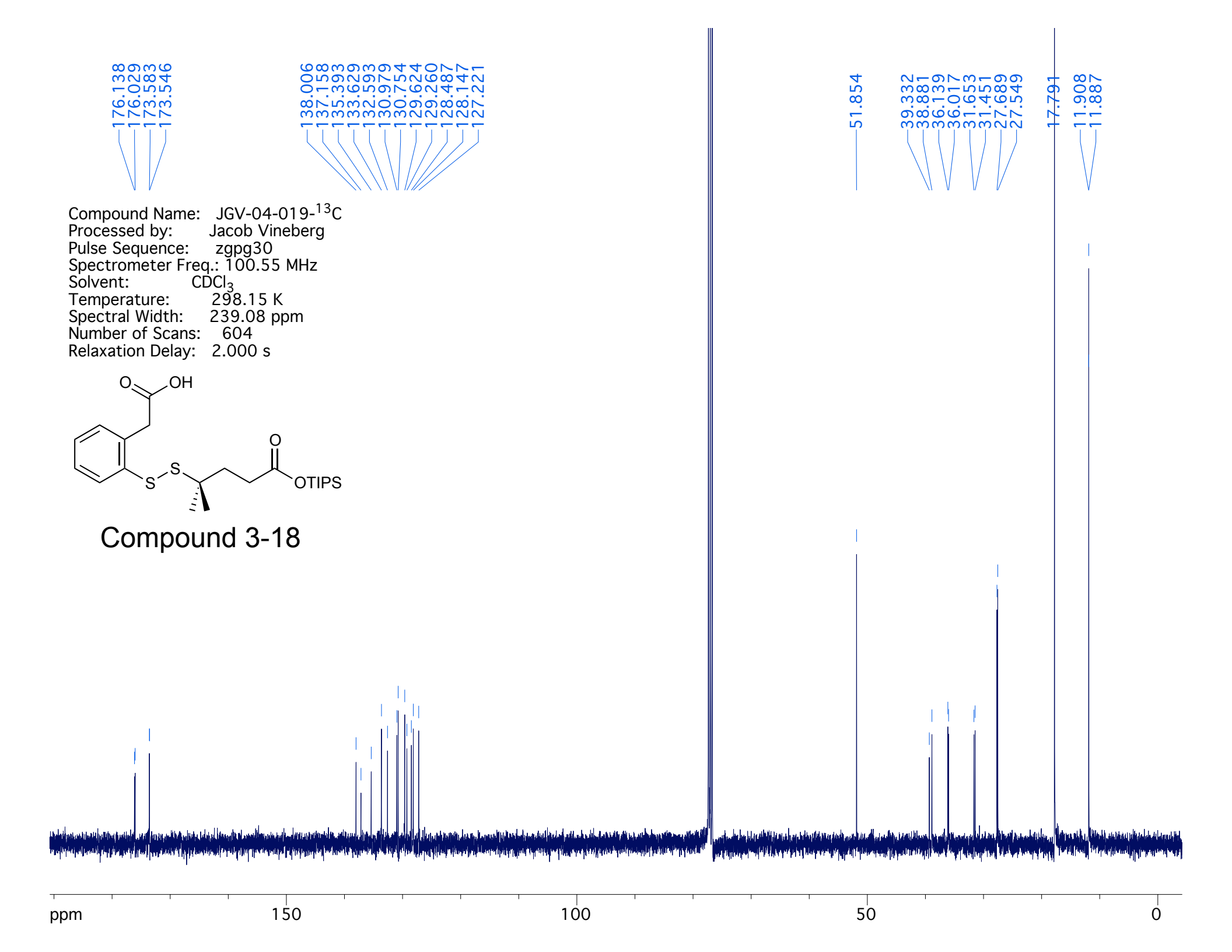
176.138
176.029
173.583
173.546
138.006
137.158
135.393
133.629
132.593
130.979
130.754
129.624
129.260
128.487
128.147
127.221
51.854
39.332
38.881
36.139
36.017
31.653
31.451
27.689
27.549
17.791
11.908
11.887
Compound Name: JGV-04-019-13C
Processed by: Jacob Vineberg
Pulse Sequence: zgpg30
Spectrometer Freq.: 100.55 MHz
Solvent: CDCl3
Temperature: 298.15 K
Spectral Width: 239.08 ppm
Number of Scans: 604
Relaxation Delay: 2.000 s
O
OH
O
S
S
OTIPS
Compound 3-18
ppm
150
100
50
0

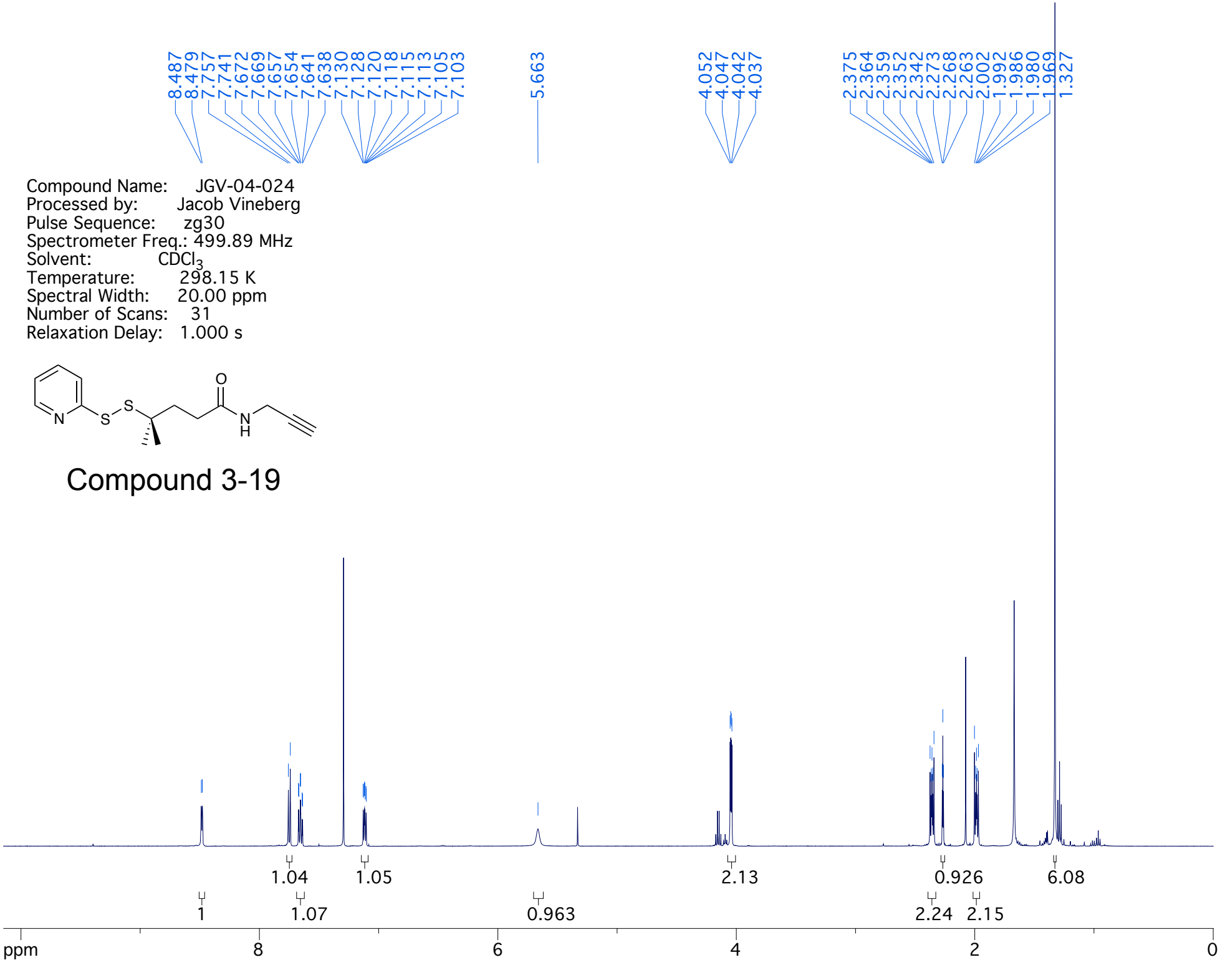
8.487
8.479
7.757
7.741
7.672
7.669
7.657
7.654
7.641
7.638
7.130
7.128
7.120
7.118
7.115
7.113
7.105
7.103
5.663
4.052
4.047
4.042
4.037
2.375
2.364
2.359
2.352
2.342
2.273
2.268
2.263
2.002
1.992
1.986
1.980
1.969
1.327
Compound Name: JGV-04-024
Processed by: Jacob Vineberg
Pulse Sequence: zg30
Spectrometer Freq.: 499.89 MHz
Solvent: CDCl3
Temperature: 298.15 K
Spectral Width: 20.00 ppm
Number of Scans: 31
Relaxation Delay: 1.000 s
O
S
S
N
S
N
H
Compound 3-19
1.04
1.05
2.13
0.926
6.08
1
1.07
0.963
2.24
2.15
ppm
8
6
4
2
0

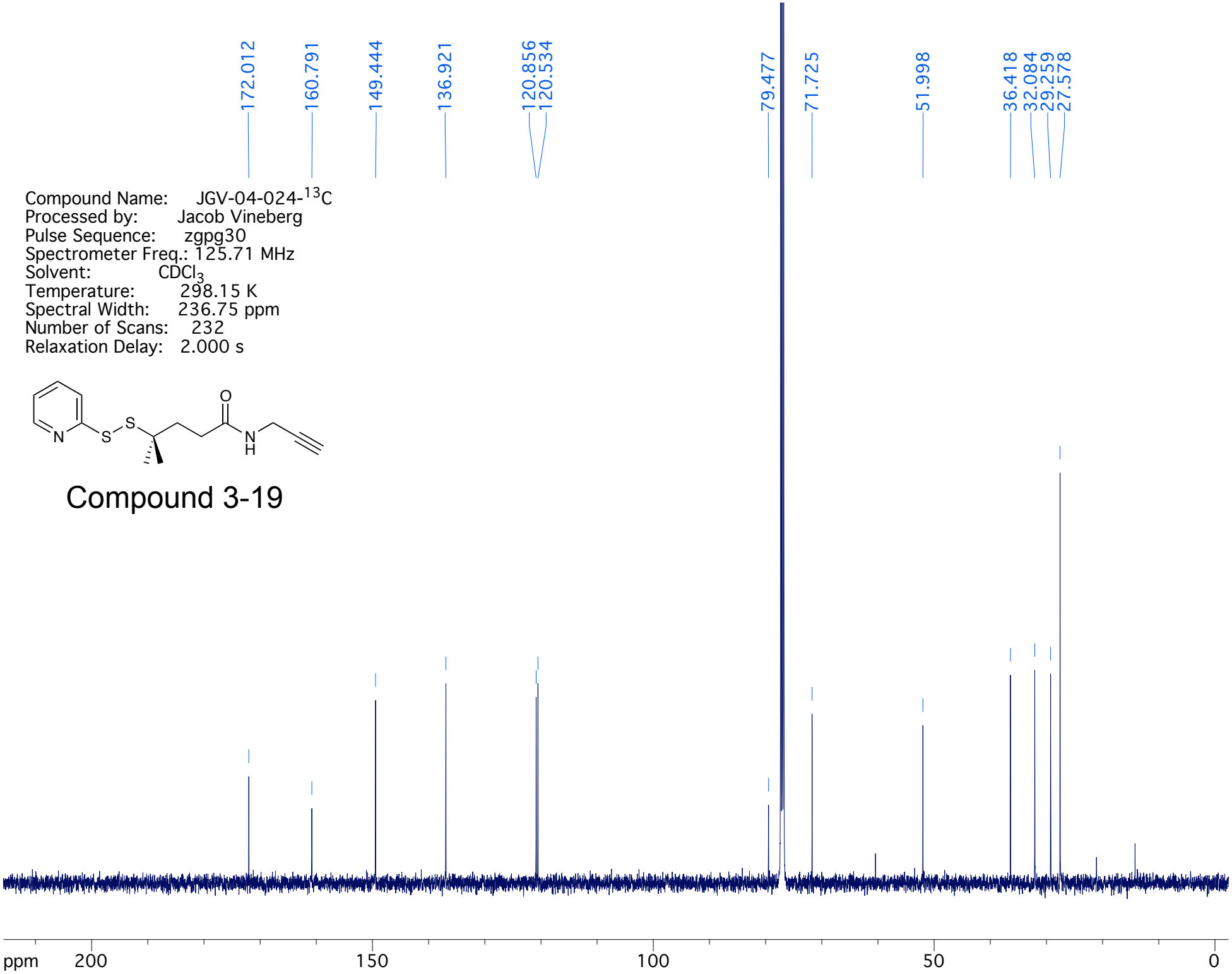
172.012
160.791
149.444
136.921
120.856
120.534
79.477
71.725
51.998
36.418
32.084
29.259
27.578
Compound Name: JGV-04-024-^{13}C
Processed by: Jacob Vineberg
Pulse Sequence: zgpg30
Spectrometer Freq.: 125.71 MHz
Solvent: $CDCl_3$
Temperature: 298.15 K
Spectral Width: 236.75 ppm
Number of Scans: 232
Relaxation Delay: 2.000 s
N
S
S
O
N
H
Compound 3-19
ppm
200
150
100
50
0

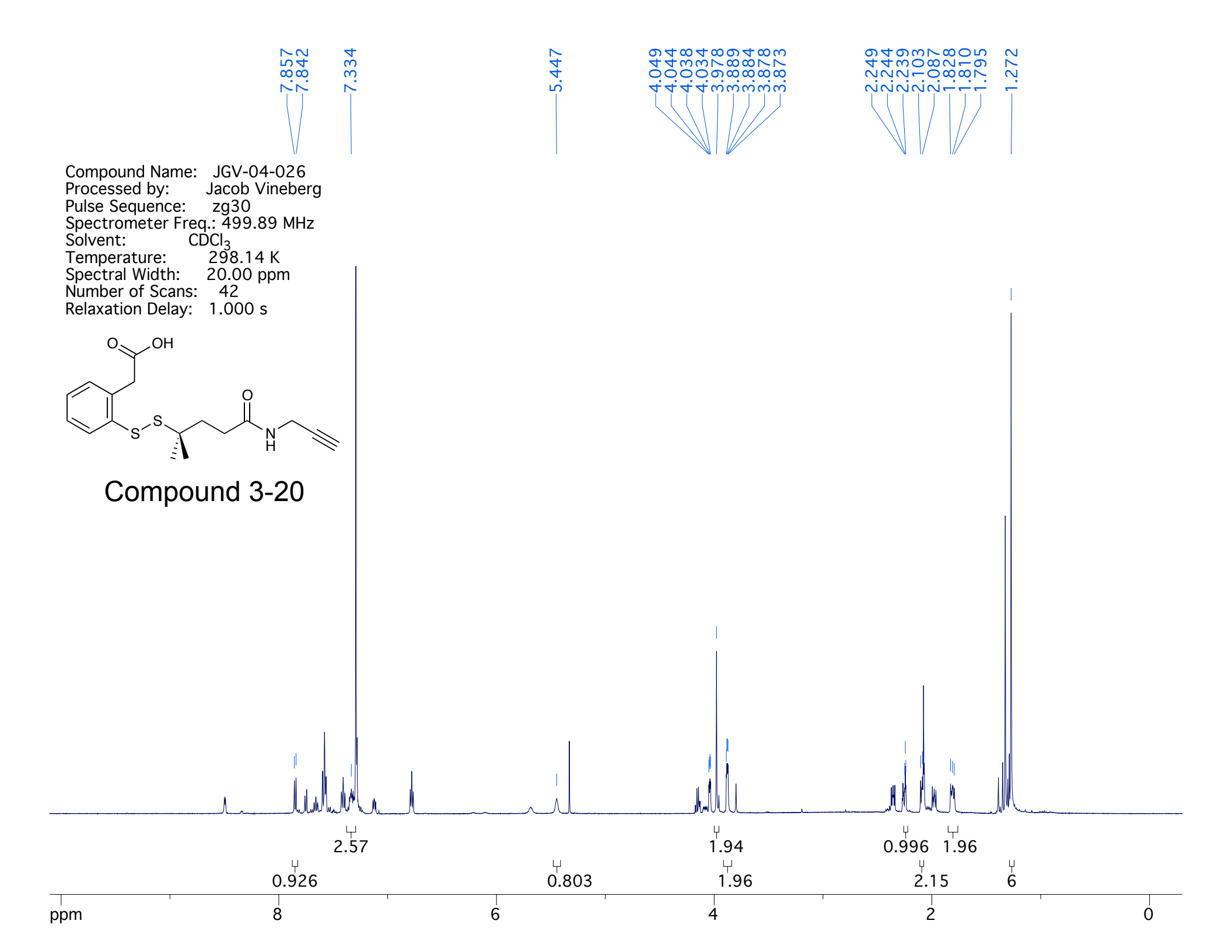
7.857
7.842
7.334
5.447
4.049
4.044
4.038
4.034
3.978
3.889
3.884
3.878
3.873
2.249
2.244
2.239
2.103
2.087
1.828
1.810
1.795
1.272
Compound Name: JGV-04-026
Processed by: Jacob Vineberg
Pulse Sequence: zg30
Spectrometer Freq.: 499.89 MHz
Solvent: CDCl3
Temperature: 298.14 K
Spectral Width: 20.00 ppm
Number of Scans: 42
Relaxation Delay: 1.000 s
O
OH
O
S
S
N
H
Compound 3-20
2.57
1.94
0.996
1.96
0.926
0.803
1.96
2.15
6
ppm
8
6
4
2
0

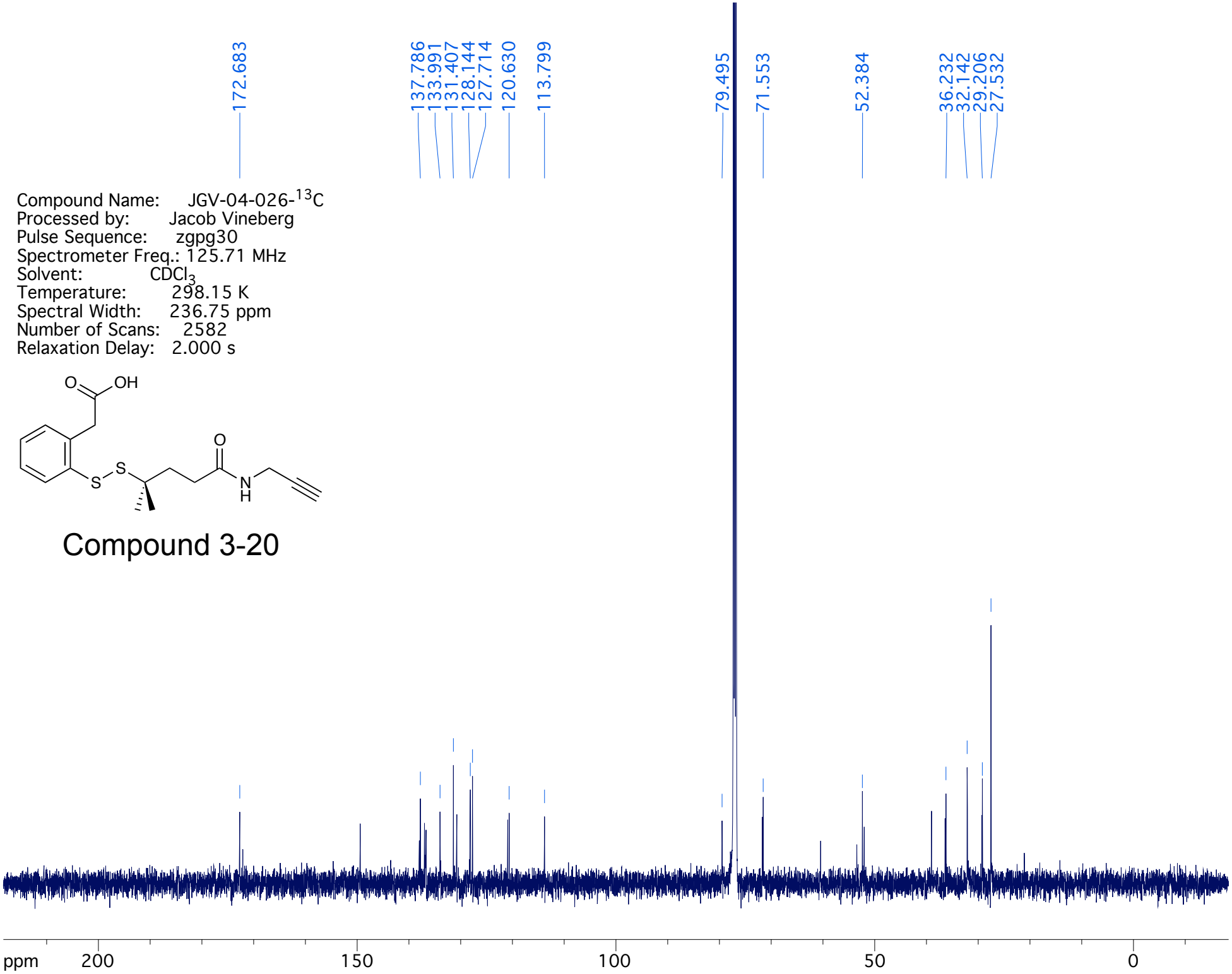
172.683
137.786
133.991
131.407
128.144
127.714
120.630
113.799
79.495
71.553
52.384
36.232
32.142
29.206
27.532
Compound Name: JGV-04-026-13C
Processed by: Jacob Vineberg
Pulse Sequence: zgpg30
Spectrometer Freq.: 125.71 MHz
Solvent: CDCl3
Temperature: 298.15 K
Spectral Width: 236.75 ppm
Number of Scans: 2582
Relaxation Delay: 2.000 s
O
OH
O
S
S
N
H
Compound 3-20
ppm
200
150
100
50
0

Compound Name: JGV-04-033
Processed by: Jacob Vineberg
Pulse Sequence: zg30
Spectrometer Freq.: 499.89 MHz
Solvent: $CDCl_3$
Temperature: 298.15 K
Spectral Width: 20.00 ppm
Number of Scans: 78
Relaxation Delay: 1.000 s

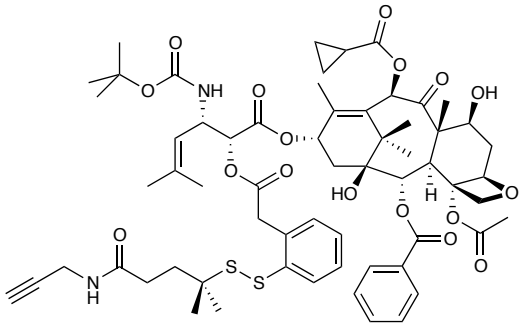

Compound 3-21

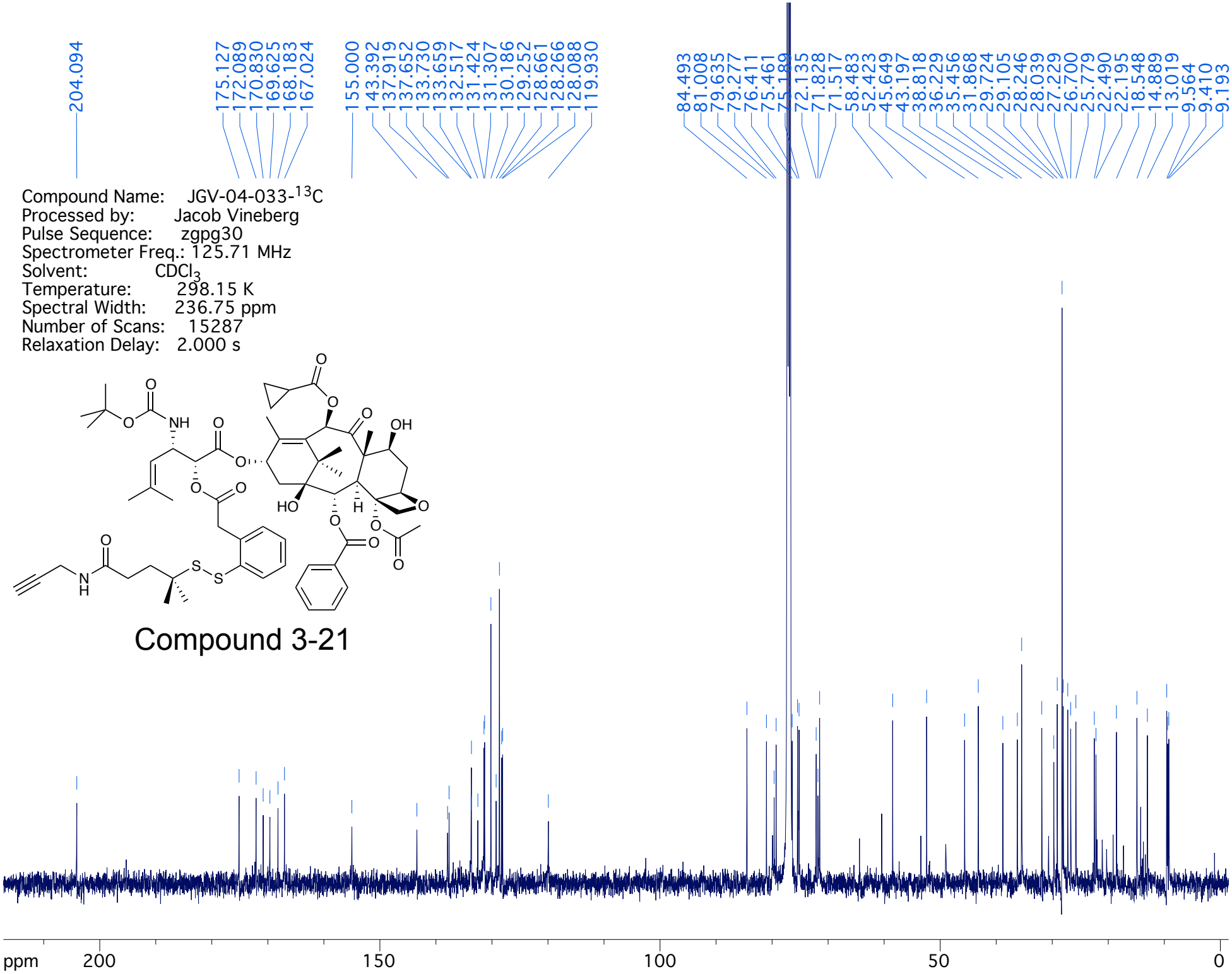
204.094
175.127
172.089
170.830
169.625
168.183
167.024
155.000
143.392
137.919
137.652
133.730
133.659
132.517
131.424
131.307
130.186
129.252
128.661
128.266
128.088
119.930
84.493
81.008
79.635
79.277
76.411
75.461
75.189
72.135
71.828
71.517
58.483
52.423
45.649
43.197
38.818
36.229
35.456
31.868
29.724
29.105
28.246
28.039
27.229
26.700
25.779
22.490
22.195
18.548
14.889
13.019
9.564
9.410
9.193
Compound Name: JGV-04-033-13C
Processed by: Jacob Vineberg
Pulse Sequence: zgpg30
Spectrometer Freq.: 125.71 MHz
Solvent: CDCl3
Temperature: 298.15 K
Spectral Width: 236.75 ppm
Number of Scans: 15287
Relaxation Delay: 2.000 s
Compound 3-21
ppm
200
150
100
50
0

Compound Name: JGV-04-010
Processed by: Jacob Vineberg
Pulse Sequence: zg30
Spectrometer Freq.: 499.89 MHz
Solvent: $CDCl_3$
Temperature: 298.14 K
Spectral Width: 20.00 ppm
Number of Scans: 54
Relaxation Delay: 1.000 s

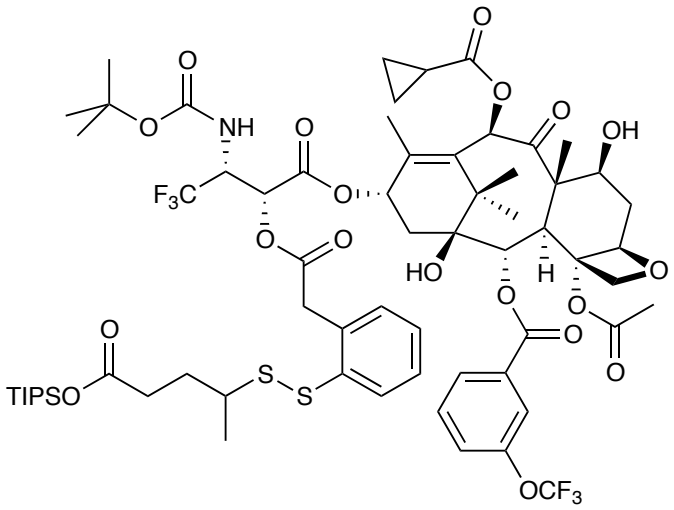

Compound 3-22

Compound Name: JGV-04-010-^{13}C
Processed by: Jacob Vineberg
Pulse Sequence: zgpg30
Spectrometer Freq.: 125.71 MHz
Solvent: $CDCl_3$
Temperature: 298.15 K
Spectral Width: 236.75 ppm
Number of Scans: 2511
Relaxation Delay: 2.000 s

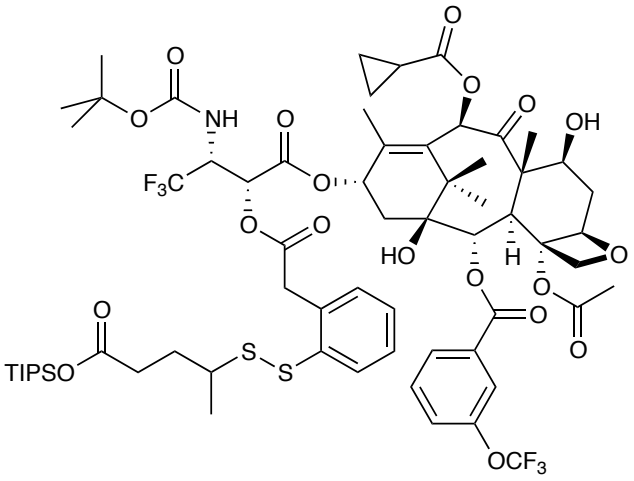

Compound 3-22

Compound Name: JGV-04-010-^{19}F
Processed by: Jacob Vineberg
Pulse Sequence: zg
Spectrometer Freq.: 470.34 MHz
Solvent: $CDCl_3$
Temperature: 298.15 K
Spectral Width: 29.97 ppm
Number of Scans: 13
Relaxation Delay: 5.000 s

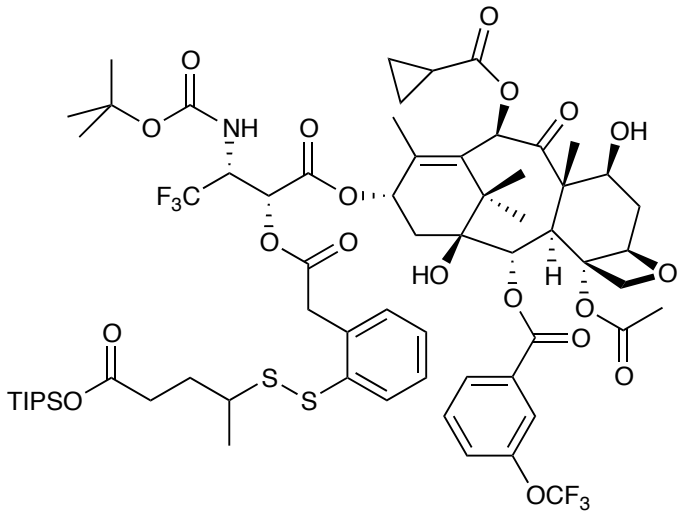

Compound 3-22

Compound Name: JGV-04-011
Processed by: Jacob Vineberg
Pulse Sequence: zg30
Spectrometer Freq.: 499.89 MHz
Solvent: $CDCl_3$
Temperature: 298.15 K
Spectral Width: 20.00 ppm
Number of Scans: 30
Relaxation Delay: 1.000 s

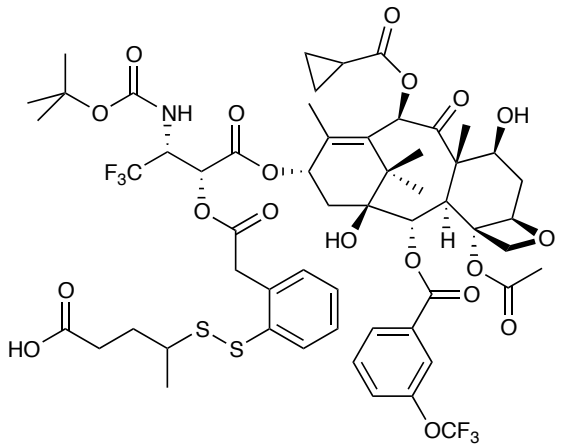

Compound 3-23

Compound Name: JGV-04-011-^{13}C
Processed by: Jacob Vineberg
Pulse Sequence: zgpg30
Spectrometer Freq.: 125.71 MHz
Solvent: $CDCl_3$
Temperature: 298.15 K
Spectral Width: 236.75 ppm
Number of Scans: 1305
Relaxation Delay: 2.000 s

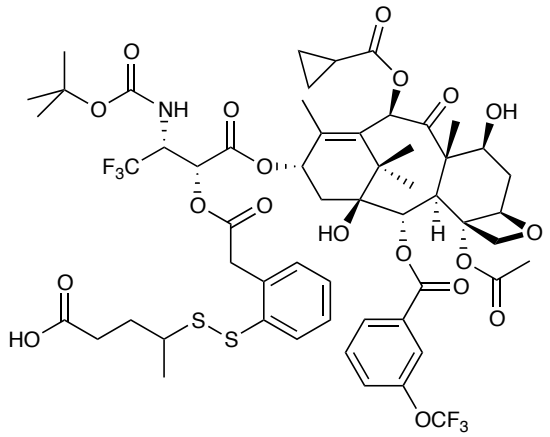

Compound 3-23

Compound Name: JGV-04-011-^{19}F
Processed by: Jacob Vineberg
Pulse Sequence: zg
Spectrometer Freq.: 470.34 MHz
Solvent: $CDCl_3$
Temperature: 298.15 K
Spectral Width: 29.97 ppm
Number of Scans: 33
Relaxation Delay: 5.000 s

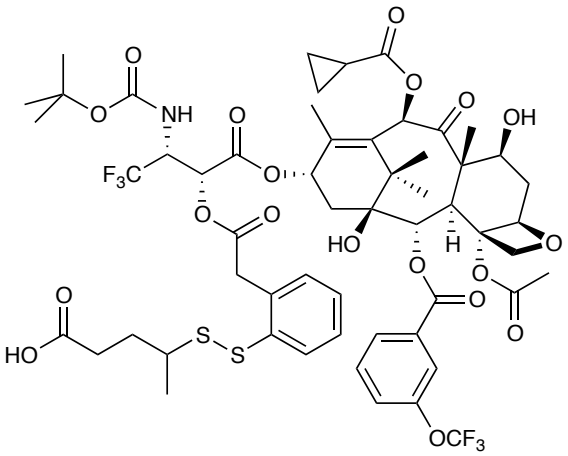

Compound 3-23

Compound Name: JGV-04-013
Processed by: Jacob Vineberg
Pulse Sequence: zg30
Spectrometer Freq.: 499.89 MHz
Solvent: $CDCl_3$
Temperature: 298.14 K
Spectral Width: 20.00 ppm
Number of Scans: 42
Relaxation Delay: 1.000 s

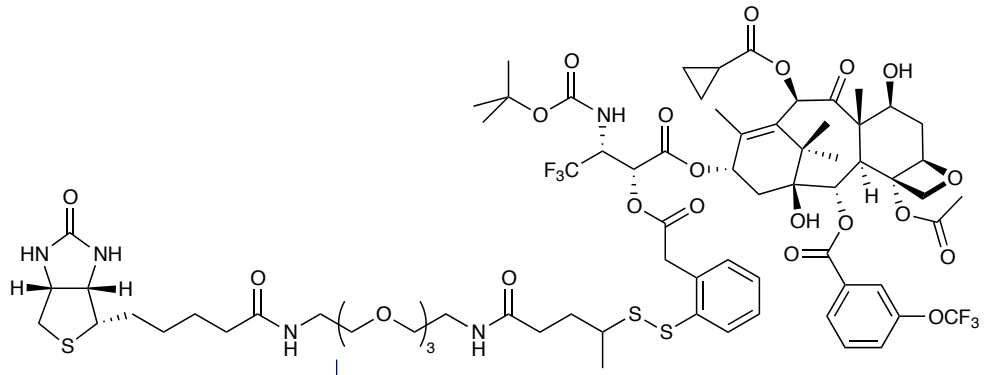

Conjugate 3-24 (BLT-S-F6)

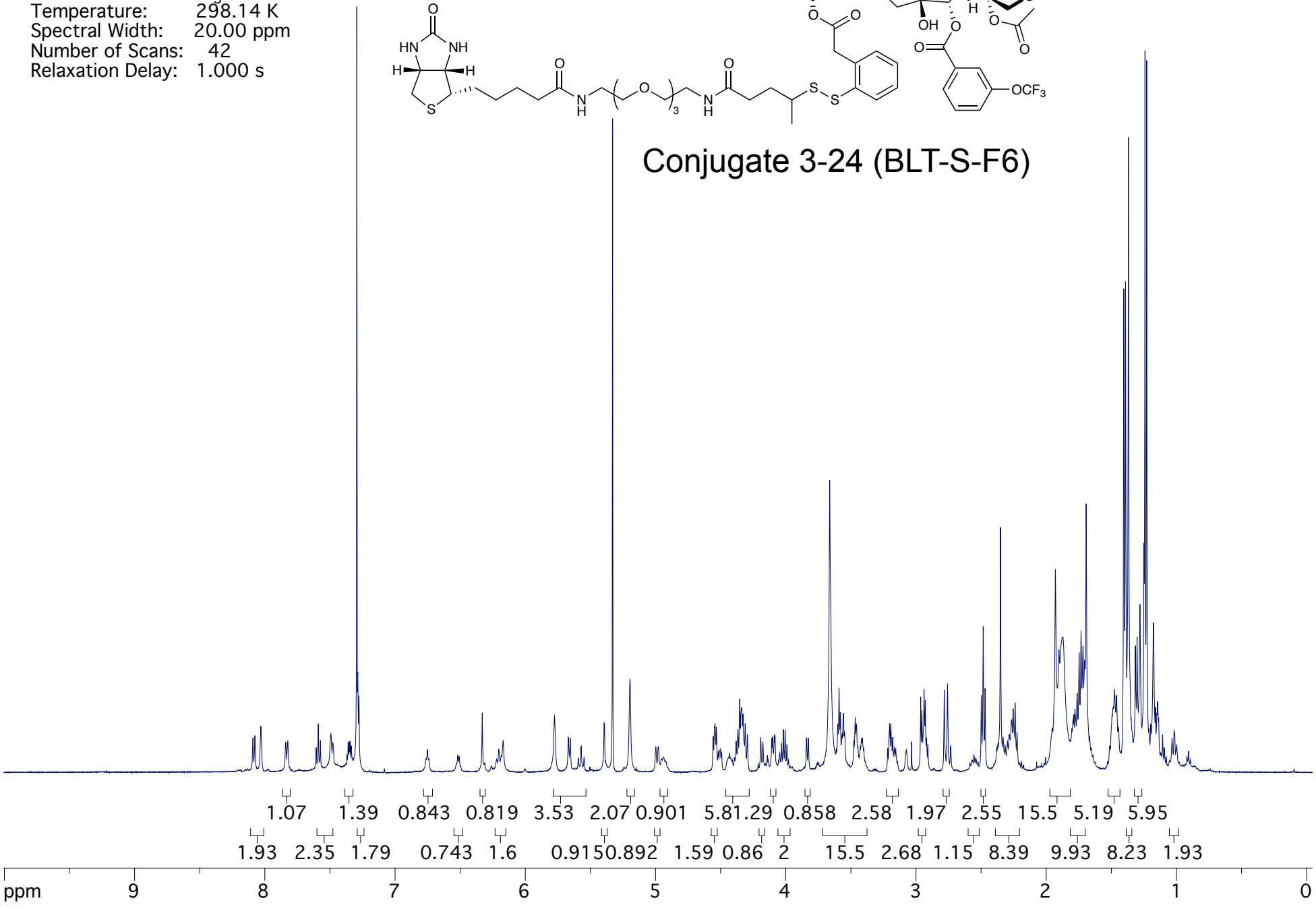

Compound Name: JGV-04-013-^{13}C
Processed by: Jacob Vineberg
Pulse Sequence: zgpg30
Spectrometer Freq.: 125.71 MHz
Solvent: $CDCl_3$
Temperature: 298.15 K
Spectral Width: 236.75 ppm
Number of Scans: 1366
Relaxation Delay: 2.000 s

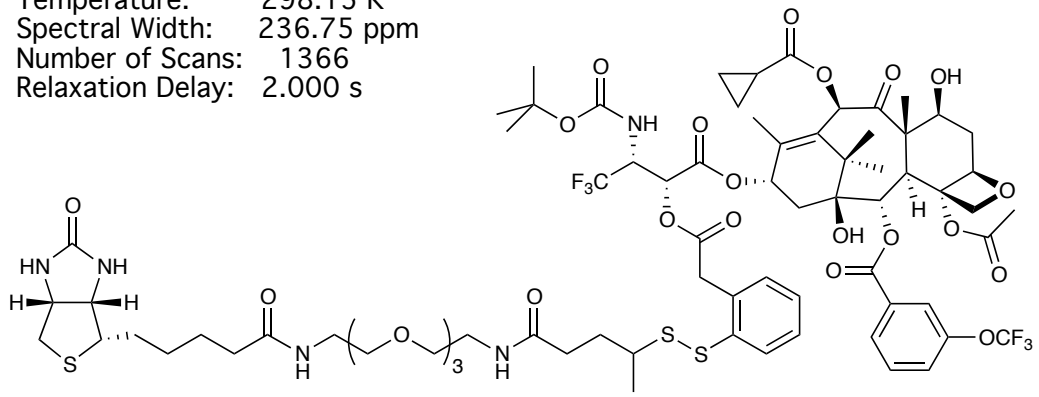

Conjugate 3-24 (BLT-S-F6)

Compound Name: JGV-04-013-^{19}F
Processed by: Jacob Vineberg
Pulse Sequence: zg
Spectrometer Freq.: 470.34 MHz
Solvent: $CDCl_3$
Temperature: 298.15 K
Spectral Width: 29.97 ppm
Number of Scans: 39
Relaxation Delay: 5.000 s

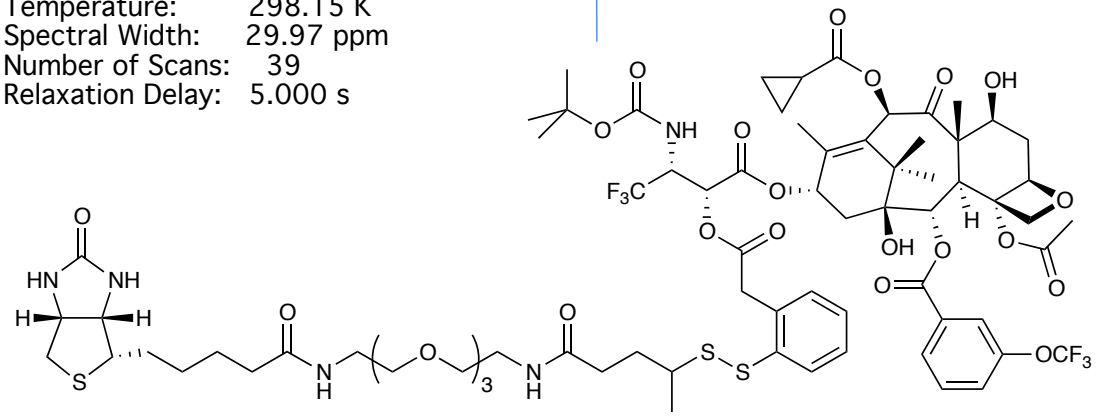

Conjugate 3-24 (BLT-S-F6)

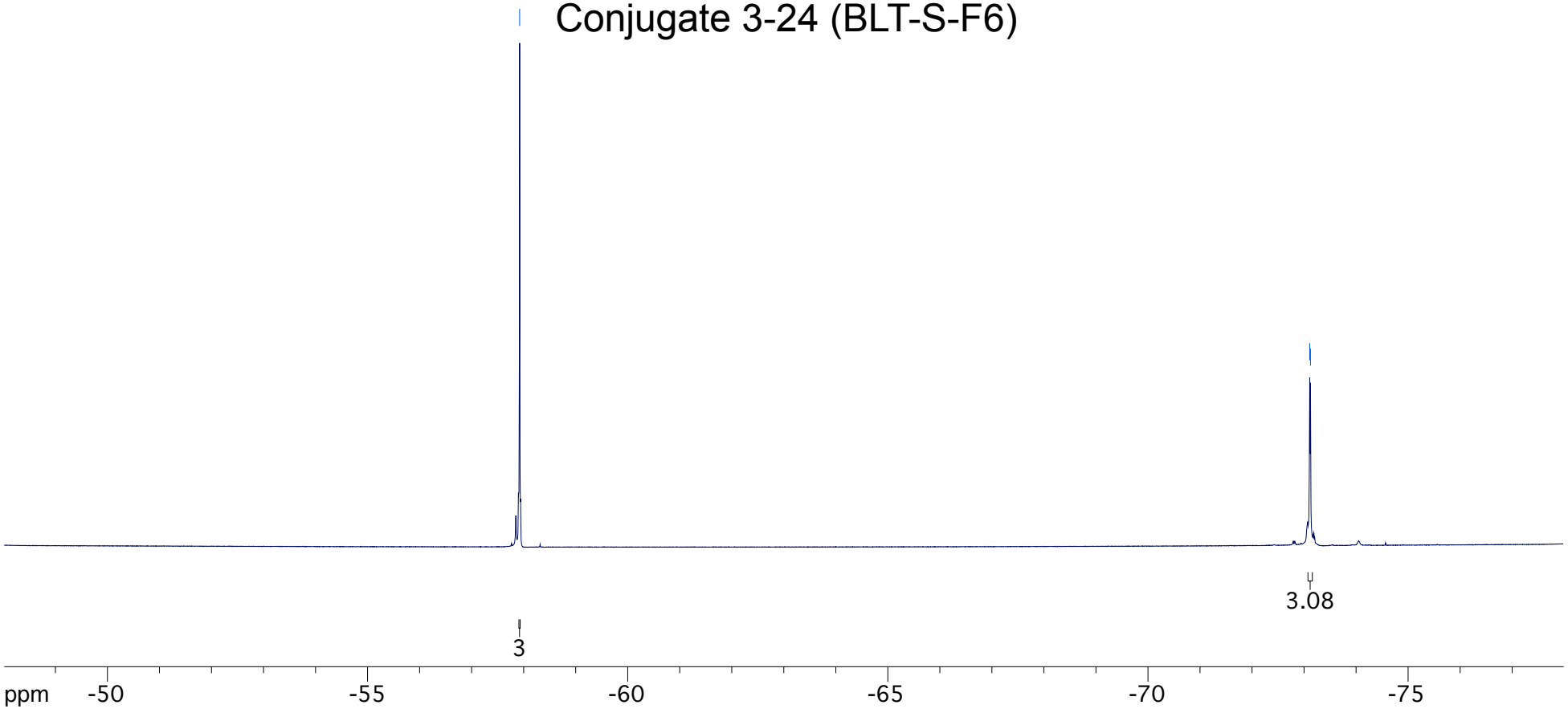

Appendix Chapter 4

Compound Name: JGV-02-036
Processed by: Jacob Vineberg
Pulse Sequence: s2pul
Spectrometer Freq.: 300.07 MHz
Solvent: $CDCl_3$
Temperature: 298.15 K
Spectral Width: 15.00 ppm
Number of Scans: 100
Relaxation Delay: 1.000 s

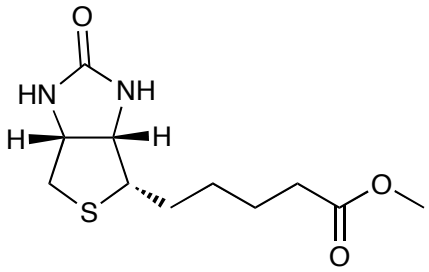

Compound 4-1

Compound Name: JGV-02-037
Processed by: Jacob Vineberg
Pulse Sequence: s2pul
Spectrometer Freq.: 300.07 MHz
Solvent: D_2O
Temperature: 298.15 K
Spectral Width: 15.00 ppm
Number of Scans: 100
Relaxation Delay: 1.000 s

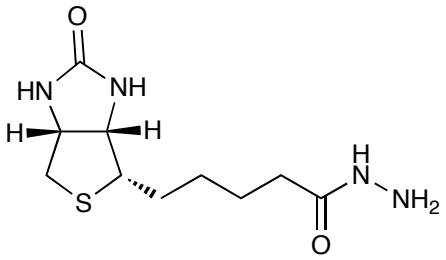

Compound 4-2

Compound Name: JGV-02-037-^{13}C
Processed by: Jacob Vineberg
Pulse Sequence: zgpg30
Spectrometer Freq.: 125.71 MHz
Solvent: DMSO
Temperature: 298.15 K
Spectral Width: 236.75 ppm
Number of Scans: 14795
Relaxation Delay: 2.000 s

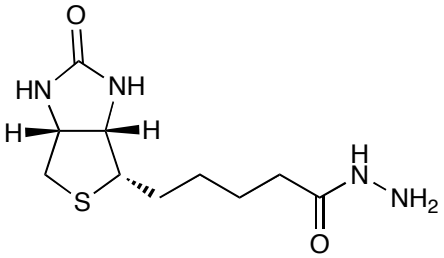

Compound 4-2

Compound Name: JGV-02-033
Processed by: Jacob Vineberg
Pulse Sequence: zg30
Spectrometer Freq.: 399.83 MHz
Solvent: MeOD
Temperature: 298.15 K
Spectral Width: 20.57 ppm
Number of Scans: 57
Relaxation Delay: 1.000 s

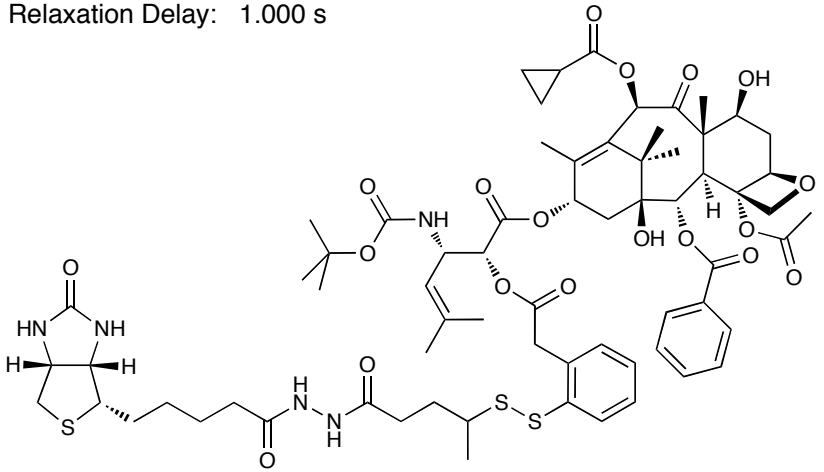

Conjugate 4-3 (BLT)

Compound Name: JGV-02-033-^{13}C
Processed by: Jacob Vineberg
Pulse Sequence: zgpg30
Spectrometer Freq.: 125.71 MHz
Solvent: MeOD
Temperature: 298.20 K
Spectral Width: 236.75 ppm
Number of Scans: 2162
Relaxation Delay: 2.000 s

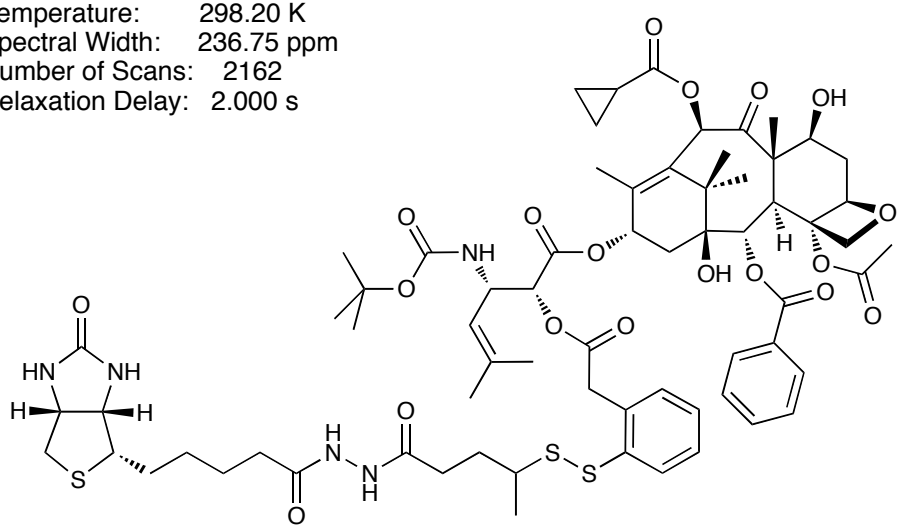

Conjugate 4-3 (BLT)

Compound Name: JGV-01-137
Processed by: Jacob Vineberg
Pulse Sequence: s2pul
Spectrometer Freq.: 599.72 MHz
Solvent: $CDCl_3$
Temperature: 298.15 K
Spectral Width: 13.34 ppm
Number of Scans: 35
Relaxation Delay: 1.000 s

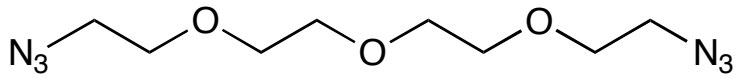

Compound 4-4

Compound Name: JGV-01-162
Processed by: Jacob Vineberg
Pulse Sequence: s2pul
Spectrometer Freq.: 599.72 MHz
Solvent: $CDCl_3$
Temperature: 298.15 K
Spectral Width: 13.34 ppm
Number of Scans: 35
Relaxation Delay: 1.000 s

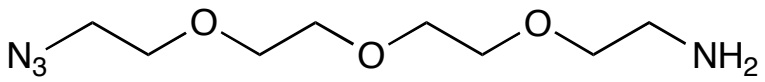

Compound 4-5

Compound Name: JGV-02-053a
Processed by: Jacob Vineberg
Pulse Sequence: s2pul
Spectrometer Freq.: 499.90 MHz
Solvent: $CDCl_3$
Temperature: 298.15 K
Spectral Width: 16.00 ppm
Number of Scans: 200
Relaxation Delay: 1.000 s

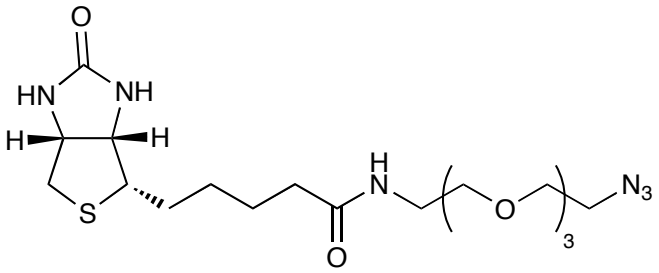

Compound 4-6

Compound Name: JGV-02-052
Processed by: Jacob Vineberg
Pulse Sequence: s2pul
Spectrometer Freq.: 300.07 MHz
Solvent: D_2O
Temperature: 298.15 K
Spectral Width: 15.00 ppm
Number of Scans: 100
Relaxation Delay: 1.000 s

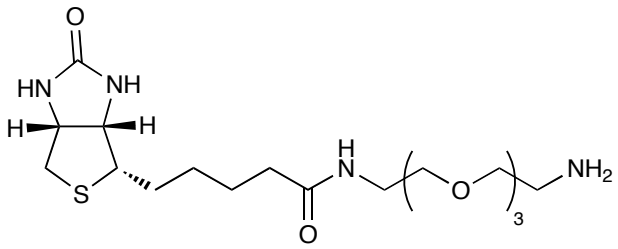

Compound 4-7

Compound Name: JGV-04-014
Processed by: Jacob Vineberg
Pulse Sequence: zg30
Spectrometer Freq.: 499.89 MHz
Solvent: MeOD
Temperature: 298.15 K
Spectral Width: 20.00 ppm
Number of Scans: 45
Relaxation Delay: 1.000 s

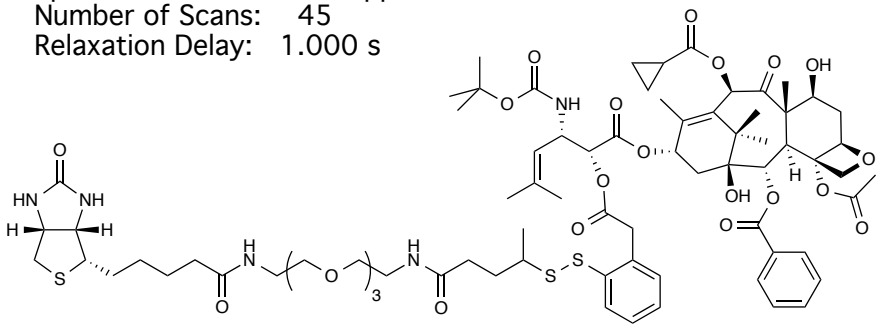

Conjugate 4-8 (BLT-S)

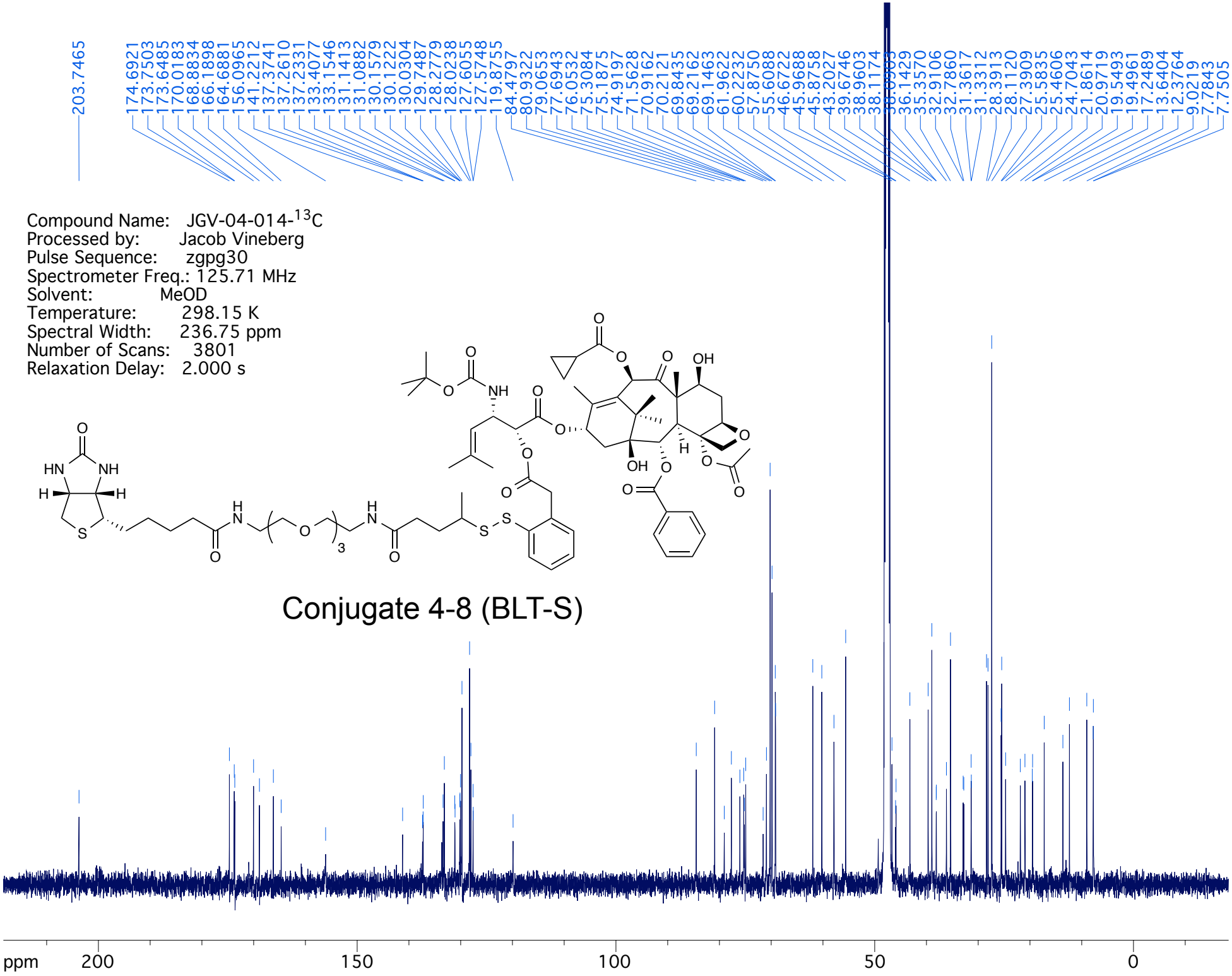
203.7465
174.6921
173.7503
173.6485
170.0183
168.8834
166.1898
164.6881
156.0965
141.2212
137.3741
137.2610
137.2331
133.4077
133.1546
131.1413
131.0882
130.1579
130.1222
130.0304
129.7487
128.2779
128.0238
127.6055
127.5748
119.8755
84.4797
80.9322
79.0653
77.6943
76.0532
75.3084
75.1875
74.9197
71.5628
70.9162
70.2121
69.8435
69.2162
69.1463
61.9622
60.2232
57.8750
55.6088
46.6722
45.9688
45.8758
43.2027
39.6746
38.9603
38.1174
36.1429
35.3570
32.9106
32.7860
31.3617
31.3312
28.3913
28.1120
27.3909
25.5835
25.4606
24.7043
21.8614
20.9719
19.5493
19.4961
17.2489
13.6404
12.3764
9.0219
7.7843
7.7505
Compound Name: JGV-04-014-13C
Processed by: Jacob Vineberg
Pulse Sequence: zgpg30
Spectrometer Freq.: 125.71 MHz
Solvent: MeOD
Temperature: 298.15 K
Spectral Width: 236.75 ppm
Number of Scans: 3801
Relaxation Delay: 2.000 s
Conjugate 4-8 (BLT-S)
ppm
200
150
100
50
0

Compound Name: JGV-03-046
Processed by: Jacob Vineberg
Pulse Sequence: zg30
Spectrometer Freq.: 499.89 MHz
Solvent: MeOD
Temperature: 298.15 K
Spectral Width: 20.00 ppm
Number of Scans: 34
Relaxation Delay: 1.000 s

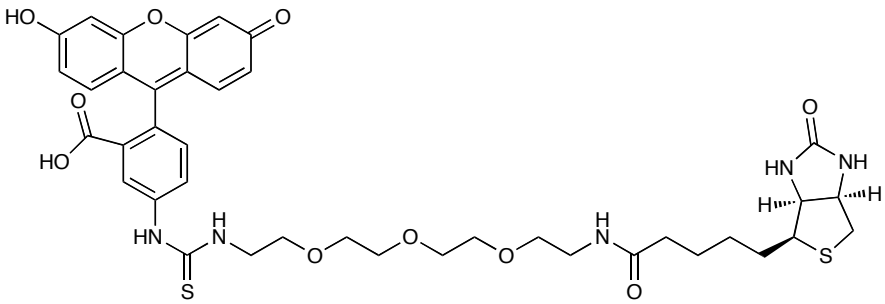

Compound 4-10
(Biotin-PEG-FITC)

Compound Name: JGV-03-046-^{13}C
Processed by: Jacob Vineberg
Pulse Sequence: zgpg30
Spectrometer Freq.: 125.71 MHz
Solvent: MeOD
Temperature: 298.15 K
Spectral Width: 236.75 ppm
Number of Scans: 23066
Relaxation Delay: 2.000 s

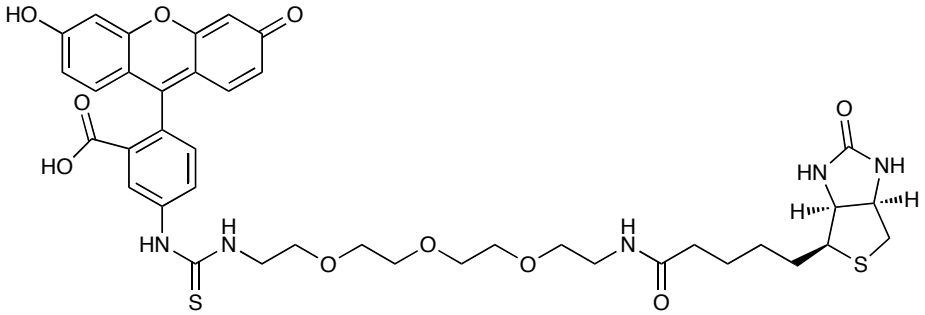

Compound 4-10
(Biotin-PEG-FITC)

Compound Name: JGV-02-065
Processed by: Jacob Vineberg
Pulse Sequence: s2pul
Spectrometer Freq.: 300.08 MHz
Solvent: DMSO
Temperature: 298.15 K
Spectral Width: 15.00 ppm
Number of Scans: 100
Relaxation Delay: 1.000 s

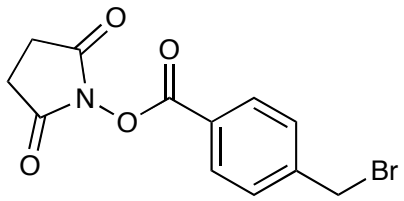

Compound 4-11

Compound Name: JGV-04-059
Processed by: Jacob Vineberg
Pulse Sequence: zg30
Spectrometer Freq.: 499.89 MHz
Solvent: MeOD
Temperature: 308.13 K
Spectral Width: 20.00 ppm
Number of Scans: 19
Relaxation Delay: 1.000 s

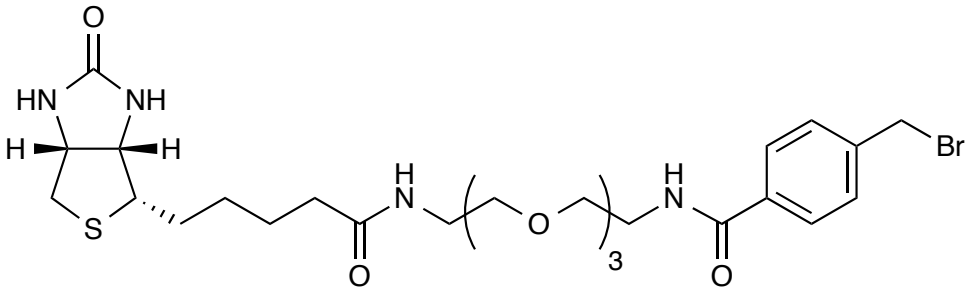

Compound 4-12

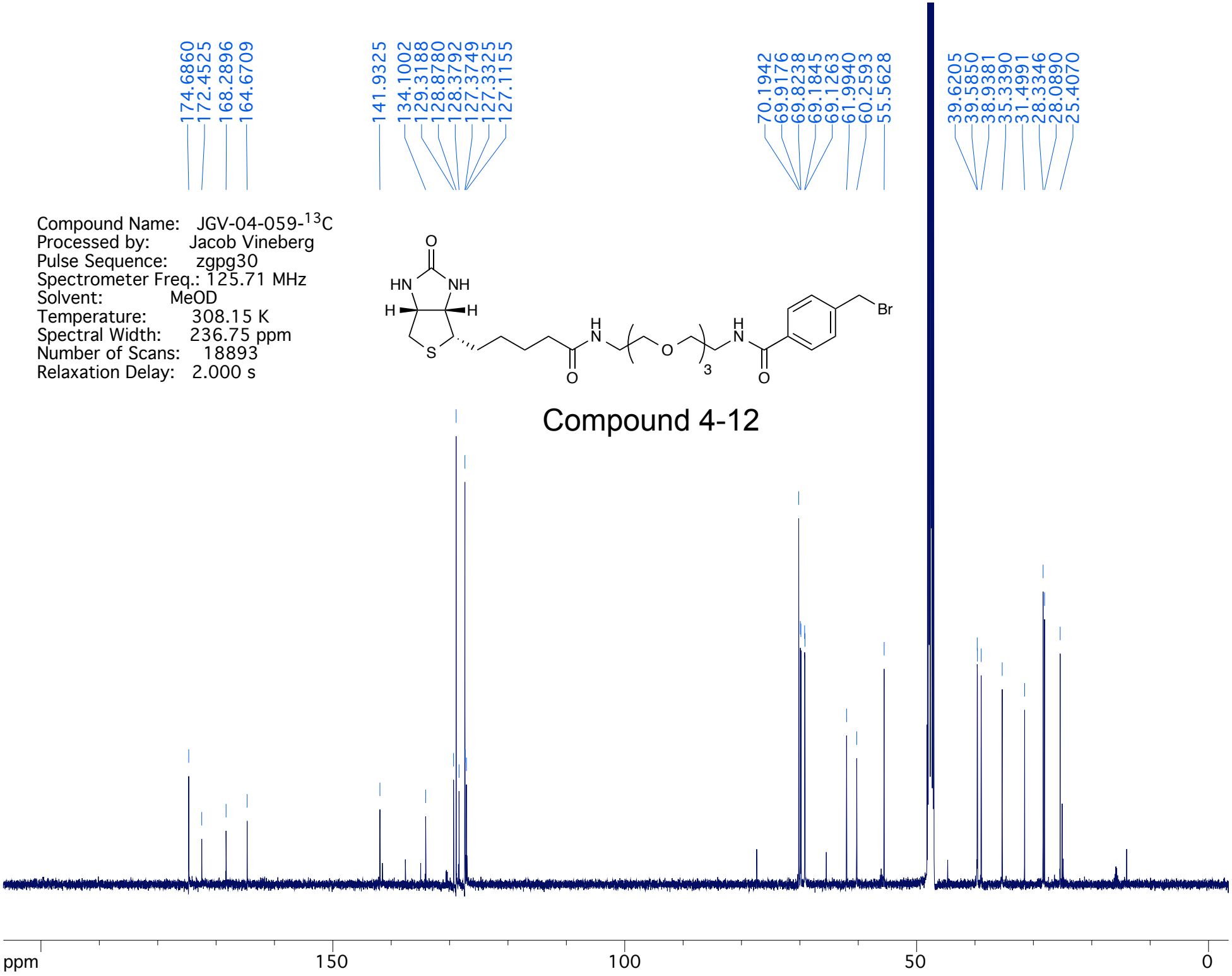
174.6860
172.4525
168.2896
164.6709
141.9325
134.1002
129.3188
128.8780
128.3792
127.3749
127.3325
127.1155
70.1942
69.9176
69.8238
69.1845
69.1263
61.9940
60.2593
55.5628
39.6205
39.5850
38.9381
35.3390
31.4991
28.3346
28.0890
25.4070
Compound Name: JGV-04-059-13C
Processed by: Jacob Vineberg
Pulse Sequence: zgpg30
Spectrometer Freq.: 125.71 MHz
Solvent: MeOD
Temperature: 308.15 K
Spectral Width: 236.75 ppm
Number of Scans: 18893
Relaxation Delay: 2.000 s
Compound 4-12
ppm
150
100
50
0

Compound Name: JGV-03-011
Processed by: Jacob Vineberg
Pulse Sequence: s2pul
Spectrometer Freq.: 300.07 MHz
Solvent: $CDCl_3$
Temperature: 298.15 K
Spectral Width: 15.00 ppm
Number of Scans: 48
Relaxation Delay: 1.000 s

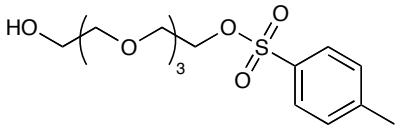

Compound 4-13

Compound Name: JGV-03-013
Processed by: Jacob Vineberg
Pulse Sequence: zg30
Spectrometer Freq.: 499.89 MHz
Solvent: $CDCl_3$
Temperature: 298.15 K
Spectral Width: 20.00 ppm
Number of Scans: 28
Relaxation Delay: 1.000 s

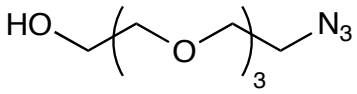

Compound 4-15

Compound Name: JGV-03-014
Processed by: Jacob Vineberg
Pulse Sequence: s2pul
Spectrometer Freq.: 300.07 MHz
Solvent: $CDCl_3$
Temperature: 298.15 K
Spectral Width: 15.00 ppm
Number of Scans: 32
Relaxation Delay: 1.000 s

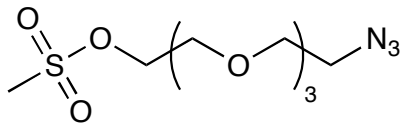

Compound 4-16

Compound Name: JGV-03-065
Processed by: Jacob Vineberg
Pulse Sequence: zg30
Spectrometer Freq.: 499.89 MHz
Solvent: MeOD
Temperature: 298.20 K
Spectral Width: 20.00 ppm
Number of Scans: 22
Relaxation Delay: 1.000 s

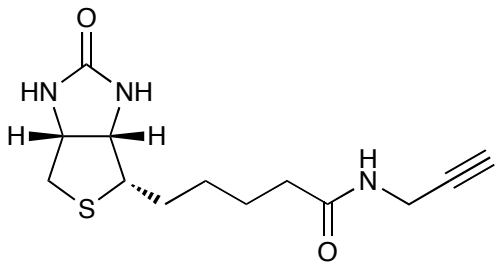

Compound 4-18

Compound Name: JGV-03-065-^{13}C
Processed by: Jacob Vineberg
Pulse Sequence: zgpg30
Spectrometer Freq.: 125.71 MHz
Solvent: MeOD
Temperature: 298.20 K
Spectral Width: 236.75 ppm
Number of Scans: 346
Relaxation Delay: 2.000 s

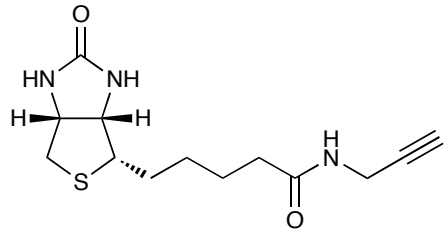

Compound 4-18

Compound Name: JGV-03-076
Processed by: Jacob Vineberg
Pulse Sequence: zg30
Spectrometer Freq.: 499.89 MHz
Solvent: MeOD
Temperature: 298.25 K
Spectral Width: 20.00 ppm
Number of Scans: 44
Relaxation Delay: 1.000 s

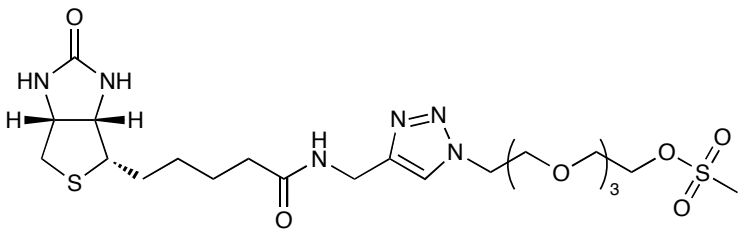

Compound 4-19

Compound Name: JGV-03-076-^{13}C
Processed by: Jacob Vineberg
Pulse Sequence: zgpg30
Spectrometer Freq.: 125.71 MHz
Solvent: MeOD
Temperature: 298.25 K
Spectral Width: 236.75 ppm
Number of Scans: 352
Relaxation Delay: 2.000 s

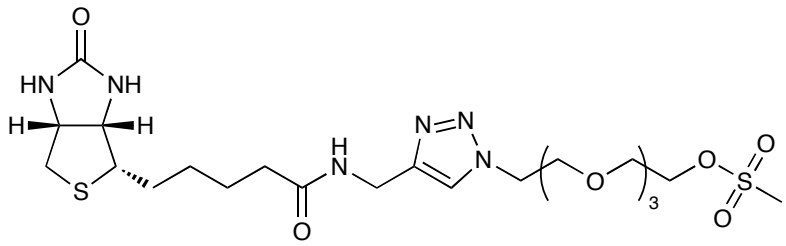

Compound 4-19

Compound Name: JGV-03-081
Processed by: Jacob Vineberg
Pulse Sequence: zg30
Spectrometer Freq.: 499.89 MHz
Solvent: MeOD
Temperature: 298.25 K
Spectral Width: 20.00 ppm
Number of Scans: 81
Relaxation Delay: 1.000 s

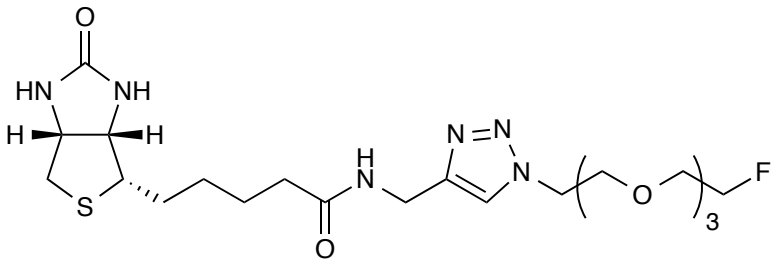

Compound 4-20

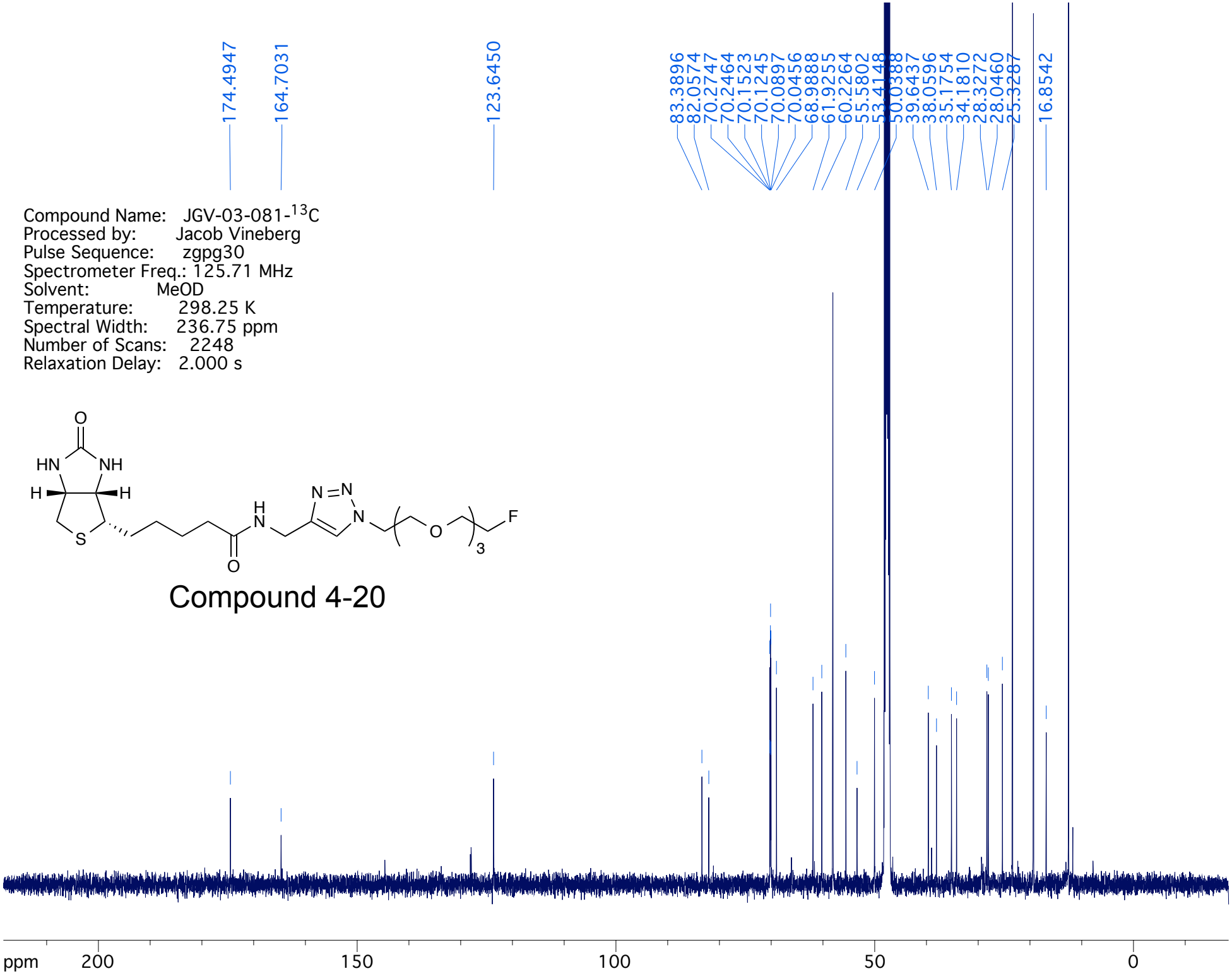
174.4947
164.7031
123.6450
83.3896
82.0574
70.2747
70.2464
70.1523
70.1245
70.0897
70.0456
68.9888
61.9255
60.2264
55.5802
53.4148
50.0388
39.6437
38.0596
35.1754
34.1810
28.3272
28.0460
25.3287
16.8542
Compound Name: JGV-03-081-13C
Processed by: Jacob Vineberg
Pulse Sequence: zgpg30
Spectrometer Freq.: 125.71 MHz
Solvent: MeOD
Temperature: 298.25 K
Spectral Width: 236.75 ppm
Number of Scans: 2248
Relaxation Delay: 2.000 s
Compound 4-20
ppm
200
150
100
50
0

Appendix Chapter 5

Compound Name: JGV-03-039
Processed by: Jacob Vineberg
Pulse Sequence: zg30
Spectrometer Freq.: 499.89 MHz
Solvent: $CDCl_3$
Temperature: 298.14 K
Spectral Width: 20.00 ppm
Number of Scans: 21
Relaxation Delay: 1.000 s

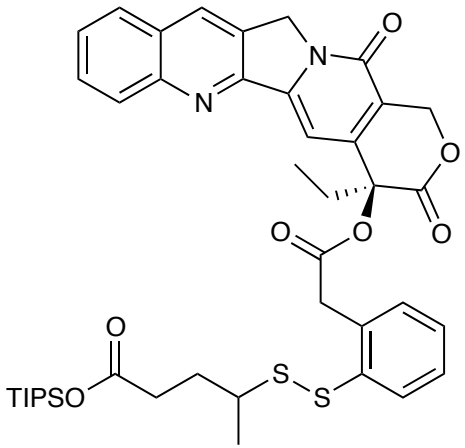

Compound 5-1

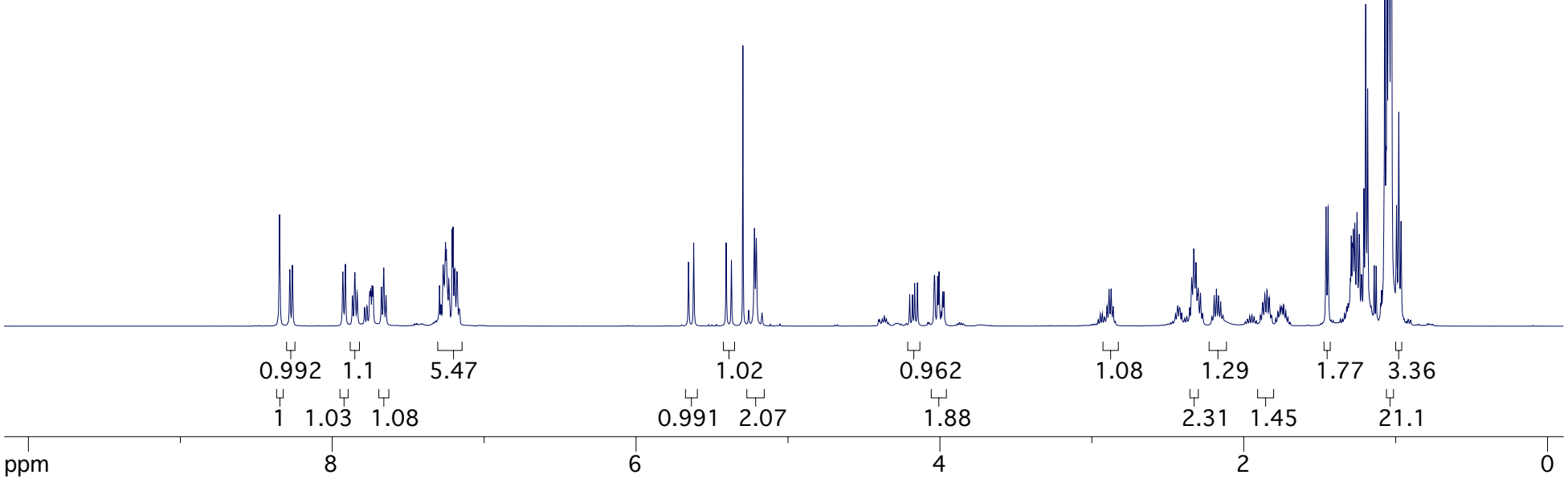

Compound Name: JGV-03-039-^{13}C
Processed by: Jacob Vineberg
Pulse Sequence: zgpg30
Spectrometer Freq.: 125.71 MHz
Solvent: $CDCl_3$
Temperature: 298.15 K
Spectral Width: 236.75 ppm
Number of Scans: 1181
Relaxation Delay: 2.000 s

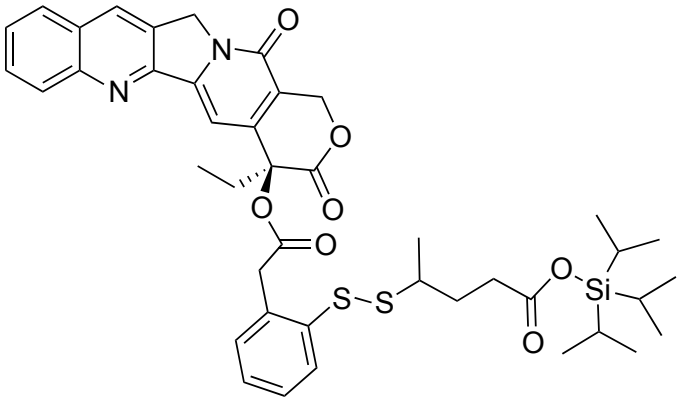

Compound 5-1

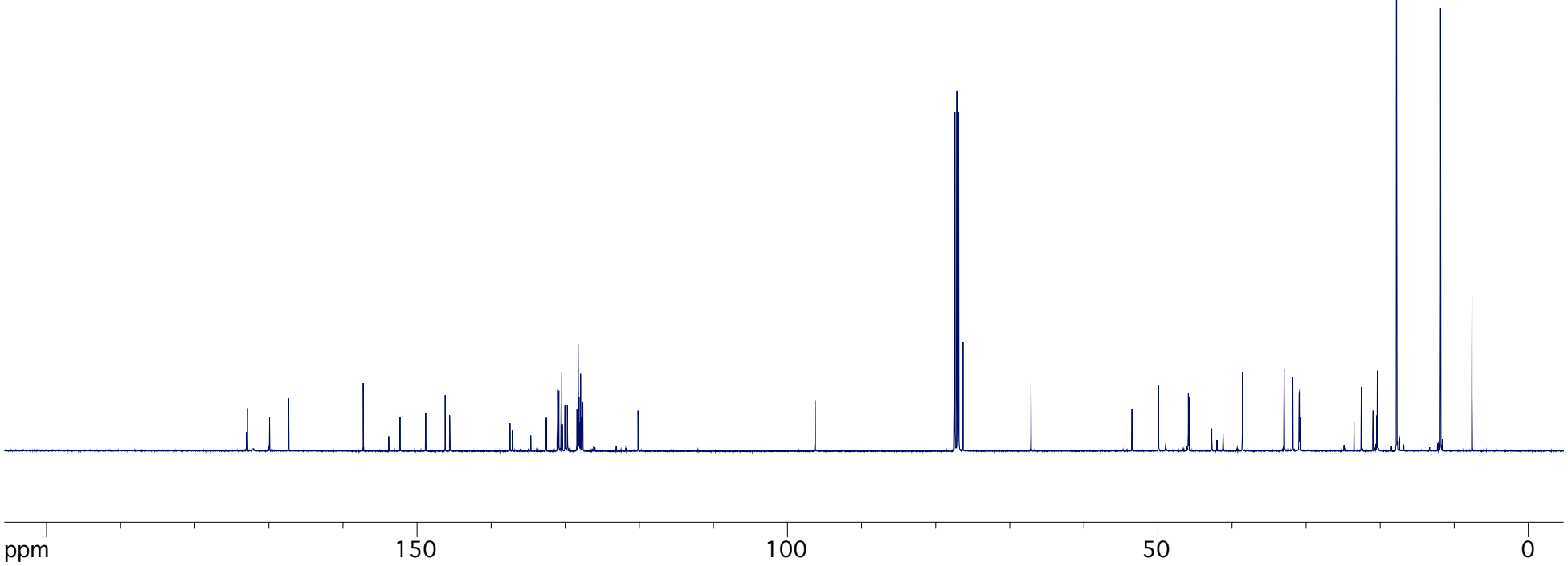

Compound Name: JGV-03-088
Processed by: Jacob Vineberg
Pulse Sequence: zg30
Spectrometer Freq.: 499.89 MHz
Solvent: DMSO
Temperature: 298.15 K
Spectral Width: 20.00 ppm
Number of Scans: 28
Relaxation Delay: 1.000 s

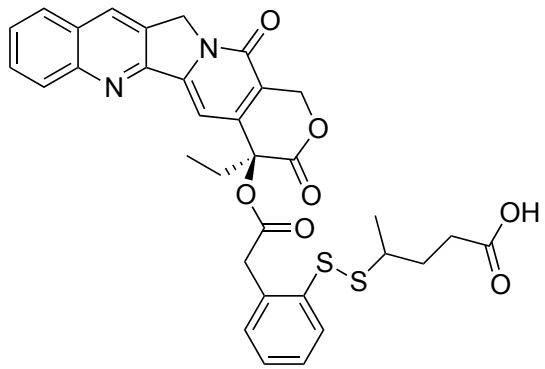

Compound 5-2

Compound Name: JGV-03-088-^{13}C
Processed by: Jacob Vineberg
Pulse Sequence: zgpg30
Spectrometer Freq.: 125.71 MHz
Solvent: DMSO
Temperature: 298.15 K
Spectral Width: 236.75 ppm
Number of Scans: 3071
Relaxation Delay: 2.000 s

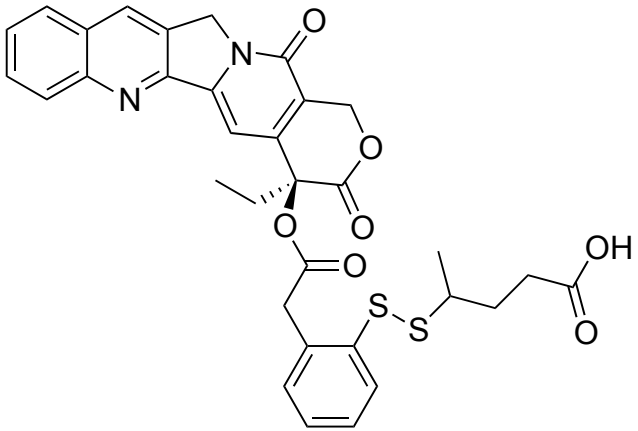

Compound 5-2

Compound Name: JGV-03-089
Processed by: Jacob Vineberg
Pulse Sequence: zg30
Spectrometer Freq.: 499.89 MHz
Solvent: $CDCl_3$
Temperature: 298.14 K
Spectral Width: 20.00 ppm
Number of Scans: 102
Relaxation Delay: 1.000 s

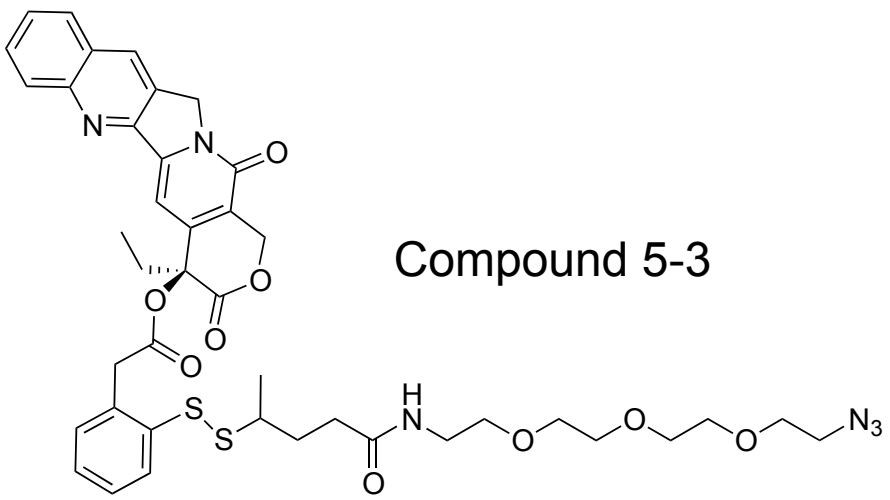

Compound 5-3

Compound Name: JGV-03-089-^{13}C
Processed by: Jacob Vineberg
Pulse Sequence: zgpg30
Spectrometer Freq.: 100.55 MHz
Solvent: $CDCl_3$
Temperature: 298.23 K
Spectral Width: 239.08 ppm
Number of Scans: 13425
Relaxation Delay: 2.000 s

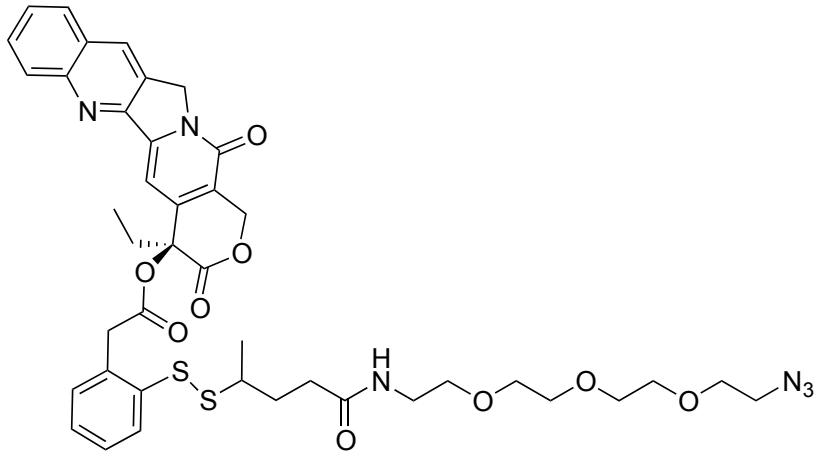

Compound 5-3

Compound Name: JGV-02-077
Processed by: Jacob Vineberg
Pulse Sequence: s2pul
Spectrometer Freq.: 300.07 MHz
Solvent: CD_3OD
Temperature: 298.15 K
Spectral Width: 15.00 ppm
Number of Scans: 50
Relaxation Delay: 1.000 s

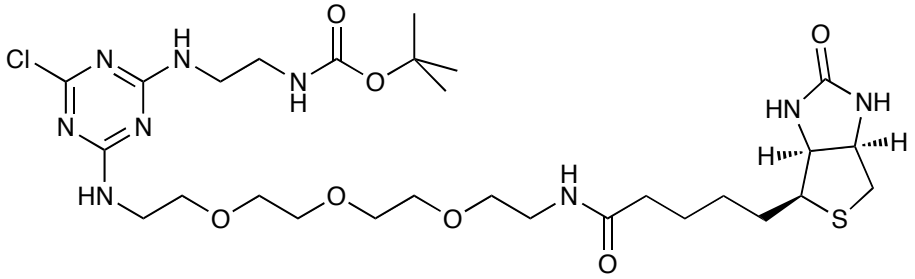

Compound 5-5

Compound Name: JGV-02-077-^{13}C
Processed by: Jacob Vineberg
Pulse Sequence: zgpg30
Spectrometer Freq.: 100.55 MHz
Solvent: MeOD
Temperature: 298.17 K
Spectral Width: 239.08 ppm
Number of Scans: 12875
Relaxation Delay: 2.000 s

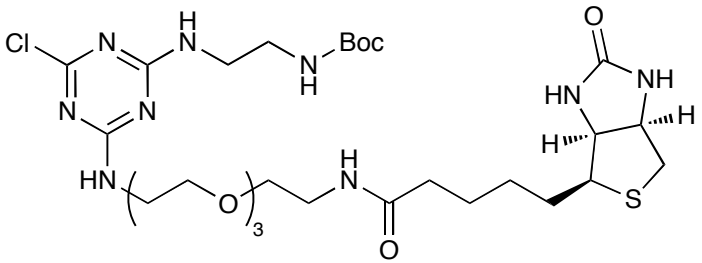

Compound 5-5

Compound Name: JGV-02-107
Processed by: Jacob Vineberg
Pulse Sequence: s2pul
Spectrometer Freq.: 300.07 MHz
Solvent: CD_3OD
Temperature: 298.15 K
Spectral Width: 15.00 ppm
Number of Scans: 100
Relaxation Delay: 1.000 s

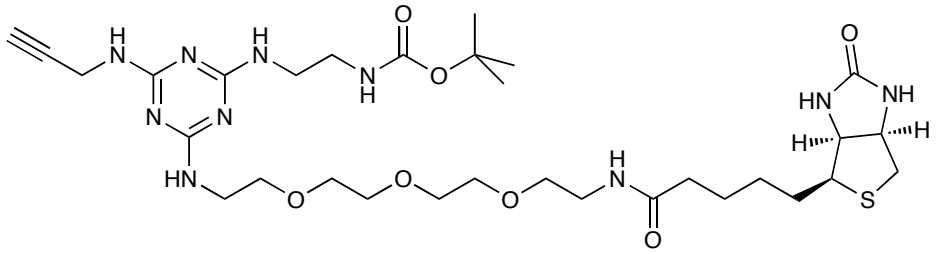

Compound 5-6

Compound Name: JGV-02-107-^{13}C
Processed by: Jacob Vineberg
Pulse Sequence: zgpg30
Spectrometer Freq.: 125.71 MHz
Solvent: MeOD
Temperature: 298.15 K
Spectral Width: 236.75 ppm
Number of Scans: 16817
Relaxation Delay: 2.000 s

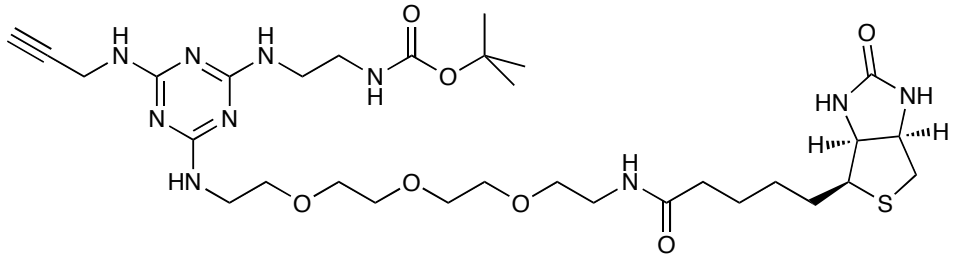

Compound 5-6

Compound Name: JGV-02-114
Processed by: Jacob Vineberg
Pulse Sequence: zg30
Spectrometer Freq.: 399.83 MHz
Solvent: MeOD
Temperature: 298.15 K
Spectral Width: 20.57 ppm
Number of Scans: 36
Relaxation Delay: 1.000 s

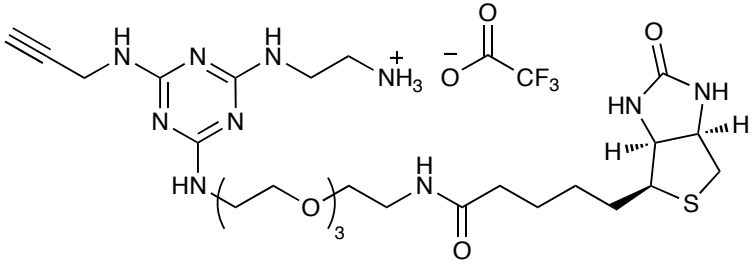

Compound 5-7

Compound Name: JGV-02-114-^{13}C
Processed by: Jacob Vineberg
Pulse Sequence: zgpg30
Spectrometer Freq.: 100.55 MHz
Solvent: MeOD
Temperature: 298.22 K
Spectral Width: 239.08 ppm
Number of Scans: 14034
Relaxation Delay: 2.000 s

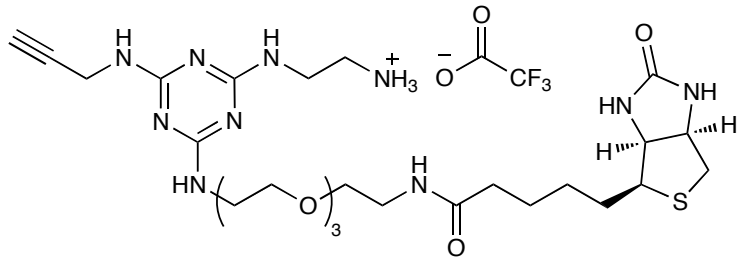

Compound 5-7

Compound Name: JGV-03-006
Processed by: Jacob Vineberg
Pulse Sequence: zg30
Spectrometer Freq.: 499.89 MHz
Solvent: MeOD
Temperature: 298.15 K
Spectral Width: 20.00 ppm
Number of Scans: 86
Relaxation Delay: 1.000 s

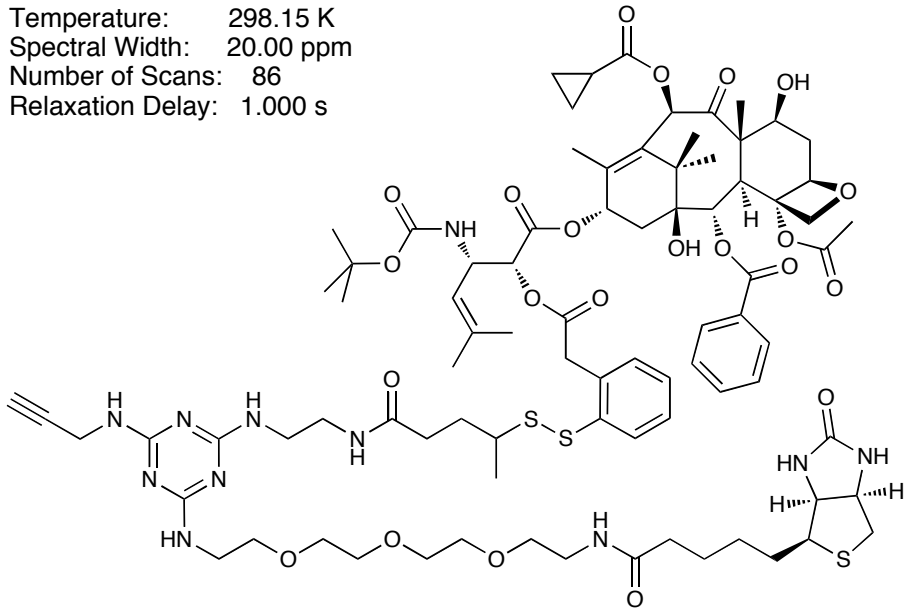

Compound 5-8

Compound Name: JGV-03-006-^{13}C
Processed by: Jacob Vineberg
Pulse Sequence: zgpg30
Spectrometer Freq.: 125.71 MHz
Solvent: CD_3OD
Temperature: 298.15 K
Spectral Width: 236.75 ppm
Number of Scans: 16260
Relaxation Delay: 2.000 s

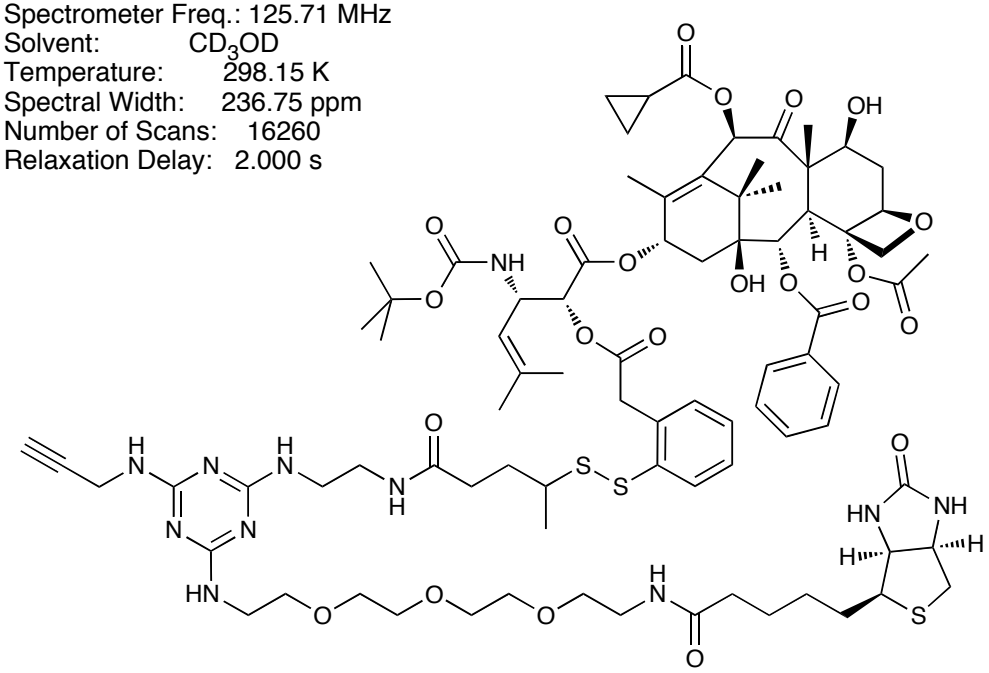

Compound 5-8

Compound Name: JGV-03-090
Processed by: Jacob Vineberg
Pulse Sequence: zg30
Spectrometer Freq.: 499.89 MHz
Solvent: MeOD
Temperature: 298.15 K
Spectral Width: 20.00 ppm
Number of Scans: 51
Relaxation Delay: 1.000 s

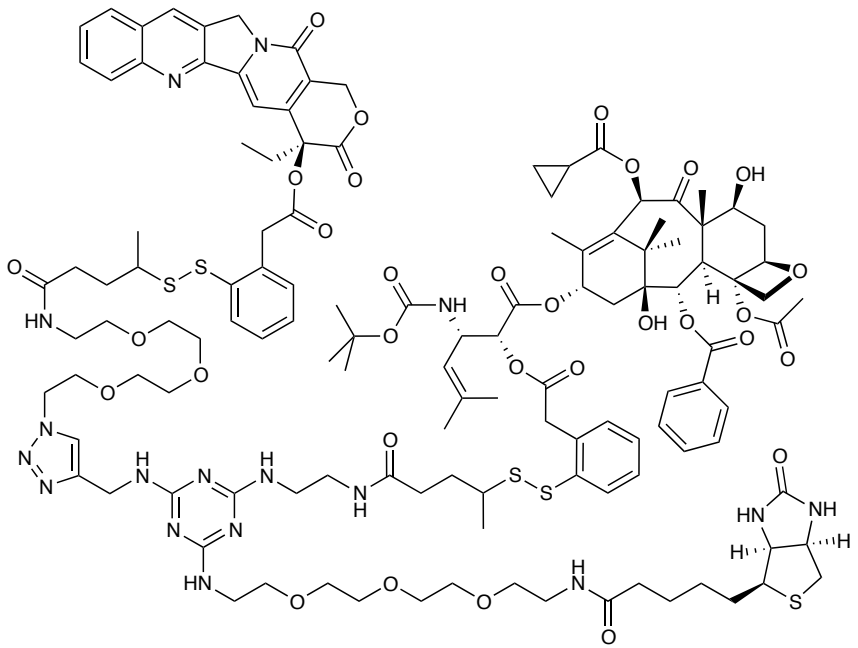

Conjugate 5-9 (DW-1)

Compound Name: JGV-03-090-^{13}C
Processed by: Jacob Vineberg
Pulse Sequence: zgpg30
Spectrometer Freq.: 125.71 MHz
Solvent: DMSO
Temperature: 298.15 K
Spectral Width: 236.75 ppm
Number of Scans: 17808
Relaxation Delay: 2.000 s

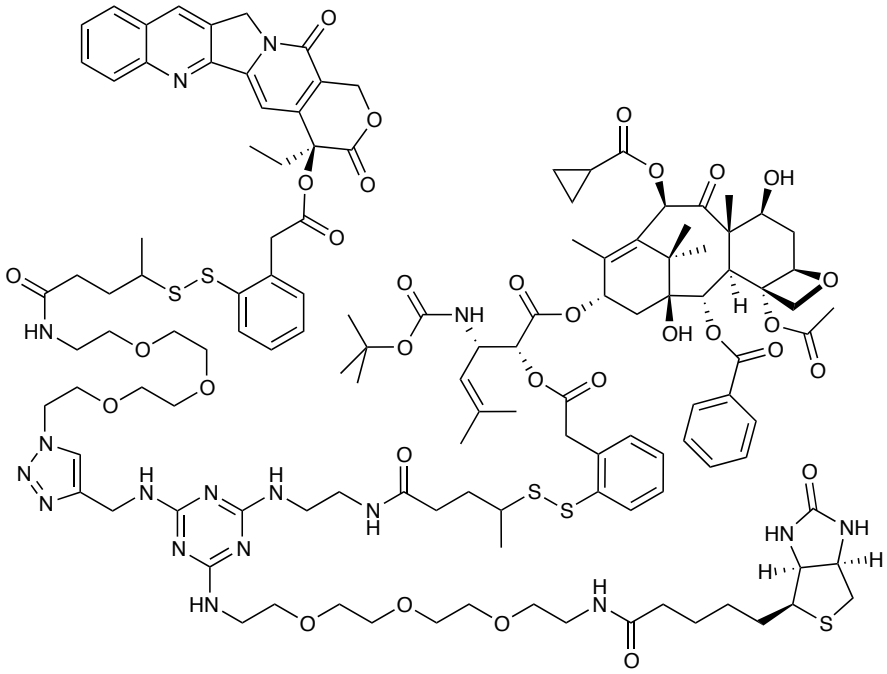

Conjugate 5-9 (DW-1)

Compound Name: JGV-03-021
Processed by: Jacob Vineberg
Pulse Sequence: zg30
Spectrometer Freq.: 499.89 MHz
Solvent: $CDCl_3$
Temperature: 298.15 K
Spectral Width: 20.00 ppm
Number of Scans: 22
Relaxation Delay: 1.000 s

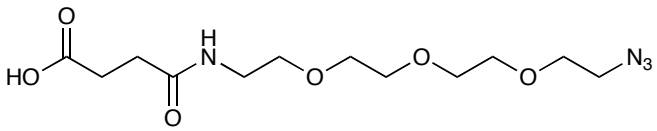

Compound 5-10

Compound Name: JGV-03-021-^{13}C
Processed by: Jacob Vineberg
Pulse Sequence: zgpg30
Spectrometer Freq.: 125.71 MHz
Solvent: $CDCl_3$
Temperature: 298.15 K
Spectral Width: 236.75 ppm
Number of Scans: 2275
Relaxation Delay: 2.000 s

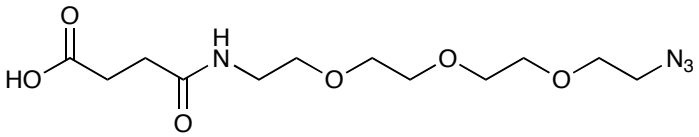

Compound 5-10

Compound Name: JGV-03-024
Processed by: Jacob Vineberg
Pulse Sequence: zg30
Spectrometer Freq.: 499.89 MHz
Solvent: $CDCl_3$
Temperature: 298.15 K
Spectral Width: 20.00 ppm
Number of Scans: 34
Relaxation Delay: 1.000 s

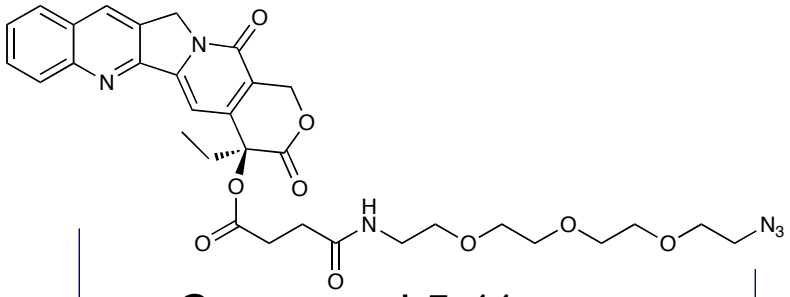

Compound 5-11

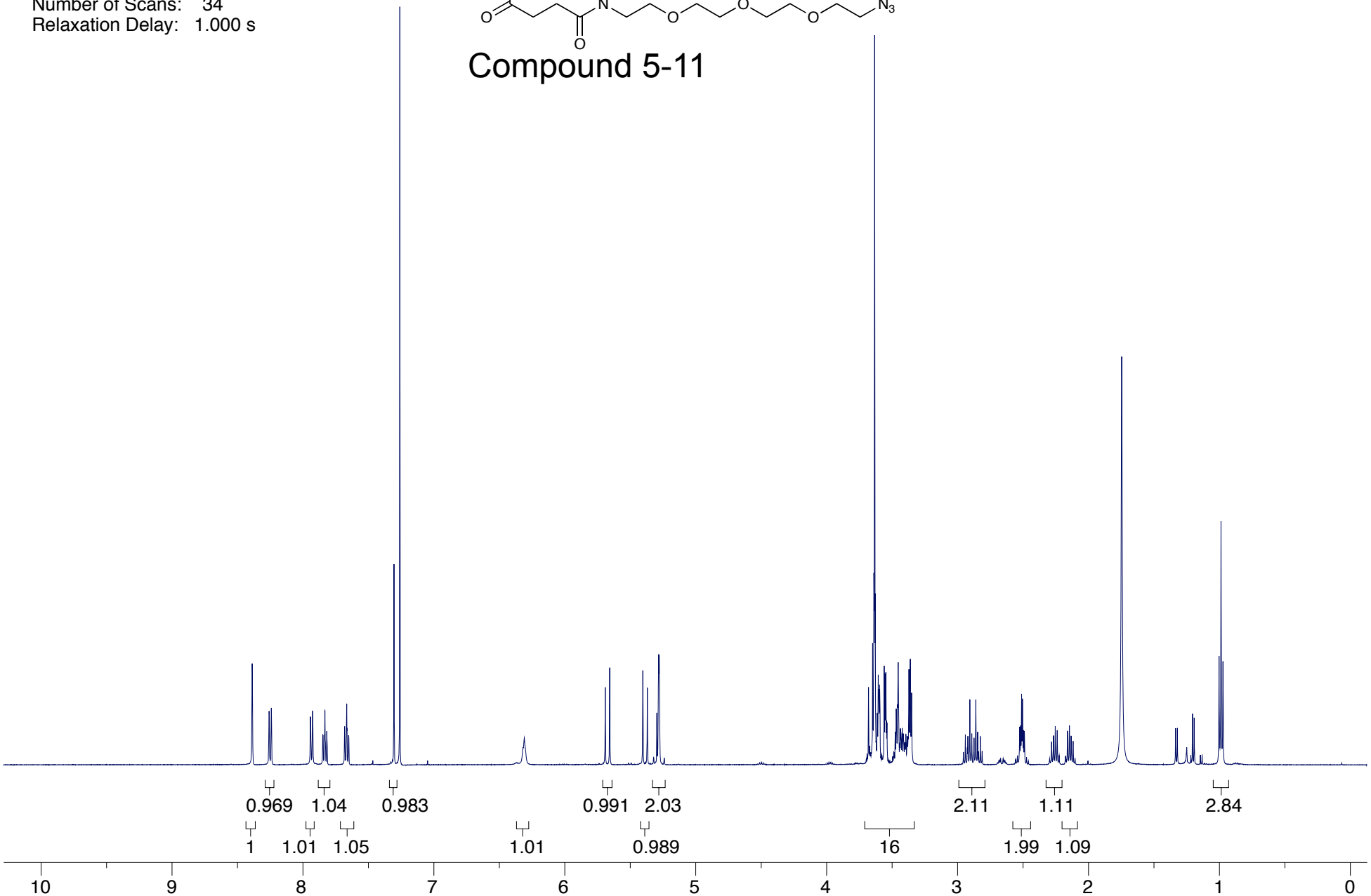

Compound Name: JGV-03-024-^{13}C
Processed by: Jacob Vineberg
Pulse Sequence: zgpg30
Spectrometer Freq.: 125.71 MHz
Solvent: $CDCl_3$
Temperature: 298.15 K
Spectral Width: 236.75 ppm
Number of Scans: 14908
Relaxation Delay: 2.000 s

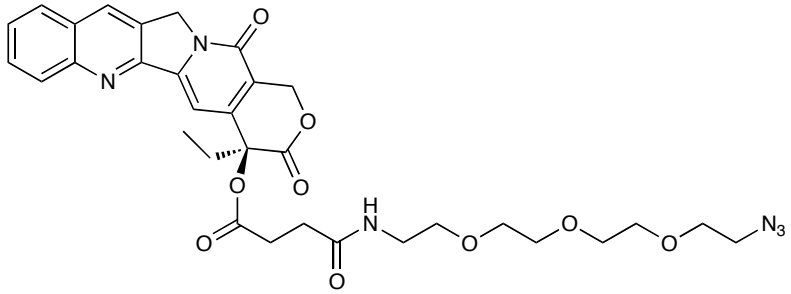

Compound 5-11

Compound Name: JGV-03-028
Processed by: Jacob Vineberg
Pulse Sequence: zg30
Spectrometer Freq.: 499.89 MHz
Solvent: MeOD
Temperature: 298.15 K
Spectral Width: 20.00 ppm
Number of Scans: 137
Relaxation Delay: 1.000 s

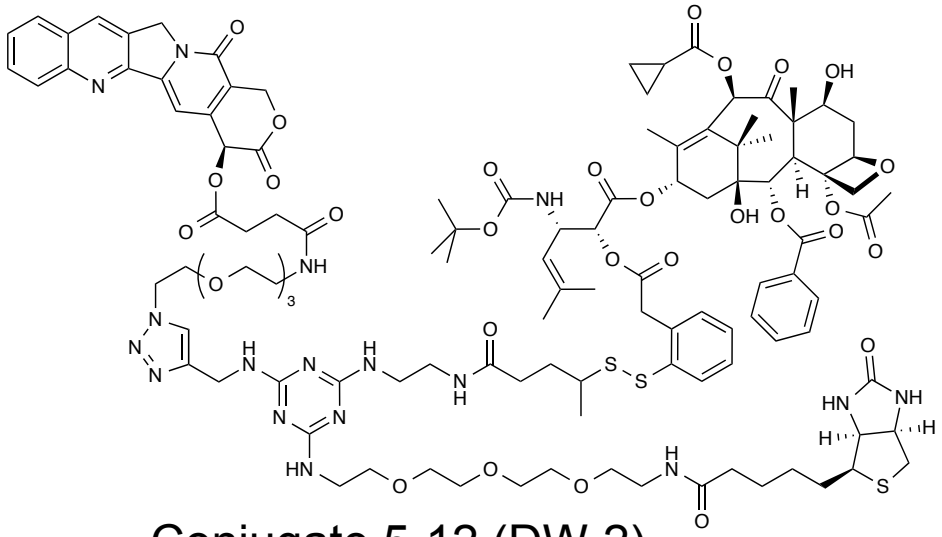

Conjugate 5-12 (DW-2)

Compound Name: JGV-03-028-^{13}C
Processed by: Jacob Vineberg
Pulse Sequence: zgpg30
Spectrometer Freq.: 125.71 MHz
Solvent: MeOD
Temperature: 298.15 K
Spectral Width: 236.75 ppm
Number of Scans: 21239
Relaxation Delay: 2.000 s

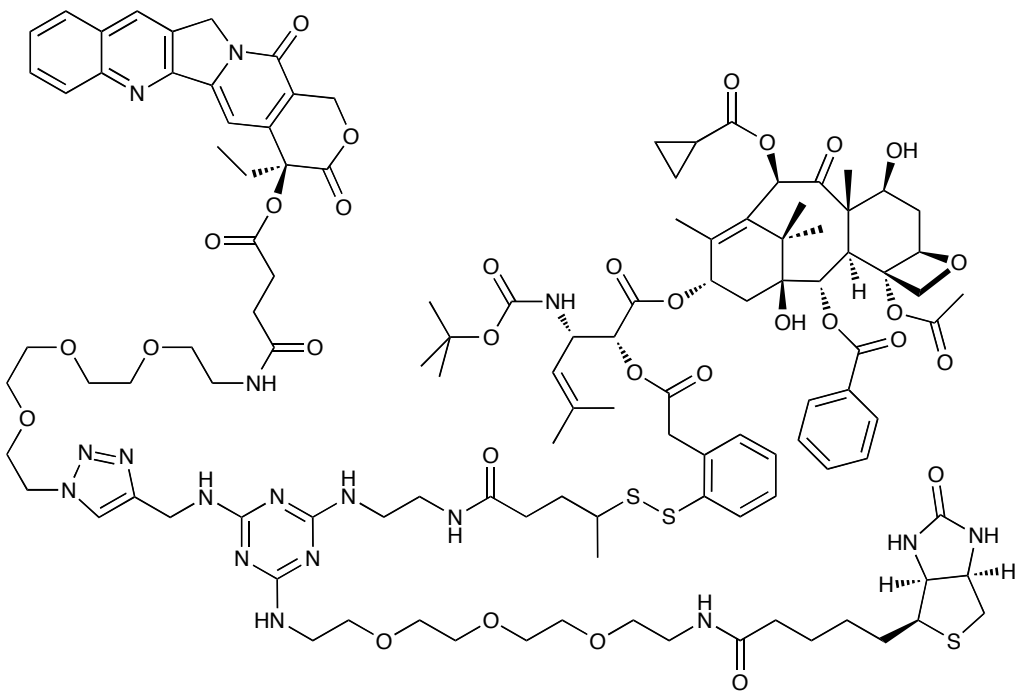

Conjugate 5-12 (DW-2)

Compound Name: JGV-03-040
Processed by: Jacob Vineberg
Pulse Sequence: zg30
Spectrometer Freq.: 399.83 MHz
Solvent: $CDCl_3$
Temperature: 298.15 K
Spectral Width: 20.57 ppm
Number of Scans: 22
Relaxation Delay: 1.000 s

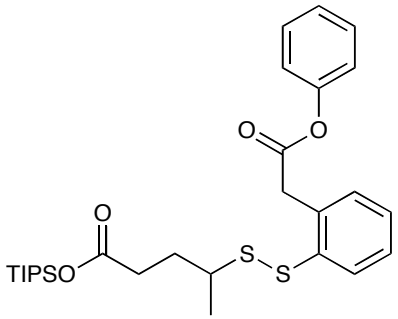

Compound 5-13

Compound Name: JGV-03-040-^{13}C
Processed by: Jacob Vineberg
Pulse Sequence: zg30
Spectrometer Freq.: 399.83 MHz
Solvent: $CDCl_3$
Temperature: 298.15 K
Spectral Width: 20.57 ppm
Number of Scans: 22
Relaxation Delay: 1.000 s

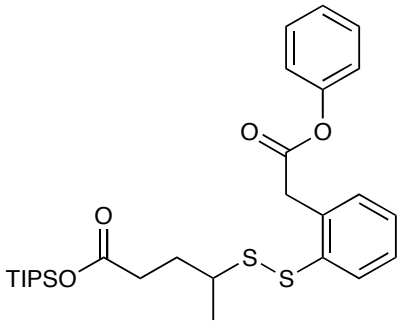

Compound 5-13

Compound Name: JGV-03-114
Processed by: Jacob Vineberg
Pulse Sequence: zg30
Spectrometer Freq.: 499.89 MHz
Solvent: $CDCl_3$
Temperature: 298.15 K
Spectral Width: 20.00 ppm
Number of Scans: 19
Relaxation Delay: 1.000 s

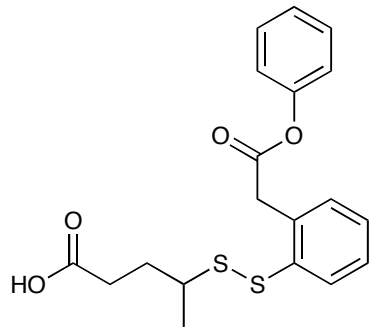

Compound 5-14

Compound Name: JGV-03-114-^{13}C
Processed by: Jacob Vineberg
Pulse Sequence: zgpg30
Spectrometer Freq.: 100.55 MHz
Solvent: $CDCl_3$
Temperature: 298.18 K
Spectral Width: 239.08 ppm
Number of Scans: 373
Relaxation Delay: 2.000 s

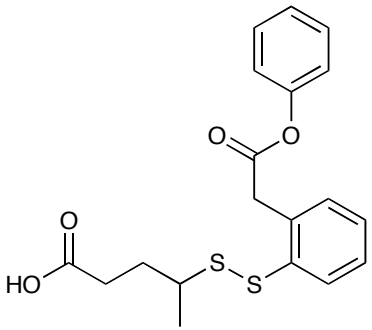

Compound 5-14

Compound Name: JGV-03-115
Processed by: Jacob Vineberg
Pulse Sequence: zg30
Spectrometer Freq.: 499.89 MHz
Solvent: $CDCl_3$
Temperature: 298.14 K
Spectral Width: 20.00 ppm
Number of Scans: 20
Relaxation Delay: 1.000 s

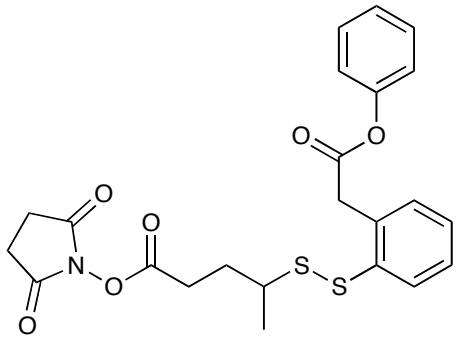

Compound 5-15

Compound Name: JGV-03-115-^{13}C
Processed by: Jacob Vineberg
Pulse Sequence: zgpg30
Spectrometer Freq.: 125.71 MHz
Solvent: $CDCl_3$
Temperature: 298.15 K
Spectral Width: 236.75 ppm
Number of Scans: 456
Relaxation Delay: 2.000 s

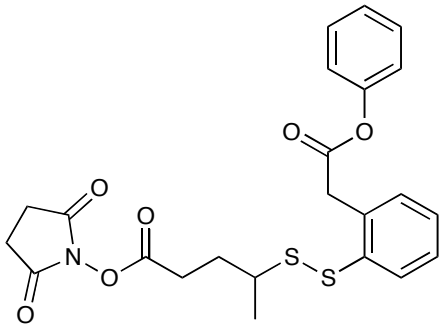

Compound 5-15

Compound Name: JGV-03-100
Processed by: Jacob Vineberg
Pulse Sequence: zg30
Spectrometer Freq.: 499.89 MHz
Solvent: $CDCl_3$
Temperature: 298.15 K
Spectral Width: 20.00 ppm
Number of Scans: 55
Relaxation Delay: 1.000 s

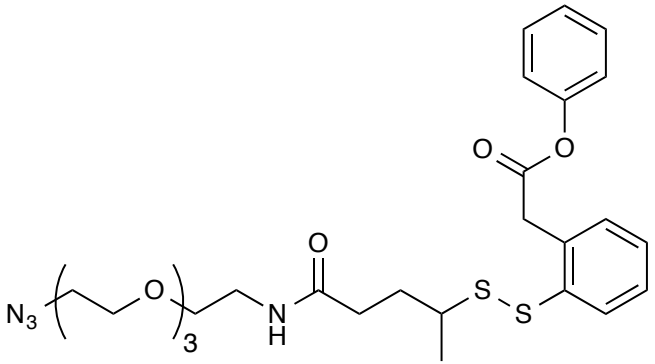

Compound 5-16

Compound Name: JGV-03-100-^{13}C
Processed by: Jacob Vineberg
Pulse Sequence: zgpg30
Spectrometer Freq.: 125.71 MHz
Solvent: $CDCl_3$
Temperature: 298.15 K
Spectral Width: 236.75 ppm
Number of Scans: 1764
Relaxation Delay: 2.000 s

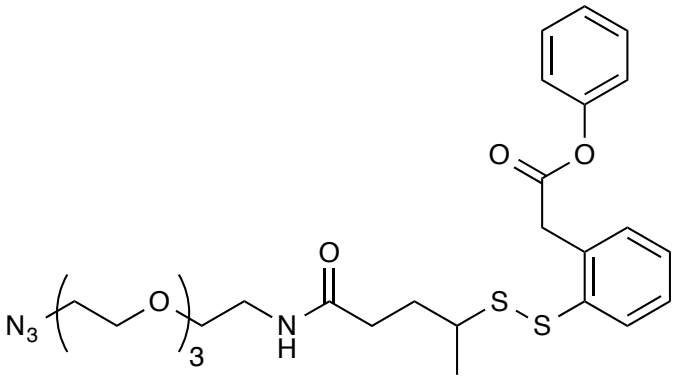

Compound 5-16

Compound Name: JGV-03-103
Processed by: Jacob Vineberg
Pulse Sequence: zg30
Spectrometer Freq.: 499.89 MHz
Solvent: $CDCl_3$
Temperature: 298.14 K
Spectral Width: 20.00 ppm
Number of Scans: 66
Relaxation Delay: 1.000 s

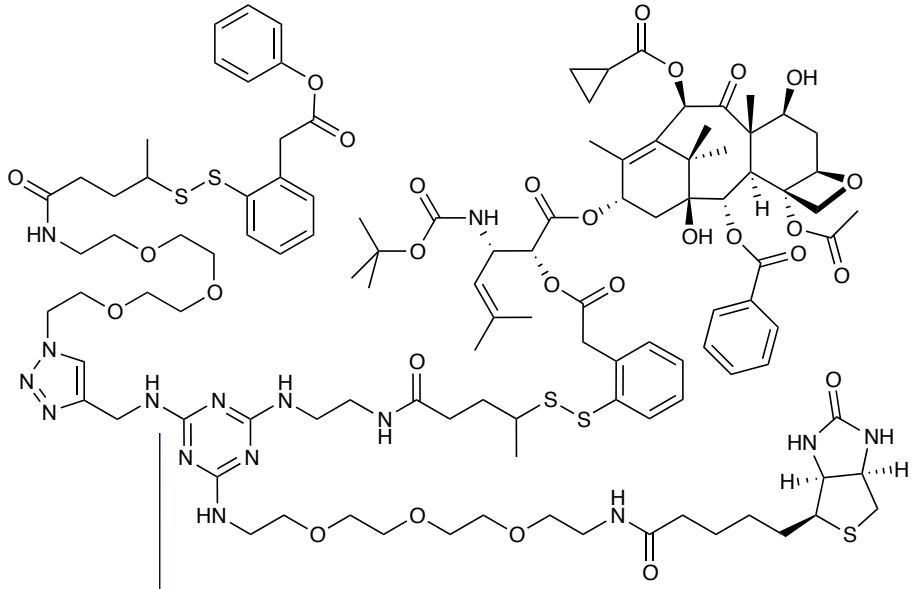

Conjugate 5-17 (SW-Tax)

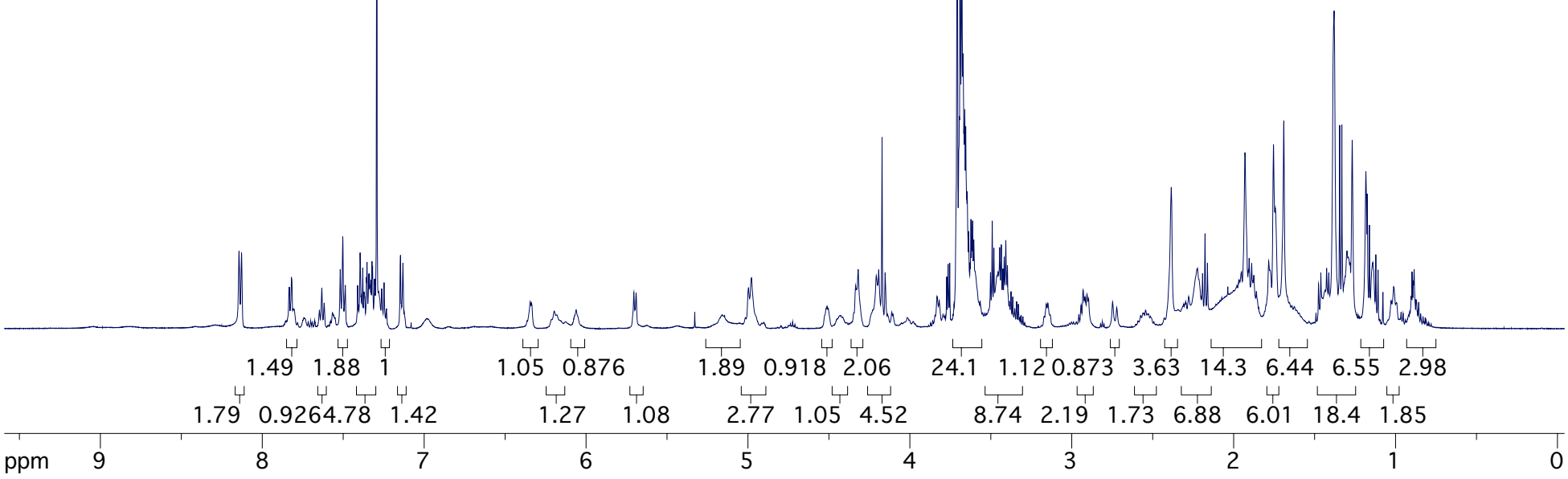

Compound Name: JGV-03-103-^{13}C
Processed by: Jacob Vineberg
Pulse Sequence: zgpg30
Spectrometer Freq.: 125.71 MHz
Solvent: $CDCl_3$
Temperature: 298.15 K
Spectral Width: 236.75 ppm
Number of Scans: 16642
Relaxation Delay: 2.000 s

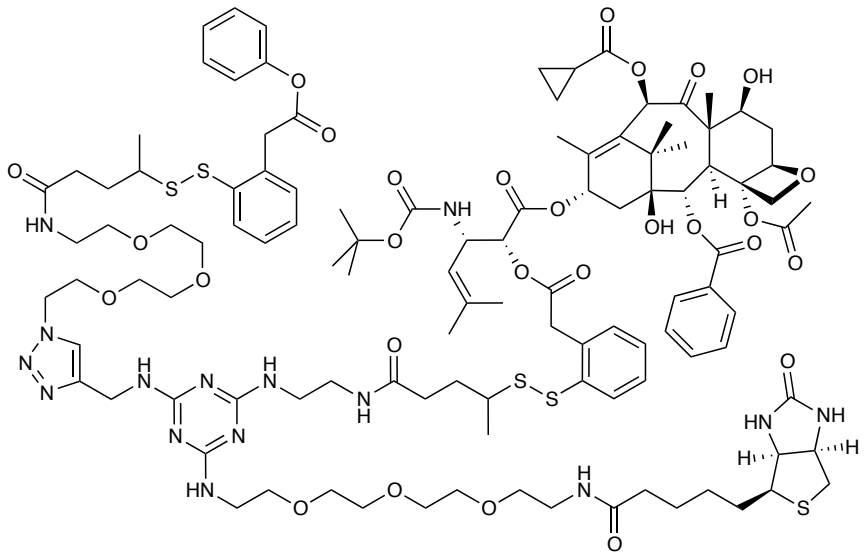

Conjugate 5-17 (SW-Tax)

Compound Name: JGV-03-106
Processed by: Jacob Vineberg
Pulse Sequence: zg30
Spectrometer Freq.: 499.89 MHz
Solvent: MeOD
Temperature: 298.15 K
Spectral Width: 20.00 ppm
Number of Scans: 37
Relaxation Delay: 1.000 s

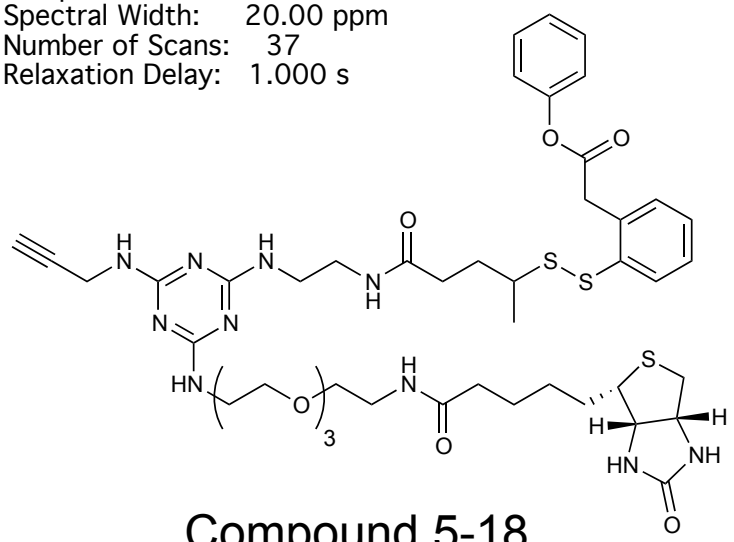

Compound 5-18

Compound Name: JGV-03-106-^{13}C
Processed by: Jacob Vineberg
Pulse Sequence: zgpg30
Spectrometer Freq.: 125.71 MHz
Solvent: MeOD
Temperature: 298.15 K
Spectral Width: 236.75 ppm
Number of Scans: 634
Relaxation Delay: 2.000 s

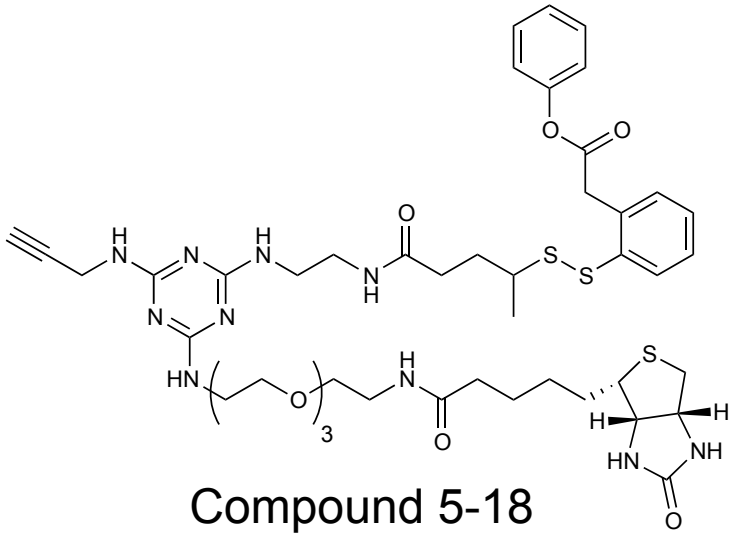

Compound 5-18

Compound Name: JGV-03-107
Processed by: Jacob Vineberg
Pulse Sequence: zg30
Spectrometer Freq.: 499.89 MHz
Solvent: DMSO
Temperature: 298.15 K
Spectral Width: 20.00 ppm
Number of Scans: 63
Relaxation Delay: 1.000 s

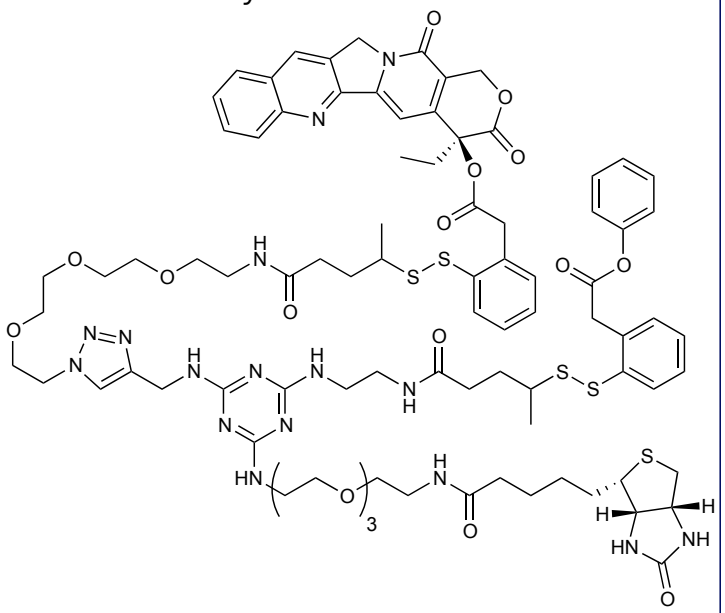

Conjugate 5-19 (SW-CPT)

Compound Name: JGV-03-107-^{13}C
Processed by: Jacob Vineberg
Pulse Sequence: zgpg30
Spectrometer Freq.: 125.71 MHz
Solvent: DMSO
Temperature: 298.15 K
Spectral Width: 236.75 ppm
Number of Scans: 15884
Relaxation Delay: 2.000 s

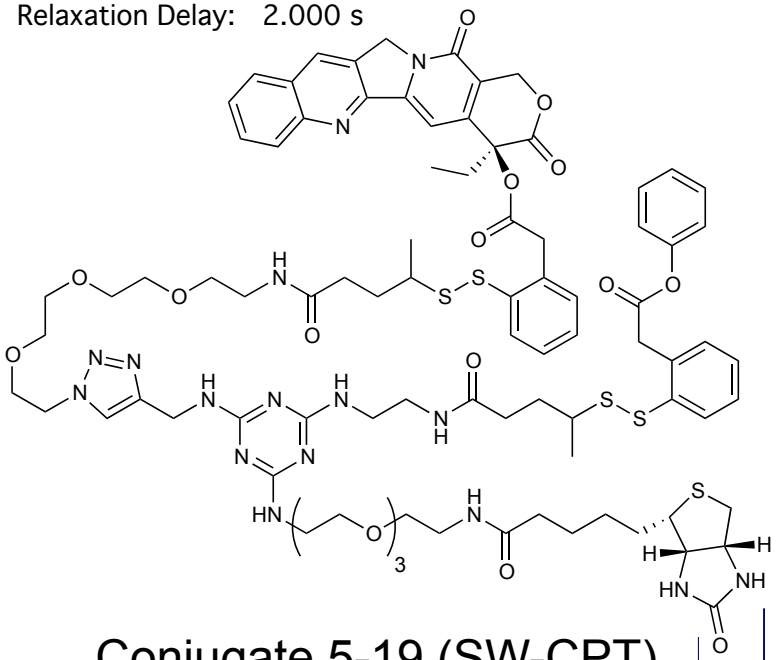

Conjugate 5-19 (SW-CPT)

Appendix Chapter 6

Compound Name: JGV-02-094
Processed by: Jacob Vineberg
Pulse Sequence: s2pul
Spectrometer Freq.: 300.08 MHz
Solvent: DMSO
Temperature: 298.15 K
Spectral Width: 15.00 ppm
Number of Scans: 50
Relaxation Delay: 1.000 s

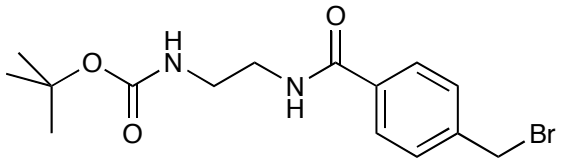

Compound 6-1

Compound Name: JGV-02-095
Processed by: Jacob Vineberg
Pulse Sequence: s2pul
Spectrometer Freq.: 300.08 MHz
Solvent: DMSO
Temperature: 298.15 K
Spectral Width: 15.00 ppm
Number of Scans: 50
Relaxation Delay: 1.000 s

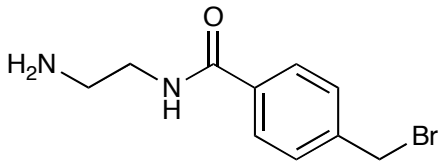

Compound 6-2

Compound Name: JGV-03-016
Processed by: Jacob Vineberg
Pulse Sequence: s2pul
Spectrometer Freq.: 300.07 MHz
Solvent: $CDCl_3$
Temperature: 298.15 K
Spectral Width: 15.00 ppm
Number of Scans: 48
Relaxation Delay: 1.000 s

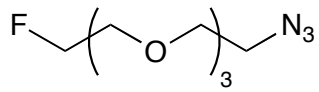

Compound 6-3

Compound Name: JGV-03-016-^{13}C
Processed by: Jacob Vineberg
Pulse Sequence: zgpg30
Spectrometer Freq.: 125.71 MHz
Solvent: $CDCl_3$
Temperature: 298.15 K
Spectral Width: 236.75 ppm
Number of Scans: 242
Relaxation Delay: 2.000 s

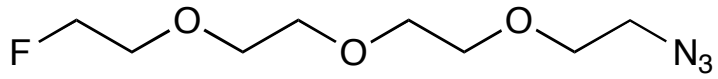

Compound 6-3

Compound Name: JGV-03-016-^{19}F
Processed by: Jacob Vineberg
Pulse Sequence: s2pul
Spectrometer Freq.: 282.32 MHz
Solvent: $CDCl_3$
Temperature: 298.15 K
Spectral Width: 177.10 ppm
Number of Scans: 200
Relaxation Delay: 4.000 s

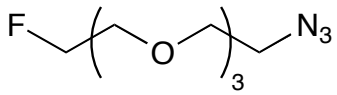

Compound 6-3

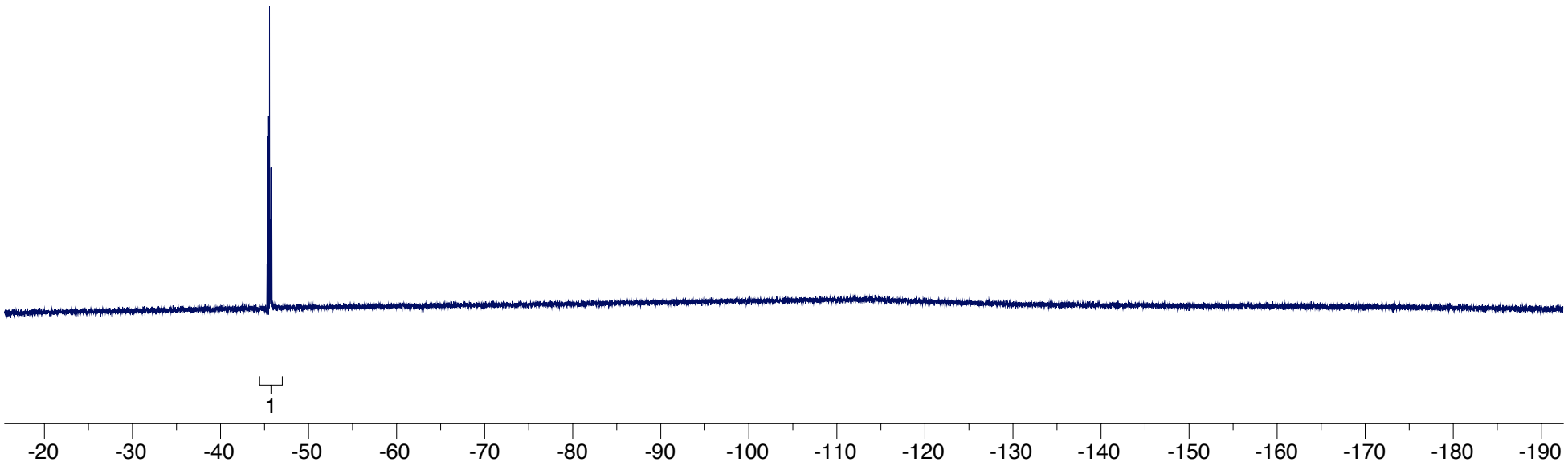

Compound Name: JGV-03-018
Processed by: Jacob Vineberg
Pulse Sequence: zg30
Spectrometer Freq.: 499.89 MHz
Solvent: MeOD
Temperature: 298.15 K
Spectral Width: 20.00 ppm
Number of Scans: 47
Relaxation Delay: 1.000 s

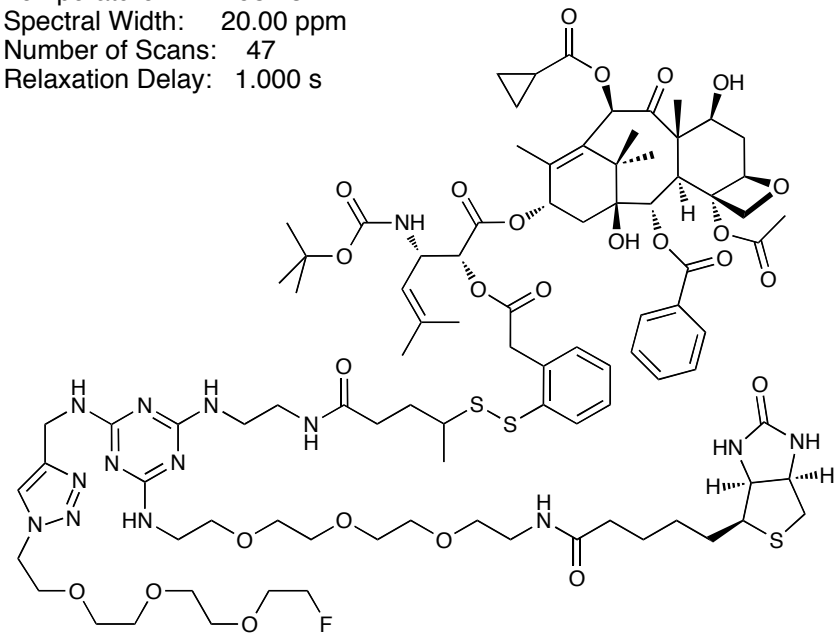

Conjugate 6-4 (BLT-F)

Compound Name: JGV-03-018-^{13}C
Processed by: Jacob Vineberg
Pulse Sequence: zgpg30
Spectrometer Freq.: 125.71 MHz
Solvent: MeOD
Temperature: 298.15 K
Spectral Width: 236.75 ppm
Number of Scans: 20216
Relaxation Delay: 2.000 s

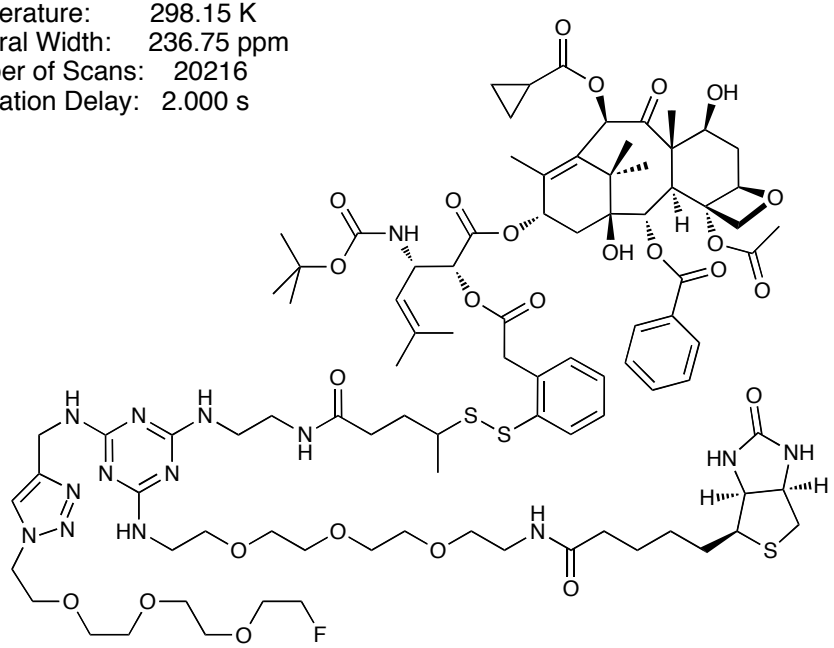

Conjugate 6-4 (BLT-F)

Acquisition Date: JGV-03-026
Processed by: Jacob Vineberg
Pulse Sequence: zg30
Spectrometer Freq.: 499.89 MHz
Solvent: DMSO
Temperature: 298.15 K
Spectral Width: 20.00 ppm
Number of Scans: 43
Relaxation Delay: 1.000 s

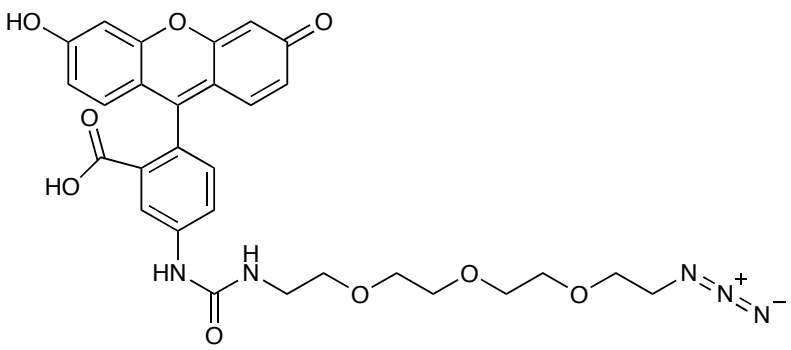

Compound 6-5

Compound Name: JGV-03-026-^{13}C
Processed by: Jacob Vineberg
Pulse Sequence: zgpg30
Spectrometer Freq.: 125.71 MHz
Solvent: DMSO
Temperature: 298.15 K
Spectral Width: 236.75 ppm
Number of Scans: 2835
Relaxation Delay: 2.000 s

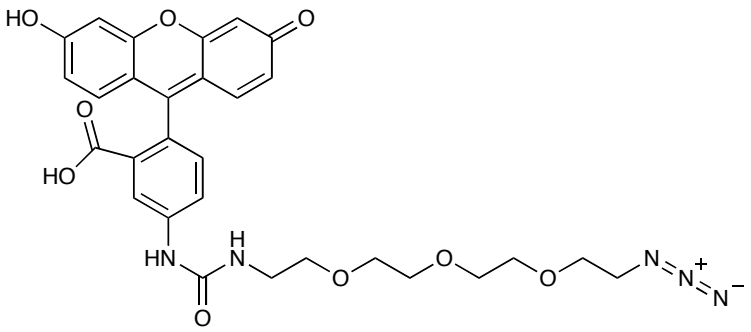

Compound 6-5

Compound Name: JGV-03-029
Processed by: Jacob Vineberg
Pulse Sequence: zg30
Spectrometer Freq.: 499.89 MHz
Solvent: DMSO
Temperature: 298.15 K
Spectral Width: 20.00 ppm
Number of Scans: 139
Relaxation Delay: 1.000 s

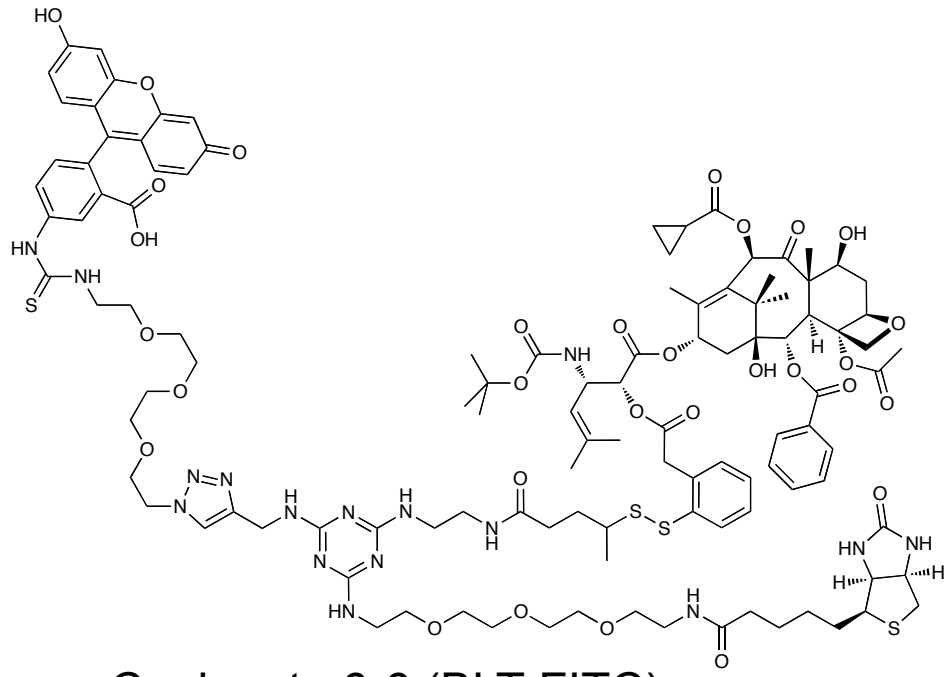

Conjugate 6-6 (BLT-FITC)

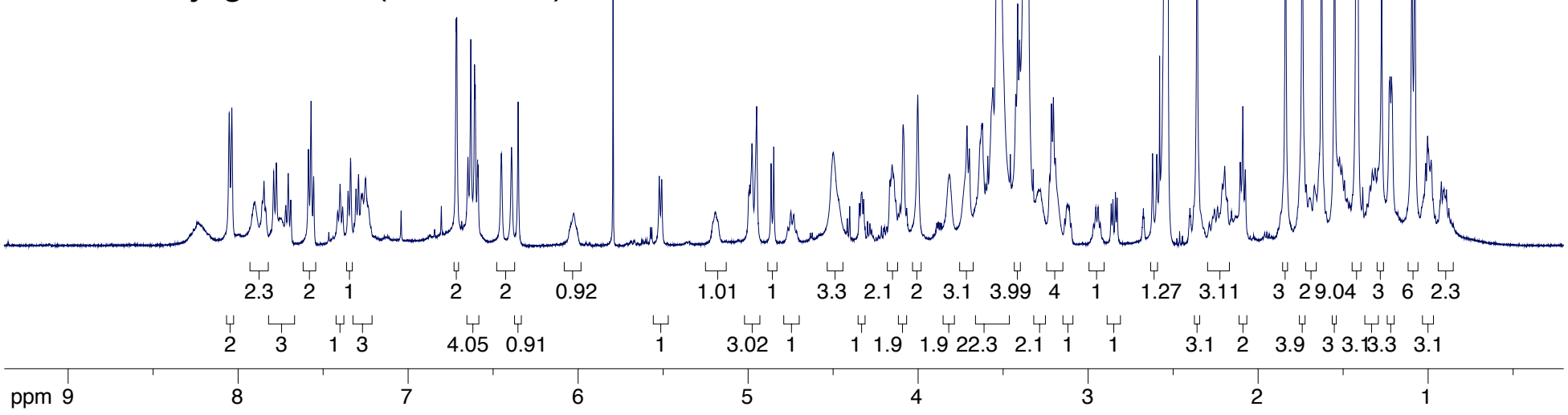

Compound Name: JGV-03-029
Processed by: Jacob Vineberg
Pulse Sequence: zgpg30
Spectrometer Freq.: 125.71 MHz
Solvent: DMSO
Temperature: 298.15 K
Spectral Width: 236.75 ppm
Number of Scans: 15586
Relaxation Delay: 2.000 s

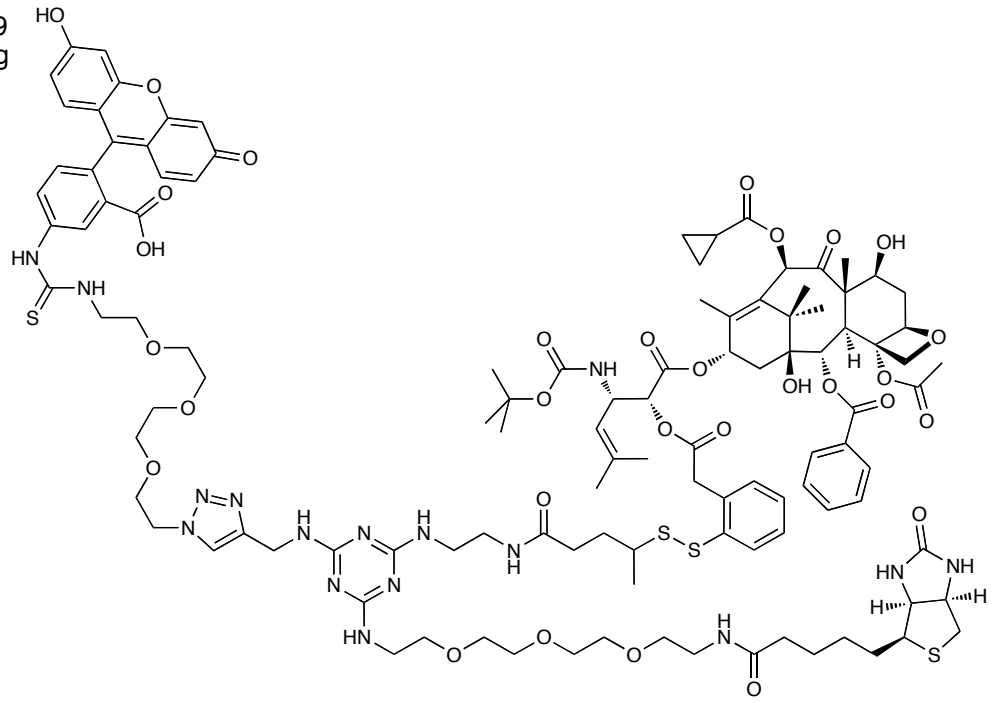

Conjugate 6-6 (BLT-FITC)

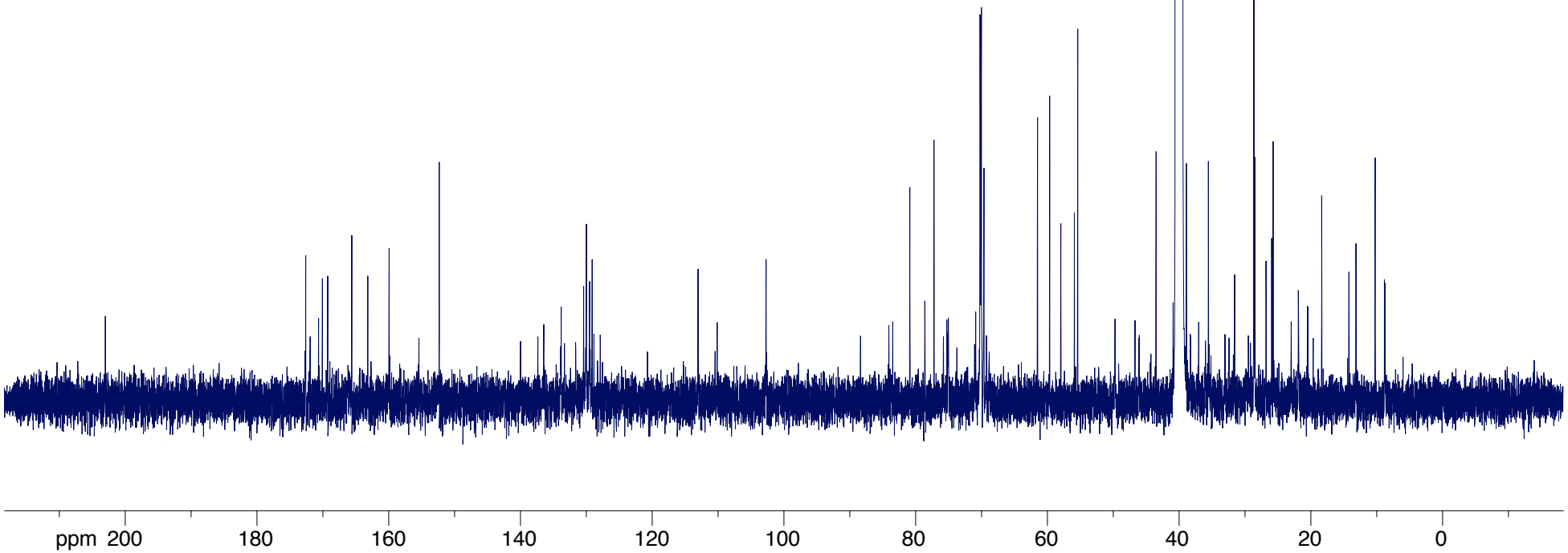

Appendix Chapter 8

Compound Name: JGV-03-075
Processed by: Jacob Vineberg
Pulse Sequence: zg30
Spectrometer Freq.: 300.18 MHz
Solvent: DMSO
Temperature: 293.45 K
Spectral Width: 20.33 ppm
Number of Scans: 78
Relaxation Delay: 1.000 s

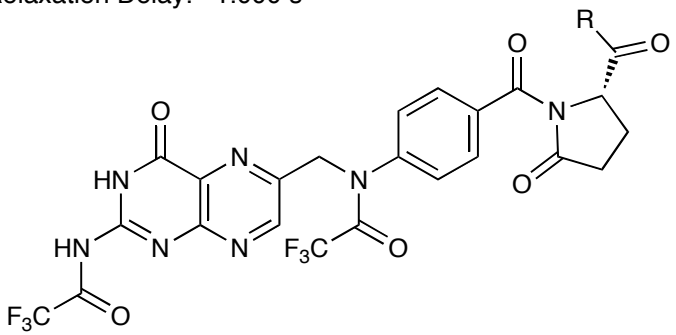

R = -OH, -OCOCF$_3$

Compound 8-1

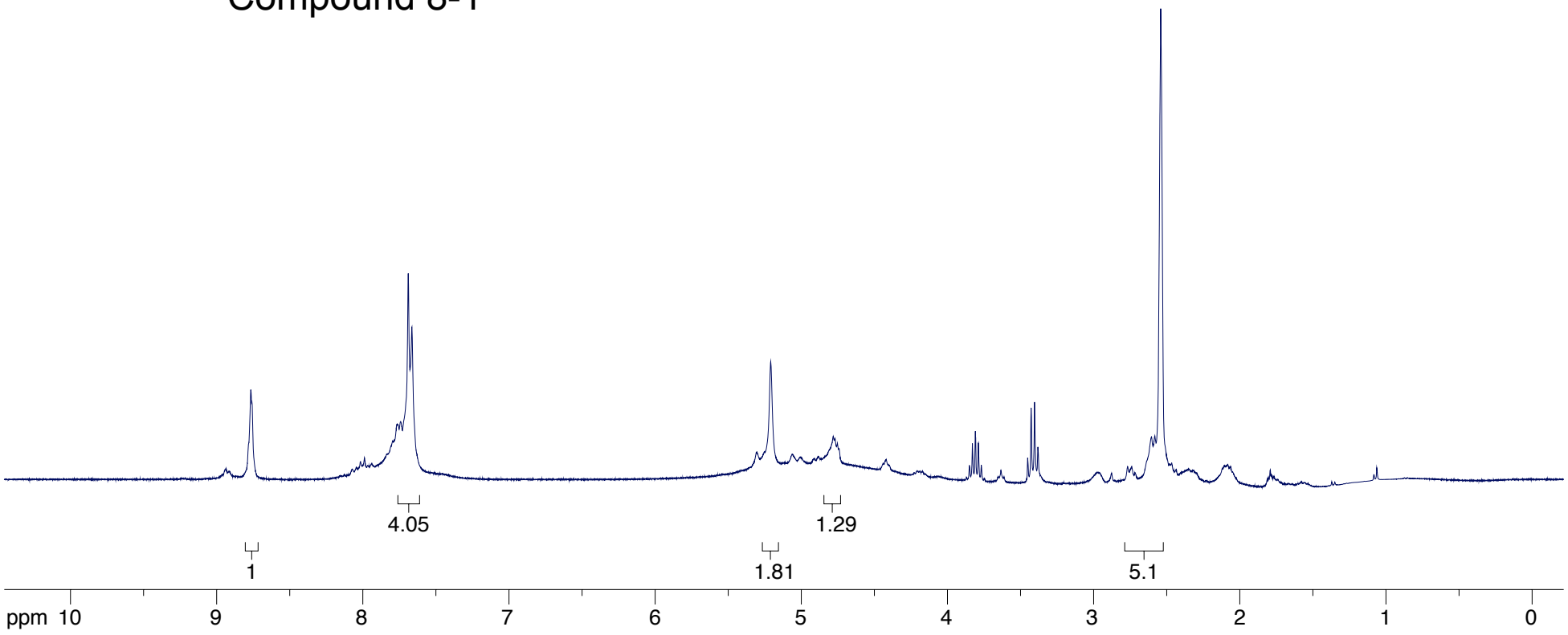

Compound Name: JGV-03-075-^{13}C
Processed by: Jacob Vineberg
Pulse Sequence: zgpg30
Spectrometer Freq.: 125.71 MHz
Solvent: DMSO
Temperature: 298.25 K
Spectral Width: 236.75 ppm
Number of Scans: 1583
Relaxation Delay: 2.000 s

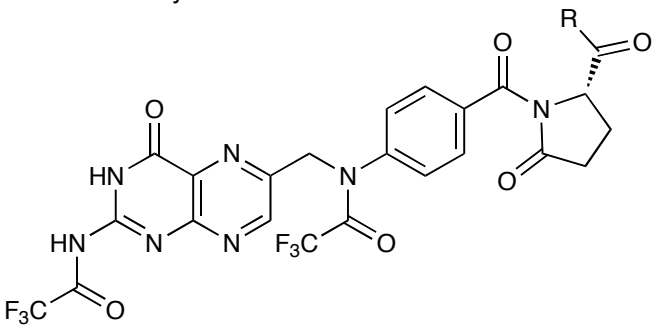

R = -OH, -OCOCF$_3$

Compound 8-1

Compound Name: JGV-03-075-^{19}F
Processed by: Jacob Vineberg
Pulse Sequence: zgflqn
Spectrometer Freq.: 376.18 MHz
Solvent: DMSO
Temperature: 298.00 K
Spectral Width: 237.35 ppm
Number of Scans: 66
Relaxation Delay: 1.000 s

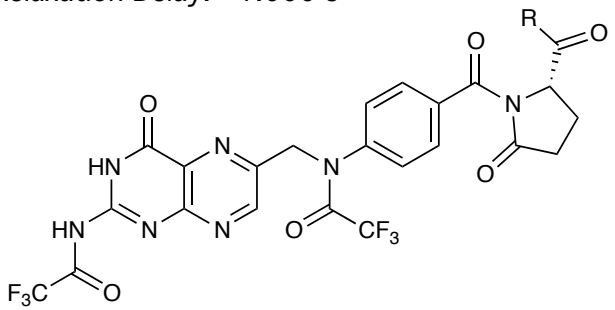

R = -OH, -OCOCF$_3$

Compound 8-1

Compound Name: JGV-03-077
Processed by: Jacob Vineberg
Pulse Sequence: zg30
Spectrometer Freq.: 499.89 MHz
Solvent: DMSO
Temperature: 298.25 K
Spectral Width: 20.00 ppm
Number of Scans: 24
Relaxation Delay: 1.000 s

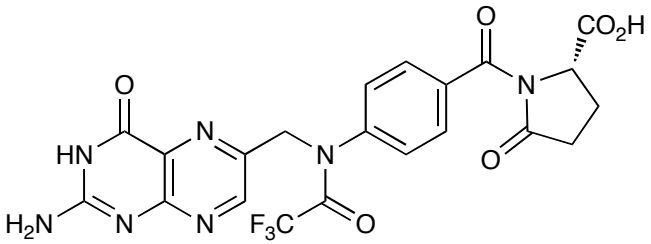

Compound 8-2

Compound Name: JGV-03-077-^{13}C
Processed by: Jacob Vineberg
Pulse Sequence: zgpg30
Spectrometer Freq.: 125.71 MHz
Solvent: DMSO
Temperature: 298.25 K
Spectral Width: 236.75 ppm
Number of Scans: 384
Relaxation Delay: 2.000 s

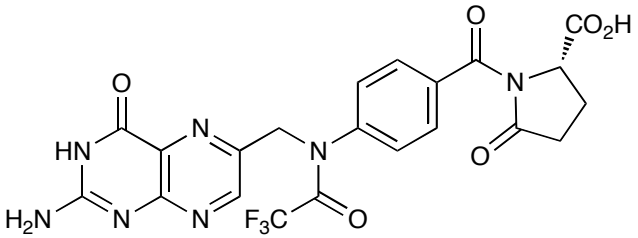

Compound 8-2

Compound Name: JGV-03-077-^{19}F
Processed by: Jacob Vineberg
Pulse Sequence: s2pul
Spectrometer Freq.: 282.32 MHz
Solvent: DMSO
Temperature: 298.15 K
Spectral Width: 177.10 ppm
Number of Scans: 1000
Relaxation Delay: 4.000 s

-66.633

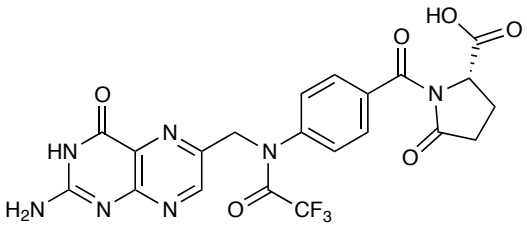

Compound 8-2

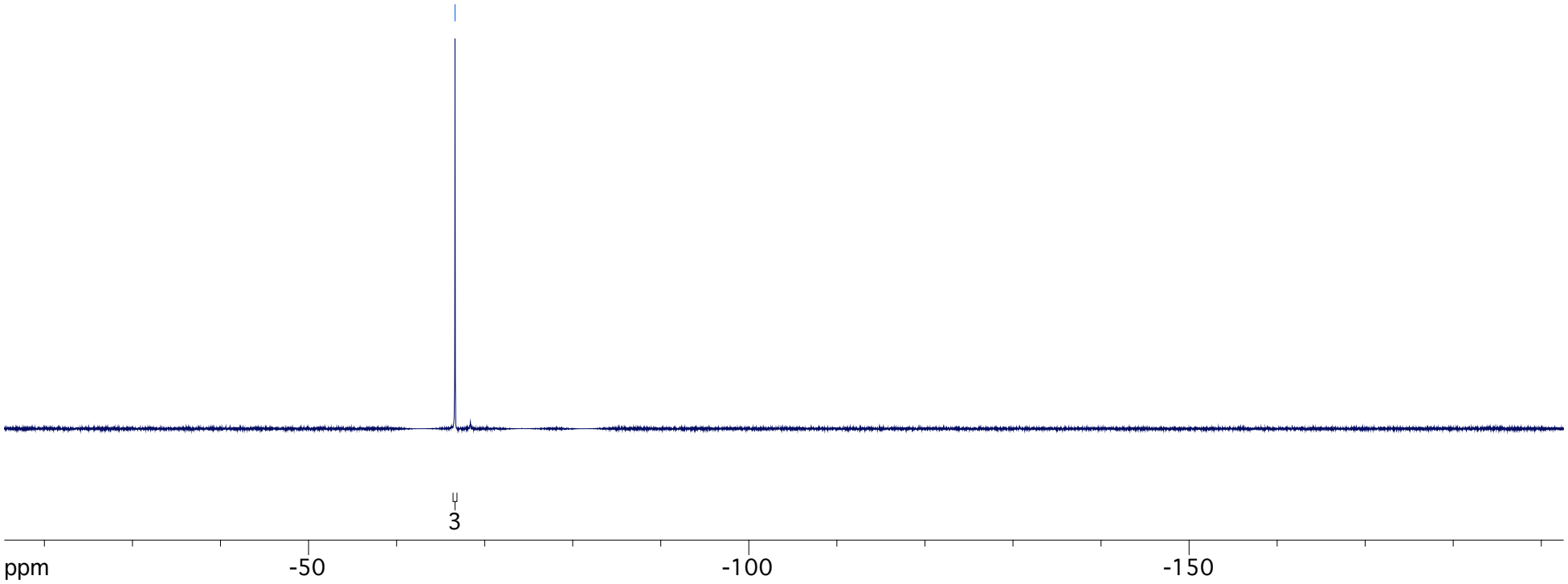

Compound Name: JGV-03-078
Processed by: Jacob Vineberg
Pulse Sequence: zg30
Spectrometer Freq.: 300.18 MHz
Solvent: DMSO
Temperature: 293.57 K
Spectral Width: 20.33 ppm
Number of Scans: 38
Relaxation Delay: 1.000 s

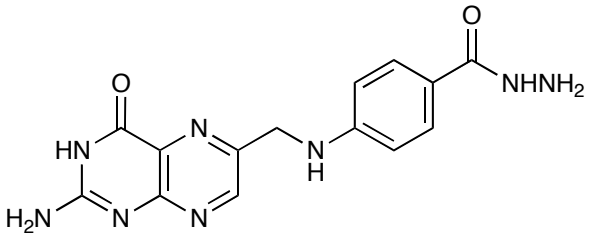

Compound 8-3

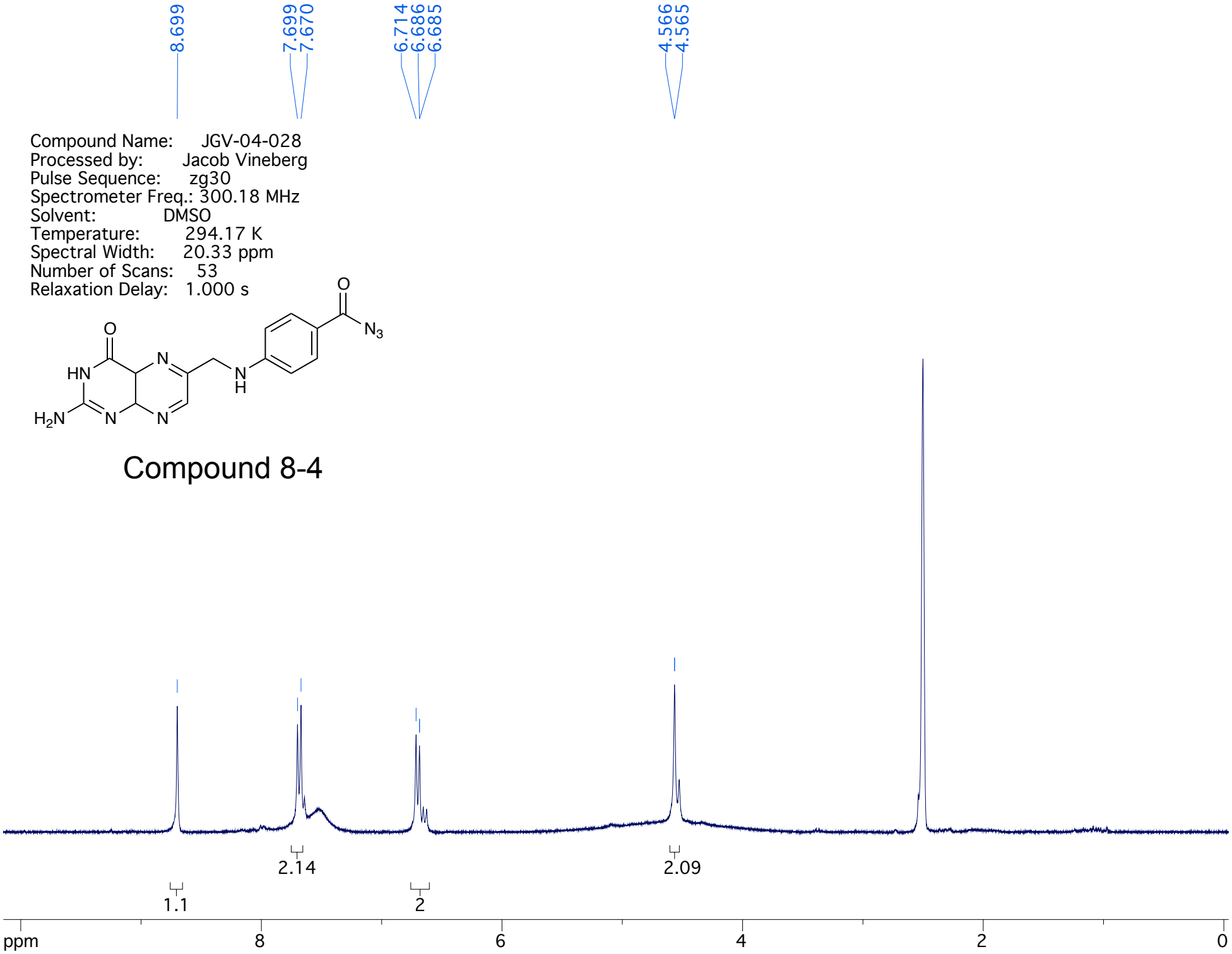
8.699
7.699
7.670
6.714
6.686
6.685
4.566
4.565
Compound Name: JGV-04-028
Processed by: Jacob Vineberg
Pulse Sequence: zg30
Spectrometer Freq.: 300.18 MHz
Solvent: DMSO
Temperature: 294.17 K
Spectral Width: 20.33 ppm
Number of Scans: 53
Relaxation Delay: 1.000 s
O
N3
O
HN
N
N
H
H2N
N
N
Compound 8-4
2.14
2.09
1.1
2
ppm
8
6
4
2
0

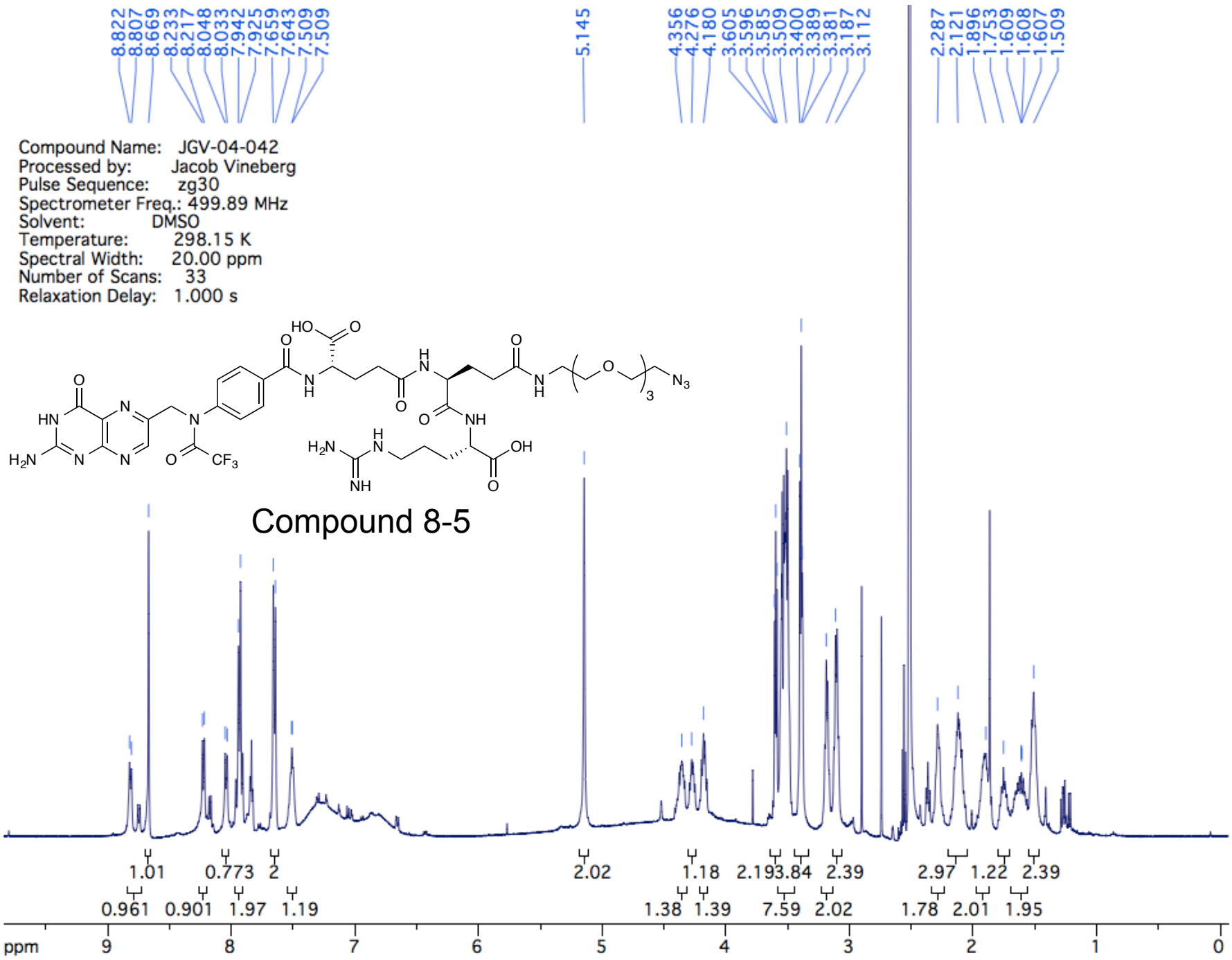
8.822
8.807
8.669
8.233
8.217
8.048
8.033
7.942
7.925
7.659
7.643
7.509
7.509
5.145
4.356
4.276
4.180
3.605
3.596
3.585
3.509
3.400
3.389
3.381
3.187
3.112
2.287
2.121
1.896
1.753
1.609
1.608
1.607
1.509
Compound Name: JGV-04-042
Processed by: Jacob Vineberg
Pulse Sequence: zg30
Spectrometer Freq.: 499.89 MHz
Solvent: DMSO
Temperature: 298.15 K
Spectral Width: 20.00 ppm
Number of Scans: 33
Relaxation Delay: 1.000 s
Compound 8-5
1.01
0.773
2
2.02
1.18
2.19
3.84
2.39
2.97
1.22
2.39
0.961
0.901
1.97
1.19
1.38
1.39
7.59
2.02
1.78
2.01
1.95
ppm
9
8
7
6
5
4
3
2
1
0

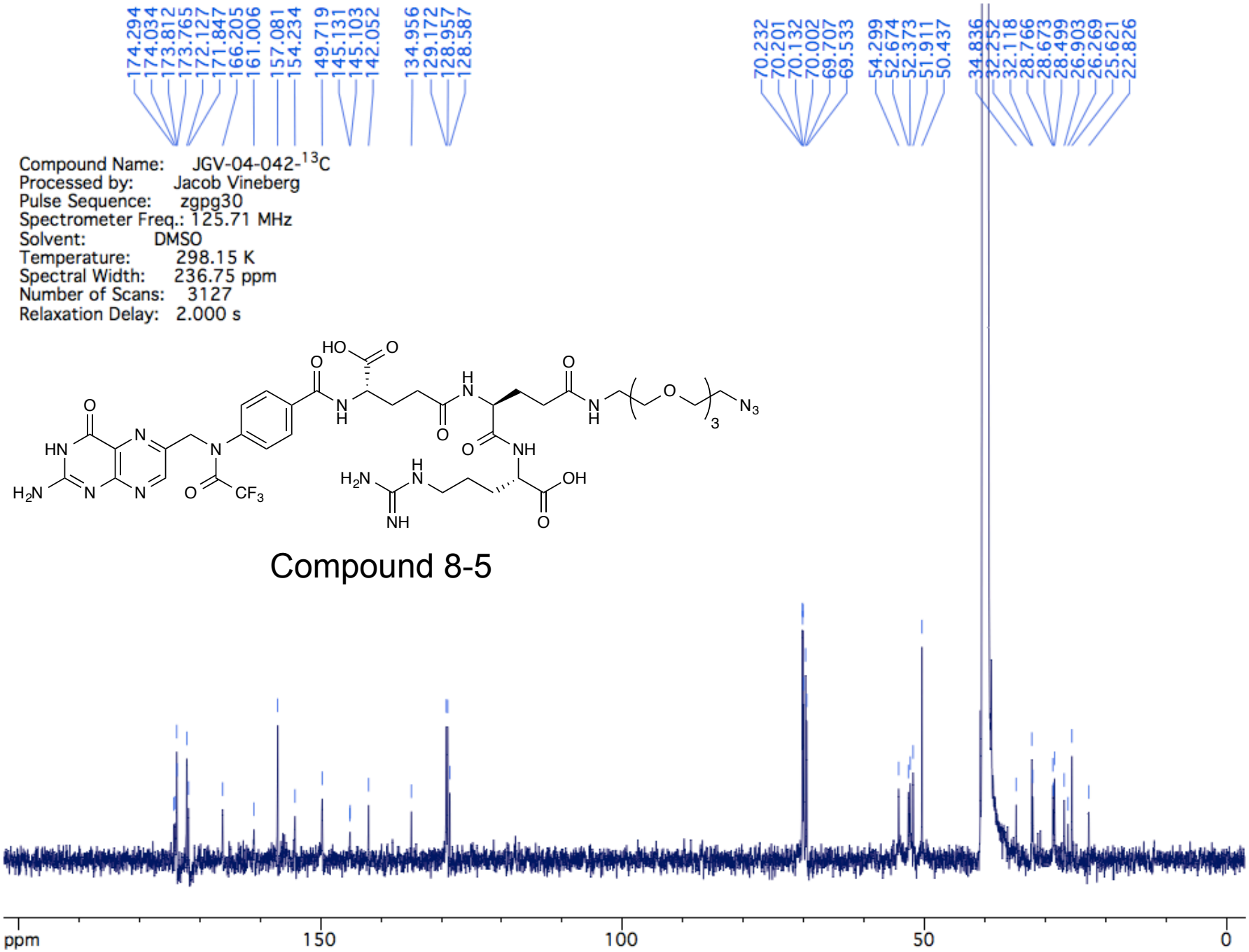
174.294
174.034
173.812
173.765
172.127
171.847
166.205
161.006
157.081
154.234
149.719
145.131
145.103
142.052
134.956
129.172
128.957
128.587
70.232
70.201
70.132
70.002
69.707
69.533
54.299
52.674
52.373
51.911
50.437
34.836
32.252
32.118
28.766
28.673
28.499
26.903
26.269
25.621
22.826
Compound Name: JGV-04-042-13C
Processed by: Jacob Vineberg
Pulse Sequence: zgpg30
Spectrometer Freq.: 125.71 MHz
Solvent: DMSO
Temperature: 298.15 K
Spectral Width: 236.75 ppm
Number of Scans: 3127
Relaxation Delay: 2.000 s
Compound 8-5
ppm
150
100
50
0

Compound Name: JGV-04-042-^{19}F
Processed by: Jacob Vineberg
Pulse Sequence: s2pul
Spectrometer Freq.: 282.32 MHz
Solvent: DMSO
Temperature: 298.15 K
Spectral Width: 177.10 ppm
Number of Scans: 16
Relaxation Delay: 4.000 s

66.581

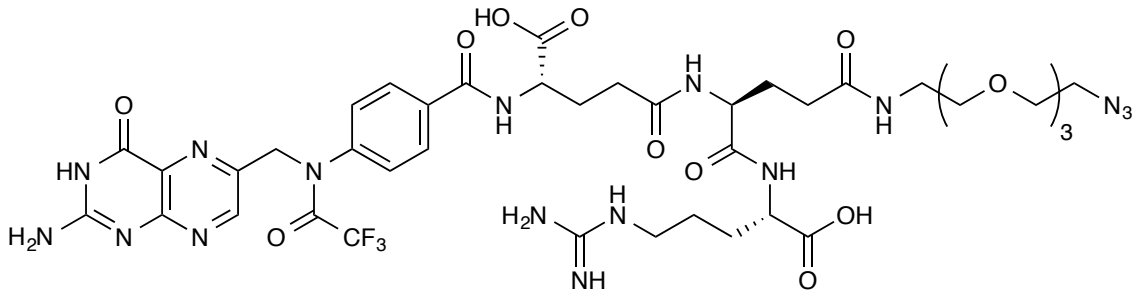

Compound 8-5

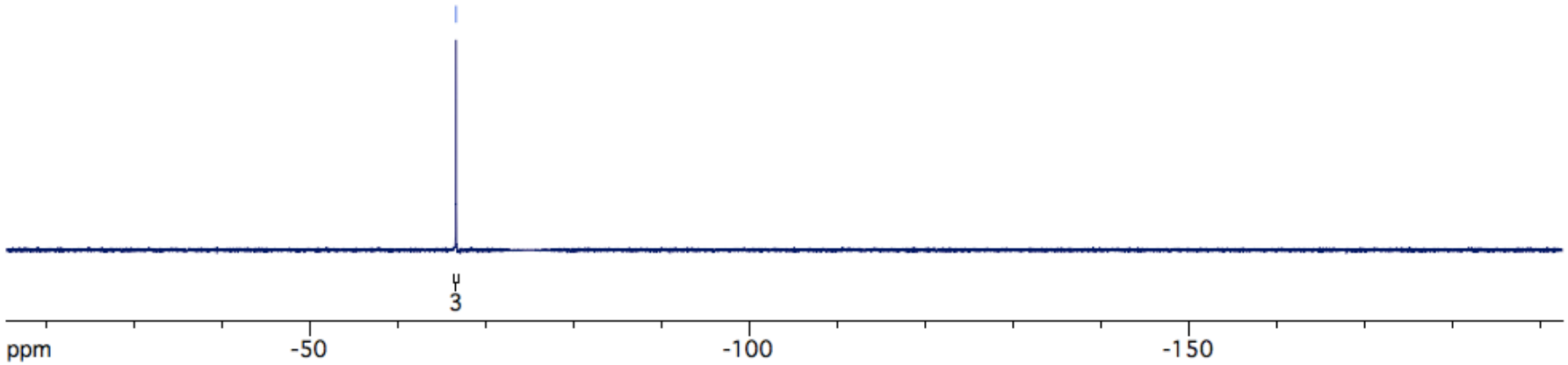

Compound Name: JGV-04-047
Processed by: Jacob Vineberg
Pulse Sequence: zg30
Spectrometer Freq.: 499.89 MHz
Solvent: DMSO
Temperature: 298.14 K
Spectral Width: 20.00 ppm
Number of Scans: 128
Relaxation Delay: 1.000 s

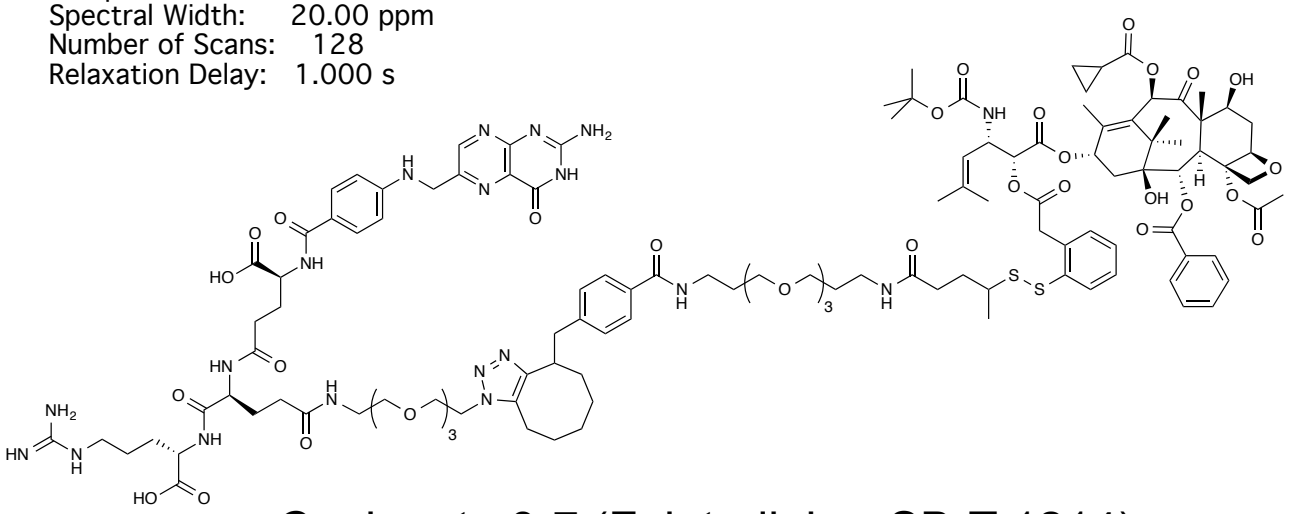

Conjugate 8-7 (Folate-linker-SB-T-1214)

Compound Name: JGV-04-047
Processed by: Jacob Vineberg
Pulse Sequence: zgpg30
Spectrometer Freq.: 125.71 MHz
Solvent: DMSO
Temperature: 298.15 K
Spectral Width: 236.75 ppm
Number of Scans: 72007
Relaxation Delay: 2.000 s

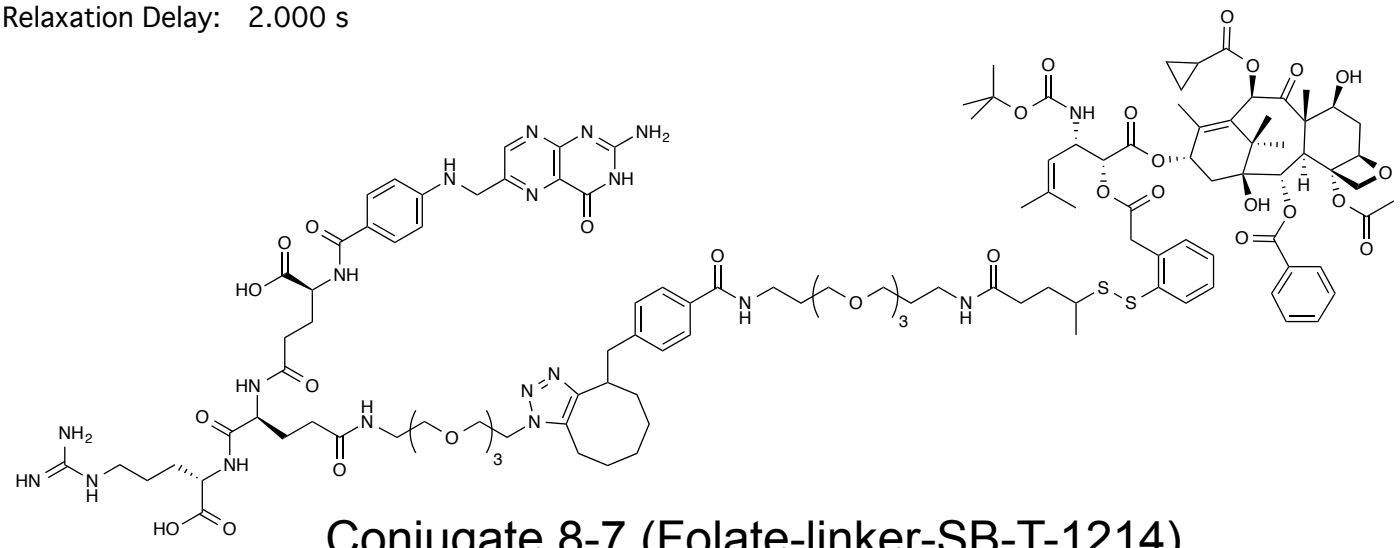

Conjugate 8-7 (Folate-linker-SB-T-1214)

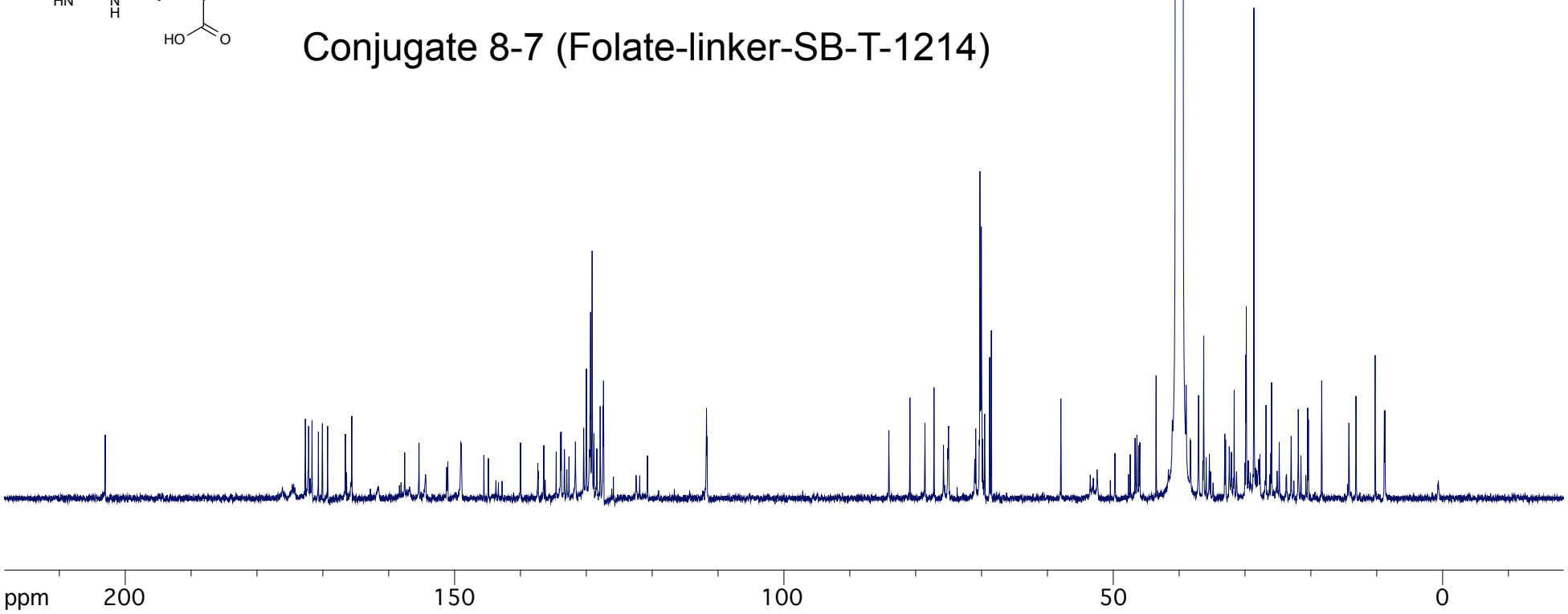

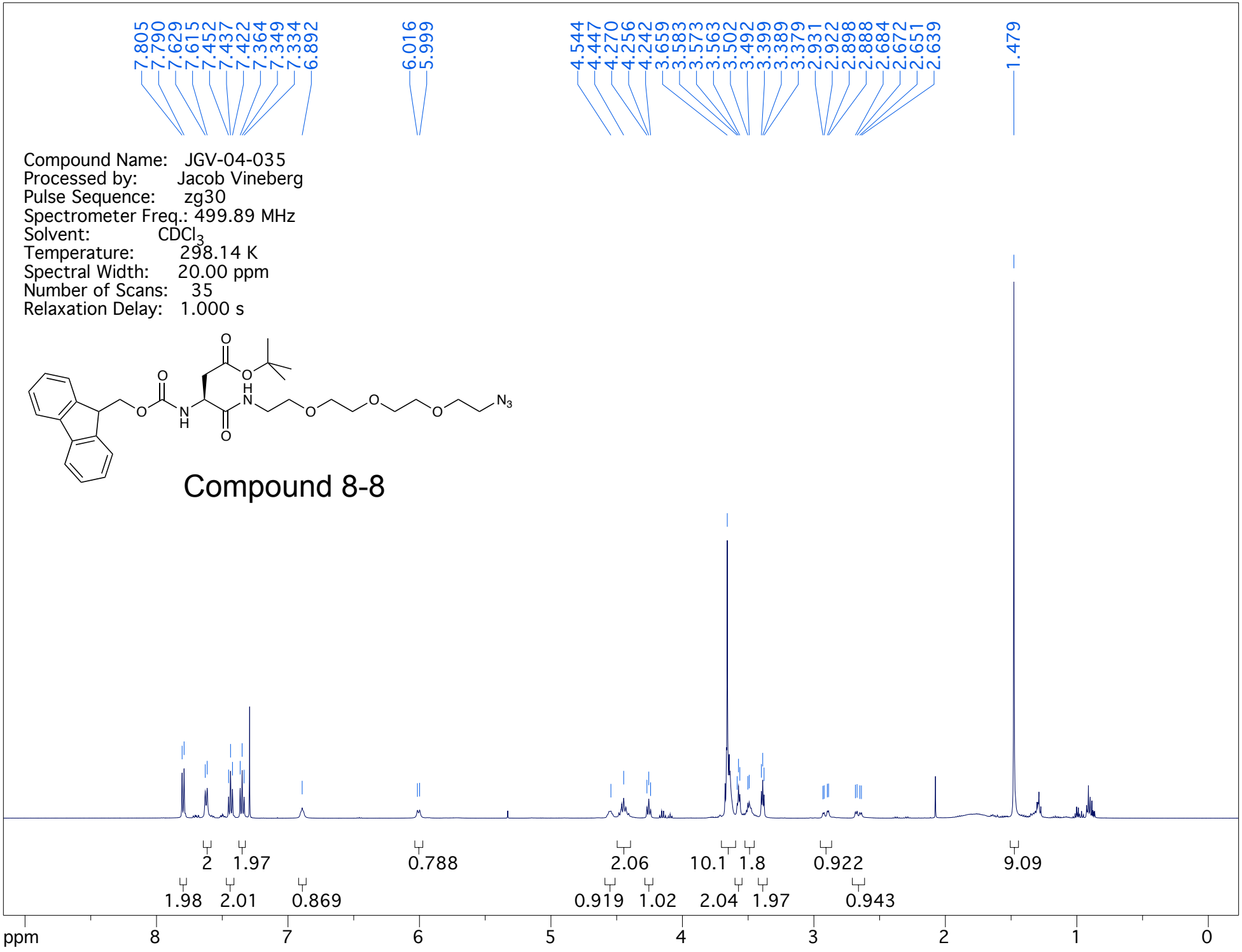
7.805
7.790
7.629
7.615
7.452
7.437
7.422
7.364
7.349
7.334
6.892
6.016
5.999
4.544
4.447
4.270
4.256
4.242
3.659
3.583
3.573
3.563
3.502
3.492
3.399
3.389
3.379
2.931
2.922
2.898
2.888
2.684
2.672
2.651
2.639
1.479
Compound Name: JGV-04-035
Processed by: Jacob Vineberg
Pulse Sequence: zg30
Spectrometer Freq.: 499.89 MHz
Solvent: $CDCl_3$
Temperature: 298.14 K
Spectral Width: 20.00 ppm
Number of Scans: 35
Relaxation Delay: 1.000 s
Compound 8-8
2
1.97
0.788
2.06
10.1
1.8
0.922
9.09
1.98
2.01
0.869
0.919
1.02
2.04
1.97
0.943
ppm
8
7
6
5
4
3
2
1
0

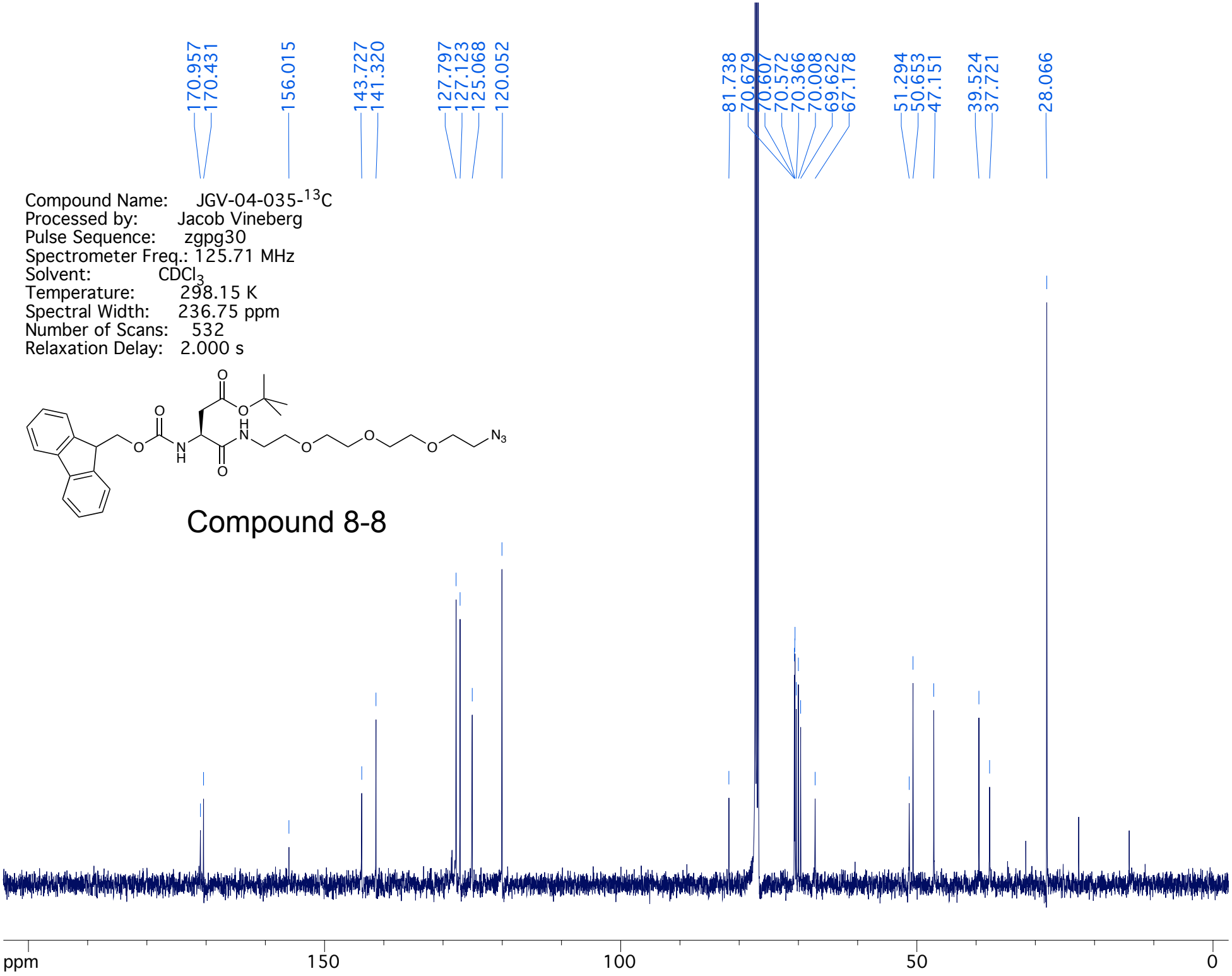
170.957
170.431
156.015
143.727
141.320
127.797
127.123
125.068
120.052
81.738
70.679
70.607
70.572
70.366
70.008
69.622
67.178
51.294
50.653
47.151
39.524
37.721
28.066
Compound Name: JGV-04-035-13C
Processed by: Jacob Vineberg
Pulse Sequence: zgpg30
Spectrometer Freq.: 125.71 MHz
Solvent: CDCl3
Temperature: 298.15 K
Spectral Width: 236.75 ppm
Number of Scans: 532
Relaxation Delay: 2.000 s
Compound 8-8
ppm
150
100
50
0

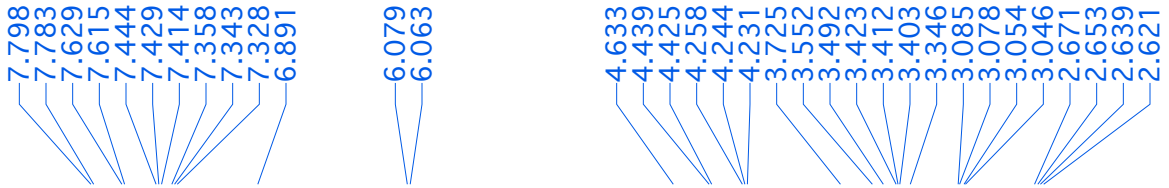

Compound Name: JGV-04-036
Processed by: Jacob Vineberg
Pulse Sequence: zg30
Spectrometer Freq.: 499.89 MHz
Solvent: $CDCl_3$
Temperature: 298.14 K
Spectral Width: 20.00 ppm
Number of Scans: 57
Relaxation Delay: 1.000 s

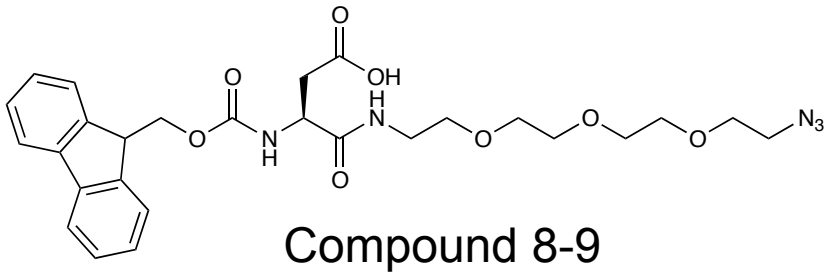

Compound 8-9

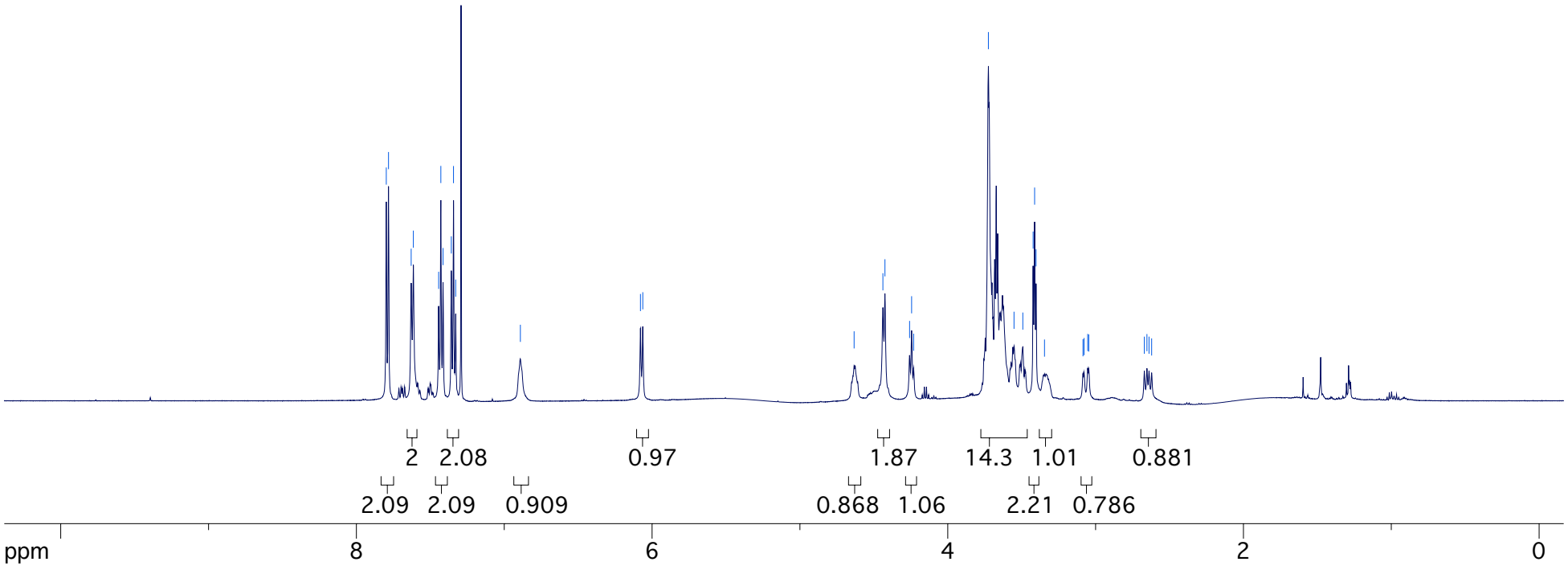

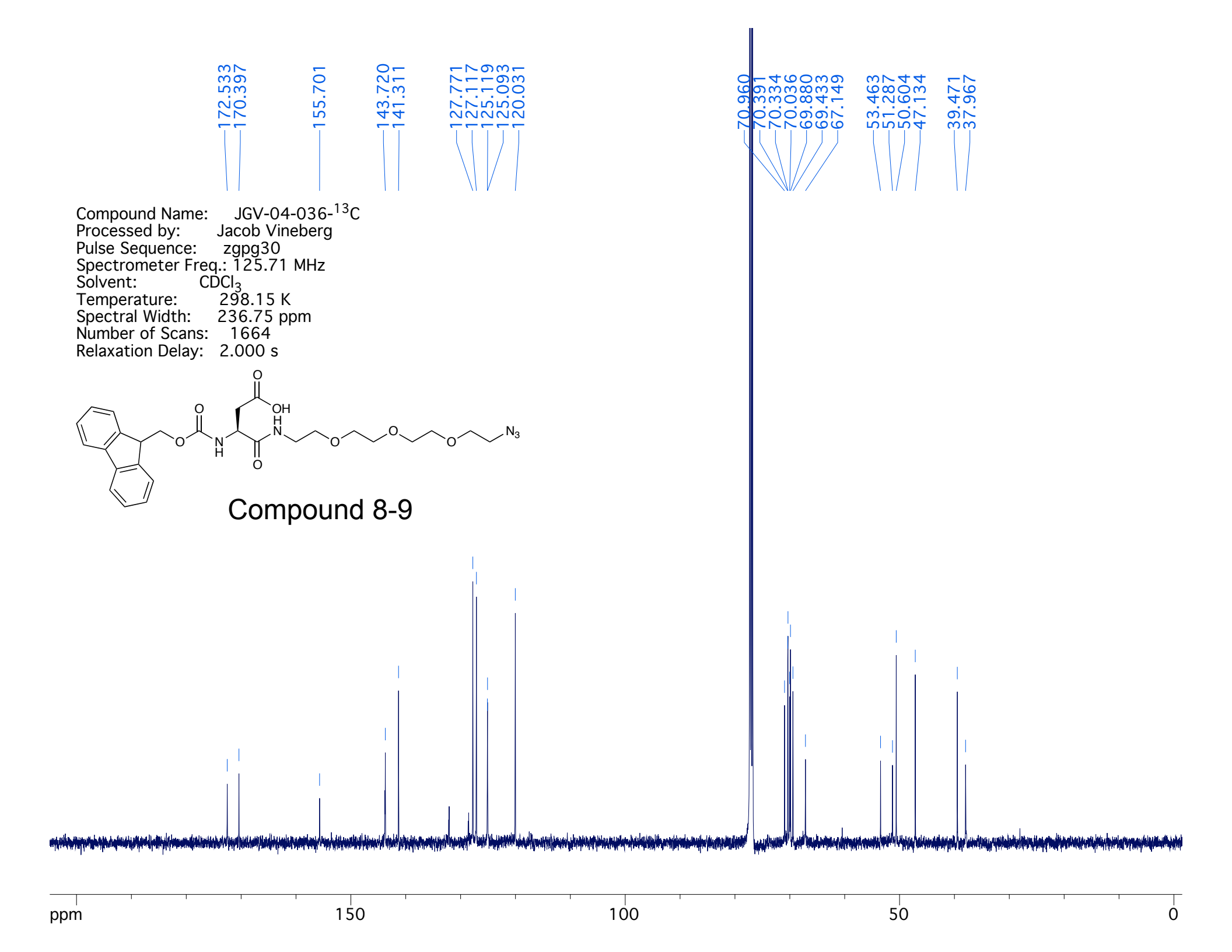
172.533
170.397
155.701
143.720
141.311
127.771
127.117
125.119
125.093
120.031
70.960
70.391
70.334
70.036
69.880
69.433
67.149
53.463
51.287
50.604
47.134
39.471
37.967
Compound Name: JGV-04-036-13C
Processed by: Jacob Vineberg
Pulse Sequence: zgpg30
Spectrometer Freq.: 125.71 MHz
Solvent: CDCl3
Temperature: 298.15 K
Spectral Width: 236.75 ppm
Number of Scans: 1664
Relaxation Delay: 2.000 s
Compound 8-9
ppm
150
100
50
0

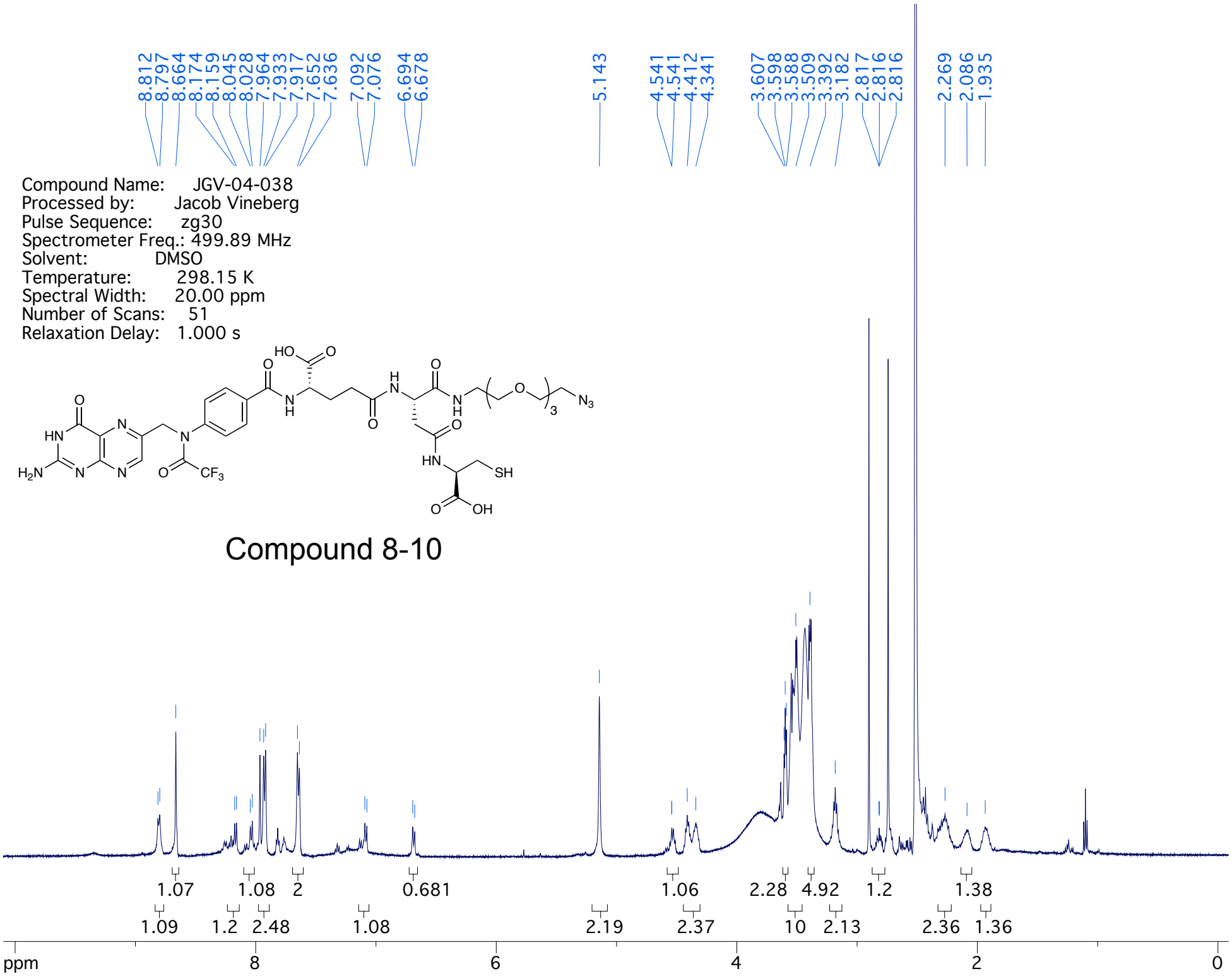
8.812
8.797
8.664
8.174
8.159
8.045
8.028
7.964
7.933
7.917
7.652
7.636
7.092
7.076
6.694
6.678
5.143
4.541
4.541
4.412
4.341
3.607
3.598
3.588
3.509
3.392
3.182
2.817
2.816
2.816
2.269
2.086
1.935
Compound Name: JGV-04-038
Processed by: Jacob Vineberg
Pulse Sequence: zg30
Spectrometer Freq.: 499.89 MHz
Solvent: DMSO
Temperature: 298.15 K
Spectral Width: 20.00 ppm
Number of Scans: 51
Relaxation Delay: 1.000 s
Compound 8-10
1.07
1.08
2
0.681
1.06
2.28
4.92
1.2
1.38
1.09
1.2
2.48
1.08
2.19
2.37
10
2.13
2.36
1.36
ppm
8
6
4
2
0

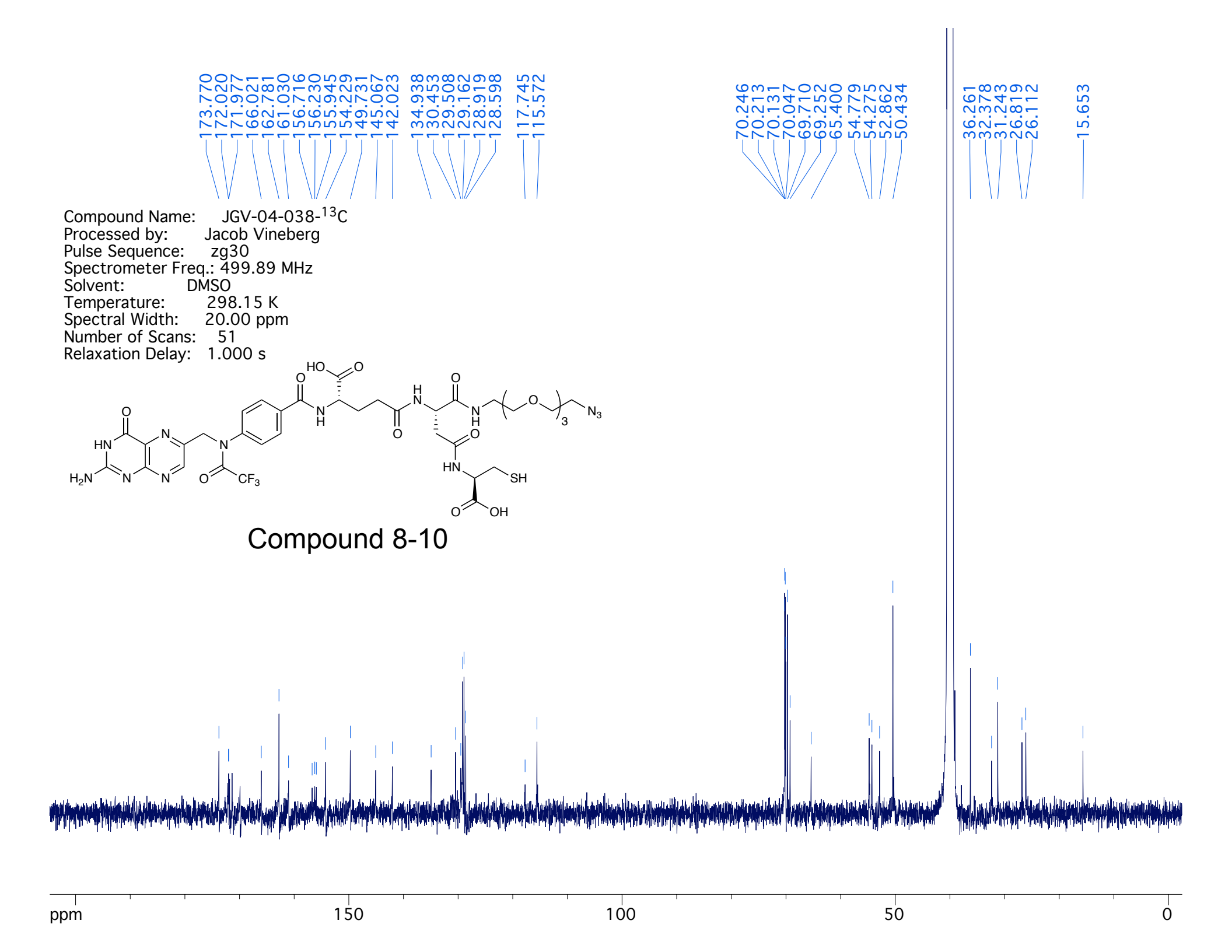
173.770
172.020
171.977
166.021
162.781
161.030
156.716
156.230
155.945
154.229
149.731
145.067
142.023
134.938
130.453
129.508
129.162
128.919
128.598
117.745
115.572
70.246
70.213
70.131
70.047
69.710
69.252
65.400
54.779
54.275
52.862
50.434
36.261
32.378
31.243
26.819
26.112
15.653
Compound Name: JGV-04-038-13C
Processed by: Jacob Vineberg
Pulse Sequence: zg30
Spectrometer Freq.: 499.89 MHz
Solvent: DMSO
Temperature: 298.15 K
Spectral Width: 20.00 ppm
Number of Scans: 51
Relaxation Delay: 1.000 s
Compound 8-10
ppm
150
100
50
0

Compound Name: JGV-04-038-^{19}F
Processed by: Jacob Vineberg
Pulse Sequence: zgflqn
Spectrometer Freq.: 376.18 MHz
Solvent: DMSO
Temperature: 298.15 K
Spectral Width: 237.35 ppm
Number of Scans: 61
Relaxation Delay: 1.000 s

-66.061

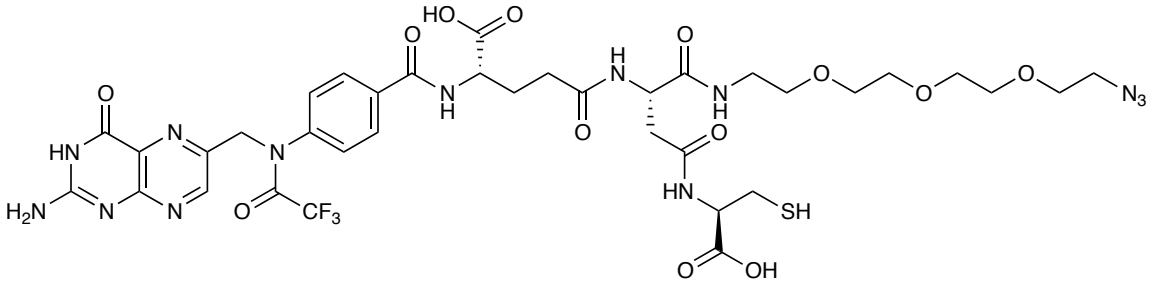

Compound 8-10

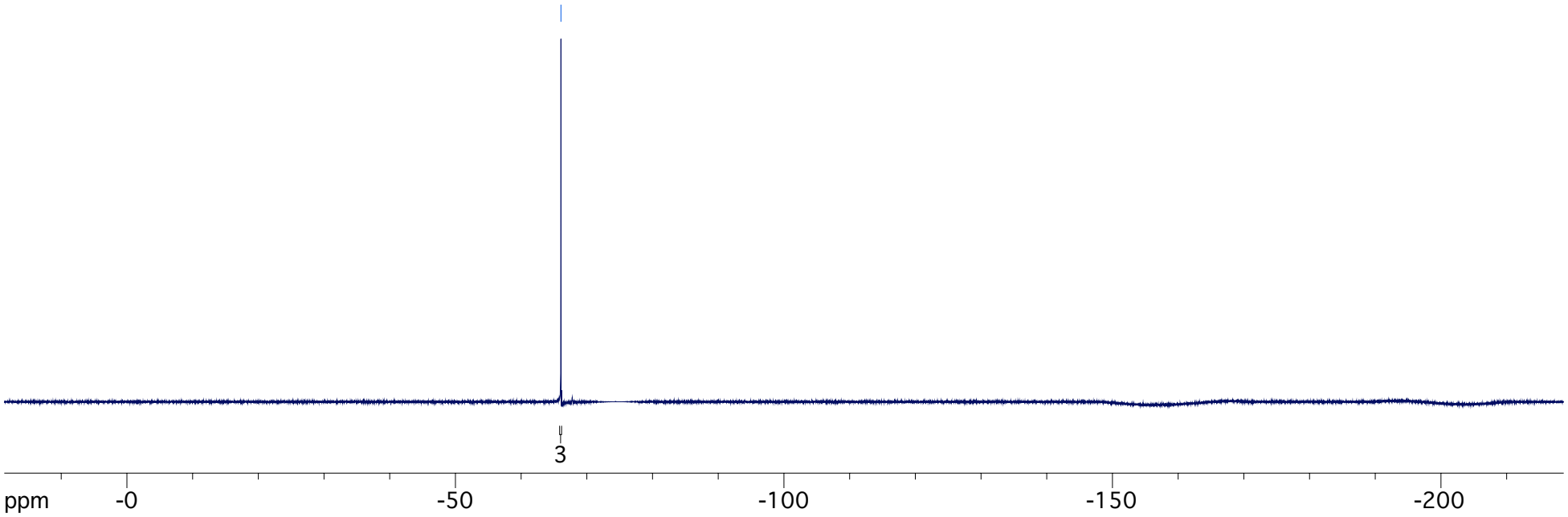

Compound Name: JGV-04-041
Processed by: Jacob Vineberg
Pulse Sequence: zg30
Spectrometer Freq.: 499.89 MHz
Solvent: DMSO
Temperature: 298.15 K
Spectral Width: 20.00 ppm
Number of Scans: 31
Relaxation Delay: 1.000 s

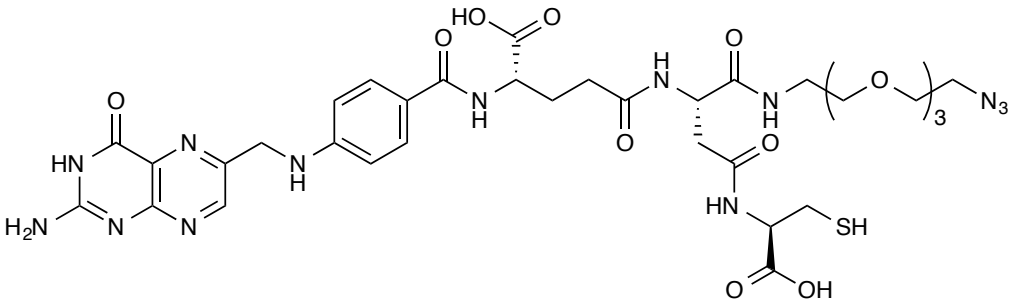

Compound 8-11

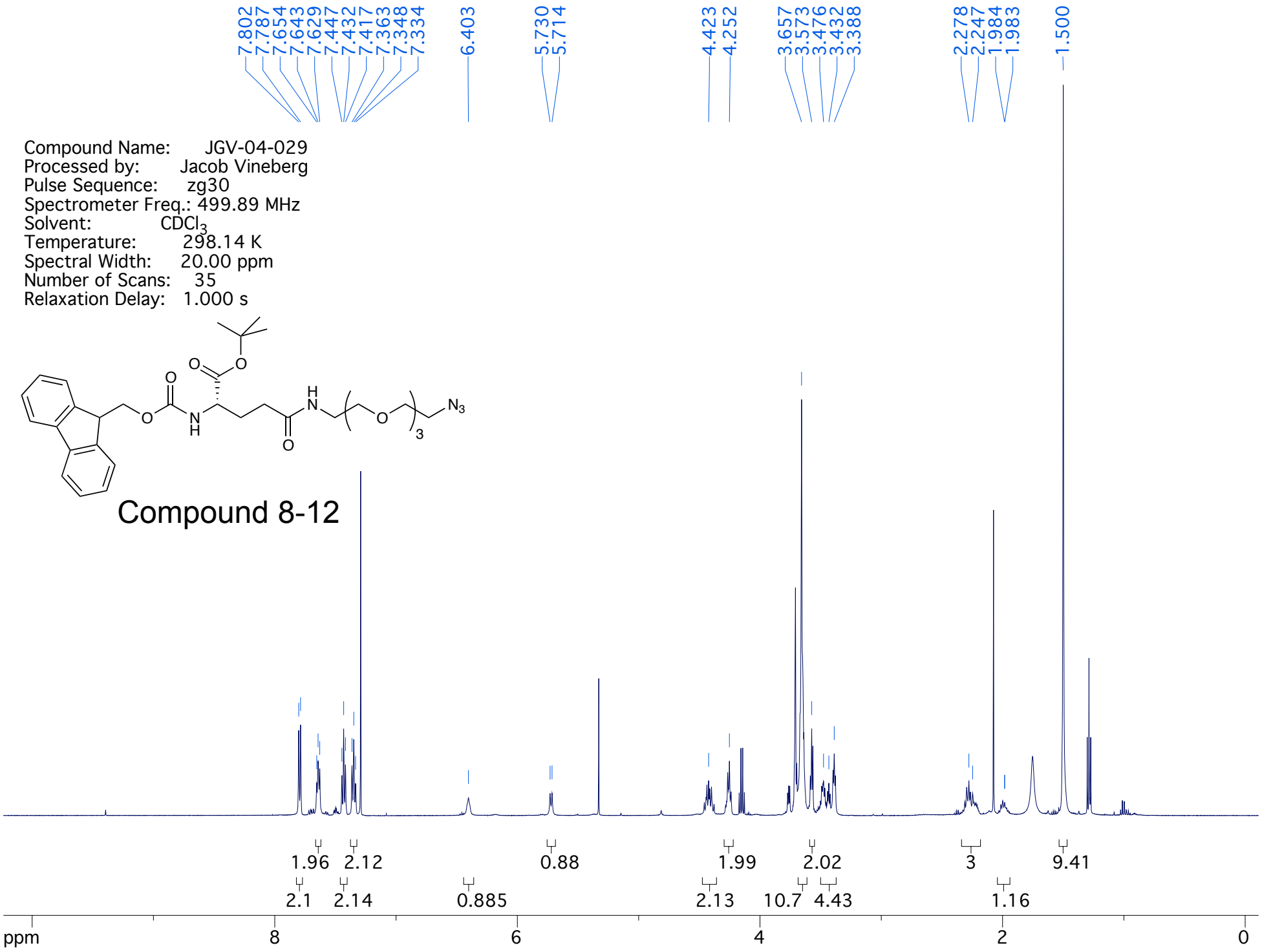
7.802
7.787
7.654
7.643
7.629
7.447
7.432
7.417
7.363
7.348
7.334
6.403
5.730
5.714
4.423
4.252
3.657
3.573
3.476
3.432
3.388
2.278
2.247
1.984
1.983
1.500
Compound Name: JGV-04-029
Processed by: Jacob Vineberg
Pulse Sequence: zg30
Spectrometer Freq.: 499.89 MHz
Solvent: $CDCl_3$
Temperature: 298.14 K
Spectral Width: 20.00 ppm
Number of Scans: 35
Relaxation Delay: 1.000 s
Compound 8-12
1.96
2.12
0.88
1.99
2.02
3
9.41
2.1
2.14
0.885
2.13
10.7
4.43
1.16
ppm
8
6
4
2
0

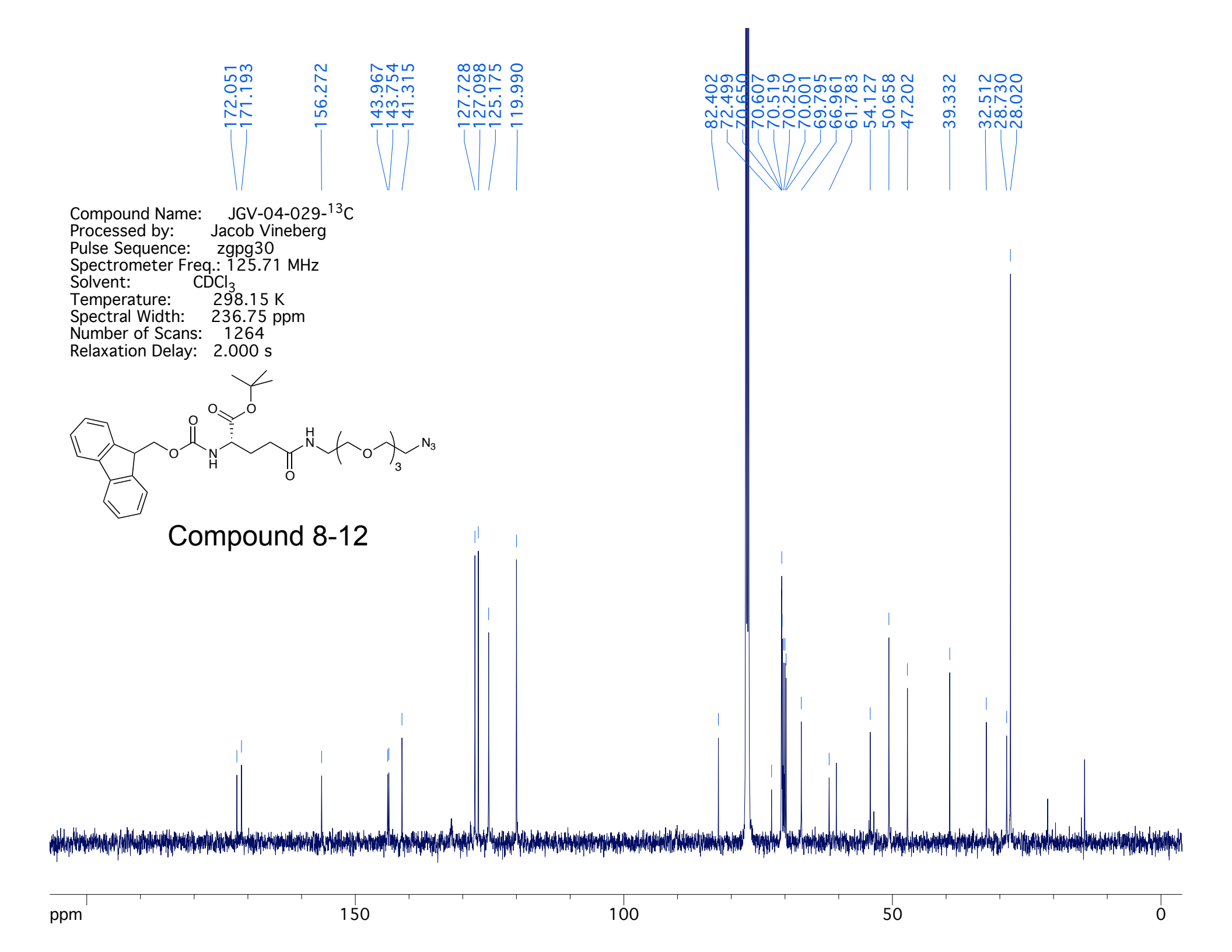
172.051
171.193
156.272
143.967
143.754
141.315
127.728
127.098
125.175
119.990
82.402
72.499
70.650
70.607
70.519
70.250
70.001
69.795
66.961
61.783
54.127
50.658
47.202
39.332
32.512
28.730
28.020
Compound Name: JGV-04-029-13C
Processed by: Jacob Vineberg
Pulse Sequence: zgpg30
Spectrometer Freq.: 125.71 MHz
Solvent: CDCl3
Temperature: 298.15 K
Spectral Width: 236.75 ppm
Number of Scans: 1264
Relaxation Delay: 2.000 s
Compound 8-12
ppm
150
100
50
0

Compound Name: JGV-04-030
Processed by: Jacob Vineberg
Pulse Sequence: zg30
Spectrometer Freq.: 499.89 MHz
Solvent: $CDCl_3$
Temperature: 298.15 K
Spectral Width: 20.00 ppm
Number of Scans: 39
Relaxation Delay: 1.000 s

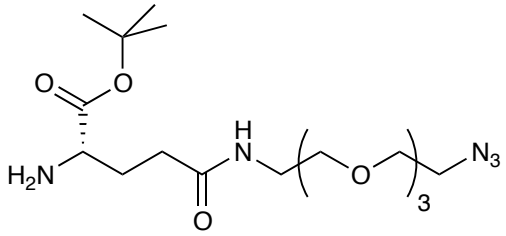

Compound 8-13

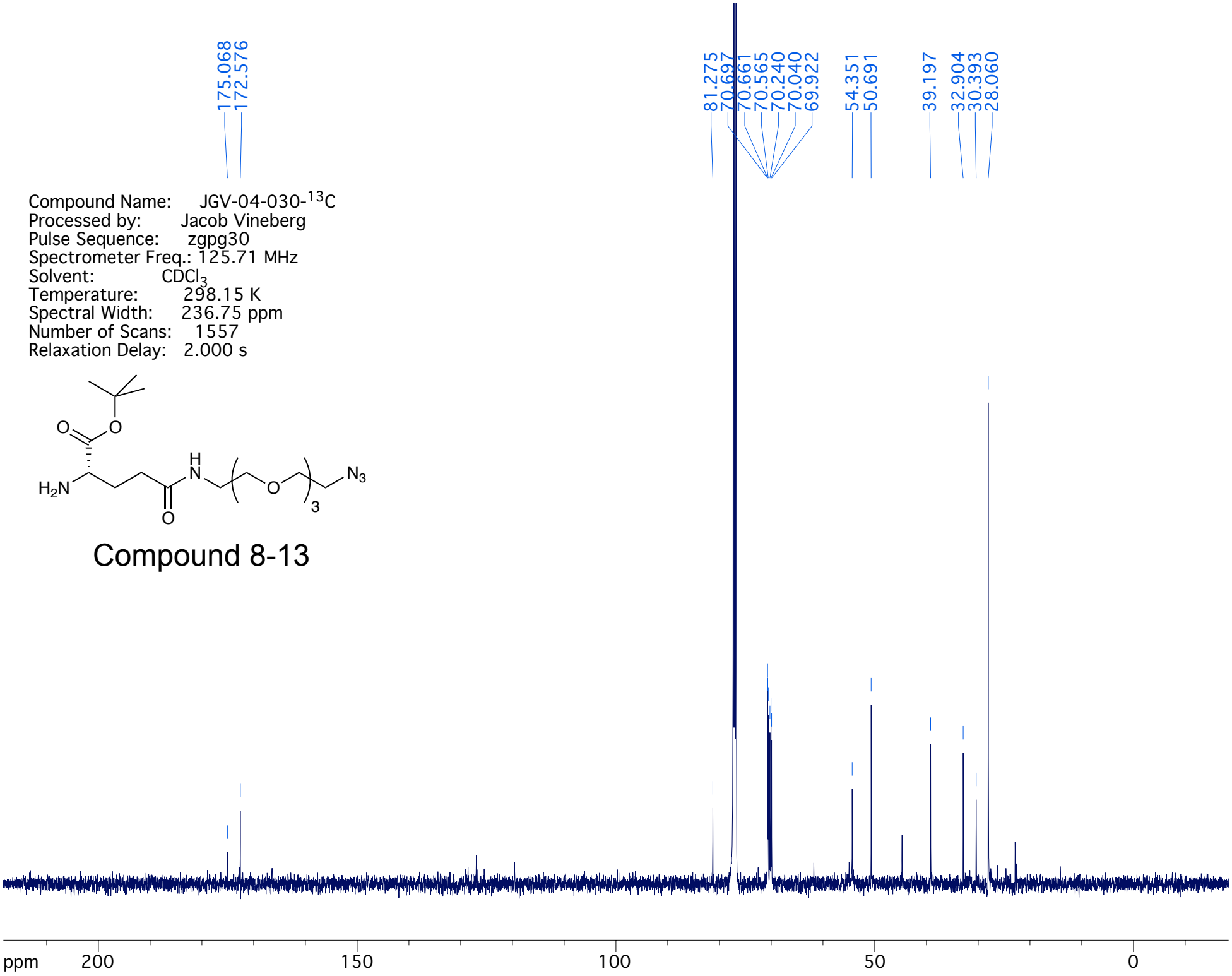
175.068
172.576
81.275
70.697
70.661
70.565
70.240
70.040
69.922
54.351
50.691
39.197
32.904
30.393
28.060
Compound Name: JGV-04-030-13C
Processed by: Jacob Vineberg
Pulse Sequence: zgpg30
Spectrometer Freq.: 125.71 MHz
Solvent: CDCl3
Temperature: 298.15 K
Spectral Width: 236.75 ppm
Number of Scans: 1557
Relaxation Delay: 2.000 s
Compound 8-13
ppm
200
150
100
50
0

Compound Name: JGV-04-078
Processed by: Jacob Vineberg
Pulse Sequence: zg30
Spectrometer Freq.: 399.83 MHz
Solvent: DMSO
Temperature: 298.15 K
Spectral Width: 20.57 ppm
Number of Scans: 100
Relaxation Delay: 1.000 s

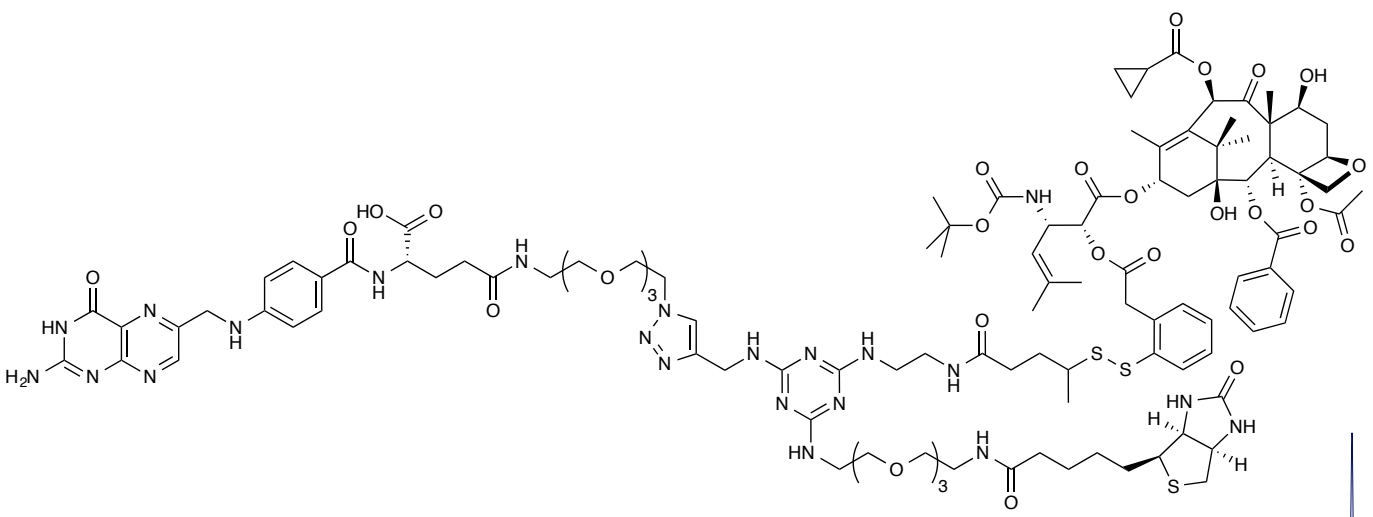

Conjugate 8-18 (DV-1)

203.0037
172.6479
170.6162
170.0606
169.2495
165.5939
163.1700
162.7617
155.3884
139.9795
137.3368
136.4641
133.8639
133.3327
131.6069
130.3905
129.9751
129.5189
129.1001
128.8241
127.9075
120.6993
111.6433
84.0546
80.8773
78.5931
77.2076
75.7740
74.9918
70.9011
70.1954
70.0604
70.0029
69.6042
61.4982
59.6587
57.9674
55.8814
49.7344
46.6858
46.0281
43.4827
38.8712
38.2548
36.9967
36.2441
35.5550
35.4082
33.0525
32.4675
31.5572
31.2337
28.6401
28.5017
26.7966
25.9382
25.7224
22.9712
21.8819
20.4994
18.3352
14.2220
14.1940
13.1414
10.2167
8.8155
8.7322

Compound Name: JGV-04-078-^{13}C
Processed by: Jacob Vineberg
Pulse Sequence: zgpg30
Spectrometer Freq.: 176.07 MHz
Solvent: DMSO
Temperature: 298.15 K
Spectral Width: 236.65 ppm
Number of Scans: 7269
Relaxation Delay: 2.000 s

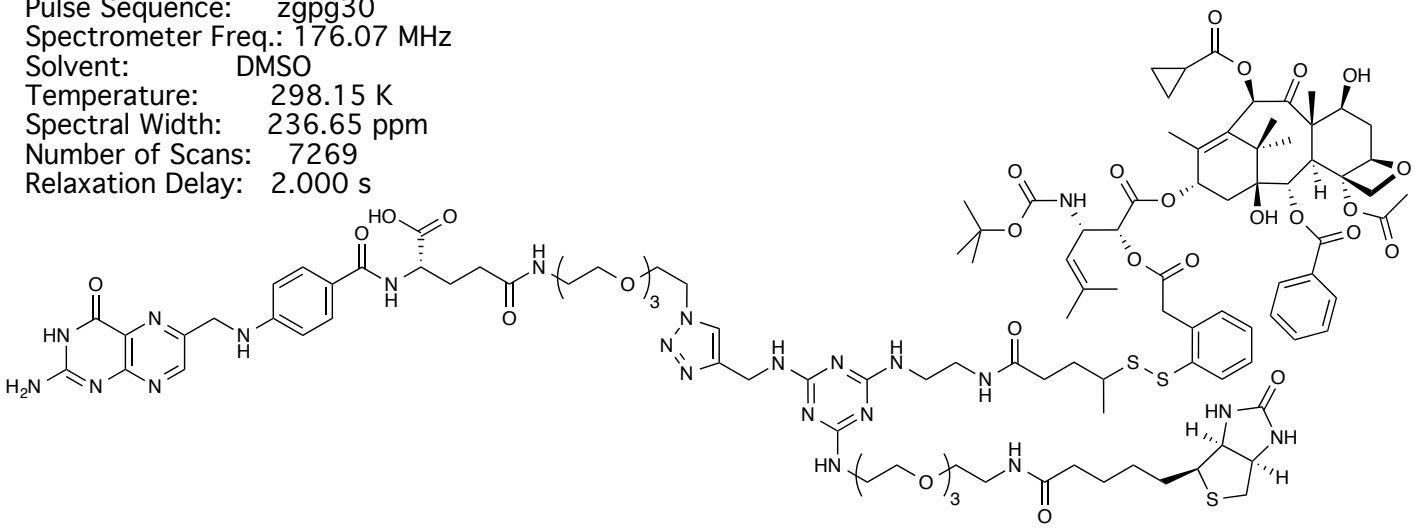

Conjugate 8-18 (DV-1)